

Geophysical Monograph Series
American Geophysical Union

Geophysical Monograph Series

A. F. SPILHAUS, JR., *managing editor*

1 Antarctica in the International Geophysical Year

A. P. CRARY, L. M. GOULD, E. O. HULBURT, HUGH ODISHAW, AND WALDO E. SMITH, *editors*

2 Geophysics and the IGY

HUGH ODISHAW AND STANLEY RUTTENBERG, *editors*

3 Atmospheric Chemistry of Chlorine and Sulfur Compounds

JAMES P. LODGE, JR., *editor*

4 Contemporary Geodesy

CHARLES A. WHITTEN AND KENNETH H. DRUMMOND, *editors*

5 Physics of Precipitation

HELMUT WIECKMANN, *editor*

6 The Crust of the Pacific Basin

GORDON A. MACDONALD AND HISASHI KUNO, *editors*

7 Antarctic Research: The Matthew Fontaine Maury Memorial Symposium

H. WEXLER, M. J. RUBIN, AND J. E. CASKEY, JR., *editors*

8 Terrestrial Heat Flow

WILLIAM H. K. LEE, *editor*

9 Gravity Anomalies: Unsurveyed Areas

HYMAN ORLIN, *editor*

10 The Earth beneath the Continents: A Volume in Honor of Merle A. Tuve

JOHN S. STEINHART AND T. JEFFERSON SMITH, *editors*

11 Isotope Techniques in the Hydrologic Cycle

GLENN E. STOUT, *editor*

12 The Crust and Upper Mantle of the Pacific Area

LEON KNOPOFF, CHARLES L. DRAKE, AND PEMBROKE J. HART, *editors*

13 The Earth's Crust and Upper Mantle

PEMBROKE J. HART, *editor*

14 The Structure and Physical Properties of the Earth's Crust

JOHN G. HEACOCK, *editor*

15 The Use of Artificial Satellites for Geodesy

SOREN W. HENRIKSEN, ARMANDO MANCINI, AND BERNARD H. CHOVITZ, *editors*

**The Use of Artificial Satellites
for Geodesy**

Based on papers presented at

The Third International Symposium on
The Use of Artificial Satellites for Geodesy
April 15-17, 1971
Washington, D.C.

Sponsored by

The American Geophysical Union
The American Institute of Aeronautics and Astronautics
National Oceanic and Atmospheric Administration
U. S. Army Topographic Command

geophysical monograph 15

***The Use of Artificial
Satellites for Geodesy***

**SOREN W. HENRIKSEN
ARMANDO MANCINI
BERNARD H. CHOVITZ
editors**

**American Geophysical Union
Washington, D. C.
1972**

*Published with the aid of a grant
from the Charles F. Kettering Foundation*

International Standard Book Number 0-87590-015-1
Copyright © 1972 by the American Geophysical Union
1707 L Street, N. W.
Washington, D. C. 20036
Library of Congress Catalog Card Number 72-88669

WILLIAM BYRD PRESS, RICHMOND, VIRGINIA

Dedication

Yrjö Väisälä
1889–1971

Who made geodesists cast their vision upward

Weikko Heiskanen
1894–1971

Who inspired the dream of a global geoid

Preface

This monograph contains 34 communications presented at the Third International Symposium on the Use of Artificial Satellites for Geodesy in 1971, and 4 invited papers on subjects that complement the others and provide continuity. All contributions represent the most recent findings in the theoretical and applied fields of satellite geodesy, including new instrumentation (satellite sensors and ground equipment) of potential use in satellite geodesy.

The two preceding symposiums were held at Washington, D.C., in 1962 and at Athens, Greece, in 1965. The Proceedings of the first were published by North-Holland Publishing Company, Amsterdam, in 1963, and the Proceedings of the second by the National Technical University, Athens, in 1967. The prime mover behind both was George Veis, and his continuing dedication to this subject was in large measure responsible for scheduling this third symposium.

It is interesting to view the shift of emphasis in satellite geodesy as one progresses through the sets of proceedings. The first had as a primary concern the development of basic methods of handling and analyzing data and results, and thus concentrated on problems in celestial mechanics. Optical tracking was the primary observing system considered. At the second symposium, it was time to harvest the fruits planted at the first. Global geodetic results in station position and geoid heights to 10- to 20-meter accuracy were announced, based mainly on optical and Doppler tracking. In this volume, the emphasis has turned in two directions: a critical analysis of past results, and an anticipation of new data gathering methods that could improve geodetic knowledge by an order of magnitude.

The papers are organized into four major subjects: geometric geodesy, physical geodesy, instrumentation and environment, and extra-terrestrial geodesy. This organization imposes some degree of order on the material, but of course it is far from perfect. We cannot expect

artificial satellites, objects used as space targets for geometric geodesy and as free-swinging pendulums for gravimetry, to lend themselves to such arbitrary categorization. Some papers, particularly those dealing with simultaneous determinations of gravity-potential coefficients and station positions and those dealing with short-arc analyses, cover both geometrical and physical geodesy. Other papers like those reporting results with new instrumentation, lasers, for example, could be placed either with instrumentation or in one of the geodesy sections. The choice of sections for these papers was made on the basis of the area stressed by the author. The short-arc papers, for example, were placed in geometrical geodesy if the main objective of the paper was determination of station position, or in physical geodesy if it was primarily concerned with determination of a physical phenomenon like polar motion.

Many noteworthy achievements emerging during the past few years are reported in this monograph. To mention a few, there are the completion of the observational phase of the Worldwide Geometric Satellite Triangulation program, the completion of the Secor Equatorial Trilateration Belt, and preliminary results from the International Satellite Geodesy Experiment, a campaign involving concentrated laser tracking on different satellites. The results achieved on some of these programs are remarkable indeed, having surpassed earlier expectations of accuracy by appreciable amounts. The problem of achieving decameter accuracy worldwide has definitely been conquered, and researchers are now addressing themselves to the 1-meter phase of geometric geodesy and its ramifications to physical geodesy and other scientific fields.

The papers on physical geodesy are equally significant. There are articles on novel representations of the fine structure of the earth's potential by sampling functions, buried masses, and simple-layer models to complement the existing spherical harmonic representation for the long-wave component of the field. On the

topics of new instrumentation and tracking, there are papers on the orbiting gravity gradiometer, satellite altimetry, and satellite-to-satellite Doppler tracking, all of which serve as alternatives for determining the gravity field components of shorter wavelength. These and other innovations are now being vigorously pursued by geodesists, so that new achievements in this field lie just over the horizon.

Significant results have also emerged from combinations of satellite and surface-gravity data and from new analyses of Doppler orbits. An article dealing with the accuracy of potential coefficients places a limit on improvements of potential coefficients expected from more surface surveys, and the Doppler orbit

results prove that satellite geodesy can presently detect polar wobble as accurately as and at shorter intervals than is possible by conventional astronomic techniques.

In keeping with the tradition of the Proceedings of the two previous symposium volumes, the editors have added a closing summary.

The editors wish to extend their appreciation to the American Geophysical Union (AGU) for its assistance in organizing the Symposium, to the AGU Geophysical Monograph Board for approving the publication of the monograph based on the symposium, and finally to the authors, not only for their individual contributions, but for their understanding and assistance in producing the edited manuscript.

SOREN W. HENRIKSEN
ARMANDO MANCINI
BERNARD H. CHOVITZ

editors

Contents

Preface

1. Geometric Geodesy: Theory

Critical Configurations for Fundamental Range Networks.....	GEORGES BLAHA	1
Geometric Accuracy Obtainable from Simultaneous Range Measurements to Satellites L. AARDOOM		9
Absolute Orientation of Satellite Triangulation.....	ANGEL A. BALDINI	19

2. Geometric Geodesy: Results

Status of Data Reduction and Analysis Methods for the Worldwide Geometric Satellite Triangulation Program.....	HELLMUT H. SCHMID	27
Geometrical Adjustment with Simultaneous Laser and Photographic Observations on the European Datum.....	A. CAZENAVE, O. DARGNIES, G. BALMINO, AND M. LEFEBVRE	43
Preliminary Results of the Secor Equatorial Network.....	ERICH H. RUTSCHEIDT	49
Geos 1 Secor Observations in the Pacific (Solution SP 7) IVAN I. MUELLER, JAMES P. REILLY, CHARLES R. SCHWARZ, AND GEORGES BLAHA		59
Mini-Arc Orbit Determination for the Geos C Altimetry Experiment ROBERT M. L. BAKER, JR.		67
Tracking-Station Coordinates from Geos 1 and Geos 2 Optical Flash Data JAMES G. MARSH, BRUCE C. DOUGLAS, AND STEVEN M. KLOSKO		77
Survey Improvement and Calibration Analysis for the Air Force Eastern Test Range with Geos C.....	NORMAN BUSH	83

3. Physical Geodesy: Theory

Analysis of Methods for Computing an Earth Gravitational Model from a Combination of Terrestrial and Satellite Data.....	JOHN HOPKINS	93
Nature of the Satellite-Determined Gravity Anomalies... MOHAMMAD ASADULLAH KHAN		99
Simple Layer Model of the Geopotential in Satellite Geodesy.... KARL-RUDOLF KOCH		107
Propagation of Errors in Orbits Computed from Density Layer Models FOSTER MORRISON		111
Representation of the Earth Potential by Buried Masses.....	GEORGES BALMINO	121
A Geopotential Representation with Sampling Functions C. A. LUNDQUIST AND G. E. O. GIACAGLIA		125
Refinement of the Gravity Field by Satellite-to-Satellite Doppler Tracking CHARLES R. SCHWARZ		133
Satellite-Satellite Tracking for Estimating Geopotential Coefficients C. F. MARTIN, T. V. MARTIN, AND DAVID E. SMITH		139

4. Physical Geodesy: Results

Improvement of Zonal Harmonics by the Use of Observations of Low-Inclination Satellites, Dial, SAS, and Peole A. CAZENAVE, F. FORESTIER, F. NOUEL, AND J. L. PIEPLU		145
---	--	-----

Accuracy of Potential Coefficients Obtained from Present and Future Gravity Data	RICHARD H. RAPP	151
Error Model for the SAO 1969 Standard Earth.....	C. F. MARTIN AND N. A. ROY	161
Detailed Gravimetric Geoid for the United States		
WILLIAM E. STRANGE, SAMIR F. VINCENT, RICHARD H. BERRY, AND JAMES G. MARSH		169
Determination of Gravity Anomalies by Satellite Geodesy.....	K. ARNOLD	177
Refined Doppler Satellite Determinations of the Earth's Polar Motion		
LARRY K. BEUGLASS AND RICHARD J. ANDERLE		181
Geodetic Studies by Laser Ranging to Satellites		
DAVID E. SMITH, RONALD KOLENKIEWICZ, AND PETER J. DUNN		187
Observed Effects of Earth-Reflected Radiation and Hydrogen Drag on the Orbital Accelerations of Balloon Satellites.....	EDWIN J. PRIOR	197
5. Instrumentation and Environment		
Rapid Global Geoid Mapping with Satellite Altimetry		
H. R. STANLEY, N. A. ROY, AND C. F. MARTIN		209
Average Return Pulse Form and Bias for the S193 Radar Altimeter on Skylab as a Function of Wave Conditions.....	WILLARD J. PIERSON, JR., AND EMANUEL MEHR	217
Accuracy of Satellite Radar Altimeter Measurements.....	ALAN H. GREENE	227
Geodesy with Orbiting Gravity Gradiometers.....	ROBERT L. FORWARD	239
Timing for Geodetic Satellites.....	W. MARKOWITZ	245
Atmospheric Correction for Troposphere and Stratosphere in Radio Ranging of Satellites.....	J. SAASTAMOINEN	247
Measured Physical and Optical Properties of the Passive Geodetic Satellite (Pageos) and Echo 1.....	DAVID S. MCDUGAL, ROBERT BENJAMIN LEE, III, AND DARYL C. ROMICK	253
6. Extraterrestrial Geodesy		
Geodesy Results Obtainable with Lunar Retroreflectors		
J. E. FALLER, P. L. BENDER, C. O. ALLEY, D. G. CURRIE, R. H. DICKE, W. M. KAULA, G. J. F. MACDONALD, J. D. MULHOLLAND, H. H. PLOTKIN, E. C. SILVERBERG, AND D. I. WILKINSON		261
Lunar Gravity Model Obtained by Using Spherical Harmonics with Maseon Terms	MARSHALL H. KAPLAN AND BOHDAN G. KUNCIW	265
Estimate of the Gravity Anomalies of Venus.....	P. BALDI, E. BOSCHI, AND M. CAPUTO	275
Prospects for Planetary Geodesy.....	WILLIAM M. KAULA	279
7. Data Management		
Considerations for an Earth Physics Information-Management Service		
ROBERT W. MARTIN AND FREDERICK D. YOUNG		283
<i>Summary</i>		289

1. Geometric Geodesy: Theory

Critical Configurations of Fundamental Range Networks

GEORGES BLAHA

*Department of Geodetic Science
Ohio State University, Columbus, Ohio 43210*

Abstract. A range network is defined to consist of ground stations and targets where only distances between the two sets of points are observed. Such a network is said to be fundamental when only those six constraints are used that are needed to define the coordinate system for an adjustment. When ground stations or targets have certain configurations, a unique adjustment in terms of coordinates may be impossible, even when the number of observations is sufficient and the coordinate system is uniquely defined. Such configurations, resulting in the singular solutions, are said to be critical. This paper, being strictly theoretical, focuses on singular solutions rather than on numerical problems in some ill-conditioned systems of fundamental range networks. Because it is a summary, the paper is not intended to pursue the cases of linear dependence of the columns in the coefficient matrix of observation equations (a straightforward but extremely lengthy procedure). The critical configurations are presented in two separate groups. The first deals with ground stations lying all in a plane and the second deals with ground stations generally distributed. The two kinds of problems require different mathematical treatments and lead to quite different conclusions. A typical critical configuration when all ground stations are in a plane arises when they all lie on one second-order curve. When ground stations are generally distributed, a typical critical configuration can be represented by all points of a network (ground stations and targets) lying on one second-order surface. Because the singular solutions are inherent to them regardless of the number of co-observing ground stations, these two cases constitute the main contribution of the fundamental range network analysis. If they and some other more complex distributions of points summarized in this paper are avoided, an adjustment of range networks yields a unique solution.

A range network, formed by a set of ground stations and a set of targets, is such that between the two sets of points only ranges are observed. As in most geodetic adjustments, the mathematical model for range observations is treated in a linearized form. The adjustment procedure applied to this model is the least squares method.

Range observations, being invariant with respect to the coordinate system, do not offer information about it; thus when an adjustment is made in terms of coordinates, a certain co-

ordinate system has to be defined. Six constraints are necessary for definition of the coordinate system; three to define its position, and three to define its orientation. Any coordinate system thus defined yields theoretically the same adjusted values of distances. In the theoretical part of this investigation, a coordinate system is chosen such that the first ground station is at its origin, the second station is on its x axis, and the third station is in its xy plane. For practical computations, the coordinate system may be the most advantageous that

renders the trace of the variance-covariance matrix for the coordinates of all or certain selected points a minimum. The constraints defining the coordinate system in this manner are called 'inner adjustment constraints.' The idea of using inner adjustment constraints was first presented by *Meissl* [1962], and recently by *Rinner* [1966, annex F], and *Meissl* [1969]. The problem of inner adjustment constraints is treated in great detail by *Blaha* [1971a]. Their application in connection with an actual adjustment was given by *Mueller et al.* [1970].

When only six constraints defining the coordinate system are used, the network is said to be fundamental. In this paper, only fundamental networks are considered. In certain cases, when ground stations or targets are in special configurations, a unique adjustment in terms of coordinates may be impossible, even if the number of observations is sufficient and the coordinate system is uniquely defined. Such critical configurations result in singular solutions, and their description is the subject of this paper. They are separated into two groups. In the first group, all ground stations are in a plane, and in the second they are generally distributed. To a limited degree these problems were also treated by *Rinner* [1966, annex A] and *Killian and Meissl* [1969]. Their detailed treatment is presented by *Blaha* [1971b], a report of which this paper is a summary.

TREATMENT OF RANGE OBSERVATIONS WITH ALL GROUND STATIONS IN A PLANE

The results of this section can be used for practical problems whenever the ground stations lie near a plane. Clearly, this happens when the ground network extends over a relatively small area.

The basic idea used in treating the networks where the ground stations are approximately in one plane is to stipulate that all ground stations are exactly in the plane and to find the critical loci of the points in the network that will result in a singular solution. Applications for practical cases (where the condition of coplanarity is only approximately fulfilled) follows from the fact that conditions leading to singularity in theory lead to near singularity in practice. Examples of the correspondence between such theoretical and practical configuration conditions are the following:

CONFIGURATIONS OF RANGE NETWORKS

a. Targets on a straight line in theory correspond to satellite positions on a relatively short pass in practice.

b. Ground stations lying on a second-order (plane) curve in theory correspond in practice to ground stations in projection on the (best-fitting) plane lying on or near a second-order curve.

c. A satellite group lying theoretically in a plane corresponds in practice to short satellite passes of approximately the same altitude. This situation can arise when the same satellite is observed on different passes.

The main result of this investigation is the detection of singularity for the theoretical cases and the establishment of rules to avoid it.

In order to present the results of these investigations, certain notations are introduced: The ground stations are denoted by numbers and letters in the sequence 1, 2, 3, 4, ..., *i*, ..., *k*, *s'*, *s''*, ..., and the satellite groups observed by these stations are denoted as *j*, ..., *j_i*, ..., *j_k*, *j_{s'}*, *j_{s''}*, ..., respectively. A satellite group consists of those satellite points (targets) that are observed by a given quadrant (quad) of stations. The convention used for the subscript of a certain satellite group is such that the index indicates the number or letter of the station in the quad observing this satellite group that has not observed any other satellite group or that is listed as the last station in the quad. For example, the quad consisting of stations 1, 2, 3, and 4 observes the satellite group *j₄*. The division of a network into quads is convenient from the practical point of view. Considering more than four co-observing stations does not affect the derivations made with the above concept.

The discussion is divided into two basic parts, according to whether the number of ground stations observing all the satellite points is three or more, or less than three. When the number of stations observing all the targets is less than three, the principle of 'station replacement' is introduced, which leads directly to the concept known in practice as 'leapfrogging.' Both concepts, the first, dealing with at least three stations observing all the targets, and the second, dealing with replacement of stations, lead to similar conclusions. The most important conclusion is that, except for certain critical configurations of points (stations or targets or

GEORGES BLAHA

both), an adjustment of range networks gives nonsingular results, in spite of the fact that all stations are in one plane. The network that can be nonsingular with the smallest number of ground stations possible is said to constitute a fundamental unit. When at least three stations observe all the targets, a fundamental unit consists of six stations. When the principle of station replacement is utilized, a fundamental unit is also six stations, except for one specific observing pattern when the number of required stations is seven.

When three stations, denoted as 1, 2, 3, are observing all the targets, the necessary and sufficient conditions for a network to be nonsingular are easy to specify. One of the configurations that makes an adjustment singular is when all the targets in one satellite group needed for the determination of a fundamental unit are in a straight line. This is only a special case of a general pattern when all satellite points within a group (e.g., j_i) are in the plane containing the corresponding ground station (i). This case, called singularity A , is illustrated in Figure 1. In a more general sense, singularity A is said to occur when all targets observed by a certain station (such targets may be contained in more than one satellite group) are in the plane with this station. When exactly three stations (1, 2, 3) observe all targets, the targets observed by any particular station besides 1, 2, 3 are all contained in one satellite group. Under the assumption that singularity A does not exist, the necessary and sufficient conditions for a network to be nonsingular are such that at least three stations in addition to those three (1, 2,

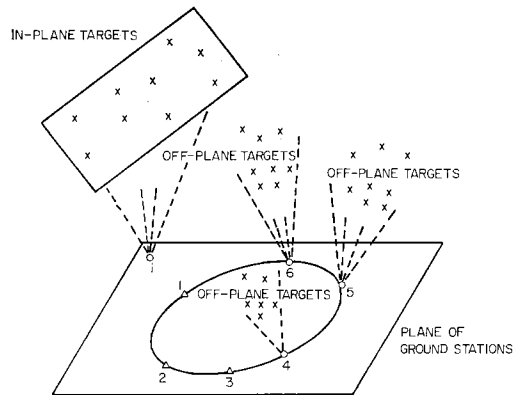


Fig. 2. Singularity C : stations 1, 2, 3 observe all targets; all stations observing off-plane targets are on a second-order curve with stations 1, 2, 3.

3) observing all the targets must observe targets that are not all in one (general) plane (off-plane targets), and these three stations must not lie on one second-order curve with stations 1, 2, 3. If these conditions are not fulfilled, it is said that singularity C has occurred; such configuration of points is illustrated in Figure 2. A special case of singularity C is singularity B , in which all the ground stations are on one second-order curve (Figure 3). From the conditions given above, it is seen that a fundamental unit consists of six ground stations. If such a fundamental unit exists, it is always possible to expand a network by adding further stations and satellite groups, the necessary and sufficient conditions being that no target should lie in the plane of the ground stations and that no station

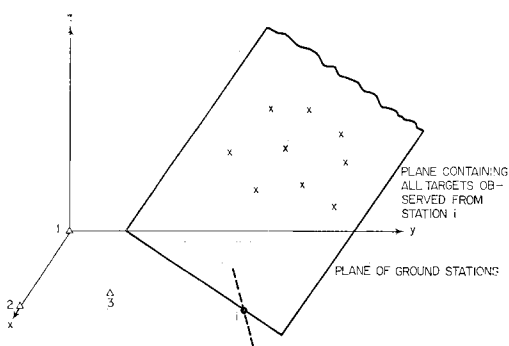


Fig. 1. Singularity A : station i is in the plane of its observed targets.

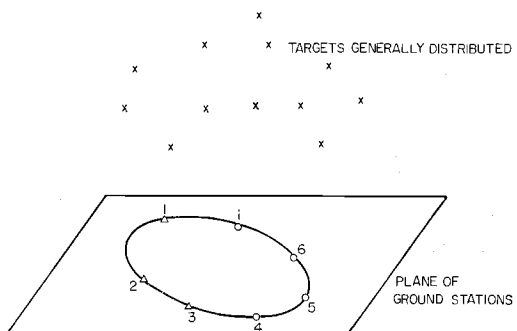


Fig. 3. Singularity B : stations 1, 2, 3 observe all targets; all stations are on a second-order curve.

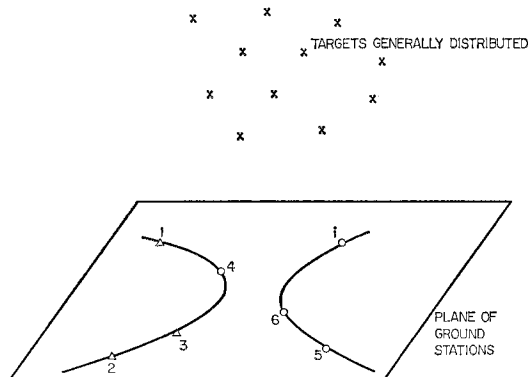


Fig. 4. Singularity C: all stations observe all targets; all stations are on a second-order curve.

should lie in a plane with all its observed targets.

If all ground stations are co-observing, then singularity in a network could occur only if all the stations are on one second-order curve, or if all the targets are in one plane (in this case, all the satellite groups coincide). These two cases are illustrated in Figures 4 and 5, respectively. Otherwise, the solution is nonsingular. Numerical results indicate that when all the stations observed simultaneously the solution was strengthened very significantly.

When dealing with the concept of station replacement, it is concluded that one replacement (leapfrogging) can be sufficient to build a fundamental unit, from which further expansion is possible under certain conditions. Therefore, a great deal of time was devoted to analyzing the problem of one replacement where the fundamental unit is assumed to include the stations 1, 2, 3, 4 and the satellite group j_4 is assumed to contain off-plane targets. After two quads (formed by stations 1, 2, 3, 4 and stations 1, 2, 3, k) have completed their observations, the first replacement will take place. It consists of station k replacing station 3 for the next observations. The satellite group $j_{s'}$ is then observed by the quad of stations 1, 2, k , s' , etc. At this point, the discussion is divided into two cases: in the first case, the satellite group j_k contains off-plane targets; in the second case, which is rather special and mainly of theoretical interest, the targets in j_k are in one plane. It is true for both cases that a network is singular if the targets in any of the satellite groups (in-

CONFIGURATIONS OF RANGE NETWORKS

cluding j_k in the second case) are in a straight line. This conclusion is similar to what was mentioned for three stations observing all the targets. It is again assumed that no satellite group lies in a plane passing through the corresponding station. Thus, singularity A cannot exist.

With the above assumption, the necessary and sufficient conditions for a nonsingular solution in the first case (j_k containing off-plane satellites) are similar to those given for three stations observing all the targets. Namely, the network is nonsingular if there is at least one more satellite group (in addition to j_4 and j_k) containing off-plane targets and if the corresponding station does not lie on a second-order curve with stations 1, 2, 3, 4, and k . In other words, at least three stations not lying on a second-order curve with stations 1, 2, 3 must observe off-plane targets. Therefore, a fundamental unit in this case consists also of six ground stations.

The second case, rather artificial, deals with such configurations when the satellite group j_k is composed of targets lying all in one plane (assumed not to pass through station k). The necessary conditions for a nonsingular network stipulate that there must be at least two additional satellite groups (besides j_4) that contain off-plane targets. Consequently, a fundamental unit in this case includes seven ground stations (i.e., two stations in addition to stations 1, 2, 3, 4, and k).

If the first replacement is successfully carried

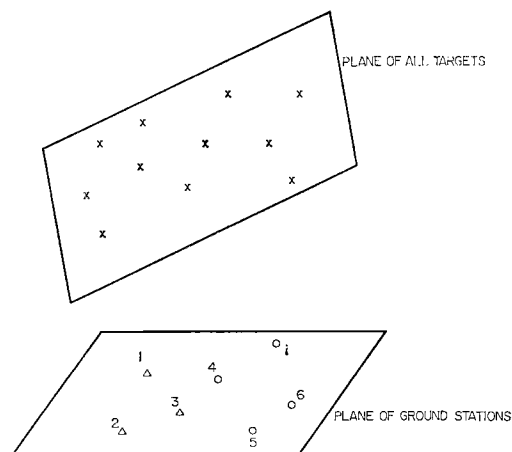


Fig. 5. Singularity C: all stations observe all targets; all targets are in a plane.

GEORGES BLAHA

TABLE 1. Necessary and Sufficient Conditions to Avoid Singular Solutions when All Ground Stations Are in a Plane

Type of Singularity	Arrangement of Observations	Necessary Conditions to Prevent Singularity	Sufficient Conditions to Prevent Singularity	Notes
Singularity A (or closely related singularity)	Any	No station should be in a plane with all its observed targets (distributed over one or more satellite groups)	No station should be in a plane with the corresponding satellite group	This singularity is assumed to be nonexistent in analysis of singularity C
Singularity C (global type of singularity)	Stations 1, 2, 3 observe all targets	Three stations in addition to 1, 2, 3 not lying on a second-order curve with them should observe off-plane targets	Same as the necessary conditions	Special case of singularity C is singularity B; it occurs when all stations are on a second-order curve
Station k replaces station 3 (satellite group j_4 contains off-plane targets)	Group j_k contains off-plane targets	One station in addition to 4 and k not lying on a second-order curve with 1, 2, 3, 4, k should observe off-plane targets	Same as the necessary conditions	
All stations observe all targets (all stations co-observe)	Group j_k contains in-plane targets	Two stations in addition to 4 should observe off-plane targets, Always avoid all stations lying on a second-order curve	More complex requirements (according to stations which observe off-plane targets)	
		Avoid all targets lying in a plane (any plane) and all stations lying on a second-order curve	Same as the necessary conditions	

out, then the resulting fundamental unit can be expanded to become a larger, nonsingular network. When new stations and satellite groups are added to it, the necessary and sufficient conditions for the new network to be nonsingular are the same as those for similar enlargement when three stations observed all the targets; namely, no target should be in the plane of the ground stations and no station should be in a plane with all its observed targets.

The main results of this section are summarized in Table 1.

Since the number of ground stations is always relatively small compared to the number of targets, the most important conclusion for all ground stations lying in a plane is that the ground stations should not be distributed on or near a second-order curve.

TREATMENT OF RANGE OBSERVATIONS WITH GROUND STATIONS GENERALLY DISTRIBUTED

In this section, the ground stations in fundamental range networks are considered to be generally distributed in space. This discussion

covers range observations made over a large territory, when ground stations are on the physical surface of the earth, departing significantly from a plane. Since the ground stations in this instance are all approximately on a sphere, their distribution in space is not completely general. However, whenever they depart from a plane, the nature of the problem is the same regardless of further specifications.

The observations are again divided into quads and notations are similar to those used previously. Whether four or more ground stations observe simultaneously has again no effect on the derivations. Most of the investigations for general distribution of ground stations have been carried out for at least three stations observing all the targets.

Perhaps the most important theoretical result in this section is that whenever all the points (ground stations and targets) of a network lie on one second-order surface the network is necessarily singular. An illustration of such configuration appears in Figure 6.

Some special cases of singular solutions arise when all the targets observed by a certain sta-

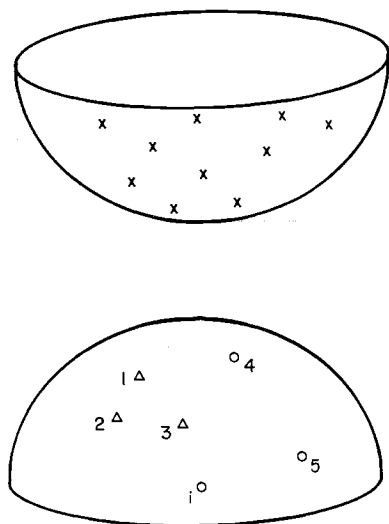


Fig. 6. Critical surfaces: all stations observe all targets; all stations and all targets are on a second-order surface.

tion (they can be in one or more satellite groups) are in a plane that contains this station (mostly called singularity *A*), or when all the targets of a network are in a plane on a second-order curve (called 'reversed singularity *B*'). When all its points lie on a second-degree surface, the network is singular even if all the ground stations co-observe; this is the only case of a singular problem when all the stations co-observe, except for the special cases when all the targets of a network are in a plane containing one ground station, or when they are all on a second-order (plane) curve. Naturally, when all the points are on one second-order surface, the network is singular no matter how the observations are arranged (e.g., leapfrogging).

When only a limited number of stations co-observe, the situation is somewhat more complicated. In practice, four stations forming quads may co-observe a set of targets. With three stations observing all the targets, it was found that an adjustment of range observations is singular if for each quad the stations and the corresponding targets lie on a specific second-order critical surface. All these critical surfaces intersect in one second-order (plane) curve containing the above three stations. This geometric property is illustrated in Figure 7. If the special singular cases due to singularity *A* or 'reverse singularity *B*' do not exist, the

CONFIGURATIONS OF RANGE NETWORKS

network has a nonsingular solution if there is at least one (satellite) point outside the corresponding critical surface.

When utilizing the concept of station replacement, it was found that besides the above two special cases singular solutions would again be associated with specific second-order surfaces. In this case, sufficient conditions for nonsingular networks stipulate that after an expansion of a nonsingular network the new network is still nonsingular if the targets of any 'new' satellite group do not lie in a plane with the three 'old' stations and that the fourth 'new' station does not lie in one plane with these targets.

The main results of this section are summarized in Table 2.

It can be concluded that, with singularity *A* and reverse singularity *B* nonexistent, a solution will be singular if certain (or all) stations, together with certain (or all) satellite points, lie on specific second-order surface(s). However, such cases are not likely to happen in practice for the following reasons:

a. Distribution of ground stations alone does not induce any type of singularity. Since the number of ground stations is always limited, their distribution presented a cause for concern in the limited-area (plane) case; it is irrelevant in the general distribution case.

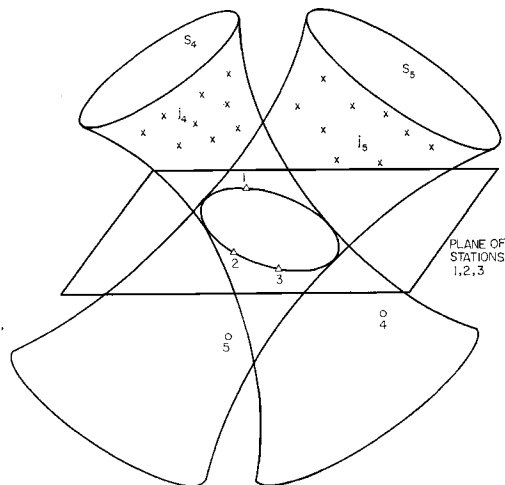


Fig. 7. Critical surfaces: stations 1, 2, 3 observe all targets; stations 4 and 5, together with their satellite groups j_4 and j_5 , are on the second-order surfaces S_4 and S_5 , respectively; stations 1, 2, 3 are on the second-order intersection curve of surfaces S_4 and S_5 .

GEORGES BLAHA

TABLE 2. Necessary and Sufficient Conditions to Avoid Singular Solutions when Ground Stations Are Generally Distributed

Type of Singularity	Arrangement of Observations	Necessary Conditions to Prevent Singularity	Sufficient Conditions to Prevent Singularity	Notes
Singularity A (or closely related singularity)	Any	No station should be in a plane with all its observed targets (distributed over one or more satellite groups)	No station should be in a plane with the corresponding satellite group	This singularity is assumed to be nonexistent in analysis of global singularity
Reversed singularity B	Any	Targets should not be all in a plane on a second-order curve	Same as the necessary conditions	This singularity is assumed to be nonexistent in analysis of global singularity
Global singularity	Stations 1, 2, 3 observe all targets	Avoid all satellite groups (one group per quad) containing targets lying all on the corresponding second-order critical surfaces (one surface per quad). Always avoid all points lying on a second-order surface	Same as the necessary conditions	All critical surfaces can be computed explicitly. They all intersect in the plane of stations 1, 2, 3 on a second-order curve containing the three stations. If four points outside this plane are common to some critical surfaces, these surfaces coincide
	Station replacement (e.g., leapfrogging)	Always avoid all points lying on a second-order surface	Avoid certain second-order surfaces not expressed explicitly	
	All stations observe all targets (all stations co-observe)	Avoid all points lying on a second-order surface	Same as the necessary conditions	

b. If a network is singular, it is caused by all the satellite points lying on certain second-order surfaces (together with some ground stations). This could seldom happen in practice, as the number of targets may be very large; thus the probability of all the targets lying on specific second-order surfaces is very small.

Results of the range investigations for ground stations in general configuration can certainly be useful when only a small number of targets are observed, because then it could happen that they all lie near one or more specific second-order surfaces. However, for the reasons cited above, these results are mainly of theoretical interest.

Acknowledgment. The work described in this paper was partly supported by NASA under contract NGL 36-008-093.

REFERENCES

Blaha, Georges, Inner adjustment constraints with emphasis on range observations, *Rep. 148*, Dep.

of Geod. Sci., Ohio State Univ., Columbus, 1971a.

Blaha, Georges, Investigations of critical configurations for fundamental range networks, *Rep. 150*, Dep. of Geod. Sci., Ohio State Univ., Columbus, 1971b.

Killian, Karl, and Peter Meissl, Einige Grun- gefährlichen Örter, Beiträge zur Theorie der gefährlichen Örter, in Beiträge zur Theorie der geodätischen Netze im Raum, ser. A, no. 61, Deutsche Geodätische Kommission, Munich, 1969.

Meissl, Peter, Die innere Genauigkeit eines Punkthaufens, *Österreichische Z. Vermess.*, 50, nos. 5 and 6, 1962.

Meissl, Peter, Zusammenfassung und Ausbau der inneren Fehlertheorie eines Punkthaufens, Beiträge zur Theorie der geodätischen Netze im Raum, ser. A, no. 61, Deutsche Geodätische Kommission, Munich, 1969.

Mueller, Ivan I., J. P. Reilly, Charles R. Schwarz, and Georges Blaha, SECOR observations in the Pacific, *Rep. 140*, Dep. of Geod. Sci., Ohio State Univ., Columbus, 1970.

Rinner, Karl, Systematic investigations of geodetic networks in space, report on contract DA-91-591-EUC-3584, U.S. Army Eng., Fort Belvoir, Virginia, 186 pp., 1966.

Geometric Accuracy Obtainable from Simultaneous Range Measurements to Satellites

L. AARDOOM

Geodetic Institute, Delft University of Technology, Delft, Netherlands

Abstract. We consider the problem of obtaining information on the internal geometry of a net of ground-based observing stations from simultaneous laser range measurements to satellites. The approach involves the measured ranges and the interstation distances only. One family of idealized four-station configurations is investigated with regard to the internal geometric accuracy attainable from simultaneous ranging. A variety of orbital heights is considered. It is found that the estimated standard deviation of the derived interstation distances will be about 5 times the standard deviation of the range measurements to the satellites, provided that the interstation distances and the orbital heights of the satellites are carefully selected and provided that a feasible observation program is presupposed.

The precision of ground-to-satellite laser ranging is at present typically 1 meter (standard error) for ranges up to a few megameters, but systems with substantially better precision are quite feasible, and there does not seem to be a physical reason why a precision of a few centimeters could not be attained. Ranges will be measured to such distant objects as geostationary satellites and even beyond that, to the moon.

The purely geometric method of simultaneous ranging to a satellite can obviously yield neither orientation in an earth-fixed frame of reference of the network nor location, but it can provide network shape and scale. A suitable combination of simultaneous camera observations and rangings would give full information on the geometry of the network except its location with respect to the mass center. For some investigations, a tie to the center of mass or even an orientation in an earth-fixed system of reference is not essential, the internal geometry of the network being more relevant. This situation can occur in studies of the dynamics of the solid earth where relative motion rather than absolute position of selected points is subject to investigation. In such studies, precise laser ranging is likely to play an important role [Kaula, 1970], and it is also likely that the technique of simultaneous ranging will be applied.

However, elementary geometric reasoning suggests poor propagation of precision from the measured station-to-satellite ranges to the derived interstation distances, and therefore it will be of interest to try to find out what accuracy can in fact be attained. Bender *et al.* [1968] and Brown [1970] have dealt with this problem, but the importance of the subject justifies another analysis.

BASIC IDEAS AND SCOPE OF INVESTIGATION

The simplest case of geometrically meaningful simultaneous station-to-satellite ranging comprises four ground stations P_i ($i = 1, \dots, 4$) and a satellite in a mutually observable position P_s (Figure 1). As was pointed out in a previous paper [Aaroom, 1970], the four measured station-to-satellite ranges l_{is} ($i = 1, \dots, 4$) and the six unknown interstation distances l_{ij} ($i, j = 1, \dots, 4; i \neq j$) are connected through the determinant relation

$$g^* \equiv |G^*| \\ = \begin{vmatrix} 1 & \cos \phi_{12}^* & \cos \phi_{13}^* & \cos \phi_{14}^* \\ \cos \phi_{21}^* & 1 & \cos \phi_{23}^* & \cos \phi_{24}^* \\ \cos \phi_{31}^* & \cos \phi_{32}^* & 1 & \cos \phi_{34}^* \\ \cos \phi_{41}^* & \cos \phi_{42}^* & \cos \phi_{43}^* & 1 \end{vmatrix} = 0 \quad (1)$$

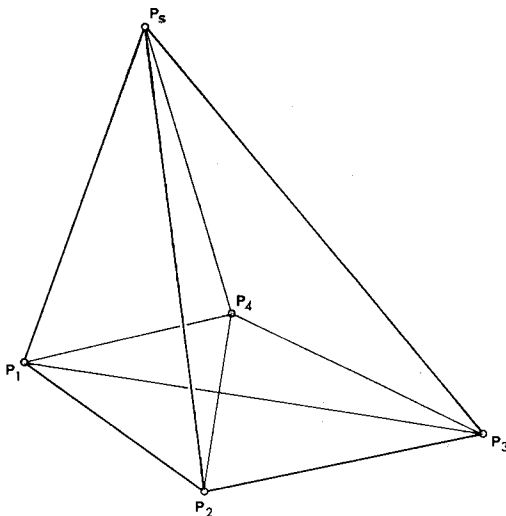


Fig. 1. Four-station geometry for simultaneous ranging to satellites.

where $\cos \phi_{is}$ stands for

$$\frac{l_{is}^2 + l_{js}^2 - l_{ij}^2}{2l_{is}l_{js}}$$

and ϕ_{is} is the unknown angle subtended at P_s by the directions to P_i and P_j , which supposedly have not been measured. Equation 1 is a nonlinear relation between six unknown l_{ij} , and in general six such relations resulting from six simultaneous observations to satellite positions P_s ($s = 1, \dots, 6$) are expected to make a set of relations that determine l_{ij} uniquely. These six interstation distances, together with their statistical properties, form the basic geometric result one wants to find from four-station simultaneous satellite ranging; hence we are not concerned with either orientation or location of the four-station network. It was also pointed out in the previous paper that the geometric conditions imposed by multiple n -station ranging, in which more than four stations participate, can be reduced to $n - 3$ independent relations of type (1).

No doubt the four-station case will be typical, because, although daylight laser ranging is quite feasible, atmospheric conditions may still severely limit the number of cases of mutual visibility. The probability of success will obviously decrease with increasing multiplicity n of stations. Therefore, in view of its relative

RANGE MEASUREMENTS TO SATELLITES

importance, it seems reasonable to restrict this initial study to four stations.

Within the limits set by this choice, a variety of four-station configurations could be considered. It is assumed that the stations P_i ($i = 1, \dots, 4$) are on a sphere of radius $R = 6370$ km, a value close enough to the mean radius of the earth. Two obvious model groupings of stations are:

- a. Four stations at the corners of a square (Figure 2a).
- b. Three stations arranged as an equilateral spherical triangle around a central station (Figure 2b).

However, the first configuration, like all coplanar four-station configurations, leads to a singularity [Killian and Meissl, 1969], indicating that such configurations are indeterminate with simultaneous satellite ranging. Therefore this first configuration will be ignored.

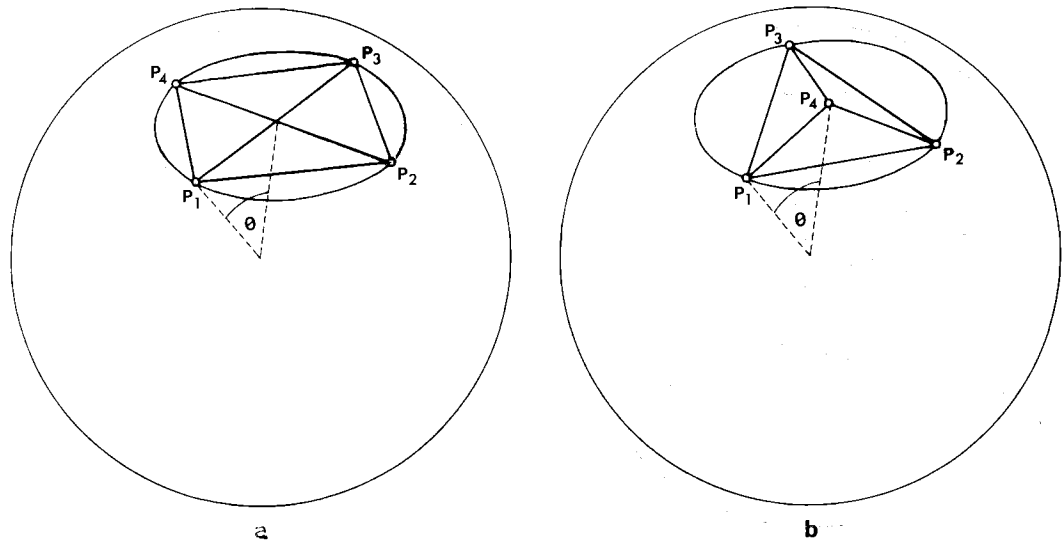
Angle θ defines through R the size of the model configuration. The zenith angle z of an optical observation will, because of atmospheric or other conditions, be limited to a maximum $\zeta < 90^\circ$. Here ζ will be varied from 60° to 85° . The domain of observable satellite positions is the interior of the circular cone with P_i as vertex, the local normal as axis, and ζ as semi vertex angle (Figure 3). This definition of the observability domain probably simplifies too much the actual situation. In general, the possibilities of laser ranging may also be geometrically restricted by conditions imposed by the optical characteristics of the retroreflector array and its location on the satellite and the type of stabilization (magnetic or gravity-gradient) applied. Intersecting the thus simplified domain by a concentric sphere of radius $R + H$, one finds the ranging domain of a satellite at height H for station P_i , on the assumption that the distance from P_i to any point of this domain is not beyond the range of observation. The spherical radius of the ranging domain at height H as seen from the center of the earth is denoted α . From Figure 3 it appears that

$$\frac{\sin \zeta}{\sin (\zeta - \alpha)} = \frac{R + H}{R} = 1 + \frac{H}{R} \quad (2)$$

Equation 2 is solved for α .

L. AARDOOM

11

Fig. 2. Obvious model station configurations; θ is geocentric angle.

To be simultaneously observable from a number of stations P_i , a satellite position at height H must be in all ranging domains associated with those stations. The set of points, if any, satisfying this condition is called the common ranging domain at height H for the stations involved. In general, the boundary of such a domain will be composed of a number of small circle arcs, but, for the symmetric model station configuration to be considered, this common domain is reasonably well approximated by a small circle inscribed in the actual domain (Figure 4). These approximating circles have geocentric radii

$$\beta = \alpha - \theta \quad (3)$$

Clearly a necessary condition for the feasibility of a simultaneous ranging is $\beta > 0$; hence $\theta < \alpha$. From this condition, maximum values $\theta_{\max} = \alpha$ for θ can be calculated by using (2). The resulting θ_{\max} sets an upper bound to the separation of the stations in the model configuration.

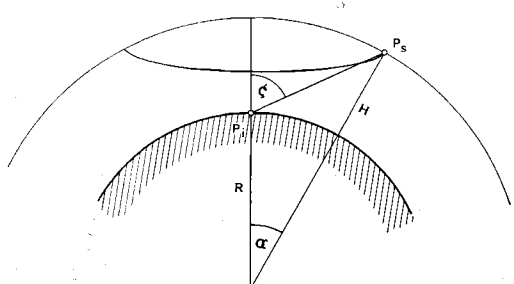
For simplicity, it is assumed that the observed satellite positions P_s are distributed in some regular way over the common ranging domain. The basic purpose of this investigation is to study numerically the statistics of interstation distances l_{ij} in the model station configuration for a variety of sizes (angles θ). A variety of both satellite heights H and satellite position

distributions within the common ranging domain are to be considered. It is assumed throughout that distances l_{ij} are determined from simultaneous ranges to satellite positions in one common ranging domain at height H only. Uniqueness of solution requires a minimum of six positions P_s in each case.

An obvious statistic to be studied is the variance-covariance matrix $V\{l_{ij}\}$ of interstation distances l_{ij} . This matrix being given, one might try to find criteria for optimization of the determination of selected geometric features of the station network, such as a selected l_{ij} or the angle between two interstation lines.

THE STOCHASTIC MODEL

The compound probability distribution of all ranges in a campaign (at least six simultaneous

Fig. 3. Geometry of ranging domain as defined by satellite altitude H and maximum zenith distance ξ .

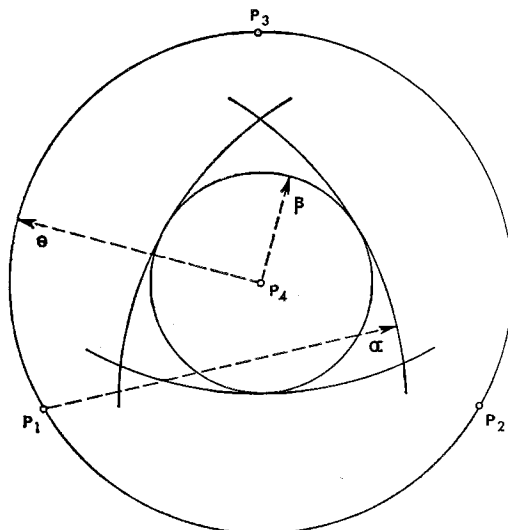


Fig. 4. Common ranging domain as defined by geocentric angle $\beta = \alpha - \theta$.

rangings from four stations) is supposed to be multidimensional Gaussian. This supposition and the assumption that relations 1 are sufficiently linear in terms of small increments dl_{is} and dl_{is} , justify least squares procedures.

Apart from its mean, the Gaussian distribution of the measured ranges l_{is} ($i = 1, \dots, 4$; $s = 1, \dots, q$) is defined by the variance-covariance matrix $V\{l_{is}\}$. Any variance-covariance matrix $V\{l_{is}\}$ can be formally associated with a Gaussian distribution, thus formally legalizing the application of the least squares apparatus, although this could be physically not fully justified.

Simultaneously measured ranges l_{is} ($i = 1, \dots, 4$), as well as consecutively measured ranges from one station l_{is} ($s = 1, \dots, q$), are assumed to be statistically independent, their individual distributions being Gaussian with a proportional range variance $\sigma^2 = (\sigma_i/l)^2$, constant for all four stations in a selected campaign as defined by the station configuration model by θ , H , and q . Here l is the range to the satellite, and σ_i is its standard deviation. The constancy of σ^2 is a working hypothesis that is not too crude, because the variability of ranges l within a selected campaign is rather limited on the assumptions made and if it is assumed that large zenith-angles, causing refraction correction problems, are avoided.

RANGE MEASUREMENTS TO SATELLITES

In practically conceivable cases, σ can be anything between 10^{-6} and 10^{-9} , the value 10^{-7} probably being characteristic for laser ranging systems of the near future. The range variance σ^2 can be interpreted as the variance of $\ln l_{is}$ ($i = 1, \dots, 4$; $s = 1, \dots, q$) and, for the variance-covariance matrix $V\{\ln l_{is}\}$ of quantities $\ln l_{is}$, we have

$$V\{\ln l_{is}\} = \sigma^2 I \quad (4)$$

where I stands for the $(4q)$ th-order unit matrix.

Whether or not (4) is a reasonable statement depends on the degree to which possibly existing correlations can be neglected. Correlation between simultaneous ranges will be weak; one could think of some through refractive and earth-tide effects. Discarding such correlation, however, a variance-covariance matrix $V\{l_{is}\}$ would be composed of $q^2 4 \times 4$ diagonal submatrices in turn arranged in a $q \times q$ compound matrix that is $V\{l_{is}\}$.

The diagonals of the off-diagonal submatrices of $V\{l_{is}\}$ represent correlation between consecutive rangings from the same station. Such correlation could easily result from an imperfect synchronization of the station's clock relative to the clocks at the other stations. Also, the incomplete correction of atmospheric effects might be a source of correlation, and there is possibly more. Nevertheless, since hardly anything sensible can be said a priori, this type of correlation has also been disregarded.

The constancy of the proportional range variance σ^2 is a supposition that is not realistic beyond the realm of a specific campaign. Indeed, the precision of conventional and some more advanced laser ranging systems operating with pulse durations of 10 nsec or longer will be range-dependent, since the amount of distortion of the return pulse and its stochastic variability will tend to increase with the range [Lehr et al., 1969]. But this range dependence will be much less than a proportionality, and, with sophisticated short-pulse systems, the range variance σ^2 will approximate a constant.

Nevertheless, the constancy of the proportional range variance throughout is adopted as a working hypothesis, and hence $V\{\ln l_{is}\}$ is used instead of $V\{l_{is}\}$.

Although it could have been more convenient to work with range variances than with proportional range variances, the latter have the ad-

L. AARDOOM

vantage that the subsequent analysis more clearly brings out how poor the situation is with regard to the propagation of scale and how much can be gained with an advanced system of approximately constant range variance.

It is assumed that σ^2 in (4) takes into account a numerical decrease due to an eventual interpolation in near-simultaneous sequences of range measurements.

THE ANALYSIS

We specify the positions of stations P_i ($i = 1, \dots, 4$) by vectors \mathbf{p}_i ($i = 1, \dots, 4$). In model configuration sub b (Figure 2b), these could be chosen as

$$\begin{aligned} \mathbf{p}_1 &= R \begin{pmatrix} \sin \theta \\ 0 \\ \cos \theta \end{pmatrix} & \mathbf{p}_2 &= R \begin{pmatrix} -\frac{1}{2} \sin \theta \\ \frac{1}{2}(3)^{1/2} \sin \theta \\ \cos \theta \end{pmatrix} \\ \mathbf{p}_3 &= R \begin{pmatrix} -\frac{1}{2} \sin \theta \\ -\frac{1}{2}(3)^{1/2} \sin \theta \\ \cos \theta \end{pmatrix} & \mathbf{p}_4 &= R \begin{pmatrix} 0 \\ 0 \\ 1 \end{pmatrix} \end{aligned} \quad (5)$$

The radius β of the common ranging domain is found from (2) and (3), ζ and H being chosen as wanted.

A reasonably uniform distribution of satellite positions P_s (geocentric colatitude ψ_{nm} , geocentric longitude λ_{nm} , P_4 being adopted as pole) within the common ranging domain is obtained by taking

$$\begin{aligned} \psi_{nm} &= n \frac{\beta}{N} \\ (n &= 0, \dots, N; m = 1, \dots, 6n) \end{aligned}$$

$$\begin{aligned} \lambda_{nm} &= \frac{m}{n} \frac{\pi}{3} \\ (n &= 1, \dots, N; m = 1, \dots, 6n) \end{aligned}$$

$$\lambda_{nm} = 0 \quad (n = 0)$$

N controls the number $q = 1 + 3N(N + 1)$ of four-station observation events.

The geocentric satellite positions are given by

$$\begin{aligned} \mathbf{r}_{nm} &= (R + H) \begin{pmatrix} \sin \psi_{nm} \cos \lambda_{nm} \\ \sin \psi_{nm} \sin \lambda_{nm} \\ \cos \psi_{nm} \end{pmatrix} \\ (n &= 0, \dots, N; m = 1, \dots, 6n) \end{aligned} \quad (6)$$

Subscripts and superscripts are merely used as useful labels and are written in suitable places. We write, relabeling, \mathbf{r}_s ($s = 1, \dots, q$) instead of \mathbf{r}_{nm} .

Station-to-satellite vectors are

$$\mathbf{l}_{is} = \mathbf{r}_s - \mathbf{p}_i$$

$$(i = 1, \dots, 4; s = 1, \dots, q)$$

These have magnitudes $l_{is} = |\mathbf{l}_{is}|$. Then

$$\cos \phi_{is}^s = \frac{\mathbf{l}_{is} \cdot \mathbf{l}_{is}}{l_{is} l_{is}} \quad (7)$$

and

$$G^s = \begin{bmatrix} 1 & \cos \phi_{12}^s & \cos \phi_{13}^s & \cos \phi_{14}^s \\ \cos \phi_{21}^s & 1 & \cos \phi_{23}^s & \cos \phi_{24}^s \\ \cos \phi_{31}^s & \cos \phi_{32}^s & 1 & \cos \phi_{34}^s \\ \cos \phi_{41}^s & \cos \phi_{42}^s & \cos \phi_{43}^s & 1 \end{bmatrix}$$

is the matrix, the determinant $g^s = |G^s|$ of which should vanish, as prescribed by (1).

On the other hand, the elements $\cos \phi_{is}^s$ can be written in terms of the measured station-to-satellite ranges l_{is} and the unknown interstation distances l_{ij} , as before:

$$\cos \phi_{is}^s = \frac{l_{is}^2 + l_{is}^2 - l_{ij}^2}{2l_{is} l_{is}} \quad (8)$$

and the first step is now to linearize (1) in small increments dl_{ij} and dl_{is} to approximated initial values $l_{ij,0}$ and measured $l_{is,0}$. This linearization is a prerequisite for the application of least-squares techniques.

The result is

$$\mathbf{a}_{ii}^s \cdot \mathbf{d} \ln l_{is} = \mathbf{b}_i^s \cdot \mathbf{d} \ln l_{is} \quad (9)$$

with

$$\mathbf{a}_{ii}^s = \begin{bmatrix} a_{12}^s \\ a_{13}^s \\ a_{14}^s \\ a_{23}^s \\ a_{24}^s \\ a_{34}^s \end{bmatrix}^T \quad \mathbf{d} \ln l_{is} = \begin{bmatrix} d \ln l_{12} \\ d \ln l_{13} \\ d \ln l_{14} \\ d \ln l_{23} \\ d \ln l_{24} \\ d \ln l_{34} \end{bmatrix}$$

$$\mathbf{b}_i^* = \begin{pmatrix} b_1^* \\ b_2^* \\ b_3^* \\ b_4^* \end{pmatrix} \quad \mathbf{d} \ln l_{is} = \begin{pmatrix} d \ln l_{1s} \\ d \ln l_{2s} \\ d \ln l_{3s} \\ d \ln l_{4s} \end{pmatrix}$$

and

$$a_{ij}^* = D_{ii,0}^{-1} \left(\frac{l_{ij}^2}{l_{is} l_{is}} \right)_0 \quad (10)$$

$$\begin{aligned} b_i^* = & \left[D_{i1}^* \frac{l_{is}}{l_{1s}} + D_{i2}^* \frac{l_{is}}{l_{2s}} \right. \\ & \left. + D_{i3}^* \frac{l_{is}}{l_{3s}} + D_{i4}^* \frac{l_{is}}{l_{4s}} \right]_0 \end{aligned} \quad (11)$$

D_{ij}^* stands for the cofactor of the corresponding element in G^* .

q four-station rangings will yield q relations of type (9); ($s = 1, \dots, q$). In matrix form

$$A \cdot \mathbf{d} \ln l_{is} = B \cdot \mathbf{d} \ln l_{is} \quad (12)$$

compound matrices A and B being defined as follows:

$$A = \begin{pmatrix} \mathbf{a}_{ii}^1 \\ \mathbf{a}_{ii}^2 \\ \vdots \\ \mathbf{a}_{ii}^q \end{pmatrix}$$

$$B = \begin{pmatrix} \mathbf{b}_i^1 & & & & & \\ \cdots & \mathbf{b}_i^2 & & & & \\ \cdots & \cdots & \mathbf{b}_i^3 & & & \\ \cdots & \cdots & \cdots & \mathbf{b}_i^4 & & \\ \cdots & \cdots & \cdots & \cdots & \mathbf{b}_i^q & \end{pmatrix}$$

RANGE MEASUREMENTS TO SATELLITES

A has q rows and six columns; B should be understood to have nonzero elements in the s th row in columns $4(s-1)+1$ to $4(s-1)+4$ only; B has q rows and $4q$ columns.

Both A and B depend on the joint geometry of the four stations and the q observed satellite positions. The present problem, given A and B and the variance matrix $V\{\ln l_{is}\}$ as given by (4), is to predict the variance-covariance matrix $V\{\ln l_{ij}\}$ for the interstation distances. The solution is standard:

$$V\{\ln l_{ij}\} = (A^T G A)^{-1} \quad (13)$$

with

$$G^{-1} = B V\{\ln l_{is}\} B^T$$

or, using (4),

$$G^{-1} = \sigma^2 B B^T \quad (14)$$

A^T is the transpose, and A^{-1} is the inverse of A .

$B B^T$ is simply the q th-order diagonal matrix, the elements of which are $\mathbf{b}_i^* \mathbf{b}_i^*^T$ ($s = 1, \dots, q$). With (14), (13) becomes

$$V\{\ln l_{ij}\} = \sigma^2 [A^T (B B^T)^{-1} A]^{-1} \equiv \sigma^2 V \quad (15)$$

Matrix $V = [A^T (B B^T)^{-1} A]^{-1}$ has been evaluated for a variety of possible combinations of values for orbital heights H , station separation angles θ , and parameters N . The latter controls the number q of four-station ranging events, uniformly distributed over the common ranging domain. To obtain $V\{\ln l_{ij}\}$, we multiply by σ^2 , if we want to take the precision of the laser ranging system into account.

Of prime interest here, however, is the matrix V , specifying, roughly speaking, the loss of proportional precision from station-to-satellite ranging through the geometry to interstation distances. In full, V reads:

$$V = \begin{pmatrix} (12, 12) & (12, 13) & (12, 14) & (12, 23) & (12, 24) & (12, 34) \\ (13, 12) & (13, 13) & (13, 14) & (13, 23) & (13, 24) & (13, 34) \\ (14, 12) & (14, 13) & (14, 14) & (14, 23) & (14, 24) & (14, 34) \\ (23, 12) & (23, 13) & (23, 14) & (23, 23) & (23, 24) & (23, 34) \\ (24, 12) & (24, 13) & (24, 14) & (24, 23) & (24, 24) & (24, 34) \\ (34, 12) & (34, 13) & (34, 14) & (34, 23) & (34, 24) & (34, 34) \end{pmatrix} \quad (16)$$

L. AARDOOM

if (ij, km) stands for the covariance between $\ln l_{ij}$ and $\ln l_{km}$, and (ij, ij) for the variance of $\ln l_{ij}$, everything divided by σ^2 .

It is the variances that are of prime interest here, although the covariances, which are often of the same order of magnitude as the variances, certainly cannot be neglected if the precision of derived quantities like angles between interstation chord lines is to be estimated.

It appears that variances (ij, ij) as evaluated for different N are roughly inversely proportional to q , as one would expect. There is some divergence from this rule, in fact up to 60%, but in terms of standard deviations this is less than 30%, and the discrepancy is neglected. The results obtained for $N = 1$ ($q = 7$) have been normalized by multiplication by 7, so that starting from these normalized values the corresponding variances for any $q \geq 6$ can be estimated with sufficient accuracy through division by q . This procedure tends to underestimate (ij, ij) by up to 60% for $N = 5$; ($q = 91$).

Each matrix V exhibits two distinct variances (see also Figure 2b):

$$(12, 12) = (13, 13) = (23, 23) = M^2$$

$$(14, 14) = (24, 24) = (34, 34) = m^2$$

It was found that

$$1 < M^2/m^2 < 2.3$$

and consequently

$$1 < M/m < 1.5$$

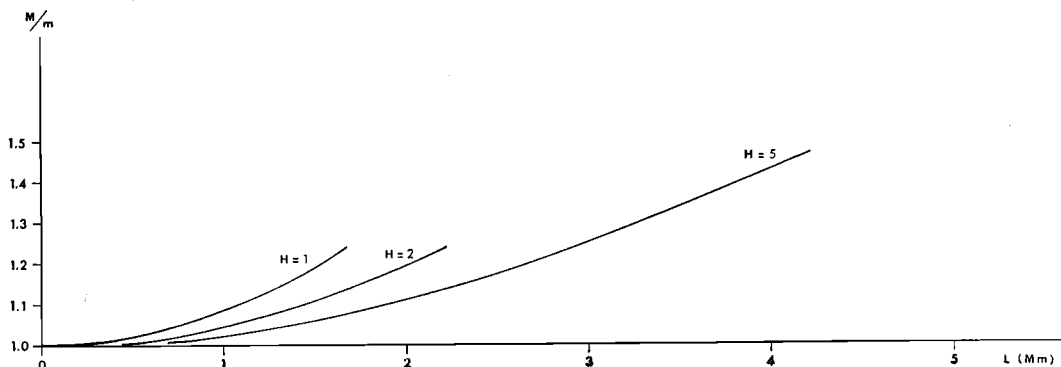


Fig. 5. Ratio M/m versus smallest ground distance L in model station configuration. M and m are the proportional standard deviations of the two numerically distinct interstation distances. Curves are valid for satellite altitudes $H = 1, 2$, and 5 megameters and maximum zenith distance $\zeta = 75^\circ$. L is given in megameters.

The ratio M/m always increases with increasing θ , H being fixed. Figure 5 illustrates this for some practical values of H . Here θ has been replaced by an equivalent surface distance L (Mm). The maximum magnitude 1.5 of the ratio justifies the adoption of M as an over-all measure of proportional precision propagation; however, this is sometimes a bit pessimistic.

Figure 6 gives normalized M for a variety of possible, though not always practical, combinations of H and L at $\zeta = 75^\circ$. $H = 0.1, 0.2$, and 0.5 represent, certainly in this context, hardly or not at all feasible satellite heights, and $H = 36$ represents the geostationary satellites. The case $H = 380$, typical for the moon, has also been studied, but for practical reasons the result is not given in Figure 6; the smallest attainable M is about 2500, which apparently makes the moon, or rather a retroreflector package on its surface, an unfavorable target for simultaneous laser ranging from the earth, if the object is to find terrestrial interstation distances. For $H = 36$, the estimates of Figure 6 will in general be too optimistic, because a uniform distribution of points P_s over the common ranging domain usually cannot be approached with geostationary satellites.

Finally, $V\{\ln l_{ij}\} = \sigma^2 V$ is the matrix of variances

$$\begin{aligned} \sigma^2 \cdot (ij, ij) &= \text{var} \{ \ln l_{ii} \} \\ &= (1/l_{ii}^2) \text{var} \{ l_{ii} \} \end{aligned}$$

and covariances

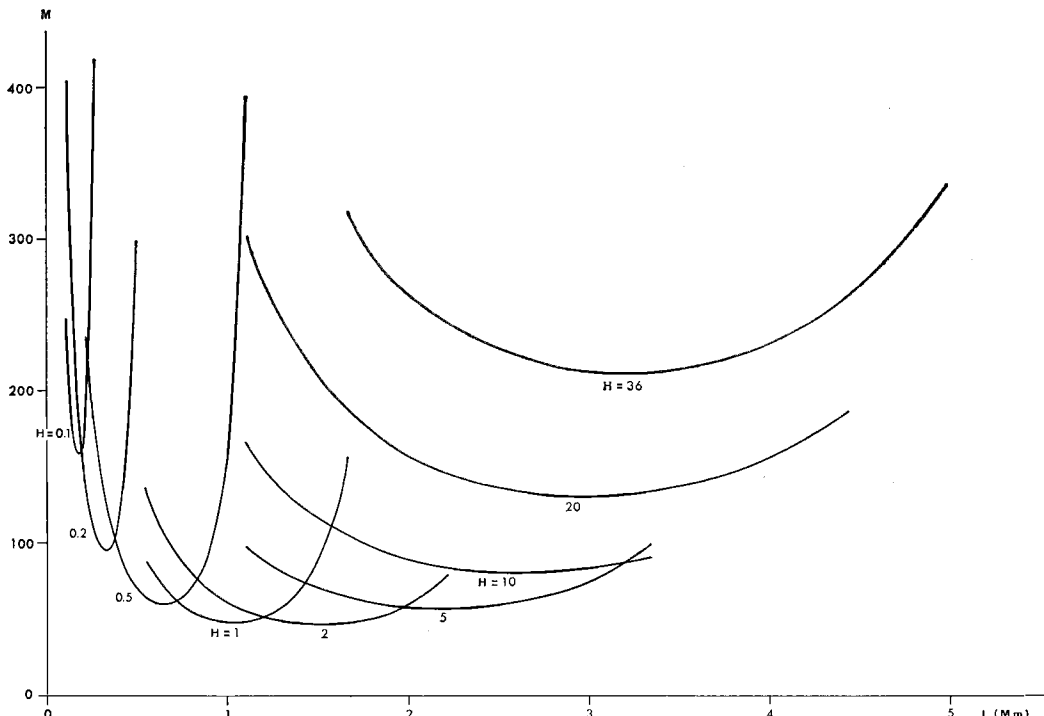


Fig. 6. Largest proportional standard deviation M of interstation distances for satellite altitudes H from 0.1 to 36 megameters and maximum zenith distance $\xi = 75^\circ$. Ground distance L is given in megameters. M is based on unit proportional ranging variance.

$$\sigma^2 \cdot (ij, km) = \text{covar} \{ \ln l_{ij}, \ln l_{km} \} \\ = (1/l_{ij}l_{km}) \text{var} \{ l_{ij}, l_{km} \}$$

Curves similar to those of Figure 6 have been obtained for maximum zenith angles $\xi = 60^\circ, 65^\circ, 70^\circ, 80^\circ$, and 85° .

The M curves of Figure 6 all show an absolute minimum; the same holds for the other values of ξ . For each ξ , these minimums have been connected by smooth curves, which have been plotted in Figure 7.

Obviously the ratio

$$M = (\text{var} \{ \ln l_{ij} \} / \text{var} \{ \ln l_{is} \})^{1/2}$$

is related to the ratio

$$\mu = (\text{var} \{ l_{ij} \} / \text{var} \{ l_{is} \})^{1/2}$$

by

$$\mu = (l_{ij}/l_{is}) M$$

where μ is a measure of absolute precision propagation. Using the approximate ratio

$$l_{ij}/l_{is} = (R/H) \sin \theta \cdot (3)^{1/2}$$

the M curves of Figure 6 have been transformed into approximated μ curves in Figure 8.

The absolute minimums of the M curves of Figure 6 must be understood to represent cases of a most favorable balance between two opposing geometric effects: the separation of the stations P_i and the separation of the ranged satellite positions P_s . The larger these separations, the smaller M , but because of optical conditions (earth's curvature and maximum zenith angle ξ) the separations are negatively correlated. The μ curves of Figure 8 demonstrate the same property. Within the limits set by the assumptions made, the minimums represent 'best' determinations of the model configuration of Figure 2b.

It is to be expected that, on the assumption of a uniform distribution of points P_i and a variance-covariance matrix of type (4), an optimum configuration of stations P_i , if any, must be a symmetric one. The only conceivable 'nonsingular' symmetric grouping of the four stations is that of model configuration sub b , and therefore this must be the optimum one.

L. AARDOOM

The minimums thus indicate 'best' determinations of this 'optimum' configuration. Here 'best' means minimum M and minimum μ , and 'optimum' is used in the sense of an over-all optimum, so that (12, 12) = (13, 13) = (23, 23) and (14, 14) = (24, 24) = (34, 34). It might be possible, however, to find a station grouping that yields a smaller individual (12, 12), say, but a study of such asymmetric cases is beyond the scope of this paper.

The M curves of Figure 6 certainly do not look promising, although Figure 7 suggests that something can be gained by increasing the maximum zenith angle. Apparently the propagation of proportional precision from measured station-to-satellite ranges into interstation distances is rather poor, particularly with low and very high satellites. With q uniformly distributed positions P_s , the characteristic standard deviation becomes $Mq^{-1/2}$. However, because of a correlation that is probably present but is neglected, this square-root rule has limited practical value, and the result must therefore be interpreted as a rather rough estimate.

Even when selecting the most favorable orbital heights, one has to be aware of a factor of at least 10 or so as the ratio between the propor-

tional standard deviation of derived interstation distances and the proportional standard deviation of (smoothed) ranging. One cannot expect to decrease this ratio substantially by increasing the number of observations, particularly since it will be rather difficult to increase that number beyond practical bounds. Such practical bounds result from two considerations. Potential applications of high-precision laser ranging systems are often there, where the possibility of relative motions of the earth's crust can no longer be denied. Depending on the expected type of relative motion, the averaging time for the observations must be necessarily limited. This, in turn, sets some practical limit to the number q , because of the general difficulty of acquiring quadruple optical simultaneities. The assumption that the ranging precision is range-independent, probably valid with future short pulse systems, causes a substantial improvement of the situation. This is immediately obvious from a comparison of the μ curves of Figure 8 with the M curves of Figure 6. Now the satellites with orbital heights over 2000 km appear as the more favorable objects to determine interstation distances from a four-station ranging campaign. In particular, the very high objects like the

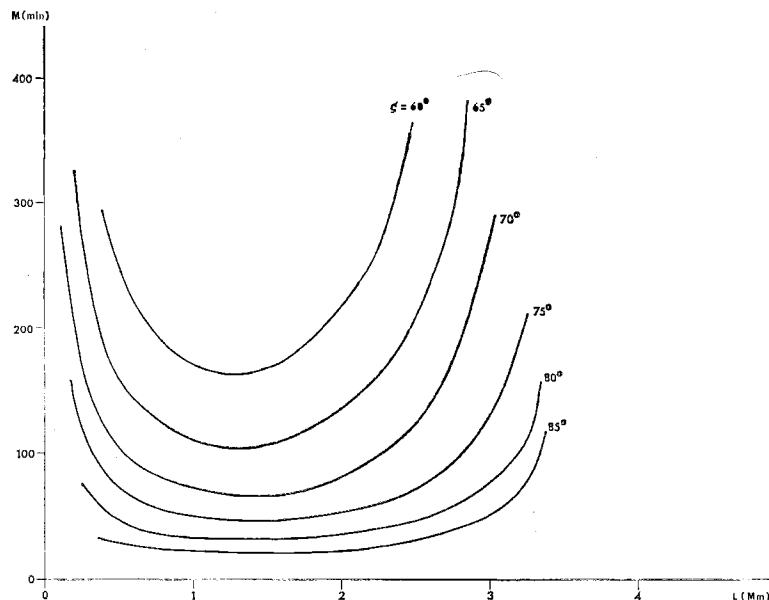


Fig. 7. Minimum values $M(\min)$ of standard deviation M of interstation distances for maximum zenith distances ξ between 60° and 85° . L is given in megameters. $M(\min)$ is based on unit proportional ranging variance.

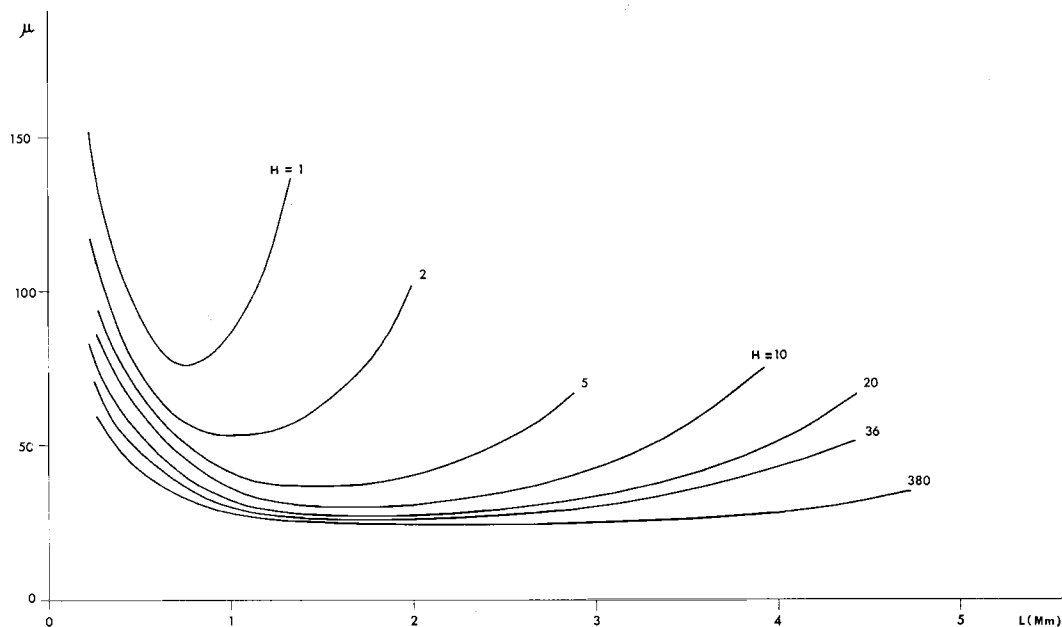


Fig. 8. Largest standard deviation μ of interstation distances for satellite altitudes H between 1 and 380 megameters and maximum zenith distance $\zeta = 75^\circ$. L is given in megameters and μ is based on unit ranging variance.

geostationary satellites and retro-reflector packages on the lunar surface come out as very useful from a purely geometric point of view.

These results indicate that the estimated standard deviation of interstation distances is well below 10 times that of the ranging, even for a relatively small number of four-station observation events, provided that the orbital height of the satellite is suitably selected. This is in fairly good agreement with the results of Bender *et al.* [1968] and Brown [1970].

Figure 7 indicates that the maximum zenith angle ζ is an important parameter. A substantial improvement is effected by an increase of this angle, especially in the range from 60° to 75° . No doubt refraction problems are enhanced by such an increase, and therefore it would be interesting to determine whether some optimum ζ can be found.

Since the ranging standard deviation might be as small as 5 cm in future sophisticated systems, it is expected that ultimately an interstation precision of some 25 cm (standard deviation) can be obtained from a rather limited observation program.

Here it is presupposed, however, that such a project be programmed with some care as to

station distribution and both height and spatial distribution of satellite positions.

The present results are tentative; multiple-station configurations are also being investigated.

Acknowledgment. Most of the calculations were performed by Mr. K. H. Otten, Geodetic Institute, Delft University of Technology.

REFERENCES

- Aardoom, L., Geometry from simultaneous satellite ranging, *Tellus*, 22(5), 572, 1970.
- Bender, P. L., et al., Satellite geodesy using laser range measurements only, *J. Geophys. Res.*, 73(16), 5355, 1968.
- Brown, D. C., Near term prospects for positional accuracies of 0.1 to 1.0 meters from satellite geodesy, *Rep. AFCRL-70-0501*, DBA Systems, Inc., Melbourne, Fla., 1970.
- Kaula, W. M. (Chairman), The terrestrial environment: Solid earth and ocean physics, *NASA Contract. Rep. 1579*, 1970.
- Killian, K., and P. Meissl, Einige Grundaufgaben der räumlichen Trilateration und ihre gefährlichen Örter, Beiträge zur Theorie der geodätischen Netze im Raum, ser. A, nos. 61 and 65, Deutsche Geod. Kommission, Munich, 1969.
- Lehr, C. G., M. R. Pearlman, J. L. Scott, and J. Wohn, Laser satellite ranging, paper presented at Symposium on Laser Applications in the Geosciences, Douglas Advanced Res. Lab., Huntington Beach, Calif., 1969.

Absolute Orientation of Satellite Triangulation

ANGEL A. BALDINI

Research Institute, U.S. Army Engineer Topographic Laboratories
Fort Belvoir, Virginia 22060

Abstract. A satellite is photographed against a star background simultaneously from several camera sites. From absolute satellite topocentric directions, derived from the photographs, and known astronomic station positions, the satellite event is reduced to a geograv coordinate system with an origin close to the earth's center of mass and axes parallel to the sidereal system. The satellite directions being known, the stations are then also reduced to this system. The directions of plumb lines are tilted to determine, to a close approximation, the earth's center of mass. A minimum of two satellite positions is required for fixing the stations to this system. The elapsed period of time between two photographs can be as short as a few seconds or as long as many hours or days. A number of systems can be combined to get a closer approximation of the earth's center of mass. This theory can also be applied to the moon, asteroids, and certain natural satellites of planets.

The topocentric position of a point in space can be reduced to a quasi-geocentric position by introducing the concept of the geograv coordinate system, with an origin close to the earth's center of mass and axes parallel to the sidereal system. A number of independent geograv systems can be tied through absolute topocentric orientations between ground stations to get a closer approximation to the earth's center of mass. The point in space can be an earth satellite, the moon's center, asteroids, or a natural satellite.

GEOGRAV POINT

A geograv point is a point that closely approximates the center of the earth's mass. The point can be defined first from the known astronomic station position and the station-to-satellite absolute directions obtained from satellite photographs taken at different camera sites. Simultaneity of observations or reduction to it is the basic condition.

GEOGRAV COORDINATE SYSTEM

As a rule, the direction of a plumb line of any station does not meet the earth's axis of rotation but passes close to it.

The astronomical meridian is a plane defined by the direction of the plumb line and a line

parallel to the earth's axis of rotation. Therefore, this plane runs parallel to the earth's axis of rotation, and its separation is always small. Consider now a set of ground stations observing at widely separated points. Two astronomic meridians intersect, and the line so formed runs parallel to the earth's axis of rotation. Therefore a set of lines so formed are all parallel, but with random positions with respect to the true earth's axis of rotation. The mean of these lines will run almost coincident with the true earth's axis of rotation. On this mean line there exists a point nearest to the plane of the true equator. This point will be called a local geograv point: a point very close to the true center of mass of the earth.

A set of station-to-satellite directions resulting from the photographs of an object in space can be referred to the local geograv point. There is one such point for each set of observing stations. Each of these points, which are considered to be the origin of a local geograv coordinate system, is taken to be a first approximation to the earth's center of mass. To obtain the geograv point, each local vertical must rotate an angle ϵ , which is not only unknown, but also varies from point to point. It is well known that the earth can be represented by an ellipsoid of revolution. Therefore, if one

chooses the shape of any known ellipsoid, the local geograv point can be defined. A first approximation for the angle ϵ can be obtained from

$$\epsilon = 696'' \sin 2\phi$$

where ϕ is the astronomic latitude.

If the observing stations are distributed on both sides of the equator, the shape of the ellipsoid used is not of importance. For any chosen flattening, the position of the geograv point will lie almost on the true equator. Therefore, a satellite photographed simultaneously from camera sites north and south of the equator with its position reduced to the geograv point would almost correspond to the true geocentric position. However, if the stations are all either north or south of the equator, the satellite coordinate in declination will have a systematic error in declination (positive or negative), the value of which will depend on the value of the flattening used.

In Figure 1, let the point S be a satellite and let A and B be two ground camera stations photographing S against a star background. The absolute orientations of lines AS and BS are expressed in terms of topocentric right ascension and declination. Let V_a and V_b be the true direction of the plumb lines at A and B , respectively. The geograv point can be defined as follows: In Figure 2, the local astronomical meridians of A and B intersect in a line MN and are parallel and close to the earth's axis of rotation. The vertical V_a is in the plane ANM , and the vertical V_b is in the plane BMN . They intersect the line MN at points A_0 and B_0 , respectively. By rotating V_a by angle ϵ_1 and V_b by angle ϵ_2 , we impose the condition that they meet at M . This point M is considered to be the geograv point.

Let M in Figure 1 be the geograv point and the center of a sphere of unit radius. We join A and B with M and let A_1 and B_1 be the points where they pierce the sphere. Through M , we draw a line parallel to AS that pierces the sphere at Q . The plane formed by the two lines AS and AM will intersect the sphere along the great circle arc A_1QR . Consequently, the satellite S , as viewed from M , must be on the arc A_1Q . Through M we draw a parallel to BS that will pierce the sphere at L . The plane formed by BM and BS intersects the sphere along the

SATELLITE TRIANGULATION

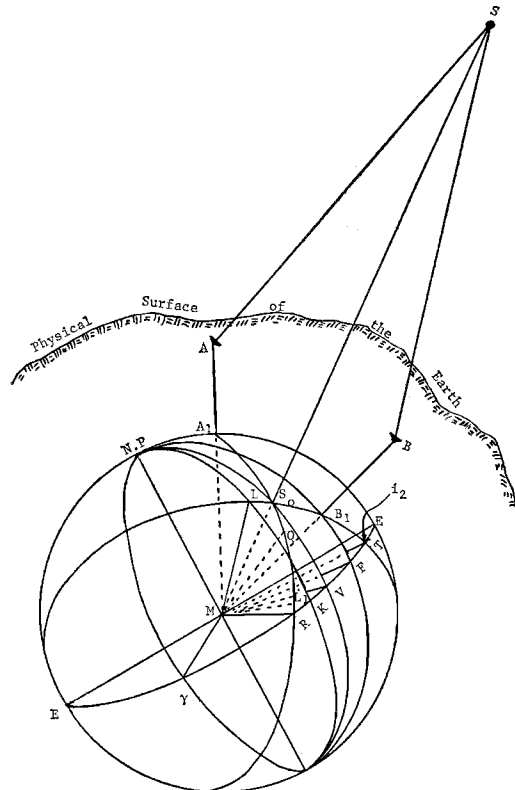


Fig. 1. Subsatellite position in the geograv system.

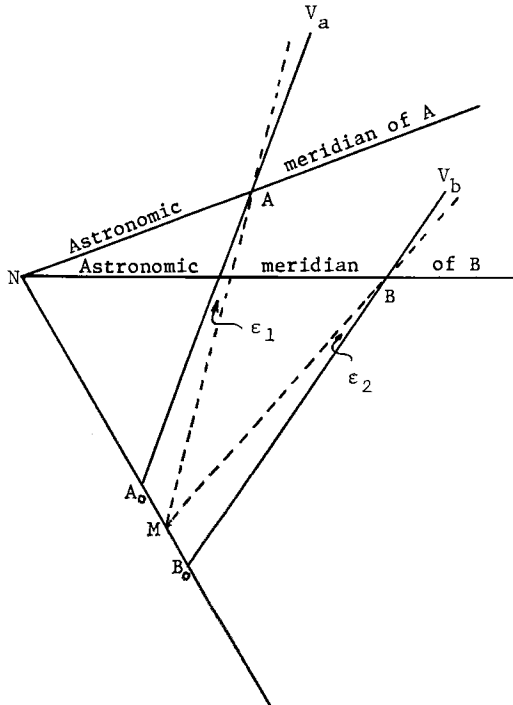
great circle arc B_1LT . The satellite S as viewed from M must also be on the great circle B_1L . Therefore the point where these two great circles A_1QR and B_1LT intersect will be the subsatellite position on the sphere as viewed from M . These considerations can be extended to any number of observing stations and any number of satellites.

Through M , we draw a line parallel to the earth's axis of rotation so that the point where it pierces the sphere corresponds to the north pole, N.P. A plane through M normal to the axis of rotation is the equatorial plane that intersects the sphere with the great circle arc ERE . The plane SAM intersects the equator at R , forming an angle of inclination i_1 , and the plane SBM intersects the equator at T with an angle of inclination i_2 , i_2 being different from i_1 .

To fix the direction MS_0 at each station, two parameters, ξ and η , related to these angles of inclination are computed.

ANGEL A. BALDINI

21

Fig. 2. Diagram showing the geograv point M .COMPUTATION OF THE PARAMETERS ξ AND η

Let line My point to the vernal equinox. If the meridians of L , S_o , and station B are drawn, they intersect the equatorial plane at points K , V , and F , respectively.

The angle γMK is the topocentric right ascension of the satellite (known from the photograph taken at B), and the angle LMK is its declination. The angles γMV and $S_o MV$ are the unknown geocentric right ascension and declination of the satellite. The angle γMF is the local sidereal time at station B when the photograph was taken. Arc $B_o F$ is the geocentric station latitude and $\Omega = \gamma MK$. Then using

- α_o geocentric right ascension of the satellite
- δ_o geocentric declination of the satellite
- α_2 topocentric right ascension from station B
- δ_2 topocentric declination from station B
- θ_2 local sidereal time at station B
- β_2 geocentric latitude of station B
- λ_2 longitude of station B , positive west
- θ_g Greenwich sidereal time

three equations follow:

$$\tan \delta_0 = \tan i_2 \sin (\alpha_0 - \Omega)$$

$$\tan \delta_2 = \tan i_2 \sin (\alpha_2 - \Omega) \quad (1)$$

$$\tan \beta_2 = \tan i_2 \sin (\theta_2 - \Omega)$$

The two parameters ξ_2 and η_2 are related to the angles i_2 and Ω through the equations:

$$\xi_2 = \tan i_2 \cos \Omega \quad (2)$$

$$\eta_2 = \tan i_2 \sin \Omega$$

$$\cot \Omega = \xi_2 / \eta_2 \quad (3)$$

$$\tan i_2 = \xi_2 \cos \Omega + \eta_2 \sin \Omega$$

Developing the sine of the differences of angles in (1) and taking into account

$$\theta_g = \theta_2 + \lambda$$

we obtain

$$\tan \delta_0 = \xi_2 \sin \alpha_0 - \eta_2 \cos \alpha_0$$

$$\tan \delta_2 = \xi_2 \sin \alpha_2 - \eta_2 \cos \alpha_2 \quad (4)$$

$$\tan \beta_2 = \xi_2 \sin (\theta_g - \lambda_2) - \eta_2 \cos (\theta_g - \lambda_2)$$

Tan β_2 can be computed from

$$\tan \beta_2 = (1 - f)^2 \tan \phi_2 + \frac{2fH}{a} \tan \phi_2 \quad (5)$$

where

ϕ_2 is the astronomic latitude.

$$f = 1/298.3.$$

$$a = 6378 \text{ km.}$$

H is the height of the station in kilometers.

The influence of H for computing $\tan \beta$ is negligible. For $\phi = 60^\circ$ and $H = 1 \text{ km}$, the second term of (5) amounts to only

$$(2FH/a) \tan \phi = 0.000001 \quad (6)$$

Thus this term can be neglected.

Since α_o and δ_o are unknown, we obtain the parameters ξ_2 and η_2 from the last two equations of (4). For any station and for a satellite event, equations similar to (4) are formed, and from these a different pair of values ξ and η are computed for those stations so that a general equation for determining α_o and δ_o can be developed; that is,

$$-\xi_i \sin \alpha_o + \eta_i \cos \alpha_o + \tan \delta_0 = 0 \quad (7)$$

$$i = 1, 2, 3, \dots, n$$

Introducing two unknown parameters X_0 and Y_0 , related to α_0 and δ_0 as

$$\sin \alpha_0 = X_0 \tan \delta_0 \quad (8)$$

$$\cos \alpha_0 = Y_0 \tan \delta_0$$

$$\tan \alpha_0 = X_0 / Y_0 \quad (9)$$

$$\tan \delta_0 = \frac{\sin \alpha_0 + \cos \alpha_0}{X_0 + Y_0} \quad (10)$$

we can rewrite equation 7 as:

$$-\xi_i X_0 + \eta_i Y_0 + 1 = 0 \quad (11)$$

Equation 11 is a condition equation with parameters ξ_i and η_i .

ADJUSTMENT OF PARAMETERS ξ_i , η_i

The sets of ξ_i , η_i as derived from equations 4 produce a first approximation for the adjustment of these parameters. Using the condition that any two pairs of values ξ , η for any two stations determine a constant C , we have

$$(\eta_m - \eta_n)/(\xi_m - \xi_n) = C \quad (12)$$

Further, we impose the condition that three sets of ξ and η must satisfy the condition that the determinant

$$\begin{vmatrix} \xi_1 & \eta_1 & 1 \\ \xi_2 & \eta_2 & 1 \\ \xi_3 & \eta_3 & 1 \end{vmatrix} = 0 \quad (13)$$

The ξ_i and η_i values, derived from equation 4, will give discrepancies in equations 13. These equations of condition must be rigorously satisfied. Therefore, we apply corrections to the ξ_i , η_i so that the discrepancies vanish.

If we set up corrections V_1 and V_2 for the first set ξ_1 and η_1 , V_3 and V_4 for the second set, and so on, we obtain for each independent set:

$$\begin{vmatrix} \xi_1 + V_1 & \eta_1 + V_1 & 1 \\ \xi_2 + V_2 & \eta_2 + V_2 & 1 \\ \xi_3 + V_3 & \eta_3 + V_3 & 1 \end{vmatrix} = 0 \quad (14)$$

The corrections V are computed according to the method of least squares, the conditional observations being correlates.

SATELLITE TRIANGULATION

DETERMINATION OF THE STATION GEOCENTRIC LATITUDE AND LONGITUDE

After the ξ and η values have been adjusted, we proceed to the determination of the ground-station positions with respect to the geograv point. The latitude and longitude of one station are related to the geograv point through the adjusted values of ξ and η by using the third equation of (4), which is now reduced to the following form:

$$\begin{aligned} \tan \beta = & \cos \lambda (\xi_i \sin \theta_{gi} - \eta_i \cos \theta_{gi}) - \sin \lambda \\ & \cdot (\eta_i \sin \theta_{gi} + \xi_i \cos \theta_{gi}) \quad (16) \end{aligned}$$

$i = 1, 2, 3$

where θ_{gi} is Greenwich sidereal time. In order to determine β and λ , we let

$$A_1 = \xi_1 \sin \theta_{g1} - \eta_1 \cos \theta_{g1} \quad (17)$$

$$B_1 = \xi_1 \cos \theta_{g1} + \eta_1 \sin \theta_{g1}$$

from the first observations and let

$$A_2 = \xi_2 \sin \theta_{g2} - \eta_2 \cos \theta_{g2} \quad (18)$$

$$B_2 = \xi_2 \cos \theta_{g2} + \eta_2 \sin \theta_{g2}$$

from the second observations.

Then from the two photographs, we find the two equations

$$\tan \beta = A_1 \cos \lambda - B_1 \sin \lambda \quad (19)$$

$$\tan \beta = A_2 \cos \lambda - B_2 \sin \lambda$$

which, by subtraction, produces

$$\cos \lambda (A_2 - A_1) - (B_2 - B_1) \sin \lambda = 0 \quad (20)$$

and allows us to determine the longitude λ from

$$\cot \lambda = (B_2 - B_1)/(A_2 - A_1) \quad (21)$$

when

$$A_2 - A_1 > B_2 - B_1$$

and

$$\tan \lambda = (A_2 - A_1)/(B_2 - B_1) \quad (22)$$

when

$$A_2 - A_1 < B_2 - B_1$$

After the longitude is known, the geocentric latitude is computed by equation 19.

ANGEL A. BALDINI

23

LEAST SQUARES SOLUTION

If one has observed more than two satellite positions, one has more than sufficient data to compute the coefficients A and B . The equations are independent; therefore, the method of least squares can be used for computing λ and β as follows:

We introduce two unknown parameters N and D , defined by

$$\begin{aligned}\sin \lambda &= N \tan \beta \\ \cos \lambda &= D \tan \beta\end{aligned}\quad (23)$$

so that the longitude is computed from

$$\tan \lambda = N/D \quad (24)$$

and the latitude β is computed from

$$\tan \beta = (\sin \lambda + \cos \lambda)/(N + D) \quad (25)$$

In order to compare β with respect to the astronomical latitude, we compute ϕ from

$$\tan \phi = (\tan \beta)/(1 - f)^2 \quad (26)$$

or if the height H of the station with respect to sea level is known, ϕ can be obtained from

$$\tan \phi = \frac{\tan \beta}{(1 - f)^2 + H/a}$$

The A_i and B_i are computed from equation 17, and the parameters N and D are computed by the method of least squares from

$$-NB_i + DA_i = 1 \quad i = 1, 2, \dots, n \quad (27)$$

It must be pointed out that at each station only one pair of ξ and η can be used for each satellite event. If n represents the number of satellite events, we will have n pairs of values of

TABLE 1. Adjusted Apparent Right Ascensions and Declinations for Anna 1B
(Flash sequence 34.)

Station	Obs.	Greenwich Sidereal Time	Right Ascension	Declination
640	1	192°07'06.70"	92°42'12.66"	21°08'44.28"
	2	08 30.10	94 11 55.22	19 50 52.23
	3	10 03.60	95 50 27.83	18 22 47.98
	4	11 27.90	97 17 23.09	17 02 59.65
	5	12 52.10	98 42 26.01	15 43 04.49
641	1	192 07 06.70	115 15 53.50	20 20 29.33
	2	08 30.10	116 24 05.86	18 55 44.31
	3	10 03.60	117 38 00.50	17 21 57.34
	4	11 27.90	118 42 20.99	15 58 43.17
	5	12 52.10	119 44 37.48	14 36 50.46
643	1	192 07 06.70	101 58 40.39	12 05 23.52
	2	08 30.10	103 15 49.20	10 49 08.18
	3	10 03.60	104 40 10.18	9 24 28.06
	4	11 27.90	105 54 12.48	8 09 07.76
	5	12 52.10	107 06 26.33	6 54 50.38
647	1	192 07 06.70	81 02 02.20	16 33 09.21
	2	08 30.10	82 28 25.34	15 25 03.28
	3	10 03.60	84 04 18.75	14 07 34.71
	4	11 27.90	85 29 46.30	12 56 56.05
	5	12 52.10	86 54 14.96	11 45 43.38
648	1	192 07 06.70	61 54 01.10	6 24 32.61
	2	08 30.10	62 55 47.52	5 36 01.17
	3	10 03.60	64 05 17.53	4 40 42.97
	4	11 27.90	65 08 05.95	3 50 06.43
	5	12 52.10	66 10 58.05	2 58 51.15
649	1	192 07 06.70	51 52 44.56	22 57 38.99
	2	08 30.10	52 54 15.33	22 21 00.49
	3	10 03.60	54 03 58.81	21 38 20.38
	4	11 27.90	55 07 20.13	20 58 26.68
	5	12 52.10	56 11 09.29	10 17 12.40

TABLE 2. Astronomic Station Coordinates

Station	Longitude	Latitude	Ht. above Sea Level, meters
640	90°40'44.47"	29°33'46.48"	2.0
641	95 09 13.04	29 35 41.42	8.2
643	92 31 31.98	31 19 17.27	26.8
647	88 04 43.21	30 14 49.22	1.2
648	81 09 13.58	32 00 08.78	12.2
649	80 04 56.33	26 57 16.90	6.8

ξ and η for each observing station. These are the values to be used in equations 16 and 17.

COMPUTATION OF UNKNOWN STATION

For a station that has only photographs of a satellite but whose astronomic position is unknown, we must use the third equation in (4), since now α_0 and δ_0 are already known through the computation from the other stations. The ξ and η values to be used are derived from the first two equations of (4). Then we proceed to compute λ and β or ϕ through equations 24, 25, and 26.

SAMPLE COMPUTATION

As an illustration of the procedure just described, a sample problem is given using five flashes from the Anna 1B geodetic satellite observed from six different camera sites. The satellite photographs were taken with PC-1000

TABLE 3. Values of ξ and η from the First Satellite Position

Station	Approximate Value	Adjusted Value
1 ξ_1	-0.3300 96 4015	-0.3301 00 1267
	1.2096 01 8166	1.2096 06 8254
2 ξ_2	-0.6236 63 3295	-0.6237 01 6648
	-0.4528 36 2070	-0.4529 10 9793
3 ξ_3	-2.1564 52 5298	-2.1568 62 9972
	-9.1324 98 5337	-9.1344 32 3010
4 ξ_4	-0.4154 62 0706	-0.4154 70 4864
	0.7261 75 3071	0.7261 97 4268
5 ξ_5	-0.4402 21 295	-0.4402 27 3263
	0.5859 86 9910	0.5860 11 8971
6 ξ_6	-0.5427 67 3714	-0.5427 64 0027
	0.0053 97 3262	0.0053 98 2826

SATELLITE TRIANGULATION

TABLE 4. Satellite Position on the Geograv System from Flash 1

Station Pair	Right Ascension	Declination
1, 2	100°00'54.721"	28°09'57.675"
1, 3	54.721	57.675
1, 4	54.721	57.675
1, 5	54.721	57.675
1, 6	54.721	57.675
2, 3	100 00 54.721	28 09 57.675
2, 4	54.721	57.675
2, 5	54.721	57.675
2, 6	54.721	57.675
3, 4	100 00 54.721	28 09 57.675
3, 5	54.721	57.675
3, 6	54.721	57.675
4, 5	100 00 54.721	28 09 57.675
4, 6	54.721	57.675
5, 6	100 00 54.721	28 09 57.675

cameras with 10° square field of view. The topocentric right ascensions and declinations resulting from the plate adjustment are shown in Table 1. These data and the astronomic coordinates of the camera sites were used for computing the satellite position in the geograv system. The station astronomic coordinates used are given in Table 2. The ξ and η values for the first satellite positions computed from equation 4 and their adjusted values resulting by applying equation 23 are shown on Table 3. From the adjusted ξ and η values, the geograv satellite coordinates were derived from the equation

$$-\xi \sin \alpha_0 + \eta \cos \alpha_0 + \tan \delta_0 = 0$$

The results obtained by using various combinations of station pairs are shown in Table 4. The values resulting for all five flashes are shown in Table 5.

TABLE 5. Geograv Satellite Position

Flash	Right Ascension	Declination
1	100°00'54.721"	28°09'57.675"
2	100 16 05.924	27 57 16.297
3	100 33 03.773	27 43 00.471
4	100 48 17.192	27 30 07.321
5	101 03 26.664	27 17 13.407

ANGEL A. BALDINI

25

TABLE 6. Geograv Station Coordinates

Station	Longitude	Latitude	
		β	ϕ
640	90°40'44.293"	29°23'56.53"	29°33'47.27"
641	95 09 14.089	29 25 51.20	29 35 42.34
643	92 31 32.011	31 09 06.12	31 19 17.53
647	88 04 42.922	30 04 51.14	30 14 50.19
648	81 09 18.940	31 49 47.17	32 00 05.96
649	80 04 57.293	26 48 00.26	26 57 16.30

GEOGRAV STATION POSITIONS

With the adjusted values of set ξ and η , the coefficients A_i , B_i were computed according to equations 17 and 18.

The longitudes were computed in accordance with equations 21 and 22 and the latitude from (19). These results are shown in Table 6. The differences between the astronomic coordinates and the geograv system coordinates are shown in Table 7.

CONCLUSIONS

The tests discussed here are very encouraging. In the writer's opinion, better results can be achieved by using large telescopes, available at many observatories, to photograph objects against the star background. Several classes of

objects are usable; (1) low-orbiting or synchronous earth satellites, (2) the Io satellite of Jupiter, (3) the moon, and (4) many of the asteroids. After a set of stations is tied to different geograv points, on the basis of an angular adjustment, the final geocentric satellite and ground station positions can be computed.

TABLE 7. Difference between Astronomic Coordinates and Geograv Coordinates

Station	$\Delta\lambda$	$\Delta\phi$
640	+0.18"	-1.79"
641	-1.05	-0.92
643	-0.03	-0.26
647	+0.29	-0.97
648	-5.36	+2.82
649	-0.96	+0.60

2. Geometric Geodesy: Results

Status of Data Reduction and Analysis Methods for the Worldwide Geometric Satellite Triangulation Program

HELLMUT H. SCHMID

National Geodetic Survey, National Ocean Survey

National Oceanic and Atmospheric Administration, Rockville, Maryland 20852

Abstract. The article discusses the status of the worldwide geometric satellite program as of April 1971. The field observations have been completed, and their distribution compares favorably with the original goal. The comparator measurements and the reduction of single-camera records have been improved, multiple synthetic directions have been introduced, and a modified model for the global adjustment has been used. The results of an error study based on the presently selected data yield a rms error of 4.1 meters per station coordinate, which is believed to indicate the accuracy of the final result.

Field observations for the worldwide geometric satellite triangulation program started shortly after the launch of the Pageos balloon satellite in June 1966. By the end of that year, there were eleven Wild BC 4 field instrumentation systems in the field. Seven of these were equipped with the 300-mm focal-length lens, the rest with the 450-mm Cosmotar lens, especially developed by Wild Heerbrugg, Ltd., for the application under consideration. The observational program was concluded in November 1970 with observations from stations in the general area of the Indian Ocean. During the later years of operation, there were up to 16 BC 4 instrumentation systems of essentially similar design in the field, all but one featuring the 450-mm lens, supplemented for a period of 14 months by two Air Force 1000-mm camera systems having a somewhat different design. In the early phase of the observation program, the satellites Echo 1 and in particular Echo 2 were also observed on shorter lines of the world net, until those targets ceased to exist in May 1968 and June 1969, respectively.

Altogether 3672 successful plates were obtained relating to 1702 successful events, composed of 1449 double-station, 238 triple-station, and 15 quadruple-station events.

During the planning phase of this program, the question of worldwide coverage being hampered by prevailing weather conditions was raised, especially over the Antarctic region. As an answer, Figures 1-6 show the distribution of all successful missions. The successfully observed satellite crossings are depicted with the locations of the center points of the observed orbital arcs, with ticks pointing toward the stations from which the specific event was photographed. There are gaps in the coverage, as can be seen by closer inspection of these figures. Characteristically, these gaps occur mainly in the area of the equatorial belt. They are not necessarily related one-to-one to weather conditions, but must be attributed partly to the fact that, because of the limited number of observation systems available, it was obviously necessary to accomplish the observation program in sequential phases. For economic and

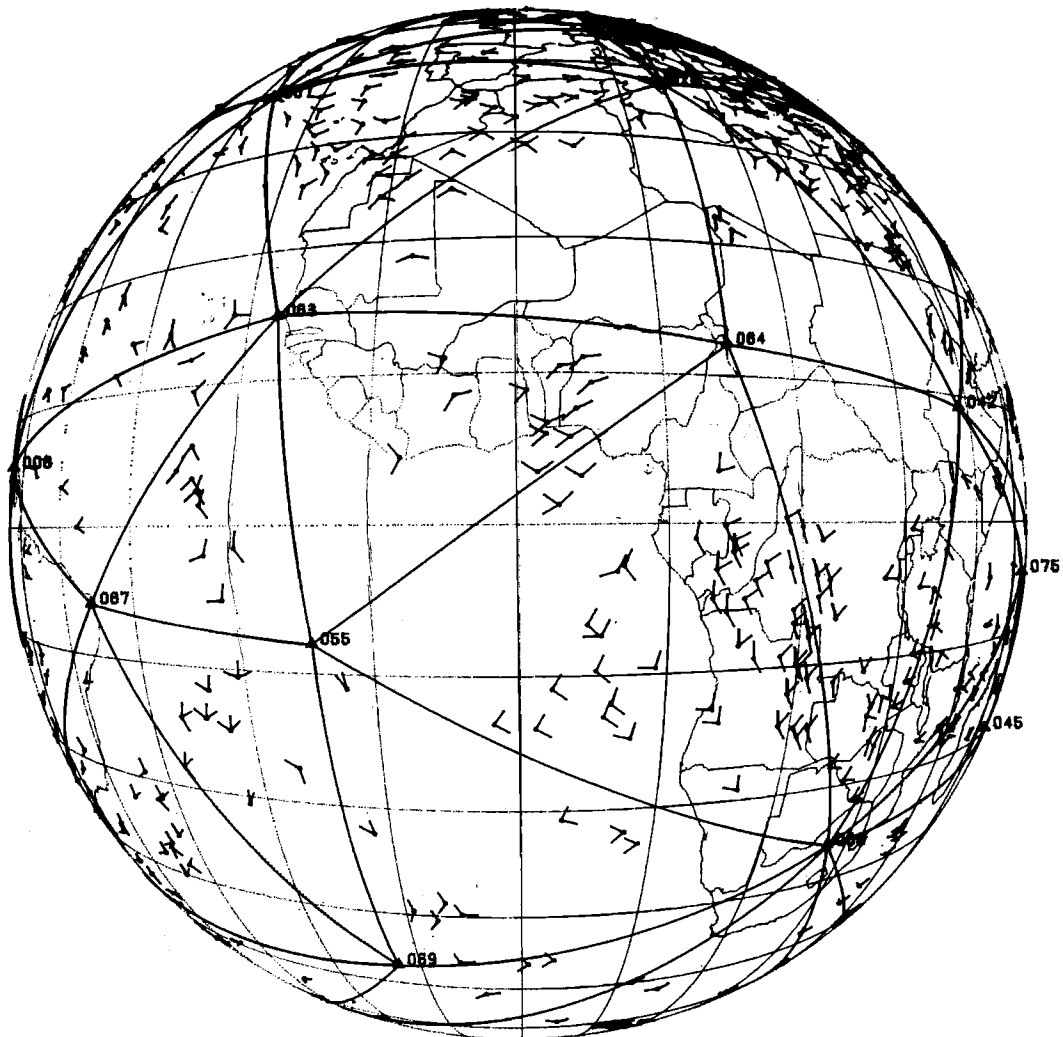


Fig. 1. Geographic distribution of stations and observations. Center of view is latitude 0, longitude 0.

political reasons, it was necessary to restrict the program to a minimum of station reoccupations. A conclusive analysis of the percentage of successfully obtained photographs versus possible opportunities in terms of weather conditions must also include all single plates obtained, which are not shown here because of their uselessness for triangulation. A partial result of such a study, which could provide information to the meteorological community on cloud coverage at night, is shown in Figure 7, presenting the number of opportunities against the failure of observation due to weather condi-

tions. The percentages for each station give the proportional loss due to weather.

Because of stringent criteria for accepting an event as 'successful,' the information available for reduction constitutes material of essentially uniform quality with respect to the photogrammetric contents of the acquired photographs. There is naturally a certain range of image quality because of local haze and, more likely, occasional very thin layers of clouds. Of greater significance for the metric quality of an individual record is a defect in the number of recorded stars caused primarily

HELLMUT H. SCHMID

29

by the lack of stars up to the 8th magnitude in certain parts of the sky and, secondly, again by the loss of the lower-magnitude stars owing to haze or clouds afflicting particularly the simultaneous photography of stars during the recording of the satellite event.

There are 125 lines associated with the basic station network, not counting the occasionally observed skip lines between stations at times up to 7000 km apart. Forty-two skip lines were obtained that contribute significantly to the strength in the final triangulation.

The minimum goal of the observation pro-

gram was to obtain, on the average, 10 missions per line, distributed evenly on both sides of each line. The number that is considered for theoretical reasons to be an optimum for a specific line is 16.

Correspondingly, the minimum goal was to obtain about 1250 double missions or about 2500 plates. Table 1 shows the actual distribution of the observations obtained with respect to the sides of the triangles formed by the station configuration; the triple and quadruple missions have been split up into a corresponding number of double missions, an approach

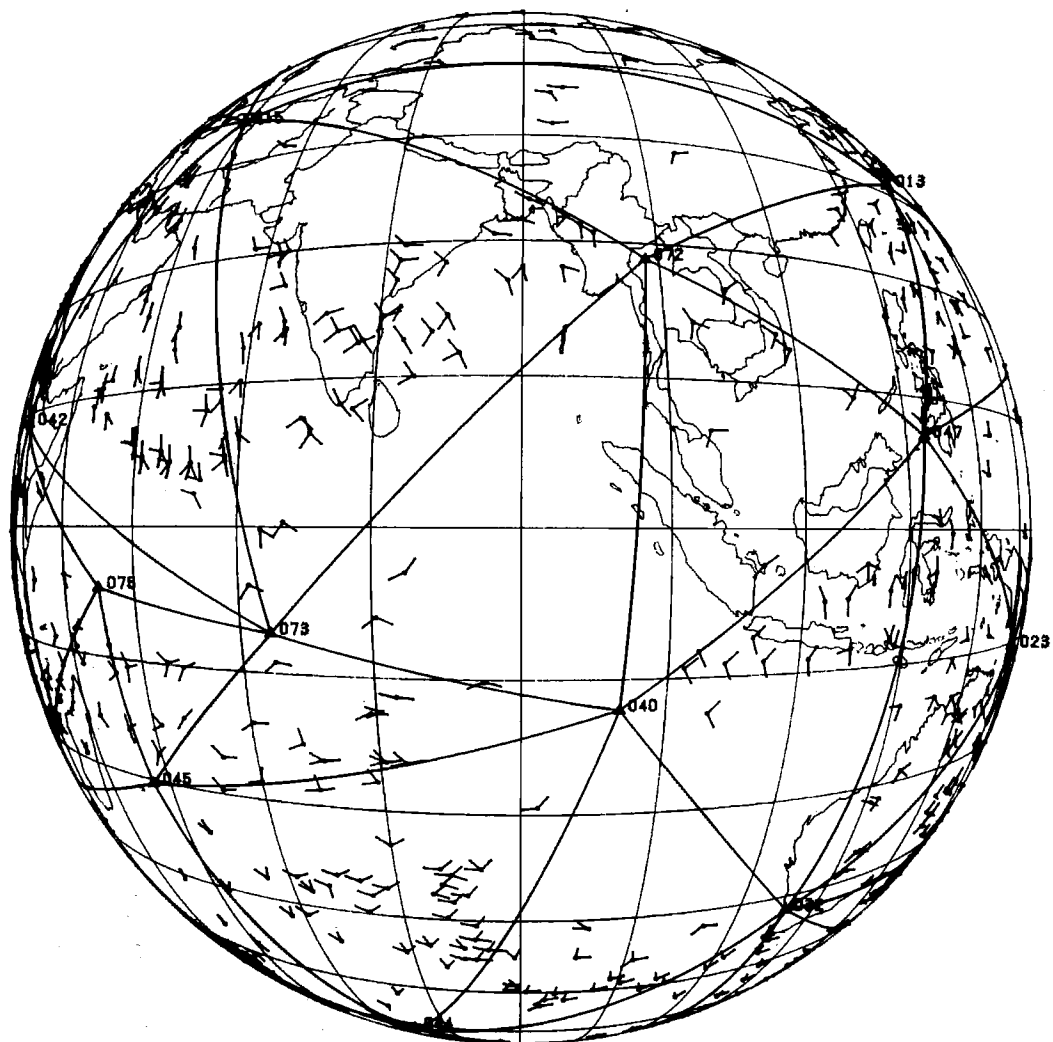


Fig. 2. Geographic distribution of stations and observations. Center of view is latitude 0, longitude 90°E.

WORLDWIDE SATELLITE TRIANGULATION

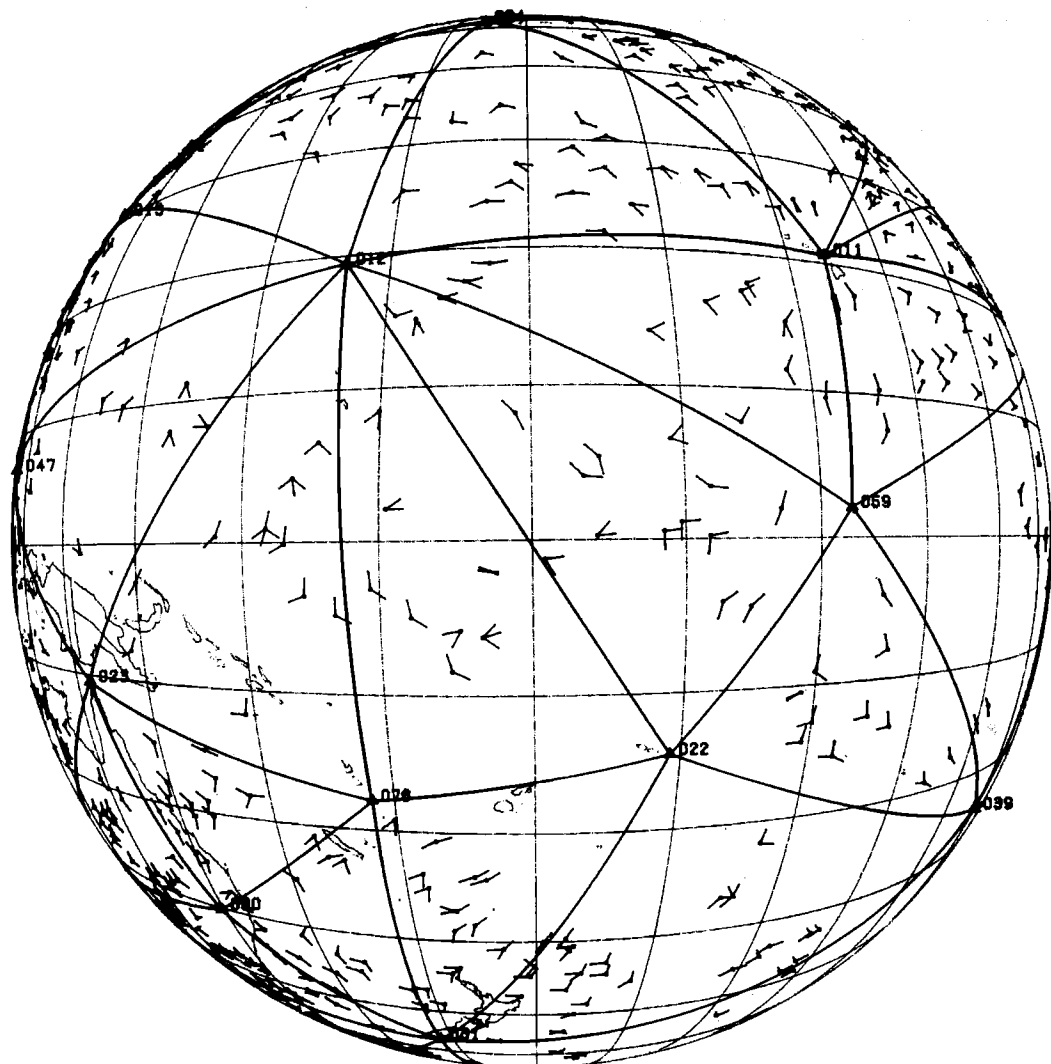


Fig. 3. Geographic distribution of stations and observations. Center of view is latitude 0, longitude 180.

that depreciates slightly the geometric strength of these missions, but leads nevertheless to a realistic presentation of the amount of material collected.

The determination of UT1 time for all star exposures to within a few milliseconds and the recording of the time of the satellite observations to a precision of better than $\pm 100 \mu\text{sec}$ for the various tracking stations relative to each other were very successful. The individual station clocks were in general tied to each other to within at least $\pm 10 \mu\text{sec}$. Because of the

availability of simultaneously received time signals, a study of propagation effects from the difference between clock time maintained station to station and the reception of radio-transmitted time signals will enable us to produce in the data reduction, as a by-product, quantitative information on atmospheric propagation effects at night over the four-year observational period.

The number of plates obtained at the individual stations is shown in Figure 8. The black areas indicate a surplus of obtained plates, and

HELLMUT H. SCHMID

31

the lined areas show the deficiency of observations. Figure 9 shows the number of plates observed at each station normalized with respect to the length of the longest single observation period, which was 654 days. The stations are plotted according to latitude, indicating the impact of weather conditions on the possibility of observing simultaneous events, as well as the availability of periods of illumination of the satellite with respect to the location of the observing stations during a specific period of occupation.

With respect to data reduction, the goal is to

develop an approach whose level of sophistication is consistent with the theoretical accuracy expectations of the method of geometric satellite triangulation. In addition, the computations are organized to provide statistical information about the individual error contributions to each reduction step, in order to test the validity of any a priori assumptions about the precision of independently introduced parameters.

In order to give some quantitative information about the results obtained through April 1971, the data-reduction system for the photogrammetric satellite triangulation method is di-

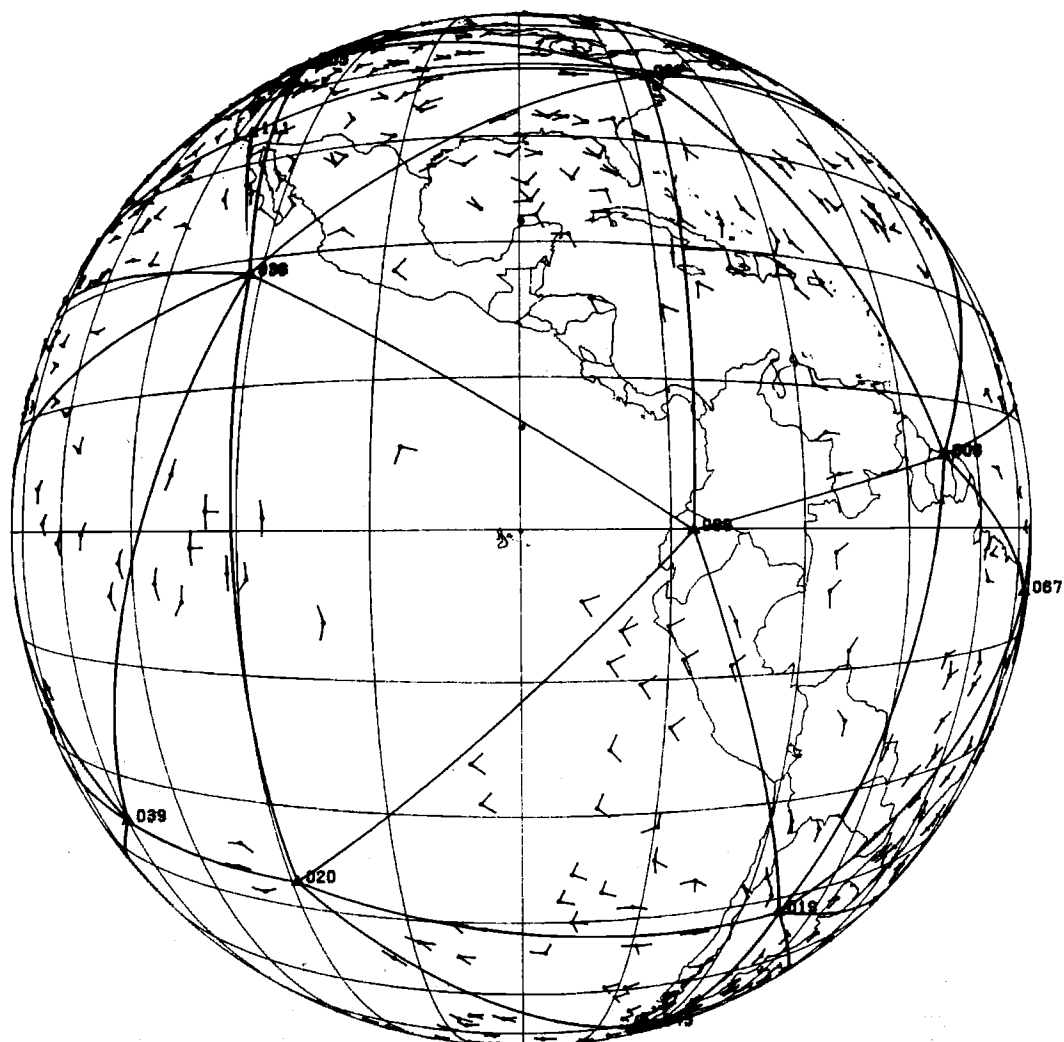


Fig. 4. Geographic distribution of stations and observations. Center of view is latitude 0, longitude 90°W.

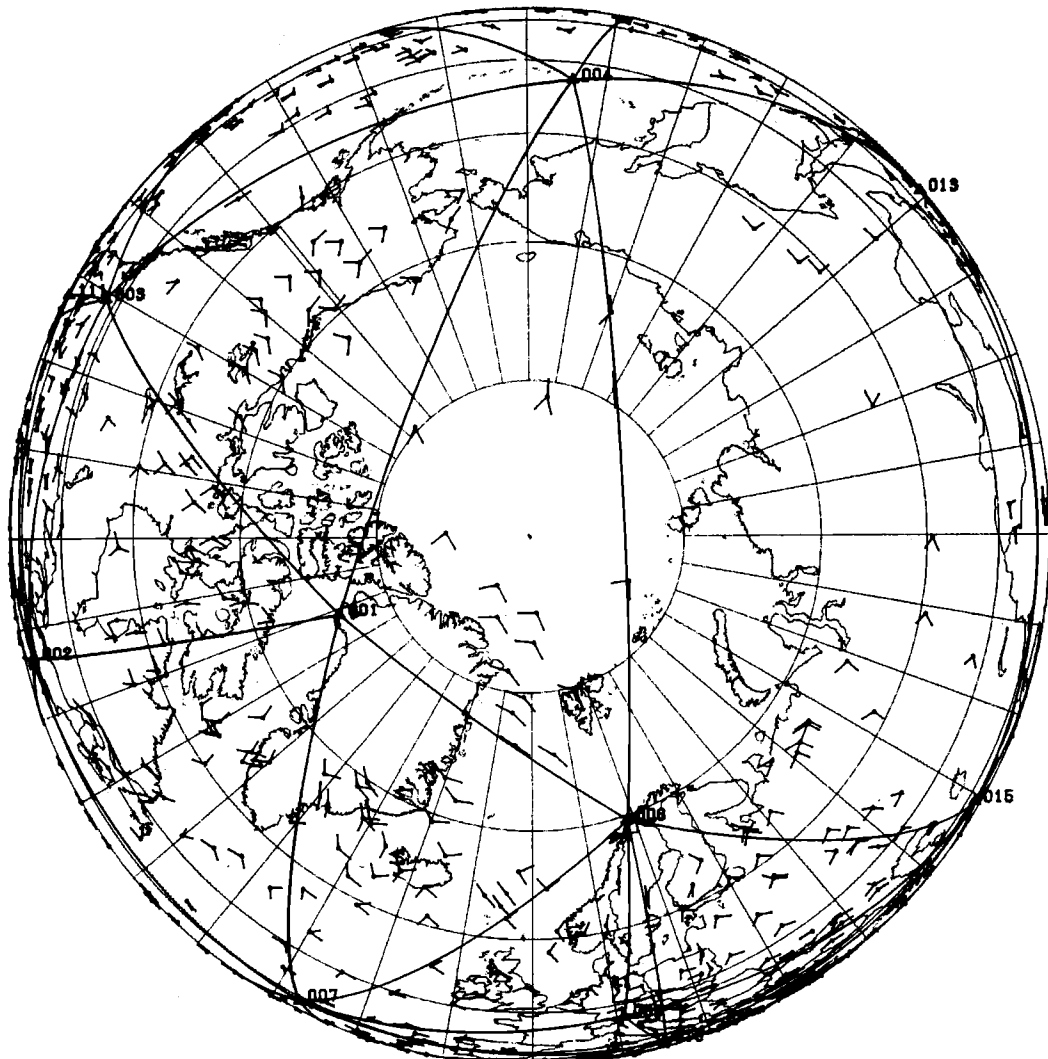


Fig. 5. Geographic distribution of stations and observations. Center of view is the north pole.

vided into four phases, which are characterized either by the computation of specific operational activities or by the computation of information suited for an analysis of specific error sources. These are:

1. The comparator measurements of the star and satellite imagery and their reduction to plate coordinates.

2. The analytical presentation of an interpolation model (analytical reconstruction of the photogrammetric bundle of a single camera) which restitutes the photographic recording

process and orients the thus re-established photogrammetric bundle of rays to either the reference system of metric astronomy for a certain epoch or to a geodetic reference frame determined by an epoch pole (e.g., the conventional origin, 1902-1903) and a chosen zero-time meridian (zero meridian of the BIH-UT1 system).

3. The process of determining the station-to-satellite directions by interpolating the satellite imagery into the model for the photogrammetric bundle.

HELLMUT H. SCHMID

33

4. The final three-dimensional triangulation of the observation stations, relative to an arbitrarily chosen origin.

An error analysis was conducted on 500 completely reduced plates with respect to the accuracy of (a) the coordinate measuring procedure, (b) the photogrammetric bundle simulation, (c) the process of interpolating the satellite imagery into the background of the fixed star field, and (d) the triangulation of single station-to-station lines. A summary of the results with respect to the first three steps is presented in

Table 2, where an attempt is made to give quantitative information about the various error sources.

The geometric satellite triangulation method is mainly affected by five randomly acting error sources. The corresponding irregular errors appear in connection with:

1. The comparator measurements of the star and satellite images (Table 2, column 2).
2. The star catalog data, used as reference parameters (Table 2, column 6).

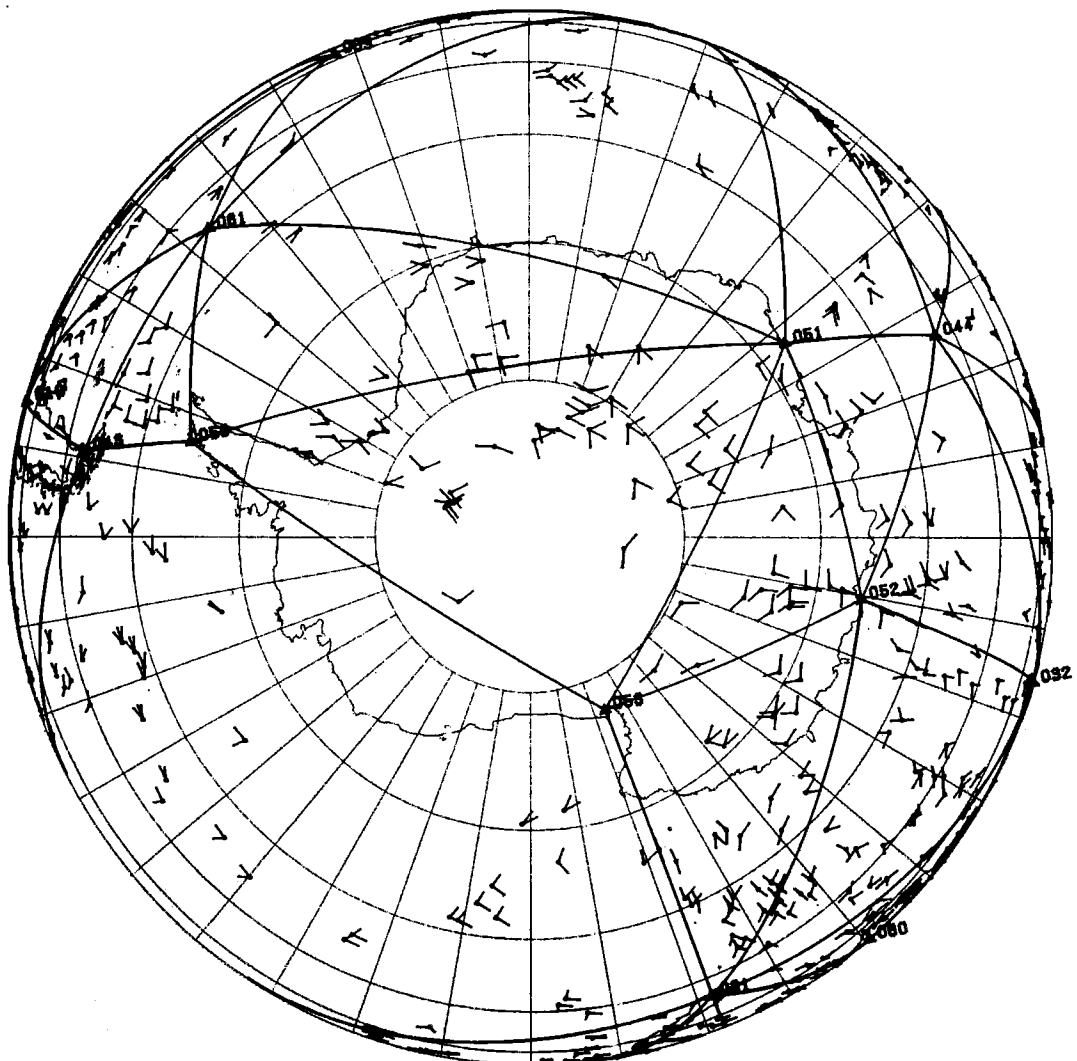


Fig. 6. Geographic distribution of stations and observations. Center of view is the south pole.

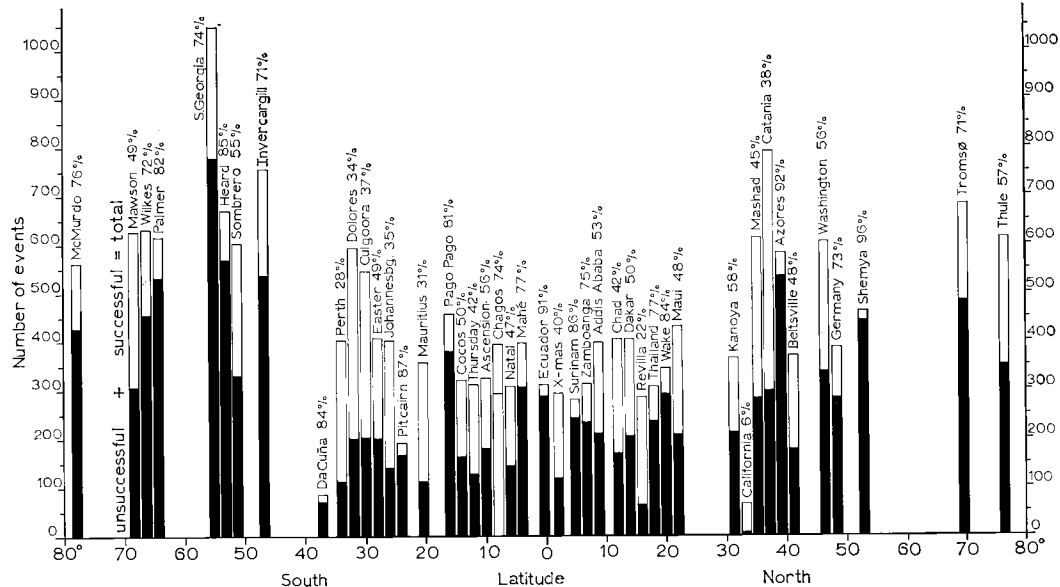


Fig. 7. Effect of cloud cover on scheduled events.

3. The time determination associated with the star and satellite image exposures.

4. The atmospheric scintillation that affects the directions toward the photographically recorded star and satellite trails (Table 2, column 4).

5. Emulsion distortion occurring during development (Table 2, column 3).

The irregular time errors for both the star and satellite photography are, typically, at least an order of magnitude below the level of the main error sources and can therefore be neglected. As is shown in Table 2, column 2, the accuracies of the comparator measurement for a double measurement of a single image are essentially equal for both the stars and the satellite images and amount to $\pm 1.8 \mu\text{m}$.

A detailed study of the coordinate measuring process based on more than a million double measurements [Schmid, 1969] showed that, despite the existing variations in precision of the measurements from plate to plate, particularly as a result of the use of up to 34 different comparator operators, all measurements are essentially Gaussian in behavior. From an examination of the individual error contributions given in Table 2, columns 2a, 3a, 4a, and 6a, it is obvious that the major error source is the

scintillation effect of the atmosphere that contributes, on the average, 75% to the total noise of the photogrammetric bundle reconstruction, as can be verified from the values given in Table 2 in columns 7a and 4a, respectively. Similarly, scintillation contributes 81% of the noise in the polynomial smoothing of the satellite images in accordance with the values given in columns 8b and 4b, respectively. Fortunately, this noise is strictly Gaussian in its distribution and can be reduced by statistical treatment, provided that enough star and satellite images are available on each photograph. This situation reveals the reason for the inadequacy of a geometric satellite triangulation based on electronic flashes, the number of which is entirely inadequate in the present state of the art; moreover, the resulting images, owing to the short duration of the flashes, are affected by even larger scintillation.

The facts just outlined are presented in more detail in Figure 10, where these results are shown for the individual 500 photographs. The lower diagram shows the average error of the comparator measurements, the middle diagram shows the mean error of the individual bundle reconstruction, and the upper diagram presents the mean scintillation. The similarity of behavior between the top and middle dia-

HELLMUT H. SCHMID

35

TABLE 1

Station-to- Station Line	Number of Successful Events	
	L	R
1 to 2	7	16
3	9	18
4	4	2
6	17	15
7	5	1
11*	0	1
15*	1	0
16*	2	1
38*	1	2
65*	3	6
2 to 3	14	19
6*	1	1
7	4	5
8	16	8
9	3	3
38	4	10
111	6	11
3 to 4	0	4
11	7	16
38	7	13
12*	0	2
111	24	20
4 to 6*	0	2
11	0	3
13	5	5
12	0	8
6 to 7	2	4
15	9	7
16	9	13
65	5	8
7 to 8	0	0
16	18	11
55*	0	2
63	23	7
64*	3	1
65	6	0
67*	2	2
8 to 9	7	1
19	7	15
61*	0	1
63	0	1
67	2	3
9 to 19	4	12
20	2	3
38	4	6
43*	2	2
11 to 22*	1	2
38	13	2
59	21	21
12	4	20
111	15	5

TABLE 1 (*continued*)

Station-to- Station Line	Number of Successful Events	
	L	R
12 to 13	1	11
22	2	5
23	7	9
59	9	2
60*	1	0
13 to 15*	2	0
23	0	0
47	8	5
72	4	1
15 to 16	31	37
40*	7	3
42	28	15
45*	9	1
64*	2	12
65	0	5
72	4	10
73	12	7
75	11	1
16 to 42	5	0
63	0	13
64	22	9
65	7	12
19 to 20	7	2
43	19	30
61	4	14
67	6	9
69*	0	2
20 to 38	11	2
39	1	2
43	4	11
22 to 23	2	3
31	14	4
39	2	5
59	9	10
60	15	4
78	0	3
23 to 31*	2	8
32	19	4
40*	1	1
47	6	3
60	20	32
72*	0	4
78	6	1
31 to 32*	10	10
39	3	0
51*	0	1
52	6	4
53	10	12
59*	0	1
60	31	25
78	2	2

WORLDWIDE SATELLITE TRIANGULATION

TABLE 1 (*continued*)

Station-to- Station Line	Number of Successful Events	
	L	R
32 to 40	26	6
44	4	4
45*	4	0
47	9	4
51*	5	0
52	5	5
53*	1	1
60	17	39
72*	0	1
38 to 39	3	2
59	1	5
111	3	8
39 to 59	6	2
40 to 44	2	0
45	26	8
47	4	3
60*	0	3
72	1	4
73	9	4
75*	6	2
42	45*	7
	64	16
	68	8
	73*	6
	75	2
43	50	3
	61	4
44 to 45	1	1
51	3	4
52	1	1
68	1	0
45 to 51*	2	5
68	13	7
73	13	18
75	22	11
47 to 60*	0	2
72	5	11
78*	1	0
50 to 51	0	1
52*	2	0
53	4	0
61	2	7
51 to 52	18	19
53	13	11
61	5	1
68	8	12
52 to 53	15	13
60	2	6
53 to 60*	3	8
61*	1	0

TABLE 1 (*continued*)

Station-to- Station Line	Number of Successful Events	
	L	R
55 to 63	21	8
64	7	8
67	13	7
68	0	2
69	6	4
61 to 67	3	0
68	1	2
69	2	2
63 to 64	9	5
67	10	3
69*	0	2
64 to 68	3	25
67 to 69	1	0
68 to 69	4	0
75	0	3

* Skip lines (between noncontiguous stations of the network).

grams is obvious and shows the significance of the error contributions of the scintillation effect. The photographs are arranged according to the latitude of the observation station (from +20° to -78°), indicating a considerable increase in the scintillation effect at higher latitude. This fact is also shown in Figure 11, where the average scintillation per station is shown again as a function of the latitude of the observing station. The number given for each point is the number of photographs used to form the average scintillation value.

From Table 2, column 7a, we see that a uniquely determined photogrammetric bundle reconstruction allows the determination of the direction of a central ray with an accuracy of $\pm 1.57''$. With the introduction of about 100 stars per plate, each photographed an average of five times, leading to about 500 star images per photograph, one can derive from the information of Table 2 the accuracy of such a direction from a corresponding adjustment to $\pm 0.25''$.

Table 3 shows results obtained for a specific photograph with 105 different reference stars and 648 star images, for rays corresponding to various positions across the plate.

HELLMUT H. SCHMID

37

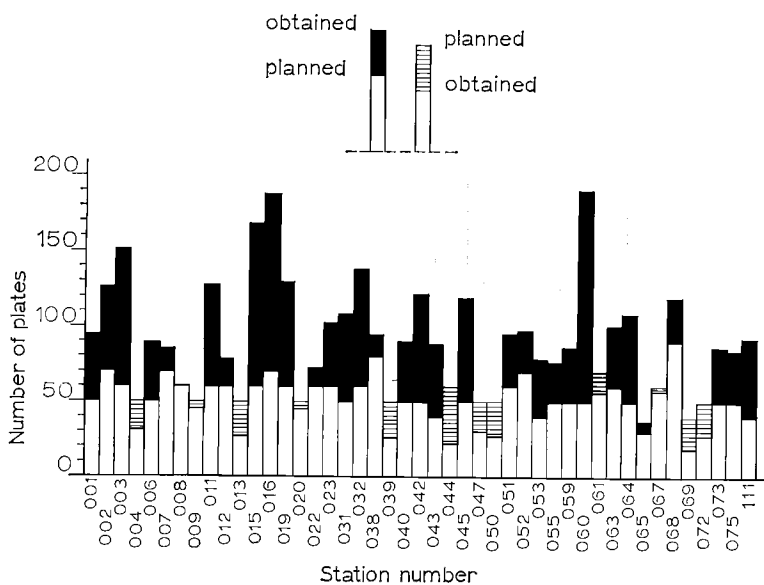


Fig. 8. Number of plates per station.

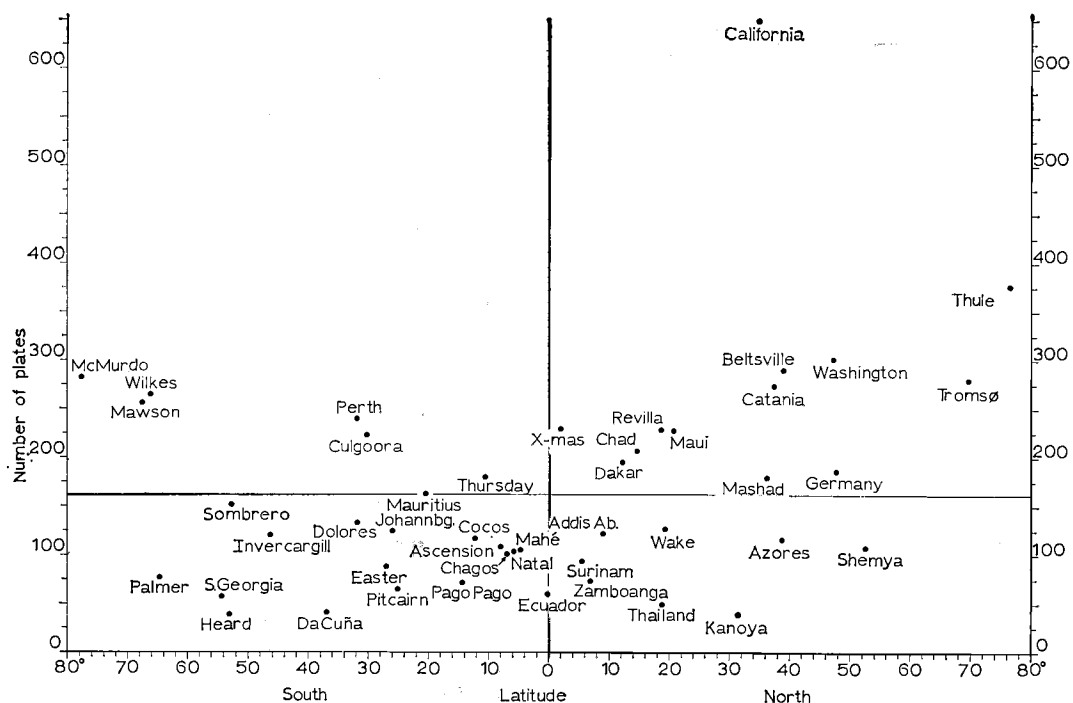


Fig. 9. Number of plates per station normalized with respect to period of 654 days.

WORLDWIDE SATELLITE TRIANGULATION

TABLE 2. Error Sources

(1) Type of Imagery	(2) Mean Errors of Comparator Measurements $m_i, \mu m$	(3) Assumed Mean of Irregular Emulsion Shift, μm	(4) Avg. of Mean Scintillation μm	(5) Mean Coordinate Error after Adjustment in Photogrammetric Bundle Simulation $[(2)^2 + (3)^2 + (4)^2]^{1/2}$ $m_i, \mu m$	(6) Introduced Mean Error of Reduced Star Catalog Data $m_i, \mu m$	(7) Total Noise in Photogrammetric Bundle Simulation Adjustment $[(2)^2 + (3)^2 + (6)^2]^{1/2}$ μm		(8) Mean Error of Polynomial Smoothing $[(2)^2 + (3)^2 + (4)^2]^{1/2}$ μm
						sec	sec	
Average values						± 0.40	± 3.42	± 1.57
<i>a</i> Stars	± 1.81	± 1.00	± 2.58	± 1.18	± 3.31	± 0.87	± 1.57	± 3.52
<i>b</i> Satellite	± 1.79	± 1.00	± 2.86	± 1.31				± 1.61
Minimal values								
<i>c</i> Stars	± 0.97	± 1.00	± 1.01	± 0.46	± 1.88	± 0.87	± 0.40	
<i>d</i> Satellite	± 0.87	± 1.00	± 1.07	± 0.47				
Maximal values								
<i>e</i> Stars	± 2.45	± 1.00	± 6.46	± 2.96	± 6.87	± 0.87	± 0.40	
<i>f</i> Satellite	± 2.68	± 1.00	± 6.84	± 3.14				

Photogrammetric cameras, Wild BC-4, lens, cosmotar, f , 450 mm; aperture, 132 mm.
 Targets, Pages balloon satellite for 496 photographs and Echo satellite for 4 photographs.

Program, world net.

Period of observation, October 1966 to September 1969.

Observation material, 500 selected photographs with corresponding time recordings from 35 stations in the world net.

HELLMUT H. SCHMID

39

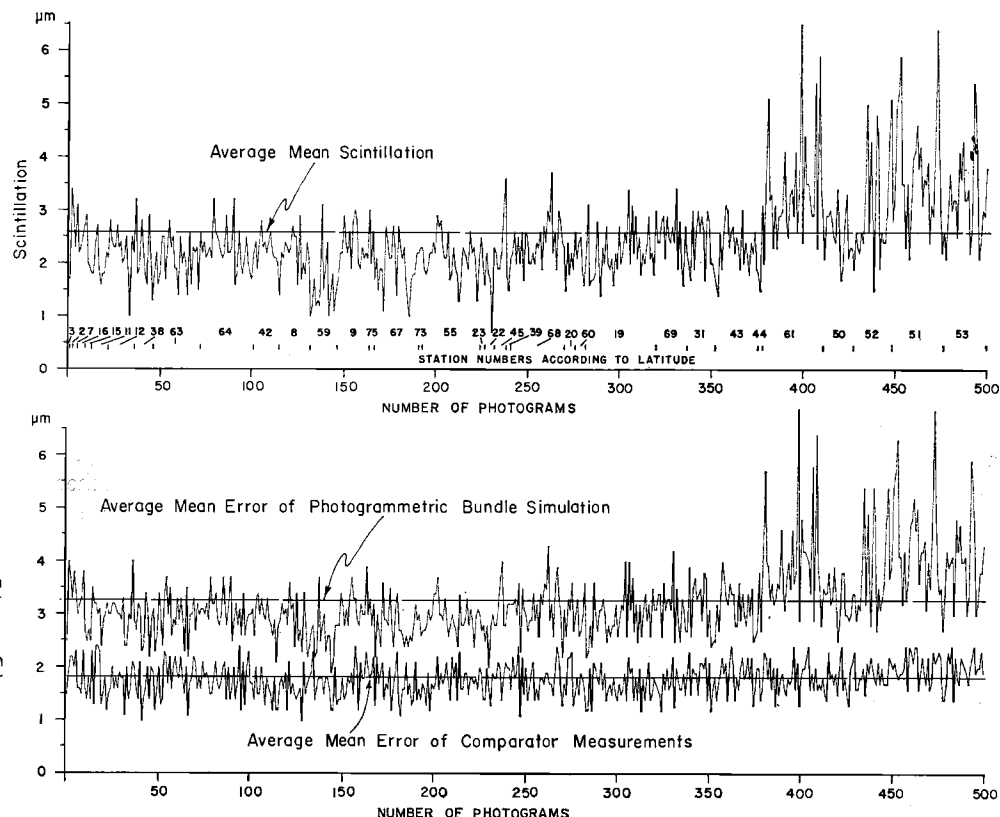


Fig. 10. Comparison of scintillation and errors in comparator measurements.

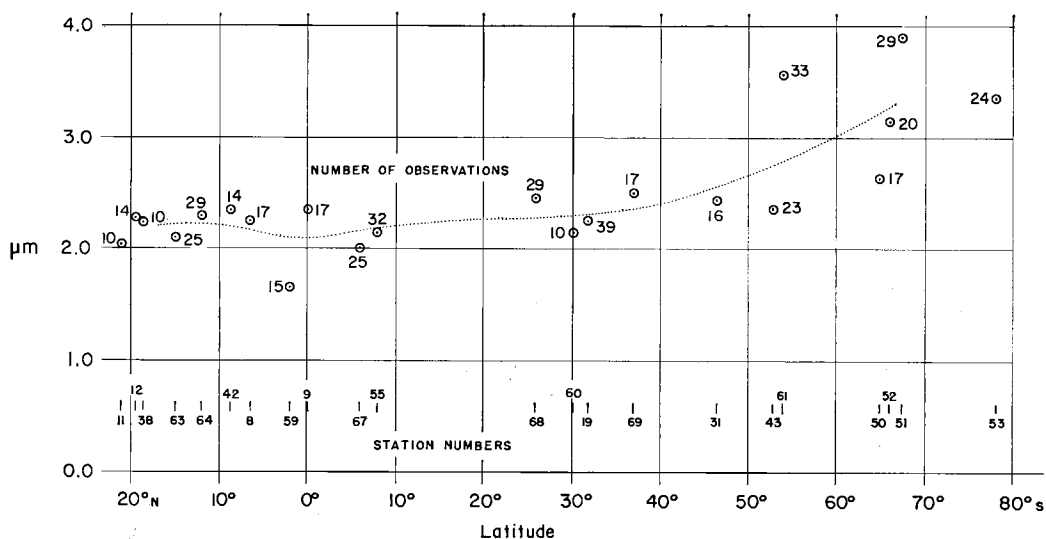


Fig. 11. Scintillation versus station latitude.

WORLDWIDE SATELLITE TRIANGULATION

TABLE 3.

Image Position on Plate, $x(\text{mm})/y(\text{mm})$	Mean Error of a Direction, sec of arc
0/0	± 0.23
10/10	± 0.25
20/20	± 0.23
30/30	± 0.19
40/40	± 0.21
50/50	± 0.25
60/60	± 0.44
70/70	± 2.77

The accuracy of $\pm 0.23''$ for the direction of a central ray ($x, y = 0$) agrees well with the $\pm 0.25''$ that was the expected value from general considerations. As with the information given in Table 2, column 8b, one also obtains for a single curve-fitted fictitious image at the center of the plate an accuracy of $\pm 0.25''$, using 300 images and independent smoothing polynomials of the sixth degree for the x and y coordinates.

The use of all seven directions that can be deduced from the sixth-degree polynomial fits contributes to an improvement of 32% over a single fictitious central direction. Because the uncertainties introduced from the bundle reconstruction and the curve-fitting computations are independent error sources, the final expected accuracy for a single fictitious direction in which all the information available on a specific photograph is combined can thus be computed to

$$68\% \text{ of } 0.25(2)^{1/2} = \pm 0.24''$$

The final triangulation algorithm is based on the justifiable assumption that the directions to the satellite obtained on a specific station are results uncorrelated to the other observing stations. Furthermore, previous studies have shown that the mean errors of the triangulated station coordinates in terms of latitude and longitude are proportional to the slant distance between observing station and satellite, and three times as large for the vertical component. This distance, in the world net, is about six

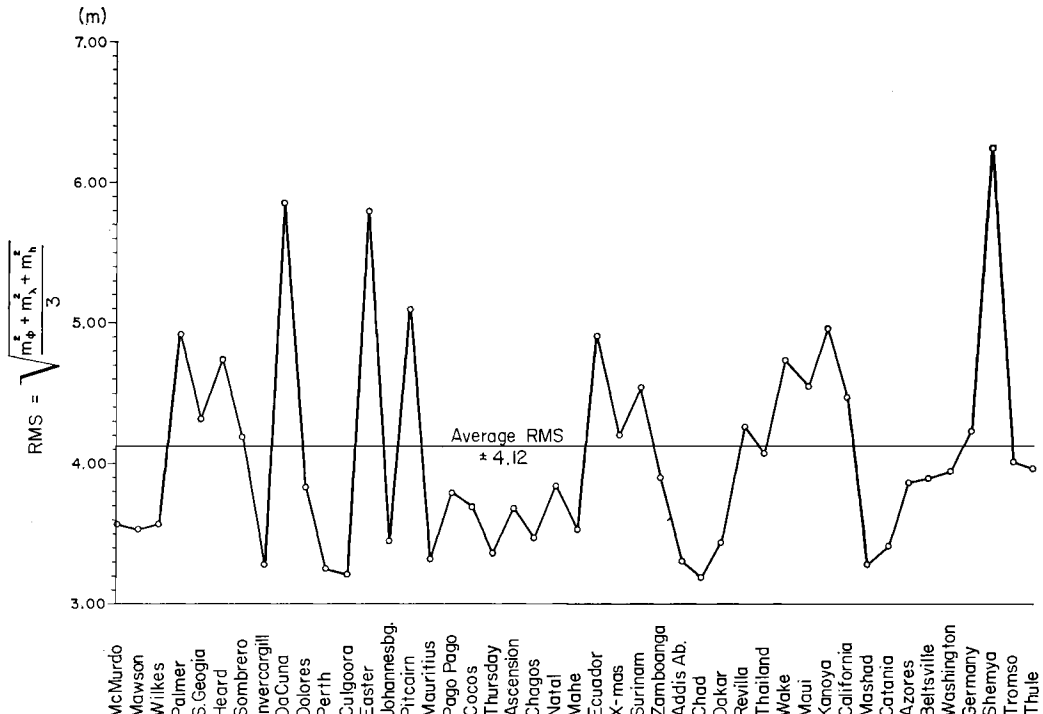


Fig. 12. Root-mean-square station errors.

HELLMUT H. SCHMID

41

million meters. Consequently, with an accuracy of $\pm 0.24''$ for a fictitious direction in which the total information available on a single plate has been combined, a mean error of ± 7.0 meters is obtained for the longitude and latitude components and ± 21 meters for the vertical component. With four base lines, each measured to about one part in a million, the latter error is reduced to ± 12.6 meters. Four such base lines have been measured, in Australia, the United States, Central Europe, and the middle of Africa. Because the presently selected observational material constitutes about five independent solutions, the expected accuracy of the triangulated station positions is obtained by dividing the previously obtained accuracy values, which refer to a unique solution, by $(5)^{1/2}$, leading to the following mean errors: in latitude and longitude, ± 3.1 meters, and, for the corresponding vertical component, ± 5.6 meters, or a rms error of

$$\left(\frac{m_\phi^2 + m_\lambda^2 + m_H^2}{3} \right)^{1/2} = \pm 4.1 \text{ meters}$$

In order to compare these expected values with the actual situation, all selected events were combined in an error study based on an adjustment algorithm. The rms errors for the station positions, as obtained from the corresponding variance-covariance matrix, are shown in Figure 12. The result was obtained by assuming $3/2$ for the ratio of the mean error of unit weight after adjustment to the mean error of unit weight before adjustment, a value which

has been marginally obtained from previous adjustments of completely reduced data.

The corresponding rms of ± 4.12 meters agrees completely with the expected rms error of ± 4.1 meters, indicating that a sufficient amount of information was collected during the observational program. A slight degradation from the theoretically expected accuracy must be expected owing to the lack of an even distribution of the observations. However, as the results show, this is counteracted by the increased strength of the triangulation due to the double and triple missions and the observation of skip lines. The increase of the mean error of unit weight after adjustment to at least $3/2$ times the mean error of unit weight before adjustment is due to unavoidable small systematic error sources that cannot be modeled.

The most obvious weakness in the solution affects the station Shemya, which influences also the stations in Japan and Wake. The remedy for this situation is on hand with the data of the current observations in the densification network in the North American continent. Shemya will then be tied with sufficient strength to the world network stations Thule and Moses Lake, and will, in turn, influence favorably the accuracy in the position of the stations in Japan and on Wake Island.

REFERENCE

Schmid, H. H., Application of photogrammetry to three-dimensional geodesy, *Eos Trans. AGU*, 50, 4, 1969.

Geometrical Adjustment with Simultaneous Laser and Photographic Observations on the European Datum

A. CAZENAVE, O. DARGNIES, G. BALMINO, AND M. LEFEBVRE

*Groupe de Recherches de Géodésie Spatiale
Bretigny, France*

Abstract. During the 1968 European geodetic observing program organized jointly by the Centre National d'Etudes Spatiales, France, and the Smithsonian Astrophysical Observatory, United States, a large number of simultaneous or quasi-simultaneous laser and optical observations were collected. Particular attention has been given to the interpolation necessary to make observations exactly simultaneous. More than 2000 independent relations have thus been obtained, linking 9 station positions. The resulting relative coordinates of these stations are compared with other determinations.

Observations of an artificial satellite against the star background and simultaneous laser range measurements make it possible to compute a geometric adjustment of the ground station network.

If, at a given time, a ground station measures one of the topocentric coordinates of a satellite (direction or distance), a relation between station and satellite coordinates can be obtained.

If several stations simultaneously measure n independent quantities, n being greater than 3, it is possible to eliminate the three coordinates of the satellite from the n relations so obtained. The remaining $n - 3$ relations linking the station coordinates are linearized in the vicinity of an a priori solution.

The set of equations is solved by a least squares procedure that may take into account several constraints, such as short and well-known vectors linking two collocated stations [Bivas, 1971; Balmino, 1969].

PROCESSING OF THE DATA

Raw observations are not used until suspicious data are eliminated through analysis of residuals in orbit computations overlapping each other. Range measurements are corrected for atmospheric refraction and calibration [Bivas, 1969]. Angular measurements giving equatorial coordinates of the satellite (deduced from the coordinates of the stars with respect to the mean

equinox of 1950.0) are corrected for parallactic refraction and annual aberration. Differential refraction is taken into account during plate reduction.

All epochs are referred to atomic time (AT) as maintained by the Bureau International de l'Heure (BIH).

COMPUTATION OF THE OBSERVATIONS RELATIONS

The angular observations are then transformed to direction cosines in a terrestrial reference system. This system is defined by the Z axis passing through the international convention origin, the x axis toward the conventional Greenwich meridian of BIH, and the y axis directly perpendicular to the zx plane.

Transformation from the inertial system to the terrestrial system is made by the following corrections [Balmino, 1969]:

Precession from 1950.0 to date of observation.

Nutation at date of observation.

Rotation of true sidereal time using UT1 values given by circular D of BIH.

Correction for polar motion as given by circular D of BIH.

Range measurements to the satellite at the exact time of optical observation are inter-

TABLE 1. Initial Coordinates, European Datum of 1950

No.	Station	Position		
		x, meters	y, meters	z, meters
Optical stations				
9004	San Fernando	5,105,680.1	-555,102.9	3,769,799.3
8015	Haute Provence	4,578,413.0	458,091	4,403,312.0
8019	Nice	4,579,554.2	586,729	4,386,535.6
9091	Dyonisos	4,595,251.6	203,957.3	3,912,795.0
9065	Delft	3,923,505.9	300,003.1	5,003,119.8
9066	Zimmerwald	4,331,390.6	567,637.4	4,633,235.9
9074	Riga	3,183,998.8	1,421,638.2	5,322,894.4
9077	Uzhgorod	3,907,494.2	1,602,533.2	4,764,034.8
9080	Malvern	3,920,250.8	-134,624.4	5,012,852.2
Laser stations				
7804	San Fernando	5,105,701.2	-555,125.7	3,769,768.3
7815	Haute Provence	4,578,457.2	458,075.2	4,403,270.0

polated through a pass-by-pass smoothing by using a simple orbit computation model.

A typical pass contains about 40 to 60 laser range observations, and this procedure is generally sufficient to reduce the residuals to noise level. The synthetic range measurement so obtained is weighted according to the amplitude of the noise, usually of the order of 1.5 meters. This process is conducted on a Control Data Corporation 250 (CDC) display unit connected to a CDC 6600 computer. All the optical observations are weighted according to an assumed accuracy of 2 arcsec.

RESULTS

Simultaneous observations of six satellites carrying laser retroreflectors (beacon B, beacon C, D1 C, D1 D, Geos 1, Geos 2) during the 1968 period have been obtained from 13 stations on the European datum.

Laser Stations

Haute Provence, France	7815
San Fernando, Spain	7804

Camera Stations

Haute Provence, France	8015
San Fernando, Spain	9004
Dyonisos, Greece	9091
Nice, France	8019
Uzhgorod, USSR	9077
Riga, Latvian SSR	9074
Delft, Netherlands	9065
Zimmerwald, Switzerland	9066
Malvern, United Kingdom	9080
Helsinki, Finland	9076
Meudon, France	8030

European datum coordinates of these stations are given in Table 1.

Several sets of observations have been re-

TABLE 2. Corrections to the European Datum Coordinates for Mediterranean Triangle

Stations		Corrections, meters				Scale Factor K
From	To	Δx	Δy	Δz	$\Delta \rho$	
<i>First Set of Observations (1400 linear independent relations)</i>						
9004	8015	8.3 ± 1.2	16 ± 1.5	9.4 ± 1.3	13.7 ± 1.0	10×10^{-6}
9004	9091	-3.0 ± 6.8	12 ± 5.3	15.4 ± 5.3	13.6 ± 4	5.1×10^{-6}
<i>Second Set of Observations (630 linear independent observations)</i>						
9004	8015	7.9 ± 3.2	14.6 ± 4.4	10.6 ± 4.4	13.3 ± 3.8	10×10^{-6}
9004	9091	-5.3 ± 4.6	20.6 ± 7.5	-8.7 ± 4.9	19.8 ± 4.8	7.5×10^{-6}

The Haute Provence-Nice vector has been kept fixed to the surveyed value.

CAZENAVE, DARGNIES, BALMINO, LEFEBVRE

45

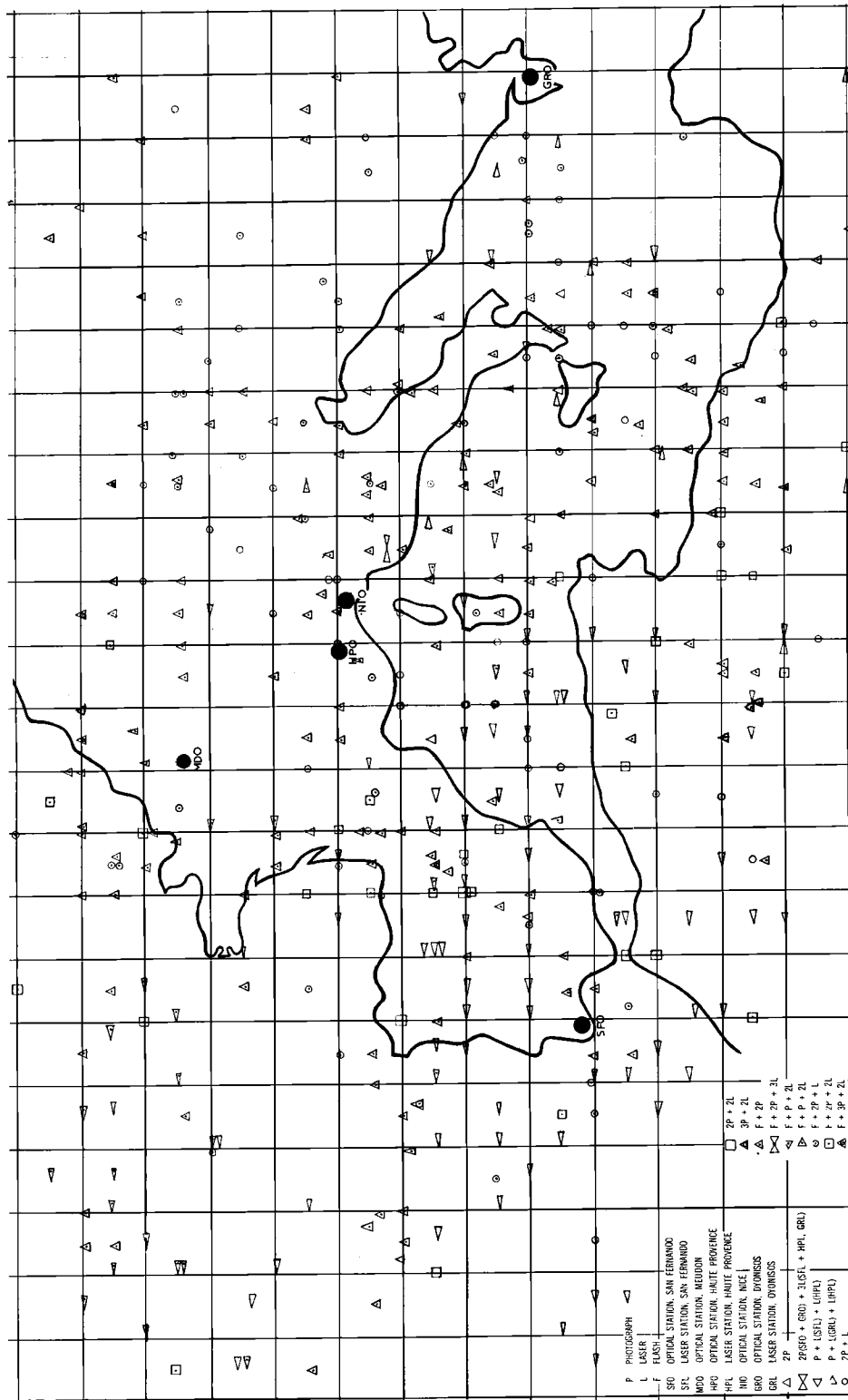


Fig. 1. Distribution of optical and laser observations during the RCP 133 campaign.

TABLE 3. Number of Simultaneous Observations Used in the 9-Site Adjustment
(An optical observation corresponds to one flash sequence of Geos 2.)

Stations	9004 7804	9091	8015 7815	8019	9065	9066	9074	9077	9080
9004		32	8	26	1	15	11	5	2
7804		3	18	9	3	11	0	3	2
9091			8	18	2	6	15	8	0
			12						
8015				20	6	14	11	4	4
7815				23	2	4	4	6	3
8019					7	22	21	6	6
9065						11	4	2	4
9066							12	7	3
9074								7	2
9077									0

duced. Two sets, involving only six stations in the Mediterranean area (Haute Provence, San Fernando, Nice, Dyonisos), lead to two solutions giving relative positions of these four sites. The distribution of observations is shown in Figure 1, and the results appear in Table 2. The results also show the associated confidence interval at the 2σ level.

A solution using observations from the 13 stations was attempted, but two stations had to be dropped, because the number of simultaneous observations was too small: they were Helsinki (9076) and Meudon (8030).

The final solution, involving more than 2000 independent linear relations, leads to the adjustment of the relative positions of the 11 remaining stations (9 sites). Table 3 shows the number of simultaneous observations used. This solution was made with observations of Geos 2 only.

The results, given in Table 4, show a very good consistency with the previous solutions in-

volving only four sites (Table 2). Table 5 gives the associated normalized covariance matrix.

CONCLUSION

The systematic difference in interstation distance gives an average scale factor difference of $+8 \times 10^{-6}$, which might be explained either by the propagation in the network of systematic bias in the laser range measurements or by a global shrinking of the European datum.

On the other hand, these results differ significantly from the results deduced from the global solution for geopotential and station coordinates obtained by the Smithsonian Astrophysical Observatory [Gaposchkin and Lambeck, 1971; Lambeck, 1971].

However, the solution presented here has been fully confirmed by the results derived at Goddard Space Flight Center using only optical observations in a dynamic solution [Marsh *et al.*, 1971]. The agreement for the chord length

TABLE 4. Corrections to the European Datum of 1950 Relative to San Fernando
(2030 linear independent equations.)

Stations		Corrections, meters				Scale Factor K
From	To	$\Delta x(2\sigma)$	$\Delta y(2\sigma)$	$\Delta z(2\sigma)$	$\Delta \rho(2\sigma)$	
9004	8015	7.7 ± 3	18.7 ± 3	13.3 ± 3	17.8 ± 2.5	13×10^{-6}
9004	8019	9.1 ± 3	14.6 ± 3	16.0 ± 3	15.5 ± 2	11×10^{-6}
9004	9091	5.8 ± 4	26.0 ± 5	-6.3 ± 4	25.0 ± 3	9×10^{-6}
9004	9065	-9.3 ± 5	15.3 ± 4	-9.3 ± 5	6.6 ± 2.5	3.5×10^{-6}
9004	9066	5.2 ± 3	14.0 ± 3	14.2 ± 3	15.0 ± 2	9.2×10^{-6}
9004	9074	-31.8 ± 5	-32.0 ± 4	46.0 ± 4	22.0 ± 3	6.9×10^{-6}
9004	9077	12.0 ± 5	27.0 ± 5	11.0 ± 5	21.0 ± 5	7.9×10^{-6}
9004	9080	25.0 ± 6	18.0 ± 5	36.0 ± 6	12.6 ± 2.5	7.1×10^{-6}

CAZENAVE, DARGNIES, BALMINO, LEFEBVRE

47

TABLE 5. Normalized Covariance Matrix for the 9-Site Adjustment

	Haute Provence 8015	Haute Provence 8015	Dyonisos 9091	Dyonisos 9091	Delft 9065	Riga 9074	Uzhgorod 9077	Malvern 9080
Haute Provence 8015	1	1	0,4	1	-0,1	1	-0,2	1
Dyonisos 9091	0,4	0,1	0,6	0,4	0,4	0,1	-0,2	1
Delft 9065	0,1	0,1	0,3	0,3	0,1	0,2	-0,1	1
Riga 9074	0,4	-0,1	-0,1	0,4	-0,2	0,1	1	
Uzhgorod 9077	0,4	-0,1	0,3	-0,5	0,4	0,1	-0,2	
Malvern 9080	0,1	0,1	0,5	0,1	0,2	0,3	0,2	1

TABLE 6. Interstation Difference Comparison to 9004 (San Fernando)
 [Goddard Space Flight Center (GSFC) to Groupe de Recherches de Géodésie Spatiale (GRGS)
 and Smithsonian Astrophysical Observatory (SAO) to GRGS.]

Station	Number	GSFC-GRGS		SAO-GRGS	
		meters	ppm	meters	ppm
Haute Provence	8015	-1.9	1.5	-20.9	16.5
Nice	8019	-1.9	1.4	-18.9	14.0
Dyonisos	9091	-14.0	5.3	-52.0	19.7
Delft	8009	+2.8	1.5	-28.6	15.3
Riga	9074	-12.7	4.0	-54.3	17.2
Zimmerwald	8010	-1.1	0.7	-23.9	15.2
Uzhgorod	9077	-3.1	1.2	-43.0	16.6
Malvern	9080	-2.5	1.4	-31.5	17.6

from San Fernando to other European stations is spectacular, with the exceptions of Greece and Riga, probably because of the small number of observations (Table 6).

This agreement most probably settles the problem of the scale of the European datum, as explained by *Marsh et al.* [1971], and provides an excellent check on the accuracy of the satellite laser ranging systems of the Groupe de Recherches de Géodésie Spatiale.

Acknowledgment. We wish to express our gratitude to the staff of the Smithsonian Astrophysical Observatory whose cooperation has permitted the CNES-SAO 1968 observation campaign to provide most of the optical data. We also wish to thank the Goddard Space Flight Center for monitoring the flashes of the Geos 2 satellite; their observations make up the better part of this analysis. Special thanks must go to all European independent stations whose valuable data have been provided to us through the Smithsonian Astrophysical Observatory. Operations of the two French laser stations and the Nice, Haute Provence, and Meudon cameras were conducted through a cooperative program, 'Recherche coopérative sur programmes 133,' under the responsibility of the Ingénieur Général

Géographe J. J. Levallois (IGN) and the scientific management of Dr. F. Barlier (Meudon Observatory). This program was supported by the Centre National de la Recherche Scientifique, the Direction des Recherches et Moyens d'Essais of the Defence Ministry, and the Centre National d'Etudes Spatiales.

REFERENCES

- Bivas, M., Méthode générale de Géodésie géométrique, *Bull. 3*, Groupe de Rech. de Géod. Spatiale, Bretigny, France, 1971.
 Balmino, G., Synthèse des premiers résultats des campagnes Diadème et RCP 133, third cycle thesis, Paris Sci. Faculty, October 3, 1969.
 Bivas, R., La télémétrie spatiale par laser: Applications géodésiques, doctoral thesis, Paris Sci. Faculty, July 9, 1969.
 Gaposchkin, E. M., and K. Lambeck, Earth's gravity field to the sixteenth degree and station coordinates from satellite and terrestrial data, *J. Geophys. Res.*, 76, 4855-4883, 1971.
 Lambeck, K., The relation of some geodetic datums to a global geocentric reference system, *Bull. Geod.*, 99, 37-53, 1971.
 Marsh, J. G., B. C. Douglas, and S. M. Klosko, A unified set of tracking station coordinates derived from geodetic satellite tracking data, *Doc. X-553-71-370*, Goddard Space Flight Center, Greenbelt, Md., July 1971.

Preliminary Results of the Secor Equatorial Network

ERICH H. RUTSCHEIDT

U.S. Army Topographic Command, Washington, D.C. 20315

Abstract. The completion of observations on the Secor equatorial network in March 1970 marked the end of one phase of the satellite geodesy program at the U.S. Army Topographic Command. This paper presents a brief history of the program, an outline of the computational procedures, and a summary and evaluation of some results of preliminary adjustments. Future plans are discussed, and specifications for a final adjustment are considered.

Field operations of the U.S. Army Secor program came to a close in March 1970 with completion of the Secor equatorial network. The objectives of the program had been to connect isolated datums and tie them into a unified world geodetic system to create basic geodetic control frameworks and to improve estimates of the earth's geodetic parameters. As a pure ranging system, Secor also offered a possible means to provide scale lines for the Pageos BC 4 network. At the present time, all Secor data have been processed and some preliminary adjustments have been completed. The results to date have been promising, but further adjustments, analysis, and evaluation must be undertaken before a final accuracy evaluation can be made.

A Secor distance-measuring station determines the range to a suitable transponder-carrying satellite by measurement of the phase shift undergone by the modulation on an electromagnetic wave in its round trip between station and satellite. Four modulation frequencies are employed, the highest frequency (shortest wavelength) yielding resolution, the lower frequencies, nonambiguity of measurement. The ground stations interrogate the transponder in sequence, but, through dynamic smoothing of the ranges without time lag, simultaneous ranges are obtained, in effect, between the stations. Because an electromagnetic wave is refracted in its passage through the ionosphere, Secor ranges are also measured on a second carrier, one-half the frequency of the first. The difference in range measured on the two frequencies reveals the

magnitude of the refraction and allows a correction to be made to the high-frequency range. The principles of Secor geodetic operations and technical details of the equipment are fully described by the *Cubic Corporation* [1964].

It is not necessary, of course, that solutions be restricted to four-station, simultaneous observations. Observations from even a single station of known position can be used to compute the orbit of a satellite. This orbit can then be used with others in a solution for an unknown site. In practice, however, it has been required that at least part of each track contain four-station, simultaneous observations before it can be included in the final Secor network solutions.

HISTORY

In April 1960, the Army Map Service, now the U.S. Army Topographic Command, contracted to purchase four prototype Secor stations from Cubic Corporation, San Diego, California. Experience with this equipment in satellite tracking had led the contractor to propose it as a geodetic system of potential high accuracy. On the strength of successful tests of the prototype stations and an aircraft-borne transponder, two additional Secor stations were purchased in June 1961. Tests conducted in the fall of 1961, however, raised questions as to the soundness of the concept. In order to resolve these questions, the Office of the Chief of Engineers directed the re-evaluation of the system by a team of scientists and engineers from the National Bureau of Standards, the Ballistic Research Laboratories, and the U.S. Army

Geodesy, Intelligence and Mapping Research Agency, now the Engineer Topographic Laboratory. This team confirmed the validity of the system concept, but recommended modifications of equipment to improve reliability and accuracy. The research and development phase of the program was subsequently assigned to the Geodesy, Intelligence and Mapping Research Agency, and, under their direction, the recommended modifications were completed.

Upon completion of tests in the southwestern part of the United States using previously established triangulation stations, six ruggedized Secor stations were shipped to Japan to begin the Secor Pacific network. The first successful operational track was not obtained until October 1964. After this the network progressed slowly, quad by quad, until its termination at Hawaii in December 1966. The network served to connect the Tokyo, Australian, and North American datums, in addition to the independent datums of the many Pacific Islands it spanned.

In the early stages of the Pacific network, stations were not moved from a site until sufficient tracks had been proven satisfactory by an actual solution. Even with six stations, four tracking and two leapfrogging ahead, delays were common. Because of the very high rate of ambiguous data, a first solution for an unknown station was sometimes exceedingly difficult to achieve. Neither long-arc fitting and prediction techniques nor short-arc self-calibration methods proved as effective as the trial and error methods of ambiguity detection that were used to grind out the site-by-site solutions. With increased experience and confidence in the equipment, however, a completed solution no longer became the criterion for station movement, and progress became more rapid. After completion of the Secor Pacific network, a preliminary adjustment was made, but final adjustment was deferred until after observation and adjustment of the Secor equatorial network.

The Secor equatorial network was designed to mesh with the Secor Pacific network with no unnecessary station movements or interruption of field operations. In its original configuration, it began at the line Maui-Midway of the Pacific net, tied to the United States through Alaska and Canada, and then extended eastward to encircle the earth and close upon itself at its

SECOR EQUATORIAL NETWORK

origin, Maui-Midway. Because of the deterioration of EGRS 7, the only high-altitude satellite in service at that time, the data collected for the tie between Hawaii and the United States were of very poor quality. After the launch of a second high-altitude satellite, EGRS 9, in June 1967, the situation was greatly improved. This fine satellite, along with new procedures that greatly improved calibration accuracy and eliminated ambiguities as a problem in range determination, provided excellent data as the network progressed eastward from the United States. For this reason, it was decided to treat the original Hawaii-United States tie as a separate project and to reobserve a second tie to close the network back to the United States. Unfortunately, severe budget cuts forced a curtailment of operations, and only a single point tie was made, at Larson AFB. Failure to close the network on at least one station of the origin precluded obtaining a completely independent Secor adjustment of the network. The North American datum tie between Larson and the origin did provide positional closure for an independent Secor adjustment of the rest of the network, but this is weakened by the lack of azimuth closure. This is not critical in a Secor solution with external constraints, since there is an abundance of BC 4 lines common to the Secor network to provide directional control; for analysis, evaluation, and comparison, however, a completely independent Secor solution of a strong network would have been desirable.

Concurrently with Secor network operations, a number of special projects were undertaken. Between November 1965 and May 1966, four Secor stations participated with other satellite systems in an intercomparison test made with the Geos 1 satellite from sites of the National Ocean Survey precise geodimeter traverse in the United States. The difference between the Secor results and the precise survey of about 6 meters total error again demonstrated the geodetic capability of Secor [Dudley and Warren, 1968].

In the spring of 1968, a single Secor station participated in a collocation experiment at Wallops Island, Virginia. Several systems simultaneously tracked the Geos 2 satellite. The standard deviation of the Secor range residuals from short-arc orbital solutions was about 2 meters, but, in comparison with laser measurements, the



Fig. 1. Present equipment at the station 31490 near the 40°40'N. latitude boundary.

frequency ranging data were lacking, it was not used to correct any ranging data in the final solutions. Only ranges that could be corrected through their dual-frequency measurements were used.

Preliminary solutions were computed quad by quad in step with the observations. Three stations were fixed, and the position of the fourth, unknown station was computed. It then became one of the fixed stations in the solution for the next unknown station. Purely geometric solutions were computed first. Their chief purpose was to clean up the data and obtain approxi-

SECOR EQUATORIAL NETWORK

mate orbital parameters for the pass observed. A second solution using a batch least-squares adjustment of orbital parameters and site coordinates [Cubic Corporation, 1966] was next made in order to incorporate nonsimultaneous ranges that could not be used in the geometric solutions. As each single quadrilateral was completed, its data, on punched cards, were stored for later network adjustments by the same orbital constraint program.

The last single quadrilateral gave the position of Larson computed through a Secor network of about 40,000 km. A comparison to the North

TABLE 1. Geocentric Coordinates (in Meters) for the SAO 1969 Standard Earth According to Secor Solution 1

Station	X	Y	Z	σ_x	σ_y	σ_z
Herndon	1088864	-4842932	3991850	0	0	0
Worthington	-449400	-4600882	4380302	0	0	0
Ft. Stewart	794694	-5360045	3353094	0	0	0
Austin	-744080	-5465222	3192484	0	0	0
Larson	-2127793	-3785908	4656006	0	0	0
Bermuda	2307997	-4873769	3394465	2	2	2
Puerto Rico	2349438	-5576031	2010358	9	8	4
Panama	1142641	-6196125	988353	3	3	1
Paramaribo	3623278	-5214219	601672	5	5	3
Azores 1	4433655	-2268157	3971621	5	3	5
Azores 2	4433647	-2268190	3971611	5	3	5
Dakar	5884476	-1853615	1612710	7	6	6
Natal	5186345	-3654278	-653047	8	7	5
Ascension	6118349	-1571831	-878611	10	9	7
Ft. Lamy	6023446	1617906	1331554	12	7	10
Catania	4896478	1316127	3856529	10	5	10
Cyprus	4363385	2862262	3655265	12	5	12
Rota	5093581	-565322	3784199	7	5	8
Roberts Field	6237374	-1140291	687680	9	7	7
Addis Ababa	4900805	3968221	966229	15	7	12
Mashhad	2604481	4444149	3750224	15	7	14
Chagos	1905200	6032244	-810830	20	11	16
Chiang Mai	-941612	5967468	2039231	18	10	19
Singapore	-1542465	6186950	151746	19	12	19
Zamboanga	-3361860	5365854	764562	18	13	20
Darwin	-4071509	4714245	-1366577	20	16	20
Manus	-5367605	3437892	-225438	18	16	20
Guam	-5059746	3591230	1472737	16	15	21
Wake	-5858514	1394529	2093860	13	15	20
Palau	-4433383	4512958	809916	17	14	21
Guadalcanal	-5915064	2146877	-1037908	19	18	19
Pago Pago	-6100010	-997357	-1568538	20	19	16
Christmas	-5885377	-2448366	221712	15	16	14
Maui	-5467760	-2381209	2254064	8	13	13
Midway	-5618703	-258179	2997263	9	14	17
Shemya	-3851714	396472	5051328	11	11	15

ERICH H. RUTSCHEIDT

53

TABLE 2. BC 4 Directional Constraints

Line	Azimuth	Elevation	σ_{Az} , meters	σ_{El} , meters
Paramaribo to Dakar	73.1106492°	-19.1093582°	10.0	10.5
Paramaribo to Ascension	107.7940767	-21.4233196	9.5	11.5
Dakar to Ascension	172.1032986	-11.4578938	7.1	7.4
Dakar to Ft. Lamy	90.6856834	-15.8506109	5.1	7.4
Dakar to Catania	45.7907963	-18.3450641	6.0	8.4
Ascension to Ft. Lamy	56.0231914	-17.7514769	7.2	10.2
Ascension to Addis Ababa	73.7838065	-27.8759284	16.5	16.8
Ft. Lamy to Catania	0.0184426	-12.6685325	4.9	7.1
Ft. Lamy to Addis Ababa	95.7396910	-11.8636358	13.1	10.8
Ft. Lamy to Mashhad	51.2301123	-23.3583542	6.5	11.5
Catania to Addis Ababa	136.6906761	-17.9259063	12.4	11.0
Catania to Mashhad	78.0127342	-17.6680093	5.0	8.8
Addis Ababa to Mashhad	31.3606786	-16.6560880	10.9	13.4
Wake to Pago Pago	144.5884786	-20.1769627	7.9	14.7
Wake to Christmas	111.5876951	-19.5975645	8.5	14.5
Wake to Shemya	8.2010889	-16.9795117	11.9	20.0
Christmas to Pago Pago	218.6774905	-10.4963164	4.7	8.5
Larson to Wake	272.2799552	-32.6026420	13.0	16.7
Larson to Shemya	303.1911246	-20.8179809	19.2	18.1

American datum (NAD) position of Larson shows, Secor - NAD: $\Delta\phi = 289$ meters, $\Delta\lambda = 784$ meters, $\Delta H = 173$ meters.

NETWORK ADJUSTMENTS

As the Secor networks were being observed, simulated and real data were being adjusted. The purpose of these investigations was to evaluate the effects of error models and external constraints on the adjustments. Attempts to reduce the position closures of the Secor equatorial network by modeling the residual biases in the Secor observations produced the opposite effect [Carlson, 1971]. The experiments with simulated data [Leroy, 1969] and with real data indicated that the position error increased systematically from the tightly constrained North American datum survey positions in the United States. The early experiments with network adjustments indicated that the position errors were reduced by the introduction of position or azimuth-elevation direction constraints or both at intervals along the Secor network.

Since the preliminary solutions indicated that the Secor equatorial network required external survey data for controlling the propagation of error, it was decided to make use of the following data:

1. North American datum positions for the five Secor stations in the United States com-

puted from conventional ties with the first-order triangulations net.

2. Ballistic camera (BC 4) azimuth and elevation angles computed between Secor stations that are collocated with BC 4 stations.

In order to make eventual use of the SAO 1969 standard earth [Gaposchkin and Lambeck, 1970] height constraints, the geocentric coordinates (X , Y , Z) of North American datum stations were translated to the SAO 1969 datum. The translation parameters were derived from 12 stations common to SAO 1969 and the North American datum. The translation parameters are, SAO 1969 - NAD: $X = -24 \pm 7$ meters, $Y = 154 \pm 8$ meters, $Z = 182 \pm 7$ meters. The shift to SAO 1969 put the Secor equatorial network on an earth-fitting ellipsoid ($a = 6378155$, $1/f = 298.25$).

The first simultaneous adjustment of the entire Secor equatorial network was carried out in the short-arc orbital mode. In this adjustment, the SAO 1969 positions of the five tracking stations in the United States were held fixed, a standard deviation σ of 1000 meters in latitude, longitude, and height were assigned to the remaining stations, and an a priori estimate of 5 meters standard deviation was assigned to each of the Secor observations. No other constraints were added to the adjustment. No attempt was made to estimate residual

SECOR EQUATORIAL NETWORK

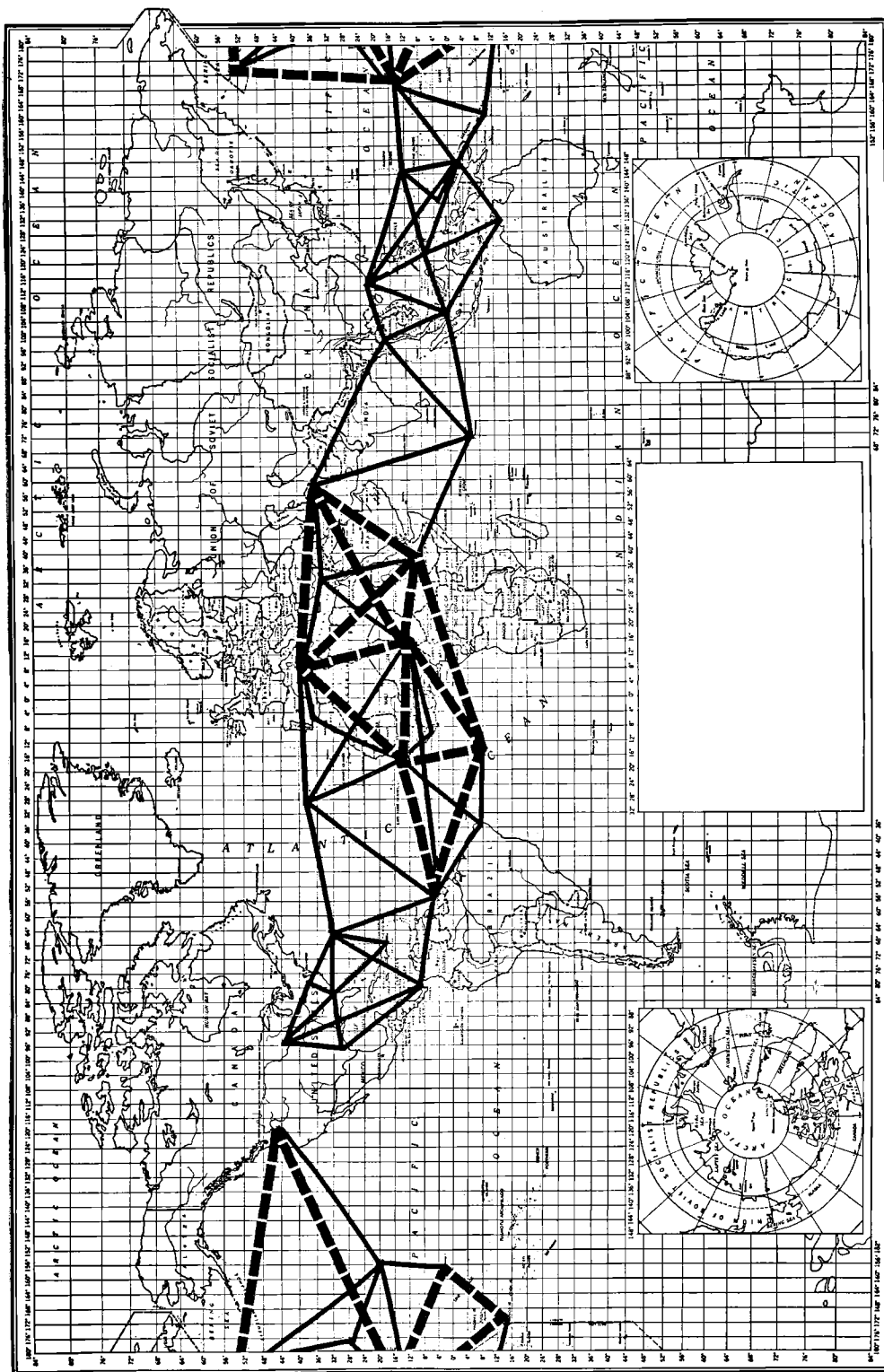


Fig. 2. BC 4 azimuthal constraints.

ERICH H. RUTSCHEIDT

55

TABLE 3. Geocentric Coordinates (in Meters) for the SAO 1969 Standard Earth According to Secor Solution 2

Station	X	Y	Z	σ_x	σ_y	σ_z
Herndon	1088864	-4842932	3991850	0	0	0
Worthington	-449400	-4600882	4380402	0	0	0
Ft. Stewart	794694	-5360045	3353094	0	0	0
Austin	-744080	-5465222	3192484	0	0	0
Larson	-2127793	-3785908	4656006	0	0	0
Bermuda	2308000	-4873758	3394476	2	2	2
Puerto Rico	2349441	-5576011	2010367	9	7	4
Panama	1142646	-6196109	988355	3	2	1
Paramaribo	3623285	-5214189	601685	4	4	2
Azores 1	4433652	-2268147	3971658	4	3	4
Azores 2	4433644	-2268180	3971648	4	3	4
Dakar	5884475	-1853585	1612753	4	4	5
Natal	5186350	-3654231	-653018	5	5	3
Ascension	6118350	-1571780	-878563	6	6	5
Ft. Lamy	6023432	1617933	1331625	6	5	6
Catania	4896460	1316124	3856596	5	5	6
Cyprus	4363357	2862253	3655338	5	5	7
Rota	5093574	-565320	3784252	4	4	5
Roberts Field	6297372	-1140252	687730	5	5	5
Addis Ababa	4900777	3968242	966311	6	5	7
Mashhad	2604437	4444124	3750294	6	5	7
Chagos	1905169	6032270	-810752	8	7	7
Chiang Mai	-941662	5967444	2039289	7	6	8
Singapore	-1542501	6186946	151802	7	7	8
Zamboanga	-3361895	5365831	763596	7	8	8
Darwin	-4071519	4714241	-1366555	8	10	7
Manus	-5367613	3437865	-225435	7	9	7
Guam	-5059774	3591188	1472743	6	8	7
Wake	-5858533	1394476	2093845	5	8	7
Palau	-4433412	4512927	809935	6	8	8
Guadalcanal	-5915050	2146852	-1037917	7	10	7
Pago Pago	-6099954	-997378	-1568565	8	11	7
Christmas	-5885337	-2448401	221676	6	10	8
Maui	-5467750	-2381252	2254032	4	8	7
Midway	-5618722	-258232	2997242	4	8	7
Shemya	-3851767	396427	5051337	5	7	7

biases in the adjustment. In all, 594 orbits encompassing 48,500 ranges were included in the adjustment. The fixed positions introduced the orientation and scale of the first-order triangulation system of the North American datum.

Positional data from the adjustment, Secor solution 1, are given in geocentric coordinates in Table 1. The rms of the range residuals is 2.65 meters. The estimated standard deviation for each adjusted tracking station position is also listed in Table 1.

Since only the geometry of the Secor equa-

tional network is determined by the intersection of measured ranges from the tracking stations to the orbiting satellite, the origin and the orientation of the configuration of the network must be determined from external survey data. The minimum constraints necessary are: one position that is latitude, longitude, and height; one azimuth-elevation direction from the fixed station to a second station in the network; and one elevation direction from the fixed point to a third station in the network. The minimum constraints for the network, however, need to be increased because of the lack of observation

TABLE 4. Geocentric Coordinate Comparison (in Meters), Solution 2 Minus Solution 1

Station	ΔX	ΔY	ΔZ
Herndon	Fixed	Fixed	Fixed
Worthington	Fixed	Fixed	Fixed
Ft. Stewart	Fixed	Fixed	Fixed
Austin	Fixed	Fixed	Fixed
Larson	Fixed	Fixed	Fixed
Bermuda	3	11	11
Puerto Rico	3	20	9
Panama	5	16	2
Paramaribo	7	30	13
Azores 1	-3	10	37
Azores 2	-3	10	37
Dakar	-1	30	43
Natal	5	47	29
Ascension	1	51	48
Ft. Lamy	-14	27	71
Catania	-18	-3	67
Cyprus	-28	-9	73
Rota	-7	2	53
Roberts Field	-2	39	50
Addis Ababa	-28	21	82
Mashhad	-44	-25	70
Chagos	-31	26	78
Chiang Mai	-50	-24	58
Singapore	-36	-4	56
Zamboanga	-35	-23	34
Darwin	-10	-4	22
Manus	-8	-27	3
Guam	-28	-42	7
Wake	-19	-53	-15
Palau	29	-31	19
Guadalcanal	14	-25	-9
Pago Pago	56	-21	-27
Christmas	40	-35	-36
Maui	10	-43	-32
Midway	-19	-53	-21
Shemya	-53	-45	9

data between Larson and Worthington. The orientation of the network in solution 1 is furnished by only four of the five survey stations in the United States. That is, Larson affects the solution only as a fixed point. By merely adjusting the network by holding fixed the five survey stations, some of the orientation error is removed, but the propagation of residual biases and random error in the observations will increase toward the middle of the network. This accumulation of error has been reduced in Secor solution 2 by adding directional constraints at intervals in the network.

SECOR EQUATORIAL NETWORK

The additional directional constraints (Table 2) in solution 2 were derived from the preliminary BC 4 special solution 1. The geocentric coordinates of the BC 4 stations collocated with the Secor stations were translated to SAO 1969 datum and then shifted further by the collocation data computed by taking the difference between the local survey coordinates of the BC 4 and Secor stations. The azimuth-elevation direction of the chords (Figure 2) between the 'BC 4 positions' of the collocated Secor stations were computed by well-known equations [Leroy and Googe, 1967]. The standard deviations for those 19 directions (Table 2) were derived from the standard deviations listed in the BC 4 special solution 1.

In order to evaluate the effects of the BC 4 directional constraints, no other constraints were added to the five position constraints in solution 1. The results of solution 2 are shown in Table 3. The rms of the range residuals changed by only 1 cm. The standard deviations of the position were reduced by factors of 2 or 3 in the African and Pacific areas of the Secor equatorial network, where the BC 4 directional constraints were introduced. The two facts indicate a weakness in the geometry of the network rather than significant errors in the observations. These facts suggest further investigations into the distribution of the observed data throughout the network. Initial investigations have indicated a gap in the observations between Larson and Worthington and a probable deficient number of observations in the Austin, Ft. Stewart, and Puerto Rico area.

A comparison of the geocentric coordinates of the two solutions is shown in Table 4. A study of Tables 1, 3, and 4 will show that the coordinate differences (ΔX , ΔY , ΔZ) are greater than the standard deviation of the position. For the stations in the middle of the network (Near East and Africa), the differences are greater than 3σ for the Z coordinate. Secor sites, in order of increasing longitude, reveal a systematic change in latitude differences ($\Delta\phi$). This is clearly shown in Figure 3, a plot of $\Delta\phi$ versus longitude. Note that the maximum and minimum $\Delta\phi$ fall in the African and Pacific areas of the network, where BC 4 directional constraints were imposed on solution 2.

One explanation for the graph is that, in solution 1, the effects of unmodeled residual

ERICH H. RUTSCHEIDT

57

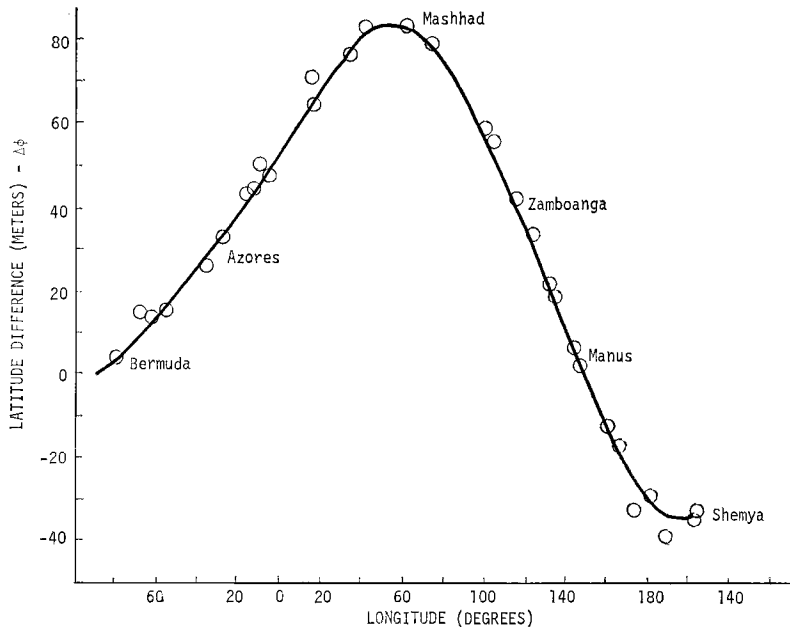


Fig. 3. Latitude comparison, solution 2 minus solution 1.

biases and random errors in the Secor observations accumulate toward the middle of the network. Therefore, the largest position errors would occur at the African-Near East tracking stations. In solution 2, BC 4 directional constraints were introduced into the African and Pacific parts of the network. A comparison of the two solutions is expected to show larger position differences at the African and Near East stations than at the Pacific stations.

The distance and azimuth of a number of individual lines distributed through the network were computed for solutions 1 and 2, respectively. The comparison of these lines is shown in Table 5. Changes in scale from imposing azimuth constraints average about 2.2 ppm. The only large anomaly, 7.5 ppm, occurs at the Shemya-Larson line. This suggests a weakness in the geometry connecting Shemya with Larson and the Pacific part of the network. The changes in azimuth are expected.

The directions of the BC 4 lines constrained in solution 2 are shown after adjustment in Table 6. The difference in meters at the ends of the lines between adjusted Secor directions and the input BC 4 directions are also shown. Examination of standard deviations in Table 2 reveals that, in many cases, they are exceeded

by the differences. This may be due, in part, to the five survey position constraints in the network and, in part, to an imbalance in the weighting of Secor ranges and BC 4 directions.

FUTURE PLANS

An immediate task is to carry out a stability analysis of the Secor equatorial network. The first step is to obtain a minimum constraint solution. In each subsequent adjustment, combinations of constraints will be added, and the results of adjustment will be compared to the

TABLE 5. Secor Line Comparisons, Solution 2 Minus Solution 1

Line	ΔDist, meters	ΔDist/Dist ($\times 10^6$)	ΔAz
Ft. Stewart to Bermuda	6	3.7	-1.87''
Bermuda to Paramaribo	3	1.0	-1.00
Bermuda to Azores	-4	1.2	-1.41
Azores 1 to Dakar	-6	2.1	-1.56
Dakar to Ft. Lamy	-9	2.5	-2.00
Catania to Ft. Lamy	-7	2.5	-2.09
Ft. Lamy to Addis Ababa	-4	1.5	-1.39
Mashhad to Chiang Mai	9	2.1	-0.04
Guam to Wake	1	0.4	2.03
Wake to Guadalcanal	4	1.2	2.63
Wake to Maui	-7	1.8	1.14
Wake to Shemya	-13	3.4	1.09
Shemya to Larson	-35	7.5	0.36

SECOR EQUATORIAL NETWORK

TABLE 6. Secor Directions of BC 4 Lines

Line	Azimuth	Elevation	ΔAz , meters	ΔEl , meters
Paramaribo to Dakar	73.1106154°	-19.1096529°	2	21
Paramaribo to Ascension	107.7940465	-21.4233743	2	4
Dakar to Ascension	172.1034044	-11.4578986	5	0
Dakar to Ft. Lamy	90.6860712	-15.8506396	24	2
Dakar to Catania	45.7909139	-18.3450359	8	2
Ascension to Ft. Lamy	56.0238076	-17.7514229	42	3
Ascension to Addis Ababa	73.7843163	-27.8758591	53	7
Ft. Lamy to Catania	0.0183724	-12.6686391	3	5
Ft. Lamy to Addis Ababa	95.7399791	-11.8633613	13	12
Ft. Lamy to Mashhad	51.2302230	-23.3581877	10	15
Catania to Addis Ababa	136.6908668	-17.9258787	13	2
Catania to Mashhad	78.0130535	-17.6676625	22	23
Addis Ababa to Mashhad	31.3606804	-16.6560456	0	3
Wake to Pago Pago	144.5880283	-20.1769115	34	4
Wake to Christmas	111.5875912	-19.5976872	8	9
Wake to Shemya	8.2005343	-16.9792049	36	20
Christmas to Pago Pago	218.6772945	-10.4955314	8	32
Larson to Wake	272.2799328	-32.6025941	3	6
Larson to Shemya	303.1909372	-20.8180421	15	6

minimum constraint solution. In this method of analysis, a system is stable if additional constraints have small effects on the minimum constraint solution. On the basis of this information, the best combination of constraints can be selected for the final adjustment of the network.

Combined Secor, BC 4, and Doppler solutions are now being investigated by means of their normal equations. A stability analysis of each of these networks will help decide the relative weights given to each system in the combined solution. Theoretically, a combined adjustment of the networks should lead to a solution in which each system contributes its greatest strength.

REFERENCES

- Berbert, J. H., and H. C. Parker, Comparison of C-band Secor and Tranet with a collocated laser on ten tracks of Geos 2, *Tech. Rep. X514-68-458*, 59 pp., Goddard Space Flight Center, Greenbelt, Md., 1968.
- Carlson, A. E., Error propagation in part of the Secor equatorial net, *Geod. Memo. 1656*, 22 pp., U.S. Army Topographic Command, Washington, D.C., 1971.
- Cubic Corp., San Diego, Calif., Orbital constraint network adjustments for geodetic solutions, final technical report, contract DA-49-018-ENG-3094, 140 pp., 1966.
- Cubic Corp., San Diego, Calif., Ruggedized geodetic Secor, final technical report, contract DA-49-018-ENG-2390, vol. 1 (300 pp.) and vol. 2 (200 pp.), 1964.
- Dudley, G. H., and M. A. Warden, Secor results of Geos A comparison tests, report to U.S. Army Map Service, Washington, D.C., 11 pp., 1968.
- Gaposchkin, E. M., and K. Lambeck, 1969 Smithsonian standard earth (II), *Smithson. Astrophys. Observ. Spec. Rep. 915*, 1970.
- Gross, J. E., Preprocessing electronic satellite observations, *NASA Contract. Rep. 1183*, 188 pp., 1968.
- Leroy, C. F., Error analysis for Secor equatorial network (SEN), *Geod. Memo. 1636*, U.S. Army Topographic Command, Washington, D.C., 17 pp., 1969.
- Leroy, C. F., and W. D. Googe, Secor network adjustment program, *Geod. Memo. 1620*, U.S. Army Map Service, Washington, D.C., 39 pp., 1967.
- Wilson, D. C., Ionospheric model refinement, *Tech. Memo. 69*, contract DACA 71-68-C-0143, part 1 (68 pp.) and part 2 (79 pp.), Cubic Corp., San Diego, Calif., 1969.

Geos 1 Secor Observations in the Pacific (Solution SP 7)

IVAN I. MUELLER, JAMES P. REILLY, CHARLES R. SCHWARZ, AND GEORGES BLAHA

Department of Geodetic Science

Ohio State University, Columbus, Ohio 43210

Abstract. Secor observations carried out by the U.S. Army Corps of Engineers define a geodetic network extending through the Pacific Ocean from Japan, with three stations on the Japanese datum, to the west coast of the United States. Thus this network was connected to major datums on both ends. However, observations on Geos 1 were taken only in the middle of the network, from Truk Island to Maui, so that the network determined by Geos 1 observations alone is not directly attached to any major geodetic datum. The adjustment of this isolated network and its indirect connection to the North American datum presented several interesting problems. A little-known procedure called 'inner adjustment' was found to be the appropriate method to define a coordinate system for the adjustment of the isolated network and to determine the inner consistency of the observations. The network was indirectly tied to the North American datum by the use of (1) satellite observing stations of other observing systems whose coordinates were previously determined, (2) relative positions of these and nearby Secor stations, as determined by local surveys, and (3) geodetic heights composed of leveled (orthometric) heights plus geoid heights obtained from a geoid map.

This paper is concerned with the use of the some 60,000 geodetic Secor observations on Geos 1 taken by the Pacific Tracking Network and available in the National Space Science Data Center. This set of data presents some interesting and unique problems.

First, the tracking stations that observed Geos 1 constitute a network that is not attached to any major datum. The Secor Pacific network as a whole was begun in Japan, with three stations on the Japanese datum, and extended through the Pacific Ocean to the west coast of the United States. However, observations on Geos 1 were only taken in the middle of the network, from Truk Island to Maui (Figure 1), so that the network determined by the Geos 1 observations alone was isolated from the major datums at the ends of the larger network. The primary satellites for the Pacific network were from the EGRS series, so that Geos 1 was not always fully observed when the primary satellites were available. Thus, the network determined by the available (Geos 1) observations alone has some weak ties, owing to insufficient numbers of observations. Our main interest was in determining whether the Geos 1 observations

could be put together into an independent rigid network and in finding indirect ties by which such a network could be related to a major geodetic datum.

A second problem lay in determining the quality of the data themselves. We expected to find evidence of systematic errors, since in its early days the Secor system was plagued by range ambiguities, calibration errors, and possibly unreliable determinations of ionospheric refraction. Theoretically, it is possible to determine station positions, orbit unknowns, and coefficients of observational error models all in one simultaneous short-arc solution. However, the data set available in the National Space Science Data Center did not include all the original data. In a great many cases, only segments of less than 2 minutes duration from a pass were included. From these short-duration segments, it is not possible to define adequately the orbit and the error model. Therefore, a large amount of the data could not be used in short-arc adjustments. For this reason, our main tool was the geometric mode adjustment in which almost all of the data could be utilized. However, short-arc orbital mode adjustments were

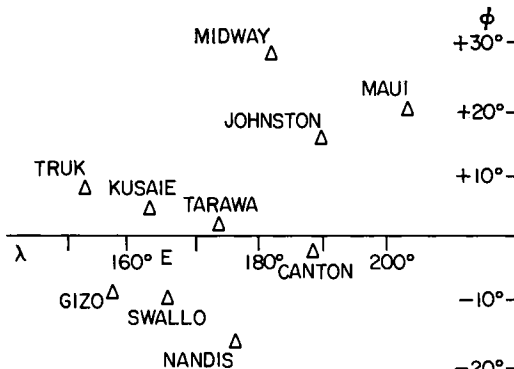


Fig. 1. Location of the Secor stations in the Pacific.

also used to recover ambiguities and calibration errors from those subsets of the data that constituted passes of reasonable length.

As a further complication, we did not have a priori knowledge of either the error model unknowns, the orbit parameters, or the station positions. Without such a priori constraints, there were just too many unknowns to afford a reasonably well-determined solution. If one has fairly good station positions, one can find and remove bad data; conversely, if one has all good data, a rigid network can be easily constructed. Having neither reliable data nor station positions, we were faced with a bootstrap operation.

Preliminary results of this investigation were presented at the Geos 2 Review Conference at NASA, Goddard Space Flight Center, in June 1970, where we reported our best solutions obtainable without modeling for systematic errors [Mueller *et al.*, 1970a].

'INNER' ADJUSTMENT

From a set of range observations between ground stations and satellite positions, one can only determine distances between pairs of points. Since range measurements are independent of the coordinate system, no actual coordinates can be determined from the ranges alone. It is possible to have an adjustment in which the unknowns are the distances between pairs of points, and it can be shown that the total number of independent distances is $3u - 6$, where u is the total number of unknown points. Geodetic solutions, however,

GEOS 1 SECOR OBSERVATIONS IN THE PACIFIC

are commonly made in terms of the actual coordinates of points, and the computer programs that accomplish these solutions operate with coordinates. To use these programs, a coordinate system for the adjustment must be defined in some manner. In many cases, a priori knowledge of some of the points in some coordinate system is available, and this external knowledge can be brought into the adjustment by weighted constraint equations. In the case of range observations, the minimum number of constraint equations necessary to define the coordinate system is six. These are interpreted geometrically as specifying three parameters to define the origin of the coordinate system and three parameters to define the orientation. The scale of the system is determined by the observations themselves. If more than six constraints are used, the constraint equations may themselves have residuals; in attempting to minimize these residuals, the adjustment process may actually increase the residuals of the range observations, thus masking the true quality of the observational material. Our first objective was to find a set of data that was internally consistent, and so we began by using a minimal set of six absolute constraints.

At first these constraints were realized by fixing the three coordinates of one station, two coordinates of a second station, and one coordinate of a third station. We performed many adjustments with this set of constraints and noticed that the selection of the coordinates held fixed had a definite effect on the characteristics of the adjustment. We found that if these were not selected with care, the coordinate system would be poorly defined, and this would result in poor error propagation characteristics, a weak network, and numerical difficulties. For example, if the origin of the system were specified by fixing a station at one extreme end of the net, stations at the other end would tend to be highly uncertain and highly correlated.

Later, we found that the best way to define the coordinate system was to use the set of constraint equations called 'inner' constraints [Rinner *et al.*, 1969]. In this sense, 'best' means resulting in the smallest covariance matrix for the unknowns. Covariance matrices can be compared by means of their traces, and the inner adjustment equations are characterized by the property that the trace of the covariance matrix

MUELLER, REILLY, SCHWARZ, BLAHA

obtained with their use is a minimum among those obtained by adjusting a given set of range observations augmented by a minimal set of six constraint equations. This property also implies that the mean square uncertainty of the unknowns is smaller when the inner adjustment equations are used.

The constraint equations are written in the form

$$CX = 0$$

where

$$C = \begin{vmatrix} C_1 \\ C_2 \end{vmatrix}$$

X is a set of corrections to the approximate coordinates of the unknown points, and

$$C_1 = \left| \begin{array}{ccc|ccc|c} 1 & 0 & 0 & 1 & 0 & 0 & \dots \\ 0 & 1 & 0 & 0 & 1 & 0 & \dots \\ 0 & 0 & 1 & 0 & 0 & 1 & \dots \end{array} \right|$$

$$C_2 = \left| \begin{array}{ccc|ccc|c} 0 & -z_1^0 & y_1^0 & 0 & -z_2^0 & y_2^0 & \dots \\ z_1^0 & 0 & -x_1^0 & z_2^0 & 0 & -x_2^0 & \dots \\ -y_1^0 & x_1^0 & 0 & -y_2^0 & x_2^0 & 0 & \dots \end{array} \right|$$

Both the C_1 and C_2 matrices are made up of similar 3×3 blocks, where each block contains the coefficients of the unknown coordinates of a point. The symbols (x_i^0, y_i^0, z_i^0) denote the approximate coordinates of the i th unknown point, where both the ground points and the satellite positions are considered.

It is also possible to design a set of constraints that will result in the best solution for only a subset of the points. In our adjustments, we were only interested in the ground-station unknowns, so that we wanted to obtain the best possible solution for these unknowns while using only six constraint equations. This implies that the trace of only the part of the covariance matrix that corresponds to the ground station unknowns is minimized; thus the variances of the satellite position unknowns are not included in the minimum sum. The constraint equations that will produce a solution which is best for only some of the unknown points have the same form as those producing the best solution for all the points; however, 3×3 blocks of zeros are inserted into those positions in C_1 and C_2 ,

which correspond to unknowns whose variances are not to be included in the minimum sum.

The inner adjustment constraint equations can be given a geometrical interpretation that appeals to intuition. Let X_i^0 denote the set of approximate coordinates of the i th unknown point, dX_i denote the corrections to these coordinates, and X_i denote the adjusted coordinates; i.e.,

$$X_i = X_i^0 + dX_i$$

The first set of constraint equations, $C_1 X = 0$, is then equivalent to the set of conditions

$$\sum_i dX_i = 0$$

The geometrical interpretation of these condi-

tions is that the center of gravity of all the points will not change after adjustment; i.e.,

$$\sum_i X_i = \sum_i X_i^0$$

The second set of constraint equations, $C_2 X = 0$, corresponds to the conditions

$$\sum_i X_i^0 \times dX_i = 0$$

If the origin of the system remains fixed, the cross products $X_i^0 \times dX_i$ reflect rotations of the points around the origin. These constraint equations insure that the sums of the rotations around all three coordinate axes are zero. The corresponding geometrical interpretation is that the mean orientation of the system of points will not change after adjustment either.

Thus the respective equations $C_1 X = 0$ and $C_2 X = 0$ effectively specify the origin and the orientation of the working coordinate system used in the adjustment. A seventh constraint equation is also available to specify the scale of the system. However, this scale equation is

GEOS 1 SECOR OBSERVATIONS IN THE PACIFIC

only used when the observations themselves do not determine the scale. This would be the case, for instance, if a set of optical satellite observations were to be adjusted.

EXTERNAL CONSTRAINTS

Although there were no direct data available on the absolute or relative position of any Secor station, we were able to find several indirect sources of positional information that could be utilized as external constraints in the adjustment (Tables 1 and 2). This information consisted of the following:

1. On Maui there were camera stations from the Coast and Geodetic Survey's worldwide geometric satellite network (BC 4), and from the Smithsonian Astrophysical Observatory's network (Baker-Nunn). Both of these stations had been tied into the local survey system, together with the Maui Secor station. The relative positions of these three stations provided $3 \times 3 = 9$ constraint equations.

2. On Johnston Island there was a PC 1000 camera, operated by the U.S. Air Force almost at the same location that had been occupied by the Secor station. This PC 1000 camera had observed Pageos, Echo 1, and Echo 2 simultaneously with BC 4 cameras on Maui, Wake, and Christmas Islands [Huber, 1969]. Since the three BC 4 stations were part of the Coast and Geodetic Survey's world net, coordinates of the Johnston PC 1000 on the North American datum, together with the direction Johnston (PC 1000) to Maui (BC 4), could be determined. The relative positions of the Johnston stations and the direction Johnston to Maui provided $3 + 2 = 5$ additional constraint equations.

3. On Midway Island there was a Tranet Doppler station that had been tied to the local survey system, as had the Midway Secor station. The coordinates of the Doppler station on the Mercury ellipsoid had been published as part of the NWL 8D solution [Anderle and Smith, 1967]. Performing a datum transformation, we were able to infer NAD coordinates for the Midway Doppler, and thus determine the direction Midway (Doppler) to Johnston (PC 1000). The relative positions of the stations on Midway and the direction Midway to Johnston provided again $3 + 2 = 5$ constraint equations.

TABLE 1. Station Coordinates Used in the Network Orientations

GOCC No.	Name	Type	Datum	Latitude	σ	Longitude East	σ	h, m	σ, m
6011	Maui*	BC 4	NAD	20°42'26.139"	0.351"	203°44'42.886"	0.396"	3001.4	12.0
9012	Maui†	Baker-Nunn	SAO 1969	20 42 25.66	0.250	203 44 33.48	0.25	3029.0	7.0
6012	Wake*	BC 4	NAD	19 17 28.247	0.470	166 36 43.564	0.515	-159.2	17.2
6059	Christmas*	BC 4	NAD	2 0 13.185	0.487	202 35 20.508	0.380	-22.4	13.3
3475	Johnston‡	PC 1000	NAD	16 43 44.209	0.254	190 28 49.931	0.313	-90.2	7.9
2724	Midway§	Doppler	Mercury	28 11 48.79		182 36 40.13		-14	
2724	Midway	Doppler	NAD	28 11 50.47		182 36 46.16		-117	

* Coast and Geodetic Survey preliminary coordinate.

† Computed from Cartesian coordinates, with $\sigma = 7$ meters for each coordinate, and referred to the SAO ellipsoid of the following parameters:

$a = 6,378,155$ meters, $1/f = 298.255$ [Gaposchkin and Lambbeck, 1970].

‡ Obtained at OSU by adjusting the ACIC optical data, weighting the coordinates of Maui, Wake, and Christmas according to their uncertainties.

§ NWL 8D Solution [Anderle and Smith, 1967, p. A16]. Uncertainty is 25 meters in each Cartesian coordinate.

|| Obtained from NWL 8D mercury datum coordinate, using translation parameters of $\Delta x = -40$ meters, $\Delta y = 163$ meters, $\Delta z = 186$ meters [Anderle and Smith, 1967, p. A16].

MUELLER, REILLY, SCHWARZ, BLAHA

63

TABLE 2. Relative Positions from Local Ground Surveys

From To	Name	Type	Δx , m	Δy , m	Δz , m	Est. σ in each coord., m
5408 3475	Johnston Johnston	Secor PC 1000	3.8	0.8	-1.2	0.5
5411 6011	Maui Maui	Secor BC 4	2001.2	-22992.3	-10965.0	0.5
5411 9012	Maui Maui	Secor BN	1951.7	-22873.4	-11000.9	0.5
6011 9012	Maui Maui	BC 4 BN	-49.5	118.9	-35.9	0.5
5410 2724	Midway Midway	Secor Doppler	-882.6	1911.2	-1481.4	0.5

4. With the above information, the relative and the SAO 1969 positions of the stations on Maui, Johnston, and Midway could be determined except for the scale, which was available only in the NAD system as propagated through the BC 4 net. These islands being at the eastern end of the network, the station positions at the western end were quite weak, especially in the vertical components. This phenomenon was attributed to the cantilever effect of error propagation. In order to reduce this effect, more external information was brought into the adjustment in the form of the geodetic heights of the ten Secor stations. These heights were determined from the SAO 1969 standard earth geoid map by adding the geoid undulations to the heights above sea level as determined from spirit leveling [Gaposchkin and Lambeck, 1970]. This procedure resulted in heights with respect to the SAO ellipsoid ($a = 6,378,155$ meters, $f = 1/298.255$). Derived from a geoid map, these heights were quite uncertain. We estimated that 15 meters was a reasonable value for the standard deviation of a single height determination and derived weights for the height constraint equations from this value. Even though they had relatively low weights, these constraint equations effectively nullified the cantilever effect and greatly improved the determination of station positions at the western end of the network.

5. The Baker-Nunn station on Maui was selected as the origin of the system. Its coordinates in the SAO 1969 standard earth system (Table 1) were constrained with weights based

on the standard deviations as given by SAO [Gaposchkin and Lambeck, 1970].

The external information described in the five items above resulted in 18 positional, 4 directional, and 10 height constraint equations.

OBSERVATIONAL DATA

As a first step in selecting our final data, it was necessary to find a set that was at least internally consistent. We performed many adjustments in the geometric mode, often deleting, and sometimes adding data until we arrived at a set of residuals that were reasonably small and fairly randomly distributed. Using the inner adjustment procedure, and after a great deal of trial and error, we obtained a set of coordinates for nine of the ten stations, from Truk Island to Midway, that was internally consistent, yielding an *a posteriori* estimate for the standard deviation of a single range observation of slightly more than 5 meters. Since all the Geos 1 data from Maui gave quite large residuals, we were not able to extend the network to Maui with the Geos 1 data available in the NASA Data Center. Therefore, we requested and received EGRS 7 data from the U.S. Army Topographic Command to connect Maui to Kusaie, Johnston, and Midway islands. These data brought the standard deviation, estimated *a posteriori*, up to about 9 meters. However, we felt that this was about the best set of data we would hope to get without error modeling, since removing any of the data with the larger residuals would have ruined the geometrical integrity of the network. With this

data and with external constraints similar to those described in the preceding section, we reached solution SP 5 [Mueller *et al.*, 1970a].

Next, we re-examined the data that had previously been deleted. We suspected that many of these were good data, except that the observations contained constant biases. These constant biases are made up of ambiguities, which occur in multiples of 256 meters, and calibration errors, which are generally less than 30–40 meters. By performing short-arc orbital mode adjustments in which the station coordinates were all constrained, we were able to solve for biases for those subsets of the data that constituted passes of reasonable length. Calibration corrections were also recovered for some of the data that had previously been used in geometric mode adjustments. The observations for which constant biases had been recovered were corrected, and were then added into the set of usable data. Since very few of the passes lasted more than 10 min and covered significant ranges in altitude, no attempt was made to solve for refraction or other error model terms.

It was also possible to make reasonable estimates of the calibration errors for some of the data that constituted only a very short segment of an arc. The residuals for a given station in the geometric mode solutions were often fairly large, constant, and of the same sign. For these observations, the mean residuals served as estimates of the calibration errors.

RESULTS

In the final (SP 7) solution, we used a total of 1188 range observations (at 4° to 60° intervals) which, with the 32 external constraint equations, resulted in 287 degrees of freedom. The adjusted station coordinates in the SAO 1969 standard earth system are presented in Table 3. The standard deviation of a single range estimated from the final solution was 3.2 meters, which indicates that most of the systematic errors have been removed.

Table 4 gives the geodetic coordinates on the NAD datum. To transform the coordinates from the SAO system to the NAD, the following translation parameters were used: $\Delta x = 38$ meters, $\Delta y = -164$ meters, $\Delta z = -175$ meters. These parameters are in the sense NAD — SAO [Badekas, 1969].

TABLE 3. Coordinates for the SAO 1969 Standard Earth, Solution SP 7

GOCC No.	Name		Coordinates, m	σ , m
5401	Truk	x	-5,576,050	12
		y	2,984,667	12
		z	822,438	15
5402	Swallo	x	-6,097,450	8
		y	1,486,518	15
		z	-1,133,224	10
5403	Kusaie	x	-6,074,527	8
		y	1,854,359	10
		z	583,838	11
5404	Gizo	x	-5,805,394	9
		y	2,485,342	14
		z	-892,882	12
5405	Tarawa	x	-6,327,924	7
		y	784,583	11
		z	150,834	9
5406	Nandis	x	-6,070,207	11
		y	270,690	18
		z	-1,932,851	11
5407	Canton	x	-6,304,308	9
		y	-917,626	13
		z	-307,106	9
5408	Johnston	x	-6,007,981	5
		y	-1,111,240	8
		z	1,824,156	7
5410	Midway	x	-5,618,721	10
		y	-258,217	10
		z	2,997,241	10
5411	Maui	x	-5,468,010	6
		y	-2,381,410	7
		z	2,253,175	7

CONCLUSIONS

Our experiences with the Secor observations of Geos 1 in the Pacific indicate that with a great deal of effort one can obtain satisfactory solutions. Since none of the observing stations were positioned on major datums, external information had to be used to tie the network into existing coordinate systems. Since ambiguity and calibration corrections can be extracted reliably only from those data subsets that constitute long passes, and only a very few of the passes are long enough to allow the use of an error model more extensive than the single constant bias term, systematic errors are still suspected to be present in some of the data.

MUELLER, REILLY, SCHWARZ, BLAHA

65

TABLE 4. Coordinates for the North American Datum, Solution SP 7

GOCC No.	Name	Latitude	σ	Longitude		Height, m	σ , m
				East	σ		
5401	Truk	7°27'27.1"	0.5"	151°50'33.2"	0.4"	-127	12
5402	Swallo	-10 18 18.7	0.3	166 18 01.1	0.5	-39	8
5403	Kusaie	5 17 10.4	0.3	163 01 32.0	0.4	-84	7
5404	Gizo	-8 06 12.7	0.4	156 49 30.1	0.5	-21	10
5405	Tarawa	1 21 45.9	0.3	172 56 0.7	0.4	-95	6
5406	Nandis	-17 45 36.8	0.3	177 26 53.6	0.6	53	11
5407	Canton	-2 46 48.8	0.3	188 16 59.0	0.4	-23	9
5408	Johnston	16 43 44.0	0.2	190 28 50.2	0.3	-105	5
5410	Midway	28 12 45.4	0.3	182 37 58.6	0.4	-121	10
5411	Maui	20 49 24.6	0.2	203 32 7.9	0.2	-24	6

The solutions for the station coordinates (Tables 3 and 4) appear to be completely valid. The standard deviations of the coordinates are all acceptable. There seems to be some rise in the standard deviations toward the western and southern parts of the network, probably because all direction control is in the northeastern part of the net. If ballistic camera data or other directional information were available from some of the stations on the western end, the whole network could be further strengthened.

More details of this investigation have been given by Mueller *et al.* [1970b].

Acknowledgment. The work described in this paper was supported by grant NGL 36-008-093 from the National Aeronautics and Space Administration.

REFERENCES

Anderle, Richard J., and Steve J. Smith, NWL-8 geodetic parameters based on Doppler satellite observations, *Tech. Rep. 2106*, Nav. Weapons Lab., Dahlgren, Va., 1967.

Badekas, John, Investigations related to the establishment of a world geodetic system, *Rep. 124*, Dep. of Geod. Sci., Ohio State Univ., Columbus, 1969.

Gaposchkin, E. M., and Kurt Lambeck, 1969 Smithsonian standard earth (II), *Smithson. Astrophys. Observ. Spec. Rep. 315*, 1970.

Huber, Donovan N., Johnston island preliminary satellite network coordinates, *Tech. Rep. 113*, Aeronaut. Chart and Inform. Center, St. Louis, Missouri, 1969.

Mueller, Ivan I., J. P. Reilly, C. R. Schwarz, and G. Blaha, Experiments with Secor observations on Geos 1, paper presented at the Geos 2 Review Conference, Goddard Space Flight Center, NASA, Greenbelt, Md., June 22-24, 1970a.

Mueller, Ivan I., James P. Reilly, Charles R. Schwarz, and Georges Blaha, Secor observations in the Pacific, *Rep. 140*, Dep. of Geod. Sci., Ohio State Univ., Columbus, 1970b.

Rinner, Karl, Karl Killian, and Peter Meissl (Eds.), Beiträge zur Theorie der geodätischen Netze im Raum, Deutsche Geodatische Kommission, ser. A, no. 61, Munich, 1969 (published in English as: Karl Rinner, Systematic investigations of geodetic networks in space, Annex F, U.S. Army European Res. Office, AD-482852, 1966).

Mini-Arc Orbit Determination for the Geos C Altimetry Experiment

ROBERT M. L. BAKER, JR.

Computer Sciences Corporation, Systems Division
Los Angeles, California 90045

Abstract. The problem is, given simultaneous observations of an altimeter-bearing geodetic satellite, from three or more high-precision radar stations, to determine its orbit to submeter accuracy in the presence of perturbations arising from strong, localized gravitational anomalies (such as the Puerto Rico trench). Accuracies within several centimeters based on observational errors of a few centimeters are documented. A new solution to this problem involves the use of an f and g series specialized to the determination of radial distance (pertinent to the satellite altimeter experiment) to process data over a very short arc (e.g., 6 sec to 10 min). Such a short arc is termed a 'mini arc.' In this approach, the data batches are connected by dynamics, rather than by the usual curve fit to a power series in time. A nonunity value of the mass factor is introduced to serve as an 'alias' for the perturbations that affect the satellite's path during the mini arc. The essence of the mini-arc approach is to include the influence of the far, or relatively lower-order, force field analytically and to solve for the remaining fine structure with accuracies that can approach a few centimeters. The method is neither restricted to high-data-rate sensors nor to simultaneous sensor data; for example, the method could be effective for a single, low-data-rate laser sensor, with centimeter accuracy.

The approach taken is to develop and investigate new or specialized methods of orbit determination that take into account the unique characteristics and requirements of the Geos C radar altimetry experiment. Initially, it was recognized that, for altimeter calibration and ocean mapping, it is more important to determine the position of the satellite as accurately as possible over a relatively small part of its orbit than to determine the entire orbit accurately. In addition, for ocean mapping (e.g., measuring the Puerto Rico trench), knowledge of the absolute satellite location is not nearly as important as knowledge of the shape of the curve that it follows. This is because for certain applications we are more interested in determining the 'shape' of the ocean's surface than its actual distance from the earth's center of mass. The satellite altimeter provides a direct method of establishing the shape of the ocean's surface, and its possible future accuracy within several centimeters necessitates submeter accuracy for orbit determinations.

It first appeared that in order to interpret the altimeter data it might not be necessary to

define the location of the satellite at all! One might instead only look at the variation of the altimeter data over short periods of time and interpret these variations as being due to localized changes in the ocean surface. Although such a procedure may, in fact, be successful, Arnold [1966] and Jackson [1970] have found that there could be an orbital-path fine structure that might either mask or cause a misinterpretation of the altimeter data. (The presence of orbital-path fine structure of a few meters during data spans of a few minutes was also demonstrated by Baker *et al.* [1970] and Stanley and Roy [1972]).

Because of the existence of orbital-path fine structure, we investigated methods for 'following' the orbit by means of processing batches of data over very short arcs that we termed 'mini arcs.' First, we require that the satellite traverse less than one radian on its orbit. Second, we require that the satellite be visible from three or more designated radar sensors over the entire arc. Both of these requirements are satisfied in the Caribbean area for the nominal Geos C orbit and for arcs of 5000 km or less.

(For other purposes, longer mini arcs would be desirable.)

An ancillary unexpected benefit arises from this method. Conventional orbit determination (e.g., minimum-variance or conventional weighted least-squares differential correction) can profit from the mini-arc approach if the mini arc is interpreted either as large-scale smoothing or as a type of 'normal place,' since we were able to reduce data having a few meters rms error into fits that exhibited a few centimeters deviation from a true orbit. Conventional differential correction may tend to 'smooth through' and mask orbital-path fine structure. The philosophy of the mini-arc technique is to 'bite off' small pieces of the orbit and compute what essentially amounts to a series of 'osculating' orbits that include first-order perturbations due to the far field. Thus, one should be able to discern orbital wiggles, or fine structure, without having to hypothesize, *a priori*, the details of the force model that would lead to such wiggles. It is true that conventional differential correction could be applied over very short arcs in emulation of the mini-arc approach (but with much more computation). However, the conventional procedure is unlike the analytical mini-arc technique in that it is difficult to 'tune' the data arc length and the extent of the perturbation model to the desired over-all, consistent accuracy. In conventional differential correction, such a tuning is a trial-and-error process, whereas it can be done analytically by using the explicit mini-arc formulas. The method is not restricted to only the determination of radial distance, to only high-data-rate sensors (we have applied the method to one sample per 5 sec of data), or to processing multiple-sensor data.

PROCESSING RADIAL-DISTANCE DATA BY USING *F* AND *G* SERIES

The basic problem to be solved involves data from three or more sensors that can simultaneously view the altimeter-bearing satellite. Although more sophisticated solutions to the multilateration problem may be desirable, for reasons of simplicity the basic computation involves a three-range solution. As stations are added beyond three (up to five in our current version), all combinations of three stations are utilized to obtain the geocentric radius vector

MINI-ARC ORBIT DETERMINATION

at the *i*th time r_i , and an average of these determinations is then taken to be the best estimate \bar{r}_i . Actually, because of geometrical effects and sensor error models, a weighted average, weighted least squares (including a covariance matrix), or a method similar to the 4- or 5-star determinant method would provide a better estimate. The weights can be easily generated numerically by applying errors to the slant ranges and defining the sensitivity (variation) of r_i on the basis of these variations. In any operational version of the mini-arc orbit determination algorithm, an alternate procedure to the one employed here to preprocess the radar data is to be recommended.

The method used for obtaining r_i from three slant ranges is a modified version of *Escoba's* [1965] procedure.

Let us now assume that we have a series of geocentric radius vectors at a succession of times. Furthermore, since we are most interested in orbital arcs of limited extent, let us consider the use of an *f* and *g* series and, therefore, explicitly include the dynamics of the orbit. That is, we will set down the equation $r_i^2 = \mathbf{r}_i \cdot \mathbf{r}_i$ in terms of such a series.

Although it may not be utilized, we will carry the *f* and *g* series out to the sixth or seventh order. Since

$$\mathbf{r}_i = f_i \mathbf{r}_0 + g_i \dot{\mathbf{r}}_0 \quad (1)$$

we have

$$r_i^2 = \mathbf{r}_i \cdot \mathbf{r}_i = f_i^2 r_0^2 + g_i^2 \dot{s}_0^2 + 2f_i g_i \dot{r}_0 \quad (2)$$

Note that

$$f_i = 1 + \sum_{k=2}^6 \tau_i^k \bar{f}_k$$

$$g_i = \tau_i \left(1 + \sum_{k=3}^7 \tau_i^{k-1} \bar{g}_k \right)$$

where τ is the canonical unit of time ($\tau \approx t(\text{sec})/807$), and \bar{f}_k and \bar{g}_k are given by *Baker* [1967, p. 139].

For most orbits of interest, $\bar{f}_k \cong \bar{g}_{k+1}$.

In order to establish an appropriate truncation point, consider the size of the coefficient of τ_i^4 in (2):

$$r_i = [r_i^2]^{1/2}$$

$$= r_0 \left[f_i^2 + g_i^2 \frac{\dot{s}_0^2}{r_0^2} + 2f_i g_i \frac{\dot{r}_0}{r_0} \right]^{1/2}$$

ROBERT M. L. BAKER, JR.

69

Let

$$\begin{aligned}\epsilon &= f_i^2 - 1 + g_i^2 \frac{\dot{s}_0^2}{\dot{r}_0^2} + s f_i g_i \frac{\dot{r}_0}{r_0} \\ &= \left(\frac{2\dot{r}_0}{r_0} \right) \tau_i + \left(2\bar{f}_2 + \frac{\dot{s}_0^2}{\dot{r}_0^2} \right) \tau_i^2 \\ &\quad + \left(2\bar{f}_3 + \frac{2\dot{r}_0}{r_0} \{ \bar{f}_2 + \bar{g}_3 \} \right) \tau_i^3 \\ &\quad + \left(2\bar{f}_4 + \bar{f}_2^2 + \frac{2\dot{s}_0^2 \bar{g}_3}{r_0} \right. \\ &\quad \left. + \frac{2r_0}{r_0} \{ \bar{f}_3 + \bar{g}_4 \} \right) \tau_i^4 \end{aligned} \quad (3)$$

We shall set

$$\epsilon = \epsilon_1 \tau_i + \epsilon_2 \tau_i^2 + \epsilon_3 \tau_i^3 + \epsilon_4 \tau_i^4 \quad (4)$$

To first order

$$r_i = r_0[1 + \epsilon/2]$$

and the effect of the τ_i^4 term due to neglect of ϵ_4 is

$$\Delta r_i \cong (r_0 \epsilon_4 \tau_i^4)/2 \quad (5)$$

As can be seen, this effect (error) will only assume the maximum value given approximately by (5) at the extremes of the mini arc.

We can now evaluate ϵ_4 for a typical Geos C satellite in which $a = 1.167R_E$ and $e = 0.01860$. We shall consider three extreme cases (minimum r_0 , maximum r_0 , and maximum \dot{r}_0). The mass quantity $\mu = m_1 + m_2$ is taken as 1.

1. $r_{0(E.R.)} = 1.146, \dot{r}_0 = 0, \epsilon_4 = -3.6(10^{-3})$.
2. $r_{0(E.R.)} = 1.187, \dot{r}_0 = 0, \epsilon_4 = +2.8(10^{-3})$.
3. $r_{0(E.R.)} = 1.166, \dot{r}_0 = 1.44 \text{ times } 10^{-2}, \epsilon_4 = -2.9(10^{-3})$.

As is to be expected, the coefficient would be the largest for the first case, since it is for perigee, and both acceleration and speed are at a maximum.

Let us consider the value of τ_i for the 10-sec and 100-sec mini arc (epoch is chosen at mid arc). For 10 sec, $\tau_i^4 = (5/807)^4 = 1.46 \times 10^{-9}$, and, for 100 sec, $\tau_i^4 = (50/807)^4 = 1.46 \times 10^{-6}$. The neglected terms are, respectively (for case 1, in which the coefficient ϵ_4 is the largest), 5.25×10^{-12} and 5.25×10^{-8} . For the 100-sec data are,

the maximum error in r_i (occurring only at the extremes of the data arc) would be $(1.146)(6.378 \times 10^8)/2 \times (5.25 \times 10^{-8}) = 0.193$ meter. It is concluded, therefore, that one can neglect the fourth-order terms in the mini-arc analysis.

For ϵ_1 , ϵ_2 , and ϵ_3 we find, by substituting for \bar{f} and \bar{g} ,

$$\begin{aligned}\epsilon_1 &= 2\dot{r}_0/r_0 \\ \epsilon_2 &= (3\mu/2r_0^3) - (\mu/r_0^2 a) \\ \epsilon_3 &= -\mu\dot{r}_0/3r_0^4\end{aligned} \quad (6)$$

Because we are concerned with a gravitational anomaly that may be most influential at the subsatellite point, it would seem reasonable to allow μ to be included in the orbital parameters. Although such an approach is unconventional, it will be shown in the next section to be appropriate for the Geos C mini-arc analysis. Let

$$\begin{aligned}p_1 &= \dot{r}_0/r_0 \\ p_2 &= \mu/r_0^3 \\ p_3 &= \mu/r_0^2 a\end{aligned}$$

We then obtain

$$\begin{aligned}\epsilon_1 &= 2p_1 \\ \epsilon_2 &= 3p_2/2 - p_3 \\ \epsilon_3 &= -p_1 p_2/3\end{aligned}$$

Applying the binomial expansion to $r = r_0(1 + \epsilon)^{1/2}$, in terms of the p 's, we have

$$\begin{aligned}r_i &= r_0 \left[1 + (p_1)\tau_i + \frac{1}{2}(p_2 - p_3 - p_1^2)\tau_i^2 \right. \\ &\quad \left. + \frac{p_1}{2}(p_3 + p_1^2 - \frac{4}{3}p_2)\tau_i^3 \right] \end{aligned} \quad (7)$$

in which r_0 can be replaced by $(\mu/p_2)^{1/3}$.

ANALYTICAL INTRODUCTION OF THE MASS FACTOR

In (7), p_2 and p_3 involve μ . We have specifically not restricted μ to its usual value of unity in the mini-arc analysis so as to allow for the analytical introduction of perturbative influences without requiring a modification of the basic equation. Although it is possible to alias various perturbative influences through μ , we will consider here only the example of the earth's gravitational field. Philosophically speak-

ing, it is the essence of the mini-arc approach to include the influence of the far, or relatively lower-order, force field (that does not contribute to fine structure) analytically and to solve for the remaining fine structure.

The radical component of the perturbation due to the aspherical earth can be singled out for the Geos C altimeter mission. Thus we can take the partial derivative with respect to r of a 4th-order representation of earth's gravitational field Φ ,

$$\begin{aligned} \frac{\partial\Phi}{\partial r} = & -\frac{\mu}{r^2} \left[1 + \frac{3J_2}{2r^2} (1 - 3U_z^2) \right. \\ & + \frac{2J_3}{r^3} U_z (3 - 5U_z^2) \\ & \left. - \frac{5J_4}{8r^4} (3 - 30U_z^2 + 35U_z^4) + \dots \right] \quad (8) \end{aligned}$$

where the J 's are the zonal harmonics, and U_z is the z component of the unit vector \mathbf{U} ($\mathbf{U} = \mathbf{r}/r$).

What we would like to do is to define μ as equal to unity plus the average of all of the perturbative influences (restricted here to the second, third, and fourth zonal harmonics, but readily expandable to any level). Thus, we might have

$$\begin{aligned} \mu = & \left[1 + \frac{3}{2} \frac{J_2}{r^2} (1 - 3\langle U_z^2 \rangle) \right. \\ & + 2 \frac{J_3}{r^3} \langle U_z \rangle (3 - 5\langle U_z^2 \rangle) \\ & \left. - \frac{5}{8} \frac{J_4}{r^4} (3 - 30\langle U_z^2 \rangle + 35\langle U_z^4 \rangle) + \dots \right] \quad (9) \end{aligned}$$

where the angle brackets indicate average values. Utilization of (9) involves the consideration of two questions: How many terms need we include in (9), and what is the sensitivity of μ (and, hence, unmodeled perturbations) to changes in r and U_z from their mean values over a mini arc?

For the sake of the current analysis (which will be a consideration in the trade-off study whose result will be the optimum mini-arc length), we will consider mini-arc lengths of 10, 100, and 1000 sec.

Since J_2 has a numerical value almost one thousand times greater than J_3 , we will first consider the effect of the radial distance caused

MINI-ARC ORBIT DETERMINATION

by the neglect of J_3 . The perturbative derivative is given by

$$\dot{r}_{J_3} = -(2J_3/r^5) \sin i \{ 3[1 - 5(\sin^2 i)/4] \sin u + 5(\sin^2 i)/4 \sin 3u \} \quad (10)$$

where i is the inclination, and u is the argument of latitude ($= \omega + v$). Although it is not truly possible, we can certainly obtain the greatest upper bound for the perturbative derivative by setting both $\sin u$ and $\sin 3u$ equal to +1 and allowing r to exhibit its minimum perigee value (which for the nominal Geos C orbit is 1.146 earth radii). We also set $i = 20^\circ$. Thus

$$\dot{r}_{J_3 \text{ max}} = 2.44 \times 10^{-6} \quad (\text{in units of } \mu/a^2)$$

We can approximately account for the change in radial distance resulting from the neglect of J_3 by using the relationship

$$\Delta r = \frac{1}{2} \dot{r} (\Delta \tau)^2 \quad (11)$$

For a 10-, 100-, and 1000-sec mini arc, we obtain $\Delta r = 0.00119$, 0.119, and 11.9 meters, respectively.

Thus for submeter accuracy, it seems reasonable that only the influence of J_2 need be included for μ for mini arcs of 100 sec or less. For longer arcs, one could easily extend (9), but for the present analysis we shall set

$$\mu = 1 + \frac{3}{2} \frac{J_2}{r^2} (1 - 3\langle U_z^2 \rangle) \quad (12)$$

Let us next consider the influence of a variation of r about $\langle r \rangle$ and U_z about $\langle U_z \rangle$ over a mini arc. Note that $\langle r \rangle$ and $\langle U_z \rangle$ would come directly from the slant range solution for r_i discussed earlier; that is,

$$\begin{aligned} \langle r \rangle &= \frac{1}{N} \sum_{i=1}^N |\mathbf{r}_i| \\ \langle U_z \rangle &= \frac{1}{N} \sum_{i=1}^N \langle U_{zi} \rangle \end{aligned}$$

Since these represent mean values and since the data come in at a uniform rate, we need only estimate a variation of r and U_z over one-half of a mini arc. We will set

$$\Delta \mu_r = |\mu(\langle r \rangle) - \mu(r)| \cong \left| \frac{\partial \mu}{\partial \langle r \rangle} \Delta r \right|$$

$$\Delta \mu_{U_z} = |\mu(\langle U_z \rangle) - \mu(U_z)| \cong \left| \frac{\partial \mu}{\partial \langle U_z \rangle} \Delta U_z \right|$$

ROBERT M. L. BAKER, JR.

where Δr and ΔU_z represent the maximum excursions of r and U_z about $\langle r \rangle$ and $\langle U_z \rangle$, respectively, over the mini arc. The partial derivatives are easily obtained from (12), and

$$\Delta r = ae \sin E \quad \Delta E \approx ae \sin E(n\Delta t)$$

where E is the eccentric anomaly, and n is the mean motion, so that the maximum variation in r will occur near $E = 90^\circ$ and 270° .

For the nominal Geos C orbit, $n = 8.74 \times 10^{-4}$ radians/sec.

Thus $\Delta r = 2.07 \times 10^{-5} \Delta t$ ($\Delta t = (1/2)$ mini-arc length in seconds) and for the three mini-arc lengths we have $\Delta r = 1.03 \times 10^{-4} R_E$ (10-sec), $1.03 \times 10^{-5} R_E$ (100-sec), and $1.03 \times 10^{-6} R_E$ (1000 sec). For a maximum value of the r partial derivative, we set $\langle U_z^2 \rangle = 0$ ($U_z^2 \leq \sin^2 = 0.117$), and compute $\partial\mu/\partial r = (2.16)(10^{-8})$, so that the maximum variations are given by $\Delta\mu_r = 2.23 \times 10^{-7}$, 2.23×10^{-6} , and 2.23×10^{-5} for the 10-, 100-, and 1000-sec mini arcs, respectively. We have

$$\Delta U_z = \sin i \cos u \Delta u$$

so that the maximum variation in U_z will occur near $U = 0$ and 180° . Over the short time intervals and for the nearly circular Geos C orbit, we can set

$$\Delta u = n \Delta t$$

Thus

$$\Delta U_z = 2.95 \times 10^{-4} \Delta t$$

($\Delta t = (1/2)$ mini-arc length in seconds), and for the three mini-arc lengths we have $\Delta U_z = 1.49 \times 10^{-3}$, 1.49×10^{-2} , and 0.149 .

In the establishment of a maximum value of the partial derivative, we have a conflict, since we found that the maximum variation of U_z , i.e., ΔU_z , occurs near $u = 0^\circ$ and 180° , whereas U_z and, hence, $\partial\mu/\partial U_z$ are zero at these points. We will therefore consider that the maximum value of $\Delta\mu_{Uz}$ occurs near $u = 45^\circ$ so that for the three mini arcs of interest we have $\Delta U_z = 1.05 \times 10^{-3}$, 1.05×10^{-2} , and 0.105 . The reference value of the partial derivative will be evaluated when $U_z = 0.241$, so that

$$\partial\mu/\partial\langle U_z \rangle = 1.78 \times 10^{-3}$$

and the maximum variations are given by $\Delta\mu_{Uz} = 2.65 \times 10^{-6}$, 2.65×10^{-5} , and 2.65×10^{-4} .

Next we must translate the variation in the correction to μ into variation in the radial distance.

From (8) we see that the perturbative acceleration due to the second harmonic (that is being accounted for by the nonunity μ) is given by

$$\dot{r}_{J_2} = (-3\mu/2r^4) J_2(1 - 3U_z^2)$$

so that

$$\Delta\dot{r}_{J_2} = (-3\Delta\mu/2r^4) J_2(1 - 3U_z^2) \quad (13)$$

$$\Delta r \cong [(\Delta\dot{r}_{J_2})/2] (\Delta\tau)^2 \quad (14)$$

By far the largest value for $\Delta\mu$ is given for the 1000-sec mini arc resulting from a variation of U_z about its mean value $\langle U_z \rangle$. Evaluation of (13) with $U_z = 0.241$ yields:

$$\Delta\dot{r}_{J_2} = 2.06 \times 10^{-7} \text{ (units of } \mu/a^2)$$

For the 1000-sec mini arc, we have $\Delta\tau = 1.24$, so that from (14) we find

$$\Delta r = 1.58 \times 10^{-7} R_E$$

or about one meter. (For a 100-sec mini-arc length, Δr would be about 1 cm.)

It is concluded, therefore, that the nonunity perturbative evaluation of μ is reasonable for submeter accuracy if mini arcs having lengths less than 1000 sec are utilized.

One question that may arise is the influence of the variation in the modified μ ($\Delta\mu$) on the purely two-body part of the mini-arc analysis. In this regard, it should be recognized that variations in r about r_0 and U_z about U_{z0} are included in the basic formulation of the f and g series. Thus, the $\Delta\mu$ only affects the perturbations that the modification of μ is intended to account for.

It may be of interest at this point to compare the mini-arc approach with conventional step-by-step numerical integration. The major difference is that numerical integration employs a computed force model (limited, perhaps), whereas the mini-arc approach involves the use of an f and g series that includes an analytical formulation of the force model. The analytical force model is developed only with enough detail so as not to involve errors greater than the desired orbital accuracy during the short mini arc. In particular, the value of μ can be developed as, say,

$$\mu = 1 + \mu_0 + \mu_1 \tau_1 + \dots$$

in which the μ_0 , μ_1 , etc., coefficients are analytical relationships (similar to general perturbations) and not subject to differential correction. As an example, μ_0 can be simply represented by (12).

For a given mini-arc length, the uncertainty in J_2 , the influence of neglected higher-order coefficients, and variations of r and U_z about their mean values $\langle r \rangle$ and $\langle U_z \rangle$ do not lead to errors larger than those desired in the orbital path. For longer arcs or higher desired accuracy, the equation for μ_0 would be extended and a $\mu_1 \tau_1$ term added. Because of the simplified form of the extended f and g series (extended to include some perturbations; see *Baker* [1964]), it involves considerably less computation than would numerical integration. The results, assuming similar force model restrictions, should be identical, but using numerical integration for such a problem would be analogous to numerically integrating a two-body orbit when its analytical solution is well known.

ORBITAL FINE-STRUCTURE MODEL

The purpose of the development of an analytical orbital, fine-structure model is to establish the degree to which the mini-arc technique can follow a realistic but hypothetical perturbed path. Although we have hypothesized the model upon the results of Arnold's and Jackson's analyses of the effect of localized gravitational anomalies, the model is rather general. In fact, a linearized analysis of the influence of any localized perturbative influence (e.g., caused by radiation when a satellite enters the umbra or caused by a localized atmospheric density variation) exhibits the same form. The linearized treatment follows that by *Baker and Forster* [1963].

As has been established by *Baker* [1964] and *Baker and Forster* [1963] and the linearized analyses, there seem to be two components to a localized fine structure induced by a gravitational anomaly. First, there is a localized transient in the orbit near the gravitational anomaly that causes a local dip (or rise) in the radial distance. Second, there is a short-period variation in the radius vector whose period is about the same as the orbital period. There are other perturbations, but their wavelengths are longer

MINI-ARC ORBIT DETERMINATION

and, according to R. J. Anderle (personal communication, 1970) they can usually be accounted for by use of a reasonably high-order (e.g., 20 by 20) gravity field.

The first variation can conveniently be represented by an exponential dip in the orbit, i.e., if Δr_1 is the gravitational anomaly perturbative displacement caused by this first effect, then

$$\Delta r_1 = K_1 \{ [\exp -K_2(E - E_1)] - 1 \} \quad (15)$$

where, for a reasonable dip (but sufficiently extreme for a good test), we can tentatively adopt

$$K_1 = 2 \text{ meters}/6,378,145 \text{ meters}$$

$$K_2 = 1/30^\circ, \text{ or } 6/\pi \text{ radians}$$

$$E_1 = E_0 - (1/K_2)/2$$

and E_0 is the epoch value of the eccentric anomaly at the point of closest approach to the anomaly.

The second of the variations can also be conveniently represented by an orbital period variation in r , Δr_2 , given by

$$\Delta r_2 = -K_3 \sin(E - E_0) \quad (16)$$

where

$$K_3 = 10 \text{ meters}/6,378,145 \text{ meters}$$

Equation 15 is introduced for $E \geq E_1$, and (16) is added for $E \geq E_0$. Thus, we can represent the radial distance (longer-period perturbations having been neglected) by

$$r = a(1 - e \cos E)$$

$$+ U\{E - E_1\} \Delta r_1 + U\{E - E_0\} \Delta r_2 \quad (17)$$

where we define the step functions $U\{x\}$ for arbitrary argument x by

$$U\{x\} = 0 \text{ for } x < 0$$

$$U\{x\} = 1 \text{ for } x \geq 0$$

(In all cases it is assumed that $E > 0$.) A graphical representation of Δr_1 and Δr_2 is given by Figure 1.

The only difficulty in the utilization of the eccentric anomaly E as an independent variable is that the data are time-ordered with constant interval (i.e., ten data points per second). Thus, in simulating the data, one is required to solve

ROBERT M. L. BAKER, JR.

73

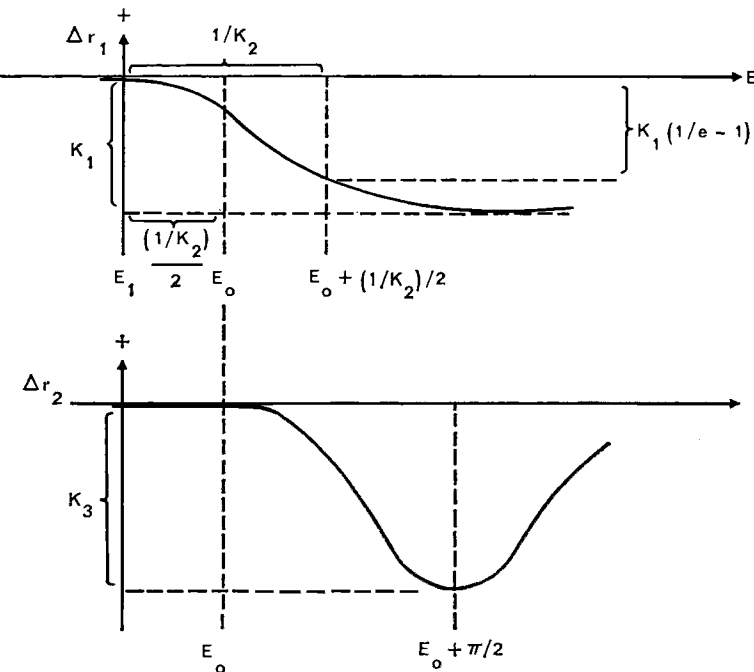


Fig. 1. Orbital path, fine-structure model.

Kepler's equation the 'hard way.' The only redeeming feature is that, for a fixed Geos C orbit, it is possible to construct a table of E and t that can be used universally for various sets of fine-structure approximations defined by different sets of K_1 , K_2 , K_3 , and E_o .

Random observational noise can be introduced by a Monte Carlo technique, i.e., we add on a random normal deviate (times the estimated standard deviation in r) to each of the r 's generated from (17) for every E and t pair. Although such a procedure is only a rough approximation to the real data, it does serve to check the mini-arc procedure.

ANALYTICAL OPTIMIZATION OF MINI-ARC INTERVAL

In any orbit determination, there are several components of the error that result in the departure of the best-fit orbit from the true orbit: random and systematic errors in the observations (including various types of noise, sensor error model uncertainty, timing errors, station-location uncertainty, etc.), errors resulting from the neglect of various perturbations, errors caused by the imperfect representation

of the perturbations that have not been neglected, and errors inherent in the numerics of the prediction technique (e.g., truncation error). In establishing the 'best' or optimum mini-arc interval, all these error components must be considered.

We have already established for a 100-sec mini arc that there is about a 12-cm error due to neglected perturbations (in μ), only a 1-cm error due to representing perturbations by mean positions, and at most a 19-cm error (at the ends of the interval) due to the truncation of τ^4 terms. Thus, for submeter accuracy of 20 to 25 cm, we require that the theoretically desired error due to observational noise should be on the order of 6 to 8 cm, say 7 cm.

Under the assumption of a Gaussian error distribution, as the number of observations is increased, the theoretical accuracy of a best estimate is likewise increased. Although a Gaussian error distribution is not a completely valid assumption, we will use it in the absence of a theory for a more realistic error distribution. The major point to be made here is that if in theory we wish to achieve a certain level of accuracy, say σ_x , then completely independent

of the accuracy of the data one can define \hat{x} to an accuracy of $\sigma\hat{x}$ by choosing the number of observations N such that

$$\sigma\hat{x} = \sigma x/(N - m)^{1/2}$$

where m is the number of dimensions of x , and $\sigma\hat{x}$ is the measurement error involved in any one measure of x . The preceding equation, therefore, sets the optimum theoretical number of observations required to define the state efficiently.

We have optimally 'tuned' the mini arc to approximately 100-sec length through consideration of the goodness of the μ fit, the influence of unmodeled perturbations, the data rate, and the data accuracy.

NUMERICAL RESULTS

Convergence. One reduces the data by utilizing the mini-arc equations and by means of conventional least-squares differential correction. An interesting feature of the mini-arc procedure, as compared with other differential correction algorithms, is that, since we are only interested in geocentric distance for the altimeter application, we need correct but three parameters (the p 's) instead of the conventional set of six or more. Furthermore, rather simple analytical partials can be developed that result in considerable computational efficiencies. These are:

$$\begin{aligned} \frac{\partial r_i}{\partial p_1} &= (\mu/p_2)^{1/3} [\tau_i + (-p_1)\tau_i^2 \\ &\quad + \frac{1}{2}(3p_1^2 - \frac{4}{3}p_2 + p_3)\tau_i^3] \end{aligned} \quad (18)$$

$$\begin{aligned} \frac{\partial r_i}{\partial p_2} &= -\frac{1}{3p_2} (\mu/p_2)^{1/3} \left[1 + (p_1)\tau_i \right. \\ &\quad - \frac{1}{2}(2p_2 + p_3 + p_1^2)\tau_i^2 \\ &\quad \left. + \frac{p_1}{2}(p_3 + p_1^2 + \frac{8}{3}p_2)\tau_i^3 \right] \end{aligned} \quad (19)$$

$$\frac{\partial r_i}{\partial p_3} = \frac{1}{2}(\mu/p_2)^{1/3} [-\tau_i^2 + p_1\tau_i^3] \quad (20)$$

Tests on a computer utilizing these partials in a least-squares differential correction indicated satisfactory convergence in examples of mini arcs representing all aspects of the problem.

The parameter p_1 seems to change the most from arc-to-arc and is also the slowest to converge. First, it should be recalled that

$$p_1 = \dot{r}_0/r_0$$

and, since we are near perigee, \dot{r}_0 starts near

MINI-ARC ORBIT DETERMINATION

zero and then increases rapidly. Second, in equation 7, r is rather insensitive to p_1 , both because of the small size of p_1 (of the order of 10^{-4}) and because of its multiplication by τ_i (the $p_1^2\tau_i^2$ and $p_1^3\tau_i^3$ terms are almost negligibly small near perigee). Thus it is reasonable to expect that p_1 would be the most slowly convergent of all of the parameters.

Fit to orbital fine structure in the presence of simulated noise. A standard deviation of the observed radial distance of two meters was introduced. As verification of the Monte Carlo approach, the standard deviation of the corrected orbit against the 'noisy' observations was always about 2 meters (at most 15 cm larger). The rms of the corrected orbit against the perturbed, simulated true orbit varied between 9 and 24 cm but, in general, was in the 10- to 15-cm submeter area. This departure could be reduced by tightening the differential-correction limit, from 0.1 meter to, say, 0.01 meter. It should be emphasized that the rms of the observations relative to the best-fit mini-arc orbit is not a measure of the accuracy of the mini arc, but simply a measure of the scatter of the raw observational data. The rms of the departures of the best-fit mini arc from the theoretically perturbed orbit is the only true measure of the mini arc's ability to follow orbital-path fine structure.

The mini arc seems to follow the orbital fine structure quite closely. As one moves from the first to the last (tenth) mini arc, p_1 changes from 6.812254×10^{-4} to 1.105204×10^{-4} ; p_2 changes from 0.6110746 to 0.5983184; and p_3 changes from 0.6000851 to 0.5916975.

The computer running time is also noteworthy. More than 40,000 observations are simulated and processed in only 400 sec of CPU time. This result is even more remarkable when it is recognized that the algorithm has not been optimally programmed, is cast in a very slow language (BASIC), and utilizes a Burroughs 5500 via a teletype, time-share terminal. The efficiency of the program emphasizes the advantages of a mini-arc technique in reducing observational data.

COMPARISON OF THE MINI-ARC TECHNIQUE TO CONVENTIONAL SMOOTHING

Although we recognize that the fundamental observations are measurements of range from

ROBERT M. L. BAKER, JR.

75

three or more stations, we will assume that such measurements have been processed and will utilize r_i as quasi-raw observational data. Thus, one could smooth such r_i data by fitting them to

$$r_i = \beta_0 + \beta_1 \tau_i + \beta_2 \tau_i^2 + \beta_3 \tau_i^3 + \dots \quad (21)$$

In more generality, we could conceive of some function of the data $f(r_i)$ and smooth it by means of the evaluation of the coefficients in a fitted curve of the form:

$$f(r_i) = \sum_{m=0}^M \beta_m \phi_m(\tau_i) \quad (22)$$

where $\phi_m(\tau)$ is a function of degree m .

When the curve fitting is completed, one has values of the coefficients β_m and can represent the data by simply quoting the numerical values of the coefficients of such an expansion.

Thus we see that smoothing has the ancillary benefit of affording 'data compression' (there being usually fewer β_m than r_i). The $\beta_m \phi_m(\tau)$ may be a simple Taylor series in time, or of a more complicated nature.

One of the major problems in the curve fitting is truncation error. An associated problem is that the fit of a large amount of data, r_i , to, say, $m = 4$ in (22) will yield values of the coefficients $\beta_0, \beta_1, \beta_2, \beta_3, \beta_4$ that may be different from the values of these coefficients when they are obtained from an even more truncated series.

Certain polynomials, called orthogonal polynomials, exhibit no change in the numerical values of the coefficients when fitted to the same data but truncated at a different point. One such set of functions having the orthogonality property is Legendre polynomials of the form:

$$f(r_i) = \sum_{m=0}^M \beta_m P_m(\tau) \quad (23)$$

where $P_m(\tau)$ is a Legendre polynomial of degree m . Such techniques are quite general in application and do not include the dynamics in the mini-arc technique via the f and g series and the nonunity value for μ .

Concern is often expressed that the smoothing process will discard valuable information from the raw data. As R. K. Merson (private com-

munication, 1965) pointed out, 95% of the information on a satellite orbit is contained in three well-spaced angular observations of the satellite. The other 5% is, of course, important for definitive orbit determination (as required for Geos C), but not in most preliminary orbit methods. One can, of course, utilize the smooth fitted curve to eliminate part of the data. Residuals (observations minus the curve fit to the observations) can be developed, the standard deviation σ can be computed, and observations that deviate more than 3σ from the fitted curve can be discarded.

Aside from the use of a nonunity μ , we still should determine the superiority of the mini-arc technique (interpreted as a smoothing process) over other data-smoothing techniques. We have used a particular quadratic fit and linear smoothing with modified epoch that involves a 16-meter departure from an unperturbed orbit and an even larger departure from a true perturbed path. We could, of course, reduce the smoothing interval down to 5 to 10 sec, but this would yield fewer data and could not reduce the error to the sub-meter range required for Geos C. A Taylor series to τ^3 could be fitted to the 1000 data points in the 100-sec interval, but this approach would require a least-squares fit to four parameters, $\beta_0, \beta_1, \beta_2$, and β_3 , rather than the three parameters p_1, p_2 , and p_3 of the mini-arc technique. Solution for four rather than three parameters involves almost twice as much computer time. Consequently, it appears that, in the context of smoothing, the mini-arc technique, with a properly 'tuned' interval, is superior to other smoothing techniques. Furthermore, the use of three rather than four parameters to represent the data yields a 25% improvement in data compression.

A mini arc could also be interpreted as a 'normal place.' Here it should be recognized that the dynamics involved in the mini-arc techniques (but missing in the conventional normal-place technique) make the mini-arc technique superior. It is even reasonable to expect a tenfold to thousandfold reduction in data processing time through use of mini arcs by utilizing them as a smoothing technique.

Acknowledgments. The research reported in this paper was accomplished under contract NAS6-1847, task order 70-12, with the guidance of R. Stanley, NASA Wallops Station, Virginia.

REFERENCES

- Arnold, K., On the influence of gravity anomalies on satellite orbits, in *Gravity Anomalies: Unsurveyed Areas, Geophys. Monogr. Ser.*, vol. 9, edited by H. Orlin, pp. 137-142, AGU, Washington, D. C., 1966.
- Baker, R. M. L., Jr., Extension of f and g series to non-two body forces, *AIAA J.*, 2(7), 1337-1339, 1964.
- Baker, R. M. L., Jr., and K. Forster, Orbit determination by linearized drag analysis, paper presented at the AIAA Astrodynamics Conference, Yale University, New Haven, Conn., August 19-21, 1963.
- Baker, R. M. L., Jr., and W. M. Makemson, *An Introduction to Astrodynamics*, 2nd ed., p. 143, Academic, New York, 1967.
- Baker, R. M. L., Jr., R. Ourston, and N. H. Schroeder, Some results of a short-arc, orbit-determination study related to the Geos C altimeter experiment, *Proceedings of the Geos 2 Program Review Meeting*, 22-24 June 1970, vol. 4, edited by Computer Sci. Corp., Falls Church, Va., 1970.
- Escobal, P., *Methods of Orbit Determination*, pp. 310 ff., John Wiley, New York, 1965.
- Jackson, F. C., Orbit uncertainty and sea-surface altimetry, *Rep. TR-70-5*, p. 5, New York Univ., New York, March, 1970.
- Merson, R. K., Some orbit determinations using visual observations, in *Trajectories of Artificial Celestial Bodies as Determined from Observations*, pp. 22-31, Springer-Verlag, Berlin, 1966.
- Stanley, H. R., N. A. Roy, and C. F. Martin, Rapid global geoid mapping with satellite altimetry, this volume, 1972.

MINI-ARC ORBIT DETERMINATION

Tracking-Station Coordinates From Geos 1 and Geos 2 Optical Flash Data

JAMES G. MARSH

Goddard Space Flight Center, Greenbelt, Maryland 20771

BRUCE C. DOUGLAS AND STEVEN M. KLOSKO

Wolf Research and Development Corporation, Riverdale, Maryland 20840

Abstract. Center-of-mass coordinates for 28 NASA MOTS and SAO Baker-Nunn camera sites have been obtained from optical flash data from Geos 1 (1965 89A) and Geos 2 (1968 002A). More than 25,000 observations in about 100 two-day arcs were used in dynamical solutions (SAO 1969 AGU gravity model). Comparison of results with local survey solutions and with solutions from deep-space vehicle tracking suggests accuracy (1σ) of about 2 meters in longitude and height and 5 meters in latitude. The relatively larger error in latitude arose from propagation of gravity-model error largely along the track of these high-inclination satellites. The results have also been compared with the solutions of the SAO 1969 standard earth for station coordinates on the North American datum. The solution of this paper is much closer to the survey results in chord length between stations. At the level of accuracy given above, the new coordinates can be regarded as uncorrelated with any particular gravity model or satellites.

The flashing lamps on the Geodetic Earth-Orbiting Satellites (Geos 1 and Geos 2) permitted literally tens of thousands of high-precision optical observations to be taken. Data coverage is excellent locally and globally, permitting both geometrical and dynamical solutions for station coordinates to be made.

The SAO 1969 standard earth [Gaposchkin and Lambeck, 1970] employs a combined method, exploiting the rich coverage of Geos 2 for geometric solutions for the North American and European datums and depending on long-arc, multiple satellite dynamical methods for other sites. In contrast, we have dynamically estimated many of the same stations from Geos data alone. There are so many optical data for Geos 1 and 2 that relatively short (2-day) orbital arcs contain enough data to determine the orbit. In addition, such arcs are so short that model error does not propagate to a large value. By combining scores of these 2-day arcs in simultaneous solutions for station coordinates, we obtained highly accurate results.

DETAILS OF SOLUTIONS

Table 1 shows the geographic distribution of the SAO Baker-Nunn and NASA Stadan and Speopt optical sites used in this study. Coverage of the North American datum is outstanding, and important contributions are also made by the Australian, South American, South African, and Tananarive datums, and many islands.

We attempted to obtain station observation geometry that would minimize the effects of model errors. This requires passes on all sides of a station and in opposite directions. Geos 1 data meet this requirement, but Geos 2 optical data do not, because they were taken primarily on S-N passes owing to satellite viewing conditions. Combined Geos 1 and 2 solutions provide very strong tracking coverage.

Table 1 also shows the number of observations used for each optical site. We examined 140 two-day arcs containing approximately 60,000 optical observations. Some 25,000 obser-

TABLE 1. Dynamically Estimated Station Positions
($a_e = 6,378,155$ meters, $1/f = 298.255$)

Location	Station	No. of Observations	Geodetic Lat.	East Long.	Spheroid Ht., meters
Blossom Point, Md.	1021	790	38°25'49.79"	282°54'48.61"	-53.7
Ft. Myers, Fla.	1022	1980	26 32 53.14	278 8 4.16	-42.0
Woomera, Australia	1024	618	-31 23 25.88	136 52 15.14	130.4
Santiago, Chile	1028	663	-33 8 58.88	289 19 53.66	710.3
Mojave, Calif.	1030	932	35 19 47.89	243 5 58.92	876.3
Johannesburg, South Africa	1031	926	-25 53 1.44	27 42 26.21	1541.0
Olifantsfontein, South Africa	9002	1544	-25 57 36.66	28 14 52.35	1570.0
St. Johns, Newfoundland	1032	179	47 44 29.27	307 16 46.14	48.0
E. Grand Forks, Minn.	1034	1869	48 1 21.53	262 59 19.51	203.2
Winkfield, England	1035	611	51 26 46.40	359 18 7.93	90.4
Rosman, N.C.	1037	1595	35 12 7.28	277 7 41.16	849.9
Orroral, Australia	1042		35 12 7.30	277 7 40.86	850.1
Woomera, Australia	1038	663	-35 37 32.68	148 57 14.85	949.6
Tananarive, Malagasy	9023	1814	-31 23 26.63	136 52 43.13	138.4
Edinburg, Texas	1043	339	-19 0 32.59	47 17 59.29	1359.8
Columbia, Mo.	7036	1139	26 22 46.52	261 40 7.25	7.8
Bermuda	7037	1540	38 53 36.24	267 47 40.87	212.5
San Juan, P.R.	7039	448	32 21 49.93	295 20 35.41	-27.0
Denver, Colo.	7040	475	18 15 28.58	294 0 23.53	-18.4
Jupiter, Fla.	7045	1371	39 38 48.14	255 23 38.47	1745.4
Sudbury, Ontario	7072	660	27 1 14.16	279 53 12.73	-37.4
Kingston, Jamaica	7075	699	46 27 21.53	279 3 10.41	221.0
Organ Pass, N.M.	7076	388	18 4 34.46	283 11 27.13	404.8
Arequipa, Peru	9001	997	32 25 24.89	253 26 48.68	1615.0
Jupiter, Fla.	9007	842	-16 27 57.21	288 30 24.53	2488.2
V. Dolores, Argentina	9010	1843	27 1 13.91	279 53 13.46	-23.0
Mount Hopkins, Ar.	9021	1024	-31 56 35.07	294 53 36.74	638.3
		497	31 41 2.95	249 7 18.36	2339.1

vations in about 100 two-day arcs were used in the final determination.

The SAO 1969 AGU gravity model [Gaposchkin and Lambeck, 1969] was used in all our work. An evaluation [Marsh and Douglas, 1971] of gravity models demonstrated the general superiority of this model before publication of the SAO 1969 standard earth [Gaposchkin and Lambeck, 1970]. The SAO 1969 standard earth produces slightly better fits to the data, but has a negligible effect on station coordinate estimation when our techniques are used.

The existence of model errors is important to any data analysis. We made a major effort to develop a strategy that would reduce the effects of model errors to a minimum. Marsh and Douglas [1971] show that satellite position error can reach 50 meters or more with even the recent SAO gravity models, largely because of uncertainty of resonant terms of the geopotential.

Model error effects of this magnitude or larger were tolerable in our solutions for two reasons. First, two-day arcs are short enough to accommodate model error, although two days is more than 1/4 of the resonant beat period for the Geos satellites. But perhaps more important is the fact that the passes were selected to be in all directions on all sites of the stations, leading to a cancelling of errors.

Since two-day orbital arcs were used for our solutions, a program to estimate geodetic parameters by Cowell's method [Martin and O'Neill, 1968] could be used with high efficiency and accuracy. A typical 60-arc solution for 20 sets of station coordinates required 3–4 hours of IBM 360/95 computer time, depending on the number of iterations required to obtain convergence. Model parameters included the complete SAO 1969 AGU gravity model, luni-

MARSH, DOUGLAS, AND KLOSKO

79

solar perturbations, radiation pressure, BIH polar motion, and UT1 data.

RESULTS

The final coordinates obtained for each station are given in Table 1. The next step is to establish reasonable estimates of the accuracy of these coordinates by comparison with other, independent solutions.

An interesting first test of station coordinates, at least on the North American datum where there are many stations, is to plot the ΔX , ΔY , ΔZ shift from the survey to center-of-mass coordinates. Figure 1 represents these transformations for the North American datum. At each station, three values are shown. The top is ΔX , the middle is ΔY , and the bottom value is ΔZ . Values are very consistent for continental stations, excluding Alaska. Among the Island sta-

tions, Jamaica and Puerto Rico also appear to be relatively consistent, but Bermuda is inconsistent, because the survey coordinates for the Bermuda camera site given in the *NASA Directory of Tracking Station Coordinates* [1970] are based on an obsolete scale (subsequently corrected by a high-precision geodimeter traverse).

The mean values and associated precision for the translation ΔX , ΔY , and ΔZ are -25.1 ± 2.8 , 162.9 ± 5.3 , and 173.5 ± 4.2 meters, respectively.

A good quantitative test of station coordinates is to compare surveyed and satellite-determined base lines. Table 2 shows the base-line differences on the North American datum for the stations given in this paper, and those obtained by *Gaposchkin and Lambeck* [1970]. It is apparent that the present solution gives better

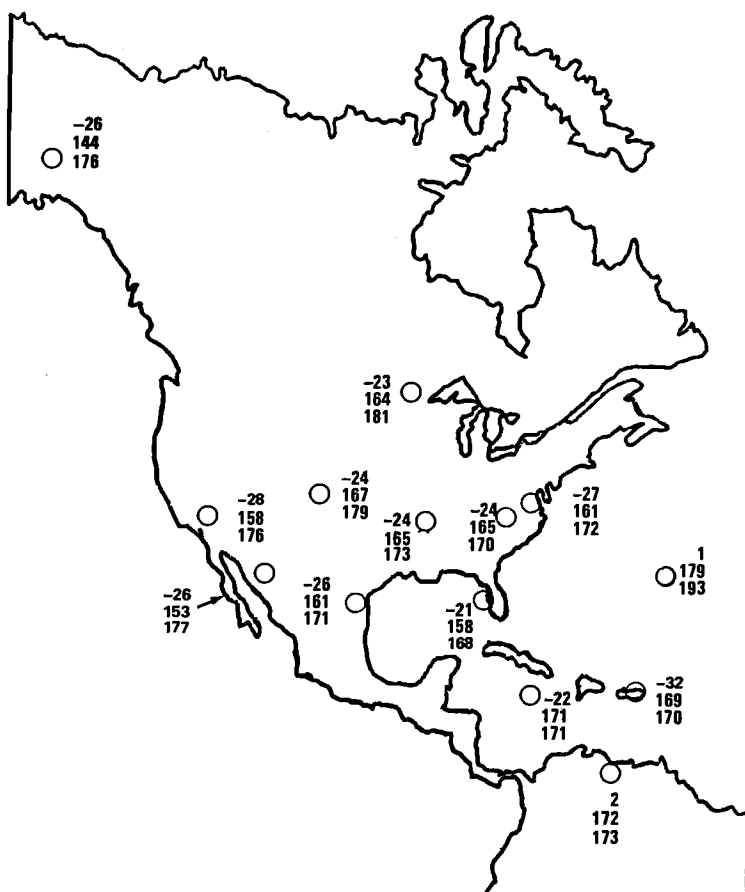


Fig. 1. NAD translations (meters) to center-of-mass coordinates.

TABLE 2. Differences in the Inter-Site Distances (meters) for Surveyed Positions on the North American Datum
(Survey minus satellite.)

GSFC									
1021*									
1030	-0.1	1030*							
1034	-0.9	-8.0	1034*						
1042	3.1	-2.0	-5.0	1042*					
7036	0.5	-2.7	-10.9	-1.8	7036*				
7037	3.5	-2.3	-4.8	-0.6	-4.4	7037*			
7045	2.9	-3.9	-0.9	-1.4	-9.3	-0.5	7045*		
7072	-3.9	-8.2	12.6	-5.5	-4.6	-7.4	-9.7	7072†	
7076	3.0	-3.3	-4.8	2.4	-2.3	-0.4	-4.5	6.5	7076‡
7040	2.4	3.2	0.2	5.6	5.1	4.7	2.7	9.4	9.9
SAO 1969 Standard Earth									
1021									
9001	-2.7	9001*							
1034	11.4	-12.8	1034						
1037	-0.8	-6.3	-2.2	1042					
7036	-11.2	-3.1	-14.9	-9.4	7036				
7037	6.7	-6.3	-6.4	0.0	-7.7	7037			
7045	3.1	-13.6	-1.6	-6.2	-16.3	-5.1	7045		
9010	-12.4	-8.9	-6.8	-1.3	-10.6	-2.2	-12.6	9010†	
7076	-30.8	-20.3	-23.9	-16.5	-18.8	-17.7	-28.9	-15.2	7076
7040	-25.5	-9.8	-12.1	-7.0	-10.3	-8.1	-16.6	-4.6	3.4

* First-order survey.

† High-precision traverse survey.

‡ First-order independent surveys transformed to the North American datum.

agreement with the survey. Of the 55 chords in Table 2 common to both solutions, only in three cases do our results differ by more than 10 meters from the survey results, and in 38 cases agreement is 5 meters or better! The SAO results show a larger random variation unrelated to chord length. It is interesting that the positions for the North American datum reported by Gaposchkin and Lambeck earlier in the AGU 1969 presentation gave slightly better agreement for intersite distances than those reported in the SAO 1969 standard earth.

A useful way to analyze interstation chords is to plot the difference between the surveyed and satellite-derived values against the interstation distance, as has been done in Figure 2 for the GSFC and SAO solutions. The GSFC E-W chords give better agreement with the survey than the others, whereas the SAO E-W chords show nothing remarkable. The situation for the GSFC solution is a result of propagation of gravity-model error largely along track, i.e., N-S for the high-inclination Geos satellites.

Also plotted in Figure 2 is Simon's rule (quoted in the *NASA Directory* [1970]) for the 1σ error to be expected for interstation distance on the North American datum. The

GSFC E-W chord differences agree very well with Simon's rule, confirming that it is an accurate estimate of the precision of surveyed interstation E-W chord lengths on the North American datum.

We have also compared our results with those obtained from tracking of deep space vehicles.

As Mottinger [1969] noted, deep space station data from interplanetary spacecraft do not yield a complete station position. The well-determined parameters are the distance of a station from the earth's spin axis and the relative longitudes of stations. The earth-fixed Z component of station position is poorly determined. Complete deep space station positions rely on independent determinations.

In no case is an optical station precisely contiguous with a deep space site. However, in all cases the stations are very close, so close that significant survey error would be regarded as unlikely. However, as is discussed later, a problem may exist with the survey for the Minitrack Optical Tracking System (MOTS) at Orroral, Australia.

The procedure used to obtain coordinates of the deep space station from the GSFC and SAO satellite solutions is as follows. The shift from

MARSH, DOUGLAS, AND KLOSKO

81

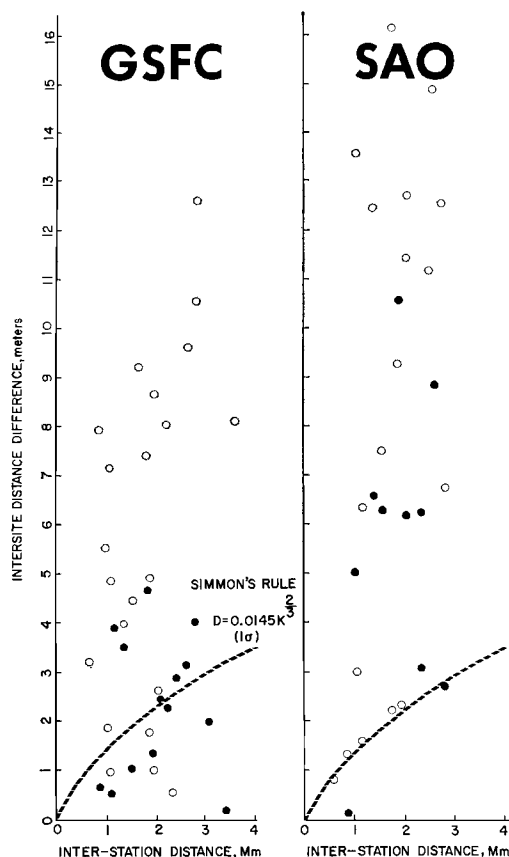


Fig. 2. Inter-site distance differences: left, GSFC; right, SAO. The solid circles represent chord differences between stations essentially east and west of one another, and the open circles are the rest.

local to center of mass in each Cartesian coordinate of the nearby satellite tracking station was calculated and then applied to the local coordinates of the deep space station. The resulting derived coordinates were then used to calculate spin-axis distances and longitude differences. A comparison of the spin-axis distances is given in Table 3 for the JPL, GSFC, and SAO solutions.

There are differences between the GSFC and SAO solutions, but the agreement is really very good. The especially close agreement of the GSFC and JPL results does suggest that the height disagreement between GSFC and SAO noted by *Marsh et al.* [1971] may be largely due to error in the SAO-determined heights. Regardless, the agreement among the investi-

gators is remarkable, especially in the light of the different techniques and satellites used.

Table 4 shows the differences in simple longitude between JPL, GSFC, and SAO positions. Here we note an inconsistency between satellite and DSS solutions. In each case, the satellite solutions are rotated with respect to the longitudes of the deep space stations, but the GSFC and JPL longitudes for Tidbinbilla are inconsistent by about $0.4''$ from the mean difference of the other three. Since the solution for Orroral alone shows a substantial inconsistency, it is possible that survey error is responsible for the discrepancy. The observed discrepancy in longitude of $0.4''$ is still rather small, being equivalent to only a little more than 10 meters. Both SAO and ourselves used optical data for the derivation of these positions, but the SAO results were obtained simultaneously with the gravity field in long (up to 30-day) multiple-arc solutions. In contrast, we were able to use short-arc (2-day) solutions in which model error does not build up excessively. The Geos flash data are so numerous that long arcs are not necessary to secure a significant amount of data.

CONCLUSIONS

Based upon the agreement with first-order surveys, tracking results from deep space stations, and gravimetrically determined heights, we conclude that our new coordinates are accurate to perhaps 2 meters in longitude and height, and 5 meters in latitude (1σ). Such errors are less than the precision of the optical data used (the rms fit being typically a little

TABLE 3. Differences between Values for Distance from the Earth's Spin Axis Obtained by Using JPL, GSFC, and SAO Solutions

Deep Space Station	No.	GSFC - JPL, meters	SAO - JPL,* meters
Goldstone	4712	-3.8	6.2
Woomera	4741	0.2	-6.3
Tidbinbilla	4742	2.0	
Johannesburg	4751	0.7	-7.0

* These values differ from those quoted by *Gaposchkin and Lambeck* [1970]. They did not use the local survey coordinates quoted in the *NASA Directory* for the JPL sites.

TABLE 4. Differences between Values for Longitude ($\Delta\lambda$) in Seconds of Arc ($0.03'' \sim 1$ meter) Obtained by Using JPL, GSFC and SAO Solutions

Deep-Space Station	No.	GSFC - JPL		SAO - JPL	
		$\Delta\lambda_1$	$(\langle\Delta\lambda\rangle - \Delta\lambda_2)^*$	$\Delta\lambda_1$	$(\langle\Delta\lambda\rangle - \Delta\lambda_1)$
Goldstone	4712	0.81	-0.03	1.04	-0.29
Woomera	4741	0.79	-0.01	0.59	0.16
Tidbinbilla	4742	0.35			
Johannesburg	4751	0.75	0.03	0.63	0.12

* Where $\langle\Delta\lambda\rangle$ is the mean longitude difference. Tidbinbilla has been excluded from the mean longitude difference calculation for GSFC; $\langle\Delta\lambda\rangle = 0.78$ for GSFC, 0.75 for SAO.

less than 2 arc sec) and less than the satellite position error resulting from uncertainty in the gravity model. Our use of multiple, relatively short-arc (2-day) solutions with passes of data taken on all sides of a station in all directions was clearly an effective way of reducing random noise and model error effects to a minimum. In addition, the comparisons with independent estimates show that it is not necessary to regard these new positions as 'belonging' in some sense to the gravity model or satellites used in their derivation.

Note added in proof. The discrepancy between our N-S chords and those of the NAD 1927 confirms the conclusion of the recent high-precision traverse that the only large error (about 10 meters) in the original North American surveys was N-S in direction from Florida up the eastern half of the United States.

Acknowledgment. We wish to acknowledge the contribution of David W. Harris of Goddard Space Flight Center. His help in analyzing the very accurate MOTS camera data was of great importance. The cooperation of the Smithsonian Astrophysical Observatory was also helpful.

REFERENCES

Gaposchkin, E. M., and K. Lambeck, New geo-

detic parameters for a standard earth (abstract), *Eos Trans. AGU*, 50, 603, 1969.

Gaposchkin, E. M., and K. Lambeck, 1969 Smithsonian standard earth (II), *Smithson. Astrophys. Observ. Spec. Rep. 315*, May 1970.

Marsh, J. G., and B. C. Douglas, Tests and comparisons of gravity models, *Celestial Mechanics*, 4, 309-325, 1971.

Marsh, J. G., B. C. Douglas, and C. F. Martin, NASA Stadan, Speopt, and laser tracking station positions derived from Geos 1 and 2 precision reduced optical and laser observations, *Space Res.*, 12, 507-514, 1971.

Martin, C. F., and B. O'Neill, The Geostar plan for geodetic parameter estimation, report on contract NAS 5-9756-132, NASA, Washington, D. C., November 1968.

Mottinger, N. A., Status of DSS location solutions for deep space probe mission: Third generation orbit determination program solutions for Mariner Mars 1969 mission, *JPL Space Programs Sum. 37-60*, vol. II, Jet Propul. Lab., Pasadena, Calif., November 30, 1969.

NASA Directory of Tracking Station Locations, prepared by Computer Sci. Corp. for Data Evaluation Branch, Manned Flight Planning and Analysis Division, Goddard Space Flight Center, Greenbelt, Md., November 1970.

Strange, W. E., S. F. Vincent, R. H. Berry, and T. G. Marsh, Detailed gravimetric geoid for the United States, this volume, 1972.

Survey Improvement and Calibration Analysis for the Air Force Eastern Test Range with Geos C

NORMAN BUSH

*Pan American World Airways, Inc., Aerospace Services Division
Patrick Air Force Base, Florida 32925*

Abstract. The results of an error analysis utilizing Geos C are presented with respect to geodetic improvement at the Air Force Eastern Test Range (AFETR) as well as at the Space and Missile Technical Evaluation Center (Samtec, which was formerly the Air Force Western Test Range). Radars were the only data source considered for the study, and data were taken from Kwajalein to Ascension. The geodetic error analysis results from a short-arc analysis are developed in terms of Cape Kennedy being the known reference station for data from Ascension to Cape Kennedy, and Vandenberg Air Force Base is the known reference station for the data from Kwajalein to the U.S. mainland. The results show that the relative survey improvement of Ascension to the Cape as well as the relative survey improvement of Kwajalein, Johnston Island, and Hawaii to Vandenberg Air Force Base can be obtained to 17 meters or better.

At the Air Force Eastern Test Range (AFETR), we have been using satellites for geodetic improvements and instrumentation calibration since 1963. Earlier projects involved the use of missiles in powered flight and free fall. A general plan utilizing satellites for geodetic improvement and calibration was formulated in 1965 [Technical Staff, 1965]. Table 1 shows a list of satellites used by AFETR from 1963 to the present time for geodetic experiments. Most recently, we completed a comprehensive geodetic improvement and radar calibration study using Geos 2, Echo 2, and Pageos [Pfingsten et al., 1970; Bush et al., 1969; Bush and Pfingsten, 1969]. For this study, we used about 75 short-arc orbits for the final survey results. The resulting survey changes for the islands of Grand Turk, Antigua, Bermuda, and Trinidad are shown in Table 2. The position changes and uncertainties are relative to Cape Kennedy.

Because of the successful use of satellites for geodetic improvement, calibration, and evaluation, particularly the Geos 2 satellite, we feel that the Geos C satellite will also contribute toward a better understanding in these areas. Since the Geos C inclination was not fixed at the writing of this paper, the geodetic error

analysis was done for the original 22° inclination as well as a 35° inclination at 1480-km orbit. The 35° inclination was chosen because it is the most favorable inclination for AFETR and the Space and Missile Technical Evaluation Center (Samtec, formerly the Air Force Western Test Range).

Because of the low inclination of Geos C, it is possible to observe from Kwajalein to Ascension in less than one arc (Figure 1). However, in this study the data from Kwajalein to the mainland are treated separately from the data from Cape Kennedy to Ascension. Restricting the analysis to two separate short arcs enables us to maintain better control for geodetic improvement and calibration, since there are fewer unknowns to contend with in separate solutions than in one comprehensive solution.

The primary AFETR objectives of Geos C are (1) to refine survey locations of pulse radar sites and to locate ship positions; and (2) to improve the calibration and evaluation of C-band pulse radar systems (land-based and shipborne).

Other objectives include a continuing study of techniques of near real-time calibration, instrumentation mathematical models, geopotential models, and refraction. This paper is only

TABLE 1. Satellites Used for AFETR Geodetic Experiments

Satellite	Orbit, km	Inclination, deg	Instrumentation	Observ. Period
Anna 1B	≈1110	50	Stellar camera	1963-1964
Geos A	≈1670	59	Stellar camera	1965-1966
Echo 1	≈1300	47	Stellar camera	1965-1966
Echo 2	575-800	81	C-band radar, stellar camera	1966-1968
Pageos	2425-5925	84	C-band radar, stellar camera	1966-1968
Geos B	1100-1600	106	C-band radar, stellar camera	1968 to present

concerned with survey location and calibration of land-based radars. The problem of ship location is treated in a separate study.

EXPERIMENTAL PLAN

There are many possible experiments that can be performed by AFETR and Samtec for geodetic improvement and instrumentation calibration. The particular experiments to be described are developed from parts of three revolutions of the 22° inclination orbit (which will be referred to as the Geos C experiment) and part of three revolutions of the 35° inclination orbit (which will be referred to as the Cal Sat experiment). Figure 1 shows the geometry for the Geos C 22° inclined orbit for three different revolutions. Of all stations of interest shown in Figure 1, only Cape Kennedy, White Sands, and Vandenberg AFB cannot observe a zenith pass. The rest of the stations are within $\pm 22^\circ$ latitude, which implies all possible geometries from an elevation angle viewpoint. Even

though Cape Kennedy cannot observe a zenith pass, there are satellite passes for which the elevation angle would be better than 40° . These same passes (good for Cape Kennedy) would also be satisfactory from Kwajalein to Ascension. Therefore, Cape Kennedy can provide a good geometric tie of Geos C to the U.S. mainland. This concept will be discussed later. Figure 2 shows the coverage for the Cal Sat 35° inclination for three different revolutions. It is possible in this case for all stations of interest to have a zenith pass. Bermuda is included in this experiment because of the higher inclination.

Although we are using the short-arc determination for geodetic ties (holding a U.S. mainland station fixed), the results will be similar to those obtained by purely geometric satellite triangulation. This was verified in our Survey Improvement Study [Bush *et al.*, 1969] using camera data. In that study, we compared survey adjustments done entirely in the intervisible

TABLE 2. AFETR Survey Changes (August 1969)

Station	Position Change,* meters	σ , meters	Uncertainty as of Aug. 1969	Uncertainty as of Sept. 1968
Grand Turk	X +0.9	2.1	1/635,000	1/330,000
	Y -6.4	1.5		
	Z -1.5	2.1		
Antigua	X +19.8	3.7	1/710,000	1/270,000
	Y -7.6	2.7		
	Z -7.9	3.4		
Bermuda †	X +21.9	4.3	1/525,000	1/270,000
	Y +4.6	2.2		
	Z +0.8	2.5		
Trinidad	X +38.4	6.1	1/480,000	1/315,000
	Y -53.9	6.7		
	Z -11.9	4.6		

* X, positive east; Y, positive north; Z, positive up.

† Changed August 1969 and September 1970.

NORMAN BUSH

85

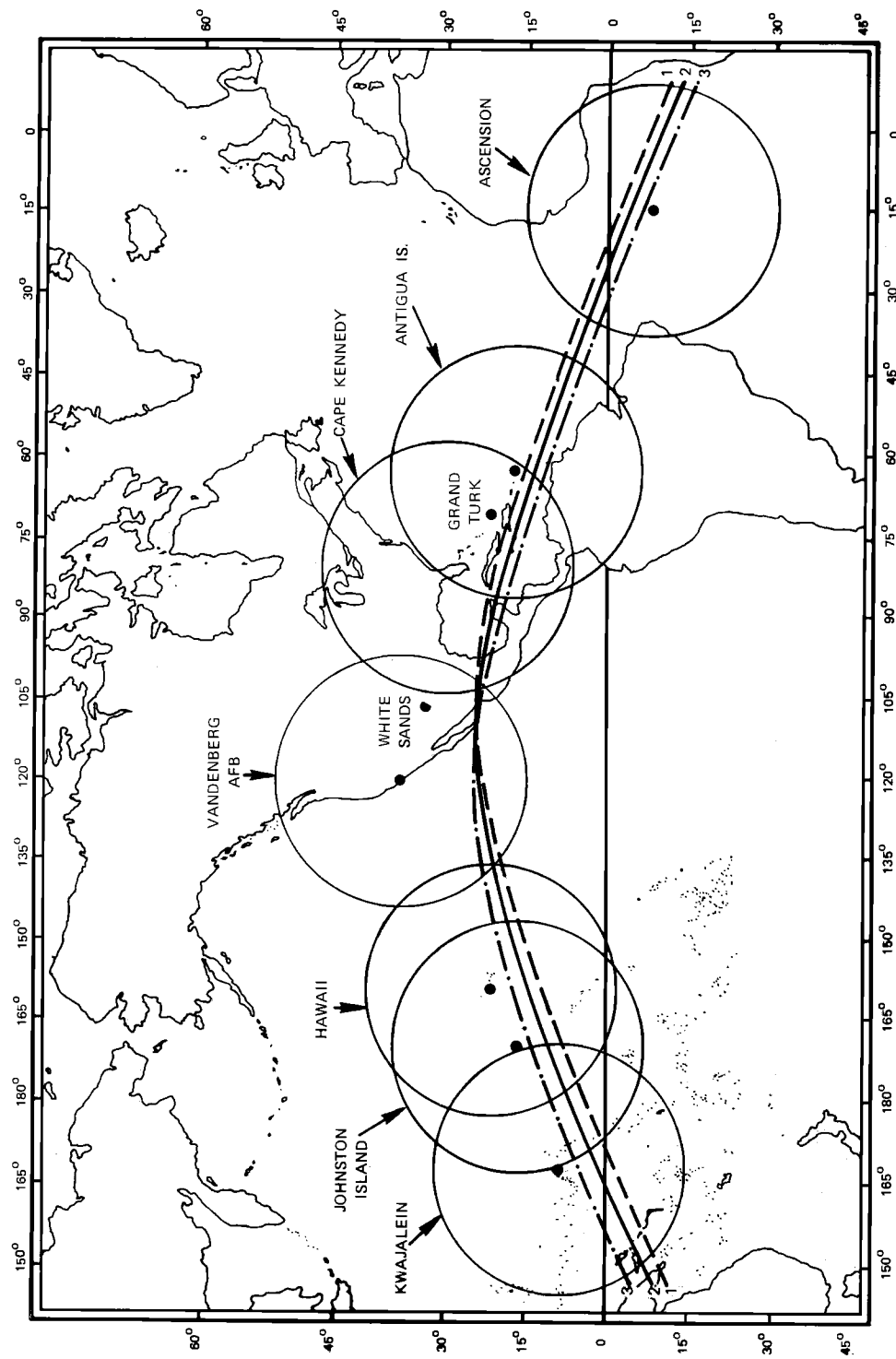


Fig. 1. Geos C coverage. Inclination, 22° ; altitude, 1110 km; minimum elevation angle, 10° .

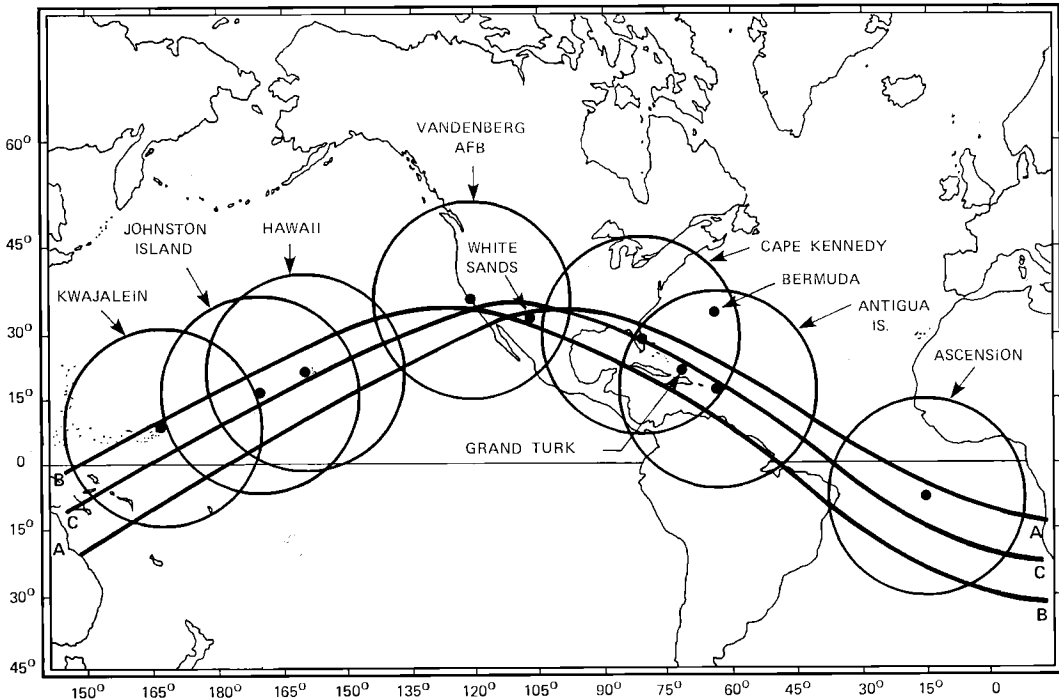


Fig. 2. Cal Sat coverage. Inclination, 35° ; altitude, 1480 km; minimum elevation angle, 10° .

mode with the survey adjustments done entirely in the orbital mode using ballistic camera data from Echo and Pageos tracks. There were no significant differences between the two solutions, indicating that, for short-arc adjustments, the orbital solution behaved like a geometric satellite triangulation. Therefore, we refer to the survey adjustments for short-arc determination as relative survey positions rather than center-of-mass positions. The long-arc techniques were not considered. If the inclination of Geos C becomes much higher than $40\text{--}45^\circ$, it will be impossible to achieve the short-arc ties described above. For example, to link Ascension to Cape Kennedy using Geos 2 (106° inclination), it is necessary to use an arc of 3 revolutions. This same problem would also occur in the Pacific for Kwajalein and the mainland.

The instrumentation considered for the short-arc experiments are pulse radars at Kwajalein, Johnston Island, Hawaii, Vandenberg AFB, White Sands, Cape Kennedy, Grand Turk, Bermuda, Antigua, and Ascension. The radar measurement uncertainties of 0.006° in azimuth, 0.007° in elevation, and 2.3 meters in range

reflect the average current values [*RCA Quality Analysis*, 1970]. It can be assumed that these values are conservative, since it might be expected that when a Geos C type satellite is in operation the measurement uncertainties would be improved.

In the experiment we are considering, there are many parameters that are solved for and there are some unmodeled effects for which we have *a priori* uncertainties. Both the adjusted parameters and the unadjusted parameters (unmodeled effects) are important in relating an accurate picture of the total uncertainty. Parameters that cannot be solved for and are considered important are carried as unmodeled effects in the error propagation. This particular decision is based on error analyses and processing of short-arc orbital data. Table 3 shows the *a priori* σ for the parameter and unmodeled effects based on current Air Force estimates. In most cases, the survey and zero set terms were carried as adjustable parameters along with the orbital elements, while refraction, geopotential, timing, and scale factors were carried as unmodeled effects. The geopotential un-

NORMAN BUSH

87

TABLE 3. Parameter and Unmodeled Effects
(*a priori* σ)

Stations	Survey σ , meters		
	X (east)	Y (north)	Z (up)
Kwajalein	51.5	51.5	28.0
Johnston Island	51.5	51.5	28.0
Hawaii	51.5	51.5	28.0
Vandenberg AFB	7.6	7.6	7.6
White Sands	1.8	1.8	1.8
Grand Turk	2.1	1.5	2.1
Antigua	3.7	2.7	3.4
Ascension	51.5	51.5	28.0
Bermuda	4.3	2.2	2.5
Azimuth	Elevation	Range	
All stations*			
Radar zero set	0.006°	0.006°	15.2 meters
Refraction†			0.03 meter
Timing			10 μ sec
Scale factor			0.5×10^{-6}

* The geopotential uncertainties are for μ , J_{22} , and K_{22} and are, respectively, 0.1×10^{-6} , 0.02×10^{-6} , and 0.09×10^{-6} .

† This uncertainty represents the residual refraction after the major correction for refraction has been applied. Measurement data is only used above 10° elevation.

modeled effects were kept to a minimum because only short-arc solutions are considered. The Cape to Ascension short arcs are about 37 min, and the Kwajalein to Cape short arcs are 44 min.

The computer program Orea [Bush *et al.*, 1970] performs the orbital error analysis for the adjusted and the unmodeled effects. The Orea program is specifically oriented toward a multiple-arc error propagation. In all the error propagation runs, survey was assumed to be constant over all arcs (three in our cases), whereas the instrumentation zero sets were taken to vary from arc to arc. In an actual operation, data are collected at a rate of 10 points/sec and edited and filtered for an output of 1 point/10 sec. The filtered data at 1 point/10 sec is considered adequate for representing the geometry of the particular orbit, especially when we are using orbital constraints. Actual survey position solutions are affected more by geometry and proper mathematical modeling than by increased sample rate. The error propagation analysis for this study was

done at 1 point/30 sec, which is a more conservative procedure than processing of 1 point/10 sec.

An indication of the geometry of the three Geos C satellite passes with respect to the observing stations is given by the point of closest approach (PCA) elevation angles shown in Table 4. These elevation angles are based on an orbital height of 1110 km and an inclination of 22°. Many of the stations have PCA elevation angles above 50°. The exceptions are Vandenberg AFB, White Sands, and the Cape, which are the highest-latitude stations. Of these three stations, the Cape has the highest elevation angle, 46° in arc 1. Vandenberg AFB would of course have the lowest elevation angle (due to its latitude), and it never exceeds 30°. Therefore, of the three U.S. mainland stations, the Cape offers the closest tie to the Geos C orbits.

GEODETIC RESULTS

A number of experimental runs were made with various combinations of radar stations in order to determine optimum situations for obtaining calibration and geodetic improvements. There were two distinct experimental groups:

1. Cape to Ascension
2. Kwajalein to Cape

Since we are only considering radar track, the Cape to Ascension track consists of the Cape, Grand Turk, Bermuda, Antigua, and Ascension. This part can be adequately covered by Geos C or Cal Sat in about 37 minutes. The other grouping includes stations Kwajalein, Johnston Island, Hawaii, Vandenberg AFB, White Sands,

TABLE 4. PCA Elevation Angles for 22° Inclination (in degrees)

Station	ARC		
	1	2	3
Kwajalein	36	51	70
Johnston Island	42	57	74
Hawaii	37	48	60
Vandenberg AFB	28	29	30
White Sands	37	36	34
Cape Kennedy	46	40	33
Grand Turk	71	48	46
Antigua	82	66	50
Ascension	59	81	75

AFETR SURVEY IMPROVEMENT AND ANALYSIS WITH GEOS C

and the Cape. The short-arc coverage for this is about 44 min.

The survey accuracy results for Cape Kennedy to Ascension are shown in Table 5 for both 22° and 35° inclinations. These results are relative accuracies with respect to Cape Kennedy, and the 1 ppm accuracy of each station is also given with respect to the Cape. The major contribution to the uncertainties in the survey location are geometry, modeled and unmodeled parameters, and measurement noise. A rerun of the Cape to Ascension experiment at a higher sampling rate, 1 point/10 sec, showed a very small change in survey accuracies, indicating dependence on these other factors.

For this limited experiment, it is apparent that the geodetic accuracy of Ascension can be considerably improved. The current accuracy of Ascension is given a priori as 51.5 meters in latitude and longitude, and the results shown in Table 5 indicate a potential accuracy of 16.6 meters or less for the 22° inclined orbits and 9.8 meters or less for the 35° inclined orbit. The Bermuda station does not appear in the 22° inclination results because of the higher latitude of the station. The Grand Turk, Bermuda, and Antigua results are not as impressive, because their a priori survey uncertainties are small initially [Bush *et al.*, 1969]. In all four radar sites, the potential survey accuracies are not too

far from 1 ppm, and it is certainly expected that a more extensive experiment would yield better results.

The survey accuracy results from Kwajalein to Cape Kennedy are given in Table 6. A number of different runs were made with these radar sites. The results from the two most pertinent runs are shown in Table 6. We considered using either Cape Kennedy or Vandenberg AFB as a mainland survey origin. There is a very slight difference in the results, and the Vandenberg origin appears to be better than the Cape origin. For both origins, the Kwajalein, Johnston Island, and Hawaii results are significantly better than the a priori survey values. A comparison of these accuracies with the listed 1 ppm are also impressive. The inclusion of the White Sands station improved the ephemeris and therefore yielded better survey accuracies.

CALIBRATION

It has been well established from previous studies and experiments [*Nicola and Bush*, 1968; *Pfingsten et al.*, 1970] that angle information in a multiple radar run does not significantly contribute to determining an accurate ephemeris. This is particularly true when the radar coverage is overlapped with other radar coverage. For the Cape to Ascension group, we have some simultaneous coverage between the Cape, Grand Turk, Bermuda, and Antigua. Ascension does not overlap with Antigua because of the distances and the 10° elevation cutoff. There would be a greater angle contribution from a radar when there is no multiple coverage. However, the angle calibration is still very good in this situation, since we are able to obtain a fairly well defined orbit between the stations of interest. As Table 3 shows, all the *A* and *E* zero set biases were assumed a priori to be 0.006° and the *R* bias to be about 15 meters. The zero set bias recoveries in range for all stations in the solution varied from 2.7 to 3.7 meters.

All the angle zero set bias recoveries were excellent and indicated a potential recovery of less than 0.0017° (i.e., about 6 arc sec). In a self-calibrating situation like this one, we would not expect to obtain too much information about the range channel (since it is the determining measurement in obtaining the ephemeris), but we can do some detailed analysis on the angle

TABLE 5. Expected Survey Accuracy, Cape Kennedy to Ascension (in meters)

Station*	22°		35°	1 ppm to Cape
	Inclination σ	Inclination σ		
Grand Turk	<i>X</i> 1.4		1.1	1.22
	<i>Y</i> 1.4		1.3	1.22
	<i>Z</i> 1.6		1.4	1.22
Bermuda	<i>X</i>		2.4	1.58
	<i>Y</i>		2.0	1.58
	<i>Z</i>		2.1	1.58
Antigua	<i>X</i> 2.1		1.7	2.30
	<i>Y</i> 2.5		2.1	2.30
	<i>Z</i> 2.3		2.0	2.30
Ascension	<i>X</i> 9.0		7.7	8.23
	<i>Y</i> 16.6		9.8	8.23
	<i>Z</i> 10.6		9.2	8.23

* *X*, east; *Y*, north; *Z*, up.

NORMAN BUSH

89

measurements. The angle analysis can be very meaningful when radars are used individually to obtain missile trajectory information. Satellite-determined angle biases can be used when we have established short- or long-term stability of the error terms. In some cases, it is even possible to have near real-time calibration between satellites and, say, a missile launch. In this way, the angle calibrations become more meaningful, since they are determined the same day the missile is tested. This is the only way to assure a dynamic pre or post calibration of the radar system.

A similar situation for the radar bias recoveries is seen for the Kwajalein to Cape group. There is some overlap between Kwajalein, Johnston Island, and Hawaii, and a second overlap of Vandenberg AFB and White Sands. Cape Kennedy does not overlap White Sands, but the Cape station is important because it is the closest mainland station to the orbit. This enables a better mainland tie to Kwajalein, Johnston Island, and Hawaii. As is expected, the range bias σ 's recoveries (2.7 to 4.3 meters) are similar to the AFETR values, since the geometry is fairly similar. The angle bias σ 's were also less than 0.0017°.

As part of this error model study, the effect and possibility of meaningful recovery of other error model terms in the range channel were analyzed. The other error model terms were residual refraction, timing, and scale factor. The a priori uncertainties of these terms are given in Table 3. The error model study indicated that improvement of the a priori information of these terms with the short-arc analysis could not be achieved. The existing hypothesized biases in zero set and survey were much greater than the residual refraction, timing, and scale factor. For the angle measurements, there are some possibilities that error model terms other than the zero set bias could be recovered. Since it is possible in the angle measurement to recover angle biases to within 0.0017°, any angle error model terms that would be 0.0017° or larger might also be recovered. The successful determination of these terms is a function of the magnitude of the bias, as well as the correlation among the error model terms to be recovered. A good statistical analysis procedure that can be used is the multiple regression technique. This technique has been used and described in earlier reports [Bush, 1964; Technical Staff, 1965].

EPHEMERIS ACCURACY

The ephemeris accuracy is primarily a function of the measurement errors, the measurement bias uncertainties, survey errors, and geometry. Only one arc is used to show position accuracies from the Geos C in Figure 1 and the Cal Sat in Figure 2. Although Figures 1 and 2 show the arcs continuously going from Kwajalein to Ascension, the error analysis results were based on assuming that the arcs ended (or started) with Cape Kennedy. The adjusted or modeled parameters were the orbital elements, survey, and the zero set biases; the unmodeled parameters were generally refraction and geopotential uncertainties. One of the preliminary unmodeled studies investigated the effects of timing and scale factor and found these to be insignificant, and so they were not considered.

The total position accuracy for Geos C (22° inclination), Cape Kennedy to Ascension, is given in Figure 3. The Cal Sat (35° inclination), Cape Kennedy to Ascension, is shown in Figure 4. The time coverages for each radar station are shown at the bottom of each figure. The Cal Sat results in Figure 4 are much better than the results in Figure 3 because of the improved geometry for a higher inclination. The ephemer-

TABLE 6. Expected Survey Accuracy, Kwajalein to Cape Kennedy (in meters)
(22° inclination.)

Station*		Survey Origin		
		Cape Kennedy σ	Vandenberg AFB σ	1 ppm to Vandenberg AFB
Kwajalein	X	13.1	13.4	9.1
	Y	18.3	16.8	9.1
	Z	13.7	14.0	9.1
Johnston Island	X	7.9	8.2	6.1
	Y	14.0	12.2	6.1
	Z	9.4	9.4	6.1
Hawaii	X	6.4	6.1	5.5
	Y	13.4	11.6	5.5
	Z	9.1	8.8	5.5
Vandenberg	X	2.4		0
	Y	5.5		0
	Z	5.8		0
White Sands	X	1.5	1.2	
	Y	1.8	1.8	
	Z	1.8	1.8	
Cape Kennedy	X		3.7	
	Y		6.1	
	Z		5.8	

* X, east; Y, north; Z, up.

AFETR SURVEY IMPROVEMENT AND ANALYSIS WITH GEOS C

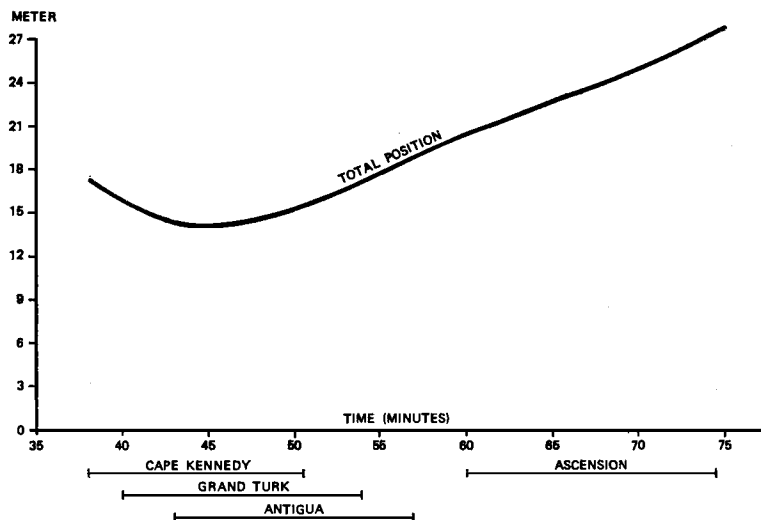


Fig. 3. Geos C ephemeris accuracy, Cape Kennedy to Ascension.

eris accuracies in Figures 3 and 4 are best over the Cape Kennedy area, where the greatest overlap between the Cape, Grand Turk, Bermuda, and Antigua occurs. Ascension is tied in with the uprange configuration through the orbital fit yielding positional uncertainties in the vicinity of 10 to 20 meters for Cal Sat and 20 to 27 meters for Geos C. The individual arc ephemeris accuracy of Ascension is not as good as the Ascension survey adjustment (Table 5), because the survey adjustment is based on data obtained from 3 arcs.

The total position accuracy for the Kwajalein

to Cape Kennedy arc is given in Figure 5. The ephemeris errors are smallest when Vandenberg AFB radar is tracking, because of the favorable geometry, and this probably explains why the survey results obtained by using Vandenberg AFB as the survey origin, are slightly better than the survey results obtained by using the Cape as the origin (Table 6).

CONCLUSIONS

The potential accuracy improvements in the geodetic and calibration areas for AFETR and Samtec make the Geos C and Cal Sat satel-

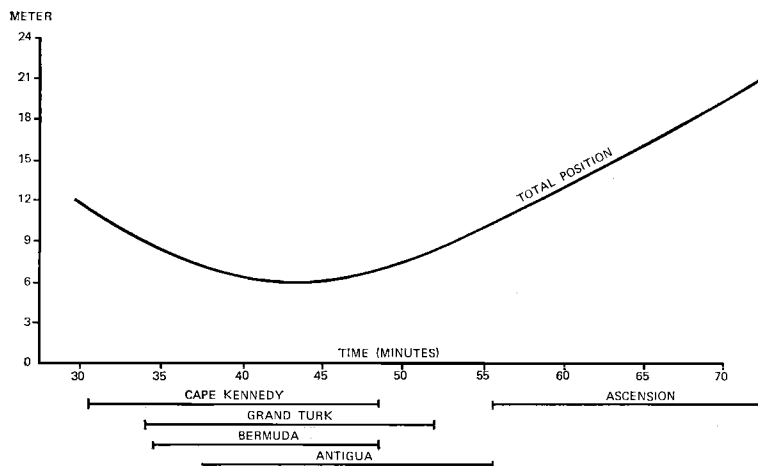


Fig. 4. Cal Sat ephemeris accuracy, Cape Kennedy to Ascension.

NORMAN BUSH

91

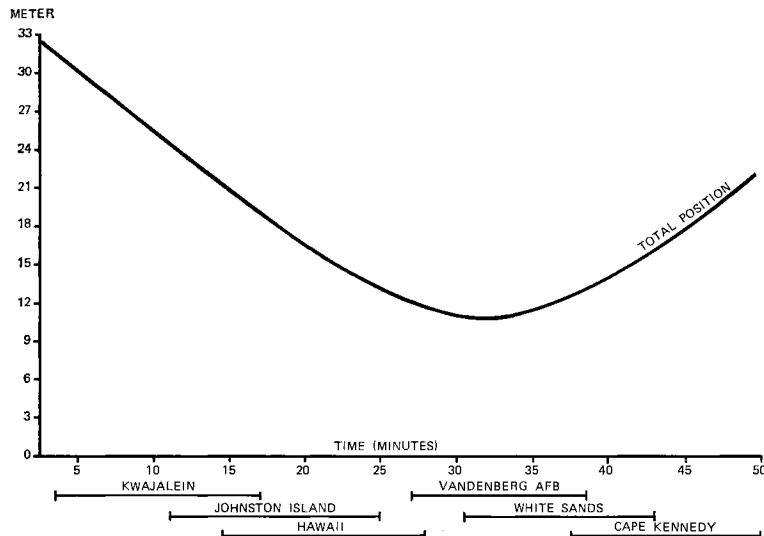


Fig. 5. Geos C ephemeris accuracy, Kwajalein to Cape Kennedy.

lites very useful objects. Even though the proposed low inclination of 22° for Geos C is not optimum for Vandenberg AFB or Cape Kennedy, it still provides a means by which geodetic improvements can be made. The more desirable inclination of 35° for Cal Sat does offer more geodetic improvements for the distant stations like Ascension and Kwajalein. Too high an inclination, like that of Geos 2 (106° or 74° retrograde), makes it impossible to tie Kwajalein to the U.S. mainland or Ascension to Cape Kennedy by short-arc techniques. The short-arc relative geodetic tie is very similar to a point-by-point geometric tie and is important for certain Air Force purposes.

The results presented in this study based on only three short arcs are impressive, so that a longer experiment would certainly be expected to yield significant geodetic improvements. It is hoped that satellites like Geos 2, Geos C, and Cal Sat are available so that a continuing geodetic calibration and evaluation program can be maintained.

Acknowledgment. I would like to thank H. L. Jury for his valuable comments and technical assistance during the preparation of this report.

REFERENCES

Bush, N., Statistical regression analysis for the STAFF program, *Tech. Memo 17, ETV-TM-*

64-10, Pan Amer. World Airways, Patrick AFB, Fla., 25 pp., 1964.

Bush, N., The effect of unmodeled errors on orbital estimation, *Rep. AFETR TR-68-9*, Pan Amer. World Airways, Patrick AFB, Fla., 31 pp., 1968.

Bush, N., and D. R. Pfingsten, Mistram MRS survey qualification study, *Rep. ETV-TM-70-47*, Pan Amer. World Airways, and RCA Int. Service Corp., Patrick AFB, Fla., 19 pp., 1969.

Bush, N., D. R. Pfingsten, J. A. Greene, et al., Mistram MRS survey improvement study, *Rep. AFETR TR-69-6*, Pan Amer. World Airways and RCA Int. Service Corp., Patrick AFB, Fla., 87 pp., 1969.

Bush, N., L. Nicola, and B. F. Young, Orea, orbital error analysis program, *Tech. Memo 114, ETV-TM-70-61*, Pan Amer. World Airways, Patrick AFB, Fla., 80 pp., 1970.

Nicola, L., and N. Bush, An investigation of orbit determination with angular data, *Tech. Staff Memo 94*, Pan Amer. World Airways, Patrick AFB, Fla., 38 pp., 1968.

Pfingsten, D. R., J. E. Pinion, J. A. Greene, and N. Bush, Radar calibration (with the use of satellites), *Rep. ETV-TM-70-98*, RCA Int. Service Corp. and Pan Amer. World Airways, Patrick AFB, Fla., 36 pp., 1970.

RCA Quality Analysis, *RCA Quality Analysis Quart. Accuracy Bull. 36*, RCA Int. Service Corp., Patrick AFB, Fla., 25 pp., 1970.

Technical Staff, Pan Amer. World Airways, ASD, and RCA Int. Service Corp., AFETR plan for use of calibration satellites for calibration and evaluation of range instrumentation, Patrick AFB, Fla., 179 pp., 1965.

3. Physical Geodesy: Theory

Analysis of Methods for Computing an Earth Gravitational Model from a Combination of Terrestrial and Satellite Data

JOHN HOPKINS

*Aeronautical Chart and Information Center
St. Louis, Missouri 63118*

Abstract. As a result of inadequate data, gravitational models derived from either terrestrial or satellite data alone do not satisfy present and anticipated needs. Since low-degree geopotential coefficients are better determined from satellite data, whereas higher-degree coefficients are better determined from terrestrial data, the best approach appears to be the combination of terrestrial and satellite data to take advantage of the best properties of each. Methods of Rapp, Kaula, Kohnlein, Ballew, Mancini, and Bjerhammar are described and tested. This analysis points to Mancini's method as the best.

Most applications of gravity data require a worldwide knowledge of the earth's gravity field. Such knowledge may take the form of a set of geopotential coefficients or mean gravity anomalies. Typical applications are the use of Stokes' formula for the determination of geoid height and the computation of gravitational force at satellite altitudes. Unfortunately, insufficient surface gravity data exist for developing mean anomalies over the entire earth's surface from observations. However, several valid methods have been used to extend gravity data into these gravimetrically unsurveyed areas, e.g., extrapolations by gravity-geophysical correlation techniques and gravity anomaly covariances. The state of the art of satellite geodesy is such that the low-degree coefficients and certain resonance-derived terms of a geopotential model can be accepted as valid and appropriate for application at satellite altitudes. However, discrepancies of undesirable magnitude are noted when different geopotential models are used on the earth's surface. An earth gravitational model

is needed that will satisfy the requirements of applications at the earth's surface and in space. Obviously, this model must be based on a combination of surface and satellite-derived data. This paper examines several of the methods that have been prepared for this purpose. Numerical results obtained are presented as the rationale for selecting the method to be used.

COMBINATIONS OF TERRESTRIAL GRAVITY DATA WITH SATELLITE-DERIVED GEOPOTENTIAL COEFFICIENTS

Several methods compare quantities derived from terrestrial data with the values of these quantities derived from the satellite coefficients as a basis for a least squares adjustment of the satellite coefficients as a basis for a least squares adjustment of the satellite coefficient set. These methods differ in the quantities that are compared.

Rapp's method. The mathematical structure of Rapp's [1967] approach is based on the comparison of terrestrial mean free-air gravity

anomalies Δg_T with similar quantities computed from a set of satellite-derived geopotential coefficients. For each available mean anomaly, there is a residual w_k . The set of residuals comprises the misclosure vector W . An individual residual is given by

$$w_k = \Delta g_T - \langle \gamma \rangle \sum_{n=2}^N (n-1) \bar{x}_n(\phi, \lambda) \quad (1)$$

where $\langle \gamma \rangle$ is the mean value of gravity over the earth's surface; $\bar{x}_n(\phi, \lambda) = \sum_{m=0}^n (\bar{C}_{nm} \cos m\lambda + \bar{S}_{nm} \sin m\lambda) \bar{P}_{nm}(\sin \phi)$; \bar{C}_{nm} , \bar{S}_{nm} are normalized geopotential coefficients; ϕ , λ are geodetic latitude and longitude of the centroid of the mean anomaly quadrangle; $\bar{P}_{nm}(\sin \phi)$ is the normalized associated Legendre function; and N is the maximum degree of satellite-derived coefficients. The elements of the observation equation matrix B (i.e., the matrix of $\partial W / \partial \bar{C}_{nm}$...) are given by

$$b_{kj} = -\langle \gamma \rangle (n-1) \bar{P}_{nm}(\sin \phi) \cos m\lambda \quad (2)$$

$$b_{kj} = -\langle \gamma \rangle (n-1) \bar{P}_{nm}(\sin \phi) \sin m\lambda$$

where the index j is defined by the sequence of geopotential coefficients $\bar{C}_{20}, \bar{C}_{21}, \bar{S}_{21}, \bar{C}_{22}, \bar{S}_{22}, \dots$.

The corrections V_x to the geopotential coefficients are given by

$$V_x = -(B^T P_0 B + P_x)^{-1} B^T P_0 W \quad (3)$$

where P_0 , P_x are the covariance matrices of observed anomalies and the satellite-derived potential coefficients, respectively. P_0 and P_x are usually assumed to be diagonal, the nonzero elements being the inverses of the a priori variances of the mean anomalies and the satellite-derived coefficients, respectively. The mean anomalies must be weighted by $\cos \phi$ if the mean anomaly quadrangles are defined in terms of a given meridian and parallel interval. The corrections given by (3) are then added to the previous values of the satellite-derived geopotential coefficients. An important distinction of Rapp's method is that a worldwide field is not required.

Kaula's method. The mathematical structure of Kaula's [1966] approach centers on the comparison of a given coefficient \bar{C}_{nm}^* or \bar{S}_{nm}^* derived from satellite data with one computed from the set of surface mean free-air anomalies, the latter being computed by

$$\begin{aligned} \bar{C}_{nm} &= \frac{1}{4\pi(n-1)\langle \gamma \rangle} \\ &\cdot \int_{\sigma} \Delta g \bar{P}_{nm}(\sin \phi) \cos m\lambda d\sigma \\ \bar{S}_{nm} &= \frac{1}{4\pi(n-1)\langle \gamma \rangle} \\ &\cdot \int_{\sigma} \Delta g \bar{P}_{nm}(\sin \phi) \sin m\lambda d\sigma \end{aligned} \quad (4)$$

where $d\sigma$ is the surface element, and integration is to be taken over the surface of the sphere. The coefficient residuals w_i are

$$\begin{aligned} w_i &= \bar{C}_{nm}^* - \bar{C}_{nm} \\ w_i &= \bar{S}_{nm}^* - \bar{S}_{nm} \end{aligned} \quad (5)$$

The elements of the observation equation matrix (the matrix of $\partial W / \partial \Delta g$ in this case) are

$$b_{ki} = -\frac{1}{4\pi(n-1)\langle \gamma \rangle} \bar{P}_{nm}(\sin \phi) \cos m\lambda d\sigma \quad (6)$$

$$b_{ki} = -\frac{1}{4\pi(n-1)\langle \gamma \rangle} \bar{P}_{nm}(\sin \phi) \sin m\lambda d\sigma$$

and the corrections to the geopotential coefficients are obtained from

$$V_x = -[(B P_0^{-1} B^T)^{-1} + P_x^{-1} (B P_0^{-1} B^T)^{-1} W] \quad (7)$$

Kaula's approach requires a worldwide surface gravity field and a priori variance of the input (satellite-derived) geopotential coefficients. If the variances are not available, corrections to the input coefficients can be found directly from (5), since (7) would reduce to

$$V_x = I W \quad (8)$$

where I is the identity matrix. The required worldwide mean gravity anomaly field can be produced by use of gravity anomaly auto-covariances or gravimetric-topographic cross-covariances in the manner discussed by Kaula [1966].

Kohnlein's method. Mathematically, Kohnlein's [1967] approach parallels that of Rapp [1967] and can be considered a refinement of it. For those quadrangles that contain adequate observational data, equation 1 can be applied directly. For quadrangles with insufficient or no gravity observations, a synthetic observation computed from

JOHN HOPKINS

95

$$\Delta g = \langle \gamma \rangle \sum_{n=2}^N (n-1) \bar{\chi}_n(\phi, \lambda) \quad (9)$$

can be used. But, this is precisely equal to the last part of the righthand side of equation 1, so that the gravity anomaly residual vanishes. The solution proceeds through (2) and (3) as in Rapp's method. To prevent these observations from biasing the solution, the corresponding elements of P_o in (3) can be adjusted to diminish their weight. Again, the corrections computed by (3) are added to the previous values of the geopotential coefficients.

COMBINATIONS OF NORMAL EQUATIONS
DERIVED FROM TERRESTRIAL DATA WITH
NORMAL EQUATIONS DERIVED FROM
SATELLITE DATA

Some methods combine normal equations computed from terrestrial data with those derived from satellite observations. *Bjerhammar* [1967] has shown that a simple summation of reduced normal equations will suffice. The resultant summed normal equations are then solved to yield corrections to an initial geopotential coefficient set.

Ballew's method. In *Ballew's* [1966] approach, the normal equations for the terrestrial gravity data are derived by comparing, as in Rapp's approach, the value of the observed mean free-air anomaly with an anomaly value computed from the input set of satellite-derived geopotential coefficients. The gravity anomaly residual $w_{\sigma k}$ is computed by an equation slightly more complicated than (1), i.e.,

$$w_{\sigma k} = \Delta g_T - \frac{GM}{r^2} \sum_{n=2}^N (n-1) \left(\frac{a_e}{r} \right)^n \bar{\chi}_n(\phi, \lambda) \quad (10)$$

where a_e is equatorial radius of the earth ellipsoid, r is the geocentric radius to a point on the ellipsoid, and GM is the gravitational constant times mass of the earth. Equation 10 reduces to 1 if a spherical approximation is used.

Corrections to the geopotential coefficients determined solely from terrestrial gravity data can be obtained by solving

$$V_x = -(B^T P_o B)^{-1} B^T P_o W_g \quad (11)$$

At this point, Ballew's method further differs from Rapp's approach in that no a priori con-

straints (the P_x matrix) are imposed in (11) as in (3). However, these are imposed after introducing the satellite-derived normal equations and any supplementary constraints. As a result, (11) now becomes

$$V_x = - \left[\alpha B_G^T P_o B_G + \sum_{i=1}^m \beta_i (B_S^T B_S)_i + \sum_{k=1}^n S_k + P_x \right]^{-1} \left[\alpha B_G^T W_g + \sum_{i=1}^m \beta_i (B_S^T W_S)_i \right] \quad (12)$$

where

B_G is the observation equation matrix for terrestrial data.

B_S is the observation equation matrix for satellite data.

S_k is the supplementary constraint (diagonal) matrix.

W_g is the vector of gravimetrically derived mean gravity anomaly residuals.

W_S is the vector of satellite-derived mean gravity anomaly residuals.

α, β are weight factors.

m is the number of satellites.

n is the number of supplementary conditions.

The initial values of the geopotential coefficients are then corrected by (12).

Ballew's approach is evidently an extension of Rapp's technique in that Ballew has added a number of independent satellite equations to the basic equations proposed by Rapp. In theory, any number of satellite normal equations can be incorporated into Ballew's final solution, thereby broadening the data base. Improved earth gravitational model solutions could be produced as new data became available.

Mancini's method. *Mancini's* [1968] method embodies the same principle as Ballew's approach, i.e., the summation of normal equations from satellite observations with those derived from terrestrial gravity data. However, Mancini's handling of the gravity data is unique among the different data combination methods. He develops a gravity residual, rather than a gravity anomaly residual, expressing it in the form

$$w_k = \frac{g_T r^2 + \omega^2 r^3 \cos^2 \phi}{GM} - 1 - \sum_{n=2}^N (n+1) \left(\frac{a_e}{r}\right)^n \tilde{x}_n(\phi, \lambda) \quad (13)$$

where g_T is the value of gravity on the earth's surface, r is the total radius vector (sum of geocentric radius vector and geoid height), and ω is the earth's angular rate of rotation. Gravity on the earth's surface is reconstructed from available surface gravity anomalies using the equation

$$g_T = \Delta g_T + \gamma - (\partial g / \partial h) h \quad (14)$$

where γ is the individual theoretical (ellipsoidal) value of gravity, h is the mean elevation of gravity anomaly quadrangle, and $\partial g / \partial h$ is the free-air gravity reduction. Geoid heights N are involved in obtaining the values of r needed in (13). N is first determined from the initial set of geopotential coefficients, improved estimates being obtained from successively corrected coefficients, from

$$N = \frac{GM}{\gamma r} \left\{ \left[\sum_{n=2}^N \left(\frac{a_e}{r}\right)^n \tilde{x}_n(\phi, \lambda) \right] - \left(\frac{a_e}{r}\right)^2 \bar{C}_{20}' \bar{P}_{20}(\sin \phi) - \left(\frac{a_e}{r}\right)^4 \bar{C}_{40}' \bar{P}_{40}(\sin \phi) \right\} \quad (15)$$

where \bar{C}_{20}' , \bar{C}_{40}' are zonal harmonic coefficients of the reference ellipsoid. Corrections to the geopotential are obtained from

$$V_x = - \left[B_G^T P_0 B_G + \sum_{i=1}^m (B_S^T B_S)_i + P_x \right]^{-1} \cdot \left[B_G^T W_G + \sum_{i=1}^m B_S^T W_S \right] \quad (16)$$

Iterations of the corrected coefficients through the solution can be made to improve the accuracy. Usually two or three iterations will suffice.

Bjerhammar's method. The philosophy of Bjerhammar's [1967] approach is to include reduced normal equations based on terrestrial gravity data, satellite triangulation results, Doppler and optical satellite data, and astrogeodetic

deflections of the vertical. The gravity anomalies are normally reduced to the geoid, the geoid initially being approximated by a sphere. Peculiar to the Bjerhammar method is the introduction of an analytical reference surface to which all free-air anomalies are reduced.

The solution is started by expressing the mean anomalies in a spherical harmonic expansion

$$\Delta g = \frac{GM}{r^2} \sum_{n=2}^N (n-1) \left(\frac{r_0}{r}\right)^n \chi_n(\phi, \lambda) \quad (17)$$

where r_0 is the radius of the reference surface, and the coefficients and Legendre functions in χ_n are not normalized.

Satellite triangulation results are incorporated in Bjerhammar's method in the form of geocentric distances (r_i):

$$r_i = a_e + \frac{GM}{r_i \gamma} \left[\sum_{n=2}^N \left(\frac{r_0}{r_i}\right)^n \chi_n(\phi, \lambda) \right] + \frac{1}{\gamma} \int_{r_0}^{r_i} g_T dh \quad (18)$$

where dh is the height differential.

The equations for computing gravimetric deflection of the vertical components using a spherical harmonic expansion and satellite-derived geopotential coefficients are:

$$\xi_i = \frac{GM}{\gamma r^2} \sum_{n=2}^N \frac{1}{r^n} \sum_{m=0}^n m(-C_{nm} \cos m\lambda + S_{nm} \sin m\lambda) \quad (19)$$

$$\eta_i = \frac{GM}{\gamma r^2} \sum_{n=2}^N \frac{1}{r^n} \cdot \sum_{m=0}^n (C_{nm} \cos m\lambda + S_{nm} \sin m\lambda) \cdot [P_{n(m+1)}(\sin \phi) - m \tan \phi P_{nm}(\sin \phi)] \quad (20)$$

After using satellite-derived geopotential coefficients in (17), (18), (19), and (20) to obtain computed quantities, residuals are formed by subtracting from the computed quantities similar values obtained from observational data.

The observation equation matrices are B_o , B_T , B_t , and B_n for terrestrial gravity, triangulation radii, and deflection component data, respectively. The solution for the corrections to the geopotential coefficients is given by

JOHN HOPKINS

97

TABLE 1. Standard Deviations for Selected Geopotential Coefficients

Coefficients	Method					
	Rapp	Kaula	Kohnlein	Ballew	Mancini	Bjerhammar
$\langle C_{21} \rangle$	2.722×10^{-8}	2.354×10^{-7}	1.211×10^{-7}	3.794×10^{-7}	2.330×10^{-12}	5.907×10^{-8}
$\langle C_{22} \rangle$	2.080×10^{-8}	2.021×10^{-7}	1.213×10^{-7}	1.955×10^{-7}	1.726×10^{-12}	3.947×10^{-8}
$\langle C_{30} \rangle$	1.629×10^{-8}	1.318×10^{-7}	5.877×10^{-8}	1.923×10^{-7}	2.090×10^{-12}	4.842×10^{-8}
$\langle C_{31} \rangle$	1.423×10^{-8}	1.232×10^{-7}	6.477×10^{-8}	1.853×10^{-7}	2.115×10^{-12}	5.885×10^{-8}
$\langle C_{32} \rangle$	1.194×10^{-8}	1.085×10^{-7}	5.807×10^{-8}	1.314×10^{-7}	1.333×10^{-12}	3.365×10^{-8}
$\langle C_{33} \rangle$	1.010×10^{-8}	9.923×10^{-8}	5.708×10^{-8}	1.221×10^{-7}	1.236×10^{-12}	3.133×10^{-8}
$\langle C_{41} \rangle$	1.084×10^{-8}	8.727×10^{-8}	4.249×10^{-8}	1.373×10^{-7}	2.012×10^{-12}	5.669×10^{-8}
$\langle C_{42} \rangle$	8.773×10^{-9}	7.940×10^{-8}	4.284×10^{-8}	1.173×10^{-7}	1.284×10^{-12}	3.643×10^{-8}
$\langle C_{43} \rangle$	7.748×10^{-9}	7.108×10^{-8}	3.794×10^{-8}	9.106×10^{-8}	9.960×10^{-13}	2.630×10^{-8}
$\langle C_{44} \rangle$	6.625×10^{-9}	6.579×10^{-8}	3.761×10^{-8}	8.971×10^{-8}	9.837×10^{-13}	2.699×10^{-8}

$$\begin{aligned}
V_x = & - \left[\alpha B_G^T P_0 B_G + \beta B_T^T B_T + \gamma B_\xi^T B_\xi \right. \\
& + \delta B_\eta^T B_\eta + \sum_{i=1}^m \epsilon_i (B_S^T B_S)_i \left. \right]^{-1} \\
& \cdot \left[\alpha B_G^T P_0 W_G + \beta B_T^T W_T + \gamma B_\xi^T W_\xi \right. \\
& + \delta B_\eta^T W_\eta + \sum_{i=1}^m \epsilon_i (B_S^T W_S)_i \left. \right] \quad (21)
\end{aligned}$$

where $\alpha, \beta, \gamma, \delta, \epsilon$ are weight factors for each class of data.

Bjerhammar also includes in his solution terms for the station coordinates with contributions from the dynamic satellite (Doppler or optical) equations and the geometric satellite triangulation equations. This approach is probably the most comprehensive of those in the literature.

NUMERICAL TESTING OF THE VARIOUS METHODS

To evaluate the several methods discussed, computer programs were written for each, and all were tested with the same data. The mean gravity anomaly field used was computed from the geopotential coefficient set associated with the 1969 Smithsonian standard earth (II) [Gaposchkin and Lambeck, 1970]. Mean anomalies were computed for the 410 equal-area 10° by 10° squares according to the scheme of Zhongolovich [1952]. The geopotential coefficients used as initial estimates were a complete set from degree (n) 2 and order (m) zero through $n = m = 10$. This set was computed by the

independent method, unknown anomalies being set to zero. Random number processes were used to assign elements to the P_0 and P_z matrices. Error covariances of the computed coefficients were determined by multiplying the elements of the inverse matrix by an unbiased estimate of the variance of unit weight [Hamilton, 1964]. With \bar{C}_{20} and \bar{C}_{40} constrained to zero by setting $\sigma \bar{C}_{20} = \sigma \bar{C}_{40} = 10^{-20}$, the coefficients selected for comparison were $\bar{C}_{n,m}$ through $n = m = 10$. Values of their accuracies are given in Table 1 for degree and order up to 4.

It is emphasized that in all these tests the quoted accuracies reflect internal consistencies only. They say nothing about the accuracy of the data that went into the computation of the parameters.

RECOMMENDED DATA COMBINATION METHOD

On the basis of the standard deviations of the geopotential coefficients shown in Table 1, Mancini's method is selected as the approach that can provide the best definition of the earth's gravitational field. It is not essential that the satellite-derived geopotential set which is to undergo correction have error variances available for each coefficient. Also, a worldwide mean gravity anomaly field is not required, but one can be obtained by extrapolating data into unobserved areas using correlation techniques or gravity anomaly covariances.

Of the several methods, one might be tempted to select that of Bjerhammar because it incorporates a variety of data types. Yet, the gravimetric and astrogeodetic data are generally from the same areas; therefore, these sources are

COMBINATION OF TERRESTRIAL AND SATELLITE DATA

somewhat correlated. There are really only two truly independent data types, surface-gravity and satellite-perturbation data (as in Ballew's method), for determining geopotential coefficients.

REFERENCES

- Ballew, R. W., *Consideration of the Error of Omission Due to Limited Parameters Derived from the Geopotential Function*, The Aeronomical Chart and Information Center, St. Louis, Mo., 1966.
- Bjerhammar, A., *A Coalescent World Geodetic System*, U.S. Army Engineer Geodesy, Intelligence and Mapping Research and Development Agency, Fort Belvoir, Va., 1967.
- Gaposchkin, E. M., and K. Lambeck, 1969 Smithsonian standard earth (II), *Smithson. Astrophys. Observ., Spec. Rep. 315*, 1970.
- Hamilton, W. C., *Statistics in Physical Science*, Ronald Press, New York, 1964.
- Heiskanen, W. A., and H. Moritz, *Physical Geodesy*, W. H. Freeman, San Francisco, Calif., 1967.
- Kaula, W. M., Tests and combinations of satellite determinations of the gravity field with gravimetry, *J. Geophys. Res.*, 71(22), 5303-5314, 1966.
- Kohnlein, W., The earth's gravitational field as derived from a combination of satellite data with gravity anomalies, paper presented to the 14th General Assembly of the IUGG, Lucerne, Switzerland, 1967.
- Mancini, A., *The Earth's Gravitational Field by Combinations of Doppler-Optical and Gravity Data*, U.S. Army Eng. Topogr. Lab., Washington, D.C., 1968.
- Rapp, R. H., *The Geopotential to (14, 14) from a Combination of Satellite and Gravimetric Data*, Dep. Geod. Sci., Ohio State Univ., Columbus, Ohio, 1967.
- Zhongolovich, J., The external gravity field of the earth and the fundamental constants connected with it, *Akad. Nauk SSSR Tr. Inst. Teoret. Astron.*, 3, 1952.

Nature of the Satellite-Determined Gravity Anomalies¹

MOHAMMAD ASADULLAH KHAN

*Hawaii Institute of Geophysics
University of Hawaii, Honolulu, Hawaii 96822*

Abstract. A mathematical model of isostatic anomaly potential of the earth is presented. These anomalies must provide an accurate index of subsurface anomalous mass distribution in the earth. It is demonstrated that the isostatic reduction is not critical for low-degree spherical harmonic solutions of satellite-determined geopotential. The correction does become important, however, for higher-degree harmonic solutions of geopotential, more so for those derived from low-altitude orbits.

An important problem in the understanding and interpretation of satellite-determined gravity results and their combination with surface gravity results is to define which of the well-known surface gravimetric anomaly types (e.g., free-air, Bouguer, isostatic, etc.) most closely equals the satellite-determined gravity anomaly. The most obvious answer, perhaps, is the free-air anomaly; but, since the mean height of most of the satellites used in the gravity-field determinations is several times greater than the depth of compensation, one must investigate how different the isostatic gravity anomaly is from the satellite-derived gravity anomaly. The solution of this problem becomes all the more important because one must assume one of the several possible isostatic compensation mechanisms in computing the isostatic reduction and thus, perhaps, run a greater risk of introducing, rather than removing, spurious factors in the gravity field.

The effect on the gravitational potential of a mass anomaly represented by a surface density $\sigma_{nm} S_{nm}$ at $r = R$ [Jeffreys, 1962] is

$$U_{nm} = \frac{4\pi G}{2n + 1} \sigma_{nm} S_{nm} \frac{R^{n+2}}{r^{n+1}} \quad (1)$$

Its compensation, located at $r = R - d$, where d is the depth of compensation, produces a potential

$$U_{nm}^c = U_{nm}[(R - d)/R]^n \quad (2)$$

In the above equations, G is the gravitational constant, and S_{nm} is the surface spherical harmonic of degree n and order m . Consequently, the potential due to the isostatic reduction is

$$U_{nm}^i = \frac{4\pi G}{2n + 1} \sigma_{nm} S_{nm} \frac{R^{n+2}}{r^{n+1}} \cdot \left[1 - \left(\frac{R - d}{R} \right)^n \right] \quad (3)$$

For small n and a reasonable depth of compensation, for example $d = 30$ km, the factor in the brackets stays close to zero. Its value is 0.005 for $n = 1$, 0.009 for $n = 2$, 0.033 for $n = 5$, 0.046 for $n = 10$, 0.068 for $n = 15$, and 0.09 for $n = 20$. For a high-altitude satellite, the potential effect of equation 3 will be further attenuated by the distance of the satellite from the source of the anomaly, i.e., a height increase of $d = 30$ km may not be significantly discernible to a satellite that is already at a height of more than 1000 km from the earth's surface and hence may not affect the type of anomaly sensed by it, since the free-air anomaly is equivalent to the isostatic anomaly at zero depth of compensation. Hence, for a small n the potential effect due to equation 3 will almost be negligible for a high-altitude satellite, i.e., the isostatic reduction will be close to zero, and the satellite will effectively be 'sensing' the isostatic anomaly for low-degree spherical harmonic

¹ Hawaii Institute of Geophysics contribution 467.

SATELLITE-DETERMINED GRAVITY ANOMALIES

TABLE 1. Fully Normalized Spherical Harmonic Coefficients of Isostatic Reduction Potential*
(In units of 10^{-6} .)

<i>n</i>	<i>m</i>	<i>C_{nm}</i>	<i>S_{nm}</i>
2	0	0.17638D 00	
	1	0.10014D 00	0.10137D 00
	2	-0.15288D 00	-0.26377D-01
3	0	-0.55929D-01	
	1	-0.26490D-01	0.51216D-01
	2	-0.16601D 00	0.15807D 00
4	3	0.37973D-01	0.22386D 00
	0	0.85853D-01	
	1	-0.57692D-01	-0.59982D-01
5	2	-0.15293D 00	0.38462D-01
	3	0.13645D 00	-0.42126D-01
	4	-0.32511D-01	0.20422D 00
6	0	-0.11080D 00	
	1	-0.16390D-01	-0.18732D-01
	2	-0.32312D-01	-0.41209D-01
	3	0.65560D-01	-0.17796D-01
	4	0.20464D 00	-0.15922D-01
7	5	-0.30906D-01	0.12035D 00
	0	0.32967D-01	
	1	-0.90340D-02	-0.51829D-01
	2	-0.52303D-02	-0.36612D-01
	3	0.35186D-01	0.58486D-01
	4	0.11459D 00	-0.71800D-01
8	5	-0.48025D-01	-0.70847D-01
	6	0.12838D-01	0.14264D-01
	0	-0.29671D-01	
	1	0.10577D-01	0.33174D-01
	2	0.49520D-01	-0.48012D-03
	3	-0.13943D-01	0.14905D-01
	4	-0.61058D-01	0.38458D-02
9	5	-0.33657D-02	-0.19237D-02
	6	-0.31250D-01	-0.47117D-01
	7	-0.28846D-01	-0.51443D-01
	0	-0.78778D-02	
	1	-0.72717D-02	-0.72717D-02
	2	0.47028D-01	-0.29087D-02
	3	0.11636D-01	0.19878D-01

TABLE 1. (continued)

<i>n</i>	<i>m</i>	<i>C_{nm}</i>	<i>S_{nm}</i>
10	0	-0.25988D-01	
	1	0.73106D-02	-0.19825D-02
	2	-0.36085D-01	-0.92681D-02
	3	-0.27504D-01	-0.18010D-01
	4	-0.39826D-01	0.25844D-01
	5	0.40957D-02	0.12491D-01
	6	0.26672D-01	-0.85016D-02
	7	0.96317D-02	0.12129D-01
	8	0.26120D-01	-0.36544D-01
	9	0.70087D-01	-0.11827D-01
	10	0.38017D-01	-0.32615D-01
	11	0	-0.84520D-02
	12	0	0.30514D-01
	13	0	-0.14791D-01
11	0	-0.61014D-02	-0.68431D-02
	1	0.55821D-02	-0.15356D-01
	2	0.22400D-01	0.12496D-01
	3	0.53871D-02	-0.96121D-03
	4	-0.55223D-02	-0.26702D-01
	5	0.38320D-01	0.17446D-01
	6	-0.15202D-01	0.38865D-01
	7	0.36484D-01	0.23102D-01
	8	0	-0.21941D-01
	9	0	-0.21811D-01
	10	0	-0.26104D-01
	11	0	0.11704D-01
12	12	0	-0.81139D-02
	1	0	-0.71189D-02
	2	0	0.23783D-03
	3	0	-0.74609D-02
	4	0	0.45206D-02
	5	0	0.31520D-01
	6	0	-0.58656D-02
	7	0	-0.11158D-01
	8	0	0.24128D-01
	9	0	0.13629D-03
	10	0	0.93796D-02
	11	0	-0.53518D-01
13	12	0	-0.37829D-01
	13	0	0.15782D-01
	1	0	0.11591D-01
	2	0	-0.18437D-02
	3	0	-0.18782D-01
	4	0	-0.12086D-01
	5	0	0.47375D-02
	6	0	0.33086D-02
	7	0	-0.53490D-02
	8	0	-0.13939D-01
14	9	0	0.45660D-02
	10	0	-0.33984D-02
	11	0	-0.21912D-01
	12	0	-0.26843D-01
	13	0	-0.39741D-01
	14	0	-0.22293D-01
	1	0	0.11008D-01
	2	0	-0.66432D-02
	3	0	-0.14841D-01
	4	0	0.13999D-01

M. A. KHAN

101

TABLE 1. (continued)

<i>n</i>	<i>m</i>	C_{nm}	S_{nm}
7		-0.52481D-02	-0.19591D-01
8		-0.72630D-02	0.31468D-02
9		0.18106D-01	0.80715D-02
10		0.40866D-01	-0.13975D-01
11		-0.90694D-02	-0.52056D-01
12		0.35183D-02	-0.43193D-01
13		0.20400D-01	-0.23599D-02
14		-0.31241D-01	-0.14057D-02
15	0	0.23152D-02	
	1	0.58209D-02	-0.43175D-02
	2	-0.12147D-01	-0.13833D-01
	3	0.14423D-01	-0.20947D-01
	4	-0.11923D-01	-0.19891D-01
	5	-0.50951D-03	0.31704D-03
	6	0.10993D-01	-0.84069D-02
	7	0.16789D-01	0.12806D-01
	8	-0.44204D-02	0.19789D-01
	9	0.13653D-01	0.25590D-01
	10	-0.71233D-02	0.16797D-02
	11	0.10087D-01	0.32796D-02
	12	-0.22560D-01	0.29689D-01
	13	-0.15798D-01	-0.19315D-01
	14	0.28706D-01	-0.18096D-01
	15	0.37793D-03	-0.80927D-02
16	0	-0.80235D-02	
	1	0.11569D-01	0.12113D-01
	2	-0.22706D-02	-0.19832D-02
	3	-0.19840D-01	-0.43733D-02
	4	-0.12283D-01	0.59508D-02

TABLE 1. (continued)

<i>n</i>	<i>m</i>	C_{nm}	S_{nm}
	5	-0.16304D-02	-0.40539D-02
	6	-0.30499D-02	-0.10741D-01
	7	0.30963D-02	-0.32988D-03
	8	-0.24620D-01	0.75107D-02
	9	-0.48175D-02	-0.14023D-01
	10	0.27698D-01	-0.44706D-02
	11	0.41806D-02	0.77210D-03
	12	0.88309D-02	0.12607D-03
	13	0.66707D-02	0.11607D-01
	14	-0.76492D-03	-0.34785D-01
	15	-0.67994D-02	-0.37743D-02
	16	-0.10457D-01	-0.13441D-01

* Computed from equation 4 using the spherical harmonic coefficients of equivalent rock topography given by Lee and Kaula [1967].

representations of the satellite-determined geopotential.

Note the sense in which the term 'isostatic reduction' is used here. It is the quantity generated by equation 3; i.e., the topography is removed, together with its compensation, and the isostatic reduction signifies the gravity anomaly expected over a topographic feature completely compensated in the manner explained above, in the absence of all other mass disturbances.

TABLE 2. Power Spectra of the Gravity Field (in milligals squared)

Degree Spectra of Isostatic Correction		Degree Spectra of Free-Air and Isostatic Gravity Anomalies		
<i>n</i>	Khan's*	Uotila's†	Free-Air‡	Isostatic§
2	0.08	0.13	7.38	8.12
3	0.46	1.02	32.96	33.38
4	0.96	2.25	20.02	16.87
5	1.30	3.69	17.85	24.55
6	0.93	2.26	15.71	12.31
7	0.58	2.16	15.55	14.34
8	1.12	2.03	6.66	6.30
9	1.33	3.11	12.70	9.37
10	1.37	3.60	12.91	11.91
11	1.02	2.97	12.28	13.14
12	1.38	2.38	5.12	7.40
13	1.48	3.75	11.16	9.98
14	1.94	2.93	7.93	6.13
15	1.40	3.42	13.26	12.43
16	1.08	4.04	13.90	11.62

* Table 1 in this paper.

† Uotila [1964].

‡ Gaposchkin and Lambeck [1970].

§ Using Gaposchkin and Lambeck's [1970] coefficients and the isostatic reduction coefficients given in Table 1 in this paper.

SATELLITE-DETERMINED GRAVITY ANOMALIES

TABLE 3. Fully Normalized Spherical Harmonic Coefficients of Isostatic Anomaly Potential*
(In units of 10^{-6} .)

<i>n</i>	<i>m</i>	C_{nm}	S_{nm}
2	0	-0.17638D 00	
	1	-0.10014D 00	-0.10137D 00
	2	0.25658D 01	-0.13377D 01
3	0	0.10152D 01	
	1	0.19963D 01	0.20893D 00
	2	0.10581D 01	-0.79275D 00
	3	0.64833D 00	0.12065D 01
4	0	-0.34185D 00	
	1	-0.47220D 00	-0.42767D 00
	2	0.48317D 00	0.66787D 00
	3	0.85298D 00	-0.11254D 00
	4	-0.47181D-01	0.13506D 00
5	0	0.18015D 00	
	1	-0.37426D-01	-0.79173D-01
	2	0.64517D 00	-0.30966D 00
	3	-0.49639D 00	-0.68867D-01
	4	-0.47157D 00	0.98932D-01
	5	0.15684D 00	-0.71945D 00
6	0	-0.17220D 00	
	1	-0.89950D-01	0.89481D-01
	2	0.60055D-01	-0.31514D 00
	3	-0.73126D-02	-0.13860D-01
	4	-0.11500D 00	-0.33208D 00
	5	-0.16340D 00	-0.45179D 00
	6	0.75855D-01	-0.89020D-01
7	0	0.12288D 00	
	1	0.23084D 00	0.82496D-01
	2	0.23354D 00	0.15693D 00
	3	0.21679D 00	-0.24938D 00
	4	-0.13621D 00	-0.11775D 00
	5	0.24955D-02	0.10038D 00
	6	-0.22722D 00	0.14921D 00
	7	0.18801D 00	-0.16267D-01
8	0	0.36498D-01	
	1	0.38526D-01	0.32968D-01
	2	0.11335D-02	0.87049D-01
	3	-0.69080D-01	-0.17919D-02
	4	-0.13730D 00	0.55872D-01
	5	-0.24250D-01	0.56787D-01
	6	-0.86870D-01	0.23845D 00
	7	-0.55301D-01	0.69290D-01
	8	-0.24519D-01	0.13548D 00
9	0	0.42882D-01	
	1	0.12941D 00	-0.32548D-01
	2	-0.15815D-01	-0.93746D-01
	3	-0.10903D 00	-0.13761D 00
	4	0.54232D-01	0.91251D-01
	5	-0.15563D-01	-0.23780D-01
	6	0.33377D-01	0.13559D 00
	7	-0.64851D-01	-0.76966D-01
	8	0.17776D 00	0.18172D-01
	9	-0.58245D-01	0.13135D 00

TABLE 3. (continued)

<i>n</i>	<i>m</i>	C_{nm}	S_{nm}
10	0	0.10324D 00	
	1	0.10520D 00	-0.99687D-01
	2	0.48599D-02	-0.95232D-01
	3	0.41578D-02	-0.12336D 00
	4	-0.83594D-02	-0.69092D-01
	5	-0.84100D-01	-0.15528D 00
	6	-0.59158D-01	-0.19303D 00
	7	0.45329D-01	0.19874D-01
	8	0.47837D-01	-0.43162D-01
	9	-0.76943D-01	0.18076D-01
11	0	0.85753D-01	0.67302D-02
	1	-0.33668D-01	
	2	-0.26124D-01	0.42692D-01
	3	0.63691D-01	-0.75326D-01
	4	-0.57146D-01	-0.12425D 00
	5	-0.35775D-01	0.69673D-01
	6	0.10123D-01	0.11965D 00
	7	0.32130D-01	0.78617D-02
	8	0.26226D-01	-0.34439D-01
	9	0.13270D 00	-0.48810D-01
12	0	-0.15384D 00	-0.42002D-01
	1	0.13979D 00	-0.18877D-01
	2	0.34504D-01	
	3	-0.57659D-01	-0.22886D-01
	4	0.34600D-01	0.68359D-01
	5	0.58624D-01	0.84779D-01
	6	-0.36188D-01	-0.21525D-01
	7	0.18854D-01	0.56251D-01
	8	-0.55388D-01	0.23261D-02
	9	0.20373D-01	0.11940D 00
13	0	0.53731D-02	0.16194D-01
	1	-0.56360D-01	0.34403D-01
	2	-0.18726D-01	0.22945D-03
	3	-0.54301D-01	-0.91724D-01
	4	0.34111D-01	-0.19942D-01
	5	0.78882D-02	
	6	-0.67633D-01	0.38275D-01
	7	-0.45612D-01	0.34419D-01
	8	0.42615D-01	-0.34396D-01
	9	-0.78938D-02	0.55925D-01
14	0	0.91900D-01	-0.55902D-01
	1	-0.86726D-01	0.68883D-01
	2	-0.46868D-01	0.17599D-01
	3	-0.27820D-01	-0.21177D-01
	4	-0.30189D-01	0.63294D-01
	5	0.89987D-01	0.28119D-01
	6	-0.11837D-01	0.76665D-01
	7	0.25520D-01	0.50032D-01
	8	-0.30547D-01	0.71289D-01
	9	0.35853D-01	
15	0	-0.34098D-01	0.34849D-01
	1	0.38763D-01	-0.28211D-01
	2	0.33883D-01	0.14923D-01
	3	-0.61970D-02	-0.25110D-01
	4	-0.19899D-01	-0.24704D-01

M. A. KHAN

103

TABLE 3. (*continued*)

<i>n</i>	<i>m</i>	C_{nm}	S_{nm}
6		0.27018D-01	-0.72501D-01
7		0.16309D-01	0.28004D-01
8		-0.23008D-01	-0.63985D-01
9		0.31433D-01	0.84273D-01
10		0.12866D-01	-0.29193D-01
11		0.36902D-01	-0.29581D-01
12		0.89627D-02	0.43193D-01
13		0.31154D-01	0.47813D-01
14		-0.20841D-01	-0.11434D-01
15	0	0.28935D-01	
	1	-0.94180D-02	0.44460D-01
	2	-0.32686D-01	-0.22229D-02
	3	-0.61215D-02	-0.26668D-01
	4	0.25839D-01	0.86535D-01
	5	0.32194D-01	0.15080D-02
	6	0.59027D-01	-0.11031D-00
	7	0.10177D-00	0.29884D-01
	8	-0.93237D-01	-0.55499D-01
	9	0.84108D-02	0.10417D-02
	10	-0.13525D-01	-0.11425D-02
	11	-0.42672D-01	0.90772D-01
	12	0.33084D-01	-0.22816D-01
	13	-0.21550D-01	0.23340D-01
	14	-0.16513D-01	-0.86900D-02
	15	0.10736D-02	-0.67093D-02
16	0	-0.24527D-01	
	1	-0.35358D-01	0.64300D-01
	2	0.23598D-01	0.32652D-01
	3	-0.27518D-01	0.36983D-01
	4	0.69212D-03	0.37050D-01
	5	-0.42571D-01	0.36284D-01
	6	-0.55389D-01	-0.32068D-01
	7	0.10281D-00	0.84307D-02
	8	-0.60118D-01	-0.99784D-02
	9	0.13818D-01	-0.92257D-01
	10	-0.57547D-01	0.39460D-02
	11	0.26696D-02	-0.71537D-01
	12	0.14003D-01	-0.34213D-01
	13	0.28804D-01	0.90760D-02
	14	-0.65941D-02	0.12159D-01
	15	-0.28686D-01	0.46156D-02
	16	-0.19065D-01	0.22062D-01

* Computed using spherical harmonic coefficients of isostatic reduction given in Table 1 in this paper and the geopotential coefficients given by *Gaposchkin and Lambeck* [1970].

For very low-altitude satellites, the effect of equation 3 must be considered. With $\sigma_{nm} = \rho_e C_{nm}(h)$, $\sigma_{nm} = \rho_e S_{nm}(h)$, the spherical harmonic coefficients of the potential U^i of isostatic reduction, on the assumptions listed in equations 1 and 2, are given as

$$C_{nm}(U^i) = \frac{3n}{2n+1} \frac{\rho_e}{\langle \rho \rangle} \frac{d}{R^2} C_{nm}(h) \quad (4)$$

$$S_{nm}(U^i) = \frac{3n}{2n+1} \frac{\rho_e}{\langle \rho \rangle} \frac{d}{R^2} S_{nm}(h)$$

where $C_{nm}(h)$ and $S_{nm}(h)$ are the spherical harmonic coefficients of equivalent rock topography, and ρ_e and $\langle \rho \rangle$ are the typical crustal and mean densities of the earth, respectively.

The spherical harmonic coefficients of isostatic correction computed from equation 4 using *Lee and Kaula's* [1967] spherical harmonic coefficients of equivalent rock topography and a compensation depth $d = 30$ km are given in Table 1. The degree power spectra of these coefficients are compared in the first and second columns of Table 2 with the power spectra of the isostatic reduction coefficients given by *Uotila* [1964], who computed his coefficients using *Jung's* [1950] method. The difference in the power spectra of the two sets of coefficients illustrates the extent to which the value of isostatic correction depends upon the nature of the isostatic reduction method used in computing the correction.

Table 3 lists the coefficients of isostatic anomaly potential. These are computed from the geopotential coefficients given by *Gaposchkin and Lambeck* [1970] and isostatic reduction coefficients given in Table 1. The geoidal heights and isostatic anomalies based on these coefficients (Table 3) are given in Figures 1 and 2, respectively. The gravity anomaly field is referred to the best-fitting satellite ellipsoid (Geodetic Reference System 1967). The power spectra of these isostatic anomaly coefficients (Table 3) are given in the fourth column of Table 2. For the sake of comparison, the power spectra of the geopotential coefficients (free-air anomalous gravity) given by *Gaposchkin and Lambeck* [1970] are listed in the third column of Table 2. The isostatic anomalies based on *Uotila's* [1964] isostatic reduction coefficients were given by *Kaula* [1970].

To sum up, the isostatic reduction is not critical for low-degree spherical harmonic solutions of satellite-determined geopotential. In fact, because of the uncertainty involved in the selection of the appropriate isostatic model, it is advisable to avoid the correction in the satel-

SATELLITE-DETERMINED GRAVITY ANOMALIES

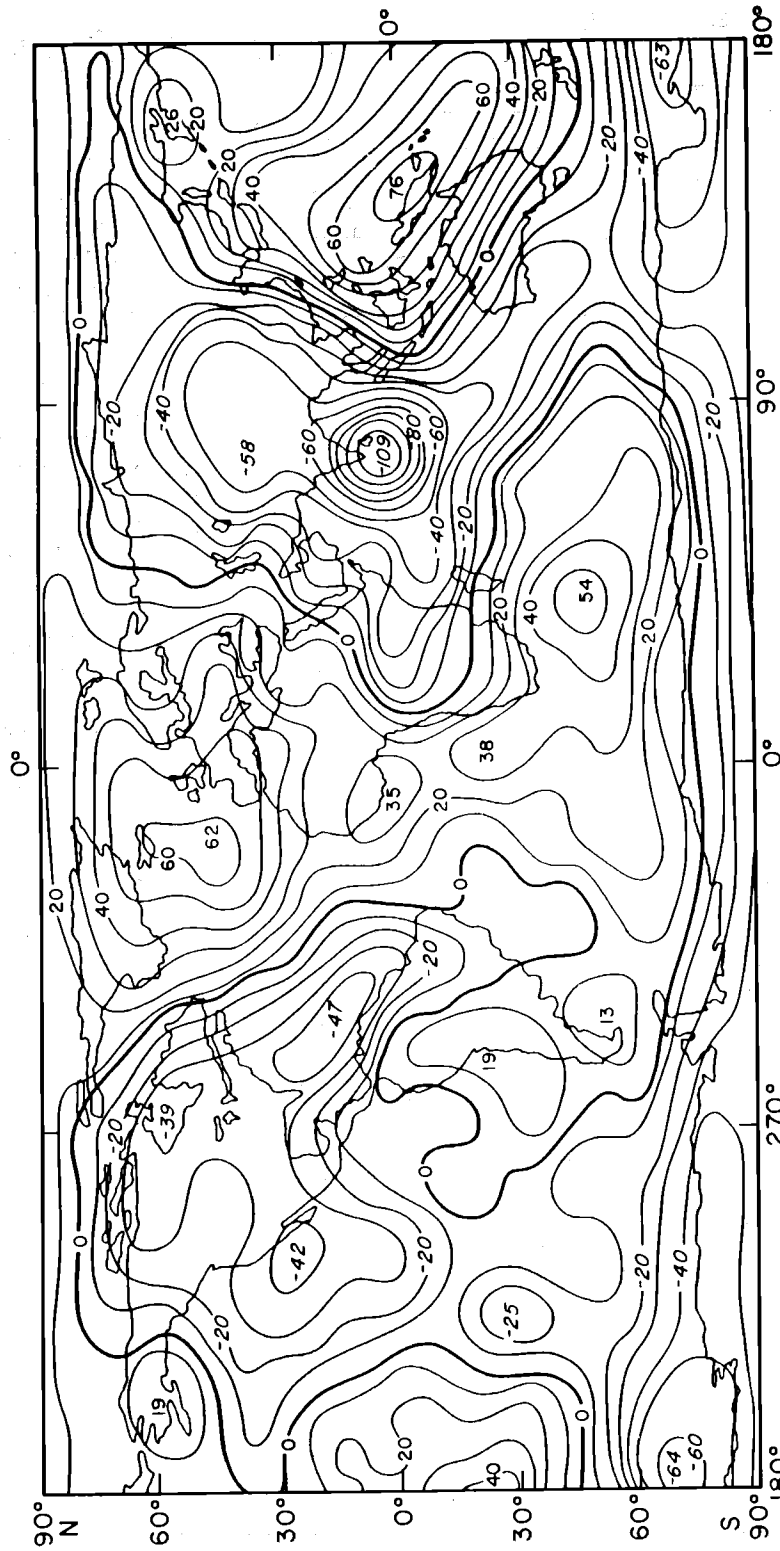


Fig. 1. Geoidal undulations (in meters) referred to the reference ellipsoid 1967 (flattening, 1/298.25) based on Khan's isostatic anomaly potential coefficient given in Table 3.

M. A. KHAN

105

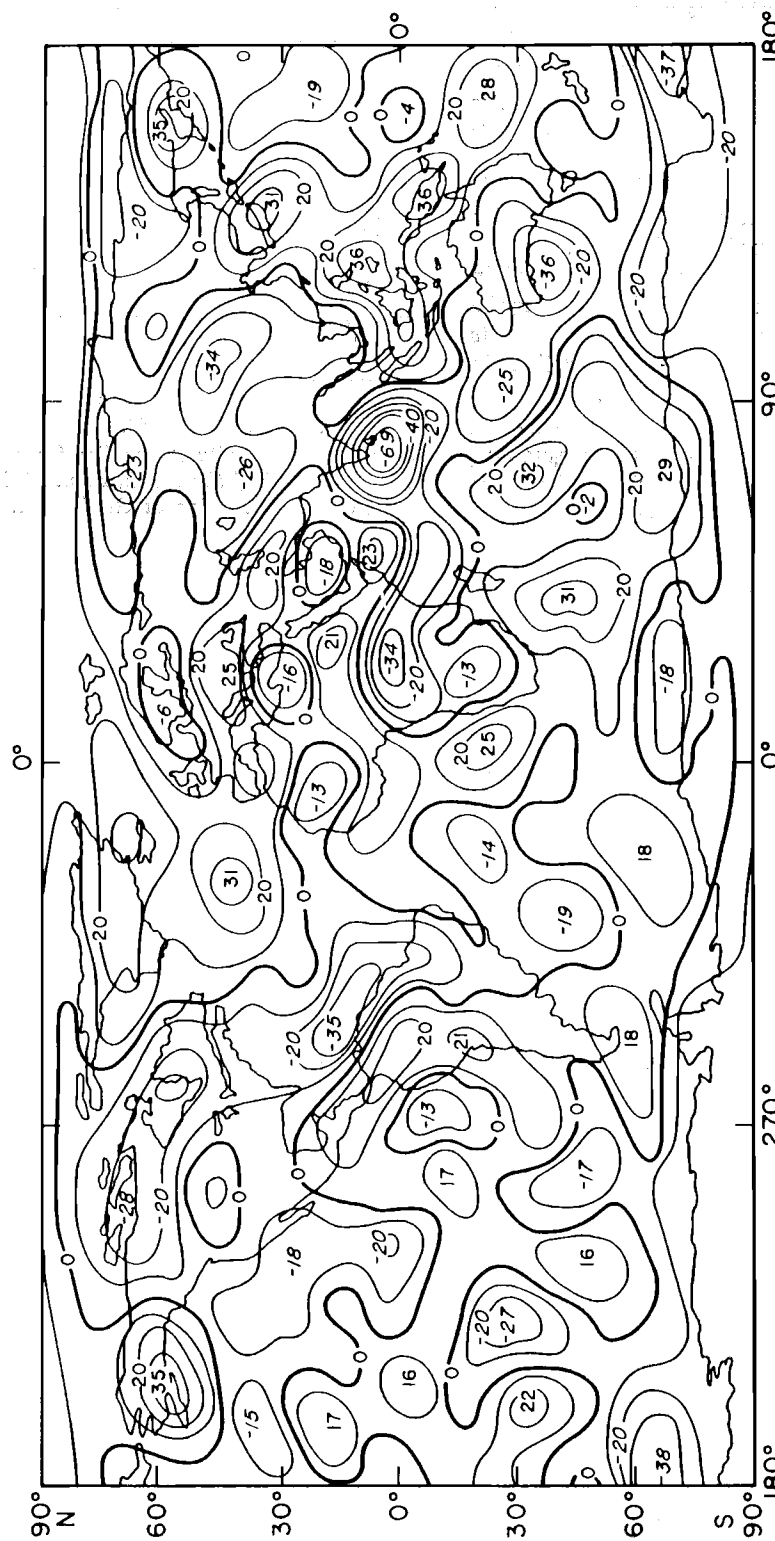


Fig. 2. Isostatic gravity anomalies in milligals referred to the reference ellipsoid 1967 (flattening, 1/298.25) based on Khan's isostatic anomaly potential coefficients given in Table 3.

SATELLITE-DETERMINED GRAVITY ANOMALIES

REFERENCES

lite gravity representations unless one is absolutely certain of its practical usefulness. The correction does become important, however, for higher-degree harmonic solutions of geopotential, more so for those derived from low-altitude orbits. The most convenient and perhaps the best method of applying the isostatic reduction seems to be via the surface density technique, as explained in this paper.

The isostatic gravity anomalies presented in Figure 2 should form the basis for assessing the subsurface anomalous mass distribution and its association with, as well as its implications in terms of, the tectonics of the earth.

Acknowledgment. I wish to thank Professor William M. Kaula of the University of California, Los Angeles, for supplying the spherical harmonic coefficients of global topography.

- Gaposchkin, E. M., and K. Lambeck, 1969 Smithsonian standard earth (II), *Smithson. Astrophys. Observ. Spec. Rep. 315*, 1970.
- Jeffreys, H., *The Earth*, Cambridge University Press, London, 1962.
- Jung, K., Die rechnerische Behandlung der AIRY-schen Isostasie mit einer Entwicklung des Quadrats der Meereshöhen nach Kugelfunktionen, *Sonderdruck aus Gerl. Beitr. Geophys.* 62(1), 1950.
- Kaula, W. M., Earth's gravity field: Relation to global tectonics, *Science*, 169, (3949), 982, 1970.
- Lee, W. H. K., and W. M. Kaula, A spherical harmonic analysis of earth's topography, *J. Geophys. Res.*, 72, 753, 1967.
- Uotila, U. A., *Gravity Anomalies for a Mathematical Model of the Earth*, Publ. 43, Isostatic Inst. of the Int. Union of Geod., 1964.

Simple Layer Model of the Geopotential in Satellite Geodesy

KARL-RUDOLF KOCH

*Institut für Theoretische Geodäsie der Universität Bonn
Bonn, Germany*

Abstract. The method of satellite geodesy that represents the earth's gravity field by the potential of a simple layer is reviewed. This model of the geopotential, which has been applied to optical satellite observations and Doppler data, is compared with different representations of the gravity field.

The representation of the earth's gravitational field in satellite geodesy by means of the potential of a simple layer has now been applied to optical satellite observations [Koch and Morrison, 1970] and to Doppler data [Koch and Witte, 1971]. Since the first proposals of this model of the geopotential [Koch, 1968a, b], the method of its application has been slightly modified because of the experience gained with practical computations. A short outline of the method as it is used now is therefore given here.

REPRESENTATION OF THE GRAVITY FIELD

The potential of gravity of the earth W is divided into the potential U , which is known and is expressed by an expansion into spherical harmonics, and into the potential T , which is unknown and is represented by a potential of a simple layer distributed over the surface of the earth. Hence

$$W = U + T \quad (1)$$

where

$$\begin{aligned} U = \frac{kM}{r} [1 + \sum_{n=2}^{n_c} \sum_{m=0}^n \left(\frac{a}{r}\right)^n \bar{P}_{nm}(\sin \phi) \\ \cdot (\bar{C}_{nm} \cos m\lambda + \bar{S}_{nm} \sin m\lambda)] \\ + (\omega^2 r^2 \cos^2 \phi)/2 \end{aligned} \quad (2)$$

Equation 2 is the well-known expansion into spherical harmonics whose coefficients \bar{C}_{nm} and \bar{S}_{nm} are taken from available results. The term with the angular velocity ω of the earth stems from the centrifugal force and equals zero outside

the earth; n_c is an integer greater than 2; and r, ϕ, λ are geocentric coordinates.

The potential T is given by

$$T = \iint_{\Sigma} \frac{\Phi}{l} d\Sigma \quad (3)$$

where Φ is the unknown density of the simple layer distributed over the surface Σ of the earth, and l denotes the distance between the fixed point and the moving point at Σ . We introduce the auxiliary density χ by

$$\chi = \Phi / \cos(f, r) \quad (4)$$

where (f, r) denotes the angle between the normal f to the earth's surface Σ and r . With the projection dE of the surface element $d\Sigma$

$$dE = d\Sigma \cos(f, r) = r^2 \cos \phi \, d\phi \, d\lambda \quad (5)$$

we obtain, instead of (3),

$$T = \iint_{\Sigma} \frac{\chi}{l} dE \quad (6)$$

The integral in (6) is now replaced by a summation over p surface elements ΔE_i of approximately equal size bordered by meridians and parallels. We assume constant densities χ_i for ΔE_i and obtain

$$T = \sum_{i=1}^p \chi_i \iint_{\Delta E_i} \frac{dE}{l} \quad (7)$$

The density values χ_i for the surface elements ΔE_i are the unknown parameters of the geopotential. They are determined from satellite observations by a numerical orbit theory based

SIMPLE LAYER MODEL OF THE GEOPOTENTIAL

on a differential correction process. This means that the equation of motion of a satellite is integrated numerically, together with the variational equations.

COMPUTATIONAL PROCEDURE

To reduce the influence of errors due to the approximation of the integral (6) by the sum (7), the potential T should be small. Hence, the expansion 2 has to be extended to a high degree and order. However, an upper limit of the degree of the expansion is given by the shortest wavelength of the harmonics in (2), which should be compatible with the sidelength of the surface elements ΔE_i . In addition to these coefficients, the resonant terms of the satellites being analyzed have to be included, in order to get optimal orbit fits.

The integral over the surface element ΔE_i in (7) is solved numerically by subdividing ΔE_i into four elements for whose midpoints the kernel of the integral is assumed to be constant. This method of numerical integration can be interpreted as using point masses instead of a surface layer [Morrison, 1971]. This integration procedure is correct if, depending on the position of the satellite, the right point at the surface element is chosen. Since the points are fixed, errors in the numerical integration of (7) cannot be avoided. However, they only enter the variational equations because, by introducing zero densities as preliminary values into (7), the potential U in (2) alone is used to compute the nominal orbits.

For the numerical integration, the surface of the earth has to be defined. This is done by means of (2). An approximate expression for the geopotential U_0 at sea level is obtained from the equation that holds for the potential at the surface of a level ellipsoid

$$U_0 = \frac{kM}{(a^2 - b^2)^{1/2}} \arctan \frac{(a^2 - b^2)^{1/2}}{b} + (\omega^2 a^2)/3 \quad (8)$$

The values for kM , a , and ω are taken from (2), and the semiminor axis b is computed from the value of \bar{C}_{20} used in (2). Setting $U = U_0$ in (2) and solving for r , the radius vector of the equipotential surface at sea level is obtained. To these values are added the topographic heights, which are published for 5° by 5° elements by Kaula *et al.* [1966].

To convert the density values into normalized harmonic coefficients, one uses [Koch, 1968b]

$$\begin{aligned} \bar{C}_{nm} &= \bar{C}_{nmu} + \frac{1}{(2n+1)kMa^n} \sum_{i=1}^P \chi_i \cdot \iint_{\Delta E_i} r^n \bar{P}_{nm}(\sin \phi) \cos m\lambda dE \\ \bar{S}_{nm} &= \bar{S}_{nmu} + \frac{1}{(2n+1)kMa^n} \sum_{i=1}^P \chi_i \cdot \iint_{\Delta E_i} r^n \bar{P}_{nm}(\sin \phi) \sin m\lambda dE \end{aligned} \quad (9)$$

where \bar{C}_{nmu} and \bar{S}_{nmu} are the harmonic coefficients of (2). The integral over ΔE_i is solved numerically by subdividing ΔE_i into nine elements. If the coordinate system of the orbit integration is a geocentric one, the density values χ_i have to be determined under the constraint that the first-degree harmonics equal zero.

The product kM of the gravitational constant and the mass of the earth is well known from space probes. Hence the transformation 9 should give a harmonic coefficient of zero degree that equals zero. If the coefficient differs from zero, it does so because the equatorial radius of the earth, and therefore U_0 , are only approximately known. With a relative error of one part in 300, we can write instead of (8)

$$U_0 = kM/a$$

so that the correction Δa of a is obtained from

$$\Delta U_0 = -(kM/a^2) \Delta a \quad (10)$$

Detailed information about the computational procedures for determining density values from Doppler data is given by Witte [1971].

COMBINATION WITH GRAVITY ANOMALIES

Knowledge of the earth's gravity field comes not only from satellite orbits but also from gravity measurements. If Δg are the gravity anomalies referred to the potential U in (2), the density values χ are obtained by [Koch, 1968b]

$$\chi = \frac{\Delta g - G}{2\pi} + \frac{3}{(4\pi)^2} \cdot \iint (\Delta g - G) S(\psi) \cos \phi d\phi d\lambda \quad (11)$$

K. R. KOCH

where

$$G = \frac{1}{4\pi} \iint \Delta g \cos \phi \, d\phi \, d\lambda$$

if the surface of the earth is approximated by the surface of a sphere. $S(\psi)$ is Stokes' function. For the combination with the satellite results, the covariances of χ have to be computed according to (11) from the given variances of Δg [Koch, 1970].

COMPARISON WITH DIFFERENT MODELS

A similar model of the geopotential is obtained if, instead of density values, gravity anomalies are used as parameters of the gravity field [Arnold, 1968; Obenson, 1970]. With such a representation, the reciprocal distance between the fixed point and the moving point in (7) is replaced by Stokes' function, which contains sine, cosine, and logarithmic functions. The evaluation of the integral corresponding to (7) is therefore more time consuming than (7), which is especially disadvantageous when satellite orbits are integrated numerically. Another point is that the surface of the earth is approximated by the surface of a sphere. This approximation is avoided with (7). However, when combining satellite and gravimetric results, the gravity anomalies can be used directly, so that transformation 11 and the computation of covariances are unnecessary.

Vinti [1968] suggested representing the potential T by the potential of a simple layer distributed over a sphere completely enclosing the earth. This proposal causes some difficulties when gravity measurements are combined with satellite results. Either the gravity anomalies have to be continued upward from the surface of the earth to the surface of the sphere or the density values have to be transferred downward from the surface of the sphere to the surface of the earth.

To determine the gravity field of the moon, Wong *et al.* [1969] expressed the potential T by point masses buried under the lunar surface. This model tries to account for the lunar mass concentrations, the so-called mascons. If applied

to the earth as has been proposed in the past [Weightman, 1967], this model again would be difficult to use for the combination of gravity anomalies with satellite observations, since point masses close to the surface of the earth will produce singularities at the surface.

REFERENCES

- Arnold, K., An attempt to determine the unknown parts of the earth's gravity field from successive satellite passages, *Bull. Geod.*, **87**, 97–101, 1968.
- Kaula, W. M., W. H. K. Lee, P. T. Taylor, and H. S. Lee, Orbital perturbations from terrestrial gravity data, *Inst. Geophys. Planet. Phys.*, Univ. Calif., Los Angeles, 1966.
- Koch, K. R., The geopotential at the earth's surface from observations of earth satellites, paper presented at 49th Annual Meeting, AGU, Washington, D. C., 1968a.
- Koch, K. R., Alternate representation of the earth's gravitational field for satellite geodesy, *Bull. Geofis.*, **10**, 318–325, 1968b.
- Koch, K. R., Surface density values for the earth from satellite and gravity observations, *Geophys. J. Roy. Astron. Soc.*, **21**, 1–12, 1970.
- Koch, K. R., and F. Morrison, A simple layer model of the geopotential from a combination of satellite and gravity data, *J. Geophys. Res.*, **75**, 1483–1492, 1970.
- Koch, K. R., and B. U. Witte, Earth's gravity field represented by a simple-layer potential from Doppler tracking of satellites, *J. Geophys. Res.*, **76**, 8471–8479, 1971.
- Morrison, F., Density layer models for the geopotential, *Bull. Geod.*, **101**, 319–328, 1971.
- Obenson, G. F. T., Direct evaluation of the earth's gravity anomaly field from orbital analysis of artificial earth satellites, *Rep. 129*, Dep. Geod. Sci., Ohio State Univ., Columbus, 1970.
- Vinti, J. P., Proposal on representation of the earth's gravitational potential (abstract), *Eos Trans. AGU*, **49**, 506, 1968.
- Weightman, J. A., Gravity, geodesy and artificial satellites, a unified analytical approach, in *The Use of Artificial Satellites for Geodesy*, vol. 2, edited by G. Veiss, pp. 467–486, National Technical University, Athens, Greece, 1967.
- Witte, B., Computational procedures for the determination of a simple layer model of the geopotential from Doppler observations, *NOAA Tech. Rep. 42*, Nat. Ocean Surv., Rockville, Md., 1971.
- Wong, L., G. Buechler, W. D. Downs, and R. H. Prislin, Dynamical determination of mascons on the moon (abstract), *Eos Trans. AGU*, **50**, 125, 1969.

Propagation of Errors in Orbits Computed from Density Layer Models

FOSTER MORRISON

*Geodetic Research and Development Laboratory
Rockville, Maryland 20852*

Abstract. Errors arise in computations of the gravitational force due to a simple density layer from the need to approximate the layer; these are essentially quadrature errors. These errors in turn cause errors in orbits computed from such a model for the geopotential. To model the quadrature errors, a disturbing potential is defined that is the difference between the potential of a pair of equal mass points and that of a single point lying midway between them and equal to their sum. The total error is constructed by the superposition of a number of such disturbing functions. Two categories of errors exist: the use of too coarse a grid of mass points to simulate the density layer, and use of grids of varying coarseness for regions of the layer close to or remote from the satellite. Procedures are given for preventing biases introduced by these quadrature errors from distorting a solution for geodetic parameters.

To use a density layer to generate the anomalous gravity field of the earth, a discrete variable model of this layer is required. In practice a network of point masses must comprise our model. It is much simpler and more practical to add more point masses than to use a more sophisticated model. Experience leads us to this conclusion. No proof of this claim will be given; counter-examples would be very welcome.

When the potential or force of gravity is being computed from a density layer model, it would seem practical to use a coarser model for distant parts of the layer than for closer ones. In a static problem, such as computing a potential using Stokes' formula, error analysis is relatively easy. But in computing a satellite orbit we are concerned with how the error will affect the orbit in time. During application of density layer models, patches of equal density have been approximated by four point masses [Koch and Morrison, 1970]. But to construct a model that is manageable, we shall study the effect of replacing a pair of equal point masses with a single mass equal to their sum and lying halfway between them. The difference between the potential field of the two points and their one-point approximation comprises the disturbing function, where the reference orbit will be that of a close satellite of

an oblate planet. Lastly, we shall consider a distribution of such pairs of point masses over the surface of the earth to be our density layer model, and that the error engendered by replacing them by single points halfway between them will indicate the quantitative and qualitative errors due to using a coarser network of points.

Consider two points of mass $M_i/2$ each, attracting a satellite at \mathbf{r} (Figure 1). The satellite is separated from the masses by distances r_A and r_B and from their center of mass by r' ; the angle γ is that between vectors directed from the center of mass to the satellite and to M_B . By the law of cosines:

$$\begin{aligned} r_B^2 &= r'^2 + s^2 - 2r's \cos \gamma \\ r_A^2 &= r'^2 + s^2 + 2r's \cos \gamma \end{aligned} \quad (1)$$

The perturbing potential we desire is proportional to

$$\frac{1}{r'} - \frac{1}{2r_A} - \frac{1}{2r_B} \quad (2)$$

Now we manipulate (1):

$$\begin{aligned} \frac{1}{2r_A} &= \frac{1}{2r'} \left(1 + \frac{s^2}{r'^2} + 2\frac{s}{r'} \cos \gamma \right)^{-1/2} \\ \frac{1}{2r_B} &= \frac{1}{2r'} \left(1 + \frac{s^2}{r'^2} - 2\frac{s}{r'} \cos \gamma \right)^{-1/2} \end{aligned}$$

ORBITS COMPUTED FROM DENSITY LAYER MODELS

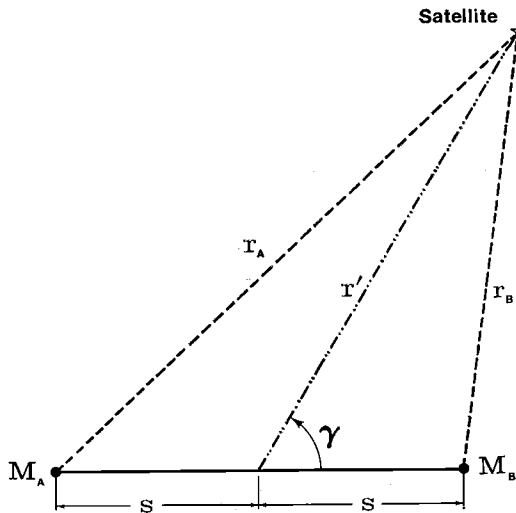


Fig. 1. Relation of the satellite position to that of the point-mass pair.

Both of these quantities can be expanded in Legendre functions [Jahnke and Emde, 1945]. Hence, it is easy to add and obtain

$$\frac{1}{2r_A} + \frac{1}{2r_B} = \frac{1}{r'} \left[1 + \sum_{i=1}^{\infty} \left(\frac{s}{r'} \right)^{2i} P_{2i}(\cos \gamma) \right] \quad (3)$$

Then it follows that

$$\frac{1}{r'} - \frac{1}{2r_A} - \frac{1}{2r_B} = \frac{1}{r'} \cdot \left[\frac{1}{2} \frac{s^2}{r'^2} - \frac{3}{2} \frac{s^2}{r'^2} \cos^2 \gamma \right] + O\left(\frac{s^4}{r'^4}\right) \quad (4)$$

To make (4) into a disturbing function, we need to multiply it by a 'GM' factor, specifically GM_i , where M_i is the combined mass of the points considered. Since M_i/M^* (M^* is earth mass) is very small, let us define a small parameter:

$$\epsilon_i = M_i/M^* \sim 10^{-6} \text{ or less}$$

and use the notation $\mu = GM^*$, so that our perturbing function is, as an increment to the Hamiltonian,

$$\Delta F_i = \frac{\epsilon_i \mu}{r'} \left[\frac{1}{2} \frac{s^2}{r'^2} - \frac{3}{2} \frac{s^2}{r'^2} \cos^2 \gamma \right] \quad (5)$$

Let us omit $O(s^4/r^4)$ from now on.

The disturbing function 5 must now be expressed in terms of orbital elements and short-period effects removed by averaging. All the quantities ϵ_i , μ , and s are constants, but r' and γ depend on both the position of the satellite and that of the center of mass of the point mass pair; in addition, γ depends on the orientation of the point mass pair. We define \mathbf{r} as the inertial satellite position, \mathbf{r}_i as the inertial position of the center of mass of the point mass pair, and $\mathbf{u}_i = (l_i, m_i, n_i)$ as the orientation vector for the point mass pair in inertial space. The basic equations are (see Figure 2)

$$r'^2 = r^2 + r_i^2 - 2\mathbf{r} \cdot \mathbf{r}_i$$

$$\cos \gamma = \frac{1}{r'} [\mathbf{u}_i \cdot (\mathbf{r} - \mathbf{r}_i)]$$

By definition $|\mathbf{u}_i| = 1$ and $||\mathbf{r} - \mathbf{r}_i|| = r'$. We will assume the point mass pair to be fixed to a rigid body (our oblate planet) centered at the origin and rotating uniformly about the 3 axis.

$$\mathbf{r}_i = \Theta \mathbf{r}_i(t_0)$$

$$\mathbf{u}_i = \Theta \mathbf{u}_i(t_0)$$

$$\Theta = \begin{bmatrix} \cos \theta & -\sin \theta & 0 \\ \sin \theta & \cos \theta & 0 \\ 0 & 0 & 1 \end{bmatrix}$$

$$\theta = \theta_0 + \theta'(t - t_0)$$

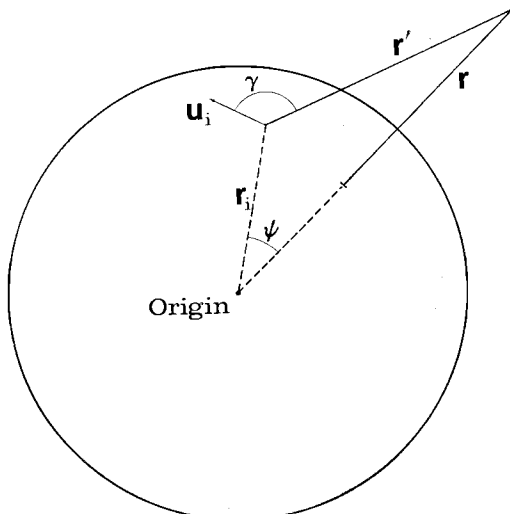


Fig. 2. Relation of the point-mass pair to the satellite and to the earth-fixed coordinates.

FOSTER MORRISON

113

The angle θ is called the sidereal angle, t is time, and θ_0 is the value of θ at $t = t_0$.

Relationships for the position of the satellite are [Danby, 1962; Hotine, 1969; Plummer, 1960]:

$$r = a \frac{1 - e^2}{1 + e \cos f}$$

$$r = a(1 - e \cos E)$$

$$\mathbf{r} = \mathbf{a}(\cos E - e) + \mathbf{b} \sin E$$

$$\mathbf{a} = a \begin{Bmatrix} \cos g \cos h - \sin g \sin h \cos I \\ \sin g \cos h \cos I + \cos g \sin h \\ \sin g \sin I \end{Bmatrix}$$

$$\mathbf{b} = b \begin{Bmatrix} -\sin g \cos h - \cos g \sin h \cos I \\ \cos g \cos h \cos I - \sin g \sin h \\ \cos g \sin I \end{Bmatrix}$$

$$b = a(1 - e^2)^{1/2}$$

The orbital elements to be used are

- a semi-major axis.
- e eccentricity.
- I inclination.
- h right ascension of ascending node.
- Λ mean anomaly.
- E eccentric anomaly.
- g argument of perigee.
- f true anomaly.
- $L = (\mu a)^{1/2}$.

AVERAGING OF FUNCTIONS

The averaging of functions is frequently an important step in a problem in celestial mechanics or differential equations. In theory we can expand such functions in trigonometric series. Often the definite integrals needed to obtain the coefficients of such a series cannot be evaluated.

Suppose we have a function $\xi(t)$ that is periodic and of period 2π . Then a function of $\xi(t)$, $\phi(\xi(t))$, is also of period 2π . We may be able to find the average value of ξ , $\langle \xi \rangle$; but it is, in general, more difficult to find the average value of ϕ , $\langle \phi \rangle$. Let us express ξ as

$$\xi = \langle \xi \rangle + (\xi - \langle \xi \rangle)$$

and expand ϕ in a Taylor series about $\langle \xi \rangle$. We can attempt to compute the average values of ϕ

by integrating this series term by term. Practical formulas are obtained using Parseval's theorem [Whittaker and Watson, 1962]. Details of the method were given by Morrison [1972].

The disturbing function 5 can be expressed as

$$\Delta F_i = \epsilon_i \mu s^2 \phi(\xi, \eta) / 2$$

a function of two periodic functions. The way ξ and η are defined will define ϕ and determine the nature of the expansion to be obtained. For this particular problem, the most natural choices are

$$\xi = r'^2$$

$$\eta = \mathbf{u}_i \cdot (\mathbf{r} - \mathbf{r}_i)$$

which imply

$$\phi = \xi^{-3/2} - 3\xi^{-5/2} \eta^2$$

The functions $\xi^{-3/2}$ and $\xi^{-5/2}$ are not the most desirable sort of thing to be expanded in Taylor series, but for a qualitative study this form of ϕ will be sufficient.

EXPANDING ξ AND η IN TERMS OF E , THE ECCENTRIC ANOMALY

We have

$$\xi = r'^2$$

$$\xi = r^2 + r_i^2 - 2\mathbf{r} \cdot \mathbf{r}_i$$

The individual terms are

$$r_i^2 = \text{constant}$$

$$r^2 = a^2(1 - e \cos E)^2$$

$$r^2 = a^2 \left(1 + \frac{e^2}{2} - 2e \cos E + \frac{e^2}{2} \cos 2E\right)$$

$$\mathbf{r} \cdot \mathbf{r}_i = \mathbf{r}_i \cdot \mathbf{a}(\cos E - e) + \mathbf{r}_i \cdot \mathbf{b} \sin E$$

We can combine the above to obtain

$$\begin{aligned} \xi &= r_i^2 + a^2 \left(1 + \frac{e^2}{2}\right) + 2e \mathbf{r}_i \cdot \mathbf{a} \\ &\quad - 2\mathbf{r}_i \cdot \mathbf{b} \sin E \\ &\quad - 2(a^2 e + \mathbf{r}_i \cdot \mathbf{a}) \cos E + \frac{1}{2} a^2 e^2 \cos 2E \end{aligned}$$

We have

$$\eta = \mathbf{u}_i \cdot \mathbf{r} - \mathbf{u}_i \cdot \mathbf{r}_i$$

Both \mathbf{u}_i and \mathbf{r}_i rotate about the z axis at the

ORBITS COMPUTED FROM DENSITY LAYER MODELS

same rate, so $\mathbf{u}_i \cdot \mathbf{r}_i = r_i \cos \xi_i = \text{constant}$. The angle ξ_i is that between a line connecting the two point masses and a radius vector to their center of mass. For point mass pairs lying on a sphere centered at the origin, $\xi = 90^\circ$ and $r_i \cos \xi_i = 0$. Using the expression for \mathbf{r} , we obtain

$$\eta = -r_i \cos \xi_i = e\mathbf{u}_i \cdot \mathbf{a} \\ + \mathbf{u}_i \cdot \mathbf{a} \cos E + \mathbf{u}_i \cdot \mathbf{b} \sin E$$

EXPANSIONS IN TERMS OF MEAN ANOMALY

Series for $\sin jE$ and $\cos jE$ in terms of the mean anomaly are well known. The coefficients are Bessel functions in the eccentricity e . Derivations are given by *Plummer* [1960]. By substituting these series in the expressions for ξ and η , we obtain the coefficients for their Fourier series in Λ , the mean anomaly. The notation remains the same as in the development for obtaining averages, except that the independent variable is Λ instead of t .

$$\langle \xi \rangle = r_i^2 + a^2(1 + 3e^2/2) + 3er_i \cdot \mathbf{a}$$

$$\langle \eta \rangle = -r_i \cos \xi_i - (3e/2)\mathbf{u}_i \cdot \mathbf{a}$$

Fourier coefficients for the functions ξ and η are readily obtained.

We now have all the results we need to construct the secular part of ΔF_i , i.e.,

$$(\Delta F_i)_s = \frac{1}{2\pi} \int_0^{2\pi} \Delta F_i d\Lambda$$

$$(\Delta F_i)_s = (\epsilon_i/2)\mu s^2([a^2(1 + 3e^2/2) + r_i^2 + 3er_i \cdot \mathbf{a}]^{-3/2} \\ - 3[a^2(1 + 3e^2/2) + r_i^2 + 3er_i \cdot \mathbf{a}]^{-5/2}[r_i \cos \xi_i + (3e/2)\mathbf{u}_i \cdot \mathbf{a}]^2 \\ + (1/16)\{15[a^2(1 + 3e^2/2) + r_i^2 + 3er_i \cdot \mathbf{a}]^{-7/2} \\ - 105[a^2(1 + 3e^2/2) + r_i^2 + 3er_i \cdot \mathbf{a}]^{-9/2}[r_i \cos \xi_i + (3e/2)\mathbf{u}_i \cdot \mathbf{a}]^2\} \\ \cdot [4a^4e^2(1 - 5e^2/4) + a^2er_i \cdot \mathbf{a}(8 - 7e^2) + 4(1 - e^2/2)(\mathbf{r}_i \cdot \mathbf{a})^2 \\ + 4(\mathbf{r}_i \cdot \mathbf{b})^2] - 15[r_i \cos \xi_i + (3e/2)\mathbf{u}_i \cdot \mathbf{a}][a^2(1 + 3e^2/2) \\ + r_i^2 + 3er_i \cdot \mathbf{a}]^{-7/2}\{2[a^2e(1 - 7e^2/4) + (1 - e^2/2)\mathbf{r}_i \cdot \mathbf{a}]\mathbf{u}_i \cdot \mathbf{a} \\ + 2(\mathbf{r}_i \cdot \mathbf{b})(\mathbf{u}_i \cdot \mathbf{b})\} - 6[a^2(1 + 3e^2/2) + r_i^2 + 3er_i \cdot \mathbf{a}]^{-5/2} \\ \cdot \{(\mathbf{u}_i \cdot \mathbf{a})^2(1 - e^2/2) + (\mathbf{u}_i \cdot \mathbf{b})^2\})] \quad (6)$$

The dominant term of $(\Delta F_i)_s$ is

$$(\Delta F_i)_0 = \frac{\epsilon_i \mu s^2}{2} (a^2 + r_i^2)^{-3/2}$$

In the Delauney variables, this is

$$(\Delta F_i)_0 = \frac{\epsilon_i \mu s^2}{2} \left(\frac{L^4}{\mu^2} + r_i^2 \right)^{-3/2}$$

The canonical equations of motion yield [*Hotine*, 1969; *Plummer*, 1960] for the change in mean motion ν

$$\Delta\nu = \Delta(d\Lambda/dt) = -\frac{\partial \Delta F}{\partial L}$$

$$\Delta\nu = \Delta(d\Lambda/dt) = -3\epsilon_i \mu s^2 \frac{L^3}{\mu^2} \left(\frac{L^4}{\mu^2} + r_i^2 \right)^{-5/2}$$

Using

$$\nu = \mu^2/L^3$$

it follows that

$$\frac{\Delta\nu}{\nu} = -3\epsilon_i \frac{s^2}{a^2} \left(1 + \frac{r_i^2}{a^2} \right)^{-5/2}$$

For most practical cases, $r_i^2/a^2 \sim 1$ and $2^{-5/2} \approx 0.18$, and so a suitable form of the above is

$$\Delta\nu/\nu = -0.53\epsilon_i s^2/a^2 \quad (7)$$

If s is equal for all point mass pairs involved in an orbit computation, this important effect can be made to cancel out by using the restriction

$$\sum_i M_i = 0 \quad (8)$$

which is a good one to require anyway, since the total mass of the earth (and of the constant μ) is left unchanged. For the case we would confront in an actual computation, where the point mass

FOSTER MORRISON

115

pairs would be replaced by single points on the far side of the earth, we could require that (8) be satisfied where the sum is taken over only those areas. A very effective way to ensure that (8) is almost true in this case is to constrain the contributions of the density layer to the low-order tesseral harmonics to be zero, since this will cause the total mass of large regular areas of the layer to be small.

All the terms of $(\Delta F_i)_*$ are readily expanded into trigonometric terms of 12- and 24-hour period, long-period (equal to the period of g or h , etc.), or into pure secular terms. Perturbations then could be computed using Von Zeipel's method or that of Lie series [Deprit, 1969].

At this point let us make some observations on the expansion of this function in orbital elements to see what can be done to minimize the effects of quadrature errors.

Let us again emphasize that $\cos \zeta$ is small, so that $[r_i \cos \zeta_i + (3e/2) \mathbf{u}_i \cdot \mathbf{a}]$ will be quite small. The term $r_i \cos \zeta_i$ is always positive, whereas $(3e/2) \mathbf{u}_i \cdot \mathbf{a}$ should be nearly random in sign, and so some canceling will occur and will reduce the magnitude of the sum.

The quantities $(\mathbf{r}_i \cdot \mathbf{a})$, $(\mathbf{u}_i \cdot \mathbf{a})$, $(\mathbf{r}_i \cdot \mathbf{a})^2$, \dots , deserve some special consideration. For one thing $\mathbf{r}_i \cdot \mathbf{a}, \dots$, are of the form

$$\begin{aligned} \mathbf{v}_i \cdot \mathbf{a} &= (\Theta \mathbf{v}) \cdot \mathbf{a} \\ \mathbf{v}_i \cdot \mathbf{a} &= (a_1 v_1 + a_2 v_2) \cos \theta \\ &\quad + (-a_1 v_2 + a_2 v_1) \sin \theta + a_3 v_3 \end{aligned} \quad (9)$$

which yields 24-hour and secular terms; secular at this stage includes terms in a_1, a_2, a_3 of long period and those linear with time.

Terms containing products of $\mathbf{r}_i \cdot \mathbf{a}$ and $\mathbf{u}_i \cdot \mathbf{a}$ never contain both \mathbf{a} and \mathbf{b} vectors, i.e., $(\mathbf{r}_i \cdot \mathbf{a})(\mathbf{r}_i \cdot \mathbf{b})$ does not occur at the order of expansion considered here, and so the generalized form is $q = [(\Theta \mathbf{v}) \cdot \mathbf{p}] [(\Theta \mathbf{w}) \cdot \mathbf{p}]$, where \mathbf{v} and \mathbf{w} are \mathbf{r}_i or \mathbf{u}_i and \mathbf{p} is \mathbf{a} or \mathbf{b} .

The result of multiplying out two products such as (9) is

$$\begin{aligned} q &= (p_1^2 + p_2^2)(v_1 w_1 + v_2 w_2) + v_3 w_3 p_3^2 \\ &\quad + [(p_1^2 + p_2^2)(v_1 w_1 - v_2 w_2)/2 \\ &\quad + p_1 p_2 (v_2 w_1 + v_1 w_2)] \cos 2\theta \\ &\quad + [(p_2^2 - p_1^2)(v_1 w_2 + w_1 v_2)] \end{aligned}$$

$$\begin{aligned} &\quad + p_1 p_2 (v_1 w_1 - v_2 w_2)] \sin 2\theta \\ &\quad + p_1 p_3 (w_1 v_3 + v_1 w_3) \cos \theta \\ &\quad - p_1 p_3 (w_2 v_3 + w_3 v_2) \sin \theta \end{aligned} \quad (10)$$

Observe that the first part of q is secular, the second is 12-hour, and the last part, 24-hour.

To analyze the possible effects of terms having the form of (9) or (10), we need to consider the functions of \mathbf{v} and \mathbf{w}

$$v_1, v_2, v_3, w_1, w_2, w_3, v_1 w_1 + v_2 w_2, v_1 w_1 - v_2 w_2,$$

$$v_2 w_1 + v_1 w_2, w_1 v_3 + v_1 w_3, w_2 v_3 + w_3 v_2, v_3 w_3$$

where $\mathbf{v} = \mathbf{r}_i$ and $\mathbf{w} = \mathbf{u}_i$, or $\mathbf{v} = \mathbf{w} = \mathbf{r}_i$ or $\mathbf{v} = \mathbf{w} = \mathbf{u}_i$. The terms p_1, p_2, p_3 are constant or very long period, so changes in their magnitude will be small during a period of a week or two.

Any one of these 36 functions of \mathbf{u}_i and \mathbf{r}_i is a function of longitude and latitude, β and λ ; let us consider any one as $D(\beta, \lambda)$ or D_i if we consider D as being defined over a set of point mass pairs. Then the total effect of any term having a factor D will be proportional to a sum or integral of products of D_i and ϵ_i . To completely eliminate quadrature error, this sum should be as near zero as possible:

$$\sum_i \epsilon_i D_i = 0 \quad (11)$$

or

$$\int_{\text{surface layer}} \epsilon(\beta, \lambda) D(\beta, \lambda) d\sigma = 0 \quad (12)$$

APPROXIMATION TO \mathbf{u}_i AND \mathbf{r}_i

Figure 3 shows the usual method for approximating a density layer. Four point masses represent the layer within a spherical rectangle bounded by lines of latitude and longitude. When all four points are replaced by one point, it is the same as having two point mass pairs replaced by two coincident points. In an actual approximation done during an integration, the two points will not exactly coincide, and the masses of the points in the pair might not be quite equal, but since we shall be averaging our effects over all or a large part of the density layer, we shall neglect these further complications.

The vector \mathbf{r}_i is given by

$$\mathbf{r}_i^T = R(\cos \beta \cos \lambda, \cos \beta \sin \lambda, \sin \beta) \quad (13)$$

ORBITS COMPUTED FROM DENSITY LAYER MODELS

where we use a spherical approximation for the density layer and assume uniform distribution of point mass pairs.

The distribution of the \mathbf{u}_i is a more complex matter. A unit vector tangent to the surface and pointing north is given by

$$\mathbf{N}^T = (-\sin \beta \cos \lambda, -\sin \beta \sin \lambda, \cos \lambda)$$

A similar vector pointing east is

$$\mathbf{O}^T = (-\sin \lambda, \cos \lambda, 0)$$

For each patch we have two \mathbf{u}_i vectors, one pointing northeast, the other northwest. These are, say,

$$\mathbf{u}_i = \frac{2^{1/2}}{2} (\mathbf{N} + \mathbf{O})$$

$$\mathbf{u}_{i+1} = \frac{2^{1/2}}{2} (\mathbf{N} - \mathbf{O})$$

where the factor is required for $\|\mathbf{u}_i\| = \|\mathbf{u}_{i+1}\| = 1$. Let us combine the above to obtain

$$\begin{aligned} \mathbf{u}_i^T &= \frac{2^{1/2}}{2} (-\sin \beta \cos \lambda \pm \sin \lambda, \\ &\quad -\sin \beta \sin \lambda \pm \cos \lambda, \cos \beta) \end{aligned} \quad (14)$$

With \mathbf{u}_i and \mathbf{r}_i obtained as continuous functions, we can use (12) provided that we consider ϵ_i as a continuous function also.

To evaluate the integrals 12, we need the functions $D(\beta, \lambda)$. They are best expressed, when possible, in sums of spherical harmonics. Only the Legendre functions up to degree 2, order 2 are needed. It turns out that all the products of components of \mathbf{r}_i can be expressed as simple spherical harmonics [Hobson, 1931]; e.g.,

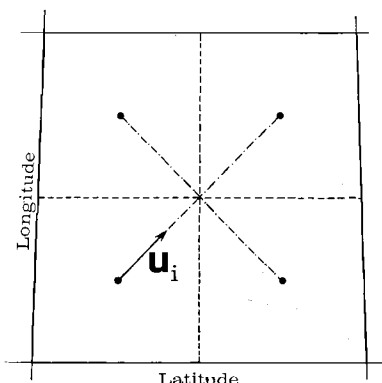


Fig. 3. A density patch represented by four point masses.

$$x_i^2 - y_i^2 = C_2^2/3 = (P_2^2/3) \cos 2\lambda \quad (15)$$

P_k^j denotes a Legendre function and C_k^j is a spherical harmonic. The products of components of \mathbf{u}_i are mostly expressible in simple spherical harmonics, but the products of components of \mathbf{u}_i with \mathbf{r}_i are not expressible in this fashion, e.g.,

$$x_i l_i - y_i m_i$$

$$= \frac{2^{1/2}}{6} P_2^1 \cos 2\lambda \pm \frac{2^{1/2}}{2} P_1^1 \sin 2\lambda \quad (16)$$

In these results, we have taken $R = 1$ for simplicity.

Referring to Figure 3, consider what happens in evaluating (12) if the point mass pairs are equal. All the terms with \pm signs (or \mp) vanish in the end result. At this point, we can say it will drastically reduce the problem of quadrature error if we constrain the contribution of the density layer to $J_2, J_1, C_1^1, S_1^1, C_2^1, S_2^1, C_2^2, S_2^2$ (the geopotential coefficients of first and second order) all to be zero, so that (12) is satisfied. If a density layer model is obtained from some geodetic data, the layer well may have such components in its gravitational potential. In that case, these components should be subtracted and put into the low-order spherical harmonic reference potential before a new iteration in the solution is done or the results are otherwise used. We already have required the contribution to J_0 to be zero by (8). So as far as (12) is concerned, the only non-zero terms are:

$$x_i l_i + y_i m_i = -\frac{2^{1/2}}{6R} P_2^1$$

$$x_i l_i - y_i m_i = \frac{2^{1/2}}{6R} P_2^1 \cos 2\lambda$$

$$x_i m_i + y_i l_i = \frac{2^{1/2}}{6R} P_2^1 \sin 2\lambda$$

$$x_i n_i + z_i l_i = \frac{2^{1/2}}{2R} (-4P_2^0/3 + 1/3) \cos \lambda$$

$$y_i n_i + z_i m_i = \frac{2^{1/2}}{2R} (-4P_2^0/3 + 1/3) \sin \lambda$$

$$z_i n_i = (1/3R) P_2^1$$

$$l_i = -P_1^0 \cos \lambda$$

$$m_i = -P_1^0 \sin \lambda$$

$$n_i = P_1^1$$

FOSTER MORRISON

117

Hence, the only quantities in (6) that will cause appreciable errors are those with factors

$$(\mathbf{u}_i \cdot \mathbf{a})$$

$$(\mathbf{u}_i \cdot \mathbf{b})$$

$$(\mathbf{r}_i \cdot \mathbf{b})(\mathbf{u}_i \cdot \mathbf{b})$$

$$(\mathbf{r}_i \cdot \mathbf{a})(\mathbf{u}_i \cdot \mathbf{a})$$

All these terms, however, have a factor $[r_i \cos \xi_i + (3e/2) \mathbf{u}_i \cdot \mathbf{a}]$, which is smaller than $R(e_E + 3e/2)$, where e_E is the eccentricity of the earth's meridians.

SHORT-PERIOD TERMS

The method of averaging used yields the short-period part of ΔF_i in a straightforward manner. All we do is subtract $\langle \varphi \rangle$ from φ and obtain

$$\varphi - \langle \varphi \rangle = \frac{\partial \varphi}{\partial \xi} (\xi - \langle \xi \rangle) + \frac{\partial \varphi}{\partial \eta} (\eta - \langle \eta \rangle) + \dots$$

When things are pleasant, we can omit all terms except those having first derivatives as factors. For our purposes, it suffices to consider

$$(\Delta F_i)_p = \frac{\partial \varphi}{\partial \xi} \sum_{i=1}^4 (a_i \cos j\Lambda + b_i \sin j\Lambda) + \frac{\partial \varphi}{\partial \eta} \sum_{i=1}^4 (\alpha_i \cos j\Lambda + \beta_i \sin j\Lambda)$$

Let us rewrite this as

$$(\Delta F_i)_p = \sum_{i=1}^4 (a_i^* \cos j\Lambda + b_i^* \sin j\Lambda) \quad (18)$$

$$a_i^* = \frac{\partial \varphi}{\partial \xi} a_i + \frac{\partial \varphi}{\partial \eta} \alpha_i$$

$$b_i^* = \frac{\partial \varphi}{\partial \xi} b_i + \frac{\partial \varphi}{\partial \eta} \beta_i$$

We can observe that the same factors of 12- and 24-hour periods that appear in the 'secular' part of ΔF_i appear in the short-period parts, so that whatever serves to minimize the effects of the long-period terms will minimize the short-period ones also. What we have sought to do is have these factors, when summed over our index i or integrated over a region of the earth's surface, sum to zero. The effect will be to make the total perturbations nil, whether these factors are contained in short-period terms having arguments upon expansion of Λ ($2\Lambda, \Lambda + \theta$,

$\Lambda - \theta, \dots$) or whether they are multiplied by secular terms, giving rise to true secular terms, very-long-period terms, or 12- and 24-hour terms with arguments like $g + \theta, g - \theta, h + g + \theta$.

CONCLUSIONS ON SIMPLE QUADRATURE ERROR

The results of this study indicate that quadrature errors from integrating satellite orbits using a density layer model can be minimized effectively by constraining the contribution of the layer to the harmonics of order and degree 2 or less to be zero; this includes the zero-order (scale) term especially. Orbital eccentricity should not be large; less than 0.055 ($\approx 2e_E/3$) would reduce the effect of orbital eccentricity below that of oblateness.

The functional form of φ is not a good one for convergence of a Taylor series, at least as far as the variable ξ is concerned. But ξ is always positive, and so formal convergence is assured. The average obtained by the theory will be good if a very close approach is not made on a particular pass, that is, as long as $(\xi - \langle \xi \rangle)$ is not very large. The problem of $(\xi - \langle \xi \rangle)$ being large is solved by using a fine mesh of points to represent the density layer directly below the satellite.

PROBLEM OF VARIABLE MESH SIZE

An obvious simplification in using density layer models for the geopotential is to approximate the part of the layer nearby with a fine mesh and the remote parts by a rather coarse one (see Figure 4). This introduces some very

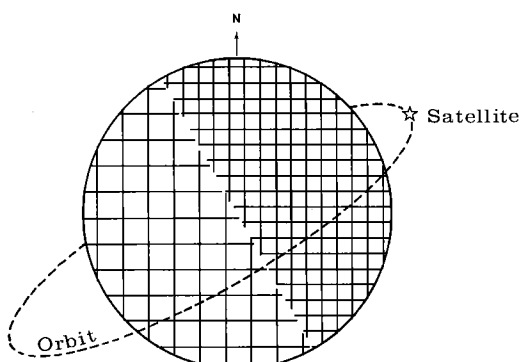


Fig. 4. Using a variable mesh size to compute the gravitational attraction of a density layer on a satellite.

interesting problems into the effects of quadrature error on satellite orbits computed.

First, it is very necessary to have the decision to use a fine or coarse mesh size based on a very simple test. If the test were complicated, the effort to perform it would exceed that needed in using a finer mesh size. The most obvious test is

$$\begin{aligned} r' < r_c &\quad \text{use fine mesh} \\ r' > r_c &\quad \text{use coarse mesh} \end{aligned}$$

where r_c is some constant.

This is a useful test, since r' probably would be needed anyway. For this analysis, we propose:

$$\begin{aligned} \psi < 90^\circ &\quad \text{use fine mesh} \\ \psi > 90^\circ &\quad \text{use coarse mesh} \end{aligned}$$

where $\cos \psi = (\mathbf{r} \cdot \mathbf{r}_i) / rr_i$. The angle ψ is that between position vectors for the satellite and the center of the point mass pair.

Using a smaller mesh size does not eliminate quadrature error, but only reduces it. The single most important effect is making s^2/r'^2 smaller. A coarse mesh has the quadrature error of the fine one in addition to its own, relative to a continuous density distribution, at least if ΔF_i is defined as we have done. If a mesh twice as fine as the original is used, the error of only the larger mesh is removed; the relative error at each step is roughly approximated by the sequence

$$1, 1/4, 1/16, 1/64, \dots, 1/4n, \dots$$

The total quadrature error is roughly proportioned to

$$\begin{aligned} \frac{s^2}{r'^2} \left(1 + \frac{1}{4} + \frac{1}{16} + \frac{1}{64} + \dots \right) \\ = \frac{s^2}{r'^2} \frac{1}{1 - 1/4} = \frac{4}{3} \frac{s^2}{r'^2} \end{aligned}$$

The reduced error is proportional to

$$\frac{s^2}{r'^2} \left[\frac{1}{4} + \frac{1}{16} + \frac{1}{64} + \dots \right] = \frac{1}{3} \frac{s^2}{r'^2}$$

The error is reduced by a factor of 4 by halving s . To account for a variable mesh size, then, the easiest thing to do is make s a function of ψ or r' . We choose to use ψ , because it is easier to create a pulse in a periodic function. If we wish to have

$$s(\psi) = s_0 \quad \psi < 90^\circ$$

$$s(\psi) = 2s_0 \quad \psi \geq 90^\circ$$

our task is very easy, formally. Let us generalize the function to the interval $[-\pi, +\pi]$ and define

$$\kappa(\psi) = s^2(\psi)/s_0^2 = 4 \quad -\pi \leq \psi < -\pi/2$$

$$\kappa(\psi) = s^2(\psi)/s_0^2 = 1 \quad -\pi/2 < \psi < +\pi/2$$

$$\kappa(\psi) = s^2(\psi)/s_0^2 = 4 \quad \pi/2 < \psi \leq \pi$$

For our purpose, we shall use the approximation

$$\kappa(\psi) = (5/2 - 3/2) \cos \psi$$

which will satisfy the conditions $\kappa(0) = 1$, $\kappa(\pi) = 4$.

Since it is only a constant, we will neglect the $4/3$ factor arising from considering all quadrature error, but keep it in mind for making comparisons with numerical results.

Obtaining the expression for $\cos \psi$ in orbital elements is laborious, but straightforward.

$$\cos \psi = \frac{\mathbf{r} \cdot \mathbf{r}_i}{rr_i} = \mathbf{r} \cdot \mathbf{r}_i \left(\frac{a}{r} \right) \frac{1}{ar_i}$$

The task of expressing $\mathbf{r} \cdot \mathbf{r}_i$ has already been done in deriving the expression for ξ . For a/r , we observe

$$\frac{a}{r} = \frac{1 + e \cos f}{1 - e^2}$$

The expansion of $\cos f$ in terms of mean anomaly is well known [Plummer, 1960]. Applying this yields the series for a/r . Now we must execute a multiplication of trigonometric series; this will not be too difficult, since we are truncating at order e^4 . The result of these calculations is the expansion of $\cos \psi$ as a Fourier series with argument Λ . To accommodate this generalization, we introduce

$$\Delta F_i^* = \kappa(\psi) \Delta F_i$$

which calls for use of a function

$$\varphi^* = \kappa \varphi$$

so that

$$\Delta F_i^* = (\epsilon_i \mu s^2 / 2) \varphi^*(\xi, \eta, \kappa)$$

The secular part of $\kappa(\psi)$ is, then,

FOSTER MORRISON

119

$$\langle \kappa \rangle = \frac{5}{2} + \frac{3}{2} e \frac{\mathbf{r}_i \cdot \mathbf{a}}{r_i a}$$

Now we can express $\kappa(\psi)$ as a Fourier series in Λ , the mean anomaly.

$$\kappa = \langle \kappa \rangle + \sum_{i=1}^4 (\alpha_i^* \cos j\Lambda + \beta_i^* \sin j\Lambda)$$

The expression for the secular part of ΔF_i^* is, in terms of previous results,

$$\begin{aligned} (\Delta F_i^*)_s &= \langle \kappa \rangle (\Delta F_i)_s \\ &+ \frac{\epsilon_i \mu s^2}{2} \frac{\partial^2 \varphi^*}{\partial \xi \partial \kappa} \left[\sum_{i=1}^4 (\alpha_i \alpha_i^* + \beta_i \beta_i^*) \right. \\ &\quad \left. + \frac{\partial^2 \varphi^*}{\partial \eta \partial \kappa} \sum_{i=1}^4 (\hat{\alpha}_i \alpha_i^* + \hat{\beta}_i \beta_i^*) \right] \end{aligned}$$

The simplifications due to the linearity of κ in φ^* are that $\partial^2 \varphi^*/\partial \kappa^2 = 0$, so that the term with that factor is to be omitted and $\langle \kappa \rangle (\Delta F_i)_s$ is of such a simple form.

CONCLUSIONS ON THE USE OF VARIABLE MESH SIZE

Although ΔF_i^* is more complicated than ΔF_i , the conditions for keeping its effects small are the same. Details are omitted for the sake of brevity, but the terms in ΔF_i^* also have the

factors enumerated in (15), (16), and (17). The magnitude of the principal secular terms is increased, and it is likely that any residual error not detected due to truncation of this theory will be larger. But the first-order errors can be minimized by using the same constraints suggested for a nonvarying mesh.

REFERENCES

- Danby, J. M. A., *Fundamentals of Celestial Mechanics*, chap. 6, Macmillan, New York, 1962.
- Deprit, A., Canonical transformations depending on a small parameter, *Celestial Mech.*, 1, 12–30, 1969.
- Hobson, E. W., *The Theory of Spherical and Ellipsoidal Harmonics*, chap. 4, Cambridge University Press, London, 1931.
- Hotine, M., *Mathematical Geodesy*, chap. 28, U.S. Government Printing Office, Washington, D.C., 1969.
- Jahnke, E., and F. Emde, *Tables of Functions*, pp. 107–118, Dover, New York, 1945.
- Koch, K. R., and F. Morrison, A simple layer model of the geopotential from a combination of satellite and gravity data, *J. Geophys. Res.*, 75(8), 1483–1492, 1970.
- Morrison, F., A novel method for averaging equations of motion, *J. Astronaut. Sci.*, in press, 1972.
- Plummer, H. C., *Dynamical Astronomy*, chap. 4 and 6, Dover, New York, 1960.
- Whittaker, E. T., and C. N. Watson, *A Course of Modern Analysis*, chap. 9, Cambridge University Press, London, 1962.

Representation of the Earth Potential by Buried Masses

GEORGES BALMINO

*Groupe de Recherches de Géodésie Spatiale
Observatoire, 92 Meudon, France*

Abstract. Some ways of representing the earth potential by point masses are explored. The 1969 standard earth model of the Smithsonian Astrophysical Observatory is used as a reference. Points regularly distributed on a sphere inside the earth have been considered, as well as nonuniform configurations. The values of the masses are derived by a least-squares fit to the SAO field. The values of the different representations obtained have been checked by computing the geoid heights, gravity anomalies, and spherical harmonics associated with the field of the masses. The best model obtained consists of 126 points, mostly at a depth of 1300 km, tied to the important gravity anomalies derived from the reference field. The mean of the residuals is 6 mgal.

The main results obtained so far in dynamical geodesy have been based on the expansion of the earth potential in spherical harmonics. The methods of analysis are complex, for they have to process numerous observations made on different satellites from many stations; in addition, the determination of the potential coefficients and station coordinates, computed at the same time, involves very large matrices that cannot be handled easily on present computers.

In the near future, the technical progress in satellite geodesy, as well as great improvements in type and accuracy of observational methods, will make it necessary to use new representations of the potential of the earth. The series of harmonic coefficients converges very slowly, and too many terms must be taken into account in order to represent small, or short-wave, variations of the field (as measured by an altimeter or determined from gravity measurements). It is desirable that new representations satisfy as many as possible of the following conditions:

1. Discrete formulation (one ‘detail’ for one function), which leads to simple programming. (Recursive formulas lead to important errors, which occur, for example, if one computes the Legendre functions up to (180, 180) to represent details of 1 degree on the geoid.)

2. Homogeneous representation on both the surface and exterior of the earth.

3. Possibility of increasing locally the number of parameters without perturbing distant regions.

4. The same formulation of the potential and its derivative on and outside the earth, so as to facilitate the combination of observations from different sources (like gravity anomalies and satellite-to-ocean altimetry).

The representation of the gravity field by buried masses, which was suggested by *Weightmann* [1967] several years ago, can satisfy these conditions under some restrictions on the configuration and depth of the points.

Theoretically, any distribution of masses inside the earth that keeps the geoid fixed gives the same field outside the geoid. Consequently, it is reasonable to distribute the mass points regularly. Nevertheless, the anomalies of the gravity field already known make us think of putting the masses at the places where particular features exist.

Taking the last standard earth model determined by *Gaposchkin and Lambeck* [1970], we have tried in our approach to attain an equivalence between this model and a configuration of mass points, in order to represent the gravimetric geoid as well as possible. The values of differently obtained representations outside the earth have been checked by integrating satellite orbits.

METHOD

One has the choice of taking a regular distribution on a sphere inside the earth, or putting the points at places corresponding to large gravity anomalies. If the anomalies of the field are not known (they are to be determined through observations), only the first point of view is valid, and a large number of mass points close to the earth's surface must be considered. One can also take surface density values [Koch, 1970], but the expression for the external field is not convenient to use for satellite motion.

Starting from an a priori configuration of points $(\mathbf{P}_i)_0$, $i = 1, 2, \dots, N$, we determine parameters ϵ_i such that:

$$\begin{aligned} U_0 &= \frac{GM}{r} \left[1 - \sum_{n=2}^{21} \left(\frac{a}{r} \right)^n J_n P_n(\sin \phi) \right. \\ &\quad + \sum_{n=2}^{22} \left(\frac{a}{r} \right)^n \sum_{k=1}^{n'} (C_{nk} \cos k\lambda \right. \\ &\quad \left. \left. + S_{nk} \sin k\lambda) P_{nk}(\sin \phi) \right] \quad (1) \end{aligned}$$

$n' = \min(n, 16)$

$$\begin{aligned} U_M &= E + T_M = E + \sum_{k=1}^N T_{Mk} \\ &= E + GM \sum_{k=1}^N \frac{\epsilon_k}{r_k} \end{aligned}$$

$$\iiint_D |U_0 - U_M|^2 dv \text{ is a minimum} \quad (2)$$

where E is a reference potential included in U_m (because terms like

$$1/r \text{ or } (1/r) J_2(a/r)^2 P_2(\sin \phi)$$

cannot be easily represented otherwise, except by deep point masses, which are without physical meaning, and D is a region of space outside the earth (e.g., between 500- and 1500-km height).

D is represented by a large number $M (> N)$ of points S , and we thus have

$$\begin{aligned} \sum_{i=1}^N \left[\left(\frac{\partial T_M}{\partial \epsilon_i} \right)_S \Delta \epsilon_i + (\nabla T_M)_S \cdot \Delta \mathbf{P}_i \right] \\ = (U_0 - U_M)_S \end{aligned}$$

with

REPRESENTING EARTH POTENTIAL

$$\Delta \mathbf{P}_i = \mathbf{P}_i - (\mathbf{P}_i)_0$$

$$\Delta \epsilon_i = \epsilon_i - (\epsilon_i)_0$$

$$(\epsilon_i)_0 = 0$$

at the first iteration.

Different weights according to the heights of S can be chosen. In addition, we add the following constraints:

$$\sum_{i=1}^N \epsilon_i = 0$$

i.e., the total mass of the earth is unchanged, and

$$\sum_{i=1}^N \epsilon_i \mathbf{g}_i = 0$$

i.e., the center of inertia is not modified.

In the above,

$$\mathbf{g}_k = \mathbf{r} - \mathbf{r}_k$$

where \mathbf{r} is the geocentric vector to S , the point at which the potential is being computed, and \mathbf{r}_k is the vector from mass point P_k to S .

Finally, we solve

$$\begin{pmatrix} [\mathbf{A}^T \mathbf{\Pi} \mathbf{A}] & \mathbf{J}^T \\ J & 0 \end{pmatrix} \begin{pmatrix} \mathbf{Y} \\ \Lambda \end{pmatrix} = \begin{pmatrix} [\mathbf{A}^T \mathbf{\Pi}] & \Delta \\ 0 & 0 \end{pmatrix} \quad (3)$$

where

\mathbf{A} is the matrix of equations of condition.

\mathbf{J} is the jacobian of constraints.

\mathbf{y} is the vector of unknowns.

Δ is the vector of Lagrange multipliers.

$\mathbf{\Pi}$ is the matrix of weights.

Δ is the vector of the quantities $(U_0 - U_M)$.

Results obtained using (3) in conjunction with (1) and (2) did not yield a satisfactory representation of the field on the earth's surface. Hence, condition (2) was replaced by:

$$\iint_{\Phi} |\Delta g_0 - \Delta g_M|^2 ds \text{ is a minimum} \quad (4)$$

where Δg_0 is the field of the gravity anomalies derived from U_0 , and

$$\Delta g_M = \frac{\partial T_M}{\partial n} - \frac{2T}{a}$$

n being the normal at the surface Φ of the reference ellipsoid whose potential here is exactly E and whose mean radius is a .

GEORGES BALMINO

123

A natural weighting is obtained by writing the condition equations on the level curves of the gravity anomalies, which gives more importance to the large anomalies. Local studies have been made to determine optimal values ϵ_i, ρ_i for large anomalies.

The adequacy of a mass-point representation obtained via (2) or (4) can be checked in the following ways:

1. Computation of the residuals $U_0 - U_M$ in D .

2. Calculation of gravity anomalies on ϕ from the formula:

$$\Delta g_Q = GM \sum_{k=1}^N \frac{\epsilon_k}{r_k^3} (a - \rho_k \cos \psi_k)$$

where Q is a point on Φ , a is the geocentric radius to Q , and ψ_k is the geocentric angle between \mathbf{g}_i and \mathbf{a} ; Δg_Q can then be compared with the actual anomaly at Q .

3. Determination of a harmonic coefficient set

$$\langle \gamma_{lm} \rangle = \sum_{k=1}^N \epsilon_k \left(\frac{\rho_k}{a} \right)^l \bar{P}_{lm}(\sin \phi_k) \cdot \left(\frac{(2 - \delta_0^m)(l - m)!}{(2l + 1)(l + m)!} \right)^{1/2} \cos m \lambda_k$$

$$\langle \sigma_{lm} \rangle = \sum_{k=1}^N \epsilon_k \left(\frac{\rho_k}{a} \right)^l \bar{P}_{lm}(\sin \phi_k) \cdot \left(\frac{(2 - \delta_0^m)(l - m)!}{(2l + 1)(l + m)!} \right)^{1/2} \sin m \lambda_k$$

where the bar denotes normalization; these can be compared with the SAO coefficients [Gaposchkin and Lambeck, 1970].

4. Comparison of numerical integration of a given orbit of a satellite in the SAO field and in the field U_M .

RESULTS

Various tests using regular distributions of mass points and condition 2 proved unsatisfactory. A model that gave a good representation of the gravity anomalies on the ellipsoid was obtained in the following manner. The reference potential E in (1) was taken to be the earth ellipsoid harmonics. Ninety-two points were positioned at the extreme values of a map of gravity anomalies based on the SAO

standard earth. Constraining the points to lie at the same depth, the best representation was obtained at a depth of 1300 km. This preliminary model was improved by adding additional points up to a total of 126 and individually adjusting the depths of the 20 largest anomalies. The results are given in Table 1. For this model,

TABLE 1. Model for 126 Mass Points

N	Lat. ϕ , deg	Long. λ , deg	Depth, km	Mass $\epsilon_i 10^{-6}$ mass of earth
1	59	-152	-1100	1.753
2	3	-176	-1300	-0.511
3	-66	-177	-1300	-1.667
4	20	-160	-1300	0.810
5	-31	-159	-1300	1.176
6	-15	-158	-1300	-0.499
7	-2	-155	-1300	0.912
8	22	-143	-1300	-1.233
9	-27	-140	-1300	-1.734
10	32	-126	-1300	-1.603
11	3	-125	-1300	-1.159
12	-19	-121	-1300	0.762
13	-46	-121	-1500	2.122
14	47	-115	-1100	0.667
15	-12	-101	-1300	0.699
16	-49	-99	-1300	-1.632
17	38	-98	-1300	-1.334
18	-76	-95	-1300	-1.265
19	-35	-85	-1300	0.579
20	-15	-85	-1000	-1.507
21	60	-89	-1300	-2.065
22	39	-71	-1300	-0.645
23	0	-71	-1300	1.868
24	-19	-69	-1300	1.667
25	-54	-69	-1500	1.048
26	19	-64	-1300	-1.713
27	24	-28	-1300	-0.175
28	9	-49	-1300	-1.275
29	-14	-52	-1300	-1.015
30	-36	-42	-2000	-0.646
31	42	-32	-1100	1.876
32	-18	-24	-1200	-1.061
33	69	-20	-1300	0.977
34	60	-175	-1300	-0.933
35	9	-11	-1300	0.974
36	22	-4	-1300	-0.665
37	-64	-25	-1500	0.753
38	39	-3	-1000	1.218
39	-39	2	-1000	-0.616
40	-50	15	-1300	0.987
41	-66	21	-1300	-1.337
42	-42	24	-1300	-0.848
43	4	25	-1000	-1.482
44	18	29	-1300	1.940
45	30	25	-1300	-2.460
46	45	26	-1000	1.498

TABLE 1. (continued)

N	Lat. ϕ , deg	Long. λ , deg	Depth, km	Mass ϵ , 10^{-6} mass of earth
47	35	46	-1300	2.707
48	21	50	-1300	-2.213
49	-6	48	-1100	-1.360
50	-43	43	-1300	2.359
51	-44	61	-1300	-1.681
52	-67	73	-1300	1.682
53	-36	74	-1300	1.603
54	4	79	-1000	-2.143
55	41	68	-1300	-1.807
56	69	76	-1300	-1.792
57	35	90	-1300	1.308
58	-49	99	-1300	1.380
59	-25	98	-1300	-1.575
60	-1	112	-1300	1.590
61	47	100	-1300	-1.931
62	62	109	-1300	2.080
63	12	124	-1300	1.110
64	-21	121	-1300	0.808
65	-38	122	-1300	-2.029
66	-63	120	-1300	-1.442
67	-4	142	-1100	1.224
68	31	141	-1300	1.625
69	-42	152	-1500	-2.374
70	1	159	-1300	-0.434
71	39	160	-1300	-1.755
72	57	158	-1300	2.384
73	-47	135	-1300	-0.178
74	-25	174	-1300	0.766
75	22	101	-1300	-0.895
76	68	133	-1300	-1.734
77	-9	30	-1300	0.498
78	16	-94	-1300	0.707
79	10	50	-1300	1.573
80	40	-112	-1300	1.519
81	58	-40	-1300	-0.578
82	58	53	-1300	1.700
83	-18	-40	-1300	1.284
84	-46	167	-1300	1.113
85	85	100	-1100	1.052
86	-42	-35	-2000	-2.932
87	-42	-16	-1300	1.248
88	26	126	-1300	-1.006
89	40	131	-1300	0.942
90	-19	160	-1200	0.684
91	39	-163	-1300	-0.595
92	42	-17	-1100	-1.040
93	43	-135	-1300	-1.365
94	33	-144	-1300	0.933
95	17	-134	-1300	1.106
96	-51	-142	-1300	-0.318
97	-34	-108	-1300	-0.378

REPRESENTING EARTH POTENTIAL

TABLE 1. (continued)

N	Lat. ϕ , deg	Long. λ , deg	Depth, km	Mass ϵ , 10^{-6} mass of earth
98	44	-89	-1300	1.252
99	77	-121	-1300	-0.334
100	82	-78	-1300	-0.857
101	85	-20	-1300	0.048
102	71	-52	-1300	1.519
103	37	-53	-1300	-0.470
104	27	-44	-1300	1.064
105	58	-5	-1300	0.667
106	-85	100	-1300	-0.010
107	4	-28	-1300	0.333
108	-6	-11	-1300	-0.127
109	-27	-16	-1300	-0.133
110	-73	-15	-1300	0.625
111	-61	-81	-1300	0.622
112	-33	-70	-1300	0.064
113	-23	-4	-1300	1.177
114	-10	4	-1300	-0.403
115	-19	30	-1300	0.091
116	28	65	-1300	0.961
117	48	43	-1300	-2.070
118	58	13	-1300	-1.057
119	16	145	-1300	-0.561
120	-47	137	-1300	0.899
121	-16	69	-1300	0.336
122	-15	112	-1300	-0.598
123	-29	145	-1300	0.153
124	23	165	-1300	-0.164
125	55	131	-1300	-0.872
126	15	14	-1300	0.990

the mean of the residuals is 6 mgal and the largest differences are of the order of 10 mgal, which is the estimated accuracy of the SAO standard earth.

REFERENCES

- Gaposchkin, E. M., and K. Lambeck, 1969 Smithsonian standard earth (II), *Smithson. Astrophys. Observ. Spec. Rep. 315*, 1970.
 Koch, K. R., Surface density values for the earth from satellite and gravity observations, *Geophys. J. Roy. Astron. Soc.*, 21, 1-12, 1970.
 Weightman, J. A., Gravity, geodesy, and artificial satellites: A unified analytical approach, in *The Use of Artificial Satellites for Geodesy*, vol. 2, edited by G. Veis, pp. 467-486, National Technical University, Athens, Greece, 1967.

Geopotential Representation with Sampling Functions

C. A. LUNDQUIST

Smithsonian Astrophysical Observatory, Cambridge, Massachusetts 02138

G. E. O. GIACAGLIA¹

University of Texas, Austin, Texas 78712

Abstract. Satellite-to-ocean altitudes measured to meter accuracy eventually can yield a geoid representation with significant short-wavelength structure over ocean areas. To cope conveniently with this expected detail, one suggested analytical technique would represent the geopotential or the geoid as an expansion in sampling functions that are linear combinations of spherical harmonics. Each of the sampling functions makes its principal contribution to the geopotential in a single geographical region. For a representation truncated after degree N , there are $(N + 1)^2$ such functions associated with a like number of points distributed nearly regularly on the globe. The features of this geopotential representation can be illustrated by considering the case $N = 22$, for which an expansion in sampling functions can be produced that is equivalent to the geopotential of the 1969 Smithsonian standard earth.

In the future, satellite instrumentation can generate observations so frequently and of such accuracy that these data will carry substantially more detailed information about the geopotential than is available from satellites today [Kaula, 1970a]. A particular example would be satellite-to-ocean altitudes measured to meter accuracy every 10 sec (about 0.6 deg of arc) along the orbit of the satellite [Kaula, 1970a, pp. 2–18]. Motivated by these expectations, several authors have examined mathematical representations of the geopotential that offer various advantages when short-wavelength features must be represented [e.g., Koch and Morrison, 1970; Obenson, 1970; Croopnick, 1970; Vinti, 1970; Lundquist and Giacaglia, 1969].

In a critical review of such suggested representations, Kaula [1970b] concludes: ‘Because of the characteristics of close satellite orbit dynamics and orbit determination from ground tracking, spherical harmonics will continue to be the most suitable representation of the main

part of the gravitational field indefinitely. However, qualitatively different satellite measurements such as precise satellite-to-satellite tracking, radar altimetry, and gravity gradiometry make appropriate spatial representations for the residual field. . . .’

Some desirable mathematical features of a representation in spherical harmonics follow from the property that this is a truncated expansion in a complete set of independent functions spanning some linear manifold in a vector space. Thus, it is instructive to examine other representations that have this same property. A representation in sampling functions is such an expansion in a complete set of independent functions, and this set can be selected to span the same linear manifold as the truncated spherical-harmonic expansion. Furthermore, the sampling-function expansion has most of the advantages of a spatial tabulation, and it is equally adaptable to representing the full or the residual field.

The sampling functions on a sphere that we will use here are given that name by analogy with the sampling functions used in information theory. The most familiar sampling function of one independent variable has the form [e.g.,

¹ On leave from the University of São Paulo, São Paulo, Brazil.

126

Shannon and Weaver, 1959, p. 53; Brillouin, 1962, p. 98; Goldman, 1953, pp. 69, 70]

$$Sa(2\pi wt) = [\sin(2\pi wt)]/2\pi wt$$

where w is the highest-frequency Fourier component in the functions to be represented. There is a similar function of one variable discussed below [Goldman, 1953, p. 83; Brillouin, 1962, p. 95], which plays the role of a sampling function for periodic functions. The sampling functions on a sphere have the same relation to spherical harmonics as sampling functions for periodic functions on a line have to sine and cosine functions.

The sampling theorem for periodic functions of one variable [Goldman, 1953, p. 83] can be stated as follows: If $f(\lambda)$ is a periodic function of period 2π and if all its Fourier coefficients vanish above the N th harmonic, then

$$f(\lambda) = \sum_{k=0}^{2N} f(\lambda_k) q_{Nk}(\lambda)$$

in which the $2N + 1$ sampling points λ_{Nk} are

$$\lambda_{Nk} = k \frac{2\pi}{2N+1} \quad k = 0 \text{ to } 2N$$

and in which the sampling functions $q_{Nk}(\lambda)$ for periodic functions are given by

$$\begin{aligned} q_{Nk}(\lambda) &= \frac{1}{2N+1} \left[1 + 2 \sum_{j=1}^N \cos j(\lambda - \lambda_k) \right] \\ &= \frac{1}{2N+1} \frac{\sin \{(2N+1)/2](\lambda - \lambda_k)\}}{\sin [(\lambda - \lambda_k)/2]} \\ &\quad k = 0 \text{ to } 2N \end{aligned}$$

(for corresponding formulas for unequally

GEOPOTENTIAL REPRESENTATION

spaced points, see Giacaglia [1970]). Thus, each of the $2N + 1$ sampling functions $q_{Nk}(\lambda)$ is expressed as a truncated Fourier series in the $2N + 1$ functions $\{\cos j\lambda, \sin j\lambda; j = 0 \text{ to } N\}$. Also, the $q_{Nk}(\lambda)$ have the same shape and differ only by a translation in multiples of $2\pi/(2N + 1)$ along the λ axis. Figure 1 illustrates this shape for $N = 22$.

The inverse of this relation is

$$\cos m\lambda = \sum_{i=0}^{2N} (\cos m\lambda_i) q_{Ni}(\lambda)$$

$$\sin m\lambda = \sum_{i=0}^{2N} (\sin m\lambda_i) q_{Ni}(\lambda)$$

$$m = 0 \text{ to } N$$

The sampling functions $q_{Nk}(\lambda)$ have the properties that

$$q_{Ni}(\lambda_k) = \delta_{ik}$$

$$\sum_{i=0}^{2N} q_{Ni}(\lambda) = 1$$

$$\sum_{i=0}^{2N} q_{Ni}(\lambda_i) q_{Nk}(\lambda_i) = \delta_{ik}$$

To formulate an analogous set of functions for a sphere, the first consideration must be the distribution of sampling points on a sphere. Through degree N , there are $(N + 1)^2$ independent spherical harmonics, so it is necessary to distribute $(N + 1)^2$ points uniformly in some sense. Of course, there are but five regular polyhedra, and only the tetrahedron has a number of vertices equal to the square of an integer. Hence, the distribution must depart somehow from ideal regularity. This is essentially the incompletely solved mathematical problem of packing a number of equal nonover-

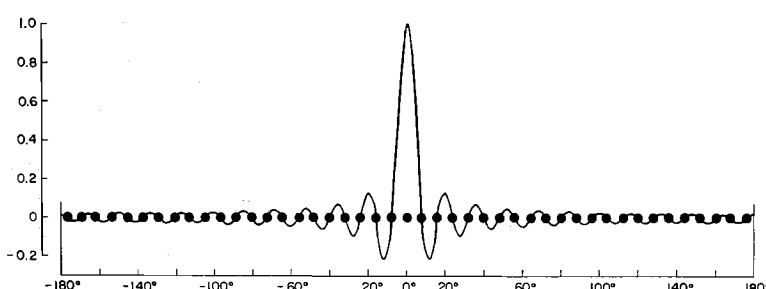


Fig. 1. The function $q_{N0}(\lambda)$ for $N = 22$.

C. A. LUNDQUIST AND G. E. O. GIACAGLIA

127

lapping circles on a sphere (for a review of this problem, see Coxeter [1962]).

For our purposes, we seek also a distribution of points for which we can find tractable mathematical expressions for the linear transformation and the inverse transformation relating the sampling functions to the spherical harmonics. Such a set is obtained by first defining $N + 1$ values of the polar angle θ , or equivalently by values of $\zeta = \cos \theta$,

$$\zeta_k = (-1)^k \cos [k\pi/(2N + 1)] \\ k = 0 \text{ to } N$$

Then, on each of the small circles corresponding to ζ_k , define $2k + 1$ points spaced uniformly in longitude λ ,

$$\lambda_{ki} = \frac{j2\pi}{2k + 1} \quad j = 0, 1, \dots, 2k$$

This distribution of points on the globe is illustrated in Figure 2. The spacing in latitude between circles of points is $2\pi/(2N + 1)$, except that the most southerly latitude is only half this distance from the south pole. This most southerly latitude circle (ζ_2) has three points. Below the single point at the north pole, (ζ_0), the next circle (ζ_2) has five points. The second most southerly circle (ζ_3) has seven points, and so forth. The latitude circle nearest the equator has the greatest number of points, $2N + 1$. Also, any meridian circle has $2N + 1$ uniformly spaced intersections with the latitude circles. In this sense, the points are spaced equally in latitude and longitude. However, this distribution does differ somewhat from the theoretical limits on interpoint spacing discussed by Coxeter [1962].

By analogy with sampling functions on a line, with this selected point distribution for a representation truncated after degree N , we define sampling functions $W_{kj}(\zeta, \lambda)$ on a sphere satisfying the conditions

$$W_{kj}(\zeta, \lambda) = \sum_{n=0}^N \sum_{m=0}^n A_{kj}{}^{nm} X_{nm}(\zeta, \lambda) \\ + B_{kj}{}^{nm} Y_{nm}(\zeta, \lambda)$$

$$X_{nm}(\zeta, \lambda) = \sum_{k=0}^N \sum_{i=0}^{2k} X_{nm}(\zeta_k, \lambda_{ki}) W_{kj}(\zeta, \lambda)$$

$$Y_{nm}(\zeta, \lambda) = \sum_{k=0}^N \sum_{i=0}^{2k} Y_{nm}(\zeta_k, \lambda_{ki}) W_{kj}(\zeta, \lambda)$$

$$W_{kj}(\zeta_h, \lambda_{hi}) = 1 \quad \text{if } (k, j) = (h, i)$$

$$W_{kj}(\zeta_h, \lambda_{hi}) = 0 \quad \text{if } (k, j) \neq (h, i)$$

where $X_{nm}(\zeta, \lambda)$ and $Y_{nm}(\zeta, \lambda)$ are the conventional spherical surface harmonics, and $A_{kj}{}^{nm}$, $B_{kj}{}^{nm}$ are constants.

The equations for the spherical harmonics as an expansion in sampling functions is a sufficient, implicit definition for the $W_{kj}(\zeta, \lambda)$. Explicit formulas for the values of $A_{kj}{}^{nm}$ and $B_{kj}{}^{nm}$ have been derived, but they are lengthy and need not be rewritten here (see Giacaglia and Lundquist [1972]; for numerical values for $N = 4, 5, 9$, see Hebb and Mair [1969]).

The functions $W_{kj}(\zeta, \lambda)$ have the additional properties that

$$\sum_{k=0}^N \sum_{i=0}^{2k} W_{kj}(\zeta, \lambda) = 1$$

$$W_{kj}(\zeta_k, \lambda) = q_{kj}(\lambda)$$

The second equation is a further demonstration that the $W_{kj}(\zeta, \lambda)$ are a natural generalization of the $q_{kj}(\lambda)$. Thus, Figure 1 is also a representation of $W_{22,0}(\zeta_{22}, \lambda)$.

Finally, and most important, if $f(\zeta, \lambda)$ is any function in the linear manifold spanned by the spherical harmonics through degree N , then

$$f(\zeta, \lambda) = \sum_{k=0}^N \sum_{i=0}^{2k} f(\zeta_k, \lambda_{ki}) W_{kj}(\zeta, \lambda)$$

For analysis of satellite-to-ocean altitudes, the geoid might be expressed advantageously in this form, as will be discussed in the following paragraphs. Alternatively, the gravitational potential itself can be represented in three dimensions by an expansion expressing the angular dependence in sampling functions [Giacaglia and Lundquist, 1971]. Similarly, the residuals between the earth's field and a reference field are conveniently written in this formulation, because the residual values at the sampling points will be just the difference between the coefficients for the full and the reference fields.

The geoid can be defined as the equipotential surface best approximating mean sea level, radius $r(\zeta, \lambda)$ being defined implicitly by the following equation (see, e.g., Rapp [1970] for a discussion of the alternative methods for the computation of geoid undulations from potential coefficients):

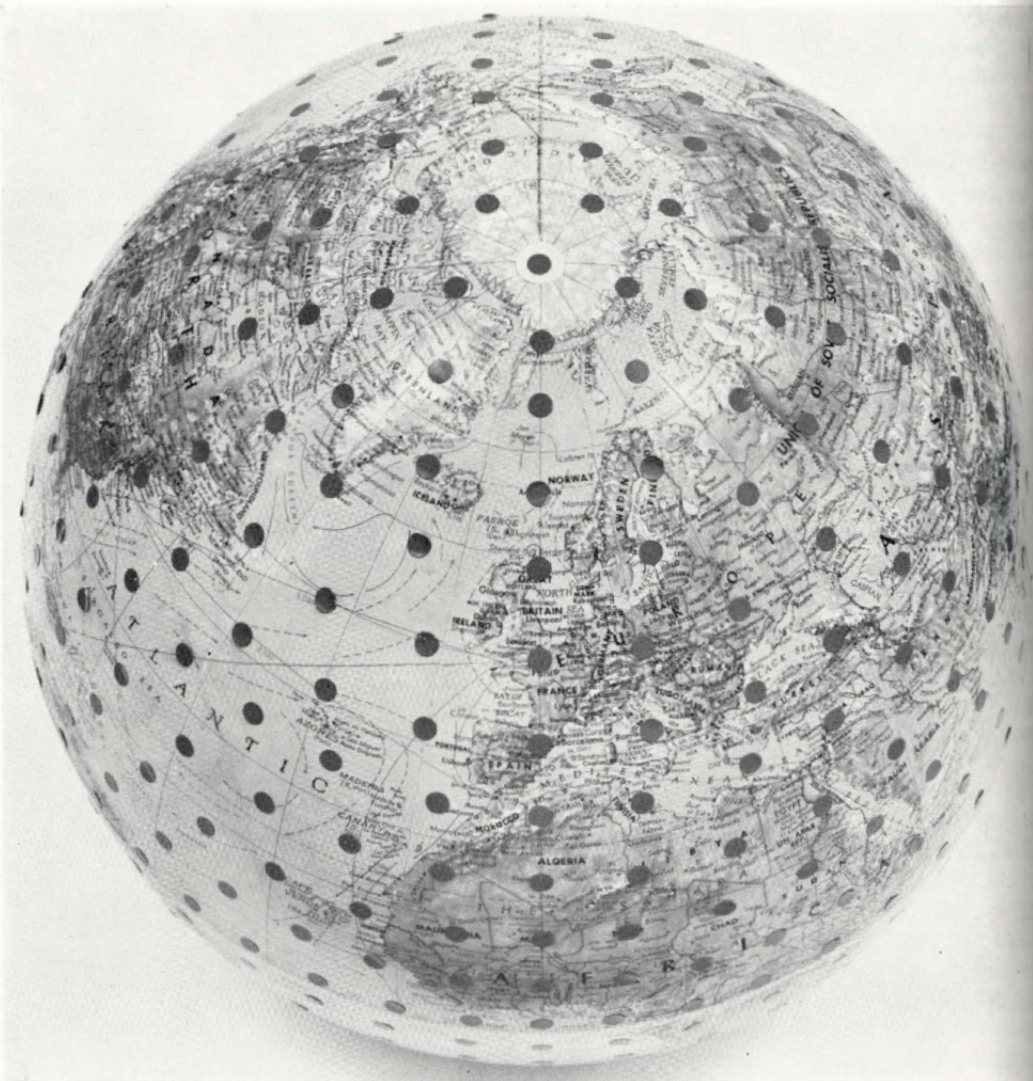


Fig. 2. The distribution of sampling points on the earth for $N = 22$.

$$r = R_0 \sum_{n=0}^N \sum_{m=0}^n \left(\frac{a}{r} \right)^n [C_{nm} X_{nm}(\xi, \lambda) + S_{nm} Y_{nm}(\xi, \lambda)] + \frac{R_0}{3} \left(\frac{r}{a} \right)^3 \sigma [(1 - X_{20}(\xi))$$

where the last term comes from the rotation of the earth with angular speed ω ; $\sigma = \omega^2 a^3 / GM$; R_0 defines the actual mean sea level (or 'best' geoid); a is, in principle, a scale factor for distances; and C_{nm} and S_{nm} are the conventional coefficients for the gravitation potential.

The solution of this for r can be written in the form (following *Burša* [1969], with slight notational changes)

$$r = R_0 \sum_{n=0}^N \sum_{m=0}^n [A_{nm} X_{nm}(\xi, \lambda) + B_{nm} Y_{nm}(\xi, \lambda)]$$

giving the radius r of the geoid at longitude λ and latitude $\phi = \arcsin \xi$, $[-\pi/2 \leq \phi \leq \pi/2]$. The coefficients A_{nm} and B_{nm} depend on the quantities $\alpha = a/R_0$, $\beta = \sigma a^{-3}$, $\gamma = -\alpha^2 C_{20}$, C_{nm} ,

C. A. LUNDQUIST AND G. E. O. GIACAGLIA

129

and S_{nm} ($n = 2, 3, \dots, N$; $m = 1, 2, \dots, n$). Such relations and their inverse can be easily obtained and are as follows (neglecting terms less than 10^{-9}):

$$A_{00} = 1 + \frac{1}{3}\beta + \frac{2}{5}\beta^2 + \frac{24}{35}\beta^3 + \frac{1}{15}\beta\gamma + \frac{8}{35}\beta^2\gamma - \frac{2}{5}\gamma^2$$

$$A_{20} = -\frac{1}{3}\beta - \frac{4}{7}\beta^2 - \frac{8}{7}\beta^3 - \frac{5}{21}\beta\gamma - \frac{4}{7}\beta^2\gamma - \gamma - \frac{4}{7}\gamma^2$$

$$A_{40} = a^4 C_{40} + \frac{6}{35}\beta^2 + \frac{6}{35}\beta\gamma - \frac{36}{35}\gamma^2 + \frac{216}{385}\beta^3 + \frac{192}{385}\beta^2\gamma$$

$$A_{60} = a^6 C_{60} + \frac{8}{77}\beta^3 - \frac{12}{77}\beta^2\gamma$$

$$A_{10} = A_{11} = B_{10} = B_{11} = A_{21} = B_{21} = 0$$

$$A_{22} = a^2 C_{22}$$

$$B_{22} = a^2 S_{22}$$

$$A_{n0} = a^n C_{n0} \quad (n = 3, 5; 7, 8, \dots, N)$$

$$A_{nm} = a^n C_{nm} \quad (n = 3, 4, 5, \dots, N); \quad (m = 1, 2, \dots, n)$$

$$B_{nm} = a^n S_{nm}$$

Let

$$u = A_{00} - 1 \simeq 10^{-3}$$

$$v = 1 - A_{00} - A_{20} \simeq 10^{-3}$$

The inverse relations are:

$$\begin{aligned} \beta &= 3u - \frac{6}{5} \left(3u - \frac{54}{5}u^2 + \frac{6}{5}v^2 - \frac{3}{5}uv \right)^2 \\ &\quad + \frac{6}{5} \left(v - \frac{54}{35}u^2 - \frac{34}{35}v^2 - \frac{18}{35}uv \right)^2 \\ &\quad - \frac{1}{5} \left(3u - \frac{54}{5}u^2 + \frac{6}{5}v^2 - \frac{3}{5}uv \right) \\ &\quad \cdot \left(v - \frac{54}{35}u^2 - \frac{34}{35}v^2 - \frac{18}{35}uv \right) \\ &\quad - \frac{1944}{35}u^3 - \frac{216}{35}u^2v \end{aligned}$$

$$\begin{aligned} \gamma &= v - \frac{54}{35} \left(3u - \frac{54}{5}u^2 + \frac{6}{5}v^2 - \frac{3}{5}uv \right)^2 \\ &\quad - \frac{34}{35} \left(v - \frac{54}{35}u^2 - \frac{34}{35}v^2 - \frac{18}{35}uv \right)^2 \\ &\quad - \frac{18}{105} \left(3u - \frac{54}{5}u^2 + \frac{6}{5}v^2 - \frac{3}{5}uv \right) \\ &\quad \cdot \left(v - \frac{54}{35}u^2 - \frac{34}{35}v^2 - \frac{18}{35}uv \right) \\ &\quad - \frac{432}{35}u^3 - \frac{108}{35}u^2v \end{aligned}$$

where terms of degree ≥ 4 in u and v can be neglected.

We finally obtain, setting $GM = \mu$,

$$R_0 = (\mu\beta/\omega^2)^{1/3} \quad a = a/R_0$$

$$C_{20} = -\gamma a^{-2} \left(\frac{\mu^2 \beta^2}{\omega^4} \right)^{1/3}$$

$$C_{40} = -\alpha^{-4} \left(-A_{40} + \frac{6}{35}\beta^2 + \frac{6}{85}\beta\gamma - \frac{36}{35}\gamma^2 + \frac{216}{385}\beta^3 + \frac{192}{385}\beta^2\gamma \right)$$

$$C_{60} = -\alpha^{-6} \left(-A_{60} - \frac{8}{77}\beta^3 - \frac{12}{77}\beta^2\gamma \right)$$

$$C_{n0} = \alpha^{-n} A_{n0} \quad (n = 3, 5; 7, 8, \dots, N)$$

$$C_{nm} = \alpha^{-n} A_{nm} \quad (n = 3, 4, 5, \dots, N);$$

$$S_{nm} = \alpha^{-n} B_{nm} \quad (m = 1, 2, \dots, n)$$

These relations serve the following purposes: Given the C_{nm} , S_{nm} , one can compute the A_{nm} , B_{nm} and subsequently the geoidal radius. Given the A_{nm} , B_{nm} , one can compute the C_{nm} , S_{nm} . It remains to be shown how the A_{nm} , B_{nm} are related to local undulations of the geoid.

Expanding r in sampling functions, one has necessarily

$$r = R_0 \sum_{k=0}^N \sum_{i=0}^{2k} \bar{r}_{ki} W_{ki}(\xi, \lambda)$$

where

$$\bar{r}_{ki} = \frac{r(\xi_k, \lambda_{ki})}{R_0}$$

It follows that

$$A_{nm} = \sum_{k=0}^N \sum_{i=0}^{2k} \bar{r}_{ki} A_{ki}{}^{nm}$$

$$B_{nm} = \sum_{k=0}^N \sum_{i=0}^{2k} \bar{r}_{ki} B_{ki}{}^{nm}$$

Reciprocally,

$$\bar{r}_{ki} = \sum_{n=0}^N \sum_{m=0}^n [A_{nm} X_{nm}(\xi_k, \lambda_{ki}) + B_{nm} Y_{nm}(\xi_k, \lambda_{ki})]$$

In summary, for the geoid expansion in sampling functions, the coefficients are just the values of the radial distance from the center of mass to the equipotential surface in the $(N+1)^2$ sampling directions (ξ_k, λ_{kj}) . This is a particularly simple and easily interpreted representation. These coefficients are easily transformed into coefficients for a spherical-harmonic expansion of the geopotential, and conversely.

To the accuracy of a few meters expected from the first satellite altimeter, mean sea level can be identified with the geoid, and a determination of sea level yields an improved geopotential. At decimeter accuracy, mean sea level departs from the geoid because of currents, winds, and other geophysical phenomena. In this case, the sea-level surface, or its departure from the geoid, can be represented by a sampling-function expansion distinct from the geoid. Also, for accurate calculations, corrections for the mass of atmospheric and solid topography above the geoid must be made.

To accommodate a sea-level profile with 1° wavelength, as will ultimately be necessary in work with satellite data, an appropriate choice is $N = 180$. There will then be 32,761 sampling directions, each of which can be associated with the center of an area of about 1 square degree on the earth's surface.

All the altitude measurements falling within any one of these areas could be aggregated statistically to give a mean radial value for the sampling direction, which is automatically the desired coefficient in the expansion. In this determination of the sea level, the satellite coordinates would depend on the geopotential at satellite altitudes, expressed most conveniently as an expansion in spherical harmonics through perhaps degree 20, depending on the orbit characteristics [Gaposchkin, 1970]. Laser ranging

GEOPOTENTIAL REPRESENTATION

from ground stations, and if necessary the altitudes themselves, could be used to determine the orbit of the satellite [Lundquist, 1967; Lundquist and Giacaglia, 1969].

Assorted iterative variants of this basic procedure are easily adapted for particular circumstances, because the linear transformations are given analytically between spherical harmonics and sampling functions. Thus, when the spectral character of the geopotential is important, as in satellite orbit theory, the spherical-harmonic form would be employed. When a tabular representation by geographical areas is convenient, the equivalent sampling-function form would be used.

Before a satellite-to-ocean altimeter is flown, the astrogeodetic geoid for continental areas might provide an instructive application of a sampling-function representation. In geographical areas where such information is available, the sampling-function coefficients could be adjusted to incorporate the short-wavelength detail of the astrogeoid. This could be a useful step toward preparation for a satellite altimeter, since some ground-based data over continents would eventually have to be used to balance the detailed altimeter data over the oceans.

Acknowledgment. This research was supported in part by grant NGR 09-015-002 from the National Aeronautics and Space Administration. One of us (Giacaglia) was partly supported by ONR contract N00014-67-A-0126-0013.

REFERENCES

- Brillouin, L., *Science and Information Theory*, 2nd ed., Academic, New York, 1962.
- Burša, M., Potential of the geoidal surface, the scale factor for lengths and earth's figure parameters from satellite observations, *Stud. Geophys. Geod.*, 13, 337-357, 1969.
- Coxeter, H. S. M., The problem of packing a number of equal nonoverlapping circles on a sphere, *Trans. N.Y. Acad. Sci.*, 24, 320-331, 1962.
- Croopnick, S. R., Orbit prediction in the presence of gravitational anomalies, Ph.D. thesis, Mass. Inst. of Tech., Cambridge, 1970.
- Gaposchkin, E. M., Future uses of laser tracking, in *Proceedings of the Geos 2 Program Review Meeting*, 22-24 June 1970, vol. 3, pp. 1-40, edited by Computer Sci. Corp., Falls Church, Va., 1970.
- Giacaglia, G. E. O., Trigonometric interpolation, in *Celestial Mechanics*, vol. 1, pp. 360-367, D. Reidel, Netherlands, 1970.

C. A. LUNDQUIST AND G. E. O. GIACAGLIA

131

- Giacaglia, G. E. O., and C. A. Lundquist, Sampling functions as an alternative to spherical harmonics, in *Special Proceedings of IAU Symposium 48, Rotation of the Earth*, edited by S. Yumi, in press, 1971.
- Giacaglia, G. E. O., and C. A. Lundquist, Sampling functions for geophysics, *Smithson. Astrophys. Observ. Spec. Rep.*, in preparation, 1972.
- Goldman, S., *Information Theory*, Prentice-Hall, New York, 1953.
- Hebb, K., and S. G. Mair, Numerical definition of localized functions on a sphere, in *Smithson. Astrophys. Observ. Spec. Rep. 294*, 45-98, 1969.
- Kaula, W. M. (Chairman), The terrestrial environment: Solid earth and ocean physics, Report of a study at Williamstown, Mass., NASA Contract. Rep. CR-1579, 1970a.
- Kaula, W. M., The appropriate representation of the gravity field for satellite geodesy, *Proceedings 4th Symposium on Mathematical Geodesy*, pp. 57-65, Com. Geod. Stal., Bologna, 1970b.
- Koch, K.-R., and F. Morrison, A simple layer model of the geopotential from a combination of satellite and gravity data, *J. Geophys. Res.*, 75, 1483-1492, 1970.
- Lundquist, C. A., Satellite altimetry and orbit determination, *Smithson. Astrophys. Observ. Spec. Rep. 248*, 14 pp., 1967.
- Lundquist, C. A., and G. E. O. Giacaglia, Possible geopotential improvement from satellite altimetry, *Smithson. Astrophys. Observ. Spec. Rep. 294*, pp. 1-44, 1969.
- Obenson, G. F. T., Direct evaluation of the earth's gravity anomaly field from orbital analysis of artificial earth satellites, *Rep. 129*, Dep. Geod. Sci., Ohio State Univ., Columbus, 1970.
- Rapp, R. H., Methods for the computation of geoid undulations from potential coefficients, *Rep. 132*, Dep. Geod. Sci., Ohio State Univ., Columbus (AFCRL-70-0281), 1970.
- Shannon, C. E., and W. Weaver, *The Mathematical Theory of Communication*, University of Illinois Press, Urbana, 1959.
- Vinti, J. P., Representation of the earth's gravitational potential, *Rep. RE-71*, Mass. Inst. of Technol., Cambridge, 1970.

Refinement of the Gravity Field by Satellite-to-Satellite Doppler Tracking

CHARLES R. SCHWARZ¹

*Department of Geodetic Science
Ohio State University, Columbus, Ohio 43210*

Abstract. The question of what resolution of the gravity field can be obtained from satellite-to-satellite Doppler tracking was investigated by performing least-squares adjustments of simulated Doppler data, solving for parameters describing the anomalous gravity field in various sized blocks. By examining the correlation between the adjusted parameters describing neighboring blocks, it was possible to judge whether a given set of data was capable of resolving blocks of a given size. Two concepts of satellite-to-satellite tracking are considered: the first involves two satellites near together in very low orbits, and the second uses geostationary satellites to track a single very low satellite. In either case, blocks 500 km on a side can be satisfactorily resolved from an orbital altitude of 700 km. From an altitude of 200 km, blocks 200 km on a side can be resolved. Because of the lower limit on altitude imposed by the presence of the earth's atmosphere, it does not appear that satellite-to-satellite Doppler tracking will be able to resolve features smaller than 200 km on a side.

Almost all our present knowledge about the broad-scale features of the gravity field (i.e., those features described by spherical harmonics of low degree and order) has been obtained from satellite gravimetry. The main advantage of using the motion of artificial satellites to determine the earth's gravity field is that satellites can sample the gravity field on a global basis, thus largely avoiding sample biases due to incomplete coverage of the earth's surface. The main disadvantage is that the magnitudes of the perturbing effects of high-degree terms in the geopotential fall off with increasing altitude, so that it is difficult to separate the many small perturbations at normal satellite altitudes. Using very low satellites would largely circumvent this difficulty; however, very low satellites are greatly perturbed by the retarding effect of the earth's atmosphere, and also require a fairly dense network of ground tracking stations to monitor their motion.

Classical surface gravimetry can resolve local features in the gravity field that are several

kilometers or tens of kilometers in extent. However, this method cannot satisfactorily survey features many hundreds or thousands of kilometers in extent; nor can it satisfactorily survey the gravity field on a global basis to determine the spectral components of the gravity field. If satellite gravimetry is to fill the gap between our present knowledge of the harmonic expansion of the gravity field and the kind of information obtained by classical gravimetry, it will be necessary to use both lower satellites and new modes of satellite tracking.

One of the new methods of satellite tracking currently being discussed is satellite-to-satellite tracking, or using one satellite to track another. Although one satellite could conceivably track another by any of the methods that have been used for tracking of satellites from the ground, the system considered here is one using the Doppler shift of a radio signal to measure the rate of change of the range between the two satellites.

There are two important advantages to using one satellite to track another. First, tracking measurements can be made on a global basis with little dependence on the location of ground tracking stations. Second, the measured radio

¹ Now at Geoscience Division, Department of Geodesy and Geophysics, U.S. Army Topographic Command, Washington, D.C. 20315.

SATELLITE-TO-SATELLITE TRACKING FOR GRAVITY FIELD

signal does not pass through the troposphere, thus circumventing the limitation imposed on ground-based measurements by the indeterminacy of the tropospheric refraction correction. It has been estimated that an accuracy of 0.3 to 1.0 mm/sec in range rate measurements could be obtained with present technology and that an accuracy of 0.03 to 0.05 mm/sec will eventually be possible [Kaula, 1970].

TWO CONCEPTS OF SATELLITE-TO-SATELLITE TRACKING

Two essentially different concepts of satellite-to-satellite tracking have been proposed. The first, proposed by Wolff [1969], envisages two satellites in the same low orbit, one behind the other by about 200 km. With this configuration, the range rate between the two satellites is insensitive to the long-wavelength features of the gravity field, since these features affect both satellites in approximately the same way, with no net effect on the range rate. However, pronounced features whose extent is less than the separation between the two satellites cause a pronounced variation in the range rate as the two satellites pass over the feature.

The second concept, described by Kaula [1970], envisages a single low satellite that can be tracked by any of an array of very high geostationary satellites. Since the very high satellites are stationary with respect to the earth, their positions can be monitored with fixed direction antennas. Furthermore, since the high satellites will be continuously visible at the monitoring stations, the Doppler measurements can be immediately relayed to the ground, thus avoiding the need for data storage and later readout from the satellite. The range rate between two satellites in this configuration contains the effects of long- and short-wavelength features. In this case, it is necessary to separate the effects of the short-wavelength features of interest from the effects of the long-wavelength features mathematically.

METHODS OF DATA REDUCTION

With two satellites in the same low orbit, pronounced variations in the gravity field are manifested by pronounced variations in the range rate. This suggests that the range rate can be used directly as a measure of the geopotential along the orbital path. Wolff [1969]

reasons that since almost all the kinetic energy of each satellite is contained in the velocity component along the line of sight between the two satellites, this would also be true for the difference in their kinetic energies; i.e., the kinetic energy difference would be proportional to the range rate between the two satellites. Assuming that total energy is conserved (which is not quite true, because the earth is rotating), this would also imply that the difference in gravitational potential at the respective positions of the two satellites is proportional to the line-of-sight range rate. If the two satellites are in exactly the same orbit, the difference in geopotential at the respective locations of the two satellites can be considered a variation of potential with position in the orbit. Thus the variation in potential divided by the variation in position would approximate the derivative of the potential along the orbit. A single integration along the orbit path would directly yield the geopotential along the path (except for a constant of integration). If the orbit is nominally circular, the values of the potential along the orbit constitute a circular profile. Given a sufficient number of such profiles, one would ultimately be able to draw a contour map of the values of the geopotential on a large sphere whose radius is that of the orbit.

Numerical simulations show the relationships discussed above to hold quite well in the presence of a simple force field and when both satellites are in exactly the same orbit. Unfortunately, they also show that these relationships break down completely when the two orbits are almost, but not exactly, identical. This is true both for the relationship between the line-of-sight range rate and the geopotential difference at the respective locations at the two satellites, and for the relationship between the potential difference and the actual potential along either orbit.

Since it is not reasonable to expect that two satellites can be maintained in precisely the same orbit, the concept of using the range rate between two orbiting satellites to map the potential field of the earth on a sphere must be abandoned. However, the concept of using the range rate between two satellites close together in similar low orbits to measure at least some function of the geopotential is still valid. Even though the potential in an area cannot be meas-

CHARLES R. SCHWARZ

135

ured directly, it is still reasonable to expect that several passes of the two satellites over an area, with some variation in their orbits, will enable one to solve for some representation of the geopotential in that area. This suggests the use of the classical least squares method, in which an observation equation is formed for each data point and all unknowns are sought in a simultaneous solution of all observation equations. This method of data reduction is valid both for two satellites close together in similar low orbits and for a single low satellite tracked by a very high satellite.

DESCRIPTION OF SIMULATIONS

The main purpose of the investigations described in this paper was to determine to what extent our knowledge of the gravity field might be refined by satellite-to-satellite Doppler tracking. The tool used to make this determination was a series of least squares adjustments of simulated satellite-to-satellite range-rate observations. The unknowns in these adjustments were the orbit elements for each pass, and a set of parameters describing the gravity field.

The gravity field was represented by the density of a fictitious layer spread on the surface of the earth. This is a local representation

of the gravity field, in the sense that each parameter is associated with a specific geographical area. As such, it is an appropriate representation to use when data are available to describe the gravity field only over certain parts of the earth's surface, in the same way that gravity anomalies are a more appropriate representation than a spherical harmonic series when the available data do not cover the whole surface of the earth. In fact, the properties of the surface-layer representation are very similar to those of the representation by gravity anomalies, and the surface-layer representation was chosen only because it is computationally more convenient for the integration of orbits than the gravity anomaly representation.

The density of surface layer was assumed to be constant in blocks of certain sizes, in the same way in which mean gravity anomalies in blocks are used. (The division was made in terms of arc rather than linear measure; however, since the simulations were carried out at low latitudes, the relation $1^\circ = 100 \text{ km}$ can be used for comparison without introducing appreciable error.) Assumed mean values of the density parameter in 92 blocks 5° by 5° are shown in Figure 1. The density parameter ϕ is the product of the gravitational constant and

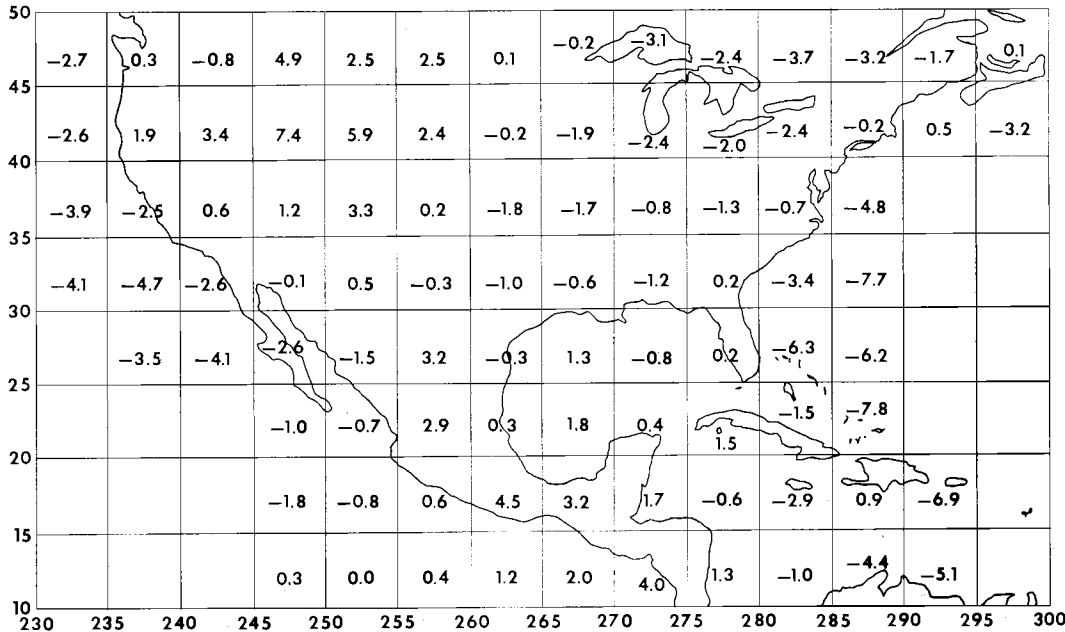


Fig. 1. Mean values of the density parameter ϕ (in milligals) for 5° by 5° blocks.

the actual surface density. The units of the density parameter are those of acceleration, and it can be conveniently measured in milligals. The value of the density parameter is about $1/2\pi$ times that of the mean gravity anomaly in the same block. Sets of mean values of the density parameter in 2° by 2° and 1° by 1° blocks were also prepared. On a worldwide basis, the rms mean value of the density parameter in a 5° by 5° block is about 3.1 mgal; for a 2° by 2° block, it is about 3.9 mgal.

For each experiment, data were generated by numerically integrating both orbits in the force field specified by the assumed values of the density of the surface layer. A series of short arcs passing over the area of interest was used. The density of the surface layer and the orbit elements were then considered to be unknown, and a least squares solution was performed for these unknowns. The variance-covariance matrix of the adjusted parameters was also computed. For each adjustment, the pertinent questions were: (1) Is the given set of data capable of determining the mean density in a block with an uncertainty less than the rms mean density? (2) Is the given set of data capable of satisfactorily separating the mean density in one block from the mean densities in neighboring blocks? The second question was answered by examining the correlation coefficients associated with the adjusted parameters.

SOLUTIONS USING SIMULATED DATA

The first question investigated was the size of blocks that could be resolved by two satellites close together in low orbits. An altitude of 700 km was first chosen. Observation equations were generated from a set of 21 passes, with the two satellites separated by 200 km in the same orbit. The uncertainties of the recovered values of the density parameters in the 92 blocks 5° by 5° range from 1 to 4 mgal. The correlation coefficient between the recovered value of the density in a block and that of its neighbor to the east or west ranged from -0.70 to -0.90. This solution was judged to be marginally satisfactory, indicating that blocks 5° by 5° can just barely be resolved from an altitude of 700 km.

Another series of solutions was performed in which the two satellites were in orbits 300 km high. Several solutions showed that it is not

always necessary to configure the two satellites so that one is always behind the other in the same orbit. Rather, it was found advantageous to introduce some variation in the relative configuration of the two satellites by using some passes in which the two satellites were roughly side by side in slightly different orbital planes, and by varying the separation between the two satellites. Figure 2 shows the uncertainties of the density parameters recovered with data from 18 passes at 300-km altitude. Typical correlations between the recovered values of the density in neighboring blocks are described by the correlation pattern below.

1.0	-0.60	0.20
0.40	-0.30	0.20
0.40	-0.30	0.15

In this pattern, positional displacement from the upper left-hand corner indicates the relative position of the two blocks to which the given correlation coefficient applies.

In all these adjustments, simulated observations of the positions of both satellites were used, as well as the simulated observations of the range rate between the two satellites. The position observations were assigned very low weights, and were included only to assign a geographic position to the gravimetric phenomenon being observed. Several adjustments showed that these position observations are necessary. However, it makes little difference to the solution for the gravity-field parameters whether the accuracy with which the positions of the satellites are observed is 10, 100, or even 1000 meters in each coordinate. These experiments showed that some ground tracking of the two satellites is necessary, although there is absolutely no need for high-accuracy tracking from the ground.

Another series of experiments used orbits 200 km high. This was judged to be about the lowest altitude at which a satellite might be kept in orbit for a reasonable lifetime, even with a drag compensation device. Satellite-to-satellite range-rate observations were generated for 10 passes over a 10° by 10° area, and solutions were made for the mean values of the density parameters in 25 blocks 2° by 2° . Table 1 shows the uncertainties in the recovered parameters when the satellites are separated by about 200 km in

CHARLES R. SCHWARZ

137

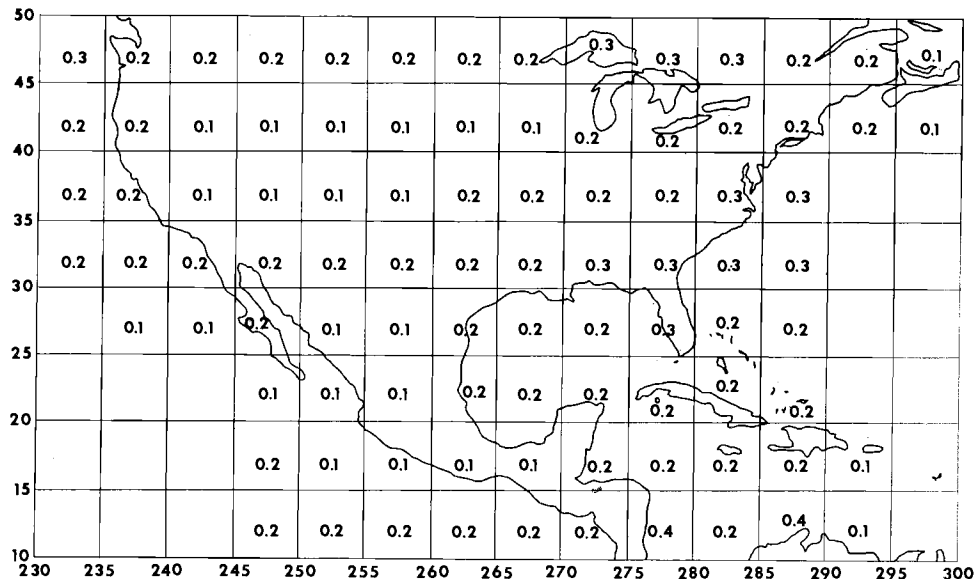


Fig. 2. Uncertainties of the recovered values of the density parameter in 5° by 5° blocks (in milligals) from 18 passes at 300 km.

200-km-high orbits. Table 2 shows the uncertainties when only one satellite is in low orbit and the other is in a geostationary orbit high above the equator. A typical pattern of correlation coefficients for the case when both satellites are in low orbits is

$$\begin{array}{ccc} 1.0 & -0.80 & +0.45 \\ -0.60 & +0.40 & -0.20 \\ +0.35 & -0.20 & +0.10 \end{array}$$

When a single low satellite is tracked by a very high satellite, the correlation between pairs of blocks is slightly larger and falls off more slowly with distance between the two blocks. Typical correlation coefficients are shown for this case by the four-block pattern

$$\begin{array}{cccc} 1.0 & -0.80 & +0.50 & -0.35 \\ -0.75 & +0.60 & -0.40 & +0.25 \\ +0.50 & -0.40 & +0.30 & -0.15 \\ -0.30 & +0.25 & -0.15 & +0.10 \end{array}$$

Both the uncertainties of the recovered parameters and the correlation coefficients indicate that better results are obtained with both satellites in low orbits. On the other hand, both

solutions could be judged to be marginally acceptable, indicating that 2° by 2° blocks can just barely be resolved from orbits 200 km high. To confirm this, several attempts were made to solve for the mean values of the density parameters in 1° by 1° blocks. These adjustments were excessively distorted by numerical error and produced completely unsatisfactory results. This remained true even when the satellite altitude was brought down to the unrealistic value of 100 km.

CONCLUSIONS

If 200 km is accepted as the lowest altitude at which a satellite can be kept in orbit for a reasonable lifetime, the gravity field can be resolved into 2° by 2° blocks, which are roughly

TABLE 1. Uncertainties of Recovered Values of the Density Parameters in 2° by 2° Blocks (in Milligals)
(Low-low configuration.)

Latitude, deg	Longitude, deg				
	240-242	242-244	244-246	246-248	248-250
45-43	0.8	1.2	1.4	1.2	0.7
43-41	1.0	1.4	1.5	1.2	0.8
41-39	1.1	1.4	1.2	1.1	0.8
39-37	0.9	1.2	1.1	1.0	0.7
37-35	0.6	0.8	0.7	0.8	0.6

SATELLITE-TO-SATELLITE TRACKING FOR GRAVITY FIELD

TABLE 2. Uncertainties of Recovered Values of the Density Parameters in 2° by 2° Blocks (in Milligals)
(High-low configuration.)

Latitude, deg	Longitude, deg				
	240-242	242-244	244-246	246-248	248-250
45-43	0.8	1.4	1.8	1.5	0.9
43-41	1.1	1.5	1.8	1.6	1.1
41-39	1.2	1.5	1.5	1.5	1.2
39-37	1.0	1.3	1.2	1.2	1.0
37-35	0.5	0.7	0.7	0.7	0.6

200 km square. A solution for blocks of this size on a global basis would be equivalent to determining the coefficients in the spherical harmonic representation of the geopotential through degree and order 90.

Larger blocks can be resolved from proportionally higher altitudes. An approximate relation-

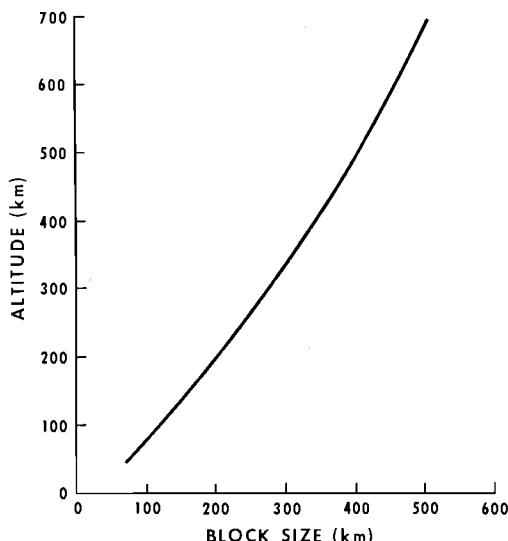


Fig. 3. Approximate maximum altitude from which the gravity field can be successfully resolved, as a function of block size.

tionship between block size and altitude is shown in Figure 3.

Although slightly better results are obtained with two low satellites than when a geostationary satellite tracks a single low satellite, many operational considerations argue strongly for the latter concept. Among these are the facts that only the low satellite would need to be equipped with a drag compensation device, and that the problem of data storage and later readout could be avoided. For these and other reasons, the concept of an array of geostationary satellites that track one or more minimum-altitude satellites is recommended.

Acknowledgments. The work described in this paper was performed by the author as part of his dissertation research at Ohio State University. Professor Ivan I. Mueller served as the author's faculty adviser. The work was partly supported by the National Aeronautics and Space Administration under contract NGL 36-008-093. A large amount of the computer time necessary for performing the numerical simulations was provided by the Instructional and Research Computer Center of Ohio State University.

REFERENCES

- Gaposchkin, E. M., The 1969 Smithsonian Standard Earth and Global Tectonics, *Proceedings of the Geos 2 Program Review Meeting, 22-24 June 1970*, vol. 1, edited by Computer Sci. Corp., Falls Church, Va., 1970.
- Kaula, W. (Chairman), The terrestrial environment: Solid earth and ocean physics, Report of a study at Williamstown, Mass., NASA Contract. Rep. CR-1579, 1970.
- Schwarz, Charles R., Gravity field refinement by satellite to satellite Doppler tracking, *Rep. 147*, Dep. of Geod. Sci., Ohio State Univ., Columbus, 1970.
- Wolff, Milo, Direct measurements of the earth's gravitational potential using a satellite pair, *J. Geophys. Res.*, 74, 5295, 1969.

Satellite-Satellite Tracking for Estimating Geopotential Coefficients

C. F. MARTIN AND T. V. MARTIN

*Wolf Research and Development Corporation
Riverdale, Maryland 20840*

DAVID E. SMITH

Goddard Space Flight Center, Greenbelt, Maryland 20771

Abstract. The tracking of artificial earth satellites by other earth satellites offers the potential for increased accuracy in estimating orbit and geopotential coefficients. The improvement in accuracy is due primarily to the near-continuous coverage possible, the addition of new geometry between tracker and tracked satellite, and the decrease in sensitivity to errors in ground-station position. This paper presents the results of simulation studies of tracking of low-altitude satellites by a high-altitude satellite using range measurements between satellites. The high-altitude satellite is tracked by ground-based range trackers. The low-altitude satellites are tracked only by the high-altitude satellites. Orbital elements for one tracking satellite and four tracked low-altitude satellites are estimated, along with a set of low degree and order geopotential coefficients. Estimation of geopotential coefficients of low degree and order is shown to be considerably more accurate using satellite-to-satellite tracking than using ground-based tracking. The use of data from one high-altitude satellite tracking four low-altitude satellites in a range of inclinations is shown to produce geopotential coefficient estimates with smaller errors than presently exist in individual coefficients or would be obtained using ground-based tracking of the same satellites. One week of continuous tracking was assumed for this simulation.

The tracking of artificial earth satellites by other satellites offers a number of advantages in the field of satellite geodesy and its application to earth physics and oceanography. These advantages consist primarily of the potential for nearly continuous tracking and the viewing geometries available for tracking low-altitude satellites. In addition, satellite-to-satellite tracking may be a more economical method of operationally maintaining orbits for scientific satellites when the tracking satellite is also a relay station for scientific data taken by satellite-borne sensors. This aspect will, however, not be considered further in the present paper.

Continuous tracking is particularly advantageous when the phenomena being observed contain large high-frequency components. That is, the determination of the parameters of a periodic motion is much easier to perform if the motion is observed for a significant fraction of a period. Except for resonance coefficients,

the dominant effects of geopotential coefficients on satellite motion have a frequency of once per day or greater. Without the use of a very large network of ground stations, it is not possible to obtain near continuous track of a low-altitude satellite from ground stations alone. Such tracking coverage can be obtained, however, by the use of only a single high-altitude tracking satellite.

In its consideration of the application of satellite-to-satellite tracking to geopotential coefficient recovery, this paper will restrict the class of coefficients to those of low degree and order. The best available sets [Lundquist and Veis, 1966; Gaposchkin and Lambeck, 1970] of these coefficients contain errors that seriously hamper the determination of highly definitive satellite orbits below altitudes of 1000 km. The nearly continuous tracking obtainable from high-altitude satellites permits the use of arc lengths considerably shorter than those that have been

used for lower-frequency data. This method should be well suited for observing the high-frequency perturbations in low-altitude satellite orbits and successfully resolving the effects of geopotential coefficients of low degree and order.

CHARACTERISTICS OF SATELLITE-SATELLITE TRACKING

In a general consideration of satellite-to-satellite tracking for orbit determination or for the estimation of geopotential coefficients, there are a large number of variables that need to be optimally chosen. These include: (1) the type of measurement made by a tracking satellite; (2) the number of tracking satellites; (3) the orbits of the tracking satellites; (4) the ground-based tracking for determining the orbit(s) of the tracking satellite(s); (5) the tracking of the low-altitude satellites by ground stations.

The first three of these variables can be fixed with a reasonable degree of confidence on the basis of a previous study [Martin, 1970a]. The conclusions reached in that study were:

1. Range and range rate measurements are of approximately equal value in both orbit determination and geopotential recovery when the effects of nominal values of range biases are included.

2. Increasing the number of tracking satellites from one to two or three does lead to improved orbit accuracy, but the improvement is only moderate.

3. A synchronous tracking satellite and a 12-hour tracking satellite are almost equally effective in determining low-altitude satellite orbits, the 12-hour satellite being slightly better.

On the basis of these results, the simulations whose results are presented in this paper are based on range data only for the intersatellite measurement and for a single tracking satellite in a near-synchronous orbit. In addition, the near-synchronous satellite is tracked by a limited but worldwide network of range trackers, and no ground stations track the low-altitude satellites.

ERROR ANALYSIS FOR SATELLITE-TO-SATELLITE TRACKING

The mathematical technique used for simulating the reduction of satellite-to-satellite track-

SATELLITE-SATELLITE TRACKING

ing data is based upon a minimum variance simultaneous estimate of the orbit elements of all satellites involved, together with an adjusted set of geopotential coefficients. That is, the data reduction process is hypothesized to estimate six orbital elements for each satellite and a set of geopotential coefficients. The data reduction process is minimum variance if these are the only errors affecting the solution other than random measurement noise. If this were the case, then the variance-covariance matrix normally produced as a part of the data reduction process could be used as a valid measure of the accuracy of geopotential coefficient recovery. Since this variance-covariance matrix is really a function only of measurement partial derivatives, and thus only on nominal orbits, it can readily be simulated.

In practice, however, the largest sources of error in orbital data reductions are unmodeled parameters. These would include, for example, measurement biases that are nonzero but assumed to be so in data reduction, errors in station position assumed not to exist, and force-model errors that are ignored. It is the unmodeled force-model errors that are normally the dominant contributors to all adjusted parameter errors for multi-revolution satellite arcs. For these reasons, it is necessary that orbital simulations properly account for the more significant unmodeled parameters, particularly force-model parameters.

With geopotential coefficients of low degree and order adjusted, the most significant unadjusted force-model parameters are errors in higher-degree geopotential coefficients, atmospheric drag, and solar radiation pressure. The relative importance of these parameters varies with the satellite altitude, the arc length, and the satellite area-to-mass ratio. For the present study, we will assume that all low-altitude satellites are geodetic satellites for which the area-to-mass ratios have been chosen small enough that model errors for solar radiation pressure and drag forces are negligible.

The technique of including the effects of errors in unadjusted parameters in simulations of data reduction for satellite-to-satellite tracking has been incorporated [Martin, 1970a] into a computer program, EASST, which will consider intersatellite or ground tracking of up to five satellites in any orbit using either range,

MARTIN, MARTIN, AND SMITH

141

range rate, or right ascension and declination data types. The EASST program was used for all the coefficient recovery simulations whose results are included in this paper.

The systematic errors whose effects were propagated in the simulations are: errors in station position, 5 meters in each coordinate; tracker (range) biases, 2 meters (constant for each radar and satellite); force-model errors, 50% of difference between SAO M1 (extended) and 1969 standard earth. The errors in station position represent the accuracy currently achievable [Douglas and Marsh, 1971], as do the radar biases for well-calibrated radars or lasers. The force-model error is based on differences between two of the best available large geopotential models: the M1E model based on the SAO M1 model [Lundquist and Veis, 1966] augmented with 13th-order resonance coefficients [Yiououlis, 1968; Douglas and Marsh, 1969] and the SAO 1969 standard earth [Gaposchkin and Lambeck, 1970]. Differencing between gravity models has been shown [Martin, 1970b] to be a valid method of modeling geopotential coefficient error. Tests of residuals for a 7-day arc of Geos 2, the arc length used for the geopotential recovery simulations, have shown that scaling the differences between these two gravity models by a factor of 0.5 does provide a model for the lack of data fit to the estimated orbit.

The geopotential model error can be viewed in an alternative but equally valid manner. If the same data reduction were performed once with the M1E model, then with the SAO 1969 standard earth, the differences in the estimated coefficients would be twice the expected error due to neglected errors in higher-degree coefficients. The EASST program computes directly the effects of these gravity-model differences on the simulated data reduction, without

having to simulate two data reductions and then difference them.

In general, measurement noise has negligible effects compared to systematic error effects and so measurement noise level and measurement frequency, within limits, do not affect the results presented in the next section.

SIMULATIONS OF GEOPOTENTIAL RECOVERY

To simulate the recovery of geopotential coefficients of low degree and order, four satellites at different inclinations and altitudes were chosen as the tracked satellites. The epoch elements for these satellites are given in Table 1, along with the tracking satellite elements. In general, the tracked satellites have circular orbits with altitudes of 400, 600, 800, and 1000 km, and inclinations varying from 25° to 90°. The tracking satellite is a low-inclination satellite, drifting around the earth approximately once every 8 days. The total tracking period used is 7 days. The locations of the ground stations tracking the high-altitude tracking satellite are given in Table 2. All stations are considered to make range measurements whenever the satellite is above 20° elevation angle. The tracking satellite in turn is considered to make range measurements to each of the tracked satellites whenever they are not occulted by the earth.

In order to have a valid comparison with possible alternative methods of estimating geopotential coefficients of low degree and order, three other simulations were made of tracking of the same four low-altitude satellites. These tracking systems were:

1. Range tracking by five globally distributed stations, given in Table 2, with tracking of all four satellites when they were above 10° elevation angle, 24 hours per day.
2. Range tracking by the same five stations and with the same cutoff angle, but with track-

TABLE 1. Orbital Elements of Satellites Used in Geopotential Recovery Simulations

Satellite	a , meters	e	i , deg	Ω , deg	ω , deg	M , deg
Tracked						
1	6,770,000	0.00001	25	0	0	45
2	6,970,000	0.00001	40	120	45	0
3	7,170,000	0.00001	65	240	135	0
4	7,370,000	0.00001	90	172	260	20
Tracking	38,000,000	0.02	3	72	340	30

SATELLITE-SATELLITE TRACKING

TABLE 2. Satellite Tracking Locations

Name	Latitude	Longitude	Ht. above Spheroid, meters
<i>Range Trackers of High-Altitude Satellites</i>			
Winkfield, England	51°26'40.7"	359°18' 8.4"	76
Pretoria, S. Africa	-25 56 37.4	-28 21 30.6	1863
Kauai, Hawaii	21 31 15.4	202 0 9.8	368
Carnarvon, Australia	-24 54 12.3	113 42 58.5	11
Wallops Is., Va.	37 51 35.3	284 29 23.9	-36
<i>Range Trackers of Low-Altitude Satellites</i>			
Wallops Is., Va.	37 51 36.69	284 29 25.92	-48
Ascension Island	-07 57 19.31	345 40 20.78	555
Carnarvon, Australia	-24 53 47.24	113 43 01.76	12
Kauai, Hawaii	22 07 23.95	200 20 04.19	1127
Madagascar	-19 00 06.47	47 08 53.02	1320
<i>Optical Trackers of Low-Altitude Satellites</i>			
Woomera, Australia	-31 06 03.07	136 47 02.82	158
Maui, Hawaii	20 42 25.67	203 44 34.12	3032
Organ Pass, N. Mex.	32 25 24.89	253 26 48.68	1615
Curacao, Netherlands Antilles	12 05 25.04	291 09 44.66	-22
Arequipa, Peru	-16 27 57.21	288 30 24.53	2488
Santiago, Chile	-33 09 6.76	289 20 00.51	727
San Fernando, Spain	36 27 46.99	353 47 36.31	55
Johannesburg, S. Africa	-25 53 01.44	27 42 26.21	1541
Naini Tal, India	29 21 33.31	79 27 27.07	1856
Tokyo, Japan	35 40 22.62	139 32 16.18	80

ing restricted to the 'working day' hours of 0800 to 1600 local time.

3. Optical tracking by 10 globally distributed optical tracking (right ascension and declination) stations, with an elevation cutoff angle of 20° and tracking restricted to the hours of 2000 to 0400 local time. The locations of these ten stations are given in Table 2.

Although all four tracking systems simulated are optimistic to some extent in terms of the simultaneous coverage of all four satellites under all weather conditions, one data point per 1 to 2 min when the tracked satellite is within view of the tracking station (and above the cutoff angle) is adequate to provide all the geometry needed for the coefficient estimation.

The estimated total uncertainty in the 34 estimated coefficients of low degree and order are given in Table 3 for the four different modes of tracking the four low-altitude satellites. Given in Table 3 also are the SAO 1969 standard earth values for the 34 coefficients and the differences between the SAO 1966 and 1969 standard earth values for these coefficients.

These differences serve as a measure of the current uncertainty in this set of coefficients. The adjusted coefficient uncertainties are due almost entirely to the geopotential coefficient error. That is, adjusted coefficient errors are due to errors in unadjusted coefficients of higher degree and order.

Two methods of summarizing the results of Table 3 can be used to indicate the coefficient recovery capability of each tracking mode. First, the number of coefficients whose adjusted σ is less than the a priori uncertainty as expressed by the differences between the two gravity models is:

- 24 satellite-to-satellite tracking
- 22 24-hour ground-based range tracking
- 7 8-hour ground-based range tracking
- 17 8-hour ground-based optical tracking

This shows that three of the four tracking modes are able to provide improvements in 50% or more of the coefficients. Satellite-to-satellite tracking is able to improve the most coefficients, and the 24-hour range tracking is not far be-

MARTIN, MARTIN, AND SMITH

143

hind. Next, the number of coefficients that each tracking mode is able to obtain best is:

- 8 a priori
- 15 satellite-to-satellite tracking
- 9 24-hour range tracking
- 0 8-hour range tracking
- 2 8-hour optical tracking

Here the satellite-to-satellite tracking mode shows a clear superiority over both the other tracking modes and the a priori values that are based on many more arcs of many more satellites than the four 1-week arcs considered here.

Several of the coefficients [e.g., $C(6, 3)$] have a rather high a priori error, as is indicated by the SAO M1 and SAO 1969 standard earth differences. In general, it is found from Table 3 that, when the a priori differences are large, the adjusted standard deviations are large for all the tracking modes. This would seem to indicate both that the coefficient is not well known and that it is difficult to determine, regardless of the type of tracking data.

CONCLUSIONS

From the results given above, particularly in Table 3, a number of conclusions can be

TABLE 3. Standard Deviations of Adjusted Geopotential Coefficients of Low Degree and Order for Different Modes of Tracking

Coefficient	SAO Stand. Earth Value	SAO M1 Stand. Earth δ	Sat-Sat Tracking	Adjusted Coefficient σ		
				8-hr Radar	24-hr Radar	8-hr Opt.
$C(2, 2) \times 10^6$	1.5580	-0.0215	0.0264	0.0252	0.0124	0.0404
$S(2, 2) \times 10^6$	-0.8805	0.0085	0.0046	0.0668	0.0094	0.0541
$C(3, 3) \times 10^7$	0.9570	-0.1750	0.1059	0.0858	0.0883	0.0709
$S(3, 3) \times 10^7$	1.9950	0.2654	0.0511	0.8144	0.0167	0.1287
$C(3, 2) \times 10^6$	0.3047	-0.0537	0.0062	0.0201	0.0088	0.0261
$S(3, 2) \times 10^6$	-0.2168	0.0328	0.0024	0.0197	0.0169	0.0257
$C(3, 1) \times 10^6$	2.1280	-0.0366	0.0122	0.1578	0.0634	0.0256
$S(3, 1) \times 10^6$	0.2810	0.0060	0.0135	0.0308	0.0272	0.0232
$C(4, 4) \times 10^9$	-1.6840	0.5638	0.2847	5.7760	0.3720	0.8744
$S(4, 4) \times 10^9$	7.1690	-2.3090	0.1004	0.4902	1.5450	0.3722
$C(4, 3) \times 10^8$	5.9130	-0.8230	0.2615	0.9407	0.3287	1.0230
$S(4, 3) \times 10^8$	-0.9243	-0.2157	0.0074	0.9644	0.3143	0.3554
$C(4, 2) \times 10^7$	0.7384	-0.0004	0.0491	0.0347	0.0248	0.0188
$S(4, 2) \times 10^7$	1.5790	-0.0994	0.0103	0.1281	0.0162	0.0426
$C(4, 1) \times 10^7$	-5.0270	-0.4030	0.3120	0.1766	0.2252	0.1721
$S(4, 1) \times 10^7$	-4.6260	0.1763	0.0425	0.7462	0.0300	0.1557
$C(5, 5) \times 10^9$	0.3101	0.0739	0.0934	0.9822	0.2171	0.3925
$S(5, 5) \times 10^9$	-1.4750	0.0151	0.1347	0.3473	0.0598	0.3299
$C(5, 4) \times 10^9$	-2.0780	0.0184	0.2331	0.9609	0.3751	1.4880
$S(5, 4) \times 10^9$	0.6463	-0.1483	0.4700	0.7290	0.9215	0.3387
$C(5, 3) \times 10^8$	-1.4230	-0.2968	0.0183	0.5655	0.1332	0.1314
$S(5, 3) \times 10^8$	-0.2863	0.3094	0.3749	0.2351	0.0454	0.0714
$C(5, 2) \times 10^8$	9.9180	0.2817	1.0010	2.6420	1.7410	1.6620
$S(5, 2) \times 10^8$	-5.6780	1.9280	0.9662	1.2510	0.5062	0.8759
$C(6, 6) \times 10^{11}$	2.0660	-2.9980	0.3956	4.3450	1.1890	0.5404
$S(6, 6) \times 10^{11}$	-1.7420	-1.8680	1.1010	6.1540	0.8832	1.1380
$C(6, 5) \times 10^{10}$	-1.7060	-0.8236	0.1801	2.4750	1.1730	1.0110
$S(6, 5) \times 10^{10}$	-4.2180	0.5181	0.0064	1.6400	0.4914	1.2970
$C(6, 4) \times 10^9$	-0.0015	-0.1655	0.0322	0.1884	0.0308	0.1965
$S(6, 4) \times 10^9$	-1.5290	-0.4311	0.0459	0.9469	0.1389	0.0566
$C(6, 3) \times 10^{10}$	5.7790	-16.9800	1.9020	41.3800	2.8500	14.5000
$S(6, 3) \times 10^{10}$	9.2530	-2.8230	5.0610	8.3010	3.1250	9.5270
$C(6, 2) \times 10^8$	0.6820	0.1760	0.1634	1.1550	0.1140	0.1299
$S(6, 2) \times 10^8$	-4.3760	-0.1741	0.1269	1.2630	0.0619	0.6569

144

drawn about the capability to estimate geopotential coefficients of low degree and order using satellite-to-satellite tracking, as well as other tracking modes.

1. Concentrated tracking of either the ground-based range, optical, or satellite-to-satellite tracking type is able to produce a geopotential model with significantly improved coefficients of low degree and order from only a few satellites at different inclinations and using arc lengths of one week (or less).

2. Satellite-to-satellite tracking is clearly superior to any of the other tracking modes for improving coefficients of low degree and order.

3. Range tracking during the normal working day alone produces insufficient data for a significant improvement in coefficients of low degree and order. On the other hand, 24-hour range tracking of the low-altitude satellites can produce significant coefficient improvements.

4. Optical tracking for an 8-hour period each day produces results that are slightly inferior to the 24-hour range tracking.

Acknowledgment. The work upon which this paper is based was sponsored in part by Goddard

SATELLITE-SATELLITE TRACKING

Space Flight Center under contract NAS5-11736 Mod 3.

REFERENCES

- Douglas, B. C., and J. G. Marsh, Geos 2 and 13th order terms of the geopotential, *NASA X-Doc. X-552-69-291*, July 1969.
- Douglas, B. C., and J. G. Marsh, Tracking station coordinates from Geos 1 and Geos 2 optical flash data, paper presented at the Third International Symposium on the Use of Artificial Satellites for Geodesy, Washington, D.C., April 1971.
- Gaposchkin, E. M., and K. Lambeck, 1969 Smithsonian standard earth, *Smithson. Astrophys. Observ. Spec. Rep. 815*, May 18, 1970.
- Lundquist, C. A., and G. Veis, Geodetic parameters for a 1966 Smithsonian Institute standard earth, *Smithson. Astrophys. Observ. Spec. Rep. 200*, vol. 1, 1966.
- Martin, C. F., Evaluation of satellites tracking satellites for orbit determination and geopotential recovery, final report, contract NAS 5-11736 Mod 3, Goddard Space Flight Center, Greenbelt, Md., June 1970a.
- Martin, C. F., Models for geopotential coefficient error (abstract), *Eos Trans. AGU*, 51, 740, 1970b.
- Yiououlis, S. M., Improved coefficients of the thirteenth-order harmonics of the geopotential derived from satellite Doppler data at three different orbital inclinations, *Rep. TG-1003*, Johns Hopkins Appl. Phys. Lab., Baltimore, Md., May 1968.

4. Physical Geodesy: Results

Improvement of Zonal Harmonics by the Use of Observations of Low-Inclination Satellites Dial, SAS, and Peole

A. CAZENAVE, F. FORESTIER, F. NOUEL, J. L. PIEPLU

*Groupe de Recherche de Géodésie Spatiale
Bretigny, France*

Abstract. Up to 1970, solutions for zonal harmonics have been obtained from observations of satellites with inclination greater than 28°. During 1970, three satellites have been launched with smaller inclinations: Peole, 7010901, with 15°; Dial, 7001701, with 5°; and SAS, 7010701, with 3°. The analysis of their orbital parameters obtained with interferometric observations leads to a set of new condition equations. When added to the Kozai set of equations, they contribute to the determination of zonal harmonics of higher degree, to which orbits of low-inclination satellites are sensitive.

From 1958 until today, the determination of zonal harmonics of the terrestrial potential has been continuously improved through the improvements in corrections for other perturbing causes, extension of the number of satellites observed, more precise data to compute orbital elements, and more various inclinations. However, before 1970, no satellites of inclination below 28° had been utilized in such a determination [Anderle, 1965; King-Hele *et al.*, 1969; Kozai, 1969]. The different sets of harmonics therefore agree for inclinations that had contributed to their determination, but differ significantly in orbit computation for lower values of the inclination.

OBSERVATIONAL DATA

During 1970, three satellites of low inclinations were put in orbit (Table 1): Dial, 7001701, launched from Kourou, French Guiana, March 10, 1970; SAS, 7010701, launched from the San Marco platform on December 12, 1970; and Peole, 7010901, launched from Kourou on December 12, 1970. These three satellites, of respective inclination 5°, 3°, and 15°, are all

equipped with tracking systems transmitting at frequencies of 136–138 MHz. They are tracked regularly by the two interferometric stations of CNES (Kourou and Pretoria, South Africa). For each of these satellites, intensive observations were made during a rotation of the argument of perigee (two rotations for Dial).

The interferometric stations Diane, which are quite similar to the Minitrack stations, are characterized by the ability to track satellites at altitudes as low as 15–20° and an accuracy of 2×10^{-4} on direction cosines. In spite of the limited number of stations and their weak geographical coverage, the observations are well distributed on the orbit. In effect, during a day, a low-altitude station is looking successively at all the parts of a near-equatorial orbit. This coverage permits rather good determination of eccentricity and argument of perigee, as well as drag effect, even for low-perigee satellites.

PROCESSING

The periods of observations, which last about 1 month, are divided into 4-day arcs with an overlapping of 2 days. Figure 1 shows the dis-

IMPROVEMENT OF ZONAL HARMONICS

TABLE 1. Low Inclination Satellites, 1970

Satellite	<i>a</i>	<i>e</i>	<i>i</i>	Perigee	Apogee	$d\omega/dt$	$d\Omega/dt$	Period of Observ.
Dial	7345	0.088	5.41	321	1613	$12.3^\circ/D$	$-6.2^\circ/D$	March 10 to April 9, April 11 to May 11
SAS	6929	0.0031	3.03	529	574	$15.0^\circ/D$	$-7.5^\circ/D$	Dec. 12 to Jan. 15
Peole	7010	0.0165	15.00	516	748	$13.2^\circ/D$	$-7.0^\circ/D$	Dec. 12 to Jan. 16

tribution in mean anomaly for each of these arcs for Peole and SAS. Excellent for Peole, it becomes very poor during the second half of the observation for SAS (it was very good for Dial). These different arcs have been processed by an analytical differential orbital improvement program using the Brouwer theory with zonal harmonics J_2 to J_5 . For Peole and SAS, the eccentricities of which are small, we took J_3 and $J_5 = 0$ to avoid numerical problems in the analytical developments. To take into account the effects of air drag, we adjust two more parameters: secular variations of a and e . The mean elements computed are corrected for the perturbing effects of luni-solar potential and solar radiation pressure by a program using the formalism of Cook [1962]. The correction for air drag was computed by assuming the invariability of the perigee height, except for

SAS, where only the variation of the semi-major axis is used, the orbit being almost circular.

Figure 2 shows the secular variation of the semimajor axis for the three satellites. For example, Figure 3 shows variations of e , after all corrections had been made, for Peole.

These elements can then be written in the following form:

$$\begin{aligned} e &= e_0 + e_1 \Delta t + A_{1e} \sin \omega \\ &\quad + A_{2e} \cos 2\omega + A_{3e} \sin 3\omega \\ \omega &= \omega_0 + \omega_1 \Delta t + A_{1\omega} \cos \omega \\ &\quad + A_{2\omega} \sin 2\omega + A_{3\omega} \cos 3\omega \\ \Omega &= \Omega_0 + \Omega_1 \Delta t + A_{1\Omega} \cos \omega \\ &\quad + A_{2\Omega} \sin 2\omega + A_{3\Omega} \cos 3\omega \end{aligned}$$

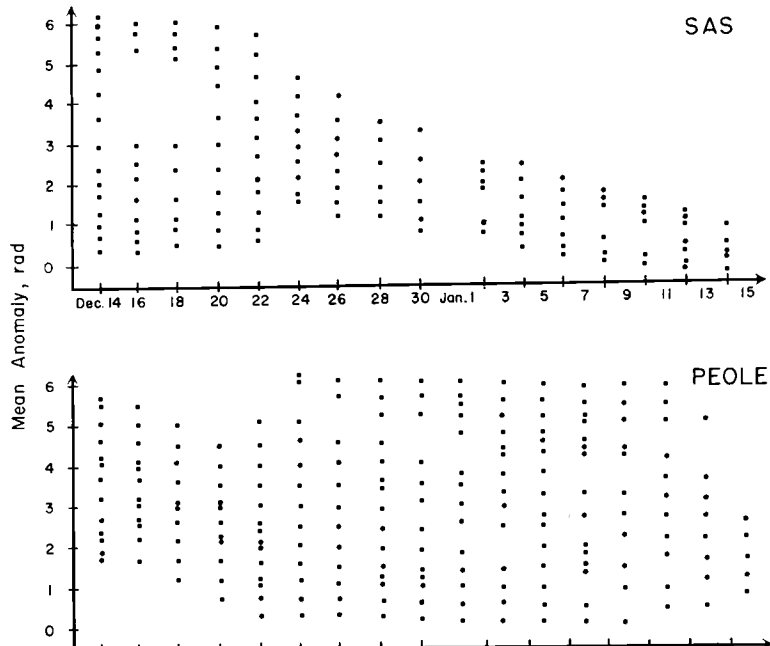


Fig. 1. Distribution of observations for SAS and Peole.

CAZENAVE, FORESTIER, NOUEL, AND PIEPLU

147

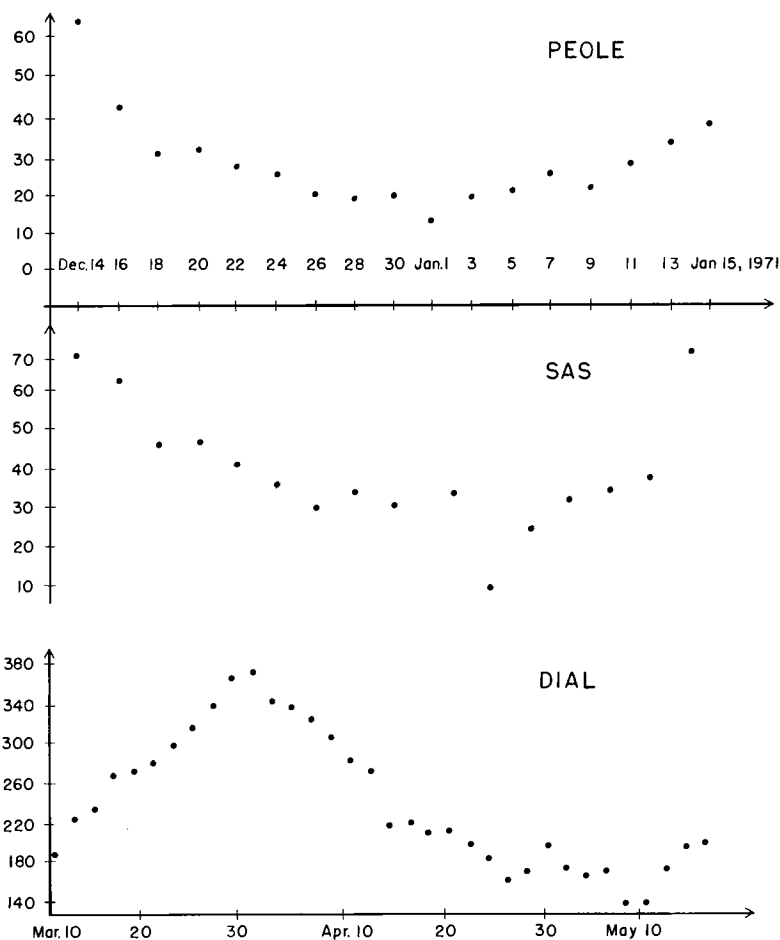


Fig. 2. Secular variations of semimajor axis (meters/day) for Peole, SAS, and Dial.

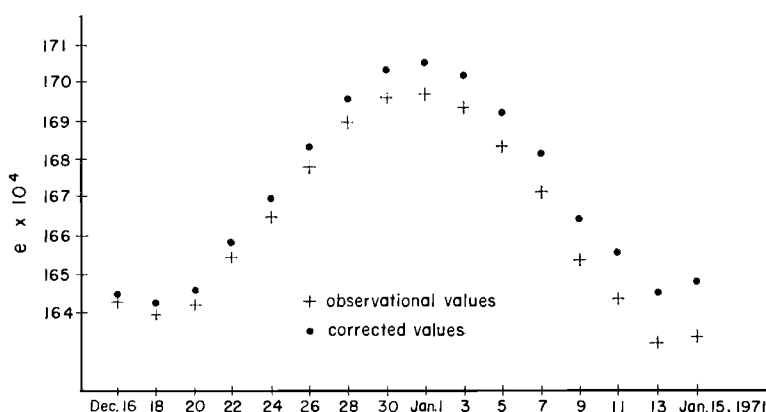


Fig. 3. Eccentricity of People.

IMPROVEMENT OF ZONAL HARMONICS

TABLE 2. Equations of Condition for Odd-Order Harmonics

Satellite	ΔJ_3	ΔJ_5	J_7	J_9	J_{11}	J_{13}	J_{15}	J_{17}	J_{19}	J_{21}
People	-108	190	-213	181	-114	39	25	-63	75	-65
Dial										$(33 \pm 12) \times 10^{-6}$
1st period	-38	71	-93	104	-108	105	-98	88	-76	65
2nd period	-38	71	-94	106	-109	106	-99	89	-77	66
										$(1 \pm 7) \times 10^{-6}$
										$(19 \pm 6) \times 10^{-6}$

Reference values: $J_3 = -2.538 \times 10^{-6}$, $J_5 = -0.230 \times 10^{-6}$.

TABLE 3. Equations of Condition for Even-Order Harmonics

Satellite	J_2	J_4	J_6	J_8	J_{10}	J_{12}	J_{14}	J_{16}	J_{18}	J_{20}
People	244.858	-417	428	-292	80	122	-252	282	-223	110
Dial	-129.066	236	-278	-253	-180	89	-5	-54	82	-81
										$(265,833 \pm 135) \times 10^{-6}$
										$(-140,300 \pm 8) \times 10^{-6}$
1st period	227.8	-427	562	-632	649	-626	576	-510	436	-360
Dial	-114.6	218	-292	337	-358	361	-350	329	-301	270
										$(248,351 \pm 71) \times 10^{-6}$
										$(-124,701 \pm 27) \times 10^{-6}$
2nd period	228.7	-430	566	-638	655	-633	583	-516	441	-363
Dial	-115.1	219	-294	340	-362	365	-354	333	-305	273
										$(248,146 \pm 95) \times 10^{-6}$
SAS	-139.338	233	-430	541	-622	674	-700	704	-690	662
										$(-125,029 \pm 56) \times 10^{-6}$
										$(-151,052 \pm 147) \times 10^{-6}$

CAZENAVE, FORESTIER, NOUEL, AND PIEPLU

149

The $e_i \Delta t$ term is introduced to compensate the rough corrections made for the air drag effects. The $A_{2e}, A_{3e}, A_{2o}, \dots$ terms are computed from the orbital elements and are subtracted from the first members of the equations. Then we determine $e_o, e_1, A_{1e}, \omega_o, \dots$ by a least squares adjustment. The poor accuracy of data does not permit a good determination of A_{1e} and A_{1o} . The small eccentricity of SAS and the bad distribution of observations lead to indeterminate values for A_{1e} and ω_1 .

EQUATIONS OF CONDITION

The parameters that had been adjusted above can be expressed in linear forms of the zonal harmonics as:

$$\begin{aligned} A_{1e} &= \sum_i \alpha_{2i+1} J_{2i+1} \\ \Omega_1 - \rho J_2^2 &= \sum_i \beta_{2i} J_{2i} \\ \omega_1 - \tau J_2^2 &= \sum_i \gamma_{2i} J_{2i} \end{aligned}$$

where ρJ_2^2 and τJ_2^2 are the effects of J_2^2 on Ω_1 and ω_1 .

The coefficients $\alpha_{2i+1}, \beta_{2i}, \gamma_{2i}$ are functions of the orbital elements and are computed by a program adapted by G. Brachet using an analytical theory developed in the Bureau des Longitudes [Challe and Laclaverie, 1969].

Finally, we obtain the equations of condition of Tables 2 and 3. It is important to note that, for odd harmonics, the ΔJ_3 and ΔJ_5 parameters are the complements of the J_3 and J_5 values used in the differential orbital program ($J_3 = -2.538 \times 10^{-6}$, $J_5 = -0.230 \times 10^{-6}$).

DETERMINATION OF A SET OF ZONAL HARMONICS

Although the observational data are of rather poor quality, it has seemed interesting to mix

TABLE 4. Odd-Order Zonal Harmonics

<i>J</i>	Our Value	Kozai, 1969
J_3	-2.543 ± 5	-2.538 ± 4
J_5	-0.226 ± 7	-0.230 ± 7
J_7	-0.365 ± 12	-0.361 ± 15
J_9	-0.118 ± 13	-0.100 ± 23
J_{11}	0.236 ± 12	0.202 ± 35
J_{13}	-0.202 ± 14	-0.123 ± 49
J_{15}	-0.081 ± 21	-0.174 ± 61
J_{17}	-0.027 ± 23	0.085 ± 65
J_{19}	-0.112 ± 23	-0.216 ± 53
J_{21}	0.106 ± 15	0.145 ± 29

TABLE 5. Even-Order Zonal Harmonics

<i>J</i>	Our Value	Kozai, 1969
J_2	1082.637 ± 4	1082.628 ± 2
J_4	-1.619 ± 10	-1.593 ± 7
J_6	0.558 ± 17	0.502 ± 14
J_8	-0.209 ± 24	-0.118 ± 20
J_{10}	-0.233 ± 26	-0.354 ± 25
J_{12}	-0.188 ± 27	-0.042 ± 27
J_{14}	0.085 ± 34	-0.073 ± 28
J_{16}	0.048 ± 43	0.187 ± 26
J_{18}	-0.137 ± 44	-0.231 ± 22
J_{20}	-0.087 ± 52	-0.005 ± 22

the present equations of condition with those given by Kozai [1969].

The weight of the new equations is computed from the standard deviation derived from the observations. This weighting is probably pessimistic and does not give the full benefit of these equations. A least squares adjustment on this set of condition equations gives the zonal harmonic values shown by Tables 4 and 5. We observe good stability in the determination of coefficients of order lower than 10.

It appears that the improvement is more significant for the odd harmonics than for the even harmonics. This fact seems surprising, the effect of the even harmonics being very large for the low-inclination satellites. In fact the effect of truncation is also very large. For the odd harmonics, on the other hand, we have all the benefit of the new equations, which permit a better decorrelation of the harmonics.

CONCLUSION

Observations of three low-inclination satellites lead to three new equations of condition for the odd-order zonal harmonics and seven new equations for the even-order zonal harmonics.

The mixing of these equations with those of Kozai [1969] yields a new set of zonal harmonics that differs significantly from Kozai's set for the harmonics beyond degree 10.

REFERENCES

- Anderle, R. J., Geodetic parameter set NWL-5E-6 based on Doppler satellite observations, *Rep. 1978*, U.S. Nav. Weapons Lab., Dahlgren, Va., 1965.
 Challe, A., and J. J. Laclaverie, Fonction perturbatrice et représentation analytique du mouvement d'un satellite, *Astron. Astrophys.*, 3, 15-28, 1969.

150

Cook, G. E., Luni-solar perturbations on the orbit
of an earth satellite, *Geophys. J. Roy. Astron.
Soc.*, 6(3), 271–291, 1962.

King-Hele, D. G., G. E. Cook, and Diana W.
Scott, Evaluation of odd zonal harmonics in the
geopotential of degree less than 33, from the

IMPROVEMENT OF ZONAL HARMONICS

analysis of 22 satellite orbits, *Planet. Space Sci.*,
17, 629–664, 1969.

Kozai, Y., Revised zonal harmonics in the geo-
potential, *Smithson. Astrophys. Observ. Spec.
Rep.* 295, 1969.

Accuracy of Potential Coefficients Obtained from Present and Future Gravity Data

RICHARD H. RAPP

*Department of Geodetic Science
Ohio State University, Columbus, Ohio 43210*

Abstract. The accuracies of recent solutions of potential coefficients as determined from satellite and from terrestrial gravity data are compared. Certain terrestrial solutions are better than others. The determination of the potential coefficients from terrestrial gravity data is considered from the point of view of the variances of the coefficients and the correlation of the coefficients. Coefficients of degree n can be strongly correlated with coefficients of degree $n + 1$ and to a lesser extent with coefficients of degree $n + 2$. For existing terrestrial gravity data, these correlations may reach 0.8. These results suggest that significant aliasing error may exist in determinations of potential coefficients from terrestrial gravity data. This error could be reduced by solving for coefficients to degree $n + 2$ and retaining only those to degree n as a useful set. Tests are made, postulating various improvements in existing surface gravity, to estimate possible corresponding improvement in the potential coefficients.

Potential coefficients used to describe the earth's gravitational field can be derived through the analysis of satellite data, through the analysis of terrestrial gravity data, or through a combination of these data. The first part of this paper will compare potential coefficient information as determined separately from recent satellite and terrestrial solutions. The second part of this paper will examine the determination of potential coefficients from terrestrial gravity with different distribution and accuracy. Such information is important when a solution of higher degree from gravity data is being considered.

DETERMINATION OF POTENTIAL COEFFICIENTS FROM TERRESTRIAL GRAVITY DATA

A comprehensive review of relevant procedures has been given by Pellinen [1966]. For applications using nonglobal gravity data, or for cases where the accuracy of a mean terrestrial gravity anomaly value is non-uniform, the following equation [Pellinen, 1969] can be used to relate potential coefficients and gravity anomalies:

$$\langle \Delta g \rangle = \Delta g_0 + \gamma \sum_{n=2}^{n_0} (n - 1) q_n \\ \cdot \sum_{m=0}^n [\langle \bar{C}_{nm} - \bar{C}_{nm,r} \rangle \cos m\lambda \\ + \bar{S}_{nm} \sin m\lambda] \bar{P}_{nm}(\sin \varphi) + \delta g_n \quad (1)$$

In equation 1,

$\langle \Delta g \rangle$ is the smoothed free-air anomaly in a specified block size.

Δg_0 is the zero-degree harmonic in the expansion of the free-air anomalies.

γ is a mean value of gravity, usually taken to be 979.8 gals.

n_0 is the highest degree being considered in the expansion.

q_n is the coefficient of smoothing.

$\bar{C}_{nm}, \bar{S}_{nm}$ are the fully normalized potential coefficients of the actual gravitational field of the earth.

$\bar{C}_{nm,r}$ are the fully normalized potential coefficients of reference ellipsoid to which the $\langle \Delta g \rangle$ have been referred.

δg_n is the influence of the $(n_0 + 1)$ and higher harmonics on $\langle \Delta g \rangle$.

POTENTIAL COEFFICIENTS FROM GRAVITY DATA

Equation 1 is used to estimate, through a weighted least squares procedure, values of \bar{C}_{nm} , \bar{S}_{nm} given values of $\langle \Delta g \rangle$.

The value of Δg_0 can be computed from the following equation [Heiskanen and Moritz, 1967, p. 111]:

$$\Delta g_0 = (\bar{\gamma}_E - \gamma_E) - \frac{1}{3}\gamma(\bar{f} - f) \quad (2)$$

where $\bar{\gamma}_E$ and \bar{f} are the equatorial gravity and flattening of the 'best' terrestrial ellipsoid, and γ_E , f are the equatorial gravity and flattening of the gravity formula to which the $\langle \Delta g \rangle$ values have been referred. If all anomalies received the same weight in the adjustment, the value of Δg_0 would not affect the determination of \bar{C}_{nm} , \bar{S}_{nm} . In practice, however, the $\langle \Delta g \rangle$ values do receive different weights, and Δg_0 should be accurately computed.

In order to estimate Δg_0 , we first note that most gravity anomalies (specifically those to be used in subsequent sections) are referred to the International Gravity Formulas so that (Potsdam system) $\gamma_E = 978.049$ gals and $f = 1/297$. Current best values are $\bar{\gamma}_E = 978.0472$ gals and $1/\bar{f} = 1/298.258$. The value of $\bar{\gamma}_E$ has been corrected for the mass of the atmosphere and has been converted to the Potsdam system by the addition of 13.7 mgal to the value given by Rapp [1970a]. When these quantities are used, $\Delta g_0 = 2.8$ mgal. In some previous computations, using older values of $\bar{\gamma}_E$ and \bar{f} , I have used [Rapp, 1969a] $\Delta g = 1.4$ mgal. The effect of the variation of Δg_0 on \bar{C}_{nm} , \bar{S}_{nm} determined in a least squares procedure will be discussed in a subsequent section.

The smoothing factor q_n depends on the degree n being considered and the procedure for estimating a mean anomaly in a given size block. When simple averaging is used to determine $\langle \Delta g \rangle$, Pellinen [1969] gives:

$$q_n = \cot \frac{\psi_0}{2} \frac{P_{n1}(\cos \psi_0)}{n(n+1)} \quad (3)$$

where ψ_0 is the radius out to which the anomalies are smoothed. For 5° blocks, the value of ψ_0 is approximately 2.15° . Table 1 gives q_n for this value of ψ_0 and for various values of n . The percentage error in the potential coefficients would be $(1 - q_n) \times 100$ if q_n were set to 1. As can be seen from Table 1, this error is relatively small for the lower degrees. It is then reasonable to set $q_n = 1$.

TABLE 1. Values of q_n with $\psi_0 = 2.15^\circ$

Degree, n	q_n	$(1 - q_n) \times 100, \%$
2	0.999	0.1
4	0.996	0.4
6	0.993	0.7
8	0.987	1.3
10	0.981	1.9
12	0.973	2.7
14	0.963	3.7
16	0.953	4.7
18	0.941	5.9
20	0.928	7.2

There are several additional pertinent facts associated with equation 1. For example, equation 1 is considered a spherical approximation to more accurate formulas. The relative error in the coefficients to this approximation is on the average nf [Ostach and Pellinen, 1966]. Values of nf considered as a percentage error are given in Table 2. These errors are on the same order as that caused by the neglect of the smoothing factor q_n . The elimination of the spherical approximation error will require more exact expressions for computing anomalies from potential coefficients. Such equations are described by Ostach and Pellinen [1966] and Hotine [1969].

Another area of concern is related to the proper terrestrial anomaly to be used on the left-hand side of equation 1. Pellinen [1969] discusses the current thinking on this matter, and he indicates that for realistic accuracy the value of $\langle \Delta g \rangle$ should be equal to the free-air anomaly plus the correction for relief (the terrain effect). Rapp [1969b] has argued that the mean terrain effect for large blocks (say 5°) will be small, so that the effect on \bar{C}_{nm} , \bar{S}_{nm} of neglecting the terrain effect

TABLE 2. Relative Error in Potential Coefficients Caused by the Spherical Approximation of Equation 1

Degree, n	$(nf) \times 100, \%$
2	0.7
4	1.3
6	2.0
8	2.7
10	3.4
12	4.0
14	4.7
16	5.4
18	6.0
20	6.7

RICHARD H. RAPP

in estimating $\langle \Delta g \rangle$ should be small. However, since no detailed studies are available, work should be continued in this area.

RECENT DETERMINATIONS AND COMPARISONS
OF POTENTIAL COEFFICIENTS FROM
TERRESTRIAL GRAVITY DATA

Bjerhammar [1969] and *Rapp* [1969a] have reported potential coefficients as derived from terrestrial gravity data. *Bjerhammar's* solution, complete through degree 8, was based on approximately 493 anomalies 10° by 10° , which represented coverage of 76% of the 648 blocks 10° by 10° covering the surface of the earth. The gravity data used by *Rapp* [1969a] consisted of 1470 anomalies 5° by 5° (57% of the 2592 blocks on the earth's surface) based on observed gravity data. Each of these anomalies was assigned a standard error. The quality and distribution of this data are shown in Figure 1. For certain computations, the blocks having no anomaly estimate based on observed terrestrial gravity data were assigned an anomaly value based on the model anomalies given by *Uotila* [1964]. These model anomalies are derived from knowledge of topographic heights and isostatic hypotheses. A standard error of ± 20 mgal was assigned to each of the model anomalies.

so as to reduce any aliasing effects on the potential coefficients being sought. This set was given, with the standard errors of the potential coefficients, by *Rapp* [1969a].

The above three potential coefficient sets, and *Bjerhammar's* set, are now compared with the newest set of potential coefficients derived from satellite data alone [*Gaposchkin*, 1969]. The comparison of the coefficient sets was carried out by computing the root mean square (rms) coefficient difference, in each degree and for the whole set, and through the correlation of the coefficients by degree and for the whole set. This correlation, as judged by the correlation coefficient r , was computed for each degree from the following expression:

$$r_n = \frac{\sum_{m=0}^n (\bar{C}_{nm} \bar{C}_{nm}' + \bar{S}_{nm} \bar{S}_{nm}')}{\left[\sum_{m=0}^n (\bar{C}_{nm}^2 + \bar{S}_{nm}^2) \sum_{m=0}^n (\bar{C}_{nm}^{2'} + \bar{S}_{nm}^{2'}) \right]^{1/2}} \quad (4)$$

where the primed coefficients are those for which the correlation coefficient with respect to the unprimed coefficients is being computed. The correlation coefficient for the complete set of coefficients to degree N is given by:

$$r = \frac{\sum_{n=2}^N \sum_{m=0}^n (\bar{C}_{nm} \bar{C}_{nm}' + \bar{S}_{nm} \bar{S}_{nm}')}{\left[\sum_{n=2}^N \sum_{m=0}^n (\bar{C}_{nm}^2 + \bar{S}_{nm}^2) \sum_{n=2}^N \sum_{m=0}^n (\bar{C}_{nm}^{2'} + \bar{S}_{nm}^{2'}) \right]^{1/2}} \quad (5)$$

Using these data, several sets of potential coefficients were derived. For this paper, three solutions based on the *Rapp* [1969a] data will be specifically described. The first solution (designated Rapp A) is based on only the observed anomaly information with $\Delta g_0 = 1.4$ mgal and is complete through degree 8. This solution should be comparable with that of *Bjerhammar*. The second solution, also complete through degree 8 (designated Rapp B) is based on the observed plus model anomalies with $\Delta g_0 = 1.4$ mgal. The third solution (designated Rapp C) is also based on the terrestrial plus model anomalies with $\Delta g_0 = 1.4$ and is considered through degree 8; however, this set of coefficients is a subset of a more complete solution carried through degree 12 and was chosen

The computation of the correlation coefficient in this manner is not meant to be a statistical measure of the agreement of two coefficient solutions, since the correlation between the coefficients is ignored. However, values of r_n and r should be helpful in judging the over-all agreement of potential coefficient solutions. The rms difference, designated Δ , and values of r_n and r are given in Table 3.

Considering Table 3, we can make the following observations:

1. From the rms coefficient difference, the *Bjerhammar* solution agrees somewhat better with the satellite solution than the comparable Rapp A solution, although the over-all correlation coefficient indicates a slightly stronger correlation of the Rapp A solution with the satel-

POTENTIAL COEFFICIENTS FROM GRAVITY DATA

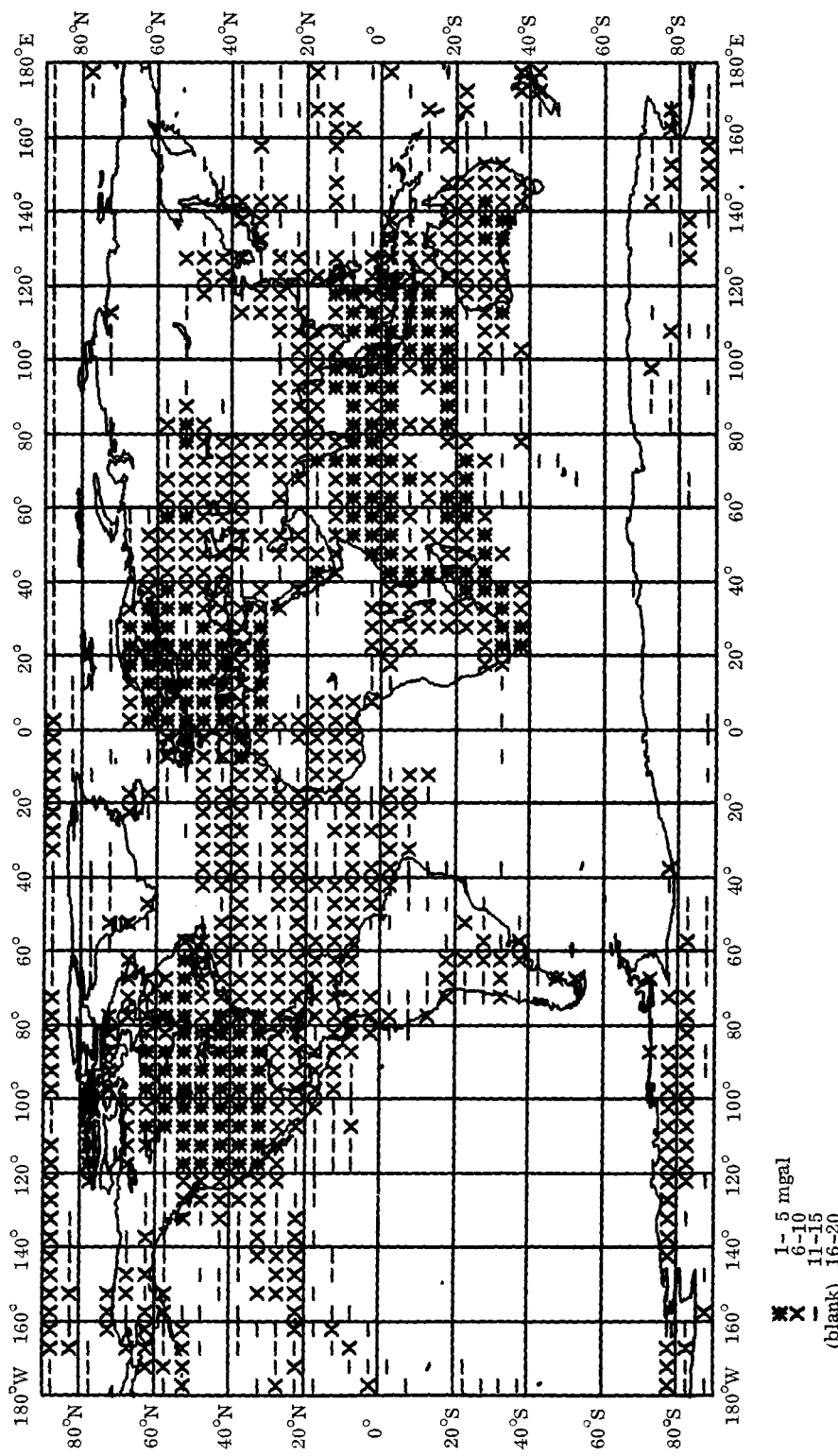


Fig. 1. Quality and distribution of terrestrial gravity data used by Rapp [1969a].

RICHARD H. RAPP

155

TABLE 3. The rms Difference Δ and Correlation Coefficients between Satellite Potential Coefficients and Coefficients Derived from Terrestrial Data

Degree, n	Bjerhammar		Rapp A		Rapp B		Rapp C	
	$\Delta \times 10^6$	r_n						
2	1.93	0.539	1.65	0.904	0.43	0.999	0.31	0.996
3	0.57	0.852	1.06	0.275	0.59	0.838	0.55	0.865
4	0.38	0.662	0.80	0.399	0.26	0.855	0.28	0.821
5	0.28	0.531	0.54	0.414	0.25	0.625	0.22	0.740
6	0.15	0.817	0.40	0.440	0.16	0.811	0.11	0.906
7	0.17	0.278	0.32	0.677	0.12	0.804	0.07	0.881
8	0.13	0.404	0.17	0.554	0.12	0.644	0.12	0.580
Over-all	0.56	0.573	0.68	0.602	0.27	0.878	0.24	0.895

lite-derived potential coefficients than the Bjerhammar solution.

2. The two solutions (Rapp B, Rapp C) incorporating model anomalies agree considerably better with the satellite potential coefficients than the solutions not incorporating model anomalies. In order to see whether the model anomalies, per se, were the cause of the better agreement, a test was run where the anomalies in the unobserved areas were set to zero with a standard error of ± 20 mgal. The rms coefficient difference between this solution and the *Gaposchkin* [1969] solution was $\pm 0.31 \times 10^{-6}$, whereas the correlation coefficient was 0.858. This indicates a slightly poorer agreement with the satellite solution than the corresponding solution using model anomalies. Thus model anomalies contribute some information to these lower-degree harmonics.

3. The Rapp C solution is slightly better than the Rapp B solution. This improvement apparently represents the reduction in the aliasing error that takes place when a subset of a higher-coefficient solution is considered.

In addition to the Rapp A and Rapp B solutions considered in Table 3, two other Rapp B solutions were run with $\Delta g_0 = 0.0$ and $\Delta g_0 = 2.8$ mgal. The purpose of these tests was to see

how changes in Δg_0 would affect the coefficients being sought. Such changes are represented in Table 4. In comparing the solution with $\Delta g_0 = 0.0$ mgal and the solution with $\Delta g_0 = 1.4$ mgal, the rms coefficient difference at degree 2 was $\pm 0.18 \times 10^{-6}$ and at degree 8 was $\pm 0.01 \times 10^{-6}$. In all solutions, the dominant effect of the changed Δg_0 was less than the standard error of the potential coefficients being sought.

ACCURACY OF POTENTIAL COEFFICIENTS FROM CURRENT TERRESTRIAL GRAVITY DATA

If a global coverage of uniform accuracy existed, the standard error (ϵ_n) of potential coefficients of degree n would be given by the following expression [Rapp, 1969c, 1970b]:

$$\epsilon_n = \frac{\epsilon_{\Delta g}}{2\gamma(n-1)} \pi^{-1/2} \theta \quad (6)$$

where $\epsilon_{\Delta g}$ is the standard error of a mean anomaly in block size θ . It is clear from equation 6 that all coefficients in a given degree should have the same accuracy, and it can also be shown that all coefficients are independently determined under the specified conditions.

From tests using actual data, such as the Rapp B solution described previously, it is found that the behavior of the standard error

TABLE 4. Comparison of Solutions Obtained with Various Δg_0 Values, rms Coefficient Differences

Solution	Rapp B Solution		
	$\Delta g_0 = 0.0$ mgal	$\Delta g_0 = 1.4$ mgal	$\Delta g_0 = 2.8$ mgal
<i>Gaposchkin</i> [1969]	$\pm 0.26 \times 10^{-6}$	$\pm 0.27 \times 10^{-6}$	$\pm 0.29 \times 10^{-6}$
Rapp B with $\Delta g_0 = 1.4$ mgal	$\pm 0.05 \times 10^{-6}$		$\pm 0.06 \times 10^{-6}$

of the potential coefficients being sought follows a decrease implied by equation 6 and is approximately constant within a given degree. This can be seen from the specific standard errors given by Rapp [1969a, c]. This fact implies that it is useful to write equation 6 in the form

$$\epsilon_n = k/(n - 1) \quad (7)$$

Knowing values of ϵ_n , we can find k by solving equation 7. Given solutions over several degrees, the most representative values of k would be the mean value as determined from all standard errors of the potential coefficients used in the solution. We can state this as follows:

$$k = \sum_{n=2}^N (n - 1) \cdot \sum_{m=0}^n (\epsilon_C + \epsilon_S)/[(N + 1)^2 - 4] \quad (8)$$

where N is the maximum degree over which the summation is to be carried. In the computations to be reported here, we have used data from the 8, 8 solutions but taking $N = 6$, so that the effect of aliasing will be reduced. The value of k for each degree, and as computed from an over-all mean using equation 8, is given in Table 5 for the Rapp A and Rapp B solutions.

We note that the results for the Rapp B solution are fairly constant, agreeing with the implications of equation 6 even though the anomalies used in Rapp B have widely varying standard errors. However, the inclusion of 1122 model anomalies at a uniform standard error of ± 20 mgal tends to unify the whole set of anomalies. The wider variations of k seen for the Rapp A solution are due to the limited gravity data used in the Rapp A solution.

TABLE 5. Values of k ($\times 10^6$) for Rapp A and Rapp B Solutions

Degree, n	Rapp A	Rapp B
2	0.605	0.326
3	0.710	0.329
4	0.774	0.335
5	0.756	0.335
6	0.696	0.331
Mean through degree 6	0.724	0.332

POTENTIAL COEFFICIENTS FROM GRAVITY DATA

The value of $k = 0.332 \times 10^{-6}$ for the Rapp B solution can be used to estimate the standard error of any potential coefficient (using equation 7) as it would be determined from the terrestrial gravity anomalies and model anomalies that have been used in these tests.

Since the standard errors of the anomalies are not uniform, and for certain types of solutions complete global coverage does not exist, the potential coefficients determined from gravity data will not be independently determined. To investigate the degree of correlation between the coefficients, a correlation coefficient matrix was computed for all solutions discussed in this paper.

For the Rapp A solution, the correlation coefficients reached -0.8 for some potential coefficients. It was seen that the strongest correlation between a given coefficient of degree n was in most cases with the similar coefficient of degree $(n + 1)$. For this specific situation, the average coefficient in this solution was approximately -0.6 . Generally the correlation between the coefficients decreased as the difference in the degree of the considered coefficients increased. In some cases, however, the correlation remained fairly high even with a degree separation of 3. We must conclude that the potential coefficients determined from existing gravity material alone will be highly correlated.

For the Rapp B solution, the maximum correlation coefficient was 0.4. For many situations the strongest correlation was between a coefficient of degree n and the similar coefficient of degree $n + 1$. The mean of the absolute values of the correlation coefficients in this case was approximately 0.3. As the degree of separation of coefficients increased, the correlation coefficients decreased at a faster rate than that found in the Rapp A solution. For example, in the Rapp A solution the correlation between $S_{3,1}$ and $S_{7,1}$ was -0.51 , whereas in the Rapp B solution the correlation between the same coefficients was only -0.04 . Clearly, the filling in of the unobserved areas with anomaly values has considerably reduced the correlation between potential coefficients being sought.

ACCURACY OF POTENTIAL COEFFICIENTS FROM NEW GRAVITY DATA

It is important to consider the improvement in potential-coefficient determination as the

RICHARD H. RAPP

157

distribution and accuracy of the terrestrial gravity data improve. If we assume uniform coverage with uniform accuracy, we can use equation 6 to determine the k defined through equation 7. For example, assuming 5° blocks, k is 0.251×10^{-6} for $\epsilon_{\Delta g} = \pm 10$ mgal, and 0.126×10^{-6} for $\epsilon_{\Delta g} = \pm 5$ mgal. For solutions involving nonuniform coverage and accuracy, it is necessary to form normal equations and carry out a solution for each individual case that is to be considered. This has been done for a number of solutions with the subsequent determination of the k values.

In some solutions, the earth was divided in four quadrants defined as follows: NW quadrant, $\varphi = 0^\circ$ to 90° , $\lambda = 180^\circ\text{W}$ to 0° ; NE quadrant, $\varphi = 0^\circ$ to 90° , $\lambda = 0^\circ$ to 180°E ; SW quadrant, $\varphi = 0^\circ$ to -90° , $\lambda = 180^\circ\text{W}$ to 0° ; SE quadrant, $\varphi = 0^\circ$ to -90° , $\lambda = 0^\circ$ to 180°E . This notation is used below to describe the various test solutions made for this paper. All solutions assume global coverage. In the descriptions, 'no standard error $>x$ mgal' refers to a solution based on the existing gravity material augmented, where necessary, by new data to meet the specified accuracy criteria.

- 1A Uniform standard error of ± 10 mgal
- 1B Uniform standard error of ± 5 mgal
- 2A No standard error >10 mgal
- 2B No standard error >5 mgal
- 3A No standard error >10 mgal in the SW quad
- 3B No standard error >5 mgal in the SW quad
- 4A No standard error >10 mgal in the NW quad
- 4B No standard error >5 mgal in the NW quad
- 5A No standard error >10 mgal in the NE quad
- 5B No standard error >5 mgal in the NE quad
- 6A No standard error >10 mgal in the SE quad
- 6B No standard error >5 mgal in the SE quad
- 7A No standard error >10 mgal in the southern hemisphere
- 7B No standard error >5 mgal in the southern hemisphere
- 8A No standard error >10 mgal in the northern hemisphere
- 8B No standard error >5 mgal in the northern hemisphere

To describe the results for these solutions, we give in Table 6 the following information for each simulation: k , the largest correlation coefficient, r_{\max} , the average values of the correlation coefficient r for the correlation of the coefficients of degree n with those of $n + 1$, and the percentage improvement in the potential coefficient determinations with respect to the current

gravity data including model anomalies. The improvement value was computed using as a reference value $k = 0.332 \times 10^{-6}$.

Of the solutions considered, the best would be 2B, where there would be a 63.3% improvement over existing determinations. In addition, the correlation between the coefficients being sought would be very small.

For the solutions in which only quadrant improvement has been considered (3 through 6), the greatest improvement would come from data collected in the SW quadrant (3). In 4 and 5, the proposed new data would yield somewhat more accurate coefficients than existing data, but the correlation between the coefficients would be increased.

Of the hemisphere solutions, 7B yields the best improvement considering k alone, but it also increases the correlation between the coefficients being sought. On the other hand, 7A shows the second best improvement in the hemisphere solutions, but it has the strong advantage that the potential coefficients will be fairly independently determined.

From these tests, it is clear that collecting gravity material in a given area will improve the accuracy of the potential coefficient solutions but that, if the data are such that the accuracy of the global data is poorly distributed, the potential coefficients computed from such data will be highly correlated. The ideal situation is

TABLE 6. Results from Simulated Gravity Coverages

Solution	$k (\times 10^6)$	r_{\max}	$\langle r \rangle$	Improvement, %
1A	0.251	0.0	0.00	24.4
1B	0.126	0.0	0.00	62.0
2A	0.220	0.2	0.08	33.7
2B	0.122	0.1	0.02	63.3
3A	0.271	0.3	0.08	18.4
3B	0.233	0.4	0.15	29.8
4A	0.318	0.5	0.33	4.2
4B	0.293	0.6	0.44	11.7
5A	0.317	0.5	0.37	4.5
5B	0.299	0.6	0.48	9.9
6A	0.304	0.4	0.17	8.4
6B	0.279	0.5	0.10	16.0
7A	0.248	0.2	0.09	25.3
7B	0.196	0.6	0.45	41.0
8A	0.304	0.5	0.41	8.4
8B	0.266	0.7	0.64	19.9

$$\sigma(\bar{C}, \bar{S}) = 10 \times 10^{-6}/n^2 \quad (12)$$

to have global uniform accuracies, the greater the accuracies, the better.

HOW HIGH CAN WE CARRY POTENTIAL-COEFFICIENT DETERMINATIONS FROM GRAVITY DATA?

Given existing data, or data postulated for the various test cases described, we need to know to what degree it makes sense to derive potential coefficients. To answer this question, we shall assume that the potential coefficients are independently determined. We then ask: at what degree can the potential coefficient be hypothesized to be zero considering the accuracy of the coefficient determinations from the terrestrial gravity information? To answer this question, we apply a single parameter hypothesis test as outlined by *Hamilton* [1964, p. 140]. We first establish a theoretical value of the F statistic F_t , depending on the degrees of freedom in the solution, and at an appropriate confidence interval. For the solutions considered here, the degrees of freedom are very large. Choosing a 95% confidence interval, $F_t = 3.84$. If we let $\sigma(\bar{C}, \bar{S})$ designate the expected rms variation of a potential coefficient, the computed F statistic, F_c , would be for the hypothesis that the estimated σ could be 0:

$$F_c = \sigma^2(\bar{C}, \bar{S})/\epsilon_n^2 \quad (9)$$

If F_c is less than F_t , the hypothesis that the coefficient is zero is accepted. We can thus say that, if F_c is greater than, or equal to, F_t , the hypothesis of zero coefficient is rejected and we can say that the coefficient is determined. Specifically, we say that a coefficient is determined if

$$\sigma^2(\bar{C}, \bar{S})/\epsilon_n^2 \geq 3.84 \quad (10)$$

or

$$\epsilon_n/\sigma(\bar{C}, \bar{S}) \leq 0.51 \quad (11)$$

In essence, equation 11 states that a potential coefficient is considered to be determined if the standard error of that coefficient is approximately one-half the expected variation of the coefficient itself.

In order to apply equation 11, we can use equation 7 for ϵ_n , but we then need a representation for $\sigma(\bar{C}, \bar{S})$. *Kaula* [1966] has given the following widely used representation of $\sigma(\bar{C}, \bar{S})$:

Pellinen [1970] has also considered the problem by deriving values for the behavior of the anomaly degree variances Δg_n^2 . Combining satellite information and gravity information, one rule suggested by *Pellinen* is

$$\Delta g_n^2 = 166/n^{1.12} \quad (13)$$

which implies a rms potential coefficient variation of

$$\sigma(\bar{C}, \bar{S}) = 9.3 \times 10^{-6}/n^{2.06} \quad (14)$$

Equations 12 and 14 can thus be used in equation 11 in combination with equation 7 to find the highest n value for which a potential coefficient can be considered determined from terrestrial gravity data. This information is given in Table 7 for both the *Kaula* and *Pellinen* rule, for the existing terrestrial and model anomaly field, as well as for the solutions listed earlier. The use of the *Pellinen* rule gives n values approximately 20% smaller than the use of the *Kaula* rule. If equation 11 were modified to the case where a potential coefficient is considered to be determined if the standard error of its determination is not greater than the expected variation in the coefficient, the numerical constant in equation 11 would be set to 1. Under this circumstance, the highest degree that could

TABLE 7. Highest-Degree Coefficient to be Found from Terrestrial Gravity Information

Solution	Kaula's Rule	Pellinen's Rule
Existing terrestrial and model anomaly data	14	12
1A	19	16
1B	39	31
2A	22	18
2B	41	32
3A	18	15
3B	21	17
4A	15	13
4B	16	14
5A	15	13
5B	16	14
6A	16	13
6B	17	14
7A	20	16
7B	25	20
8A	16	13
8B	18	15

RICHARD H. RAPP

159

be solved for could be estimated by doubling the n values given in Table 7. In this case, any $n(\max)$ greater than 36 would be a formal answer only as the maximum value of n to be found from 5° anomalies is considered to be 36 from wavelength considerations.

The values given in Table 7 have ignored the correlation between the potential coefficients that arises in most of the solutions. Because of this correlation, there will be an aliasing effect, so that potential coefficients should be computed to 2 or 3 degrees higher than that indicated in Table 7. In cases 1A and 1B, however, uniform accuracy has been assumed, so that no aliasing effects exist. In addition, because the correlation coefficients (as seen from Table 6) are small, the following solutions should have minimal aliasing effects: 2A, 2B, 3A, 3B, 6A, 6B, and 7A.

If we wish to determine the potential coefficients up to degree 25 from terrestrial gravity data, the following cases of improved gravity collection will yield the desired result (using Pellinen's rule): 1B and 2B. Each of these cases required anomaly determination to ± 5 mgal.

CONCLUSIONS

Existing solutions for potential coefficients based on existing terrestrial information generally agree with the satellite determinations within the standard errors from each result. However, exceptions to this agreement for some coefficients have been pointed out by Badekas [1969].

If we intend to extend determinations of potential coefficients from terrestrial gravity from the relatively low degrees up to the higher degrees (somewhat ill-defined as greater than 20), it is imperative that consideration be given to the minor effects heretofore neglected, such as: the smoothing factor, numerical integration error, error due to using a spherical reference surface, and the neglect of the mean terrain effect in free-air anomalies used in the solutions.

The estimation of the highest degree to which we can go depends on two factors: first, what criteria do we use to decide when a coefficient is actually determined, and second, what rule should be used to describe the behavior of the potential coefficients of higher degree? In this paper, we used a criterion for potential coefficient determinations that has a standard error approximately half the expected variation in

the potential coefficient itself. This indicates that the highest degree to which we should go with existing terrestrial information is 12 to 14. If we state that a coefficient is determined up to the point where the ratio of the standard error to the expected coefficient variation is 1, current material could be used to go up to the range of $n = 23$ to 29. This latter criterion has been used by Rapp [1968], Gaposchkin [1970], and Lambeck [1971].

Finally, it should be emphasized that simplistic approaches to finding the highest reasonable degree ignore the strong correlation between coefficients that may rise in certain types of gravity distribution and accuracy. In order to consider the complete determination, tests can be developed to compare the complete inverse matrices of various solutions instead of only comparing, in effect, the diagonal elements.

Acknowledgment. The computer time used in this study was made available through the Instruction and Research Computer Center of Ohio State University. Parts of this study were supported by the Air Force Cambridge Research Laboratories under contract F19628-69-C-0127.

REFERENCES

- Badekas, J., Investigations related to the establishment of a world geodetic system, *Rep. 124*, Dep. Geod. Sci., Ohio State Univ., Columbus, 1969.
- Bjerhammar, A., Studies of a coalescent world geodetic system, *Tellus*, 21(4), 517-548, 1969.
- Gaposchkin, E. M., Improved values for the tesseral harmonics of the geopotential and station coordinates, paper presented at the 12th Meeting of Cospar, Prague, May 1969.
- Gaposchkin, E. M., Future uses of laser tracking, in *Proceedings of the Geos 2 Program Review Meeting*, 22-24 June 1970, edited by Computer Sci. Corp., Falls Church, Va., 1970.
- Hamilton, W. C., *Statistics in Physical Science*, Ronald Press, New York, 1964.
- Heiskanen, W., and H. Moritz, *Physical Geodesy*, W. H. Freeman, San Francisco, Calif., 1967.
- Hotine, M., *Mathematical Geodesy, Monogr. Ser.*, vol. 2, Environ. Sci. Serv. Admin., Washington, D.C., 1969.
- Kaula, W. M., *Theory of Satellite Geodesy*, Blaisdell, Waltham, Mass., 1966.
- Lambeck, K., Comparison and combination of surface gravity data with satellite data, *Bull. Geod.*, 100, 203-219, 1971.
- Ostach, A. M., and L. P. Pellinen, The effect of the earth's ellipticity on its Stokes' constants, *Trans. Cent. Sci. Res. Inst. Geod. Aerial Surv. Cartogr.*, no. 171, 1966 (translated by Aeronaut.

POTENTIAL COEFFICIENTS FROM GRAVITY DATA

- Chart Inform. Center, TC-1282, pp. 117-126, 1966, AD661810).
- Pellinen, L. P., A method for expanding the gravity potential of the earth in spherical functions, *Trans. Cent. Sci. Res. Inst. Geod. Aerial Surv. Cartogr.*, no. 171, 1966 (translated by Aeronaut. Chart Inform. Center, TC-1292, pp. 65-116, 1966, AD661810).
- Pellinen, L. P., Joint adjustment of gravimetric and satellite data in the determination of the earth's gravitational field, *Byull. Sta. Opt. Nablyudeniya Iskusstv. Sputnikov Zemli*, no. 55, 58-68, 1969 (translated by Aeronaut. Chart Inform. Center, TC-1650, pp. 1-21, 1970, AD715152).
- Pellinen, L. P., Estimation and application of degree variances of gravity, *Stud. Geophys. Geod.*, 14, 168-173, 1970.
- Rapp, R. H., A global $5^\circ \times 5^\circ$ anomaly field (abstract), *Eos Trans. AGU*, 49, 507, 1968.
- Rapp, R. H., Gravitational potential coefficients from gravity data alone (abstract), *Eos Trans. AGU*, 50, 117, 1969a.
- Rapp, R. H., Corrections to a mean free-air surface anomaly to be used in the combination of gravimetric and satellite data, paper presented at the 4th Symposium on Mathematical Geodesy, Ital. Geod. Comm., Trieste, May 1969b.
- Rapp, R. H., Analytical and numerical differences between two methods for the combination of gravimetric and satellite data, *Boll. Geofis.*, 11(41-42), 108-118, 1969c.
- Rapp, R. H., Methods for the computation of geoid undulations from potential coefficients, *Rep. 132*, Dep. Geod. Sci., Ohio State Univ., Columbus, 1970a.
- Rapp, R. H., The role of gravity data in determination of the gravitational potential of the earth, *Rep. 134*, Dep. Geod. Sci., Ohio State Univ., Columbus, 1970b.
- Uotila, U. A., *Gravity Anomalies for a Mathematical Model of the Earth*, Publ. 43, Isostatic Inst., Int. Ass. Geod., Helsinki, 1964.

Error Model for the SAO 1969 Standard Earth

C. F. MARTIN AND N. A. ROY

*Wolf Research and Development Corporation
Riverdale, Maryland 20840*

Abstract. A method is developed for estimating an error model for geopotential coefficients using satellite tracking data. A single station's apparent timing error for each pass is attributed to geopotential errors. The root sum of the residuals for each station also depends on the geopotential errors, and these are used to select an error model. The model chosen is $\frac{1}{4}$ of the difference between the SAO M1 and the APL 3.5 geopotential.

One of the largest sources of uncertainty in almost all low-altitude satellite orbits consists of errors in the set of geopotential coefficients used for the orbit generation and estimation. If the satellite arc length is a few days or less, the predominant errors are due to terms of low degree and order. For arc lengths of 1 week or longer, errors in terms of high degree and order that are resonant may become the dominant errors.

In this paper, a method is proposed for estimating the effects of geopotential coefficient errors on any data reduction or orbit generation involving satellite orbits. The method involves differencing existing geopotential models and is basically no more difficult than integrating an orbit using the normal spherical harmonic expansion. The geopotential error model is calibrated using Geos 2 tracking data and the SAO 1969 standard earth [Gaposchkin and Lambeck, 1970] as the model whose accuracy is being assessed.

METHODS OF GEOPOTENTIAL MODEL EVALUATION

The determination of definitive satellite orbits requires an accurate description of the forces acting on the satellite. Accurate predictions of satellite position are even more dependent upon a good model for all significant satellite perturbations. In reality, each of the entire set of geopotential coefficients used for any orbit estimation or prediction contains errors that can produce discernable effects. The actual magni-

tude of the effects depends upon a number of factors, including the length of arc, the amount and distribution of tracking data, and the true coefficient errors. The large number of coefficients in error generally precludes the possibility of adjusting any such parameters (particularly of low degree and order) in most data reductions. The result is that the average orbit estimation must accept a geopotential model from the best available source, complete with whatever errors the coefficients contain.

The geopotential models now available include several sets developed by the Smithsonian Astrophysical Observatory [Gaposchkin, 1966; Gaposchkin and Lambeck, 1970], as well as somewhat older models developed by the Naval Weapons Laboratory [Anderle, 1965] and the Johns Hopkins Applied Physics Laboratory [Guier and Newton, 1965], and recent models developed by Rapp [1969] and Kohnlein [1967]. These models vary somewhat in size, but typically are complete to about (8, 8) with zonals to degree 16–20 and selected tesseral as high as degree 22. The total number of non-zero coefficients is of the order of several hundred. There is a wide variation in the orbit generation accuracy that the models are capable of producing. The correlation of accuracy with size is not exactly one to one, although a very accurate model must, of necessity, be quite large.

One of the most important aspects of any statement of orbit accuracy, as well as the geopotential model that produces this accuracy, is

the length of the arc over which the accuracy will hold. For arcs of approximately 2 days and less, resonance coefficient errors in general provide only an almost negligible contribution to the total orbit uncertainty. On the other hand, for arc lengths comparable to the shortest resonant beat period (approximately 6 days in the case of Geos 2) resonance coefficient errors may have effects of hundreds of meters and may be the predominant source of error. It follows that tests and comparisons of geopotential models over arcs of 1 or more weeks may provide tests of the accuracy of only a few resonance coefficients and may provide limited information on the accuracy (as a set) of the approximately 100 coefficients of lowest degree that most significantly affect shorter arcs.

ESTIMATION OF GEOPOTENTIAL ERRORS USING DIFFERENT GRAVITY MODELS

Since the satellite moves according to the true geopotential, a comparison of actual tracking data with results obtained using a particular model of the geopotential can be used for analyzing the true model accuracy. Suppose now that accuracy estimates are desired for a hypothetical satellite and a hypothetical distribution of data. Some extrapolation is thus necessary from those satellites for which data exist to the new satellite. The manner in which this extrapolation is to be made is the primary subject here. It requires that some model be derived for errors in geopotential coefficients. Such a model can be intuitively derived in the following manner.

Let us assume that two geopotential models of the same size and using comparable amounts of data from different satellites are obtained by investigators working completely independently. Assuming neither investigator to have any particular advantage, we might expect the two models to be of comparable accuracy. It is certain, however, that the two investigators will not obtain the same answers and that the models derived will not generate the same orbit. Let us assume that the models are of comparable accuracy and that at any given time the position errors that the force-model errors induce on a specified orbit are ϵ_1 and ϵ_2 , respectively. Further, let us assume that these errors each have an expected value of zero, that they are independent, and that they have the same standard

deviation σ . The standard deviation of the geopotential-model difference effects can then be obtained from the expected value of the square of the differences,

$$\begin{aligned} E[(\epsilon_2 - \epsilon_1)^2] &= E(\epsilon_2^2 - 2\epsilon_1\epsilon_2 + \epsilon_1^2) \\ &= \sigma^2(\epsilon_2) - 0 + \sigma^2(\epsilon_1) = 2\sigma^2 \end{aligned} \quad (1)$$

or

$$\sigma(\epsilon_2 - \epsilon_1) = (2)^{1/2}\sigma \quad (2)$$

We thus deduce that the set of differences between independent gravity models is a measure of the error in the individual models, with a variance higher than either by a factor of 2. If the models are not of comparable accuracy, we still have the result that

$$\text{var } (\epsilon_1 - \epsilon_2) = \text{var } (\epsilon_1) + \text{var } (\epsilon_2) \quad (3)$$

based only on the independence assumption. We have then our basic result that differences between geopotential models can provide a measure of the actual geopotential error. Some scaling factor may be necessary to account for one of the models being more accurate than the other. The procedure for incorporating this error model into a more complete error analysis will be seen in the next section.

GENERAL ERROR ANALYSIS OF ORBIT ESTIMATION

The measurement model upon which is based the least squares (or Bayesian least squares) type of orbit estimation can be expressed as

$$\delta m = A \delta a + K \delta \gamma + \epsilon \quad (4)$$

where δm is the set of measurement residuals, δa is a set of needed adjustments to an adjusted parameter set, $\delta \gamma$ is a set of errors in parameters that are in error but are not being adjusted, ϵ is the set of random noise errors in measurements, and A and K are partial derivative matrices of the measurements with respect to the a and γ parameters, respectively. With the γ parameters assumed to be known, and thus $\delta \gamma = 0$, the least squares solution for δa is

$$\delta \hat{a} = (A^T W A)^{-1} A^T W \delta m \quad (5)$$

where

$$W^{-1} = E(\epsilon \epsilon^T) \quad (6)$$

MARTIN AND ROY

163

A straightforward estimate of the variance of this estimate gives

$$\begin{aligned} \text{var}(\delta\hat{a}) &= (A^T W A)^{-1} \\ &+ [(A^T W A)^{-1} A^T W K] \\ &\cdot \text{var} \delta\gamma[(A^T W A)^{-1} A^T W K]^T \quad (7) \end{aligned}$$

Using (7), we are able to transform measurement and model variances into variances of estimated parameters. We need to consider a situation, however, in which we know the variance of the estimated parameters but do not completely know the variances of the model errors. To this end, let us compute the expected rms of residuals. From (4), the residuals after the a parameters are estimated are given by

$$r = \delta m - A \delta\hat{a} \quad (8)$$

with $\delta\hat{a}$ given by (5). Substituting from (5), we obtain

$$\begin{aligned} r &= (K + A \partial\hat{a}/\partial\gamma) \delta\gamma \\ &+ [I - A(A^T W A)^{-1} A^T W] \epsilon \quad (9) \end{aligned}$$

with

$$\partial\hat{a}/\partial\gamma \equiv -(A^T W A)^{-1} A^T W K \quad (10)$$

Since the expected values of $\delta\gamma$ and ϵ are both zero, the expected value of r is thus also zero.

In practice, one of the best available measures of the actual model errors is obtained from the root sum of squares (rss) of measurement residuals. The sum of N squared residuals to be expected on the basis of measurement and model errors can be obtained using (9) and

$$\sum_{i=1}^N r_i^2 = r^T r \quad (11)$$

with r_i denoting the i th component of the residual vector. Letting γ_i denote the components of γ , and assuming that $\text{var}(\delta\gamma)$ is diagonal, the expected value of $r^T r$ is found to be

$$\begin{aligned} E(r^T r) &= \sum_{i,k} \left(\frac{\partial r_i}{\partial \gamma_k} \delta\gamma_k \right)^2 \\ &+ Tr(W^{-1}) - Tr[A(A^T W A)^{-1} A^T] \quad (12) \end{aligned}$$

where

$$\delta r/\delta\gamma = -K - A \partial\hat{a}/\partial\gamma \quad (13)$$

and Tr denotes the trace. The trace of W^{-1} can also be written as

$$Tr(W^{-1}) = Tr[E(\epsilon\epsilon^T)] = E(\sum \epsilon_i^2)$$

and is thus the expected value of the squared components of measurement noise.

NUMERICAL EVALUATION OF GEOPOTENTIAL ERROR EFFECTS

Two methods of evaluating geopotential coefficient error effects will now be utilized to 'calibrate' the SAO 1969 standard earth for geopotential coefficient error. The geopotential error models will be based on differences between geopotential models as was explained above, and the two methods of calibration will be based on the analysis and derivations given.

The geopotential models used as the basis of the geopotential error model are:

SAO	SAO M1 model truncated at 12th-degree zonals and 8th-degree tesserals [Gaposchkin, 1966]
M1E	SAO M1 model augmented with APL [Yiououlis, 1968] and Wolf [Douglas and Marsh, 1969] 13th-order resonance coefficients
STD	SAO 1969 standard earth [Gaposchkin and Lambeck, 1970]
NWL	NWL 5E-6 truncated at 12th-degree zonals and 8th-order tesserals [Anderele, 1965]
APL	APL 3.5 model truncated at 12th-degree zonals and 8th-order tesserals [Guier and Newton, 1965]
ST8	SAO 1969 standard earth truncated at 12th-degree zonals and 8th-order tesserals

They include both 'complete' and truncated models. In addition, the set of models includes coefficient sets that are indeed of independent origin, differing in the satellites upon which they are based, the tracking measurement types, and the mathematical procedures for orbit and coefficient estimation. Among this set of models should be several pairs that are very nearly independent.

Model error evaluation from timing errors. The first method that will be used to calibrate the gravity model differences as models of geopotential coefficient error is based upon the estimation of known parameters in an orbital

data reduction. In particular, 1- to 2-day arcs of Geos 2 tracking data from the FPQ 6 radars at Wallops Island, Bermuda, and Merritt Island were reduced with the estimation of a set of 6 epoch elements for each arc and an independent timing bias for Bermuda for each pass. Actual timing errors at Bermuda are known to be of the order of fractions of a millisecond or less. The estimation of nonzero timing errors must then be due either to measurement noise or systematic measurement or model errors. The extent to which the recovered timing errors are not explicable as measurement bias (the only significant systematic measurement error) or station position error is thus an indication of the effects of force-model errors. Since the Geos 2 arcs chosen are not significantly affected by atmospheric drag, errors in solar radiation pressure, or errors in coefficients of high degree and order, the most significant force-model error is error in geopotential coefficients from terms of low degree and order.

Table 1 shows the timing biases that were estimated using the Noname [Williamson *et al.*, 1971] program and the SAO 1969 standard earth geopotential model. The table also gives the differences in timing error that would be estimated from four different combinations of the geopotential models. Except for NWL-SAO, the model differences tend to predict a large timing bias at the same time that a large timing bias was recovered. However, the model difference would be expected to predict the actual error only in the statistical sense. On this basis, the root sum of squares was taken for the Noname recovered timing biases and was compared with the root sum of squares predicted

by the model differences. These quantities are shown in the next to last line of Table 1, and the ratio of the root sum of squares from the model differences to the rss from Noname is shown on the last line.

Table 2 shows results of the same type as those of Table 1, but for a 48-hour arc. In this case, all the Noname recovered timing biases are of comparable magnitude. For the most part, the gravity model differences all predict this type of behavior. With the exception of the APL-SAO gravity model difference, however, the ratios to Noname for the rss's differ rather substantially from those shown in Table 1. The APL-SAO model difference is within about 10% of its predicted rms ratio for these two arcs.

Model error evaluation from residuals. The second method of calibration of the geopotential error model is based on the comparison of residuals from actual data reductions with the prediction of the various gravity model differences. In order to provide a satisfactory model for geopotential coefficient error, the calibration constants obtained here must be in reasonable agreement with those obtained in the preceding section.

It follows from the derivations above that the rss of residuals from an orbital data reduction can be expressed as a sum of contributions from independent error sources. This result is expressed mathematically by (12), with the last two terms due to measurement noise and the first summation due to the various error sources that are unmodeled in the data reduction. With the use of high-quality radar range measurements, and arc lengths of more than a few revo-

TABLE 1. Bermuda Timing Bias Recoveries, in Milliseconds, from Three-Station Radar Solution (Wallops, Bermuda, Merritt Island)
(38-hour Geos 2 Arc.)

Pass	Noname	SAO-ST8	M1E-STD	APL-SAO	NWL-SAO
1	-0.597	-0.658	3.217	0.092	-8.12
2	3.945	-8.44	-14.016	15.80	-2.389
3	-0.987	-0.31	-2.427	1.398	15.353
4	-0.0002	6.00	2.131	-1.894	10.526
5	-0.494	1.50	2.698	-3.40	-19.568
6	3.804	-9.67	-12.396	16.69	-10.292
7	-1.024	0.09	2.672	0.891	13.007
rss	5.715	14.266	19.635	23.369	32.805
Ratio to Noname		0.401	0.291	0.245	0.174

MARTIN AND ROY

165

TABLE 2. Bermuda Timing Bias, in Milliseconds, from Three-Station Radar Solution (Wallops, Bermuda, Merritt Island)
(2-day Geos 2 arc.)

Pass	Noname	SAO-ST8	M1E-STD	APL-SAO	NWL-SAO
1	-2.563	0.007	1.144	-0.529	-11.100
2	5.224	6.753	14.326	-22.786	-4.731
3	-3.371	6.884	12.592	-12.417	-20.400
4	-4.054	5.652	10.143	-28.700	-58.454
5	2.197	-4.685	-8.733	12.139	9.861
6	3.308	1.561	2.282	2.025	11.505
rss	8.799	12.220	23.440	40.605	64.871
Ratio to Noname		0.720	0.375	0.217	0.136

lutions, measurement noise contribution to the residual rss is essentially negligible.

The effects on measurement residuals due to any unmodeled systematic errors can be calculated by (13). Since at least nominal values for the errors in radar station position and range biases are known, it is possible to calculate their contributions to measurement residuals. In general, such effects are considerably larger than measurement noise effects, but still small compared to observed residuals for 1- to 2-day arcs.

Equation 12 can thus be written as

$$\text{rss}_{\text{obs}} = \text{rss}_{\text{noise}} + \text{rss}_{\text{bias}} + \text{rss}_{\text{sta. position}} + \text{rss}_{\text{gravity}}$$

Transferring those terms that can be reliably

calculated to one side of the equation, this can be written

$$\text{rss}_{\text{gravity}} = \text{rss}_{\text{obs}} - \text{rss}_{\text{bias}} - \text{rss}_{\text{sta. position}} - \text{rss}_{\text{noise}} \quad (14)$$

The first term on the right is obtained from a data reduction and the other components can be computed using (13) and estimates of biases, station position errors, and measurement noise. The gravity contribution to the residual rss can be computed using differences between a pair of the gravity models. The scaling factor necessary for the gravity error model is then obtained by equating the two sides of (14).

Table 3 shows the results for a 2-day arc of Geos 2 for geopotential error effects with a worldwide distribution of tracking stations. The

TABLE 3. Two-Day Geos 2 Arc 1 Residual Fit
(rss in meters.)

Models	Station				
	Wallops FPS-16	Wallops FPQ-6	Woomera	Antigua	Bermuda
Observed rss SAO-ST8	4.750	8.690	11.970	5.920	8.830
rss	9.940	14.760	24.810	12.960	14.590
Ratio	0.478	0.589	0.482	0.457	0.605
M1E-STD					
rss	16.410	24.440	23.470	22.240	23.210
Ratio	0.289	0.356	0.510	0.266	0.380
APL-SAO					
rss	23.620	30.570	85.930	34.330	31.720
Ratio	0.201	0.284	0.139	0.172	0.278
NWL-APL					
rss	68.820	83.890	55.520	57.870	54.100
Ratio	0.069	0.104	0.216	0.102	0.163

ERROR MODEL FOR SAO 1969 STANDARD EARTH

TABLE 4. Two-Day Geos 2 Arc 2 Residual Fit
(rss in meters.)

Models	Station				
	Wallopss FPS-16	Wallopss FPQ-6	Antigua	Ascension	Bermuda
Observed rss SAO-ST8	8.380	5.600	7.180	10.200	6.770
rss	4.710	13.160	14.070	19.700	12.790
Ratio	1.779	0.426	0.510	0.518	0.529
M1E-STD					
rss	10.330	22.540	22.490	34.190	22.040
Ratio	0.811	0.248	0.319	0.298	0.307
NWL-APL					
rss	73.970	80.420	39.550	68.310	52.650
Ratio	0.113	0.070	0.181	0.149	0.129
APL-SAO					
rss	21.920	33.540	42.700	59.590	36.450
Ratio	0.382	0.167	0.168	0.171	0.186

observed rss is the actual rss obtained for each station in a Noname data reduction, after modification for nominal values of measurement biases, station position errors, and measurement noise according to the right-hand side of (14). For each of the gravity-model differences, the rss is the root sum of squares of the effects that the set of geopotential coefficient differences would have on the residuals for each station. Dividing this effect on residuals by the rss obtained for each station in the data reduction gives the ratios shown on the second line for

each set of geopotential differences. For the corresponding gravity model differences, the ratios in Table 3 should be about the same as those of Tables 1 and 2 if the coefficient differences do indeed provide a valid model for geopotential error. Again, however, the agreement need be only in the statistical sense, and the degree of validity thus depends upon the expected value of residual ratios.

For two different 2-day arcs of Geos 2, Tables 4 and 5 present the residual rss's and residual ratios corresponding to those of Table 3. Some what similar results are obtained. Table 6 summarizes the ratio results from Tables 3 through 5, giving the mean ratio and its 1σ standard deviation based upon these three 2-day arcs. Comparing this summary with the ratios from Tables 1 and 2, we find rather close agreement between Tables 2 and 6 for several of the model differences. The best consistency between Tables 1, 2, and 6, however, is obtained from the APL-SAO differences, with a ratio on the order of 0.25.

TABLE 5. Two-Day Geos 2 Arc 3 Residual Fit
(rss in meters.)

Models	Station			
	Wallopss FPS-16	Wallopss FPQ-6	Antigua	Bermuda
Observed SAO-ST8	9.840	8.260	9.860	4.870
rss	13.920	12.220	19.050	9.140
Ratio	0.707	0.676	0.518	0.533
M1E-STD				
rss	23.330	21.160	36.690	14.410
Ratio	0.422	0.390	0.269	0.338
APL-SAO				
rss	30.300	28.140	42.170	20.790
Ratio	0.325	0.217	0.234	0.234
NWL-APL				
rss	75.980	78.050	52.300	47.580
Ratio	0.130	0.106	0.189	0.102

TABLE 6. Residual Ratio Summary

Model Difference	Mean Ratio	σ Ratio
SAO-ST8	0.629	0.328
M1E-STD	0.372	0.139
APL-SAO	0.226	0.066
NWL-APL	0.130	0.043

MARTIN AND ROY

167

CONCLUSIONS

The results from the preceding section have shown that one-fourth of the differences between the truncated SAO M1 and APL 3.5 gravity models produces a good estimate of the effects of geopotential coefficient errors when the data reduction is performed using the SAO 1969 standard earth set of geopotential coefficients. The restriction to the Geos 2 satellite does need to be investigated by using data from other satellites in the same manner. However, the results should be equally applicable to other satellite arcs that are not significantly affected by resonance.

Acknowledgment. The work upon which this paper is based was sponsored in part by NASA Wallops Station under contract NAS6-1628.

REFERENCES

Anderle, R. J., Geodetic parameter set NWL 5E-6 based on Doppler satellite observations, *Rep. 1977*, Nav. Weapons Lab., Dahlgren, Va., 1965.

Douglas, B. C., and J. G. Marsh, Geos 2 and

- 13th order terms of the geopotential, *NASA X-Doc. X-552-69-291*, July 1969.
- Gaposchkin, E. M., *Smithson. Astrophys. Observ. Spec. Rep. 200*, vol. 2, 1966.
- Gaposchkin, E. M., and K. Lambeck, 1969 Smithsonian standard earth, *Smithson. Astrophys. Observ. Spec. Rep. 315*, May 18, 1970.
- Guier, W. H., and R. R. Newton, The earth's gravitational field as deduced from the Doppler tracking of five satellites, *J. Geophys. Res.*, 70(18), 4613-4626, 1965.
- Kohnlein, W., The earth's gravitational field as derived from a combination of satellite data with gravity anomalies, paper presented at the IUGG 14th General Assembly, Switzerland, October 1967.
- Rapp, R. H., The geopotential to (14, 14) from a combination of satellite and gravimetric data, *Bull. Géod.*, no. 91, 47-80, 1969.
- Williamson, R., et al., NONAME system, prepared for National Aeronautics and Space Administration, Goddard Space Flight Center, Greenbelt, Md., contract NAS 5-11736 MOD92, 1971.
- Yiououlis, S. M., Improved coefficients of the thirteenth-order harmonics of the geopotential derived from satellite Doppler data at three different orbital inclinations, *Rep. TG-1003*, Johns Hopkins Appl. Phys. Lab., Baltimore, Md., May 1968.

Detailed Gravimetric Geoid for the United States

WILLIAM E. STRANGE, SAMIR F. VINCENT, AND RICHARD H. BERRY

Computer Sciences Corporation, Falls Church, Virginia 22046

JAMES G. MARSH

Goddard Space Flight Center, NASA, Greenbelt, Maryland 20771

Abstract. A detailed gravimetric geoid was computed for the United States using a combination of satellite-derived spherical harmonic coefficients and 1° by 1° mean gravity values from surface gravimetry. Comparisons of this geoid with astrogeodetic geoid data indicate that a precision of ± 2 meters has been obtained. Translations only were used to convert the NAD astrogeodetic geoid heights to geocentric astrogeodetic heights. On the basis of the agreement between the geocentric astrogeodetic geoid heights and the gravimetric geoid heights, no evidence is found for rotation in the North American datum. The value of the zero-order undulation can vary by 10 to 20 meters, depending on which investigator's station positions are used to establish it.

One of the classical objectives of geodesy has been the determination of detailed geoids of the land areas of the world. Recent years have seen an extensive increase in the amount of surface gravity data available and the advent of satellite gravity data on a worldwide basis. The data are therefore now in hand to permit construction of detailed gravimetric geoids for a number of land areas of the world through a combination of surface and satellite gravity data. Initial computations of this type have been carried out for part of the Western United States by *Rapp* [1967] and *Needham* [1972] and for Australia by *Mather* [1970]. This paper presents a detailed gravimetric geoid for the United States, obtained from a combination of surface and satellite gravity data, that is believed to have a precision of ± 2 meters.

METHOD OF COMPUTATION

The geoidal undulation at any point P on the earth can be computed using the well known Stokes' formula:

$$N(\varphi, \lambda) = \frac{R^3}{4\pi G} \cdot \int_{\lambda'=0}^{2\pi} \int_{\varphi'=-\pi/2}^{\pi/2} \Delta g_r(\varphi', \lambda') S(\Psi) \cdot \cos \varphi' d\varphi' d\lambda' \quad (1)$$

where

φ, λ are the latitude and longitude, respectively, of the computation point.

φ', λ' are the latitude and longitude, respectively, of the variable integration point.

$N(\varphi, \lambda)$ is the geoid undulation at φ, λ .

R is the mean radius of the earth.

G is the product of the universal gravitational constant and the mass of the earth.

$\Delta g_r(\varphi', \lambda')$ is the free-air gravity anomaly at the variable point φ', λ' .

$$S(\Psi) = \frac{1}{\sin(\Psi/2)} - 6 \sin(\Psi/2) + 1 - 5 \cos\Psi - 3 \cos\Psi \ln[\sin(\Psi/2)] + \sin^2(\Psi/2)]$$

where

$$\Psi = \cos^{-1} [\sin \varphi \sin \varphi' + \cos \varphi \cos \varphi' \cos(\lambda - \lambda')]$$

In order to combine surface and satellite gravity data for geoid computation, the earth was divided into two areas, a local area (A_1)

GRAVIMETRIC GEOID FOR THE UNITED STATES

surrounding the point P , and the rest of the earth (A_2). Also, the free-air gravity anomalies in each area were partitioned into two parts represented by the symbols Δg_s and Δg_2 . The Δg_s component of anomalous gravity is defined as that part of the anomalous gravity field represented by coefficients in a satellite-derived spherical harmonic expansion of the gravitational potential. The Δg_2 values are defined as the rest of the anomalous gravity field. Using the division of the earth's surface into two areas and of the anomalous gravity into two components, we can write equation 1 in the form

$$N(\varphi, \lambda) = N_1 + N_2 + N_3 \quad (2)$$

$$N_1 = \frac{R^3}{4\pi G} \left[\int_0^{2\pi} \int_{-\pi/2}^{\pi/2} \Delta g_s(\varphi', \lambda') \cdot S(\Psi) \cos \varphi' d\varphi' d\lambda' \right] \quad (3)$$

$$N_2 = \frac{R^3}{4\pi G} \left[\int_{A_1} \int \Delta g_2(\varphi', \lambda') \cdot S(\Psi) \cos \varphi' d\varphi' d\lambda' \right] \quad (3)$$

$$N_3 = \frac{R^3}{4\pi G} \left[\int_{A_2} \int \Delta g_2(\varphi', \lambda') \cdot S(\Psi) \cos \varphi' d\varphi' d\lambda' \right] \quad (3)$$

Given a set of satellite-derived coefficients in the spherical harmonic expansion of the gravitational potential, a number of methods exist for computation of the N_1 component of the geoid undulation.

The computation of N_1 was not carried out in the present case by using the integration indicated in equation 3. Rather, the procedure described by Bacon *et al.* [1970] was used. This procedure consists of fixing a value of the geoid potential W_0 and computing the component N_1 as

$$N_1 = R_G - R_E \quad (4)$$

where R_G is the radial distance to the equipotential surface defined by W_0 and a set of satellite derived spherical harmonic potential coefficients, and R_E is the radial distance to a selected reference ellipsoid defined by a semimajor axis a_e and flattening f .

The radial distance R_G to the equipotential surface W_0 at a particular latitude and longitude θ_1 , λ_1 is determined by using the equation

$$W_0 = \frac{GM}{r} \left[1 + \sum_{n=2}^{\infty} \sum_{m=0}^n (a_e/r)^n [C_{nm} \sin m\lambda_1 + S_{nm} \sin m\lambda_1] P_{nm}(\theta_1) \right] \quad (5)$$

where C_{nm} and S_{nm} are the normalized spherical harmonic potential coefficients, and the $P_{nm}(\theta_1)$ are the standard spherical harmonic functions.

The only unknown in this equation is r . Using an iterative three-point inverse interpolation scheme, the value of r (i.e., $r = R_G$) that will make equation 5 an identity is determined. Using this value of R_G , and R_E computed using the input values of a_e and f of the reference ellipsoid, a geoid undulation component N_1 is computed.

For the computations described in this paper, the area A_1 consisted of a 20° by 20° area centered on each computation point. The computational formula used to determine N_2 was

$$N_2 = \frac{R^3}{4\pi G} \sum_{j=1}^{400} \Delta g_2(\varphi_j, \lambda_j) \cdot S(\Psi_j) \cos \varphi_j \Delta \varphi' \partial \lambda' \quad (6)$$

where $\Delta g_2(\varphi_j, \lambda_j)$ is the mean gravity difference within the j th 1° by 1° square, $S(\Psi_j)$ is the value of Stokes' function at the center of the j th 1° by 1° square, and $\Delta \varphi' = \Delta \lambda' = 1^\circ$.

The value of Δg_2 used for each 1° by 1° square was computed using the formula

$$\Delta g_2 = \Delta g_e - \Delta g_s \quad (7)$$

The Δg_e values were mean 1° by 1° free-air anomalies provided by surface gravity data. These surface gravity data were made compatible with the harmonic coefficients by adding a latitude correction.

The Δg_s values are that part of the mean 1° by 1° free-air anomalies represented by the satellite harmonic coefficients used in computing N_1 . The Δg_s values were approximated by evaluating at the center of each 1° by 1° square the formula

$$\Delta g_s = \gamma_e \sum_{n=2}^k \sum_{m=0}^n (n-1) [C_{nm} \cos m\lambda' + S_{nm} \sin m\lambda'] P_{nm}(\varphi') \quad (8)$$

STRANGE, VINCENT, BERRY, MARSH

171

where γ_e is the approximate equatorial gravity in milligals (0.98×10^6 mgal), C_{nm} , S_{nm} are the normalized geopotential spherical harmonic potential coefficients of degree n and order m (i.e., C_{nm} , S_{nm}) except for C_{20} and C_{40} , and k is the upper limit on degree and order of the geopotential model.

In equation 8, the C_{20} and C_{40} terms do not represent the complete coefficients, but rather ΔC_{20} and ΔC_{40} , the difference between the complete coefficients and the coefficients compatible with the ellipsoid used in computing N_1 . In order for the procedure to produce correct results, the quantities Δg_e , Δg_s , and the a_e and f that define the ellipsoid used to compute N_1 must all be compatible. Compatibility implies that the values of C_{20} and C_{40} used to compute the values of theoretical gravity needed to obtain Δg_e and Δg_s are the same as the values of C_{20} and C_{40} implied by the reference ellipsoid. Correct results in an absolute sense are also dependent upon the value of W_o being chosen to represent the true value of the potential of the geoid. The effects of not making Δg_e , Δg_s , a_e , and f compatible are twofold. First, all the computed geoid heights may be in error by a constant; in addition, there will be a systematic error as a function of latitude. The effect of selecting an incorrect value of W_o would be to introduce a constant error in all geoid heights.

In the calculations described here, the term N_s in equation 2 is set equal to zero. This was done after tests showed that N_s normally contributed less than 1 meter to the geoid height. This is equivalent to assuming that the satellite-derived approximation to the gravity field is adequate for the area A_2 at a distance of greater than 10° from the computation point.

RESULTS OF GEOID COMPUTATION

Using the methodology described above, a detailed gravimetric geoid was computed for the United States and is presented in Figure 1. The geoid is referenced to an ellipsoid with a flattening given by $f = 1/298.255$. In carrying out the geoid computations, R_g was computed using $W_o = 6,263,675.7$ kgal m [Rapp, 1966] and the C_{nm} , S_{nm} coefficients of the SAO 1969 standard earth [Gaposchkin and Lambeck, 1970]. R_g was computed using the ellipsoid parameters $1/f = 298.255$ and $a = 6378.155$. These two quantities, R_g and R_B , provided N_1 . For the

computation of N_s , the values of the satellite gravity anomalies, Δg_s , were made compatible with the chosen flattening by using $\Delta C_{20} = 0.08 \times 10^{-6}$ and $\Delta C_{40} = -0.756 \times 10^{-6}$ (unnormed values). The values of Δg_e were made compatible by using a theoretical gravity formula compatible with the chosen flattening, i.e.,

$$g_T = 978.0421(1 + 0.00530241 \sin^2 \varphi - 0.0000059 \sin^2 2\varphi) \quad (9)$$

It was recognized that the value of W_o used in the initial computation was not exactly accurate. The effect of using an incorrect value of W_o is to produce a constant error in the computed geoid heights analogous to the zero-order undulation of Rapp [1966]. Another potential source of constant geoid height error lies in the possibility that the Δg_e values used may contribute to a systematic error. Thus, if the geoid heights presented in Figure 1 are thought of as referenced to an ellipsoid of semimajor axis 6378.155 km, they are in error by a constant. In order to determine the constant required to remove the effects of errors in W_o and Δg_e , comparisons with satellite-derived geocentric station positions were made. Two different sets of station positions were used, those derived as a part of the SAO 1969 standard earth [Gaposchkin and Lambeck, 1970] and those derived at Goddard Space Flight Center by long-arc analyses [Marsh et al. 1970, 1971]. Table 1 presents a comparison of the geoid heights relative to an ellipsoid with $1/f = 298.255$ and $a_e = 6378.155$ km derived from the SAO station position data and the geoid heights computed in the present analysis. Table 1 also presents a similar comparison with the GSFC station position data. The magnitude of the constant correction factor indicated by comparison with the SAO data is 18 meters. The comparison with the GSFC data leads to a correction factor of magnitude 31 meters. The difference in correction factors is in agreement with previously noted systematic differences between the radial component of station positions derived by the two sets of investigators [Marsh et al., 1970]. The correction factors can be applied to the gravimetric geoid heights in one of two ways. Either the constants can be added to the geoid heights presented in Figure 1, or they can be subtracted

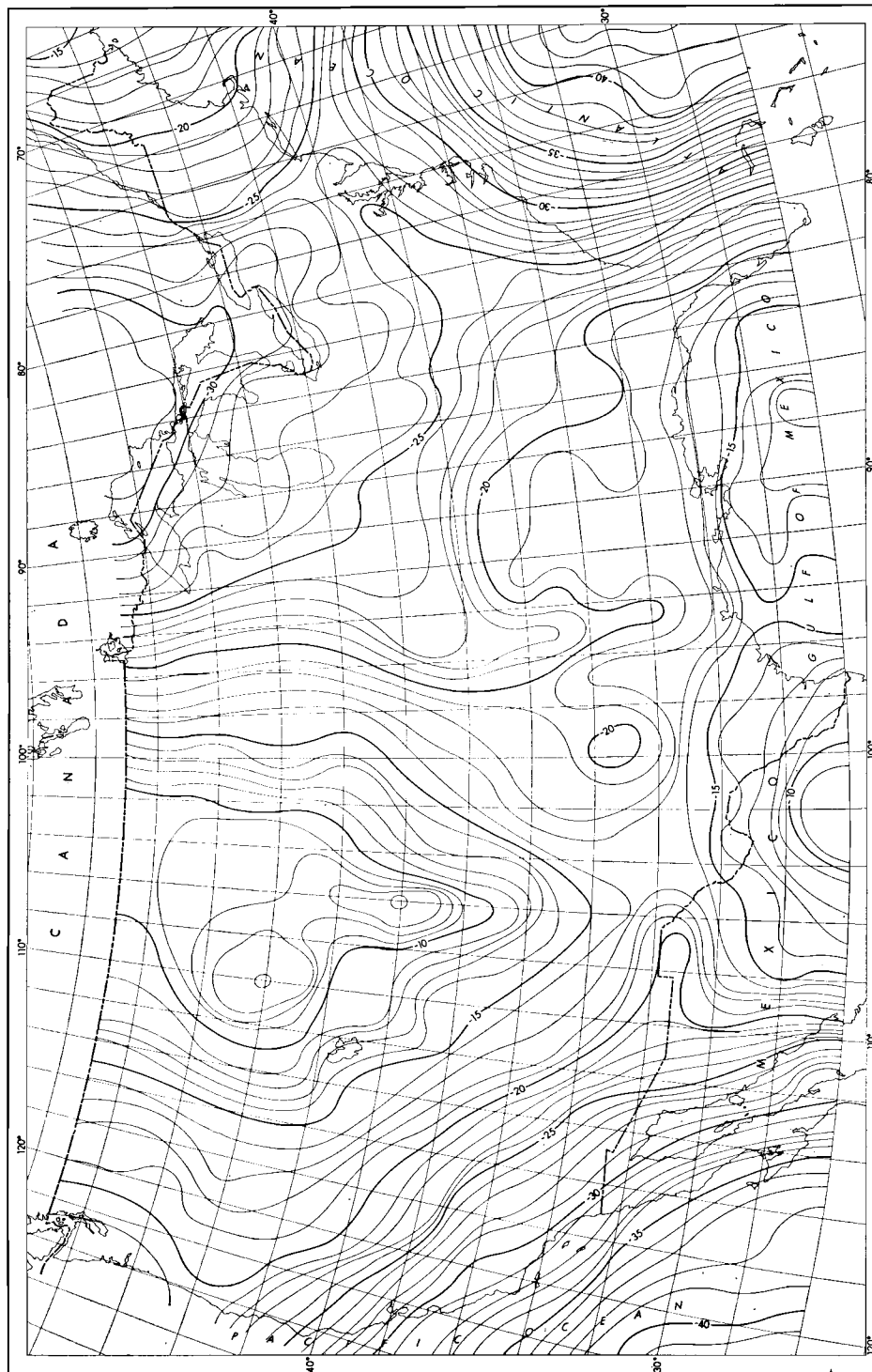


Fig. 1. Gravimetric geoid of the United States referenced to ellipsoid with flattening $f = 1/298.255$. Contour interval, one meter.

STRANGE, VINCENT, BERRY, MARSH

173

TABLE 1. Comparison of Geoid Heights at Tracking Stations

Station	Location		Geoid Height, meters		
	Lat.	Long.	GSFC	SAO	Gravity
1021	38°25'	77°6'	-55	-42	-25
1022	26°32'	81°52'	-50	-48	-18
1030	35°19'	116°55'	-53	-58	-28
1034	48°1'	97°1'	-53	-32	-18
1042	35°12'	82°53'	-57	-49	-21
7037	38°53'	92°13'	-60	-42	-23
7045	39°38'	104°37'	-44	-21	-11
7050	39°1'	76°50'	-52	-42	-24
7072	27°1'	80°7'	-53	-26	-26
7075	46°27'	80°57'	-60	-52	-29
9001	32°25'	106°34'	-35	-21	-21
9010	27°1'	80°7'	-39	-26	-26
9021	31°41'	110°53'	-42	-24	-24
9050	42°30'	71°34'	-46	-19	-19
9113	34°57'	117°55'	-37	-29	-29

from the semimajor axis of the ellipsoid to which it is assumed the geoid heights of Figure 1 refer. The latter approach is taken here. If the correction factor derived from the SAO station positions is accepted, the geoid heights of Figure 1 should be considered as referenced to an ellipsoid of semimajor axis 6378.137 km. If the GSFC correction factor is accepted, the geoid heights should be considered as referenced to an ellipsoid of semimajor axis 6378.124 km.

EVALUATION AND ANALYSIS OF RESULTS

The most obvious method of evaluating the accuracy of the gravimetric geoid of Figure 1 is through comparison with detailed astrogeodetic geoid data. Two sources of astrogeodetic geoid data exist, the astrogeodetic geoid map of Fischer [1967] and the station geoid heights of D. A. Rice (Adjustment of geoidal sections in the United States, 1927 North American

datum, unpublished map, 1970) obtained at closure points of detailed astrogeodetic profiles. A complication arises in making comparisons. The astrogeodetic data must be transformed from the NAD to a geocentric system before comparisons can be made. The degree of agreement between the astrogeodetic and gravimetric geoids is a function of the transformation constants used. In carrying out comparisons, four sets of transformation constants were examined. These sets of transformations are presented in Table 2. These sets were those obtained by Marsh *et al.* [1970], Lambeck [1971], Fischer [1968], and those associated with the 1966 SAO standard earth solution. Finally, the original transformation parameters used by Fischer [1968] to transform the NAD astrogeodetic geoid heights to geocentric geoid heights were used. Comparisons of the gravimetric geoid heights of Figure 1 with Fischer's

TABLE 2. Comparison of Gravimetric and Astrogeodetic Geoid Heights Obtained by Using Different Transformations

Solution	Transformation Constants, meters			Astrogeod. minus Gravi. Geoid Diff., meters	
	Δx	Δy	Δz	Constant Diff.	Avg. Random Diff.
GSFC	-25	163	172.5	34	1.75
Lambeck	-26	168	167	42	1.90
SAO (1966)	-30	152	176	24	2.10
Fischer	-18	145	183	15	1.5

GRAVIMETRIC GEOID FOR THE UNITED STATES

transformed astrogeodetic geoid heights was carried out at 2° intervals using each of the four transformations. The average magnitudes of the differences are given in Table 2. These average absolute differences were computed in each case in the following way. The astrogeodetic geoid heights were transformed to geocentric geoid heights relative to an ellipsoid with $1/f = 298.255$ and $a = 6378.155$ km. A mean difference between the gravimetric and astrogeodetic geoid values was computed, and this difference was added to the gravimetric geoid values before the magnitudes of the average differences were computed. These constants are indicated in Table 2.

Several points can be made about the values in Table 2. First, it is clear that, leaving aside the question of the corrective constants, the astrogeodetic and gravimetric geoids agree on the average to within ± 2 meters, regardless of which of the transformations is used. Second, the original Δx , Δy , and Δz derived by Fischer in 1968 remain the best set of values for transforming the astrogeodetic geoid to obtain a best fit with the gravimetric geoid.

Relative to the constant differences, several facts are of interest. The constant obtained by using the transformations of *Marsh et al.* [1970] is, as one would expect, essentially the same as the constant factor derived by using the station positions in Table 1. The problems with the transformation constants of *Lambeck* [1971] can be seen by noting that the constant value of 42 meters presented in Table 2 using his transformation differs by 24 meters from the 18-meter constant derived in Table 1 by using the same SAO station positions.

From the above considerations, it would appear that the transformation values of *Marsh et al.* [1970] give a conversion that is both in agreement with the results of satellite-derived geocentric tracking station positions and provides good agreement between the gravimetric and astrogeodetic geoids. It is therefore well to consider in greater detail how *Fischer's* [1968] transformation constants provide a better fit when used to convert the astrogeodetic data. An examination of the areal distribution of the differences shows that both transformations give equally good agreement except in the SW part of the United States. This is indicated in Figure 2, where geoid profiles at 40° and 45° N latitude

are presented, comparing the gravimetric geoid with Fischer's astrogeodetic geoid using both sets of transformations. Results similar to those on the 40° N profile also can be seen on a profile along 35° N.

A second source of astrogeodetic information is the unpublished map of Rice (1970). These results consist of point astrogeodetic geoid height intersections of astrogeodetic profiles having deflection stations every 10 to 20 km. One should expect these point geoid heights to be somewhat more accurate than the average geoid height from Fischer's map, since the map of necessity involves interpolation. The two sets of astrogeodetic results differ from one another systematically in that Rice's geoid heights are on the average two meters more negative than the geoid heights of Fischer. If this systematic deviation of 2 meters is removed, the average difference between the two sets of results is less than 1 meter. As might be expected from this close agreement between the two sets of astrogeodetic results, comparisons of Rice's astrogeodetic data with the gravimetric geoid produces results that are essentially identical with the results obtained by comparing with Fischer's geoid heights.

CONCLUSIONS

A gravimetric geoid has been produced for the United States having a relative accuracy of ± 2 meters. The absolute accuracy of the geoid is dependent upon the accuracy of the scale provided by the dynamically derived tracking station locations. The two investigators whose results were used to provide scales differ by 10 to 15 meters in the scales they gave.

By using translations only to convert the NAD astrogeodetic geoid heights to geocentric geoid heights, excellent agreement can be obtained between these geoid heights and the gravimetric geoid heights. This indicates that any rotations required to convert the NAD to a geocentric system, if they exist, are extremely small. This conclusion is supported by the profiles of Figure 2 and by Figure 3, in which the differences between the astrogeodetic geoid heights of Rice (which have been converted to geocentric using the transformation constants of *Marsh et al.*) and the gravimetric geoid heights are plotted as a function of latitude and longitude. No discernable trend can be seen in Figure

STRANGE, VINCENT, BERRY, MARSH

175

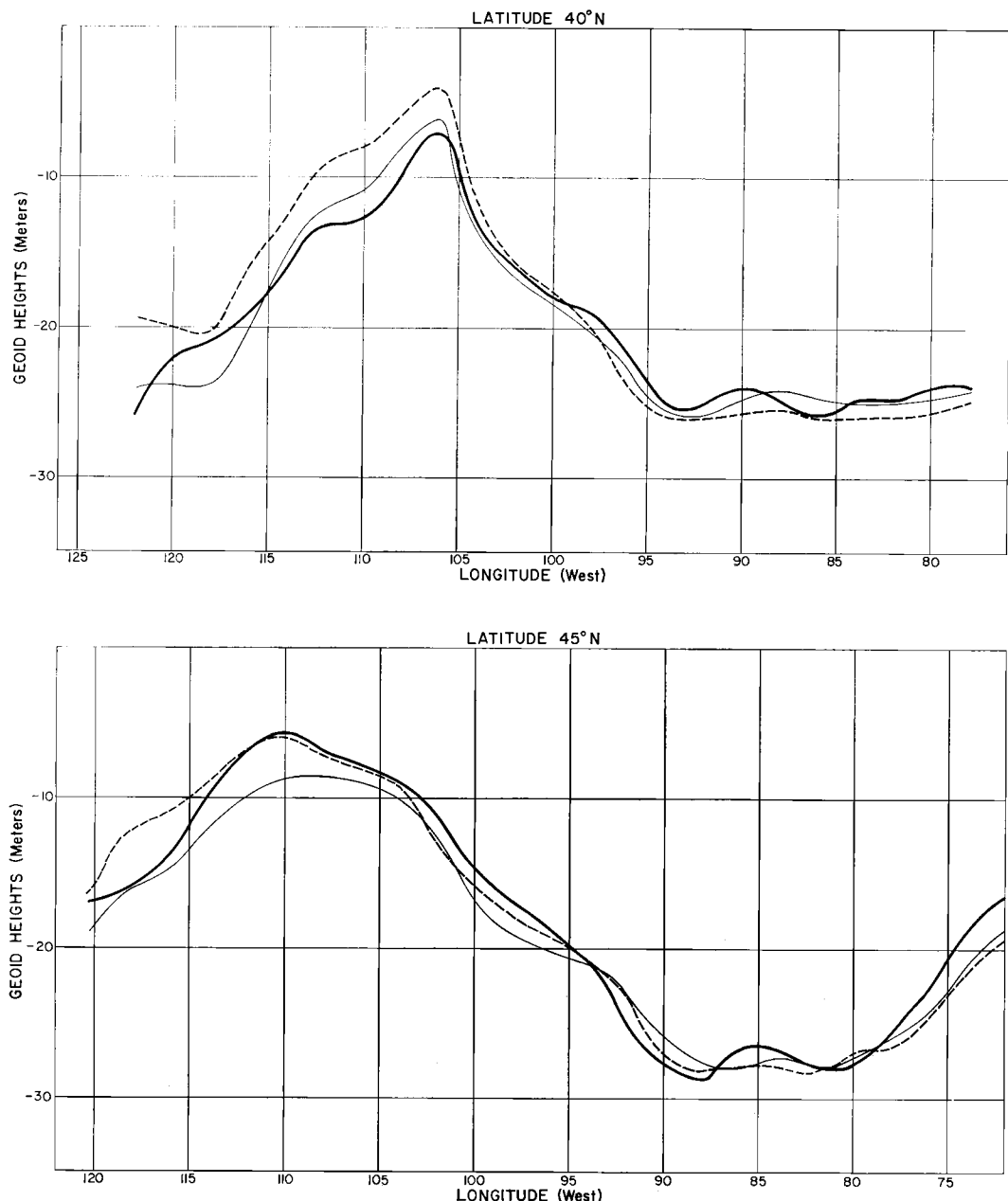


Fig. 2. Comparison of gravimetric and astrogeodetic geoid profiles along latitudes 40°N and 45°N. Heavy solid line, gravimetric geoid; dotted line, Fischer's astrogeodetic geoid transformed to geocentric using $\Delta x = -25$, $\Delta y = +162$, $\Delta z = +173$; light solid line, Fischer's astrogeodetic geoid transformed to geocentric using $\Delta x = -18$, $\Delta y = +145$, $\Delta z = +183$ (all Δx , Δy , Δz in meters).

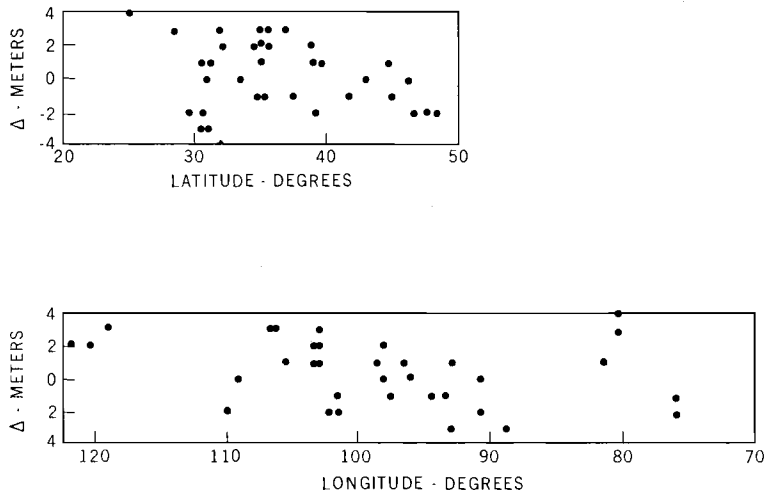


Fig. 3. Differences between astrogeodetic and gravimetric geoid heights as a function of latitude and longitude. Astrogeodetic geoid heights transformed to geocentric using $\Delta x = -26$ meters, $\Delta y = 162$ meters, $\Delta z = 173$ meters.

3, which would indicate the need for a rotation.

Finally, it should be noted from Table 1 that, after accounting for the constant difference of 31 meters, the gravimetric geoid heights and the geoid heights obtained by using the geocentric station positions of *Marsh et al.* [1970, 1971] have an average difference of only 3.6 meters. This provides a strong indication that current dynamic analyses are capable of providing the radial component of station positions with an average accuracy of the order of 5 meters, provided that the correct scale is used.

REFERENCES

- Bacon, D., R. Green, R. LeSchack, and H. Quintal, Geoid representation from satellite determined coefficients, *Doc. TR-70-3*, IBM, Gaithersburg, Md., 1970.
- Fischer, I., Geoid contours in North America from astrogeodetic deflections, 1927 North American datum, Sheet 2, Map, U.S. Army Map Service, Washington, D.C., 1967.
- Fischer, I., A modification of the mercury datum, *Tech. Rep. 67*, U.S. Army Map Service, Washington, D.C., 53 pp., 1968.
- Gaposchkin, E. M., and K. Lambeck, 1969 Smithsonian standard earth (II), *Smithson. Astrophys. Observ. Spec. Rep. 315*, 1970.
- Lambeck, K., The relation of some geodetic datums to a global geocentric reference system, *Bull. Geod.*, no. 99, 37-54, 1971.
- Marsh, J. G., B. C. Douglas, and C. F. Martin, NASA Stadan, Scepto, and Laser tracking station position derived from Geos 1 and Geos 2 precision reduced optical and laser observations, in *Proceedings of the Geos 2 Program Review Meeting, 22-24 June 1970*, vol. 1, pp. 187-214, edited by Computer Sci. Corp., Falls Church, Va., 1970.
- Marsh, J. G., B. C. Douglas, and S. M. Klosko, Goddard range and range rate and laser station coordinates from Geos 2 data, *Rep. X-552-71-52*, Goddard Space Flight Center, Greenbelt, Maryland, 23 pp., 1971.
- Mather, R. S., The Australian geodetic datum in earth space, *UNISURV Rep. 19*, University of New South Wales, Kensington, Australia, 1970.
- Needham, P., The formation and evaluation of detailed geopotential models based on point masses, *Rep. 149*, Dep. Geod. Sci., Ohio State Univ., Columbus, in press, 1972.
- Rapp, R. H., The equatorial radius and the zero-order undulation of the geoid, *Rep. 78*, Dept. of Geod. Sci., Ohio State Univ., Columbus, Ohio, 26 pp., 1966.
- Rapp, R. H., Combination of satellite and terrestrial data for a detailed geoid (abstract), *Eos Trans. AGU*, 48, 54, 1967.

Determination of Gravity Anomalies by Satellite Geodesy

K. ARNOLD

*Central Earth Physics Institute, Potsdam
German Democratic Republic*

Abstract. The satellite orbit perturbations are expressed in free-air anomalies. The station coordinates, the constant errors in the orbital elements, and the atmospheric perturbations are eliminated automatically by the method. Some of the ground anomalies are introduced as given values. Along these lines, it is possible to derive special observation equations that contain only the unknown gravity anomalies as variable parameters to be obtained by the method of least squares.

In the field of dynamical satellite geodesy, the unknown ground gravity anomalies were determined by analyzing 360° satellite orbits, introducing some ground gravity anomalies as given values. In the perturbation equations, the disturbing components of the anomalous gravity field were introduced, i.e. the radial component, the force perpendicular to the orbit, and the component orthogonal to both these forces in the direction of the satellite path. These components K_1 , K_2 , K_3 are computed from the free-air gravity anomalies on the earth's surface according to the Stokes theory [Arnold, 1965a, b, 1966a, b, 1967a, b, c, 1968, 1969, 1970a, b; Arnold and Stange, 1968; Arnold et al., 1970].

$$\begin{aligned} K_1 &= K_1(\Delta g_F) = \sum_i \kappa_{1i}(\Delta g_F)_i \\ K_2 &= K_2(\Delta g_F) = \sum_i \kappa_{2i}(\Delta g_F)_i \\ K_3 &= K_3(\Delta g_F) = \sum_i \kappa_{3i}(\Delta g_F)_i \end{aligned}$$

The Δg_F values are averaged means over $20^\circ \times 20^\circ$ compartments. The earth's surface was divided into 101 such compartments; 49 mean values were introduced as given values, and the remaining 52 mean values were determined from 360° satellite orbits, analyzing subsequent satellite passages.

If \mathbf{x}_s is the satellite position, \mathbf{x}_q is the camera position in the geodetic system, \mathbf{a} is the observed

unit vector, S is the distance from the camera to the satellite, and θ is the sidereal time, it follows for two passages in the astronomic system

$$\mathbf{x}_{s1} + S_1 \mathbf{a}_1 = \mathbf{x}_q(\theta_1)$$

$$\mathbf{x}_{s2} + S_2 \mathbf{a}_2 = \mathbf{x}_q(\theta_2)$$

Their difference is

$$\mathbf{x}_{s2} + S_2 \mathbf{a}_2 - \mathbf{x}_{s1} - S_1 \mathbf{a}_1$$

$$= [\mathbf{R}_z(\theta_2 - \theta_1) - \mathbf{E}] \mathbf{R}(\theta_1) \mathbf{x}_q$$

where \mathbf{R}_z is the rotation matrix, and \mathbf{E} is the unit matrix. After some transformations, the following error equation for the Δg_F values is reached:

$$\begin{aligned} v &= -\frac{1}{(S_1^2 + S_2^2)^{1/2}} \frac{\mathbf{n}_{12}}{|\mathbf{n}_{12}|} \sum_i \mathbf{w}_i \Delta g_F i \\ &\quad - \frac{1}{(S_1^2 + S_2^2)^{1/2}} \frac{\mathbf{n}_{12}}{|\mathbf{n}_{12}|} [(\mathbf{x}_{s2} - \mathbf{x}_{s1})_0 \\ &\quad - \{\mathbf{R}_z(\theta_2 - \theta_1) - \mathbf{E}\} \mathbf{R}_z(\theta_1) \mathbf{x}_q] \\ \mathbf{n}_{12} &= \mathbf{a}_1 \times \mathbf{a}_2 \end{aligned}$$

where $(\mathbf{x}_{s1})_0$ and $(\mathbf{x}_{s2})_0$ come from the mean orbital elements. Gravity anomalies are the only unknowns of the method, the other unknowns (stations and mean orbital elements) being eliminated by the method automatically. A total of 1182 error equations of this type were analyzed,

	200°	240°	280°	320°	0°	40°	80°	120°	160°	90°
	<u>+10</u>				<u>+2</u>				<u>+10</u>	
<u>+8</u>	0	<u>-17 ± 5</u>	<u>+32 ± 4</u>		<u>+6</u>	<u>+4</u>	<u>-3</u>	<u>-11 ± 6</u>	<u>+35 ± 6</u>	
<u>+1</u>	<u>-6</u>	<u>+8</u>	<u>-8</u>	<u>+6</u>	<u>+13</u>	<u>+9</u>	<u>+3</u>	<u>-6</u>	<u>-5 ± 3</u>	<u>+9</u>
<u>+7</u>	<u>-21 ± 3</u>	<u>-6</u>	<u>-2</u>	<u>+6</u>	<u>-23</u>	<u>-15</u>	<u>-6</u>	<u>+7</u>	<u>+8</u>	<u>+2</u>
<u>-3 ± 3</u>	<u>-4 ± 4</u>	<u>-11 ± 4</u>	<u>+5 ± 4</u>	<u>-6 ± 4</u>	<u>+7</u>	<u>-10</u>	<u>-4</u>	<u>0</u>	<u>+1</u>	<u>-3 ± 3</u>
<u>+1</u>	<u>-22 ± 4</u>	<u>-8 ± 4</u>	<u>+10 ± 4</u>	<u>-26 ± 3</u>	<u>+9</u>	<u>+27 ± 3</u>	<u>-7 ± 3</u>	<u>-3 ± 3</u>	<u>+6</u>	<u>+3</u>
	<u>+19 ± 4</u>	<u>+4 ± 4</u>	<u>-8 ± 3</u>	<u>+3</u>		<u>-21 ± 4</u>	<u>+18 ± 3</u>	<u>+9 ± 4</u>	<u>+10 ± 3</u>	<u>+6 ± 3</u>
<u>-11 ± 6</u>		<u>+33 ± 8</u>	<u>-13 ± 7</u>		<u>+22 ± 7</u>	<u>-7 ± 6</u>	<u>-6 ± 6</u>	<u>+33 ± 6</u>	<u>+6 ± 7</u>	<u>-25 ± 6</u>
	<u>-10</u>				<u>+4</u>				<u>+2</u>	

Fig. 1. Free-air anomalies.

based on Baker-Nunn observations of Vanguard 2, Vanguard 3, Telstar 1, Transit 4A, Injun 1, and Anna 1B.

Figure 1 shows the resulting free-air anomalies with their standard deviations. The underlined values are satellite-determined anomalies. The other values come from gravimeter measurements on the earth's surface, referred to the

Cassini standard gravity of 1932. The precision of the satellite-determined anomalies is about 3 mgal. It has the same order as the precision of the terrestrially given anomalies. Therefore, the latter values should be introduced as random variates if the observation material is enlarged. The geoid resulting from the free-air anomalies of Figure 1 is given in Figure 2.

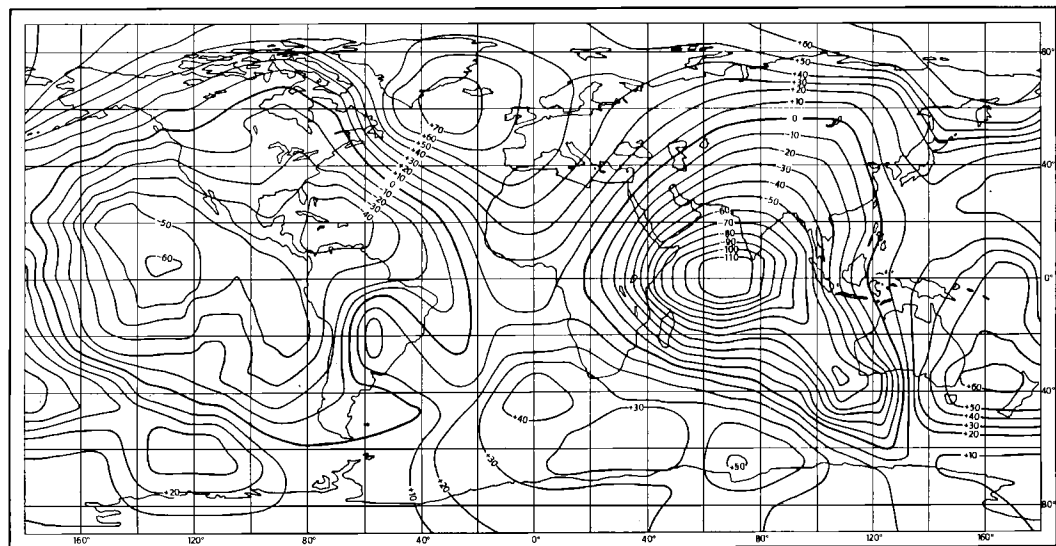


Fig. 2. Geoid from satellite observations and terrestrial data referring to the Cassini standard gravity of 1932.

K. ARNOLD

179

REFERENCES

- Arnold, K., Die Bahnen der künstlichen Erdsatelliten in ihrer Abhängigkeit von den Schwerkraum-anomalien, *Veröff. 27 des Geod. Inst. Potsdam*, Akademie-Verlag, Berlin, 1965a.
- Arnold, K., Der Einfluss der mittleren Schwerkraum-anomalien von $10^\circ \times 10^\circ$: Flächenelementen auf die Satellitenbahnen, *Gerlands Beitr. Geophys.*, 74(4), 265–270, 1965b.
- Arnold, K., On the influence of gravity anomalies on satellite orbits, in *Gravity Anomalies, Unsurveyed Areas*, *Geophys. Monogr. Ser.*, vol. 9, edited by H. Orlin, pp. 137–142, AGU, Washington, D. C., 1966a.
- Arnold, K., An attempt to determine the unknown parts of the earth's gravitation field from successive satellite passages, *Space Res.*, 7, 2, 1966b.
- Arnold, K., The use of satellites for geodetic studies, *Space Sci. Rev.*, 7, 4–68, 1967a.
- Arnold, K., Analytische Integration der durch die Schwerkraum-anomalien hervorgerufenen Satellitenbahnstörungen, *Gerlands Beitr. Geophys.*, 76, 343–348, 1967b.
- Arnold, K., Determination of the gravity field of the earth by successive passages of satellites, in *The Use of Artificial Satellites for Geodesy*, vol. 2, edited by G. Veis, pp. 185–195, National Technical University, Athens, Greece, 1967c.
- Arnold, K., An attempt to determine the unknown parts of the Earth's gravity field from successive satellite passages, *Bull. Geod.*, 87, 97–101, 1968.
- Arnold, K., *Zur Bestimmung von Schwerkraum-anomalien aus Satellitenbeobachtungen*, Vermessungs-technik 11, Berlin, 1969.
- Arnold, K., *Methoden der Satellitengeodäsie*, 231 pp., Akademie-Verlag, Berlin, 1970a.
- Arnold, K., Zur Auswertung aufeinanderfolgender Satellitendurchgänge, *Gerlands Beitr. Geophys.*, 79, 2, 1970b.
- Arnold, K., and L. Stange, Ein Versuch zur Bestimmung der unbekannten Teile des Schwerkraufeldes der Erde aus Beobachtungen aufeinanderfolgender Satellitendurchgänge, *Gerlands Beitr. Geophys.*, 77(3), 185–190, 1968.
- Arnold, K., P. Franzke, and L. Stange, *Zur Bestimmung der Schwerkraum-anomalien und Geoidundulationen aus aufeinanderfolgenden Satellitendurchgängen in den Jahren 1967, 1968 und 1969*, *Vermessungstechnik* 12, Berlin, 1970.

Refined Doppler Satellite Determinations of the Earth's Polar Motion

LARRY K. BEUGLASS AND RICHARD J. ANDERLE

Naval Weapons Laboratory, Dahlgren, Virginia

Abstract. Coordinates of the earth's pole have been recomputed for 1970. The computations were performed by using revised station coordinates that are consistent to within about 1 meter. Additional data from observing stations that were not included in previous determinations of the Doppler pole positions were also used. The new coordinates give polar motion results that are more consistent with pole positions defined by Bureau International de L'Heure 1970 data. The revised coordinates and added stations increase polar motion accuracy by about 20%.

The motion of the earth's polar axis has been determined for Doppler measurements made on Navy navigation satellites since 1969 [Anderle and Beuglass, 1970a]. The results, based on observations made by about thirteen stations during 24-hour time spans, had standard errors of approximately 1 meter and a bias of about 1 to 2 meters in the *Y* component of pole position. During 1970, one of the observing stations was moved from Hawaii to Wake Island, and antennas at three additional sites were relocated. Since a reduced station net and inconsistent coordinates could produce significant errors in the computed pole positions [Anderle and Beuglass, 1970b], it was desirable to determine the positions of the four sites in a coordinate system consistent with that for the other nine stations. However, because of the large number of stations moved in a short time and suspected small errors in the positions of the remaining sites, it was doubtful that the coordinate system (called NWL 8) could be maintained to centimeter accuracy. Consequently, it was decided that all sites would be repositioned in a new coordinate system (called NWL 9), and the 1970 pole positions would be determined in the new coordinate system.

PROCEDURE

The satellite ephemeris upon which the polar motion calculations are based is obtained by a least squares fit to observations made by about

twenty stations over a 48-hour time span. The parameters of the least squares fit include the 6 constants of integration, a drag scaling factor, the positions of observing stations that have been recently occupied, and instrument biases. The ephemeris is computed by twelfth-order Cowell numerical integration in a reference frame that is the mean equator and equinox at the start of the first day of observation. The force field included atmospheric drag, radiation pressure, the earth's gravitational field expressed in a harmonic series including 480 terms, solar and lunar gravitational attraction, and solar and lunar solid earth tides. The effect of tides on the potential is computed using a value of 0.3 for Love's number and zero lag. No corrections to station positions are made for tidal effects. Nominal values for pole positions used in the computations are obtained by extrapolating values computed in preceding months. Corrections to UT1 are based upon extrapolations of determinations by the Bureau International de L'Heure (BIH). Additional details on the observing and computing system are given by Anderle [1970b].

NWL 9C COORDINATE SYSTEM

Refined positions of the observing stations were obtained by analyzing four spans of observational data relative to the satellite ephemerides computed in the above manner. The four time spans in 1970 were days

TABLE 1. Consistency of Solution for North American Datum Stations
(rms of differences of individual solutions from mean solution.)

Sta.	Lat., meters	Long., meters	Height, meters
14	1.1	0.8	1.5
18	0.8	1.1	0.4
103	1.1	2.2	0.4
111	1.2	1.8	0.8
311	0.5	1.0	0.4
321	0.8	1.6	1.2
330	1.2	1.1	0.4
rms	0.9	1.4	0.8

110-119

157-166

187-196

227-236

A least squares solution for the position of each station was made relative to the satellite ephemerides for each span. The average difference was then obtained for each span between the nominal pole position used in computing the ephemeris and the preliminary pole position reported by the BIH in Circulaire D. The computed coordinates for each span were then rotated to correct for these differences. The averages of the coordinates obtained for each span are denoted NWL 9C. The root mean squares of the differences for each span from the mean solutions were 1.3 meters in longitude, 0.9 meter in latitude, and 0.8 meter in height (Tables 1

TABLE 2. Consistency of Solution for Isolated Stations
(rms of differences of individual solutions from mean solution.)

Sta.	Lat., meters	Long., meters	Height, meters
13	0.5	1.1	1.1
106	1.5	0.8	0.5
115	1.5	1.0	1.0
340	1.2	1.1	0.8
112	0.5	1.5	0.4
121	1.5	1.7	0.4
117	1.3	1.9	1.1
8	0.8	1.1	0.0
19	0.7	0.5	0.7
rms	0.8	1.2	0.7

and 2). This 1-meter consistency in station coordinates is a slight improvement over previous results in the NWL 8 system [Anderle, 1970a].

The NWL 9C coordinates were also compared with local survey coordinates. The positions of stations on the North American datum were transformed to the Mercury ellipsoid using the average datum shifts for the stations. The standard deviation of the differences between surveyed and satellite-determined components of station position were 5 meters, 9 meters, and 4 meters in latitude, longitude, and height, respectively (see Table 3). These differences are within the accuracy of the survey.

In another test of the new coordinates, a series of computations were made using observations for days 111-120, 226-235, and 266-

TABLE 3. Differences in Station Positions: North American Datum Satellite Minus Survey*

Station	Lat., sec	Long., sec	Lat., meters	Long., meters	Height, meters
Alaska	0.12	1.25	4	20	-4
New Mexico	-0.23	-0.11	-7	-1	-3
Maryland	0.16	-0.10	-5	-1	0
Maine	0.28	-0.37	9	-6	-5
Minnesota: 1	-0.07	-0.02	-2	2	0
2	-0.12	0.08	-4	4	0
California: 1	-0.04	-0.40	-1	-9	6
2	-0.12	-0.34	-4	-7	2
Std. dev.	0.17	0.54	5.3	9.5	3.6
Std. error of mean	0.06	0.19	1.9	3.4	1.3

* Transferred to the Mercury ellipsoid having semi-major axis $a = 6,378,166$ meters, rectangular flattening of 298.3.

BEUGLASS AND ANDERLE

183

TABLE 4. Effects of NWL 9 Coordinate System and Added Stations on the Standard Error (in Meters) of Pole Position

No. of Stations	Std. Error in X		Std. Error in Y		Coordinate System
<i>Days 111-120, 1970</i>					
	Day 113	Day 118	Day 113	Day 118	
13	1.22	1.18	1.44	1.34	NWL 8
13	1.08	1.01	1.26	1.14	NWL 9
17	0.92	0.88	0.93	0.86	NWL 9
<i>Days 226-235, 1970</i>					
	Day 228	Day 233	Day 228	Day 233	
13	1.37	1.52	1.33	1.46	NWL 8
13	1.29	1.42	1.25	1.37	NWL 9
17	0.94	1.06	0.83	0.93	NWL 9
<i>Days 266-275, 1970</i>					
	Day 268	Day 273	Day 268	Day 273	
13	1.42	1.44	1.35	1.26	NWL 8
13	1.36	1.38	1.30	1.22	NWL 9
17	1.14	1.04	1.03	0.89	NWL 9

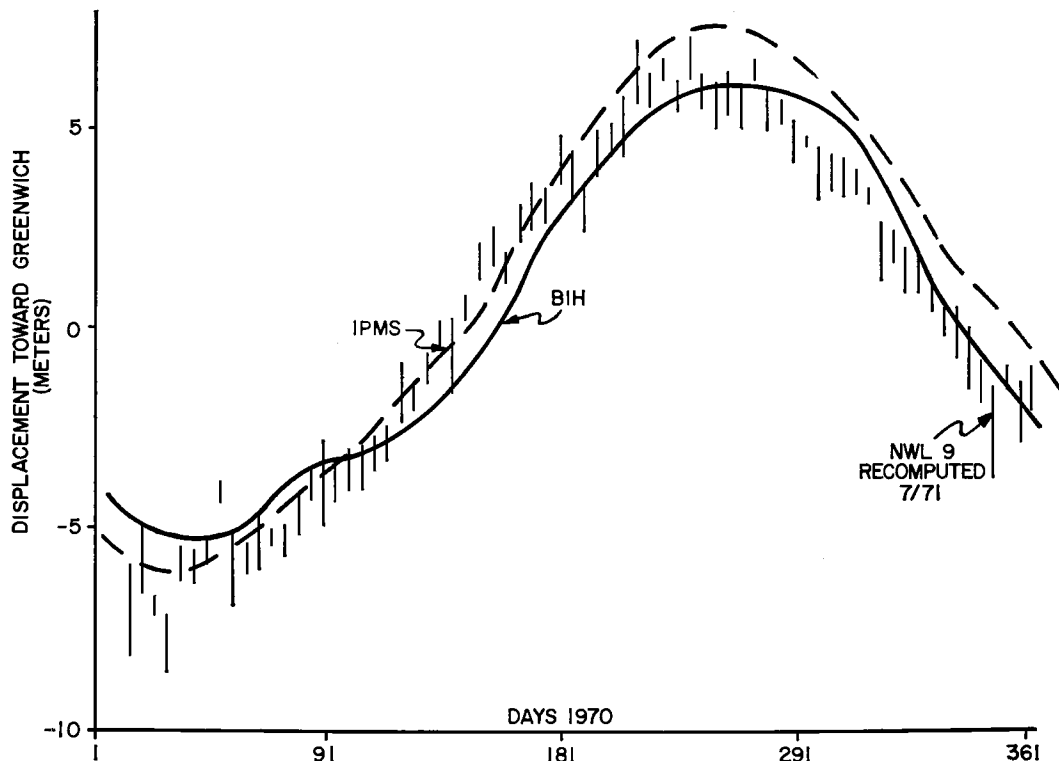


Fig. 1. X component of pole position for 1970.

184

275 of 1970. Three solutions for pole position were obtained using different numbers of stations and the two different coordinate systems. The standard error in pole positions corresponding to the residuals of fit for the three test conditions are shown in Table 4. The results show that the smaller residuals of fit obtained with the NWL 9C station coordinates improve the standard error in pole position by about 8%. The increased number of stations yields the expected additional improvement in standard error of about 10%.

NWL 9C POLE POSITION FOR 1970

The NWL 9C coordinate system was adopted for orbit computations and polar motion calculations on day 354, 1970. The library of residuals with respect to satellite ephemerides computed earlier in the year were then adjusted for the differences between the NWL 8 and NWL

EARTH'S POLAR MOTION

9 station coordinates. Figures 1 and 2 show the displacement toward Greenwich (X component) and the displacement toward 90° W (Y component), respectively, as a function of time based on five-day means. Standard errors of the mean (bars) are about 1 meter or less using the NWL 9 residuals. There is a 2-meter change in the Y component of pole position between the NWL 8 and NWL 9 solutions that reflects the correction for the bias between astronomic (BIH and International Polar Motion Service) and NWL 8 Doppler solutions reported earlier [Anderle, 1970b]. The 1970 pole path (Figure 3) is also shown for BIH, IPMS, and NWL 9 solutions.

It has been assumed in the adjustment that a satellite ephemeris based on well distributed observations from many stations is independent of the pole position. This is a reasonable assumption, since incorrect pole positions pro-

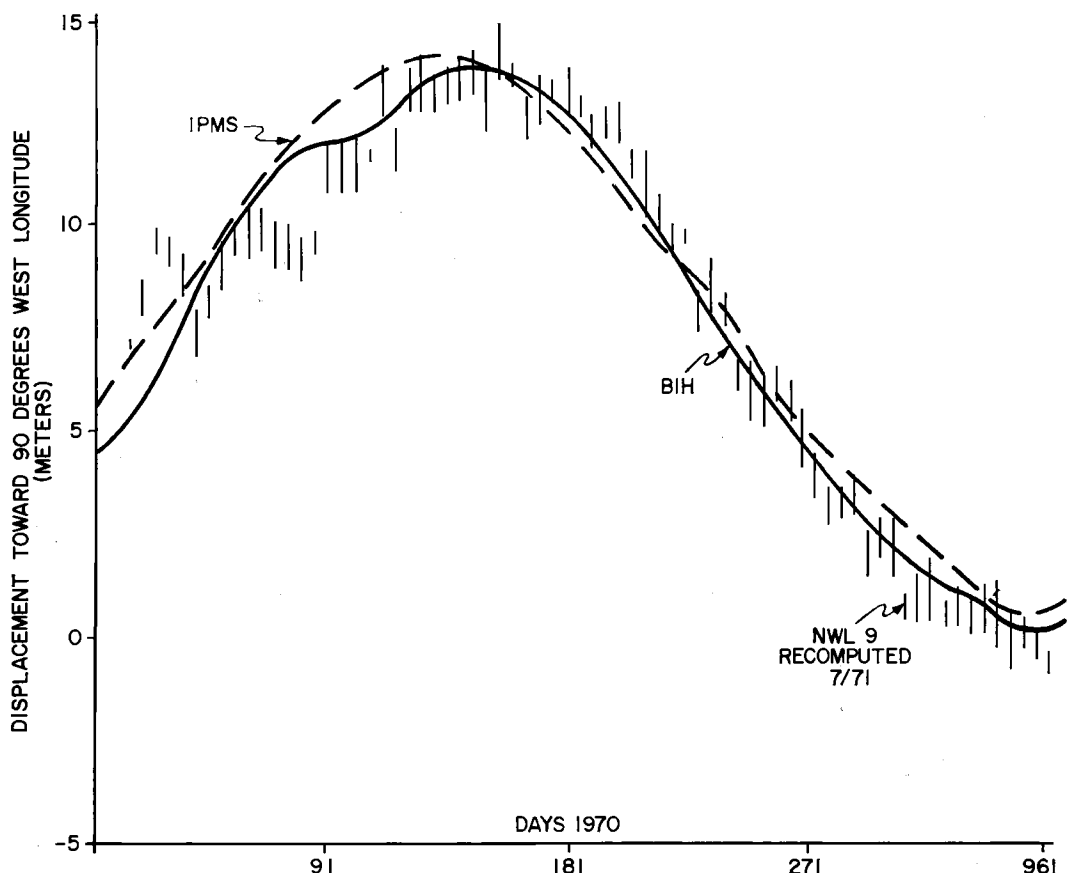


Fig. 2. Y component of pole position for 1970.

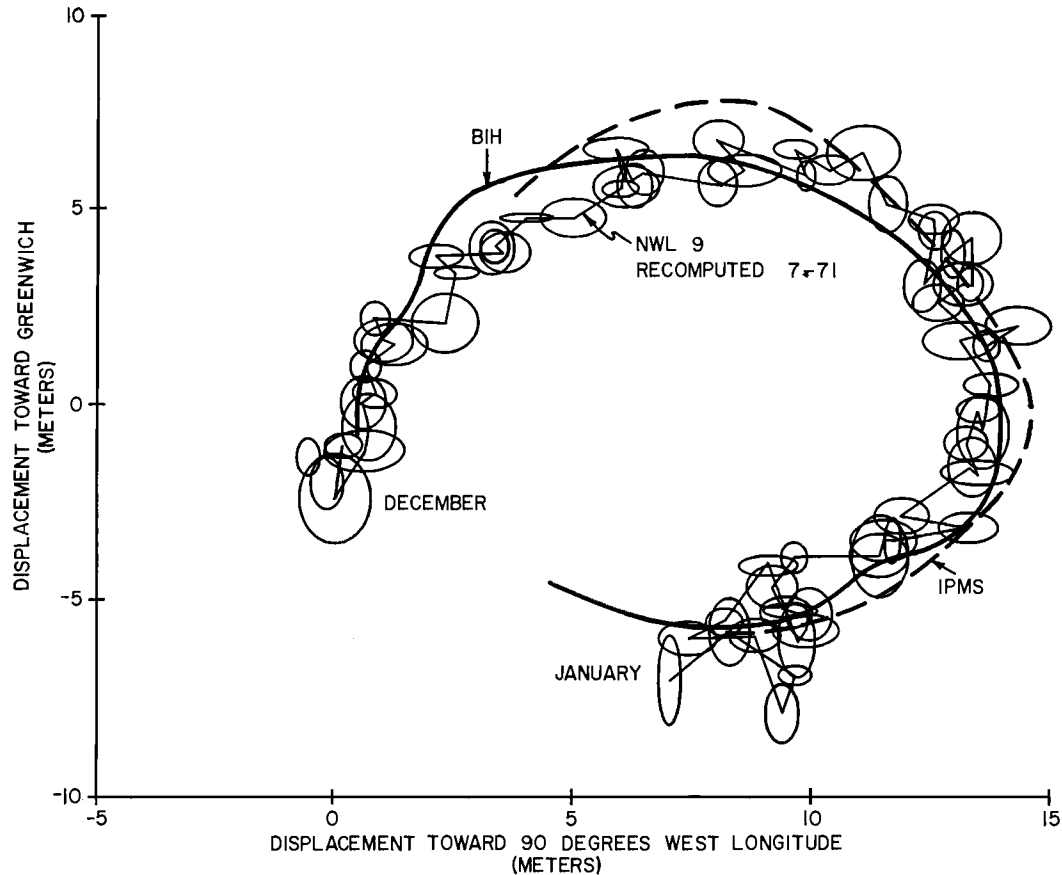


Fig. 3. Polar motion for 1970.

duce residuals of observation with a 24-hour period, whereas an error in orbit constants produces either secular residuals or residuals of observation with about a two-hour period.

SYSTEMATIC ERRORS

In a search for systematic errors, *Anderle* [1971] computed the mean latitude for each station based on each five days of observations of one satellite throughout 1970. Though the solutions were frequently consistent with the expected one-meter standard error of the mean, significant biases were found for some stations at some time during the year. The worst cases occurred when mean latitudes were computed from only north-south passes of the satellite over the station or from only south-north passes. In such cases, the deviations from the mean solution occasionally reached 6 meters. Such

differences can be expected occasionally, considering the effects of gravity errors reported by *Anderle et al.* [1969]. Consequently, under most circumstances it would be prudent to allow about 2 meters for the effect of biases on computed station positions.

SUMMARY

A set of station coordinates has been found that have a consistency of about 1 meter. These coordinates, plus some data from additional sites, have been used to produce 1970 polar motion results with standard errors of 1 meter or less. The revised pole positions agree with BIH and IPMS astronomical determinations to within about 1 meter.

REFERENCES

- Anderle, R. J., Reduction of errors in computed satellite orbits due to uncertainties in gravity coefficients, Proceedings of the Geos 2 Program*

EARTH'S POLAR MOTION

- Review Meeting, 22-24 June 1970*, vol. 9, pp. 119-139, edited by Computer Sci. Corp., Falls Church, Va., 1970.
- Anderle, R. J., Polar motion determinations by U.S. Navy Doppler satellite observations, *Tech. Rep. 2432*, Nav. Weapons Lab., Dahlgren, Va., 1970b.
- Anderle, R. J., Accuracy of Doppler determinations of station positions, *Tech. Rep. 2559*, Nav. Weapons Lab., Dahlgren, Va., 1971.
- Anderle, R. J., and L. K. Beuglass, Doppler satelite observations of polar motion, *Bull. Geod.*, 96, 125-141, June 1970a.
- Anderle, R. J., and L. K. Beuglass, Polar motion for 1967 and 1968 derived from Doppler satellite observations (abstract), *Eos Trans. AGU*, 51(4), 266, 1970b.
- Anderle, R. J., C. A. Malyevac, and H. L. Green, Jr., Effect of neglected gravity coefficients on computed satellite orbits and geodetic parameters, *J. Spacecraft Rockets*, 6(8), 951-954, August 1969.

Geodetic Studies by Laser Ranging to Satellites

DAVID E. SMITH AND RONALD KOLENKIEWICZ

Goddard Space Flight Center, Greenbelt, Maryland 20771

PETER J. DUNN

Wolf Research and Development Corporation

Riverdale, Maryland 20771

Abstract. For three months in 1970, two Goddard Space Flight Center (GSFC) laser tracking systems were used to try to detect the motion of the pole of rotation of the earth. One tracking station was at GSFC, and the other was about 400 km due north near Seneca Lake in New York State. More than two hundred passes of the Beacon Explorer C spacecraft were observed as it passed between the two stations, fifty of which were simultaneous, and these data were used to determine the orbital inclination of the spacecraft. The analysis required the accurate determination of the relative positions of the two tracking stations and the identification of the perturbations to the spacecraft orbit, in particular, those due to the gravitational fields of the earth, sun, and moon and those caused by the solid-earth tides. The results to date indicate that the GSFC laser systems can determine interstation distances with a repeatability of about 25 cm and that a new value of the Love number k that represents the distortion of the earth's gravity field caused by the tidal deformation of the earth is 0.35 ± 0.05 .

During the summer of 1970, Goddard Space Flight Center (GSFC) conducted a preliminary polar-motion experiment using its two precision laser tracking stations. The prime purpose of the experiment was to determine whether, with the present systems, it was possible to detect the motion of the pole of the earth from the analysis of laser observations of earth satellites and, if so, to what accuracy. Additional very important objectives were the determination of the capability of the two laser systems to measure interstation distances over hundreds of kilometers using satellites and also to recover the second-degree Love number k from the analysis of the solid-earth tidal perturbations. Analysis of the data collected during this experiment is still continuing, but the results to date, those concerned with the interstation distance and the tidal perturbations, are presented here.

The principle behind the polar-motion experiment is the following. If a satellite is tracked with considerable precision through the apex of its orbit (the point of maximum latitude),

the osculating orbital inclination can be very precisely determined. Further, if the tracking is continued on a regular basis, changes in the latitudes of the tracking stations due to motion of the pole in the meridians containing the stations will appear as perturbations in the observed osculating orbital inclinations.

For the experiment, the two GSFC laser tracking stations were located (see Figure 1) on the same meridian, one at the Goddard optical site (Godlas) and the other about 408 km due north near Seneca Lake in New York State (Senlas). The geodetic latitudes of Godlas and Senlas were $39^{\circ}01'N$ and $42^{\circ}42'N$, respectively, and, as such, were well placed to simultaneously track three satellites through the northern apex position of the orbits. These three satellites were Beacon Explorer C (BE-C), and two French satellites D1-C and D1-D, all with orbital inclinations of about 41° , so that the maximum northerly latitude reached by them was slightly north of the latitude of Godlas but slightly south of Senlas. All three satellites carried

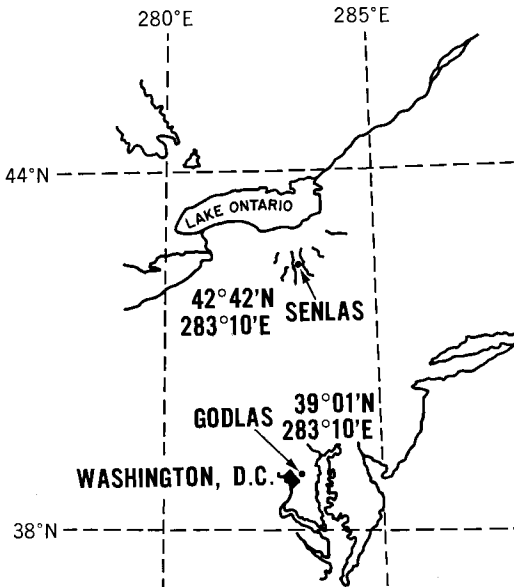


Fig. 1. One laser tracking station was at Goddard Space Flight Center (Godlas), and the other was in the Seneca Lakes region of New York State (Senlas). Senlas is 408 km due north of Godlas.

corner-cube reflectors and could therefore be tracked by lasers.

The observation program was started on June 17, 1970, and continued three months. The tracking stations were operated 10 hours a day, 6 days a week. The two GSFC laser systems are pulsed ruby lasers with a power output of about 1 joule and a pulse rate of 1/sec [Johnson *et al.*, 1967].

During the observation period, only the BE-C spacecraft was tracked with reliability. Both D1-C and D1-D were very difficult spacecraft to observe, owing entirely to our inability to provide the tracking stations with predictions of sufficient accuracy. The predictions for BE-C were considerably better, partly because of the availability of Minitrack observations and partly because of the much smaller drag perturbations of BE-C than either of the other spacecraft. Both D1-C and D1-D have perigee heights below 600 km compared to nearly 1000 km for BE-C, and are therefore much more sensitive to changes in air density. The Geos 2 spacecraft was also tracked during the experiment. The data collected are summarized in

LASER RANGING TO SATELLITES

Table 1. So far, only the data on BE-C has been analyzed.

On a clear day or night, the two tracking stations could hope to observe four consecutive passes of the BE-C spacecraft; indeed, on one occasion Senlas observed five consecutive passes but, in general, weather did not permit such extensive coverage. However, one day or night's observations was a convenient length of arc for determining the spacecraft orbit, and these arcs were referred to as mini-arcs. From the observations collected during the experiment, 22 mini-arcs were formed containing 4 to 6 hours of observations from both sites. In addition, a further 15 arcs of the same length were formed from observations at only one of the two sites when weather did not permit simultaneous tracking. Approximately 80% of all these arcs have been analyzed so far.

LASER RANGE DATA

The basic quantity that is measured by the laser ranging system is the time interval between the outgoing and returning pulse. This time interval is adjusted according to calibration measurements taken immediately before the pass, transformed into a range measurement, and corrected for atmospheric refraction. In addition, electronic and mathematical corrections are applied to ensure that the time interval measurement is taken between identical positions on the outgoing and returning pulse. These procedures, which are of fundamental importance to the interpretation of the measurements, will be described in detail in a separate publication that will describe the complete laser tracking system, including the pre-processing of the data and the final production of a range measurement.

Part of the pre-processing of a pass of laser observations is to fit an orbit through the data to determine whether any of the individual range measurements are outside the acceptance

TABLE 1. Summary of Observational Data

Spacecraft	Passes Observed	Observations	Simultaneous Passes
BE-C	168	52,264	48
D1-C and D1-D	18	3,766	1
Geos 2	18	6,157	8

SMITH, KOLENKIEWICZ, AND DUNN

189

level of 5σ , where σ is the rms of the residuals about the 5- to 10-min short-arc pass of data. Such a procedure provides a very strong indication of the precision of the laser system on a pass-by-pass basis and separately for each station. At the beginning of the experiment, the Godlas laser ranges had a rms noise of 30 to 40 cm, but toward the end of the experiment this increased to 50 to 60 cm, owing to unintentional changes in the transmitted pulse length. Senlas, however, began the experiment with a rms noise of about 1 meter, but after modifications were incorporated to make the system similar to the Godlas laser, the rms fell to 20 to 30 cm. These values only reflect the inherent precision of the system; it is almost impossible to assess the size of any bias that may exist in either of the systems. However, because of the lack of evidence of any tangible biases in these present systems, it has been assumed that the biases are a few tens of centimeters, that is, comparable to the rms noise values. There is further discussion of possible biases in the system in later sections.

Figure 2 shows the ground track of mini-arc 18 on September 2, 1970, when four consecutive passes were observed simultaneously at Godlas

and Senlas. Mini-arc 18 is certainly not typical, because of its remarkable coverage from both stations, but it does demonstrate the successive drift of the passes westward each day past the tracking stations. Figure 3 shows the range residuals from Godlas and Senlas to an orbital fit through mini-arc 18. The rms noise fit of 30 to 40 cm to each individual pass is clearly evident, but so also is the very large quasi-periodic variation of the residuals about the fit to the mini-arc. The rms noise from the mini-arc was about 3 meters for both Godlas and Senlas, but Figures 3 and 4 show the peak-to-peak variation to be about 12 meters. These residuals are presumably due largely to deficiencies in the gravitational model used in the orbit determination program, but there may also be contributions from errors in station location and measurement biases. However, it is difficult to see how they could introduce the patterns and amplitudes shown in Figure 3, particularly since the coordinates of the two stations have been adjusted to deliberately minimize the contributions from station errors to the orbital fits.

The gravitational model used in the orbit determination program is the 1969 standard

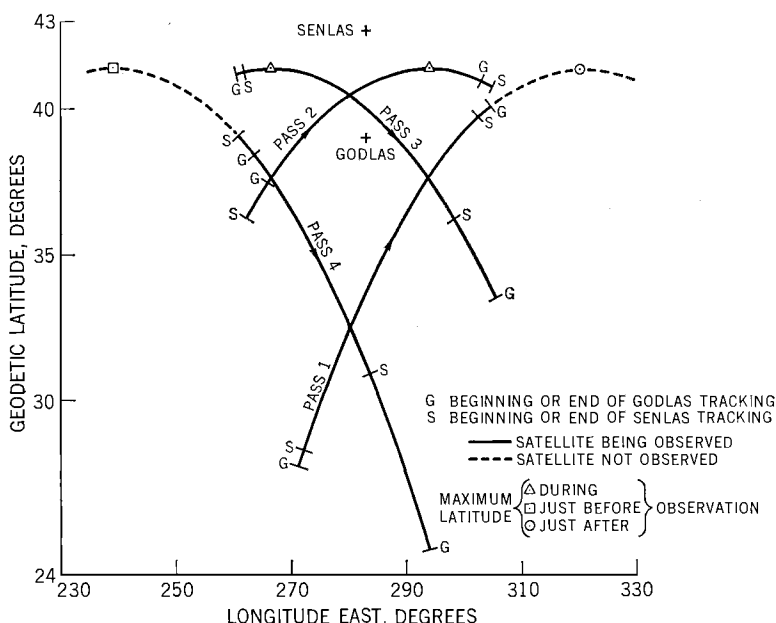


Fig. 2. As the earth rotates, the passes of the BE-C spacecraft drift successively westward. The maximum number of observable passes on any day is usually four.

LASER RANGING TO SATELLITES

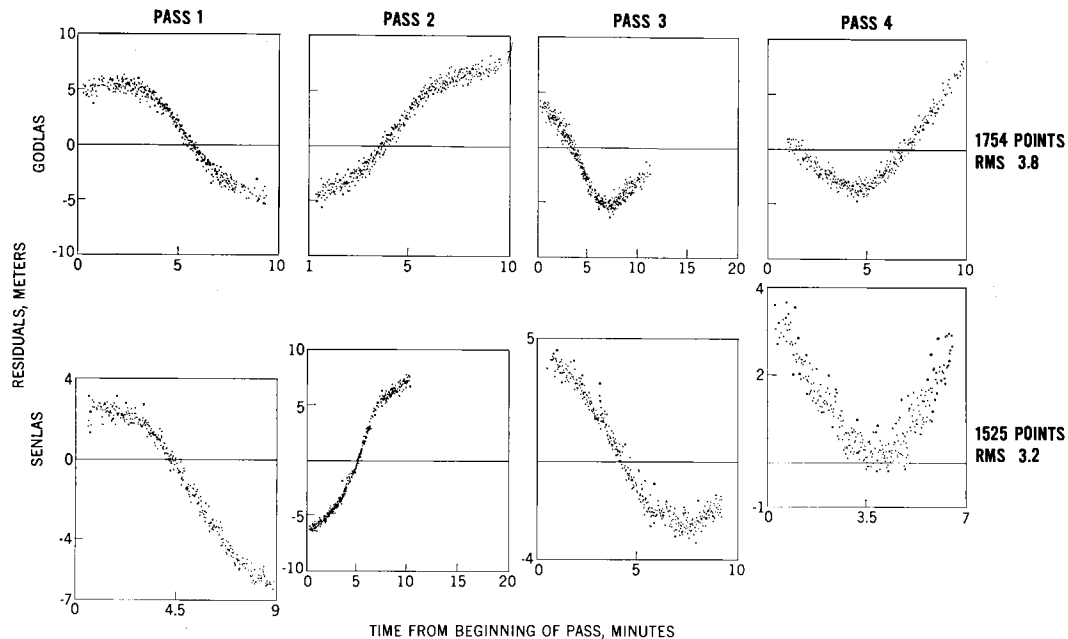


Fig. 3. The range residuals to an orbit fitted through four consecutive passes show systematic trends and patterns caused by deficiencies in the model of the earth's gravitational field.

earth (II) model of the Smithsonian Astrophysical Observatory [Gaposchkin and Lambek, 1970], and it naturally is of considerable interest to know what coefficients, if any, are causing the patterns shown in Figure 3. The patterns of the residuals suggest that each pass sees about one-half of a cycle, and therefore the period of the perturbation may be about 20 min, implying that coefficients of order 5 or 6 may be the cause. However, the least squares process in the orbit determination program will minimize the residuals and in so doing may appear to artificially reduce the period of the perturbation. The coefficients responsible could therefore be of even lower than order 5. An examination of the residual patterns in all the mini-arcs is in progress, and it is already evident that the pattern seen in mini-arc 18 is in no way unique.

NORMALIZED STATION COORDINATES

Because neither the gravitational field nor the tracking station locations were known with accuracies comparable to the laser measurements, an attempt was made to recover 'normalized' station coordinates for both Godlas

and Senlas from the data obtained during the polar motion experiment. These normalized positions would only be valid when used in conjunction with the gravitational field used to derive them (standard earth II) and only for the BE-C spacecraft, but these positions would have absorbed components of the systematic

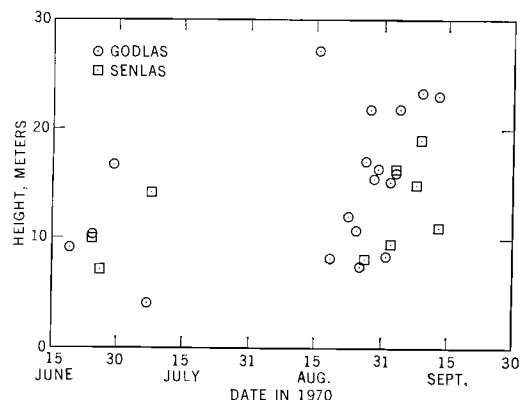


Fig. 4. Estimates of the height adjustments of the Godlas and Senlas stations obtained separately from 4- to 6-hour arcs of data.

SMITH, KOLENKIEWICZ, AND DUNN

191

errors in the orbit caused by errors in the gravitational model.

The method of deriving these normalized coordinates was as follows. Short-arc orbits were fitted through each individual pass of BE-C Godlas data for days when three or more consecutive passes were observed. Short-arc orbits were then fitted through the first two consecutive passes of each observing period, and it was evident in all cases that the orbital fit through two consecutive passes was as good as that through each pass separately. For Godlas, this was typically a rms of 30 to 50 cm. The orbital fit was then extended to three passes and then to four passes where possible. For three passes, the rms fit was nearly always larger than 1 meter, and for four passes jumped to about 4 meters. In addition to the larger rms fits, the three- and four-pass orbits also showed the average residual to be several tens of centimeters, compared to near zero for the shortest arcs, indicating that the residuals were no longer random and that there was a biasing of the orbit caused by the dynamical constraints of the gravitational model.

The recovery of Godlas' latitude, as well as the orbital elements, through the three- and four-pass orbital arcs had little or no effect on the rms or the average residual, but the recovery of the Godlas height reduced the rms of the range residuals to about 80 cm on 3-pass orbital arcs and to 2 or 3 meters on 4-pass orbital arcs. In both cases, the average residual fell to a few centimeters. We have analyzed 21 three- and four-pass orbital arcs from Godlas in this way, and the height adjustments obtained have ranged from a low of +4 meters to a high of +27 meters, with the exception of two values that are completely different for, as yet, unknown reasons. The significance of the adjustment being so large and all values being positive is not clear, but the possibility of the radius of the earth at Godlas being several meters larger than expected cannot be ruled out. The contributions to the errors in height recovery are discussed later.

In order to obtain one best-height adjustment to Godlas from the Godlas data, a multi-arc solution was performed for all 21 three- and four-pass orbital arcs in which 6 orbital elements were recovered for each arc, together with one parameter common to all arcs, the Godlas

height. The multi-arc solution for the adjustment of the Godlas height was +14.8 meters, which gives the normalized Godlas height as +18.8 meters above the ellipsoid of the standard earth II. The values of the Godlas height obtained by the Smithsonian Astrophysical Observatory, Marsh et al., and the normalized value obtained here, all based on the standard earth II, are:

<i>Gaposchkin and Lambeck [1970]</i>	+9 meters
<i>Marsh et al. [1971]</i>	+4
This paper	+18.8

A similar treatment of the data collected at Senlas provided 9 adjustments to the Senlas height from three- and four-pass orbital arcs, all of which lay between +7 and +19 meters with a multi-arc solution from all 9 arcs of +15.4 meters. This adjustment is almost identical to that obtained for Godlas and probably indicates that these adjustments are due to errors in the present earth model rather than in the measurement systems themselves. A plot of the Godlas and Senlas height adjustments that were obtained from the data are shown in Figure 4.

The dependence of the normalized height on the latitude of the station is shown in Figure 5 for Godlas. The latitude that was adopted throughout the calculations was $39^{\circ} 01' 13.88''$, but the normalized height was recovered using several values of the latitude, and Figure 5 shows that the 15-meter height adjustment required by both sets of laser data cannot be explained by merely changing the latitude of Godlas by any reasonable amount.

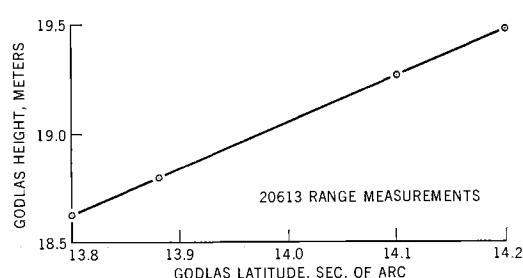


Fig. 5. The height of the Godlas station obtained from the Godlas laser ranges is almost independent of the assumed latitude of the station.

The effects of dynamic and observational errors on the adjustments of the Godlas and Senlas height have been estimated by using an error analysis program and also by making additional solutions for the heights with different values of some of the parameters in the earth model. The resulting contributions to errors in Godlas height are as follows:

Gravity model error (1/4 X SAO — APL)	6.7 meters
GM error (1 part in 10^{-6})	2.8
Godlas range bias (1 meter)	3.8
Godlas refraction error (5%)	1.3
Godlas latitude error (10 meters)	0.7

The largest contributor to height error at Godlas is seen to be the gravity field. The measure of the gravity model error that was used was a quarter of the difference between the SAO 1966 standard earth model [Lundquist and Veis, 1966] and the APL 3.5 model [Guier and Newton, 1965]. This difference has been shown by Martin and Roy [1972] to be a reasonable measure of the geopotential error of the standard earth II model for the Geos 2 orbit. Although we must be cautious in using the same error model for BE-C, it probably suffices to indicate the general size of the error.

If the errors in the models shown in Figure 3 are reasonable, it is difficult to account for the 15-meter adjustment at both sites. Furthermore, the range bias of 1 meter is probably rather generous and is more probably of the order of 25 cm. Thus there appears to be some evidence to suggest that the radius to the geoid at the stations is larger than is indicated by the earth model. However, it is important to remember that the SAO solution for the Godlas height is 5 meters larger than that obtained by Marsh *et al.* [1971] and that the difference between the SAO solution and that given here is only 10 meters and could be explainable from the error contributions shown above.

At this stage the coordinates of Godlas were fixed at the a priori values for latitude and longitude and with the recovered height of 18.8 meters; these were the 'normalized' Godlas coordinates for this experiment.

'Normalized' coordinates for Senlas were derived from a multi-arc solution of 29 short arcs of no longer than 6 hours composed of Godlas

LASER RANGING TO SATELLITES

and Senlas observations. The normalized coordinates of Godlas were used and were kept fixed in the calculations, and from the multi-arc solution values of the Senlas latitude, longitude, and height were obtained and were designated the Senlas normalized coordinates. The final normalized coordinates on the earth model of the standard earth II [Gaposchkin and Lambeck, 1970] were:

Godlas, $39^{\circ}01'13.880''N$, $283^{\circ}10'18.500''E$,
18.8 meters.
Senlas, $42^{\circ}42'04.881''N$, $283^{\circ}10'17.203''E$,
200.0 meters.

As a check on the precision of the recovery of the Senlas position, the data were divided into two sections; those observations that were obtained during the first six weeks of the experiment and those obtained during the second six weeks; and a new position for Senlas was determined from each section of data. In addition, the data collected in two consecutive 8-day periods, at the end of August and the beginning of September 1970, were analyzed to provide estimates of the Senlas position. The importance of these two data sets was that they constituted the data collected during a period of relatively fine weather; each data set contained five mini-arcs of data and could be expected to provide an indication of the results obtainable under normal working conditions in a good climate. The five sets of Cartesian coordinates for Senlas are shown in Table 2. Solution 1 is that obtained from all the data (normalized position); solutions 2 and 3 are from the first and second halves of the data; and solutions 4 and 5 are from the two 8-day periods.

Table 2 shows that the range of values of each of the three coordinates is spread over about 1 to 1.3 meters, the best solution using all the data in the middle. From these values it appears that the Senlas position has been determined with a precision of about 60 cm in each coordinate. A fact, however, that is not obvious from Table 2 is immediately evident in Table 3, which gives the chord distance between Godlas and Senlas for each of the solutions. This is that the five Senlas positions lie between two concentric spheres differing in radius by only 53 cm. Thus, although Senlas appears to be equally well determined in each of the three Cartesian coordinates it is, in effect, better de-

SMITH, KOLENKIEWICZ, AND DUNN

193

TABLE 2. Coordinates (in Meters) of the Senlas Tracking Station

Solution	X	Y	Z
1	1,069,755.44	-4,571,171.67	4,303,326.88
2	1,069,754.69	-4,571,172.56	4,303,327.04
3	1,069,755.62	-4,571,171.27	4,303,326.75
4	1,069,755.75	-4,571,171.81	4,303,327.38
5	1,069,755.26	-4,571,171.34	4,303,326.18

terminated in radial distance from Godlas than in the tangential directions by at least a factor of 2. For determining the orbital inclination of the BE-C satellite, the chord distance between the stations is a fundamental parameter of the experiment, and from Table 3 this appears to have been determined with a precision (or repeatability) of 25 to 30 cm.

Also shown in Table 3 is the estimate of the chord distance between the stations obtained by ground survey. This value differs by only 43 cm from the best solution (solution 1) obtained here and is probably less than the accuracy of either result. The estimated contributions to the error in the satellite solution are shown below, where the largest contributor is seen to be the gravity field.

Gravity model error (1/4 ×	
SAO — APL)	2.5 meters
GM error (1 part in 10^{-6})	0.2
Godlas range bias (1 meter)	0.3
Senlas range bias (1 meter)	-0.3
Godlas refraction error (5%)	0.1
Senlas refraction error (5%)	0.1
Godlas height (10 meters)	1.6

We estimate the total error of the recovered chord distance to be 2 to 3 meters. The values above also indicate why the chord distance measurement has such a good repeatability. For a nearly circular orbit, like that of BE-C, all but the range biases will contribute in the same way by about the same amount in every solution. Furthermore, if the range biases are the same and constant, they have no effect on the solution.

THE LOVE NUMBER, k_2

The locations of the laser tracking stations were chosen so as to optimize the tracking of the

BE-C spacecraft through the most northerly section of its orbit, thus providing the opportunity of precisely measuring the osculating inclination. The initial analysis of the laser ranges was based on fitting an orbit through 4 to 6 hours of data (a mini-arc) and then determining the maximum latitudes reached by the spacecraft from an ephemeris generated through the data based on the recovered orbit. Thus, for a four-pass mini-arc, four values of the maximum latitude were obtained, but usually the spacecraft was only under observation when it passed through the maximum latitude position on 1 or 2 of those passes. On approximately 30 days, enough data were available to form 4- to 6-hour orbital arcs from which the osculating values of the inclination were obtained. The values of maximum geodetic latitude (directly related to the osculating inclination) are shown in Figure 6, from which two effects are apparent. First, there is a large variation in maximum latitude, amounting to more than $30''$, during the 3 months of the experiment, and, second, there is a large change in maximum latitude from one pass to the next. The spread of maximum latitudes representing a systematic increase in the orbital inclination (during a 4- to 6-hour period) from one pass to the next as the earth rotates underneath the orbit is clearly evident in nearly all the arcs. This increase in the inclination amounts to 5 to 10 sec of arc in about 6 hours.

Both the long- and the short-term changes in the orbital inclination can be ascribed to gravitational forces; the large long-period effect is caused by the sun and moon, and the short-term effect is caused by the low degree and order tesseral harmonics of the earth. Fortunately, these effects can be calculated with adequate accuracy so that they do not sub-

TABLE 3. Godlas-Senlas Chord Distance

Solution	Chord Distance, meters	Survey Difference, cm
1	408,699.20	+43
2	408,698.87	+10
3	408,699.33	+56
4	408,699.44	+67
5	408,698.91	+14
Ground survey	408,698.77	

stantially inhibit the study of the unmodeled perturbations, such as earth tides. However, this is not to say that our knowledge of the earth's gravitational field is not one of the limiting factors in studies of unmodeled forces. On the contrary, it is believed to be an important limitation, but it is not thought to be a limitation on the short 4- to 6-hour arcs, only on the long 3-month arc.

This fact is demonstrated in Figure 7, in which the differences between the maximum latitudes obtained from the mini-arcs (4 to 6 hours) and the maximum latitudes obtained from one single long arc of 3 months are shown. The long-term variation in inclination shown in Figure 6 has now been reduced by a factor of about 10 (Figure 7), but the basic shape of the two curves (Figures 6 and 7) is the same. In addition, only one value is given in Figure 7 for each short arc; this is because, after having subtracted the long-arc maximum latitudes from the short-arc maximum latitudes, the resulting differences are the same for each pass of a short arc to within about a hundredth of a second of arc (about 30 cm on the earth's surface).

The single 3-month arc fitted to all the data was obtained after considerable difficulty had been experienced with the convergence of the

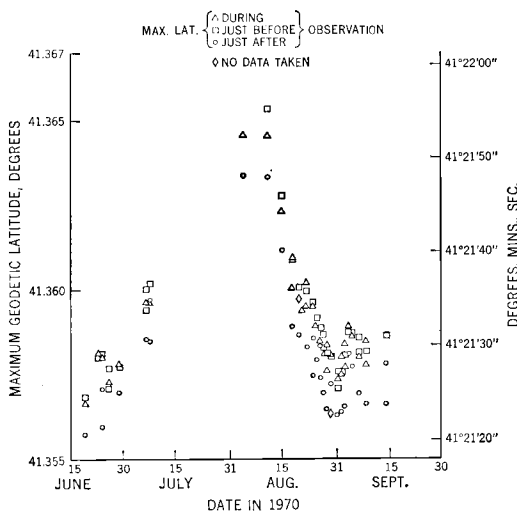


Fig. 6. The maximum latitude reached by the BE-C spacecraft shows a variation of about 30° caused by the gravitational attractions of the sun and moon during the experiment.

LASER RANGING TO SATELLITES

solution. These difficulties, which were overcome by increasing the arc length by about a week at a time, were probably caused by errors in the force models, the observations, and, to a lesser extent, by the precision of the computational procedures and are reflected in the poor fit of the laser ranges to the orbit, which had a rms of the residuals of nearly 2 km. With this size of rms, the precision of the laser observations is completely lost and, in fact, an equally good orbit was obtained for the same period from minitrack interferometer observations.

The purpose of fitting an orbit to 3 months' data was to derive an orbit for the whole period of the experiment that smoothed through all the unmodeled perturbations. When this orbit was subtracted from a short arc, which was forced to absorb the unmodeled perturbation, the residuals would reflect the unmodeled perturbations. Thus, maximum latitudes for the long arc were generated, they were subtracted from the short arc values, and the residuals are shown in Figure 7.

The residual pattern in Figure 7 can be largely ascribed to the perturbation of the orbit by the solid earth tide. The sun and moon raise a tide on the earth that changes the gravitational field, which in turn causes a perturbation of the orbit. This change in the gravitational field of the earth can be represented by the Love number k_2 , which is a dimensionless parameter conveniently describing some of the elastic properties of the earth.

Figure 7 shows the tidal perturbation of the orbital inclination for $k_2 = 0.3$ and 0.4. The large increase in the residuals at the end of July is largely due to the solar tide, whereas the small, quasi-sinusoidal oscillations in early September are caused by the lunar tide. The cause of the scatter of the points about the two curves is uncertain, but it is probably due to modeling errors and to lack of geometry in the short-arc orbits. Two types of result are given in Figure 7; the first contains data from both laser stations and is referred to as a multistation observation, and the second is a single-station observation, composed of only Godlas or Senlas data. The latter is obviously the weaker solution, because with range data from only one station there is much greater freedom for the adjustment of the orbit with almost no constraint except for the gravitational field. It is

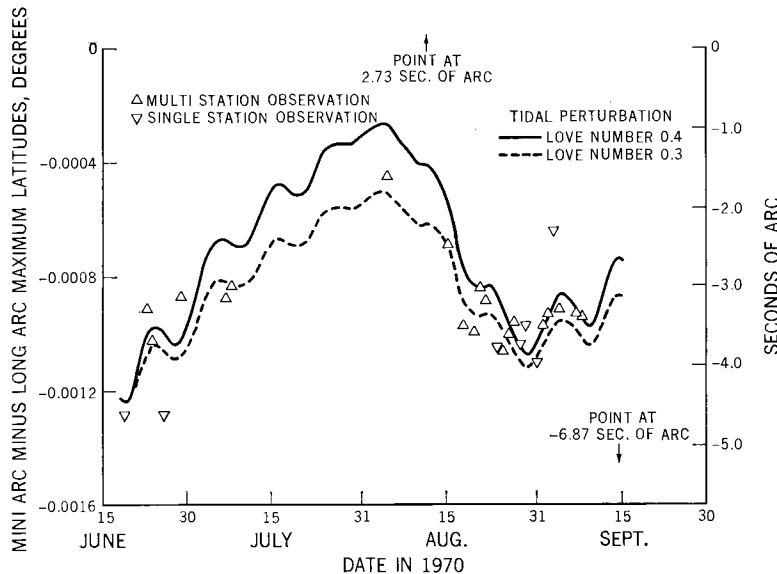


Fig. 7. The tidal perturbations of the orbital inclination for two values of the Love number k_2 are shown superimposed on the observed variation in maximum latitude after all gravitational and luni-solar perturbations have been removed.

therefore not surprising that the majority of 'bad' points in Figure 7, including those two off the Figure, are single-station solutions.

An analysis of the residuals in Figure 7 leads to the preliminary result

$$k_2 = 0.35 \pm 0.05$$

as the best value for the second-degree Love number. This method of measuring k_2 provides a mean global value of the parameter, since it is sensing the change in the gravitational field at an altitude of about 1000 km and by a technique that integrates a perturbation over many revolutions of the spacecraft. The value obtained here compares favorably with the two other global measures of k_2 , 0.29 [Kozai, 1968] and 0.34 [Newton, 1968]. However, the Love number k_2 is related to the period of the Chandler wobble of the earth on its axis by the relationship [Munk and MacDonald, 1960]

$$\sigma_0/\sigma_r = 1 - k_2/k_{2s}$$

where σ_0 is the frequency of the Chandler wobble, σ_r is the frequency of the free nutation of a rigid earth, and k_{2s} is the secular Love number. The value of σ_r is related to the moments of inertia of the earth about its principal axes and is determinable with considerable pre-

cision, whereas k_{2s} , the secular Love number, is believed to be about 0.95 on the basis of recent earth models. Thus, a value of k_2 implies a Chandler period, and the value of k_2 obtained here suggests a period about 10% larger than is actually observed if the secular Love number is taken to be about 0.95. A value of k_2 nearer 0.30 would satisfy present earth models and is just within the acceptable range of 1σ from the preliminary result obtained here.

CONCLUSIONS

The initial analysis of the laser tracking data obtained during the experiment has shown that the present GSFC lasers can provide data of sufficient quality to permit the determination of site locations with a repeatability of better than 1 meter and to detect and measure the distortion of the earth's gravitation field by the solid earth tides. These results, obtained with only two ground stations, demonstrate the important contribution that laser tracking of earth satellites can be expected to make to our knowledge of the earth's shape, gravitational field, and dynamical behavior in the next few years.

Our present ability to determine interstation distances with a precision of 25 to 30 cm, as demonstrated during this experiment, opens up

the possibility of measuring the motions of tectonic plates and the movements along fault lines over a number of years. Such experiments become even more attractive when one remembers that the present GSFC laser systems could improve by a factor of 2 or 3 in the next few years and that the largest source of error, the gravity field, can be expected to undergo comparable improvements.

The analysis of the data collected during the preliminary polar motion experiment is continuing and will provide an indication of our ability to observe the motion of the pole of rotation of the earth in the meridian containing the station. However, we feel that the results to date already indicate that the present systems and the techniques described here can profitably be used in our study of the solid earth.

Acknowledgments. The authors would like to acknowledge the advice and assistance of T. S. Johnson and D. Premo of the Advanced Data Systems Division of Goddard Space Flight Center in the organizing of the Preliminary Polar Motion Experiment. They were also responsible for the high-quality performance of the laser tracking systems, and without them the experiment could never have been conducted.

In addition, we wish to thank Dr. D. E. Smylie and Dr. L. Mansinha, National Academy of Science Research Associates at Goddard, for the

LASER RANGING TO SATELLITES

very many useful discussions on the subject of the tidal distortion of the earth.

REFERENCES

- Gaposchkin, E. M., and K. Lambeck, 1969 Smithsonian standard earth (II), *Smithson. Astrophys. Observ., Spec. Rep. 315*, 1970.
- Guier, W. H., and R. R. Newton, The earth's gravitational field deduced from the Doppler tracking of five satellites, *J. Geophys. Res.*, 70(18), 4613-4626, 1965.
- Johnson, T. C., H. H. Plotkin, and P. L. Spadin, A laser satellite ranging system, I, Equipment description, *IEEE J. Quantum Electron., QE-3*(11), 435-439, 1967.
- Kozai, Y., Love's number of the earth derived from satellite observations, *Publ. Astron. Soc. Jap.*, 20(1), 24-26, 1968.
- Lundquist, C. A., and G. Veis (Eds.), *Geodetic Parameters for a 1966 Smithsonian Institution Standard Earth*, vol. 1, Smithsonian Astrophysical Observatory, Cambridge, Mass., 1966.
- Marsh, J. G., B. C. Douglas, and S. M. Klosko, Goddard range and range rate laser station coordinates from Geos 2 data, *Rep. X-552-71-52*, Goddard Space Flight Center, Greenbelt, Md., 1971.
- Martin, C. F., and N. A. Roy, An error model for the SAO 1969 standard earth, this volume, 1972.
- Munk, W. H., and G. J. F. MacDonald, *The Rotation of the Earth*, Cambridge University Press, London, 1960.
- Newton, R. R., A satellite determination of tidal parameters and earth deceleration, *Geophys. J. Roy. Astron. Soc.*, 14, 505, 1968.

Observed Effects of Earth-Reflected Radiation and Hydrogen Drag on the Orbital Accelerations of Balloon Satellites

EDWIN J. PRIOR

NASA Langley Research Center, Hampton, Virginia 23365

Abstract. From March through May 1967, the high-altitude balloon satellites Pageos (1966 56A) and Dash 2 (1963 30D) were both in continuous sunlight orbits; hence their orbital energies were essentially unaffected by direct solar radiation, and the effects of other forces could be isolated during this period. Observed variations in the orbital accelerations of both satellites are found to be due primarily to a combination of the perturbing effects of earth albedo radiation and atmospheric drag. An equation based on diffuse Lambertian reflection of sunlight from the earth predicts quite well the observed trend of orbital accelerations for both satellites due to the force of earth albedo radiation. After correcting for this effect, the remaining orbital energy changes are found to be consistent with atmospheric drag perturbations, making it possible to deduce mean exospheric densities above 2300 km. The results indicate that hydrogen concentrations during the observation period were about 3 times greater than that given by the *U.S. Standard Atmosphere Supplements* (1966).

The orbital perturbations of balloon satellites due to earth albedo radiation force have in the past proved difficult to isolate [Baker, 1966; Sehnal, 1970]. The primary reason for this difficulty has been the effect on the orbit of direct solar radiation force, which is generally an order of magnitude greater than the effect of albedo force. A further complication is that the orbital perturbations due to the two types of radiation forces tend to be synchronized [Prior, 1970]. It is thus necessary to account very accurately for perturbations caused by solar radiation before attempting to isolate the perturbations caused by albedo force. That the perturbation would eventually be identified was predicted by Wyatt [1963], who concluded that 'the diffuse component of the earth albedo radiation might alter the orbits of earth satellites by small but detectable amounts.'

An even more elusive perturbation to detect has been the effect on a satellite orbit of hydrogen drag. A primary difficulty is that a satellite orbit that is sensitive to the small drag effect of hydrogen would also be sensitive to the force of direct solar radiation, as well as the force of earth albedo radiation, the important effect of which has not been accounted for

in previous drag studies of the exosphere [Fee, 1966; Smith, 1970]. The detection of hydrogen drag is therefore dependent on the accuracy with which we can account for these radiation force perturbations.

The two balloon satellites used in this study were designed to have extremely high area-to-mass (A/M) ratios, and thus were expected to be quite sensitive to orbital perturbations by both radiation forces and atmospheric drag. Pageos (Figure 1), a 100-foot-diameter (30.48-meter) inflatable sphere, was launched in June 1966 and was planned for primarily geodetic applications. Dash 2, an 8-foot diameter balloon, was placed in orbit in 1963; by the time of the observation period of this study in March-May 1967, both satellites were in very similar orbits. Both orbits had eccentricities of about 0.12 during this time and were in continuous sunlight, so that changes in the mean motion (n) due to direct solar radiation force were negligible. Thus, it was possible to isolate the perturbations of atmospheric drag, as well as albedo radiation force. The orbital data used in this analysis was obtained from the Smithsonian Astrophysical Observatory. The values for the time rate of change of the mean motion (dn/dt)

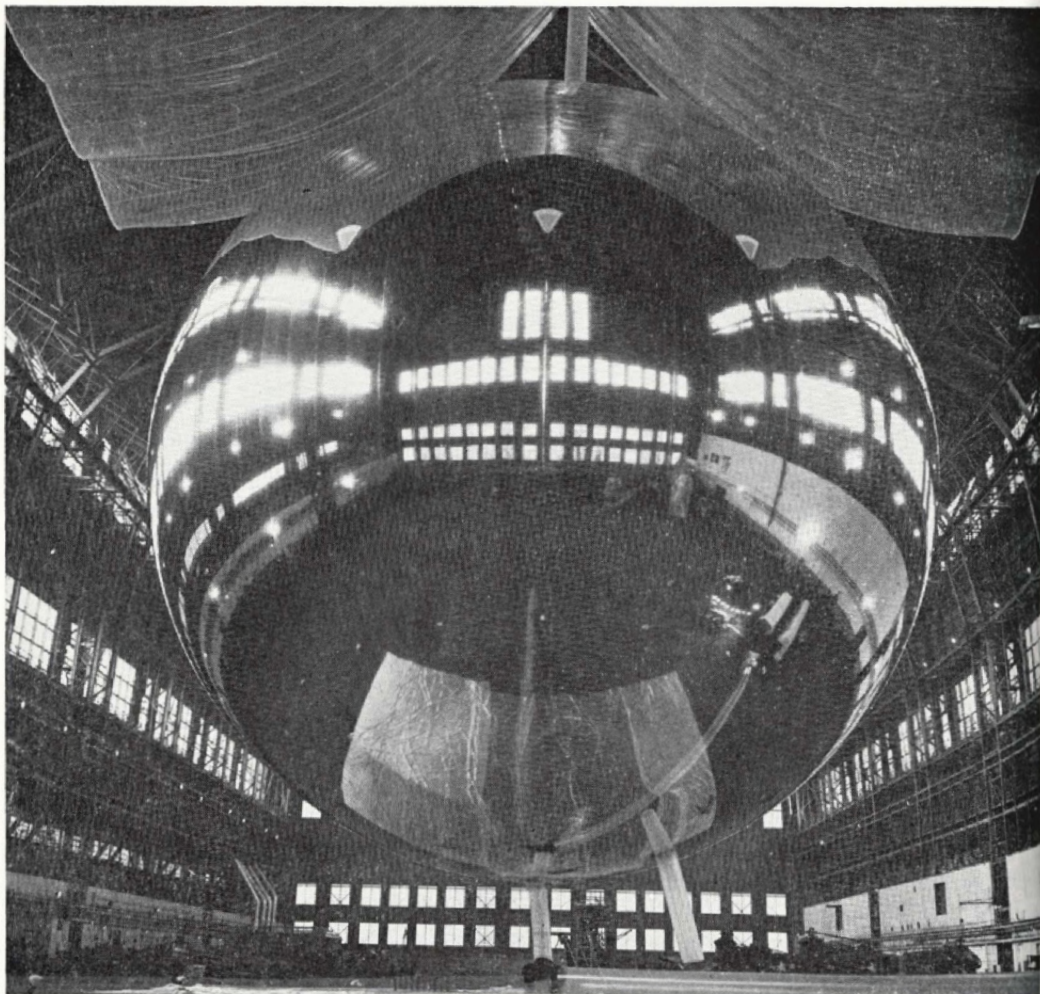


Fig. 1. Pageos.

had been corrected for the spurious effect of the motion of the perigee (J. W. Slowey, personal communication, 1971), which has been discussed in detail by *Fea and Smith* [1970].

PERTURBATIONS CAUSED BY EARTH ALBEDO RADIATION

The model for earth albedo radiation pressure in this paper has been used by *Prior* [1970]. The assumptions used in generating the model are shown in Figure 2. Earth albedo radiation flux diffusely reflected in the direction of the satellite from a unit area ds of the earth is determined using the Lambert cosine law. There is also earth-emitted radiation (or infrared radiation) emanating from the surface of the earth,

in addition to the reflected radiation. However, *Wyatt* [1963] showed that the orbital perturbations of a satellite due to earth-emitted radiation are zero or small because of the essential symmetry of infrared radiation from the earth. In contrast, *Wyatt* found that earth-reflected radiation would result in detectable orbital perturbations because of its strong dependence on solar geometry. The albedo of a unit area will be defined in this paper as the reflected total flux of radiation at all the wavelengths in the reflected spectrum, divided by the incident total solar flux. Both the radial and transverse components of the radiation pressure on the satellite due to this flux are found. The radial component is directed along the earth-satellite line, and

EDWIN J. PRIOR

199

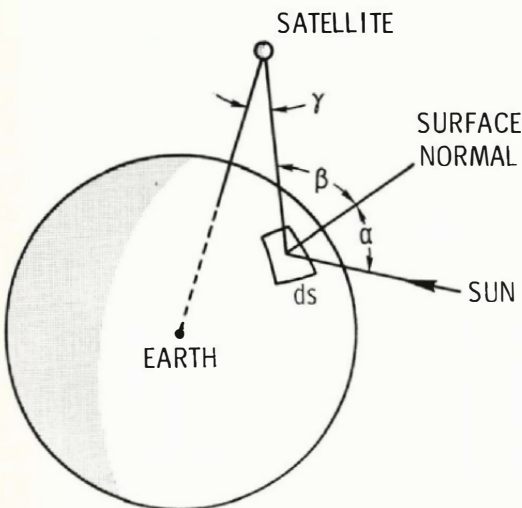


Fig. 2. Diffuse albedo model. The flux of earth albedo radiation on the satellite in the radial direction is $(Ia \cos \alpha \cos \beta \cos \gamma ds)/\pi r^2$, where a is the albedo, I is the solar flux, and r is the distance from the surface of the element to the satellite.

the transverse component lies along the direction perpendicular to the earth-satellite line and within the sun-earth-satellite plane, as shown in Figure 3. Numerical integration is performed to determine the components of the total albedo radiation flux from the entire earth.

The magnitude of the albedo radiation pressure on a satellite is directly proportional to the radiation scattering constant K [Zadunaisky et al., 1961] of the satellite surface. Pageos, a specular reflector, had a $K(A/M)$ of $135 \text{ cm}^2 \text{ g}^{-1}$ [Teichmann, 1968]; for Dash 2, a value for $K(A/M)$ of $40 \text{ cm}^2 \text{ g}^{-1}$ was deduced by Fea and Smith [1970] from an orbital analysis. Recent studies have indicated an oscillating effect on the radiation pressure orbital perturbations of a satellite due to its nonsphericity. Fortunately, the oscillating effect on the perturbation of solar radiation pressure does not occur during continuous sunlight orbits (the only periods studied in this paper) [Smith and Kissell, 1971]. There is no evidence that an oscillating effect on albedo radiation perturbations exists, possibly because the albedo radiation comes from a large finite source, whereas solar radiation emanates from a tiny source.

The albedo of the earth is known to increase from the equator to the polar regions. However,

for this paper, the first-order perturbations of albedo radiation pressure on a satellite orbit have been determined using a global annual average albedo. This albedo is taken as 0.32 ± 0.01 based on Tiros 7 satellite measurements [Levine and Arking, 1967]. The basic equations used for the integration are given by Cunningham [1963]. The specular component of earth albedo radiation is so small that it was not included here [Wyatt, 1963]. The results of the numerical integration to determine the radial component S and transverse component T of earth albedo radiation pressure are shown in Figure 3 as a function of distance r in earth radii and phase angle θ_s . It is evident that T is generally an order of magnitude smaller than S .

In the appendix of this paper, an expression is developed for the orbital acceleration dn/dt (where n is the mean motion) of a satellite due to earth albedo radiation force. This equation includes only the effect of the radial component, since it greatly predominates over the transverse. In order to obtain the perturbation equation, the following expression was used, assuming $K = 1$ to describe the variation of S with θ_s and r [Prior, 1970].

$$S = \frac{1.5 \times 10^{-5}}{r^2} \cos \theta_s \quad 0 \leq \theta_s \leq 90^\circ \quad (1)$$

$$S = 0 \quad 90^\circ < \theta_s$$

S as given by this expression (curve E) is com-

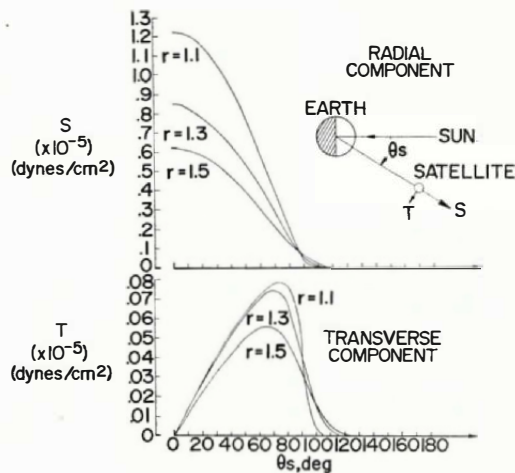


Fig. 3. Radial and transverse components of earth albedo radiation pressure.

pared with the actual Lambert variation (curve L) in Figure 4. Also shown is the variation of S that corresponds to the albedo radiation model determined by *Wyatt* [1963] from Danjon's observations of earthshine reflected from the moon's dark hemisphere. All three curves are shown at a distance of $1.4 R_E$ from the earth's center (about 2500-km altitude). The Danjon curve D shows a greater magnitude for S near the terminator ($\theta_s = 90^\circ$) than would be expected for Lambert reflection.

In this paper, the orbital accelerations due to earth albedo radiation are evaluated by numerical integration of both the radial and transverse components for diffuse Lambertian reflection from the earth. However, the simple equation 11 of the appendix gives results that are very similar. The orbital accelerations predicted by numerical integration of the Lambert model

and that predicted for the Danjon model are compared with those given by equation 11 in Figure 5. The circles represent the predictions for Pageos during the continuous sunlight observation period of March–May 1967 as the circles. Also shown are the theoretical values of dn/dt due to the force of the numerically evaluated radial component assuming Lambertian reflection (the squares), as well as the perturbations that would occur as a result of the Danjon albedo radiation model (the triangles). The solid curve in the figure represents the values of dn/dt that would occur as a result of only the numerically evaluated transverse component assuming Lambertian reflection. A number of interesting properties of albedo radiation force perturbations are apparent from Figure 5.

The effect of the transverse component is seen to be generally an order of magnitude

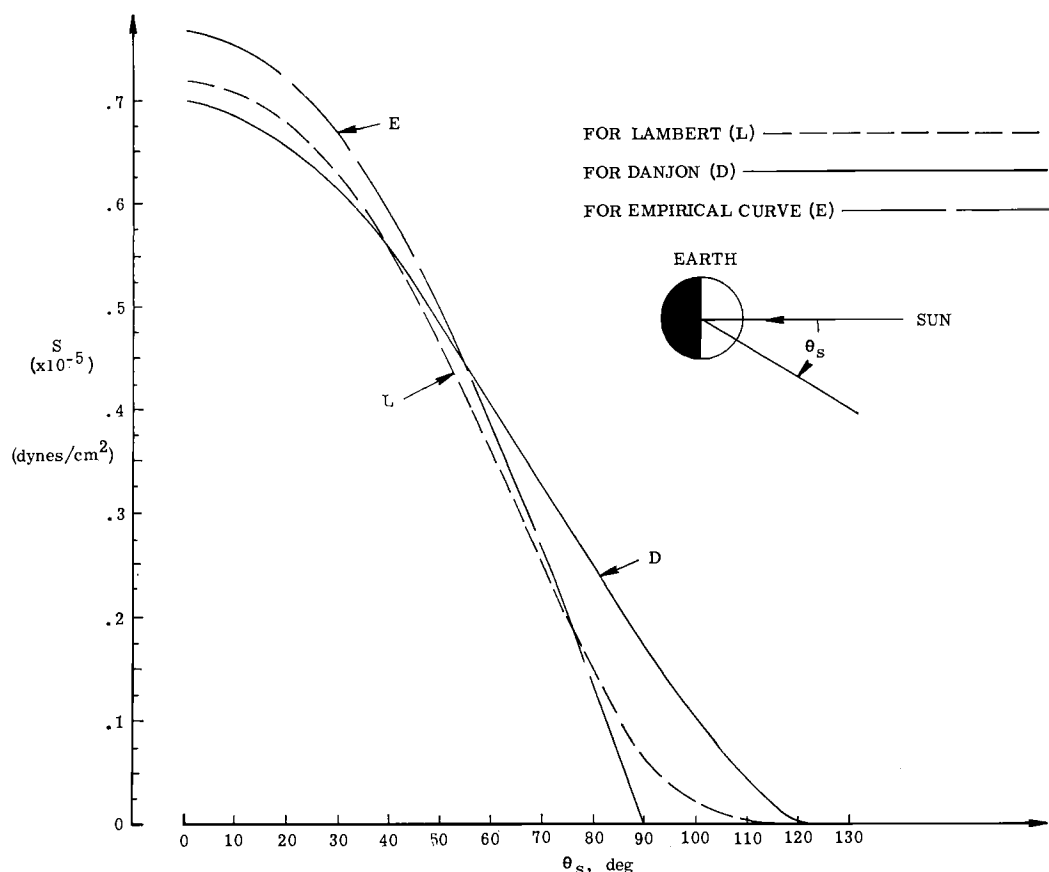


Fig. 4. Radial component of albedo radiation pressure at $1.4 R_E$ as a function of solar phase angle θ_s for different models.

EDWIN J. PRIOR

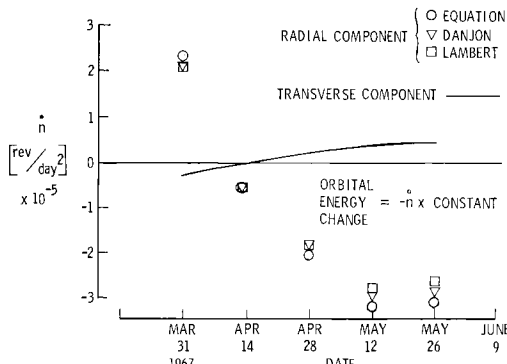


Fig. 5. Orbital perturbations of Pageos due to components of albedo radiation force.

smaller than that of the radial. In addition, the magnitudes of the predicted perturbations caused by the radial component of each model are quite close, despite the fact that the triangular data points were determined using an albedo radiation model based on observations of earth-reflected radiation, whereas the other data points were associated with the theoretical Lambert cosine variation. Finally, we note the general trend of the albedo radiation perturbations is to cause a steady decrease in $d\dot{n}/dt$ from a positive value near the beginning of the interval to a minimum near the middle of May.

Figure 6 shows the observed and predicted $d\dot{n}/dt$ variation for the Dash 2 satellite in March–May 1967. The SAO $d\dot{n}/dt$ data used here are of high quality, with an uncertainty smaller than $\pm 0.1 \times 10^{-5}$ rev day $^{-2}$ [Fea, 1970]. The uncertainty is therefore actually smaller than the size of the data points used to represent the data in the figures. The observations are given as open squares; the predictions, using Lambertian reflection and numerically integrating both the radial and transverse components for maximum accuracy, are shown as the closed squares. It is apparent that the observed data follow the trend predicted due to albedo radiation force. Both the observations and the predictions of $d\dot{n}/dt$ decrease from a positive value near the beginning of continuous sunlight to a negative value near the end. The last three observed values of $d\dot{n}/dt$ are all negative, indicating an orbital energy increase (see appendix), as do the predicted values. However, we note that all the observations are above the predictions. This suggests there are phenomena affect-

ing the mean motion in addition to albedo radiation, phenomena that increase the orbital acceleration and therefore decrease the orbital energy of the Dash 2 satellite.

In Figure 7 are shown the observed and predicted values of $d\dot{n}/dt$ for the Pageos satellite over the same time period as the Dash 2. The observations are shown as open circles. The Lambert predictions are shown as the closed circles. Again we note the observed trend of $d\dot{n}/dt$ changing from positive to negative values, following the predicted trend quite well. As for Dash 2, we see that the observations are above the predictions, suggesting again that some other phenomena are increasing the orbital acceleration of the satellite. Such a result would be consistent with drag effects.

As has been noted [Cook, 1962], there is no first-order perturbation of n due to direct solar radiation over the observation period. There is a second-order effect due to the fact that the orbit is not completely closed, but this effect is extremely small during the interval according to the expression given by Fea and Smith [1970]. Gravitational perturbations of n are negligible for both these satellites [Fea, 1970]. We have essentially eliminated variations due to lunar gravity by using 14-day epochs, the period of this minor perturbation [Fea and Smith, 1970]. Therefore, it appears that drag effects are indeed the primary cause of the mean difference between the observed and predicted values of $d\dot{n}/dt$. For the Pageos, this mean difference over the entire observation interval is approximately 1.7×10^{-5} rev day $^{-2}$, whereas

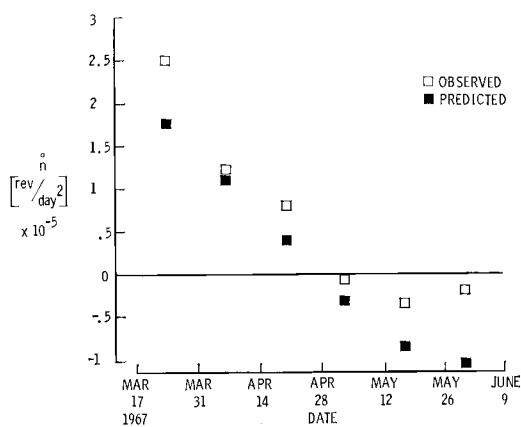


Fig. 6. Variation of mean motion for Dash 2.

ACCELERATIONS FROM EARTH ALBEDO AND HYDROGEN DRAG

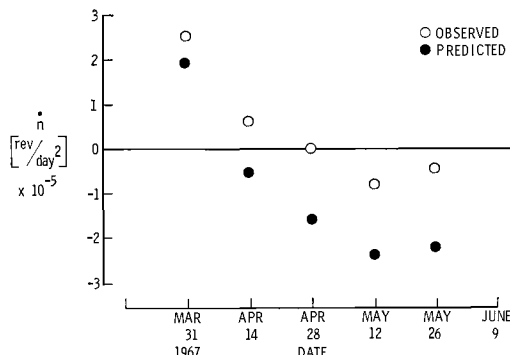


Fig. 7. Variation of mean motion for Pageos.

for Dash 2 the difference is about 0.54×10^{-5} rev day $^{-2}$. Taking these mean differences as being due primarily to drag presents the opportunity of deducing atmospheric densities at extremely high altitudes in the exosphere. As can be seen in Figure 8, the altitudes are so great that both satellite perigees were expected to be in predominantly hydrogen regimes.

Shown as a function of altitude are the number densities of atmospheric constituents for an exospheric temperature of 900°K, according to the U.S. Standard Atmosphere Supplements [1966]. These density-altitude profiles are based on the static models of Jacchia [1964] and have proven extremely useful in satellite drag studies. At both the Pageos altitude (near 2900 km) and the Dash 2 altitude (near 2300 km), hydrogen (H) is shown to predominate over helium (He) as the primary neutral constituent. All the other neutral constituents are negligible.

HYDROGEN DRAG

The techniques used for determining atmospheric densities near the satellite perigee from drag measurements of the Air Density Explorer satellites have been described in detail by Keating and Prior [1967] and Mullins et al. [1966]. In the calculation of atmospheric density by the drag technique, it is necessary to assume a drag coefficient and a variation of density along the satellite orbit. The calculation is then refined by using the initially deduced density to improve these assumptions. For this paper, the variation of neutral density initially assumed along the orbits of Pageos and Dash 2 is given by the U.S. Standard Atmosphere Supple-

ments [1966] (USSAS), with two exceptions. Instead of a temperature maximum fixed at the equator, peak temperatures are assumed to follow the latitude of the sun [Keating and Prior, 1968]. In addition, the effect of the winter helium bulge is included by using the expression developed by Keating et al. [1970]. For the drag coefficients, a value of 4 was used for hydrogen [Fee, 1965] and 2.8 for helium [Cook, 1969]. In the derivation of these coefficients, the random thermal motion of the constituent had been considered. The relative model proportions of these two constituents at the satellite perigees resulted in a drag coefficient of 3.9 for Pageos, with a somewhat lower value of 3.6 for Dash 2 due to the higher proportion of helium at its perigee.

Using a global atmospheric model based on the measurements of the lower-altitude Explorer 19 and Explorer 24 satellites [Keating et al., 1969], a mean USSAS density-altitude profile appropriate for the March–May 1967 observation period was determined for the mean latitudes and local solar times of the Pageos and Dash 2 perigees. This mean profile corresponds approximately to the 900°K USSAS profile. This density-altitude variation was then assumed initially at the perigees, with the variability of density along the orbits given by the USSAS with the exceptions noted previously.

At the extreme altitudes we are investigating, there is another drag effect that must be considered before neutral densities can be deduced. Ions are an important drag constituent of the exosphere in the altitude regime of this study (R. Cohen, personal communication, 1971). The effective cross sectional area for ion collisions is only about 10% greater than the geometric cross section area [Hohl and Wood, 1963], allowing us to treat H $^{+}$ as another drag constituent. In the calculation of atmospheric density, the hydrogen ion model assumed is based on the measurements of Brinton et al. [1969] (1×10^4 ions/cm 3 at 2700 km); the scale height of the ions is taken to be twice that of neutral hydrogen [Heikkila and Axford, 1965]. After determining the densities, the contribution of the H $^{+}$ is subtracted, leaving neutral atmospheric densities that we can compare to the USSAS. This is done in Figure 9.

As is shown, the deduced log $_{10}$ of the densities in grams per cubic centimeter (-19.13 for the

EDWIN J. PRIOR

203

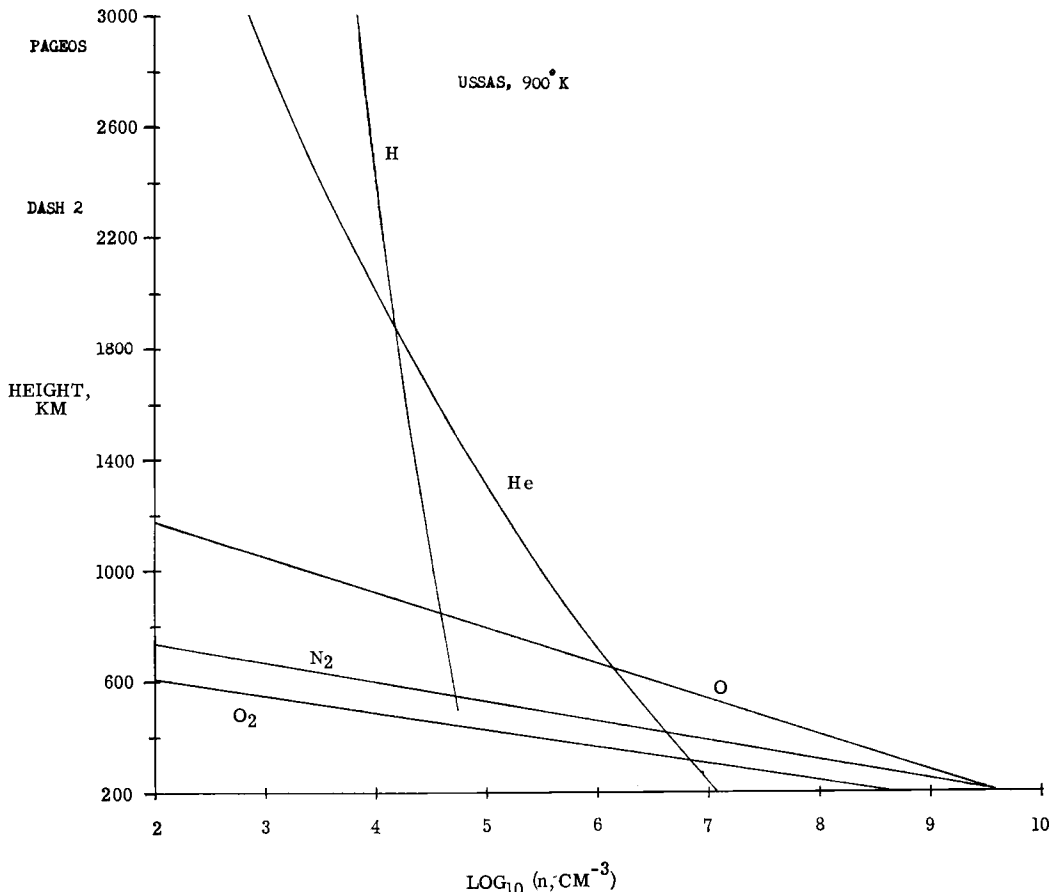


Fig. 8. Neutral atmospheric constituents at 900°K.

Dash 2 at 2325 km, and -19.23 for Pageos at 2872 km) are both much higher than values given by the USSAS. The dashed curve represents the USSAS profile with neutral hydrogen concentrations increased by a factor of 3. This density-altitude profile was most consistent with the deduced densities and was used to refine the density calculations. The closed circle represents the \log_{10} of density deduced from Pageos (-19.38) after correcting for the effect of magnetic induction drag using the estimate by Slabinski [1970] based on the theory of *Hohl and Wood* [1963]. This effect is probably negligible for Dash 2 because of its much smaller size.

The mean local solar times of the Pageos and Dash 2 perigees were within one hour of 0600 over the observation period, whereas the mean

perigee latitudes were separated by only 20 deg. Thus, since the Pageos perigee was nearly directly above that of the Dash 2, it was possible to deduce a third parameter of the exosphere from these measurements: the mean density scale height. It is seen in Figure 9 that the density scale height of about 950 km deduced from the measurements would be very near the scale height given by the excess hydrogen USSAS model (dashed line) if Slabinski's estimate is close to the actual induction drag effect. It should be pointed out that the hydrogen drag coefficient used here assumes that the satellite surfaces have not acquired an outer layer of hydrogen atoms. If such a layer had actually formed, the drag coefficient would be somewhat less than 4 [Cook, 1965; K. Moe, personal communication, 1971], and the exospheric densities

ACCELERATIONS FROM EARTH ALBEDO AND HYDROGEN DRAG

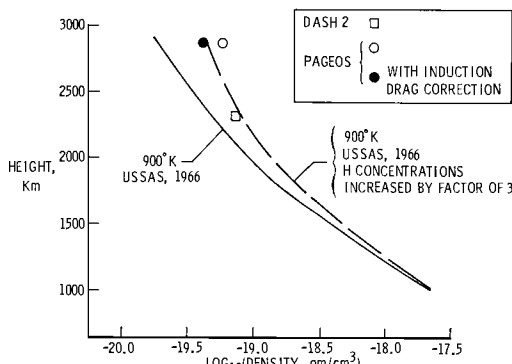


Fig. 9. Mean neutral exospheric densities near 0600 hours LST at low latitudes, April-May 1967.

and the excess hydrogen concentrations deduced in this study would be even greater.

CONCLUSIONS

The orbital mean motions of two balloon satellites, Pageos and Dash 2, have been studied during a period when both were in continuous sunlight. From a simultaneous comparison of the observed variations of the mean motion with the predicted variations due to earth albedo radiation and atmospheric drag, it can be concluded that:

1. The orbital acceleration of a satellite due to the forces of earth albedo radiation pressure was computed by numerically integrating both the radial and transverse components of diffuse Lambertian reflection all along the orbit. The observed orbital accelerations agreed with the predicted trends computed for both satellites.

2. Residuals between the observed and predicted values of the orbital accelerations for both satellites can be attributed primarily to atmospheric drag, with magnetic induction drag causing a secondary effect in the case of Pageos.

3. Exospheric densities deduced at altitudes above 2300 km from these residuals for the Pageos and Dash 2 satellites indicate that neutral hydrogen concentrations were about 3 times greater than values given by the *U.S. Standard Atmosphere Supplements* [1966]. These results were obtained at low latitudes near a local solar time of 0600 hours in April-May 1967.

4. The technique developed in this paper allows meaningful drag measurements to be

obtained at extremely high altitudes in the exosphere.

APPENDIX

To develop an expression for the variations of the mean motion n due to the radial component of albedo radiation force, we can begin with the basic perturbation equation of *Cook* [1962]:

$$\frac{da}{d\theta} = \frac{2r^2 R^2 e}{n^2 a^2 (1 - e^2)} \left(\frac{A}{M} \right) S \sin \theta \quad (A1)$$

where a is the semi-major axis in centimeters, R is the earth radius in centimeters, A/M is the area-to-mass ratio of the satellite in square centimeters per gram, e is the eccentricity, S is the radial component of earth albedo radiation pressure in dynes per square centimeter, and n has units of radians per second. The relationship between the semi-major axis and the mean motion is given by

$$n = (\mu)^{1/2} / a^{3/2} \text{ rad sec}^{-1} \quad (A2)$$

where μ is the gravitational constant times the mass of earth. The incremental change in n after one orbit is

$$\Delta n = -\frac{3}{2} \frac{(\mu)^{1/2}}{a^{5/2}} \Delta a \\ = -\frac{3}{2} \frac{n}{a} \Delta a \text{ rad sec}^{-1} \text{ rev}^{-1} \quad (A3)$$

Orbital energy changes can be related to changes in the semi-major axis to within 1% by [*Keating et al.*, 1965]

$$\Delta E = \mu M \Delta a / 2a^2 \quad (A4)$$

Where ΔE is the orbital energy change over one orbit. Thus, changes in n can also be related to changes in the orbital energy by

$$\Delta n = -\frac{3na}{\mu M} \Delta E \text{ rad sec}^{-1} \text{ rev}^{-1} \quad (A5)$$

We can use equation A1 for the change in a after one revolution:

$$\Delta a = \frac{2R^2 e}{n^2 a^2 (1 - e^2)} \frac{A}{M} \\ \cdot \int_0^{2\pi} S r^2 \sin \theta d\theta \text{ cm rev}^{-1}$$

and, using equation A3 to determine the change

EDWIN J. PRIOR

205

in mean motion and remembering that $n^2 = \mu/a^3$,

$$\Delta n = -\frac{3nR^2e}{\mu(1-e^2)} \frac{A}{M} \\ \cdot \int_{\gamma}^{2\pi} S r^2 \sin \theta d\theta \text{ rad sec}^{-1} \text{ rev}^{-1} \quad (\text{A6})$$

Substituting equation 1,

$$\Delta n = \frac{-3nR^2e}{\mu(1-e^2)} (1.5 \times 10^{-5}) \frac{A}{M} \\ \cdot \int_{\gamma}^{\tau} \cos \theta_s \sin \theta d\theta \text{ rad sec}^{-1} \text{ rev}^{-1} \quad (\text{A7})$$

In this expression, γ and τ represent the two values of true anomaly θ at which the orbit intersects the plane of the terminator ($\theta_s = 90^\circ$) in Figure A1. The straight line pq represents the intersection of the orbital plane and the plane of the terminator. It is apparent that $\tau - \gamma = \pi$ radians.

The integration is performed along the arc of the orbit that lies on the sunlit side of the terminator, where $\cos \theta_s$ has a positive value. The integration over the rest of the orbit contributes nothing, since equation 1 gives $S = 0$ along that portion of the satellite path.

In order to solve the integral and make the expression tractable, it is necessary to determine θ_s as a function of θ . First, we shall convert equation A7 so that the units for n and its time rate of change dn/dt are consistent with those provided by the Smithsonian Astrophysical Observatory (revolutions per day and revolutions per day squared, respectively). Changing equation A7 from $\text{rad sec}^{-1} \text{ rev}^{-1}$, we find that the orbital acceleration is given by

$$\frac{dn}{dt} = -\frac{3R^2(86400)^2}{4\pi^2 a^3} \left(\frac{e}{1-e^2} \right) 1.5 \times 10^{-5}$$

$$\cdot \left(\frac{A}{M} \right) \int_{\gamma}^{\tau} \cos \theta_s \sin \theta d\theta \text{ rev day}^{-2}$$

or, simplifying,

$$\frac{dn}{dt} = -8.4 \times 10^4 \left(\frac{R^2}{\pi^2 a^3} \right) \frac{e}{1-e^2}$$

$$\cdot \left(\frac{A}{M} \right) \int_{\gamma}^{\tau} \cos \theta_s \sin \theta d\theta \text{ rev day}^{-2} \quad (\text{A8})$$

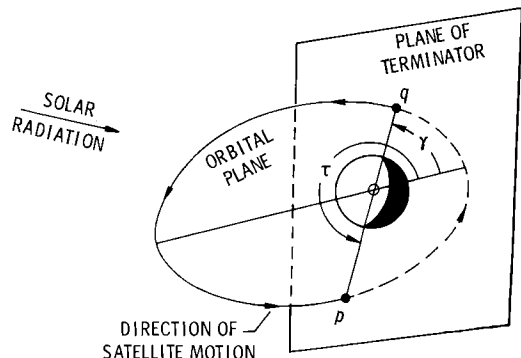


Fig. A1. Terminator-orbital plane geometry.

The relationship between θ and θ_s can be understood by looking at Figure A2, which represents the celestial sphere with the earth at its center. The point at which the orbital plane crosses the celestial equator so that the satellite is moving south to north is called the ascending node and has right ascension Ω . The right ascension of the sun is given by α_s . The arc length along the equator between the ascending node and the solar right ascension is then $(\alpha_s - \Omega)$. The arc length from the equator along the orbit to a particular position of the satellite is just $(\omega + \theta)$. The declination of the sun is given by δ_s . The arc length θ_s is the minimum angle between the earth-sun line and the earth-satellite line. We shall designate the arc length between the ascending node and the subsolar point as η . By use of spherical trigonometry, we will develop a relationship between θ and θ_s and determine the values of γ and τ in order to solve equation A8.

Using the law of cosines for a spherical triangle, we see that

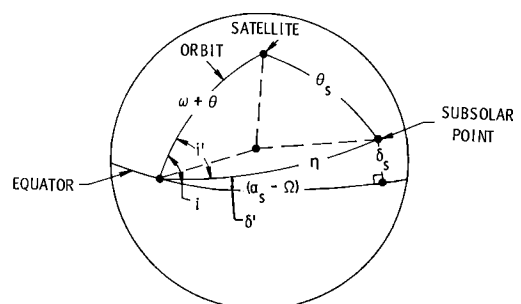


Fig. A2. Satellite-solar geometry.

$$\cos \eta = \cos (\alpha_s - \Omega) \cos \delta_s$$

$$dn/dt = (FH/2)\pi \text{ rev day}^{-2}$$

$$\begin{aligned}\cos \theta_s &= \cos (\omega + \theta) \cos \eta \\ &\quad + \sin (\omega + \theta) \sin \eta \cos i'\end{aligned}$$

Since

$$\sin \eta = [1 - \cos^2 (\alpha_s - \Omega) \cos^2 \delta_s]^{1/2} = X$$

$$\cos \eta = Y = \cos (\alpha_s - \Omega) \cos \delta_s$$

$$\cos (\omega + \theta) = \cos \omega \cos \theta - \sin \omega \sin \theta$$

$$\sin (\omega + \theta) = \sin \omega \cos \theta + \cos \omega \sin \theta$$

Then

$$\begin{aligned}\cos \theta_s &= (Y \cos \omega + X \sin \omega \cos i') \cos \theta \\ &\quad + (-Y \sin \omega + Y \cos \omega \cos i') \sin \theta\end{aligned}$$

We can define

$$G = Y \cos \omega + X \sin \omega \cos i'$$

$$H = -Y \sin \omega + Y \cos \omega \cos i'$$

Substituting back into the integral,

$$\frac{dn}{dt} = -8.4 \times 10^4 \left(\frac{R^2}{\pi^2 a^3} \right) \frac{e}{1 - e^2} \left(\frac{A}{M} \right)$$

$$\cdot \int_{\gamma}^{\tau} (G \cos \theta \sin \theta + H \sin^2 \theta) d\theta \quad (A9)$$

Calling

$$F = -8.4 \times 10^4 \left(\frac{R^2}{\pi^2 a^3} \right) \frac{e}{1 - e^2} \left(\frac{A}{M} \right)$$

we will proceed to evaluate the integrals.

$$\begin{aligned}\frac{dn}{dt} &= F \int_{\gamma}^{\tau} G \cos \theta \sin \theta d\theta \\ &\quad + F \int_{\gamma}^{\tau} H \sin^2 \theta d\theta\end{aligned}$$

$$\frac{dn}{dt} = \frac{FG}{2} (\sin^2 \tau - \sin^2 \gamma)$$

$$+ \frac{FH}{2} [\tau - \gamma - (\sin 2\tau)/2 + (\sin 2\gamma)/2] \quad (A10)$$

Using the relationship $\tau - \gamma = \pi$, equation A10 simplifies to

$$\begin{aligned}\frac{dn}{dt} &= 4.2 \times 10^4 \left(\frac{R^2}{\pi^2 a^3} \right) \frac{e}{1 - e^2} \left(\frac{A}{M} \right) \\ &\quad \cdot \{ \cos (\alpha_s - \Omega) \cos \delta_s \sin \omega \\ &\quad - [1 - \cos^2 (\alpha_s - \Omega) \cos^2 \delta_s]^{1/2} \\ &\quad \cdot \cos \omega \cos i' \} \quad (A11)\end{aligned}$$

We can determine the value of i' to use in equation A11 from the relation

$$i = i' + \delta'$$

where, from Figure A2, we have

$$\begin{aligned}\sin \delta' &= \frac{\sin \delta_s}{\sin \eta} \\ &= \frac{\sin \delta_s}{[1 - \cos^2 (\alpha_s - \Omega) \cos^2 \delta_s]^{1/2}}\end{aligned}$$

Acknowledgment. The author would like to thank for their advice and encouragement all the members of the Aeronomy Section in the Atmospheres Branch of the NASA Langley Research Center. Much of this work was done for the author's graduate studies at the University of Virginia with the helpful advice of Dr. Nelson Limber.

REFERENCES

- Baker, R. M. L., Jr., Radiation on a satellite in the presence of partly diffuse and partly specular reflecting body, in *Trajectories of Artificial Celestial Bodies*, pp. 85-150, Springer, New York, 1966.
- Brinton, H. C., R. A. Pickett, and H. A. Taylor, Diurnal and seasonal variation of atmospheric ion composition, Correlation with solar zenith angle, *J. Geophys. Res.*, 74, 4064, 1969.
- Cook, G. E., Luni-solar perturbations of the orbit of an earth satellite, *Geophys. J. Roy. Astron. Soc.*, 6, 271-291, 1962.
- Cook, G. E., Satellite drag coefficients, *Planet. Space Sci.*, 13, 929, 1965.
- Cook, G. E., Variations in exospheric density during 1967-8, as revealed by Echo 2, *Tech. Rep. 69127*, Roy Aircraft Estab., Farnborough Hants, England, June 1969.
- Cunningham, F. G., Earth-reflected solar radiation incident upon spherical satellites in general elliptical orbits, *NASA Tech. Note D-1472*, 1963.
- Fea, K., Exospheric conditions to a height of 3500 km, derived from satellite accelerations in 1964, *Planet. Space Sci.*, 14, 291, 1966.
- Fea, K., Determination of the density of air at an altitude of 3500 km, *Nature*, 205, 379, 1965.

EDWIN J. PRIOR

207

- Fea, K., The orbital accelerations of high balloon satellites, in *Cospar Symposium, Dynamics of Satellites (1969)*, Springer, New York, 1970.
- Fea, K. H., and D. E. Smith, Some further studies of perturbations of satellites at great altitude, *Planet. Space Sci.*, 18, 1499, 1970.
- Heikkila, W. J., and W. I. Axford, The outer ionospheric regions, in *Physics of the Earth's Upper Atmosphere*, pp. 96-129, Prentice-Hall, Englewood Cliffs, N.J., 1965.
- Hohl, F., and G. P. Wood, The electrostatic and electromagnetic drag forces on a spherical satellite in a rarefied partially ionized atmosphere, in *Proceedings of the Third International Symposium on Rarefied Gas Dynamics*, vol. 2, Academic, New York 1963.
- Jacchia, L. G., Static diffusion models of the upper atmosphere with empirical temperature profiles, *Smithson. Astrophys. Observ. Spec. Rep.* 170, 1964.
- Keating, G. M., and E. J. Prior, Latitudinal and seasonal variations in atmospheric densities obtained during low solar activity by means of the inflatable air density satellites, *Space Res.*, 7, 1120-1130, 1967.
- Keating, G. M., and E. J. Prior, The winter helium bulge, *Space Res.*, 8, 983-992, 1968.
- Keating, G. M., J. A. Mullins, C. W. Coffee, and D. S. McDougal, Determination of mean atmospheric densities from the Explorer 9 satellite, *NASA Tech. Note D-2895*, 1965.
- Keating, G. M., J. A. Mullins, and E. J. Prior, The polar exosphere near solar maximum, paper presented at Twelfth Plenary Meeting of Cospar, Prague, Czechoslovakia, May 1969.
- Keating, G. M., J. A. Mullins, and E. J. Prior, Simultaneous measurements of exospheric densities near opposite poles, paper presented at 11th International Space Science Symposium of Cospar, Leningrad, USSR, May, 1970.
- Levine, J. S., and A. Arking, Earth albedo measurements, July 1963 to June 1964, *J. Atmos. Sci.*, 24, 721-724, 1967.
- Mullins, J. A., G. M. Keating, D. S. McDougal, and E. J. Prior, Determination of mean atmospheric densities during minimum solar activity by means of the Explorer 19 satellite, *NASA Tech. Note D-3432*, 1966.
- Prior, E. J., Earth albedo effects on the orbital variations of Echo 1 and Pageos 1, in *Cospar Symposium, Dynamics of Satellites (1969)*, Springer, New York, 1970.
- Sehnal, L., Radiation pressure effects in the motion of artificial satellites, in *Cospar Symposium, Dynamics of Satellites (1969)*, Springer, New York, 1970.
- Slabinski, V. J., Induction drag on large echo-type satellites: Observational evidence, Ph.D. thesis, Case Western Reserve Univ., Cleveland, Ohio, Jan. 1970.
- Smith, D. E., Earth-reflected radiation pressure, in *Cospar Symposium, Dynamics of Satellites (1969)*, Springer, New York, 1970.
- Smith, D. E., and K. H. Fea, Radiation pressure effects on the acceleration of high altitude balloon satellites, *Doc. X-550-70-92*, Goddard Space Flight Center, Greenbelt, Md., 1970.
- Smith, D. E. and K. E. Kissell, Orbital accelerations of the Pageos spacecraft, paper presented at Fourteenth Plenary Meeting of Cospar, Seattle, Washington, June 1971.
- Teichmann, L. A., The fabrication and testing of Pageos 1, *NASA Tech. Note D-4596*, 1968.
- U.S. Standard Atmosphere Supplements, 1966*, ESSA, NASA, and U.S. Air Force, Dec. 1966.
- Wyatt, S. P., The effect of terrestrial radiation pressure on satellite orbits, in *IUTAM Symposium, Dynamics of Satellites, Paris, May 28-31, 1962*, Springer, New York, 1963.
- Zadunaisky, P. E., I. I. Shapiro, and H. M. Jones, Experimental and theoretical results on the orbit of Echo 1, *Smithson. Astrophys. Observ. Spec. Rep.* 61, 1961.

5. Instrumentation and Environment

Rapid Global Geoid Mapping with Satellite Altimetry

H. R. STANLEY

NASA Wallops Station, Wallops Island, Virginia 23337

N. A. ROY

*Wolf Research and Development Corporation
Pocomoke City, Maryland 21851*

C. F. MARTIN

*Wolf Research and Development Corporation
Riverdale, Maryland 20840*

Abstract. An orbiting altimeter with an instrumentation accuracy of better than 50 cm and noise levels of 20 cm can be built and flown within a relatively short time. With proper pre-mission analysis and careful scheduling, a 1° by 1° global geoidal map of 1- to 2-meter resolution can be obtained within an 18- to 20-day period by using a high-inclination orbit.

The purpose of this paper is to demonstrate, from a theoretical point of view, that it is feasible to build, fly, calibrate, and evaluate an orbiting altimeter system to provide accurate geoidal mapping on a global scale. We shall discuss the problems involved both in instrumentation and orbit determination.

Starting with a description of the Skylab altimeter characteristics, a more advanced design is postulated. This new design should not be construed as a firm recommendation for the ultimate altimeter. However, we feel that it does reasonably represent current technology and is a system that could be built and flown within a reasonable time.

INSTRUMENTATION SYSTEMS

The first problem encountered in any evaluation of a prototype system is the gathering

and analysis of engineering information about the internal performance of the system in the environment in which it will be used. The instrumentation selected for Skylab (see Table 1) and the mission plan for its use are designed specifically for this purpose. The system has a great deal of flexibility and several modes of operation. This will allow evaluation of different tracking techniques, pulse compression versus conventional techniques, and the possible advantages of various pulse widths and signal-to-noise ratios. In addition, the collected data should be sufficient to determine the correct value for the radar backscatter coefficient (σ_0), the maximum decorrelation time, and the potential of altimetry to satisfy oceanographic needs (sea-state versus wave form). The Skylab instrumentation should therefore provide valuable scientific information, as well as an evalua-

TABLE 1. Instrumentation for Skylab and for Proposed System

Altimeter Characteristics	Skylab S-193	Proposed System
Transmitter type	TWT	TWT
Peak power, kw	2	2
Frequency, GHz	13.9	13.9
PRF	350 (plus double pulse mode)	2000
Antenna	Parabolic	Parabolic
Diameter, cm	113	86.5
Gain, db	41	39.8
Beamwidth, deg	1.5	1.75
Receiver type	Coherent	Incoherent
Noise figure, db	5	5
System losses, db	5	5
Processor	Threshold or split gate	Split gate
Data	Return waveform and altitude	Return waveform and altitude
Compression type and ratio	Digital, 13 to 1	Frequency, 100 to 1
Pulsewidth (compressed mode), nsec	10	10
Receiver bandwidth, mHz	100	100
Signal-to-noise ratio, db	~20	~10

ation of hardware techniques necessary for an evolutionary altimetry development program. However, this instrumentation flexibility and the fact that data-taking periods are constrained to 5 min or less obviously preclude any global operations.

The altimeter design characteristics that could better perform accurate geoidal mapping on a global scale are also listed in Table 1. The striking similarities between this design and the Skylab design are obvious. There are some differences, however, and the rationale for the changes should be explained. The higher pulse repetition frequency (PRF) will allow more averaging and therefore improve accuracy. The smaller antenna decreases the stabilization-induced errors, provides better pulse-leading edge linearity, and thus improves accuracy. Other loop-gain changes are equalized by changes in pulse width, orbit height, and lower signal-to-noise ratio.

The performance criteria for this altimeter design, the Skylab, and the proposed Geos C designs are presented in Table 2.

The instrument performance values in Table 2 refer to laboratory conditions. In orbit, these values will be modified by propagation path errors, satellite stabilization and antenna pattern effects, sea-state bias effects, and orbit determination errors. *Godbey et al.* [1969] and others have shown that propagation path errors can be corrected to produce a residual standard error of less than 10 cm. *Miller and Hayne*

[1971] have shown that for a system stabilized to within $\pm 0.5^\circ$ the antenna pointing and pattern effects can be reduced to near 5 cm. *Miller and Hayne* [1971] also have shown that a worst-case condition with rms wave height of 3 meters and a skewness of 0.4 results in an altitude error of only 12 cm for a 50-nsec pulse-width. Therefore, except for orbit computation problems, the altimeter system capabilities will degrade, at most, from ± 20 cm to approximately ± 30 cm when in orbit. The following error budget summarizes these expected errors:

Instrumentation Errors

Signal fluctuations and thermal noise	
residual errors	11 cm
System time delay uncertainty	6
Nonlinearity range tracker and signal processor errors	12
Tracker granularity and clock uncertainty	10

Propagation-Dependent Errors

Corrected data	10
----------------	----

TABLE 2. Altimeter Performance Criteria (in centimeters)

System	Over-All Design Accuracy	Instrument Accuracy	Instrument Precision
Skylab	± 500	± 300	± 200
Geos C	± 500	± 100	± 50
Proposed system	± 300	± 50	± 20

STANLEY, ROY, AND MARTIN

211

Ocean Scattering Effects

Residual stabilization errors	< 4
Residual leading edge linearity assumption error	6
Electromagnetic MSL bias	< 12
rms error	26

The only remaining error source, which is by far the dominant one, is the process by which the altimeter measurements are verified, i.e., determination of the distance between the satellite and the mean sea surface by an independent method. The degree to which this can be accomplished by present orbit determination techniques and the subsequent uses of the calibrated data are discussed next.

ORBITAL TRADE-OFF STUDIES

Oceanographers and geophysicists have stated, with strong scientific justification, that an orbiting altimeter should be flown in a nearly polar circular orbit. In this way, coarse-grained profiles of the geoid are obtained every 12 hours. The altimeter engineer has a different point of view, however. He is primarily interested in an orbit that will allow him to calibrate and verify the altimeter performance at regular intervals and at locations where there is sufficient ground truth data to corroborate his analyses. Orbits of medium inclination would suit him better, since they could provide consecutive arc crossing points in the vicinity of well-determined ground tracking stations and where surface gravity determinations are of relatively high density. The question is whether a good compromise orbit can be devised that will provide maximum scientific information and allow for calibration and verification of the instrumentation.

First, a low inclination orbit ($i = 22^\circ$) yields the following results. Once per week, a single revolution of the satellite will provide an intersection point approximately 60 miles NE of the island of Grand Turk in the Caribbean. In essence, the satellite crosses over the same geographic point within a 2-hour period. Ground truth data (e.g., weather, sea state) can be monitored by aircraft and ships in the calibration area, which is also in an area where extensive surface gravity observations are available. Since it is not probable for sea conditions to drastically change during this period, it may be

possible to calibrate the short-term (2-hour) drift of the system. Since this particular intersection occurs on a weekly basis, long-term drift and sea-state effects could be established by the analysis of multiple passes over an extended period of time. The contribution of ground-station errors in one-revolution solutions are small in comparison to gravity-model uncertainties. The obvious disadvantage of an orbit of this type, however, is that the ocean areas profiled by the altimeter are limited to latitudes 22° N and S of the equator.

In the case of $i = 40^\circ$, the same type of intersection condition occurs in the Wallops-Bermuda area, where essentially the same ground truth conditions exist. Good, single-revolution tracking is available from a network of existing stations, so that calibration results are comparable to the low-inclination case.

All subsequent discussion refers to an orbit with an inclination of 99.1° , eccentricity 0.001, altitude 925 km, and period 103 min.

It was decided to select an orbit weighted in favor of the scientific applications of the altimeter and to determine whether calibration and verification could be performed to the satisfaction of the altimeter design engineer. The ground tracks on successive days are very nearly contiguous, their actual separation being approximately 1.3° of longitude. The separation of consecutive passes is approximately 24° of longitude, so that geographic coverage (using N-S passes) is completed in an 18-day period. The use of all pass combinations (N-S, S-N) could in theory shorten the coverage period by one-half. From a calibration viewpoint, this orbit does not appear to afford the potential that lower-inclination orbits provide. The consecutive arc intersections occur at latitudes of 81° . Existing ground-tracking stations and good ground truth areas are not abundant in these areas, nor is the climate conducive for obtaining these data (either from aircraft, ships, or tower instrumentation) on a regular basis. This means that short-term calibrations must be performed at two locations rather than one, in effect doubling the effort of gathering ground truth data. The orbit also causes rather complex scheduling of ground tracking for calibration and verification. Crossing arcs, useful for longer-term calibrations, occur at 12-hour intervals requiring multiple-shift tracking. If we can

forget the economics of the situation for the moment, however, the following sections will demonstrate that it is technically feasible to calibrate and evaluate the altimeter with high-inclination orbits and that the resulting profiles should provide significant improvement of our knowledge of the geoid.

CALIBRATION AND VERIFICATION

Certain types of error sources have to be considered only when altimeter accuracies, precision, and resolution are in the centimeter range. For example, in arcs of one to two revolutions in length, the gravity model is the predominant error source, but in arcs of less than one revolution the ground-station tracking errors dominate. Estimates of sea-state and attitude effects on the height measurement have been shown to be pulse and beamwidth dependent; however, these effects are negligible for the altimeter discussed even under the worst conditions. Tropospheric refraction model errors are also estimated to be only in the 10- to 15-cm range. Therefore, ground-tracking station errors and gravity-model errors are the most serious effects by far, their contributions varying as a function of arc length used in the orbit determination. Preliminary studies by us indicate that well-tracked orbits of one to two revolu-

RAPID GLOBAL GEOID MAPPING

tions in length might well provide the best calibration and verification.

Simulations for the high-inclination orbit were carried out as follows. First, a tracking complement was devised as shown in Table 3. This configuration was assumed to be representative of the geographic coverage that might be available for orbiting altimeter tracking. Each station was assumed to have a 5-meter station position error in each coordinate (ϕ, λ, H) relative to the center of mass and to have the capability of measuring range to the satellite with a noise of 1 meter rms and a bias of 1 meter. These are reasonable estimates of the capabilities of a well-calibrated range measuring system. In addition to the above, an error of 1 part in 10^6 was assumed in the value of GM and a gravity-model error of 25% of the difference between the APL and SAO coefficients up to and including 8, 8 was assigned. This model should be an accurate description of the gravity-model errors that can be expected in an orbit of this type.

A 10-day orbit was simulated. The results show that for most of this period the largest tracking gap is of the order of 30 min, the average gap being of the order of 12 to 16 min. In rare instances, the gap grew to 60 min, which indicates that a complete profiling effort

TABLE 3. Altimeter Orbit Simulation, Tracking Complement

Station	ϕ	λ (East)	Height, meters
White Sands, N. M.	32°21'29"	253°37'48"	1193
Point Pillar, Calif.	37 29 52	237 30 01	-7
Ely, Nev.	39 18 31	244 54 46	2787
Tananarive, M.R.	-19 00 07	47 18 53	1326
Kauai, Hawaii	22 07 24	200 20 04	1131
Pretoria, R.S.A.	-25 56 38	28 21 28	1598
Canton Island	-2 44 00	188 16 00	2
Johnston Island	16 45 45	190 29 01	17
Aberporth, G.B.	52 07 41	355 25 52	174
Ascension Island	-7 58 23	345 35 54	105
Kwajalein Island	9 10 00	167 20 00	100
Canary Island	27 45 42	344 22 05	165
Woomera, Australia	-30 49 07	136 50 17	122
Kyushu, Japan	32 00 00	131 00 00	1000
Kourou, French Guiana	5 06 46	307 29 19	169
Carnarvon, Australia	-24 53 48	113 43 02	20
Wallop's Island, Va.	37 51 37	284 29 26	-47
Bermuda	32 20 53	295 20 48	-38
Merritt Is., Fla.	28 25 29	279 20 07	-44
Antigua Is., B.W.I.	17 08 38	298 12 26	-7
Makaha Ridge, Hawaii	22 08 03	200 16 19	451

STANLEY, ROY, AND MARTIN

213

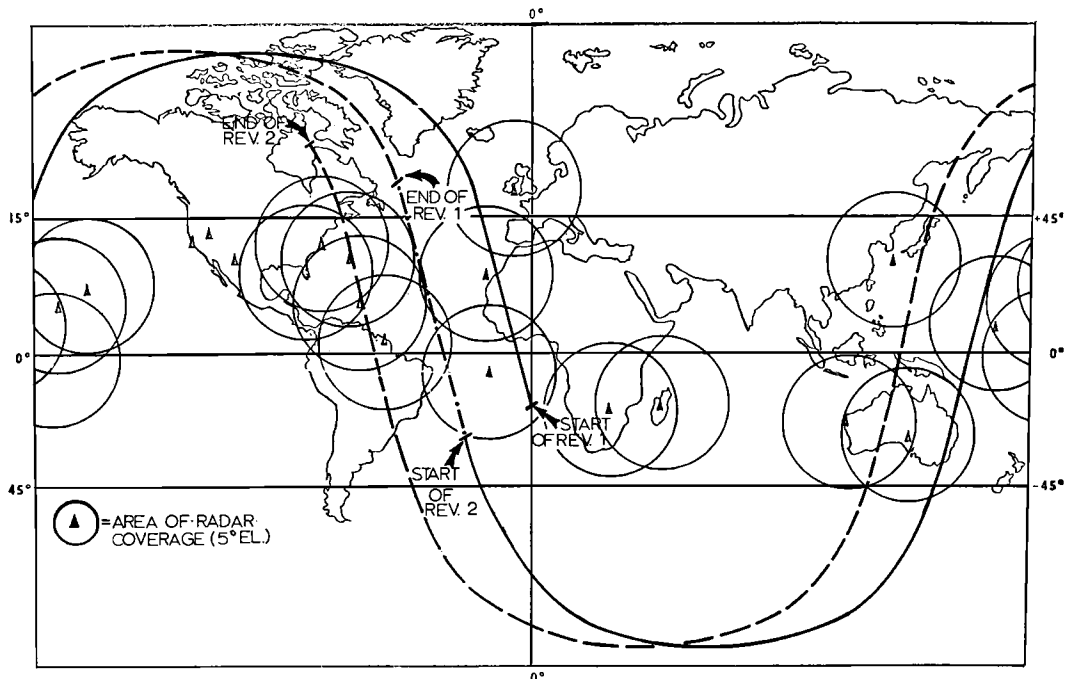


Fig. 1. Ground trace of arc 1.

within a 10-day period might require additional tracking stations. The 10-day orbit was then divided into solutions of two revolutions in length, and ten of these arcs were selected at random for further analysis. These arcs were

further subdivided into solutions of one revolution in length. Figure 1 shows the ground trace of one of these two-revolution solutions (arc 1). The ground stations tracking and the density of coverage are shown by the circles, which ap-

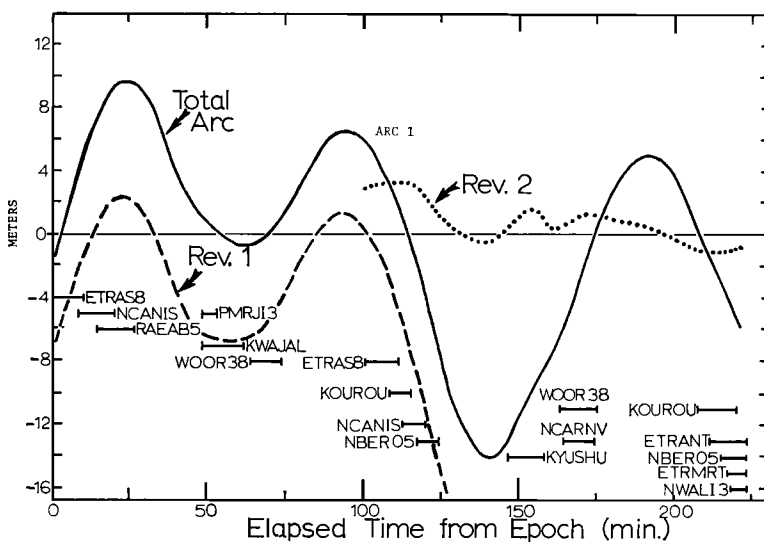


Fig. 2. Effects of gravity model errors on orbital height for arc 1.

214

proximate the tracking zones for each site based upon a 5° elevation cutoff.

Figure 2 shows the effects of the gravity-model error on the height component of the orbit. The two-revolution solution (solid line in Figure 2) poses quite serious problems from both a profiling and calibration point of view. The periodicity and amplitude of the effect seriously degrade the accuracy of profiles obtained from the solution, since the satellite position in height is ill determined. Calibrations attempted during parts of the orbit are also degraded, since it would be extremely difficult to resolve altimeter drift effects from the orbital effects. Also shown in Figure 2 are the effects when the same tracking data are used in two independent one-revolution solutions. These results demonstrate an important mission planning problem that will be encountered in the orbiting altimeter program. Single revolution profiles are not uniformly accurate, and although it is possible to perform accurate profiling and calibration missions by using single-revolution orbit determinations, it is necessary to perform pre-mission planning analyses to qualify the

RAPID GLOBAL GEOID MAPPING

results to be expected. The rev. 1 solution provides no improvement over the two-revolution solution. The rev. 2 solution does, however, show a marked improvement over the two-revolution solution. The effects of station position errors and range biases are not plotted in Figure 2, since their effects are small in comparison to the gravity model error. In an RSS sense, their combined effects add less than 1 meter to the orbital height uncertainty. The GM error, as might be expected, induces a constant bias of approximately 2.5 meters. The total orbital height uncertainty, including all the errors discussed above, is approximately 3 meters. Since a large part of this uncertainty is due to the GM-induced bias, we can conclude that the profile resolution obtained will be significantly better than 3 meters.

There is another point of interest in these results. In the two-revolution solution and the rev. 1 solution, the gravity model errors exhibit roughly one revolution period, as might be expected. In the rev. 2 solution, this periodicity is not apparent, and there is an irregularity in the effects at 160 min. Upon close examina-

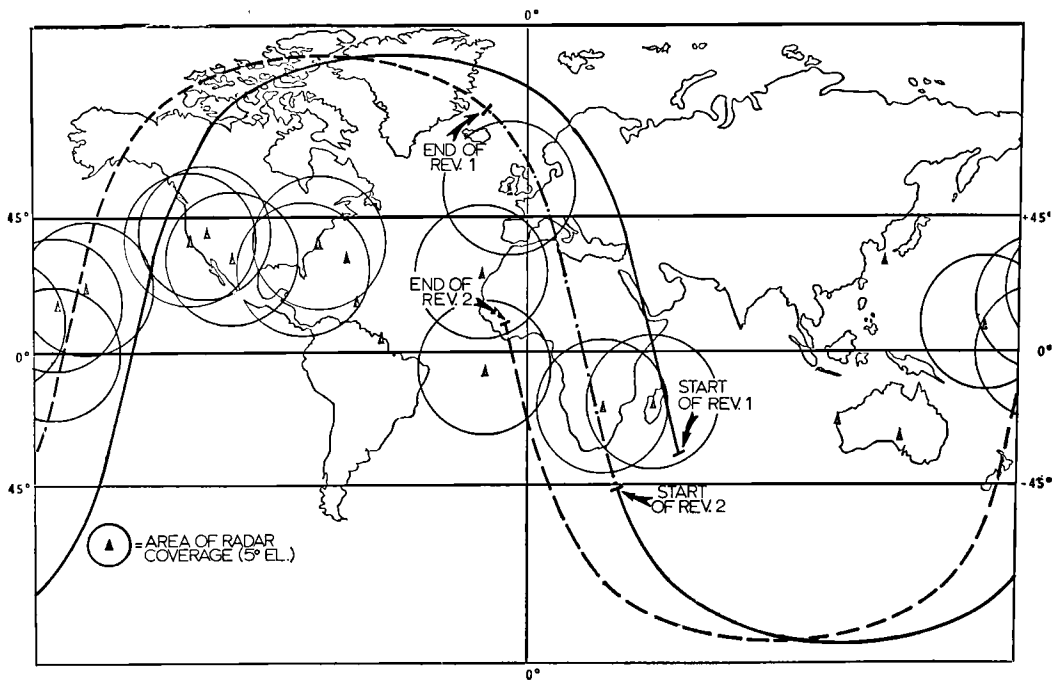


Fig. 3. Ground trace of arc 2.

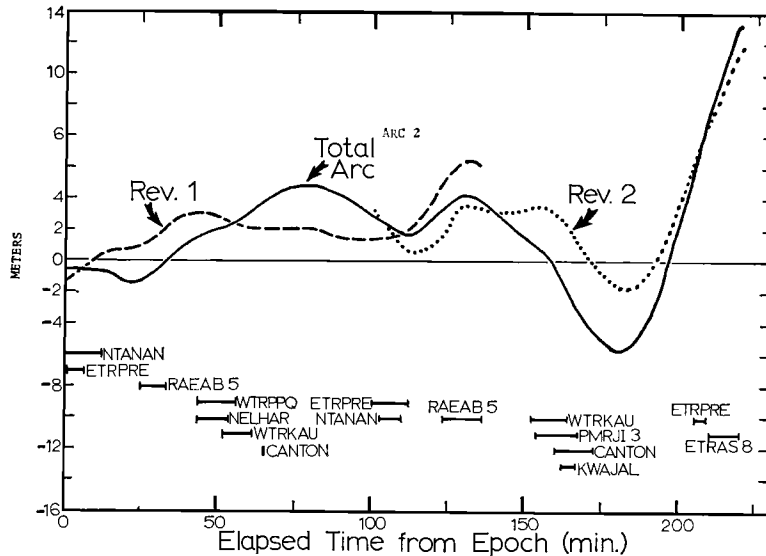


Fig. 4. Effects of gravity model errors on orbital height for arc 2.

tion, one can see this same irregularity in the two-revolution solution, although it is somewhat less well defined owing to the sharp slope in this region. It is apparent that the forces that would be computed by using the two gravity models comprising our error model differ significantly in this area.

Figure 3 shows the ground trace of another of the two-revolution solutions (arc 2) selected for analysis.

Figure 4 shows the effects of the gravity-model error on the height component of the orbit. The results are quite similar to those just discussed. The rev. 1 solution shows excellent profiling and calibration potential. The first 60 min of the rev. 2 solution can also be used for these purposes. If short-term calibration of the altimeter turns out to be necessary, this combination of solutions may prove to be fruitful, since it would be possible to calibrate over the Hawaii area twice within a period of one revolution (50–150 min). The difference in gravity-model effects for these two periods of time is approximately 1 meter. It may be possible to further reduce this by selecting a single-revolution solution that starts at 50 min and continues through 170 min.

These typical results demonstrate that it is possible to determine orbits for the altimeter

well enough to provide good calibration and verification information, as well as significant geoidal profiles, in a relatively short period of time. The problem of mission planning and scheduling will be complex and somewhat tedious, but it is a problem that can be solved. The ground truth problem for short- and long-term calibration can be solved by selecting two, or possibly more, areas that can be instrumented to provide the necessary information on a regularly scheduled basis. Two potential areas, Wallops Island and Hawaii, are suggested by the analyses performed so far.

GLOBAL MAPPING APPLICATIONS

The orbital height errors propagated are true center-of-mass errors and should be an accurate reflection of the quality of the profiles in an 'absolute' rather than a relative sense. From an orbital point of view, the profiles can be determined with a resolution of better than 2 meters, and a bias of less than 2.5–3 meters. These estimates are based on current evaluation of errors in the gravity model, GM, station positions, ground-tracking systems, and sea-state effects. Since the altimeter could not fly before 1974–1975, it is reasonable to expect that improvements in each of these areas would be realized before the first altimeter flight.

216

It is possible to obtain at least two profiles of this quality per day for extended periods of time and complete coverage of the oceans within an 18-day period. Since the satellite should have an expected lifetime of at least 1 year, it should be possible to perform correlation studies of similar profiles taken over an extended period of time and in this way further improve their accuracies.

RAPID GLOBAL GEOID MAPPING

REFERENCES

- Godbey, T. W., et al., Equipment specifications for a space rated altimeter, General Electric Co., Aerospace Electronics, Utica, N.Y., January 1969.
- Miller, L. S., and G. S. Hayne, System study of the geodetic altimeter concept, Res. Triangle Inst., Research Triangle Park, N.C., March 1971.

Average Return Pulse Form and Bias for the S193 Radar Altimeter on Skylab as a Function of Wave Conditions¹

WILLARD J. PIERSON, JR. AND EMANUEL MEHR

New York University, University Heights, Bronx, New York 10453

Abstract. The average return echo power for the radar altimeter (S193) on Skylab will be beam limited, so that it will rise to peak return in 100 nsec and fall to nearly zero in about another 400 nsec once the altimeter has searched out the nadir direction. A split-gate tracking loop with the gates separated by 50 nsec will be used. The effects of varying wave height and wave spectra on the shape of the return pulse and on the measurement of the range are calculated in terms of a convolution involving the probability density function of the wave elevations and the shape of the radar signal. The assumptions made in the calculations have been verified by measurements made by others from aircraft and towers.

The idea of using an altimeter on a spacecraft was presented by *Godfrey* [1964], among others, and its oceanographic applications were treated in a report edited by *Ewing* [1965]. *Greenwood et al.* [1969a] described a radar altimeter for use over the oceans and its geodetics applications, and *Greenwood et al.* [1969b] discussed various oceanographic applications of such an altimeter. Further study in August 1969 led to refinements in the concept of altimeter and additional requirements on the size of the ranging error [*Kauda*, 1969].

Plans for the further determination of the geoid and the position of the ocean surface relative to the geoid require radar altimeters on a succession of spacecraft capable of measuring the distance between the spacecraft and the surface of the ocean to increasing accuracies of 1 meter, $\frac{1}{2}$ meter, and finally 10 cm. Obtaining such ranging accuracies requires timing accuracies of 1 nsec or so, since a 1-nsec change in round-trip time for the radar pulse amounts to a 15-cm change in distance.

For these radar altimeters, a very short pulse of radar-frequency energy (10 GHz or higher) is transmitted from the altimeter on the spacecraft with an antenna directed toward the sea surface. The pulse is altered upon striking the

sea surface and is scattered back toward the spacecraft incoherently in such a way that the detected signal from each pulse is highly irregular from nanosecond to nanosecond, owing to phase reinforcements and phase cancellations. Averaging a great many pulses reduces the errors caused by the irregularity from pulse to pulse if successive pulses are independent.

Since the altitude of a spacecraft is fairly well known, there can be many separate pulses on the way down to the ocean surface and the way back up to the spacecraft after being reflected by the sea surface. Stated another way, a redundant pulse repetition frequency can be used so that perhaps as many as 2000 pulses per second could be transmitted from the spacecraft. It is not clear whether the successive pulses would be independent at high pulse-repetition frequencies.

The expected value of the return detected power as a function of time is, however, a concept based on the idea of averaging a very large number of return pulses. The shape of this function of time is used to design the electronic circuitry that will decide that the pulse has returned to the radar and count the number of, say, nanoseconds that have elapsed since the pulse was transmitted.

The design of an altimeter good to, say, 10 cm from spacecraft altitudes requires (1) knowledge of the effects of waves on the shape of the average return altimeter pulse, (2)

¹Contribution 111, New York University, Geophysical Sciences Laboratory.

RETURN PULSE FROM SKYLAB ALTIMETER

knowledge of the maximum pulse repetition frequency such that successive pulses are still independent, and (3) a determination of whether or not changes in the average return altimeter pulse due to waves causes the electronic circuits that decide on the range to overestimate, or underestimate, this range consistently and thus introduce a bias in the measurements. Sampling variability due to pulse variations eventually averages out, but consistent biases such as those discussed here, and others, need to be identified and removed theoretically.

EXPERIMENT S193

A follow-up on the Apollo program called Skylab is scheduled for launch in May 1973 [Naugle, 1970]. On it will be an earth-resources experimental package, of which experiment S193 will be a part. Experiment S193 consists of a scanning pencil-beam radar radiometer and an altimeter. The purposes of the altimeter are numerous, one being the proof of the concept of altimetry from space. The instrument has many special features that permit detailed studies of the return pulses that might not be needed on an operational instrument.

PURPOSES OF THIS PAPER

In this paper, the shape of the average return pulse from a flat, but rough, surface will be discussed, and the changes in the shape of this return pulse as a function of the height of the waves on the underlying sea surface will be derived. The effects of receiver bandwidth on further modifying the average return pulse will be discussed. Finally, the range will be determined by tracking the return pulses by means of a divided split gate. The effect of waves in possibly biasing the range measurements will be discussed. Minor modifications of the altimeter design so as to measure the changes in the shape of the average return pulse would make it possible to measure wave heights over the ocean with the altimeter.

TRANSMITTED AND RETURN PULSES

The S193 altimeter has many features. The procedure for acquiring true vertical and the results that could be obtained by studying the 10-nsec transmitted pulse will not be discussed. Instead, the 100-nsec pulse will be studied. In one mode of operation, the S193 altimeter

transmits a pulse of radio frequency energy at 13.9 GHz lasting 100 nsec from a parabolic antenna pointing straight down. The pulse amplitude attains a constant value during the first 2 nsec and remains constant during the next 98 nsec. The wave fronts as they propagate away from the antenna are spherical and eventually strike a roughly spherical ocean surface with a curvature of the opposite sense.

If the ocean surface is considered spherical and rough, in the sense that it has bumps and hollows on it of the order of 2.25 cm equally scattered up and down about the average surface, the wave front will first strike the ocean surface at the closest point to the spacecraft. A circle of illumination will open up with time for 100 nsec. If the beamwidth of the antenna is large enough, a hole will open up in the middle and an annulus will radiate outward from the subsatellite point such that the illuminated area remains constant for several times the pulse duration [Greenwood *et al.*, 1969a].

Under these conditions, and with an idealized square transmitted pulse τ nanoseconds long, the normalized average power coming back to the altimeter is given by equation 1:

$$\begin{aligned} f_1(t) &= 0 & -\infty < t < 0 \\ f_1(t) &= t/\tau & 0 < t < \tau \\ f_1(t) &= 1 & \tau < t < \infty \end{aligned} \quad (1)$$

Various range decision circuits have been designed based on this idealization.

However, the antenna beamwidth of S193 is quite narrow, and the pulse requires 2 nsec or so to grow to full power. For these reasons, the rise to full power is not linear, and the limited beamwidth causes the average return power to begin to fall off just as the peak is reached for the 100-nsec pulse.

The function $f_2(t)$ that represents the average return power for S193 is therefore quite complicated in form. It has been given in both a graphical and quasi-analytical form by the designers of S193. We will compare the effects of waves on this actual return pulse with the effects on the idealized pulse given above. In each case, $t = 0$ corresponds to the instant that the first part of the signal would return to the altimeter after making the round trip to the sea surface and back.

PIERSON AND MEHR

219

EFFECTS OF WAVES AND DETECTION CIRCUITS

Two effects modify $f_1(t)$ and $f_2(t)$. The first is brought about by waves on the sea surface with amplitudes of several meters, and the second is brought about by the need to detect the return signal, heterodyne it down to an appropriate intermediate frequency, and square-law detect it so as to obtain a nonoscillatory positive signal to be fed into the range discrimination circuitry. This detection procedure requires a finite amount of time, especially when measured in nanoseconds, and adds a constant amount of delay that must be calibrated out of the instrument.

If $f(t)$ represents either $f_1(t)$ or $f_2(t)$, the effects of waves can be treated as a convolution on $f(t)$ as in equation 2.

$$F(t) = \int_{-\infty}^{\infty} f(t^*)g(t - t^*) dt^* \quad (2)$$

The additional effects of detection can be treated as a second convolution on $F(t)$ so as to obtain the shape of the average power function that would be used to decide on the range to the sea surface as in equation 3.

$$F_D(t) = \int_{-\infty}^0 F(t^*)h(t - t^*) dt^* \quad (3)$$

In our studies, the form of $g(t - t^*)$ has been obtained and $F(t)$ has been computed for both an idealized altimeter and the S193 altimeter. Possible forms for $h(t - t^*)$, which could be improved given more information on the receiver design, have been assumed, and, finally, various range-decision techniques have been applied to see how the effect of waves modifies the decision on range.

THE EFFECTS OF WAVES

In developing this theory of the effect of waves, it has to be assumed that the shape of $f_1(t)$ and $f_2(t)$ is given, which is another way to say that the characteristics of the transmitted pulse and the antenna pattern are known. It is also assumed that a large number of returns can be averaged, so that the average, or expected, signal power has a meaning. The sampling variability problems and the scatter about the true, or average, range has been studied by Lee [1969].

It must further be assumed that one pulse samples a large enough area of the sea surface with many individual waves in the illuminated area. This assumption is probably doubtful for extremely high waves, and for such conditions individual surfaces would have to be constructed by Monte Carlo methods from which the character of the return signal would have to be computed.

An important study by Yaplee *et al.* [1970] has shown that it is correct to assume that all points on the sea surface, $\eta(x, y, t)$, at any t are equally good as reflectors of microwave energy, no matter how far they are above or below the mean sea surface. In that study, a 1-nsec pulse was transmitted over a path of several tens of meters from a tower to the sea surface and then detected on its return. The return power was correlated with wave elevation for an illuminated patch about 1 meter in diameter and was found to be normally distributed to a high degree of accuracy. There were dropouts of the return signal when the illuminated patch was near zero elevation and was tilted on the side of a big wave, but these dropouts were so rare compared to the strong signals that came back when the surface was nearly level and near the mean (a property of a Gaussian sea surface) that the limited number of dropouts did not detectably alter the totals.

Given all the above, it simply needs to be noted that the portions of the transmitted signal that strike the sea surface above the mean elevation will start back to the altimeter sooner than those that travel on to the mean water level, and those that go past mean water level and strike the troughs of the waves will start back later. It is simply necessary to quantify these effects by means of an appropriate derivation of the form of $g(t - t^*)$.

In an elegant derivation, Longuet-Higgins [1963] has shown that equation 4 describes the probability density function correct to second order for points picked at random from a wavy surface.

$$p(\eta) d\eta = \frac{\exp{-(\eta^2/\sigma^2)/2}}{(2\pi)^{1/2}} \cdot \left[1 + \frac{\lambda}{6} \left(\frac{\eta^3}{\sigma^3} - \frac{3\eta}{\sigma} \right) \right] \frac{d\eta}{\sigma} \quad (4)$$

This *pdf* was obtained using the concept of cumulants and cumulant-generating functions,

220

and its form is intimately connected with the hydrodynamic equations that govern gravity-wave motion. Moreover, the parameters σ and λ are both obtained as operations on the wave spectrum.

This function has the following properties:

$$p(\eta) > 0$$

except for

$$1 + \frac{\lambda}{6} \left(\frac{\eta^3}{\sigma^3} - \frac{3\eta}{\sigma} \right) < 0 \quad (5)$$

(i.e., for large negative η). It is therefore almost a *pdf* under the usual definition. The negative area is extremely small and can be neglected for typical values of λ .

$$\int_{-\infty}^{+\infty} p(\eta) d\eta = 1 \quad (6)$$

(by inspection, since odd powers of η times the exponential function integrate to zero).

$$\int_{-\infty}^{+\infty} \eta p(\eta) d\eta = 0 \quad (7)$$

(The apt choice of the term in parentheses accomplishes this.)

$$\int_{-\infty}^{+\infty} \eta^2 p(\eta) d\eta = \sigma^2 \quad (8)$$

(by inspection) and

RETURN PULSE FROM SKYLAB ALTIMETER

$$\int_{-\infty}^{+\infty} \eta^3 p(\eta) d\eta = \lambda \sigma^3 \quad (9)$$

(again owing to the apt choice of the term in parentheses).

This function thus has essentially unit area, zero mean, a variance of σ^2 , and a skewness of λ . Figure 1 shows graphs of equation 4 for $\sigma = 1$ and $\lambda = 0, 0.3$, and 0.5 .

The term $\{1 + \lambda[(\eta^3/\sigma^3) - 3(\eta/\sigma)]/6\}$ equals 1 at $\eta = 0$ and at $\eta = \pm(3\sigma)^{1/2}$. It is less than 1 for $-\infty < \eta < -(3\sigma)^{1/2}$, greater than 1 for $-(3\sigma)^{1/2} < \eta < 0$, less than 1 for $0 < \eta < (3\sigma)^{1/2}$, and greater than 1 for $(3\sigma)^{1/2} < \eta < \infty$. The second-order nonlinear properties of waves are thus that deep troughs are less probable than would be expected from a normal density, shallow troughs are more probable, low crests are less probable, and high crests are more probable.

If part of the electromagnetic wave front strikes a small piece of the sea that is at a distance η away from the mean surface $\eta = 0$, the time it would have taken to travel from η to zero is given by

$$\eta = ct''$$

and the time it would have taken to travel from zero back to η is the same, so that the total time is

$$2\eta = ct'$$

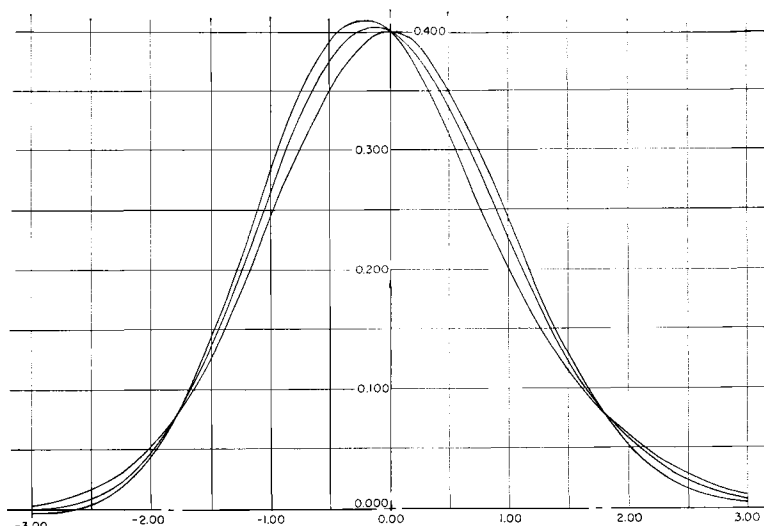


Fig. 1. Nonlinear wave elevation *pdf* for $\sigma = 1$ and $\lambda = 0, 0.3$, and 0.5 .

PIERSON AND MEHR

221

That part of the sea surface that is at a distance of η away from the mean thus shortens (or lengthens) the round-trip time by t' nanoseconds, if η is in meters and c is in meters per nanoseconds ($c = 0.3 \text{ m/nsec}$).

The probability distribution of these times is given by

$$p(t') dt' = \frac{1}{(2\sigma)^{1/2}} \frac{c}{2\sigma} \exp [-(ct'/2\sigma)^2/2] \cdot \left\{ 1 + \frac{\lambda}{6} \left[\left(\frac{ct'}{2\sigma} \right) - \frac{3ct'}{2\sigma} \right] \right\} dt' \quad (10)$$

The combined effect of all of the different elevations is given by a simple convolution and can be written as equation 2, where $g(t - t^*) = p(t - t^*) = p(t')$.

For $f_1(t)$ given by equation 1, the convolution can be evaluated analytically. For $f_2(t)$, which corresponds to the S193 altimeter design considerations, the convolution has been carried out on a computer. The analytical result for $f_1(t)$ is given by equation 11 for a pulse duration τ of 50 nsec, where $B = 2\sigma/c$.

$$F(t) = \frac{1}{(2\pi)^{1/2}} \frac{t}{50} \int_{-\tau/B}^{(50-t)/B} \exp(-\xi^2/2) d\xi + \frac{1}{(2\pi)^{1/2}} \int_{(50-t)/B}^{\infty} \exp(-\xi^2/2) d\xi + \frac{1}{(2\pi)^{1/2}} \exp[-(t^2/B^2)/2] \left[\frac{B}{50} - \frac{\lambda}{6} \frac{t}{50} \right] - \frac{1}{(2\pi)^{1/2}} \exp \left[-\frac{(50-t)^2/B^2}{2} \right] \cdot \left[\frac{B}{50} - \frac{\lambda}{6} \frac{(t-50)}{50} \right] \quad (11)$$

Graphs of equation 1 for a pulse length of 50 nsec, for an extreme skewness ($\lambda = 0.4$), and for $\sigma = 0.1, 1, 3$, and 4 are shown in Figure 2. These values of σ correspond to significant wave heights of 0.4, 4, 12, and 16 meters. The graph for $\sigma = 0.1$ is essentially the graph of equation 1. For $\sigma = 4$, however, the echoes from the sea surface begin to arrive as much as 40 nsec ahead of the time they would arrive from a flat but rough surface. Also, because of the wave troughs, full amplitude of unity is not reached until another 40 nsec after the 'no-wave' condition.

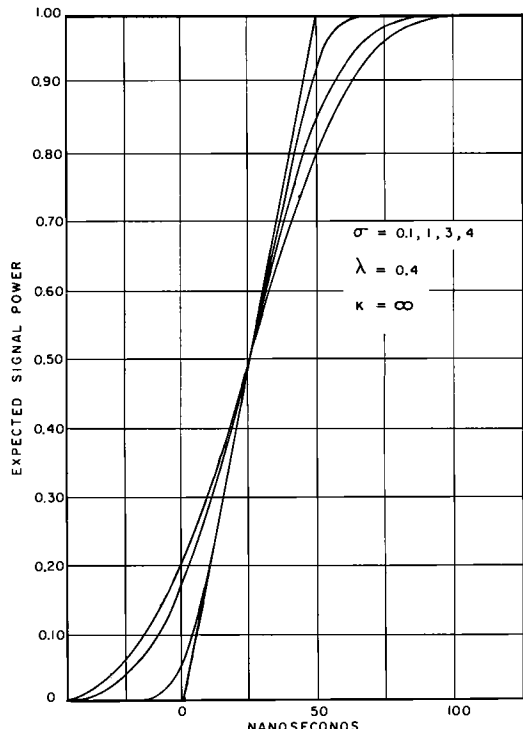


Fig. 2. Graph of equation 1 for $\sigma = 0.1, 1, 3$, and 4 and $\lambda = 4$.

The effects of waves on the average return pulse for the S193 altimeter are shown in Figures 3 and 4. Figure 3 shows the 50 nsec before zero arrival time and the first 200 nsec of the return pulse. The curve for $\sigma = 0$ gives the shape of the undisturbed pulse. For $\sigma = 4$, the signal is detectable out to 50 nsec ahead of the 'zero' time for no waves. Figure 4 shows the full pulse out to 600 nsec. The effect of the waves is to reduce the peak and to provide early returns as much as 50 nsec ahead of the true zero arrival line for a flat but rough surface. The function $f_2(t)$ discussed above is essentially the $\sigma = 0$ curve from Figure 3 and its continuation in Figure 4 past 200 nsec.

It is clear that the waves have to be fairly high before the pulse shape will be different from that for no waves. Genest [1970] reported measurements of pulse shapes from an aircraft that look quite a bit like those of Figures 3 and 4, but the data were obtained over such low waves that variations due to the waves are slight.

RETURN PULSE FROM SKYLAB ALTIMETER

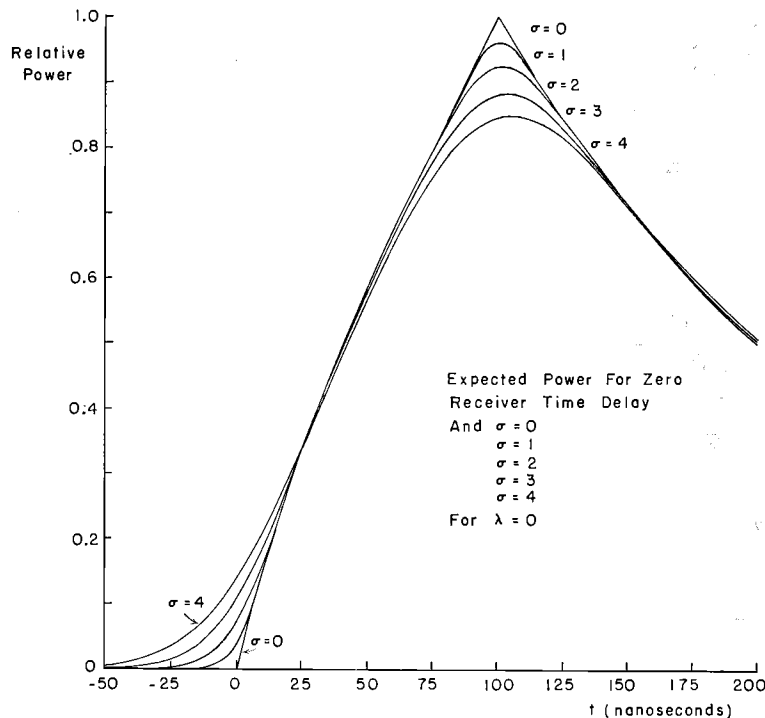


Fig. 3. Average return power for the S193 altimeter for various values of σ and no skewness for the first 200 nsec.

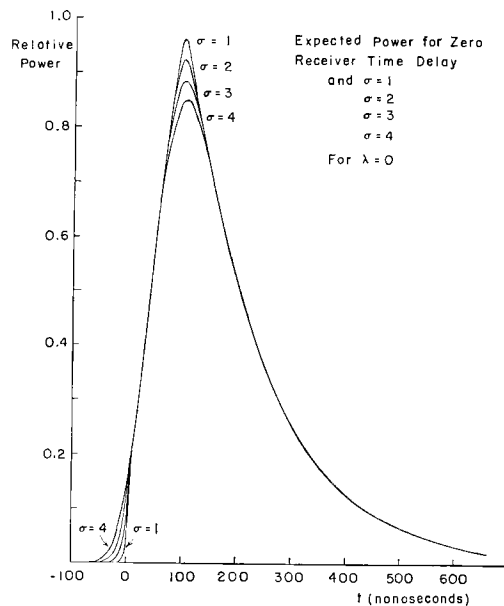


Fig. 4. Average return power for the S193 altimeter over the full range of time.

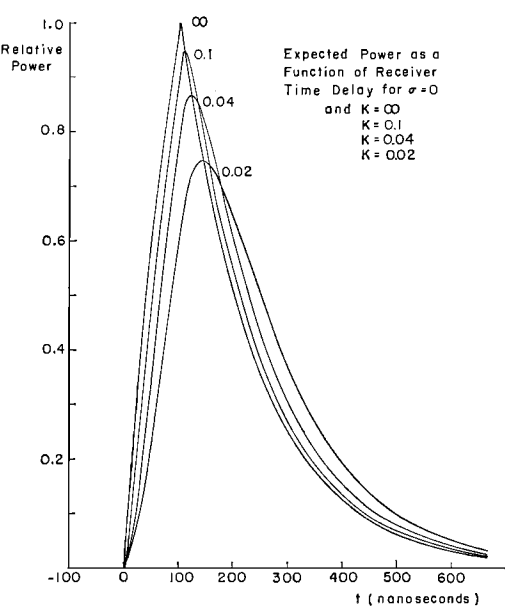


Fig. 5. Expected power as a function of receiver time delay for $\sigma = 0$ and various K .

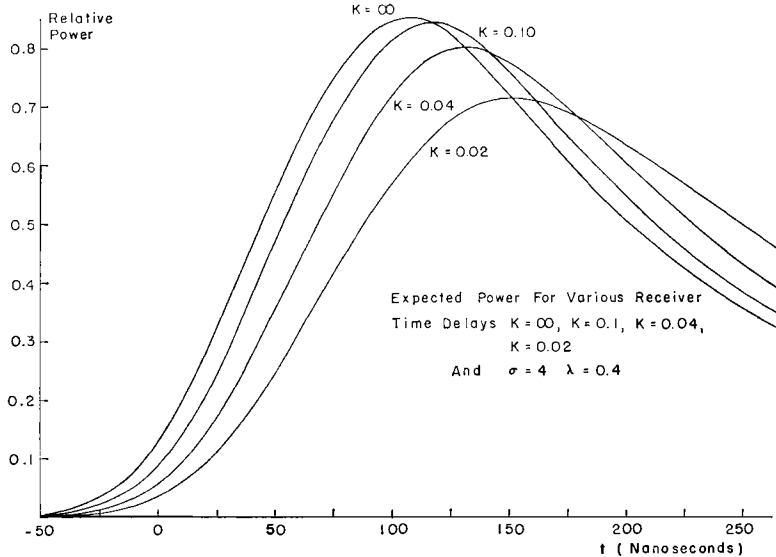


Fig. 6. Expected power for various receiver time delays and nonlinear waves with a significant wave height of 16 meters.

EFFECTS OF THE RECEIVER

As was described above, the signal that returns to the altimeter has to be detected before various kinds of circuits can be used to decide on the time elapsed between the transmission and return of the pulse. A mathematical model of this part of the altimeter is more in the province of electrical engineering than geophysics, and certainly more sophisticated models than the one to be used here need to be devised. Some of the effects of detection are illustrated, however, by a function of the form

$$h(t^* - t) = K \exp K(t^* - t) \quad -\infty < t^* < t \\ h(t^* - t) = 0 \quad t < t^* < \infty \quad (12)$$

to be applied to equation 3.

The parameter K can be thought of in terms of the bandwidth of the receiver. Infinite K yields the undisturbed signal, and as K decreases the receiver delays the signal more and more. The effect of K on the S193 altimeter signal is shown in Figure 5 for very small waves and various K 's and for very high nonlinear waves in Figure 6. Indications are that K is approximately 0.1 for the S193 altimeter.

RANGE DETECTION

The result of all these calculations is thus a set of curves representing the average, or expected, power as a function of time for a variety of wave conditions and receiver bandwidths. Once the final design is complete, the bandwidths will no longer change, but the waves will vary over a considerable range of σ and λ .

Based on the shape of these functions, there are many circuits that could be designed to decide on the exact time the pulse returned to the altimeter. One possible range decision method, for example, is threshold detection after the use of an automatic gain control circuit (AGC). In this method, the peak of the signal is normalized to a constant value by varying the gain of the detection circuit, and the pulse is decided to have arrived at the instant when the power first exceeds some part of the normalized peak, say 0.1 to 0.2 times the peak value. Decreasing bandwidth delays a decision of this nature, and increasing wave height advances a decision of this nature. For the idealized altimeter with the ramp step defined by equation 1 and a K of 0.10, a threshold detector at 0.1 would decide that the pulse returned 12 nsec early for waves with a σ of 3 meters (Figure 7).

RETURN PULSE FROM SKYLAB ALTIMETER

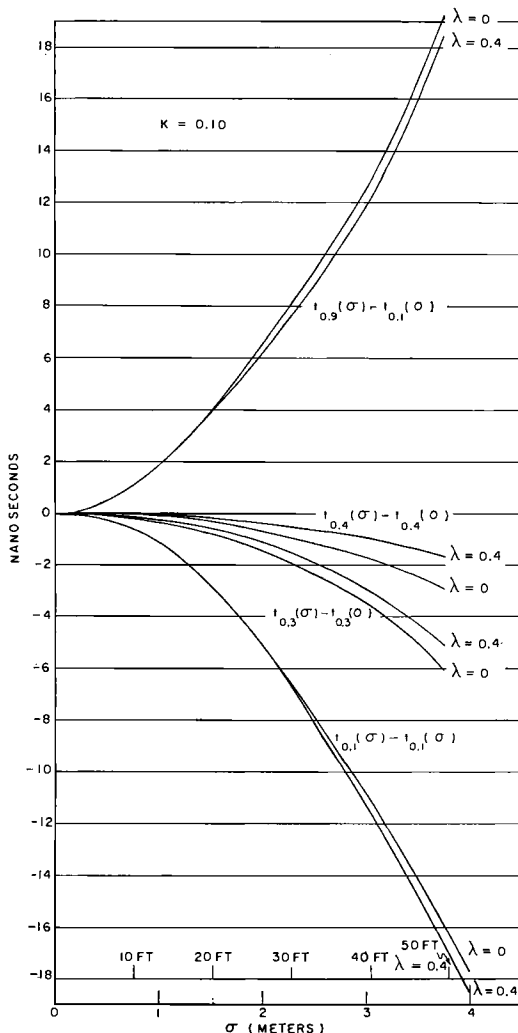


Fig. 7. Bias due to waves alone after removal of any constant receiver delay for threshold detection as a function of σ and λ ($K = 0.1$).

This would correspond to a bias of 12×15 cm or 1.8 meters, and the reported range would be too small by this amount. Other thresholds of 0.3, 0.4, and 0.9 are also illustrated after the effects due to everything in the design except the waves are removed.

The use of an automatic gain control circuit followed by threshold detection for the altimeter mode of S193, as shown by Figure 3, for a typical bandwidth would introduce little bias due

to waves for thresholds between about 0.4 and 0.6. For a threshold of 0.1, the bias would be a strong function of wave height.

For the S193 altimeter, the range tracking loop will operate in a rather unique way defined by a divided split gate. The tracking loop will shift back and forth so that the quantity $p(t)$ defined by equation (12) will be made close to zero.

$$p(t) = 2 \int_t^{t+100} F_w(t^*) dt^* - \int_{t+150}^{t+250} F_w(t^*) dt^* \quad (12)$$

This time, referred to the true pulse arrival time as zero, has been calculated for various receiver bandwidths and values of the parameter λ as a function of σ . The results for $K = 0.02$, 0.04, and ∞ are shown in Figure 8. For $K = \infty$, the arrival time decision for the pulse is biased early by about 28 nsec, or 4.2 meters. The additional effects of waves are very small; high waves with a highly nonlinear probability density function for elevation might decrease the bias by 15 cm.

For the actual S193 design, the results will be somewhere between those for $K = \infty$ and $K = 0.04$, so that the bias will be weakly de-

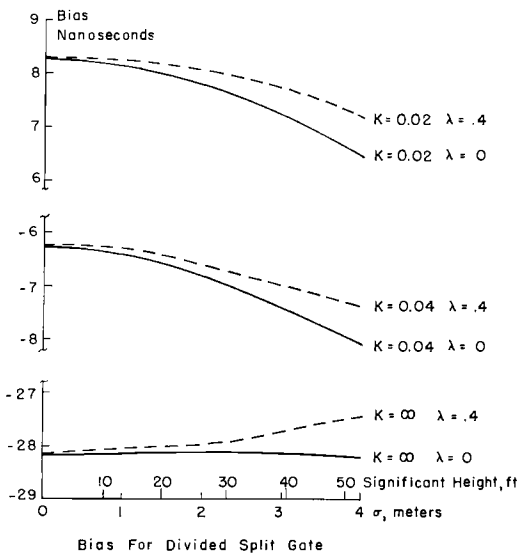


Fig. 8. Bias for the divided split gate on S193 as a function of σ and λ for various values of K .

PIERSON AND MEHR

225

pendent on wave height. The actual effects of the receiver and a more realistic convolution function need to be determined more carefully as the design of the altimeter proceeds. There is practically no bias as a function of wave conditions for the idealized return and a divided split gate as reported by *Pierson and Mehr* [1970].

WAVE VARIABILITY OVER THE OCEANS

The possible range of σ is documented in terms of the analysis of 2400 ocean wave records obtained by the Tucker shipborne wave recorder [Tucker, 1956] and analyzed at the National Institute of Oceanography in Great Britain. A report by *Draper and Squires* [1967] provides an analysis of conditions at Ocean Weather Ship *India* (59°N , 19°W) that can be used to interpret this study.

The relationship between significant wave height and the parameter σ is given in Table 1.

At Ocean Weather Ship *India*, the wave data gathered at NIO yield the results shown in Table 2. Spring and fall data are about halfway between the values given in Table 2.

OWS *India* is representative of the northwest part of the North Atlantic. For the 15 years of record, as of 1967, the highest recorded significant wave height was obtained on February 10, 1962. The significant wave height was estimated at 54.7 feet (16.7 meters), with a 90% fiducial confidence interval of 67.4 to 44.5 feet (20.5 to 13.6 meters), based on analysis techniques described by *Neumann and Pierson* [1966].

From Table 2, for example, it can be concluded that a σ of 2 meters would be exceeded about 13% of the time in the winter over this region of the North Atlantic. A σ of 4 meters

TABLE 2. Percentage of Time at OWS *India* That the Significant Wave Height Exceeded the Values Given

% of Time	Wave Height, feet		Wave Height, meters	
	Winter	Summer	Winter	Summer
100	3	0	0.9	0
90	8	3	2.4	0.9
80	9	4	2.7	1.2
70	10	5	3.1	1.5
60	12	6	3.7	1.8
50	14	7	4.3	2.1
40	16	8	4.9	2.4
30	19	9	5.8	2.7
20	21	9	6.4	2.7
10	28	12	8.5	3.7
1	42	20	12.8	6.1

would be expected once for 3 or 4 hours in 15 years, or so.

When high waves occur in the ocean, they extend over horizontal distances of several hundreds of kilometers at a given time. Thirty-foot (9.1-meter) waves and higher could easily cover an area 800 km on a side during the peak of an extratropical cyclone over the North Atlantic.

Extreme waves in the North Pacific have been described by *Rudnick and Hasse* [1971] on the basis of motion pictures made of high waves passing Flip. The significant wave height was estimated as 49 feet (14.9 meters).

The subtropical high regions in the two hemispheres would have waves 5 feet (1.5 meters) high, or so, and the trade-wind regions could have waves 6 to 12 feet (2 to 4 meters) high, depending on the local strength of the trades.

On a global basis, the southern oceans between Antarctica and 40°S during the southern hemisphere winter will have waves during the most intense cyclones in excess of 55 feet (16.8 meters). In the southern hemisphere summer, the wave-height distributions will be comparable to the summer values in Table 2 over large areas. The most valuable data for geodetic purposes will be obtained during the summer of each hemisphere.

The parameter λ requires a knowledge of the vector wave-number spectrum, presently

TABLE 1. Relationship between σ and Significant Wave Height

σ , meters	$H_{1/3}$, meters	$H_{1/3}$, feet
0.1	0.4	1.3
1	4	13.1
2	8	26.2
3	12	39.3
4	16	52.4

RETURN PULSE FROM SKYLAB ALTIMETER

REFERENCES

- poorly observed. For wind seas it can be about 0.4, and for swell it approaches zero. It can be estimated from wave hindcasting and forecasting methods on a global scale.
- #### THE ALTIMETER AS A WAVE RECORDER
- Data on waves from the open ocean are presently available only from a limited number of ships equipped with wave recorders. An additional data channel on an operational altimeter should make it possible to obtain information on wave height, along with the altimeter data. The difference in the times between a threshold detector at 0.1 and the times determined by the divided split-gate detector could be a measure of wave height. An operational altimeter that transmitted data after several orbits would, if desired, provide data on wave height over the oceans, say, every 100 km along the subsatellite track, yielding about 3000 measurements each day. These data would be of tremendous value in the development and improvement of computer-based wave-forecasting procedures as described by Pierson [1971].
- #### CONCLUDING REMARKS
- The analysis given above illustrates a procedure for predicting the form of the signals to be detected by the altimeter mode of S193. Based on the final design of the instrument, they need an additional iteration on a theoretical basis, especially with reference to the characteristics of the receiver. However, it is quite possible to predict the pulse forms that the instrument will detect well before Skylab is launched. The sample and hold circuits of the instrument will provide the data to verify these predictions. The variation in average return power as a function of wave conditions provides information on wave height, and serious consideration should be given to obtaining both range and wave-height information from an operational instrument.
- Acknowledgments.** The studies described in this paper have been sponsored by the Spacecraft Oceanography Project of the U.S. Naval Oceanographic Office under contract N63206-70-A-0075.0005.
- We thank Mr. T. Godbey for providing us with the design information on the S193 return pulse in the absence of waves and on the gating circuit. Discussions of this problem with him and with Dr. E. Posmentier were most helpful.
- Draper, L., and E. M. Squires, Waves at Ocean Weather Ship India (59°N , 19°W), *Trans. Roy. Inst. Nav. Architect.*, 109, 85–93, 1967.
- Ewing, G. (Editor), *Oceanography from Space*, Woods Hole Oceanographic Institution, Woods Hole, Mass., Ref. 65-10, 469 pp., 1965.
- Genest, E., Space geodesy aircraft experiment, final report, Raytheon Co., Sudbury, Mass., 1970.
- Godbey, T. W., Continuous orbital guidance system, unsolicited proposal to NASA, Gen. Elec. Co., Utica, N.Y., 1964.
- Greenwood, J. A., A. Nathan, G. Neumann, W. J. Pierson, F. C. Jackson, and T. E. Pease, Radar altimetry from a spacecraft and its potential application to geodesy, *Remote Sensing Environ.*, 1, 59–70, 1969a.
- Greenwood, J. A., A. Nathan, G. Neumann, W. J. Pierson, F. C. Jackson, and T. E. Pease, Oceanographic applications of radar altimetry from a spacecraft, *Remote Sensing Environ.*, 1, 71–80, 1969b.
- Kaula, W., et al., The terrestrial environment, solid earth and ocean physics, application of space and astronomic techniques, *NASA Contract. Rep. 1579*, 1970.
- Lee, H. L., The range error statistics of a satellite radar altimeter, *Tech. Rep. 112-2*, Remote Sensing Lab., Univ. of Kans. Center for Res., Lawrence, Kansas, 1969.
- Longuet-Higgins, M. S., The effect of nonlinearities on the statistical distributions of the theory of sea waves, 3, *J. Fluid Mech.*, 17, 459–480, 1963.
- Naugle, J. E., Opportunities for participation in space flight investigations, *Memo Change 33*, NASA, Washington, D.C., Dec. 22, 1970.
- Neumann, G., and W. J. Pierson, *Principles of Physical Oceanography*, Prentice-Hall, Englewood Cliffs, N.J., 1966.
- Pierson, W. J., Spectral wave forecasts, in *Proceedings of the 8th U.S. Navy Symposium on Military Oceanography*, U.S. Navy Postgraduate School, Monterey, Calif., 1971.
- Pierson, W. J., and E. Mehr, Bias errors in a divided gate tracking loop for a radar altimeter (abstract), *Eos Trans. AGU*, 51(4), 263, 1970.
- Rudnick, P., and R. W. Hasse, Extreme Pacific waves, December 1969, *J. Geophys. Res.*, 76(3), 742–744, 1971.
- Tucker, M. J., A shipborne wave recorder, *Trans. Inst. Nav. Architects*, 98, 236–250, 1956.
- Yaplee, B. S., A. Shapiro, D. L. Hammond, and E. A. Vliana, Nanosecond observations of the ocean surface from a stable platform, in *Proceedings of the Third Annual Earth Resources Program Review*, MSC 03742, Manned Space Center, NASA, Houston, Texas, 1970.

Accuracy of Satellite Radar Altimeter Measurements

ALAN H. GREENE

Raytheon Company, Wayland, Massachusetts 01778

Abstract. A K_u -band pulsed radar altimeter installed in a satellite can be used to measure instantaneous satellite altitude above the surface of the ocean to high accuracy. Major sources of measurement error can be grouped as follows: radar altimeter, propagation, and ocean surface and geometry. Each group contains random and bias errors. These are discussed and evaluated, the major emphasis being on residual errors that accrue from physical phenomena not under the control of the altimeter designer or user.

There is considerable interest in using a satellite-mounted radar altimeter to provide highly accurate measurements for mapping the shape of the ocean. Experimental radars on satellites of the near future, like Geos C, are expected to operate at K_u band (12.5 to 18 GHz) in a pulsed mode to gather ocean data. Each should yield information on ocean reflectivity and signal statistics, which will help in designing a highly accurate radar altimeter for satellite use. Such an altimeter system, providing refined information about the earth's gravity field and the oceans, could be ready for use by 1976 or 1977 [Hudson, 1971]. The accuracy goal for the experimental radars is less than 1 meter. For the advanced system, 10-cm accuracy is desired.

The sources of random and bias errors are discussed here. The magnitudes of these errors are estimated on the basis of available information.

SATELLITE RADAR ALTIMETER

The antenna diameter for the Geos C radar altimeter is limited to approximately 61 cm and is expected to be stabilized most of the time to within 1 deg of the local vertical. The frequency will be 13.9 GHz, which corresponds to an electromagnetic wavelength of 2.16 cm. The beamwidth therefore will be about 2 deg between half-power points.

The advanced radar is likely to incorporate the same basic parameters and be capable of pulse compression, accomplished, for example,

through dispersive delay lines, together with a modulated traveling wave tube (TWT) transmitter. The radar processor accepts the (compressed) video signal and derives from it average pulse shape and altitude (radar range) information by the use of sampling and tracking gates. The apparent ocean backscatter coefficient (σ^0) is implied by the AGC level.

Altitude is determined with a closed-loop tracker containing several gates for developing an error signal and a digital clock that precisely reads the position of the gates.

Major sources of altitude measurement error are: (1) radar, (2) propagation, (3) ocean surface and geometry. For each there are rapidly varying random components and slowly varying changes. Many of the latter can be made negligible by calibration. Those remaining can be considered bias errors.

Radar

Radar random errors are caused by thermal noise and instrumentation limitations. The principal instrumentation effect is timing jitter affecting transmitter trigger and relative tracker gate placement. In general, such instrumentation errors can be kept below other random effects. However, as accuracy requirements become more severe, the complexity and weight of instrumentation will rise rapidly. Bias errors are due to slowly varying drift of the timing clock or improper interpretation of tracking gate position with respect to true altitude. Both of these effects are related to geometric con-

siderations discussed below, and minimization of such errors depends upon good design and an accurate calibration technique that is independent of the radar altimeter system.

Propagation

Propagation errors can be considerable if uncompensated. Calculations based upon material given by *Barton and Ward* [1969] and *Bean and Dutton* [1966] show that tropospheric and ionospheric refraction effects can introduce a radar error of about 5 meters at 13.9 GHz, the major contribution being due to the troposphere. Most of this error can be removed if air pressure, temperature, and relative humidity at sea level are monitored near the region of the altitude measurement. The rms value of the residual error is then reduced to 8 cm at the specified frequency.

Ocean Surface and Geometry

The ocean surface appears to be quite rough at 13.9 GHz and causes each individual radar return pulse to have a random shape. Only the average of many pulse returns in a group can be predicted. The variation in return pulse shapes gives rise to a random error. The average shape is dependent upon radar design, sea state, orbital altitude, and satellite angular orientation. Although the influence of radar parameters, which are known for each mode, can be minimized by calibration, variations in sea state and geometry will be largely unpredictable, and therefore will introduce a bias error.

Certain errors cannot be removed by calibration. These are classed as either random or bias errors. The former include random effects due to radar internal noise, sea roughness, and propagation. The latter are due to uncertainties in sea state and instantaneous satellite orientation. It is apparent that the effects of propagation can be reduced to a negligible factor for the experimental systems. But in designing the advanced system, with its objective of 10-cm accuracy, we must, of course, recognize the 8-cm residual uncertainty that is now considered to be realistic.

RANDOM ERRORS

To gather precise altitude data, the leading edge of the return pulse must be tracked. The pulse from the ocean is detected with a matched

SATELLITE RADAR ALTIMETER ACCURACY

filter and a square-law envelope detector. The average leading edge of the detected waveform $v(t)$ is tracked with a closed-loop servo that develops its internal error signal using a three-gate leading-edge detector, or time discriminator. Tracking can be performed analog fashion, or, equivalently, raw data can be gathered in bunches and then processed by a computer that tracks via an appropriate algorithm. Figure 1 sketches representative waveforms and provides a functional diagram of the leading-edge detector.

If the transmitted pulse is rectangular, as illustrated, the envelope of the return, $v(t)$, will be approximately as shown, having a leading edge of about 2 pulse widths. For an idealized situation in which the impulse response of the ocean is a perfect step function, the tail of the return envelope remains constant with time. For real conditions, the tails of both the impulse response and the resulting detected return fall slowly toward zero as time becomes relatively large, owing to range attenuation, beam pattern, and ocean reflectivity. The leading edge of the average impulse response is slightly rounded owing to the randomness of the ocean surface. A good approximation to random variations can be obtained, however, assuming a single return pattern. An analytical description has been developed using a fixed waveform based upon the convolution of a rectangular transmitter

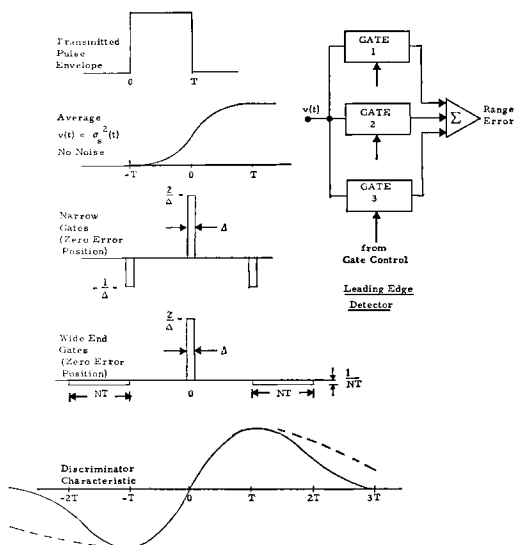


Fig. 1. Parameters of the signal processor.

ALAN H. GREENE

229

pulse envelope, a receiving filter matched to this waveform, and a step function for the impulse response of the ocean.

When the return waveform is passed through a three-gate detector, the error characteristic will take the general form illustrated in Figure 1. The gated detector is a device that takes the second difference of the return envelope in the region of the leading edge. As is shown, it is an approximation to the second derivative of the waveform. Two cases are shown. In the first, all gates are narrow with respect to a transmitted pulse width. In the second, the end gates have been widened to many times the transmitted pulse width. For each, the gains associated with the end gates are equal and the gain of the center gate is twice that of the others but with opposite sign, as is required by the second-difference criterion. These gains apply to the average of the signal in each gate, since instantaneous gain at a given gate is inversely proportional to gate width.

Error Equations

Analytical expressions have been developed for the single-pulse rms error of the leading-edge detector [Williams, 1970] on the basis of the following assumptions:

1. The matched filter output $x(t)$ consists of the ocean-return signal pulse $s(t)$ corrupted by receiver thermal noise $n(t)$. The signals $s(t)$ and $n(t)$ are each represented as narrow-band Gaussian processes, $n(t)$ being stationary, while $s(t)$ is not.

2. The means of $s(t)$ and $n(t)$ are zero.
3. The variance of $n(t)$ is the receiver noise power σ_n^2 .

4. The variance of $s(t)$ is $\sigma_s^2(t)$. It appears at the output of the square law detector in the absence of noise. A typical waveform is shown in Figure 1.

5. The autocorrelation function of $n(t)$, $R_{nn}(\tau)$, is determined by the matched receiver bandwidth and can be represented by

$$\phi_{nn}(\tau) = \sigma_n^2 \rho_n(\tau) \quad (1)$$

where

$$\rho_n(\tau) = 1 - |\tau/T| \quad |\tau| \leq T$$

$$\rho_n(\tau) = 0 \quad |\tau| \geq T$$

6. The autocorrelation function of $s(t)$, $R_{ss}(t_1, t_2)$, is determined by the transmitter bandwidth, the matched filter bandwidth, and the random nature of the ocean target. It is approximated by

$$\phi_{ss}(t_1, t_2) = \sigma_s(t_1)\sigma_s(t_2)\rho_s(t_1, t_2) \quad (2)$$

where

$$\rho_s(t_1, t_2) = \left[1 - \frac{|t_1 - t_2|}{2T} \right]^2 \quad |t_1 - t_2| \leq 2T$$

$$\rho_s(t_1, t_2) = 0 \quad |t_1 - t_2| \geq 2T$$

This formulation of ϕ_{ss} implies that random variations in wave height are negligible compared to the range equivalent of pulse width. For very narrow pulse widths, ϕ_{ss} will be wider than is indicated, since wave height becomes an important factor. Table 1 lists pulse width and equivalent range variation. If the range variation is interpreted as wave height, the sea state is given in the last column. When sea state grows to the value tabulated for a given pulse width, wave height can no longer be neglected.

The following accuracy formulas for observation of a single return result from the above assumptions. For narrow end gates, the rms error σ_{rn} in range is

$$\sigma_{rn} = \frac{cT}{4} \left(1 + \frac{3.23}{S/N} + \frac{3.18}{(S/N)^2} \right)^{1/2} \quad (3)$$

where c is the velocity of light, T is the transmitted pulse width, and S/N is the signal-to-noise ratio (N is equal to σ_n^2 , and S is the value of $\sigma_s^2(t)$ at the peak of the return waveform).

For wide end gates, the rms error, σ_{rw} , in range is

$$\sigma_{rw} = \frac{cT}{6} \left(1 + \frac{4}{S/N} + \frac{4}{(S/N)^2} \right)^{1/2} \quad (4)$$

Because the target return fluctuates, a significant error always exists no matter how high the signal-to-noise ratio. In the limit, the rms error is equivalent to half the pulse width for the narrow gates and one-third for the wide end gates, if wave height effects can be neglected. If not, as Table 1 indicates, accuracy is limited by the wave height. For example, a wave height of 4.5 meters implies that accuracy is no better than is indicated by the use of $T = 30$ nsec, even though the actual pulse

TABLE 1. Pulse Width versus Comparable Sea State

Pulse Width, nsec	Range Variation (Wave Height), meters	Equivalent Sea State
10	1.5	3 Moderate
20	3.0	5 Very rough
30	4.5	6 High
40	6.0	6-7
50	7.5	7 Very high
100	15.0	8 Precipitous

width may be narrower in equations 3 and 4. The effect described is equivalent to the rounding of the leading edge of the average impulse response. An exact treatment must consider the convolution of the leading edge with the pulse shape and receiver filter functions. For such an analysis, more accurate data on the impulse response of the leading edge than are currently available will be required.

When tracking is achieved, the error can be lessened by integrating the pulses. The ideal error, σ_{ri} , then becomes

$$\sigma_{ri} = \sigma_r / (n)^{1/2} \quad (5)$$

where σ_r is the applicable rms single pulse error, and n is the number of independent pulses integrated.

The number of pulses integrated is given by

$$m = f_r T_i$$

where f_r is the radar pulse repetition rate, and T_i is the integration time associated with tracker bandwidth.

Integration will not, however, improve the value of σ_{ri} if successive pulses are correlated and single-pulse S/N is reasonably high. The pulse repetition frequency f_{re} above which significant correlation begins to occur is given by

$$f_{re} = \frac{KV}{\lambda} \left(\frac{cT}{h(r_e + h)} \right)^{1/2} \quad (6)$$

where K is a constant in the neighborhood of 2, V is the satellite horizontal velocity, λ is the rf wavelength, r_e is the earth radius, and h is the satellite altitude.

The value of K depends on the pulse shape, receiver filter, beam pattern, and a precise definition of how much correlation is significant.

Equation 6 can be derived by application of the van Cittert-Zernike theorem, wherein a random surface, uniformly illuminated by a rectangular pulse, produces a spatial correlation distance that, when translated into time via the satellite velocity, results in a K of 1.64 [Born and Wolf, 1959]. When the receiver is assumed to have a filter matched to the transmitted rectangular pulse, the value changes to $K = 1.96$. If the transmitted pulse has a Gaussian shape and an appropriate matched filter is used, the effective surface area illuminated is increased and the value becomes $K = 2.5$.

In using (5), n is defined by

$$\begin{aligned} n &= m = f_r T_i & f_r < f_{re} \\ n &= f_{re} T_i & f_r \geq f_{re} \end{aligned} \quad (7)$$

For a satellite in circular orbit at 1000-km altitude, f_{re} is 1100 Hz with a 10-nsec pulse width (given $K = 2$). Wider pulse widths give correspondingly larger values of f_{re} .

In Figure 2, the ideal error is plotted versus S/N for an integration time of 0.5 sec and pulse widths of 10 nsec to 3 μ sec and a pulse repetition frequency of 1000 Hz, which is below f_{re} for even the narrowest pulse. Estimated maximum sea state [SS] for the accuracy at each pulse

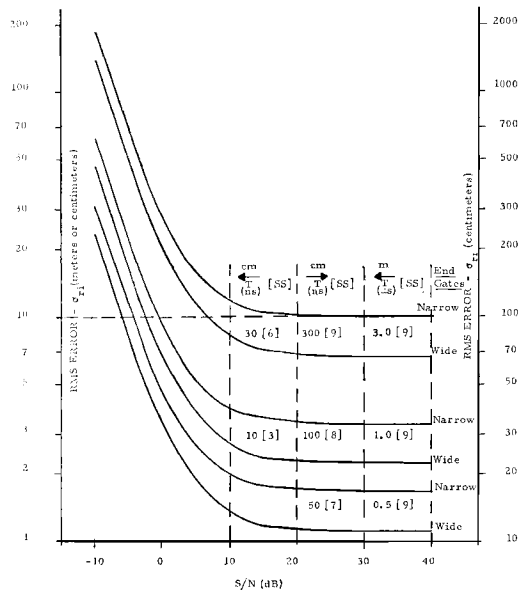


Fig. 2. Ideal random track error, $f_r = 1000$ Hz, $T_i = 0.5$ sec.

ALAN H. GREENE

231

width is given in brackets. It is clear that the most important factor affecting rms accuracy is pulse width, given a reasonably high S/N and a sufficiently calm sea. There is evidently no difficulty in meeting the experimental objective of less than 1-meter accuracy with a 100-nsec pulse, as far as errors due to the random surface are concerned. Better than 10-cm rms accuracy may be obtainable as well, but there are severe constraints in finding a suitable combination of parameters. Typical constraints are pulse repetition frequency limits imposed by equation 6, maximum integration time dictated by surface contours to be observed, sea state, and signal-to-noise ratio (S/N) achievable with a practical radar.

S/N Formation

To fully interpret the curves of Figure 2, the S/N for the altimeter must be determined. The formulas required are derived from the basic radar equation

$$\frac{S}{N} = \frac{P_t G^2 \lambda^2 \sigma}{(4\pi)^3 r^4 k T_a B N_F L_s} \quad (8)$$

where S/N is the signal-to-noise power ratio, P_t is the transmitted power, σ is the cross section of the radar target, r is the range to target, k is the Boltzmann constant, T_a is the absolute reference temperature of the receiver, B is the intermediate-frequency bandwidth in the receiver; N_F is the noise figure referred to T_a ; and L_s is the sum of all system losses.

Since the target is always directly below, we let $r = h$, where h is radar altitude above the ocean. The radar cross section is given by $\sigma = \sigma^* A$, where σ^* is the normalized backscatter coefficient, and A is the effective ocean surface area seen by the radar.

In addition, if pulse compression is used, the effective transmitted power is increased by the compression ratio (y). The basic radar equation for the altimeter is therefore

$$\frac{S}{N} = \frac{y P_t G^2 \lambda^2 \sigma^* A}{(4\pi)^3 h^4 k T_a B N_F L_s} \quad (9)$$

The surface area A is a function of radar beam geometry and transmitted pulse shape. To simplify calculations, it is assumed here that the direction of beam maximum is perpendicular to the ocean surface. Thus, effects of satellite

roll or pitch from nominal orientation must be estimated by calculations auxiliary to equations 8 and 9.

Two altitude regions must be recognized. These are pulse limited and beam limited. For the pulse-limited region, A is determined primarily by the width of the effective pulse as it spreads to its full extent upon the surface. For a given set of radar parameters, this condition exists for all altitudes h greater than the crossover altitude h_0 . For h below h_0 , the condition is said to be beam limited, since A is determined primarily by beam dimensions. These definitions apply strictly only for a symmetrical pencil beam shape and for the fixed satellite orientation mentioned above.

To calculate A as a function of altitude (h) and to find h_0 , we consider Figure 3. Because of beam symmetry, it is sufficient to examine only a vertical cross section. An ideal rectangular pulse shape of duration T is assumed. For cases where pulse compression is used, the rectangular shape is an approximation to the received compressed pulse. In the figure, O represents the center of the earth, S is the satellite position, and the hatched arc segment is the ocean surface. In addition, r_e is the earth radius, and $\Delta\theta$ is the 3-db antenna beam width. It can be shown that the apparent beam width for calculation of effective backscatter area is $\Delta\theta/[2 \ln(2)]^{1/2}$ [Probert-Jones, 1962]. Hence that angle is used in the diagrams. From the geometry, the following expressions for A can be derived:

Pulse limited

$$A = \pi h c T \left(\frac{r_e}{r_e + h} \right) \quad h > h_0, \quad (10)$$

$cT \ll h$

Beam limited

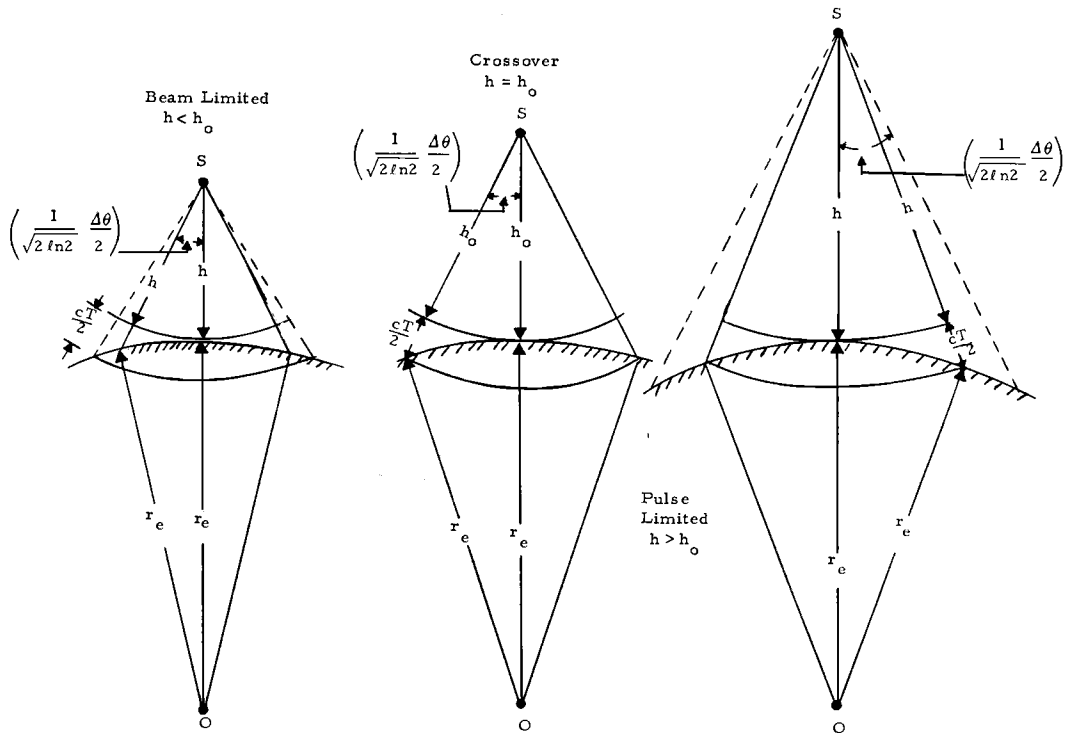
$$A = \pi h^2 \left(\frac{(\Delta\theta)^2}{8 \ln(2)} \right) \quad h < h_0, \quad (11)$$

$\Delta\theta \ll 1$

The crossover altitude is related to beam width and pulse width by

$$\left(\frac{\Delta\theta}{2} \right)^2 = \frac{(2 \ln 2) c T r_e}{h_0 (h_0 + r_e)} \quad cT \ll h \quad (12)$$

Substituting (10) into (9) and letting $B = 1/T$, where T is the compressed pulse width,

Fig. 3. S/N calculation geometry.

to indicate use of matched filter processing, results in the S/N ratio for the pulse-limited condition:

$$\frac{S}{N} = \frac{yP_t G^2 \lambda^2 \sigma^0 c T^2 \pi r_e}{h^3 N_F L_S k T_a (4\pi)^3 (r_e + h)} \quad h > h_0 \quad (13)$$

Similarly, substituting (11) into (9), and assuming matched filtering, gives the S/N ratio for the beam-limited condition;

$$\frac{S}{N} = \frac{yP_t G^2 \lambda^2 \sigma^0 (\Delta\theta)^2 T \pi}{h^2 N_F L_S k T_a (4\pi)^3 8 \ln 2} \quad h < h_0 \quad (14)$$

Noting that

$$G = (\pi d/\lambda)^2 \eta_a$$

$$\Delta\theta = 1.02\lambda/d$$

for a uniformly illuminated circular dish antenna, an alternate beam-limited expression is

$$\frac{S}{N} = \frac{yP_t d^2 \eta_a^2 \sigma^0 T \pi^2 (1.02)^2}{h^2 N_F L_S k T (512) \ln 2} \quad h < h_0 \quad (15)$$

where d is antenna diameter and η_a is antenna efficiency.

Numerical Calculations

Given the above relations, S/N has been calculated for the radar parameters listed below as an example of an experimental version. The earth's radius used is 6377 km, and the velocity of light is 3.0×10^8 m/sec.

$$P_t = 2 \text{ kw}$$

$$d = 59.0 \text{ cm}$$

$$f = 13.9 \text{ GHz}, \lambda = 2.16 \text{ cm}$$

$$G = 36.4 \text{ db}, \eta_a = 0.6$$

$$\Delta\theta = 2.15 \text{ deg}$$

$$kT_a = 4 \times 10^{-21} \text{ w/Hz}$$

$$\sigma^0 = +6.0 \text{ db}, \text{ assumed to be constant over the small angular region of interest}$$

$$N_F = 5.5 \text{ db}$$

$$L_S = 3.6 \text{ db for } y = 1, 4.1 \text{ db for } y > 1$$

Typical values of factors contributing to system loss appear in Table 2.

The S/N values calculated are listed in Table 3 for widths of 10, 50, and 100 nsec, and for 1.0 and 3.0 μ sec. For the narrower pulses, the S/N improvement due to pulse compression is included. Crossover altitudes are also listed.

ALAN H. GREENE

233

The angle between beam maximum direction and vertical has been designated θ_s . Thus the S/N for $\theta_s = 0^\circ$ apply for beam maximum pointing along the vertical. The last column gives values for a 1-deg variation in attitude of the satellite from vertical, an expected extreme situation. Examination of calculated radar impulse response for θ_s values of 0° and 1° suggests a signal-to-noise reduction of 5 db for very short effective pulses. For longer pulses, the variation should become less as the beam-limited condition is reached and exceeded. For a 1- μ sec pulse, the reduction has been estimated as 2 db. For the 3- μ sec pulse, it is probably negligible.

Comparison with Figure 2 illustrates that, on the basis of constraints of the radar example, the uncompressed 100-nsec pulse could meet the 1-meter criterion if rms error predominates over all others. The result is satisfactory for the worst case of narrow end gates and $\theta_s = 1^\circ$. Narrowing of pulse width does not improve rms errors because of S/N reduction. Substantial improvement in accuracy requires the use of pulse compression.

BIAS ERRORS

Variations in ocean reflectivity (related to variations in sea state) and changes in satellite orientation can cause bias errors to appear in altitude measurements. Such errors may be difficult to compensate, since independent accurate measures of the causes will be difficult to obtain routinely. The average return pulse shape has been modeled, and computerized results have been obtained to assess the perturbing effects. The model assumes that the impulse response of the ocean has an initial nonzero

TABLE 2. Radar System Losses

Factor	Loss, db
<i>Equipment losses</i>	
Duplexer (transmit)	0.4
Waveguide (duplexer to antenna, 2-way)	0.1
Waveguide (duplexer to tunnel diode amplifier)	0.1
Duplexer (receive)	1.2
Receiver matching loss $y = 1$	0.5
$y > 1$	1.0
Totals $y = 1$	2.3
$y > 1$	2.8
<i>Propagation losses (2-way)</i>	
Tropospheric attenuation	0.3
Moderate rain	0.8
Clouds	0.2
Total	1.3
Total losses (L_S) $y = 1$	3.6
$y > 1$	4.1

value. This assumption may be somewhat in error, but a quantitative description of the relationship of slope of the leading edge of the average impulse response to sea state depends upon the results of experiments yet to be performed. This possible source of error has been ignored, although once verified it can be easily added to the evaluation technique described below.

Return Waveform Simulation

It has been shown by *Moore and Williams* [1957] that the following holds for a flat earth:

$$\langle P_r(t) \rangle = \frac{\lambda^2}{(4\pi)^3} \cdot \int_{A(t)} \frac{P(t - 2r/c) G^2(\theta, \phi) \sigma^0(\theta, \phi) dA}{r^4} \quad (16)$$

TABLE 3. Experimental Altimeter Signal-to-Noise Ratios
($h = 1000$ km)

Compressed Pulse, nsec	Compression Ratio	Transmitter Pulse, nsec	Cross Alt. (h_0), km	S/N [$\theta_s = 0^\circ$], db	S/N [$\theta_s = 1^\circ$], db
3000	1	3000	2550	34.3	34.3
1000	1	1000	1010	29.5	27.5
100	1	100	118	9.5	4.5
100	30	3000	118	23.8	18.8
50	1	50	59	3.5	-1.5
50	60	3000	59	20.8	15.8
10	1	10	11.8	-10.5	-15.5
10	300	3000	11.8	13.8	8.8

SATELLITE RADAR ALTIMETER ACCURACY

where $\langle P_r(t) \rangle$ is the average power in the return waveform as a function of time (t), A is the area illuminated on the surface, θ is the angle to element of area dA , referred to local vertical, ϕ is the angle between two vertical planes containing the satellite, one a reference plane, the other containing the line of direction from satellite to area element dA , $G(\theta, \phi)$ is the antenna gain pattern referred to local vertical; $\sigma^0(\theta, \phi)$ is the normalized backscatter coefficient of the ocean; $P(t)$ is the wave shape of transmitted power, and t is the time after start of transmitted pulse.

Note that $G(\theta, \phi)$ is a function of both antenna pattern and satellite orientation. The antenna pattern normally has circular symmetry about its boresight axis, so that the gain can be expressed as $G(\theta_a)$, where θ_a is the angle off the boresight axis. Then

$$\cos \theta_a = \cos \theta \cos \theta_s + \sin \theta \sin \theta_s \cos \phi \quad (17)$$

where θ_s is the angle between antenna boresight and vertical. Hence $G(\theta, \phi)$ can be computed if θ_s is supplied.

Following the treatment of *Moore and Williams* [1957], but adapting to a spherical earth, we obtain for equation 16

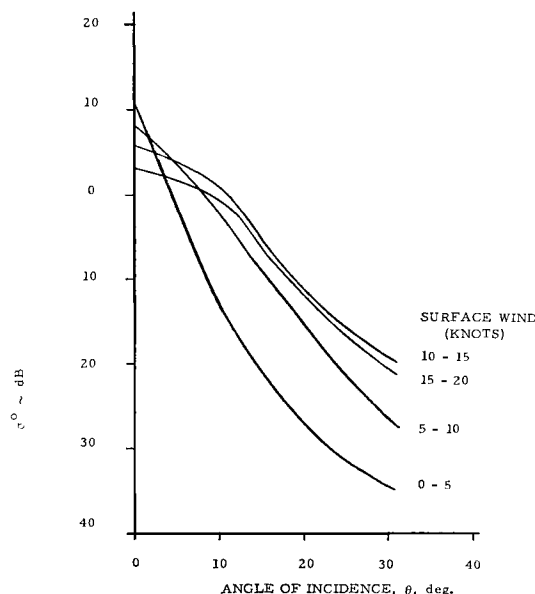


Fig. 4. Estimated σ^0 versus angle of incidence for various surface wind speeds at 13.9 GHz.

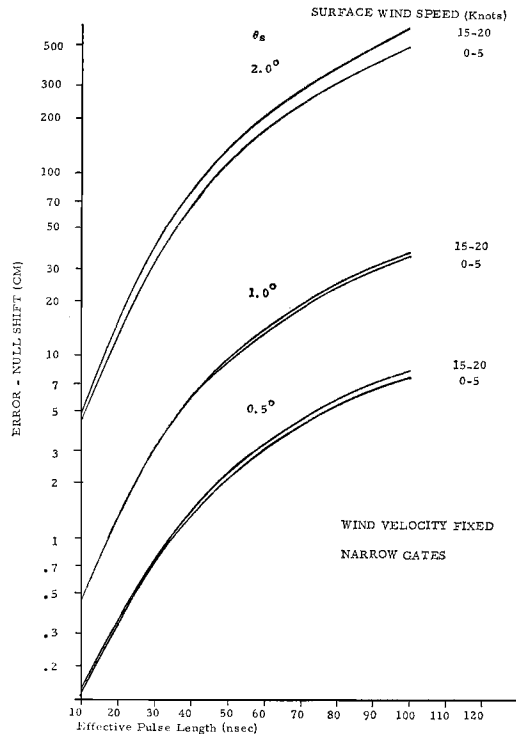


Fig. 5. Discriminator null shift for θ_s variations from 0° , narrow end.

$$\begin{aligned} \langle P_r(t_1) \rangle &= \left(\frac{r_e}{h + r_e} \right) \frac{c\lambda^2}{2(4\pi)^3} \\ &\cdot \int_0^{2\pi} \int_0^{t_1} \frac{P(t_1 - \tau) G^2(\theta, \phi) \sigma^0(\theta, \phi)}{r^3} d\tau d\phi \end{aligned} \quad (18)$$

where $t_1 = t - (2/c)h$ is time measured from the instant when the beginning of the transmitted waveform is returned from the nearest point (at altitude h). This can be rewritten as

$$\langle P_r(t_1) \rangle = \int_0^{t_1} P(t_1 - \tau) B_s(\tau) d\tau \quad (19)$$

The effect of the radar receiver filter must be included when equation 19 is evaluated. The ocean surface is random and the rf wavelength is very small compared to the surface diameter covered by a single narrow pulse (e.g., for 1000-km altitude, a 10-nsec pulse illuminates a surface area with diameter 1.02 km; see equation 10). To obtain the average power-return waveform, the receiver filter impulse response can therefore be convolved in an order different

ALAN H. GREENE

235

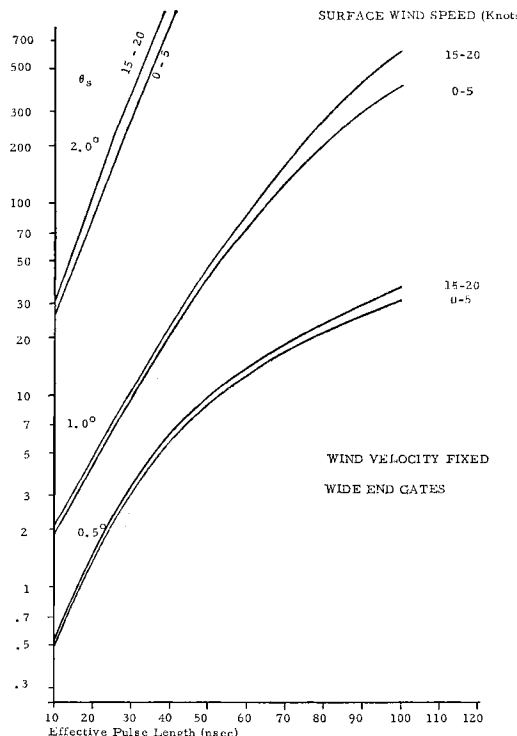


Fig. 6. Discriminator null shift for θ_s variations from 0° , wide end.

from what a cursory examination of the geometry would indicate. $P(t)$ then becomes the power wave shape of the transmitted waveform as modified by the receiver filter characteristic. If the altimeter is properly designed, $P(t)$ will be the result of passing the transmitted signal through the proper matched filter. For pulse compression, for example, $P(t)$ represents the compressed waveform obtained after passing the received signal from a point target through the compression filter and a square law detector.

The impulse response function of the ocean to the radar altimeter is given by

$$B_s(\tau) = \left(\frac{r_e}{h + r_e} \right) \frac{c\lambda^2}{2(4\pi)^3 r^3} \int_0^{2\pi} G^2(\theta, \phi) \sigma^0(\theta, \phi) d\phi \quad (20)$$

$$\tau \geq 0$$

$$B_s(\tau) = 0 \quad \tau < 0$$

The simulation computes equation 19 on a digital computer for specified functions G , σ^0 , and P . Note that r can be expressed either as a function of t or θ from the geometry. In the simulation, r is first expressed in terms of θ so that $B_s(\theta)$ is obtained. Since

$$\tau \cong \frac{\theta^2 h}{c} \left(\frac{h + r_e}{r_s} \right) \quad (21)$$

$B_s(\tau)$ is used to carry out the convolution of equation 19.

Bias Calculations

Using the altimeter parameters listed above, bias errors have been evaluated for combinations of the following: pulse lengths of 10, 50, and 100 nsec; σ^0 for wind speeds of 0-5 and 15-20 knots at the ocean surface; $\theta_s = 0, 0.5, 1.0$, and 2.0 deg. All transmitted pulses are rectangular and are received through an appropriate matched filter. The σ^0 is taken from Figure 4, and is based on Grant and Yaplee data [Skolnick, 1970] interpolated to 13.9 GHz. A θ_s of 1.0 deg swings the antenna boresight about one-half beamwidth from vertical. This causes considerable distortion of the return pattern. A 2 -deg swing causes major changes.

Calculated bias errors are shown in Figures 5, 6, and 7. The simulation was used to generate

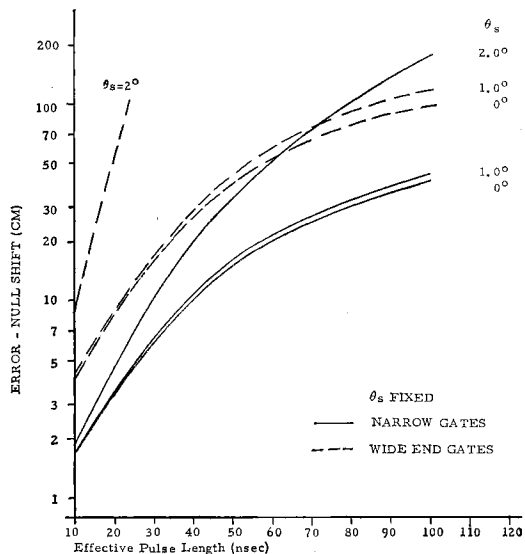


Fig. 7. Discriminator null shift for surface wind change from 0-5 to 15-20 knots.

SATELLITE RADAR ALTIMETER ACCURACY

the return waveform $v(t)$. This was then passed through a three-gate processor modeled on the computer, and the position of the set of gates was found for the null. The gate configurations illustrated in Figure 1 were used. For the narrow gates, a single point on the return waveform was selected by each gate for processing. For the wide end-gate group, the center gate selected a single point, and the end gates were chosen such that $N = 6$, so that averaging occurred over six times the pulse width.

Figures 5 and 6 show the relative error due to satellite swings from the vertical for fixed values of sea state (wind velocity). The effect of the sea state is small, showing the relative independence of the θ_s and sea-state effects. Marked improvement is obtained with pulse width and end-gate narrowing. Also, errors

climb rapidly once the half beam width point ($\theta_s = 1^\circ$) is exceeded, owing to severe distortion of the impulse response.

Figure 7 displays the effect of changes in wind velocity for fixed values of θ_s . For θ_s within a half beam width, wind velocity changes are relatively independent of θ_s . This independence disappears, however, for larger values of θ_s . The marked advantages of narrow gates and pulses are equally evident for this display of the data.

Figure 8 gives the convolved signal waveform $v(t)$ and related discriminator outputs for both narrow and wide end gates. Pulse length is 100 μ sec, wind velocity 0–5 knots, and antenna orientation vertical. The discriminator curve abscissa is the relative time of the leading edge of gate 3 (see Figure 1). The further

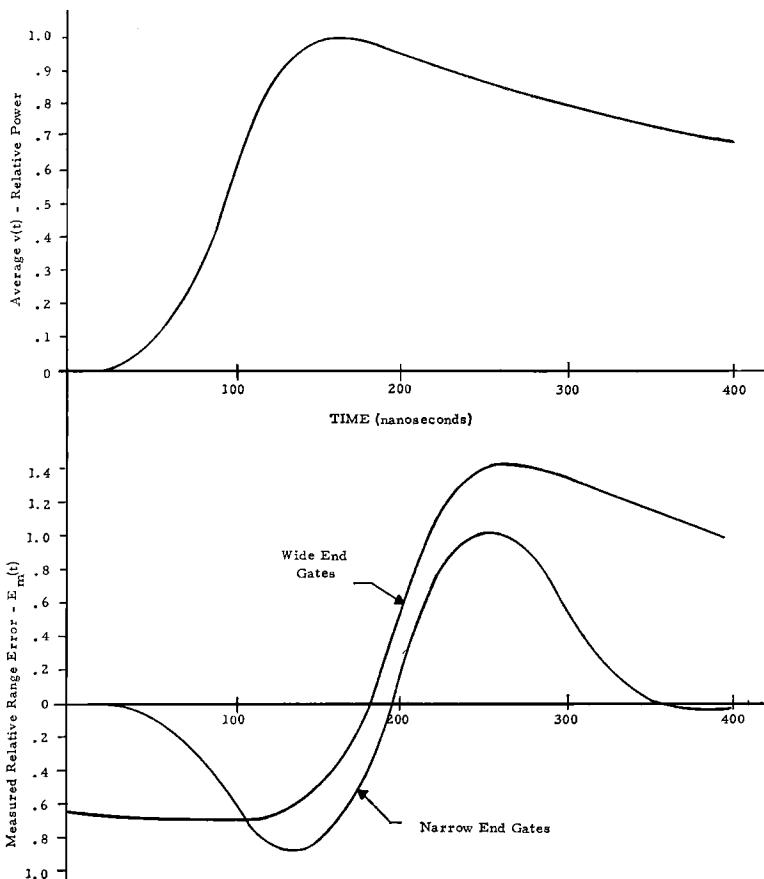


Fig. 8. Average return pulse shape and discriminator characteristic. Wind speed, 0–5 knots; effective pulse length, 100 nsec; $\theta_s = 0$.

ALAN H. GREENE

237

TABLE 4. Comparison of Errors Caused by Narrow and Wide End Gates

Pulse Width, sec	Pulse Compression (y)	Narrow End Gate		Wide End Gate	
		rms Error, cm	Bias Error, cm	rms Error, cm	Bias Error, cm
100	1	53	±50	38	±300
50	1	58	±15	43	±50
20	150	7.4	±3	5.0	±8

displacement to the left with wide end gates results from gate 3 integrating a large part of the tail. In general, the greater sensitivity of the wide-gate discriminator to parameter variation is due to this factor, since a large proportion of impulse response changes are reflected in the tail of the $v(t)$ waveform.

SUMMARY AND CONCLUSIONS

Figures 5, 6, and 7 show that narrow end gates are much to be preferred over wide end gates when small bias errors are desired. The bias effect often outweighs the opposite trend for rms errors illustrated in Figure 2. Each type of error is reduced, however, by narrowing the pulse width until limitations due to sea state occur. The effect of limitations in the sea state upon rms errors appears to dictate a minimum pulse width of approximately 20 nsec, assuming that sea states up to 5 are frequently encountered.

For the radar example chosen, the relative values of both types of error are illustrated in Table 4. S/N values for the worst case were chosen in calculating rms errors. It appears that an error of less than 1 meter can be achieved without pulse compression if a 50-nsec pulse is used with narrow end gates. Other error sources will not add greatly to those tabulated. Propagation errors, when compensated, have been estimated at 8 cm rms. Errors of available instrumentation have been estimated at 20 cm rms [Stanley *et al.*, 1971]. Absolute calibration may be a problem, but the desired relative accuracy of measurements appears to be feasible.

The operational objective of 10 cm is a more formidable goal. The 20-nsec compressed pulse width may permit the goal to be approached. Propagation errors currently estimated at 8 cm

rms are a problem. Further experimental and analytical information on ocean radar returns is needed. It is clear that the effort will require a very careful tradeoff of all processing parameters, considerable attention to stable timing circuitry, and the development of a precise calibration technique to eliminate instrumentation and processing biases.

Acknowledgments. I wish to thank L. K. Williams and W. Fordon for useful information on error sources, and E. F. Hudson for a helpful critical review. I am particularly indebted to F. C. Benham, who developed the simulation for bias errors and provided the data reported.

REFERENCES

- Barton, D. K., and H. R. Ward, *Handbook of Radar Measurement*, Prentice-Hall, Englewood Cliffs, N. J., 1969.
- Bean, B. R., and E. J. Dutton, *Radio Meteorology*, NBS Monogr. Ser., vol. 92, U.S. Government Printing Office, Washington, D.C., 1966.
- Born, M., and E. Wolf, *Principles of Optics*, Pergamon, New York, 1959.
- Hudson, E. F., A geodetic and oceanographic satellite altimeter system, paper presented at AIAA Space Systems Meeting, Denver, Colo., 1971.
- Moore, R. K., and C. W. Williams, Jr., Radar terrain return at near vertical incidence, *Proc. IRE*, 45(2), 228-238, 1957.
- Probert-Jones, J. R., The radar equation in meteorology, *Quart. J. Roy. Meteorol. Soc.*, 88, 485-495, 1962.
- Skolnick, M. (Ed.), *Radar Handbook*, chap. 26, p. 9, McGraw-Hill, New York, 1970.
- Stanley, H. R., N. A. Roy, and C. F. Martin, Rapid global geoid mapping with satellite altimetry, this volume, 1972.
- Williams, L. K., A Comparison of leading edge processors for the Geos C altimeter, *Tech. Memo. LKW-5*, Raytheon Co., Advan. Develop. Lab., Wayland, Mass., June 2, 1970.

Geodesy with Orbiting Gravity Gradiometers

ROBERT L. FORWARD

Exploratory Studies Department

Hughes Research Laboratories, Malibu, California 90265

Abstract. A new instrument for sensing the earth's gravity field, the rotating gravity gradiometer, has been demonstrated in the laboratory. A design with sensitivity adequate for geodesy from low earth orbit is under development by NASA. The gravity gradiometer measures the gradient of the gravity force field rather than the field itself. The sensor does not respond to acceleration and can operate in free fall or in accelerating environments where the usual gravity meters cannot work. A gradiometer in a spin-stabilized satellite in a low polar orbit will make a significant contribution to the geodetic mapping program presently being carried out by satellite tracking, since it preferentially senses the higher harmonics (>35) of the earth's field, where the Doppler tracking signals fall off rapidly.

ROTATING GRAVITY GRADIOMETER

The rotating gravity gradient sensor that has been developed at the Hughes Research Laboratories [Bell, 1970] is a device for measurement of the second-order gradient of the total gravity potential field. Since the instrument concept has been described in detail in other publications (see references given by Bell [1970]), we will only briefly outline its basic characteristics in this paper. The sensor configuration consists of a resonant cruciform mass-spring system with a torsional vibrational mode (see Figure 1). In operation, the sensor is rotated about its torsionally resonant axis at an angular rate ω that is exactly one-half the torsional resonant frequency. When a gravitational field is present, the differential forces on the sensor resulting from the gradients of the gravitational field excite the sensor structure at twice the rotation frequency [Forward, 1965]. Only the differential torque ΔT between the sensor arms at the doubled frequency is coupled into the sensor output. Piezoelectric transducers attached to the central torsional flexure suffice to convert the gravitationally induced differential torques into measurable voltages.

STATUS OF INSTRUMENTATION

The objectives of our initial research programs were to investigate the engineering feasi-

bility of the basic sensor concept, to develop sensor structures that would operate at a high sensitivity level both in free fall and in $1 G$ environment, to measure the sensor's sensitivity to gravitational fields, and to investigate the sources of noise produced by the rotation of the sensor. A torsionally flexible structure utilizing piezoelectric readout was found to be a suitable design and offers a significant improvement over other possible gradiometer designs (see extensive bibliography given by Bell [1970]). It has demonstrated the capability of being operated in an earthbound laboratory environment while maintaining a high sensitivity and low signal-to-noise ratio. The present noise level of this sensor is ± 1 Eotvos unit (EU) = 10^{-9} gal/cm (1 σ at an integration time of 10 sec) and is limited by background noise in the laboratory. Using this sensor, we recently carried out an experimental simulation, measuring in real time gravity gradient fields that had exactly the same magnitude and time variation as the gravity gradient signals that would be expected from an orbiting vehicle around the moon [Bell, 1970].

One of our programs, to begin shortly under NASA sponsorship, is for the design of an earth-orbiting gravity gradient sensor (Figure 2). For the orbital case, the optimum method is to fabricate a sensor with a relatively low resonant frequency (2 to 8 Hz), attach it directly to the

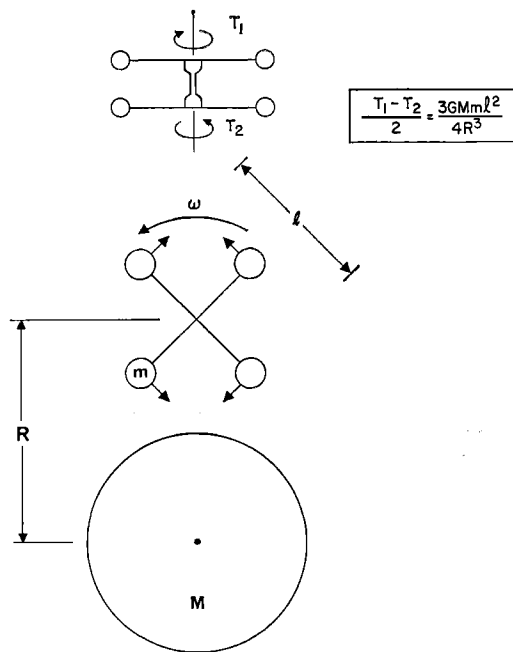


Fig. 1. Method of operation of torsional gravity gradiometer.

spacecraft, and spin the spacecraft itself at the desired spin speed (1 to 4 rev/sec). This mode of operation has two significant advantages. There are no bearing noise problems, which are the primary source of difficulty in earthbound operation, and, most important, since the spacecraft is rotating along with the sensor, the gravity gradient field of the spacecraft is stationary in the frame of reference of the sensor and the sensor does not sense the gravity field of the spacecraft, only the gravity gradient field of the earth. The objective of the program is to develop a sensor system capable of measuring gravitational gradients at a level of 0.01 EU with a 30-sec integration time.

The effective resolution of a gradiometer at an altitude of 250 km is approximately 250 km. If a gradiometer were placed in a near polar orbit with suitably chosen orbital parameters, it would pass within 250 km of every point on the earth in 80 orbits, thus completely mapping the earth in 5 days.

GEODESY WITH ORBITING GRADIOMETERS

The application of orbiting gravity gradient sensors to geodesy is straightforward. An ob-

ORBITING GRAVITY GRADIOMETERS

jective of geodesy is to determine the variations of the earth's gravitational potential, which can be expressed in terms of spherical harmonics:

$$V = \frac{GM}{r} \left[1 + \sum_{n=2}^{\infty} \left(\frac{a}{r} \right)^n \sum_{m=0}^{\infty} P_{nm}(\sin \phi) \cdot \{ C_{nm} \cos m\lambda + S_{nm} \sin m\lambda \} \right] \quad (1)$$

where a is the mean radius of the earth, P_{nm} is the normalized Legendre polynomial, C_{nm} and S_{nm} are the coefficients of the harmonic terms, and (r, ϕ, λ) are the coordinate positions of the instrument.

In the present satellite geodesy programs, orbital perturbation methods of obtaining the gravitational potential harmonics have led to the determination of the harmonics through the fourteenth degree and order [Rapp, 1968]. In theory, this technique can be extended to obtain all higher orders of the gravitational potential; however, it is anticipated that it will be difficult to obtain the higher-order components [Kaula, 1970].

The advantage of gradiometer techniques in obtaining the higher-order harmonics of the earth's gravitational field is straightforward. Terms with increasing n correspond to small-scale features on or near the surface. Although the contribution of these harmonic components to the gravitational potential is quite small, their contribution to the gravitational force gradient at a point above them is a substantial fraction of the gravitational gradient of the entire earth.

To illustrate the behavior of the gravitational force gradient, let us examine the gradient that is predicted for higher orders of n . A typical term in the gravitational potential

$$V_{nm} = (GM/a)(a/r)^{n+1} P_{nm}(\sin \phi) C_{nm} \cos m\lambda \quad (2)$$

gives rise to a radial gravity of

$$g_r = \frac{\partial V}{\partial r}$$

$$= (n+1) \frac{GM}{a^2} \left(\frac{a}{r} \right)^{n+2} P_{nm} C_{nm} \cos m\lambda \quad (3)$$

and a radial gravity gradient of

ROBERT L. FORWARD

241

$$\Gamma_{rr} = \frac{\partial^2 V}{\partial r^2} = (n+1)(n+2) \cdot \frac{GM}{a^3} \left(\frac{a}{r}\right)^{n+3} P_{nm} C_{nm} \cos m\lambda \quad (4)$$

The present technique for measurement of the gravitational field from orbit utilizes Doppler velocity tracking of the orbiting vehicle, either from the ground or from other spacecraft. The part of the differential Doppler velocity due to the higher orders of the gravitational field is given by the time integral of the acceleration field. For the radial Doppler velocity, we take the time integral of the radial acceleration

$$\Delta v_r = \int g_r dt = \frac{n+1}{n} \frac{GM}{av} \left(\frac{a}{r}\right)^{n+2} P_{nm} C_{nm} \sin m\lambda \quad (5)$$

where we have used the fact that the maximum spatial periodic variation ($m = n$) has a time variation due to the orbital velocity v given by

$$\cos_{\max} m\lambda = \cos n\lambda$$

$$= \cos \left(n \frac{x}{a} \right) = \cos \left(\frac{nv}{a} t \right)$$

If we assume that the strength of the components follows the statistical law $\langle S_{nm} \rangle \sim \langle C_{nm} \rangle \sim 10^{-5}/n^2$ [Kaula, 1968], and that $(2n+1)$ terms contribute to each degree, we can calculate the Doppler velocity, gravity, and gravity gradient as a function of the harmonic degree. These are plotted in Figure 3 for 250-km altitude.

The Doppler velocity data in Figure 3 are correct, although they differ by 2 orders of magnitude from what would be calculated from

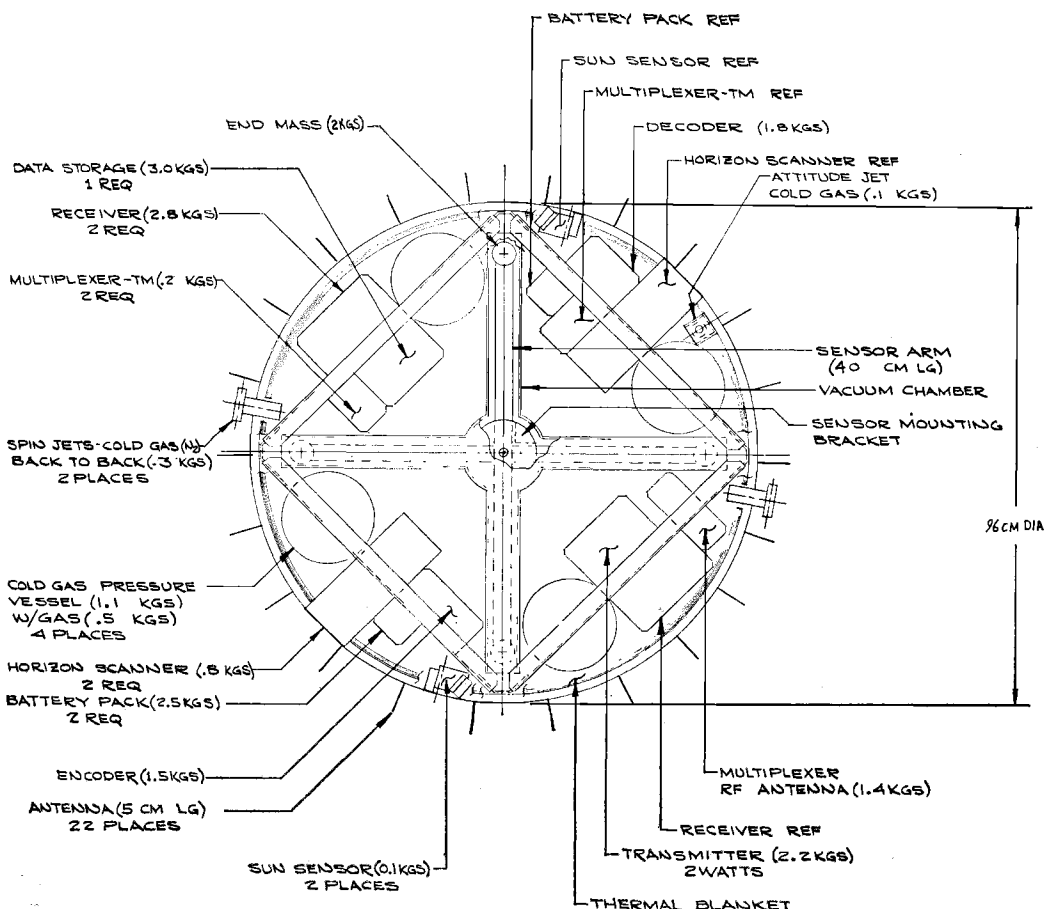


Fig. 2. Spacecraft configuration for earth geodesy experiment.

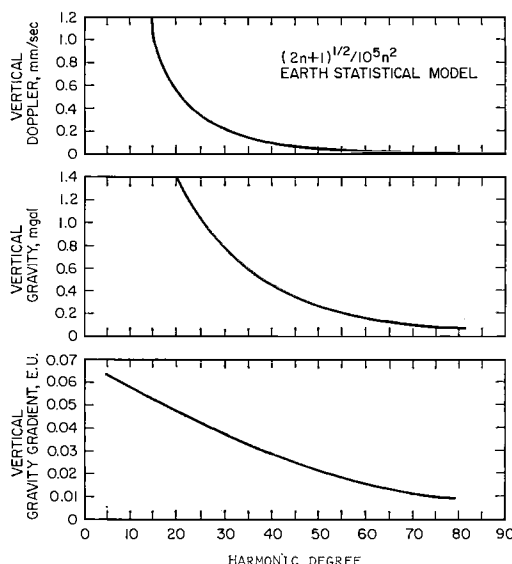


Fig. 3. Vertical Doppler velocity, gravity, and gravity gradient in 250-km orbit.

Figure 5-7, page 5-28 of the Williamstown report [Kaula, 1970] as presently published. Recently Kaula (private communication, 1971) has brought to our attention the fact that the right-hand ordinate of Figure 5-7 in the Williamstown report should read 10^{-2} mm/sec rather than mm/sec.

Figure 3 indicates that if satellite-to-satellite Doppler tracking techniques attain their anticipated sensitivity level of 0.05 mm/sec at 30 sec, Doppler tracking will be able to extract gravity data up to degree 50, and if a gravity gradiometer with an 0.01-EU sensitivity at 30 sec can be flown it will contribute significant information out to degree 75. The comparative signal-to-noise of the two techniques crosses over at degree 35. We thus see that the two techniques are complementary rather than competitive, since below degree 35 Doppler tracking has a better signal level, whereas above degree 35 the gradiometer gives better data.

The average strength of the higher-order gravity variations predicted in our Figure 3 and in Figure 5-7 of the Williamstown report use a statistical model based on the autocovariance analysis of a large variety of samples of gravimetry [Kaula, 1963, p. 524] and are estimated to be correct within $\pm 30\%$. A statistical model

ORBITING GRAVITY GRADIOMETERS

assumes that the phases of the various harmonics are not correlated, whereas we might expect some correlation in phases to occur at the position of significant geophysical anomalies, such as mountain ranges. To obtain some feeling for this possibility, we have also looked at the gravity fields to be expected at altitude for reasonable mass anomalies on the surface.

PERIODIC MASS MODELS

In an attempt to study further the relative sensitivity of Doppler velocity tracking measurements and gravity gradiometer measurements for the higher-order gravity fields, a massive disc model was used to generate gravity data, and the signals expected for both a single disc and a periodic array of discs were calculated.

In the single-disc model, we chose a disc radius of 150 km or disc diameter of 300 km. The disc density contrast was chosen so that the differential gravity at the surface was 10 mgal. This particular choice of density contrast is not important to the question of the relative sensitivity, since the gravity, gravity gradient, and Doppler velocity signals all vary directly as the density, and if the real anomaly is different all the curves should be changed by the same factor.

The results are plotted in Figure 4, which indicates that a disc with diameter 300 km, thickness 15 km, mass of 1.7×10^{16} kg, and density contrast of 0.016 g/cc will create at an altitude of 250 km the following signals:

Vertical gravity of 1.5 mgal peak.

Vertical gravity gradient variation of 0.11 EU.

Vertical Doppler velocity shift of 1.0 mm/sec.

The analysis of a single disc is, however, not a close analogy to the periodic variation in the gravity field that is implied by the usual harmonic representation of the field. The disc model analysis was therefore expanded to a calculation of the signals expected over a periodic array of disc anomalies. The density contrast (positive or negative) was assumed to be the same as in the single-disc analysis. The curves in Figure 5 are extrapolations of the data from the center portion of the disc array to eliminate end effects. The periodic signals were

ROBERT L. FORWARD

243

Vertical gravity	$\pm 0.65 \text{ mgal}$
Vertical gravity	$\pm 0.1 \text{ EU}$
gradient	
Vertical Doppler	$\pm 0.08 \text{ mm/sec}$
velocity shift	

We notice that the magnitude of the gravity gradient is almost the same for the single disc. This is because the gravity gradient signal, being the spatial derivative of the acceleration, has a sharp cutoff, and the signal from an adjacent disc of opposite mass actually contributes slightly to the total signal. The magnitude of the periodic vertical gravity signal is slightly less from the single disc signal. The broad signature of the vertical gravity signal causes signals from adjacent discs of opposite sign to partially cancel.

Finally, the vertical Doppler velocity signal from the single disc is more than an order of magnitude smaller than that from the periodic disc. This is because the Doppler velocity sig-

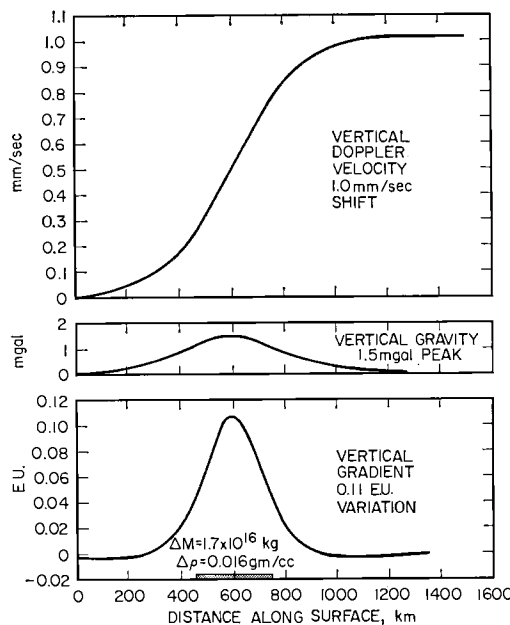


Fig. 4. Gravity signals of single 300-km diameter disc at 250-km altitude.

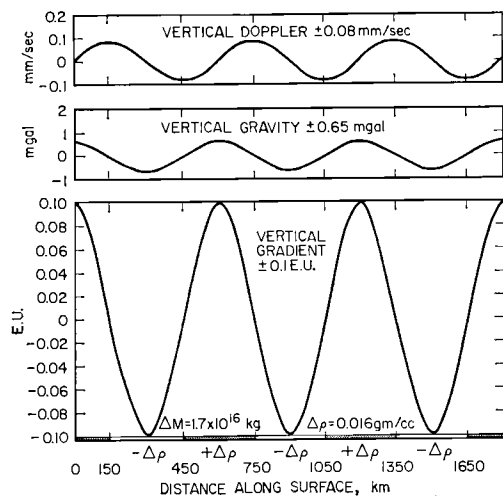


Fig. 5. Gravity signals at 250-km altitude from periodic disc array.

nal is the integral of the acceleration signal, and the integration tends to smooth out the periodic variation that we are looking for.

Acknowledgments. I would like to acknowledge many valuable discussions with E. Sherry, P. Muller, and J. Whitcomb.

REFERENCES

- Bell, C. C., R. L. Forward, and H. P. Williams, Simulated terrain mapping with the rotating gravity gradiometer, in *Proceedings of the Symposium on Dynamic Gravity*, edited by W. T. Kantner, pp. 115-128, Instrum. Soc. Amer., Pittsburgh, Pa., 1971.
- Forward, R. L., Rotating gravitational and inertial sensors, in *Proceedings of the AIAA Unmanned Spacecraft Meeting*, pp. 346-351, AIAA, New York, 1965.
- Kaula, W. M., Determination of the earth's gravitational field, *Rev. Geophys. Space Phys.*, 1, 507-551, 1963.
- Kaula, W. M., *An Introduction to Planetary Physics*, John Wiley, New York, 1968.
- Kaula, W. M. (Chairman), The terrestrial environment: Solid earth and ocean physics, Report of a Study at Williamstown, Mass., NASA Contract. Rep. CR-1579, 1970.
- Rapp, R. H., Gravitational potential of the earth determined from a combination of satellite, observed, and model anomalies, *J. Geophys. Res.*, 73, 6555-6562, 1968.

Timing for Geodetic Satellites

W. MARKOWITZ

Department of Physics, Marquette University
Milwaukee, Wisconsin 53233

Abstract. Timing accuracies available for observation of geodetic satellites are: 1 to 20 μ sec with Loran C and 0.1 to 1.0 μ sec with portable atomic clocks. Higher accuracies may be developed with very-long-baseline interferometry. Leap seconds will be introduced in 1972.

Concurrent observations of geodetic satellites made about the world require that the epochs of observation be referred to a common reference. An accuracy of about 1 msec can be obtained through use of high-frequency radio signals. Higher accuracies are generally obtained by use of Loran C and portable clocks. This report reviews high precision techniques in current use and under development.

Loran C. Precise epoch timing and frequency are provided over a large part of the world by Loran C. Synchronization with respect to the U.S. Naval Observatory master clock can be obtained to about 2 μ sec in Atlantic areas (United States and Europe) and to about 5 μ sec in Pacific areas. Plans are underway to provide an accuracy of about 1 μ sec in both areas.

Either a visual or a phase-coherent receiver can be used. A constant error of 1 or 2 cycles, equal to 10 or 20 μ sec, respectively, may occur with the visual receiver, but frequency is not affected. Generally the constant error is not important, and the visual receiver, whose cost is relatively low, can be used.

The National Ocean Service uses visual Loran-C receivers and portable quartz-crystal clocks to maintain synchronization of its geodetic satellite network to within 20 μ sec; the accuracy requirement is 40 μ sec. A visual receiver was installed at the Wallops Island satellite tracking station of NASA to resolve a timing problem, and a coherent receiver at the MacDonald Observatory of the University of Texas, Ft. Davis, for synchronizing lunar laser observations.

Artificial satellites. Satellites can be used for the distribution of time and frequency through (a) transmissions originating from a clock in the satellite, and (b) use as a relay for the two-way exchange of signals from ground stations.

Method *a* involves the difficulty that the geometric positions of both the satellite in its orbit and the receiving station on the rotating earth must be known with high precision for the instant of reception. These positions cannot generally be obtained currently, even when the satellite is in a synchronous orbit. An error of 1 km in range causes an error of 3.3 μ sec in epoch. An error of 1 m/sec in range rate causes an error of 3.3×10^{-9} in frequency.

The use of communications satellites to provide synchronization to within 0.1 μ sec through two-way transmissions is being developed by the Naval Research Laboratory and the Naval Observatory. This technique will be used for increasing the accuracy of Loran-C synchronization around the world.

Portable atomic clocks. The U.S. Naval Observatory uses portable cesium-beam atomic clocks, flown in airplanes, to provide synchronization around the world with an accuracy of 0.1 to 1.0 μ sec.

VLF stations and Omega. Synchronization can be maintained to about 5 μ sec by VLF communication stations and Omega. However, initial synchronization must be provided by other means, e.g., portable atomic clocks.

Lasers and VLBI. Lasers and VLBI can provide synchronization in the nanosecond and subnanosecond regions. Experiments with VLBI

246

have already given results in the subnanosecond region, but a difficulty yet to be solved is that of removing cycle ambiguity.

Leap seconds. Time signals are broadcast on Universal Coordinated Time (UTC), which is maintained close to UT1. Beginning January 1, 1972, the frequency of UTC has been kept con-

TIMING FOR GEODETIC SATELLITES

stant at the frequency defined by the cesium atomic clock, namely 9,192,631,770 oscillations = 1 sec. To maintain a close relation between UTC and UT1, to within 0.7 sec, leap seconds will be introduced. It is expected that about 1 leap second will be added each year for some years to come, on July 1 or January 1 if needed.

Atmospheric Correction for the Troposphere and Stratosphere in Radio Ranging of Satellites

J. SAASTAMOINEN

*Photogrammetric Research, Division of Physics
National Research Council of Canada, Ottawa, Ontario, Canada*

Abstract. Since the barometer measures the weight of the overlying atmosphere, it follows by the law of Gladstone and Dale that the height integral $\int(n - 1)dr$ of the atmospheric refractivity for radio microwaves, taken from ground level up to the top of the stratosphere, is in a dry atmosphere directly proportional to ground pressure. The refractivity integral, therefore, can be determined without detailed knowledge of the height distribution of the refractive index, which not only simplifies the derivation of refraction formulas in which atmospheric models have been used hitherto, but also improves their accuracy. The range correction for troposphere and stratosphere to be subtracted from the observed microwave distance will be given by the formula

$$\Delta s(\text{meters}) = 0.002277 \sec z [p + (1255/T + 0.05)e - 1.16 \tan^2 z]$$

where z is the zenith distance, p is the total barometric pressure and e is the partial pressure of water vapor, both in millibars, and T is the absolute temperature in degrees Kelvin.

Using the notation in Figure 1, the retarding effect of the electrically nonconducting layers of the lower atmosphere on the propagation of electromagnetic waves is found to equal distance:

$$\begin{aligned} \Delta s &= \int_{(P_1 P')} (n - 1) ds \\ &= \int_{r_1}^{r'} (n - 1) \sec z dr \quad (1) \end{aligned}$$

This correction must be subtracted from the observed electromagnetic range to obtain the true measured length of the effective ray path.

Since z is not, in general, constant along the ray path but depends upon the refractive index according to the law of refraction

$$nr \sin z = n_1 r_1 \sin z_1 = \text{const} \quad (2)$$

it will be necessary to find a suitable expression for $\sec z$ that makes (1) integrable. Setting $nr/(n_1 r_1) = y$ for brevity, we have, from (2),

$$\sin^2 z = (\sec^2 z_1 - 1)/(y^2 \sec^2 z_1)$$

$$\begin{aligned} \cos^2 z &= (y^2 \sec^2 z_1 - \sec^2 z_1 \\ &\quad + 1)/(y^2 \sec^2 z_1) \end{aligned}$$

$$\begin{aligned} \sec z &= y \sec z_1 [1 + \sec^2 z_1 (y^2 - 1)]^{-1/2} \\ &= y \sec z_1 \\ &\quad - [y(y^2 - 1) \sec^3 z_1]/2 + \dots \end{aligned}$$

Considering further that

$$\begin{aligned} y &\cong \frac{r}{r_1} = 1 + \frac{1}{r_1}(r - r_1) \\ y(y^2 - 1) &\cong \frac{2}{r_1}(r - r_1) \end{aligned}$$

we have as a first approximation

$$\begin{aligned} \sec z &= \sec z_1 - (1/r_1) \\ &\quad \cdot (\sec^3 z_1 - \sec z_1)(r - r_1) \quad (3) \end{aligned}$$

Equation 1 now becomes

$$\begin{aligned} \Delta s &= \sec z_1 \int_{r_1}^{r'} (n - 1) dr - \frac{\sec z_1 \tan^2 z_1}{r_1} \\ &\quad \cdot \int_{r_1}^{r'} (n - 1)(r - r_1) dr \quad (4) \end{aligned}$$

which expresses the range correction as a function of two atmospheric integrals. The values of the above integrals can be determined, as follows.

ATMOSPHERIC CORRECTION FOR RADIO RANGING

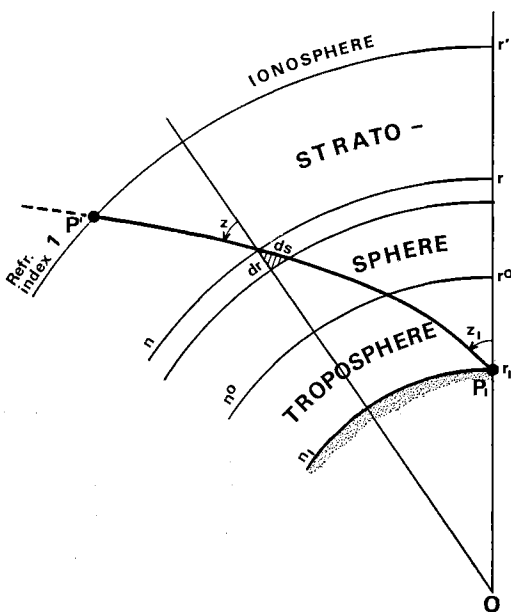


Fig. 1. Schematic illustration of electromagnetic ray path in a spherically layered atmosphere.

Integral $\int_{r_1}^{r'} (n - 1) dr$

In physical meteorology, the atmosphere can be thought of as a mixture of two ideal gases, dry air and water vapor. If we denote the total pressure by p , the partial pressure of water vapor by e , and the absolute temperature by T , the densities of the dry-air and water-vapor components are, as stated by the perfect gas law,

$$\rho_d = \frac{p - e}{RT} \quad \rho_w = \frac{e}{R_w T}$$

where R and R_w stand for the appropriate gas constants. The density of the mixture is, of course, equal to $\rho_d + \rho_w$, or

$$\rho = \frac{p}{RT} - \left(1 - \frac{R}{R_w}\right) \frac{e}{RT}$$

The atmosphere being in hydrostatic equilibrium, pressure p measured at any height level is equal to the total weight of the air contained in a vertical column of unit cross section, reaching from the point of observation up to the top of the atmosphere. Consequently,

$$\begin{aligned} \int_{r_1}^{r'} \rho dr &= \frac{1}{R} \int_{r_1}^{r'} \left(\frac{p}{T}\right) dr - \frac{1}{R} \left(1 - \frac{R}{R_w}\right) \\ &\cdot \int_{r_1}^{r'} \left(\frac{e}{T}\right) dr = \frac{p_1}{g} \end{aligned} \quad (5)$$

where g is the local value of gravity at the centroid of the atmospheric column.

The refractivity of moist air for electromagnetic radiation can be written

$$\begin{aligned} n - 1 &= \frac{(n_0 - 1)T_0}{p_0} \left(\frac{p}{T}\right) - c_w(e/T) \\ &+ c_w'(e/T^2) \end{aligned} \quad (6)$$

where n_0 is the refractive index of dry air at pressure p_0 and temperature T_0 , and c_w and c_w' are constants. The corresponding height integral

$$\begin{aligned} \int_{r_1}^{r'} (n - 1) dr &= \frac{(n_0 - 1)T_0}{p_0} \int_{r_1}^{r'} \left(\frac{p}{T}\right) dr \\ &- c_w \int_{r_1}^{r'} \left(\frac{e}{T}\right) dr + c_w' \int_{r_1}^{r'} \left(\frac{e}{T^2}\right) dr \end{aligned}$$

can be readily determined with the aid of equation 5. This gives

$$\begin{aligned} \int_{r_1}^{r'} (n - 1) dr &= \frac{(n_0 - 1)RT_0}{p_0 g} p_1 \\ &+ \left[\frac{(n_0 - 1)T_0}{p_0} \left(1 - \frac{R}{R_w}\right) - c_w \right] \\ &\cdot \int_{r_1}^{r'} \left(\frac{e}{T}\right) dr + c_w' \int_{r_1}^{r'} \left(\frac{e}{T^2}\right) dr \end{aligned} \quad (7)$$

Equation 7 expresses the value of the refractivity integral in terms of ground pressure p_1 , with corrections included due to the presence of water vapor in the air. Omitting the humidity terms, which even under extreme conditions are unlikely to contribute more than about 10% to the total refractivity integral, we have from (7) and (6)

$$\int_{r_1}^{r'} (n - 1) dr \cong \frac{R}{g} (n_1 - 1) T_1 \quad (7a)$$

for the approximate value of the refractivity integral.

Integral $\int_{r_1}^{r'} (n - 1) (r - r_1) dr$

This integral requires some consideration of the prevailing vertical state of the atmosphere.

J. SAASTAMOINEN

249

Since the refraction term dependent on it is fairly small, a general idea of the vertical distribution of pressure and temperature in the atmosphere will be sufficient.

Through most of the troposphere, or the lower atmosphere from sea level up to a height of about ten kilometers, the temperature decreases with height at a fairly uniform rate, which varies slightly with latitude and season, although in the polar regions there is a permanent inversion in the lower troposphere where the actual temperatures increase with height. Integration of the hydrostatic equation for fluids, $dp = -g\rho dr$, on the conditions $\rho = p/(RT)$ and

$$T = T_1 + \beta(r - r_1) \quad (8)$$

where the vertical gradient of temperature, $\beta = dT/dr$, is assumed to be constant, gives the pressure as

$$p = p_1(T/T_1)^{-g/(R\beta)} \quad (9)$$

and the pressure-temperature ratio as $p/T = (p_1/T_1)(T/T_1)^{m'}$, where $m' = -g/(R\beta) - 1$ is constant. The refractive index is now given by

$$n - 1 = (n_1 - 1)(T/T_1)^{m'} \quad (10)$$

Since from (8)

$$r - r_1 = \frac{T - T_1}{\beta} = \frac{T_1}{\beta}(T/T_1 - 1)$$

we have

$$\int (n - 1)(r - r_1) dr = \frac{(n_1 - 1)}{\beta^2} \cdot \int (T/T_1 - 1)(T/T_1)^{m'} dT$$

The solution of the above integral can be obtained by elementary functions. Performing the integration and transforming the result, we obtain the value of the tropospheric integral

$$\begin{aligned} \int_{r_1}^{r^0} (n - 1)(r - r_1) dr &= \frac{R^2}{g^2(1 - R\beta/g)} \\ &\cdot [(n_1 - 1)T_1^2 - (n^0 - 1)T^{0^2}] \\ &- \frac{R}{g}(n^0 - 1)(r^0 - r_1)T^0 \end{aligned} \quad (11)$$

which holds for any constant value of $\beta \neq g/R$, including $\beta = 0$.

Above the troposphere is a thermally distinct layer in which the temperature remains approximately constant or even increases with height. As far as the refraction of radio waves is concerned, this isothermal region, the stratosphere, extends up to the base of the ionosphere or to a height of about 50 km. It is separated from the troposphere by a surface called the tropopause at which tropospheric temperature gradient β rather abruptly becomes zero.

Denoting the state of the atmosphere at the tropopause by p^0, T^0, \dots , and integrating the hydrostatic equation on the condition $\rho = p/(RT^0)$, the pressure is obtained as

$$p = p^0 e^{m(r - r^0)} \quad (12)$$

where e is the base of natural logarithms, and $m = -g/(RT^0)$ is constant. Similarly,

$$n - 1 = (n^0 - 1)e^{m(r - r^0)} \quad (13)$$

Since identically

$$r - r_1 = (r - r^0) + (r^0 - r_1)$$

we have first

$$\begin{aligned} \int_{r^0}^{r'} (n - 1)(r - r_1) dr &= \int_{r^0}^{r'} (n - 1)(r - r^0) dr \\ &+ (r^0 - r_1) \int_{r^0}^{r'} (n - 1) dr \end{aligned}$$

For $\beta = 0$ in the stratosphere, equation 11 gives

$$\int_{r^0}^{r'} (n - 1)(r - r^0) dr = \frac{R^2}{g^2}(n^0 - 1)T^{0^2}$$

and further, in view of (7a), we obtain the total stratospheric integral

$$\begin{aligned} \int_{r_1}^{r^0} (n - 1)(r - r_1) dr &= \frac{R^2}{g^2}(n^0 - 1)T^{0^2} \\ &+ \frac{R}{g}(n^0 - 1)(r^0 - r_1)T^0 \end{aligned} \quad (14)$$

The sum of (11) and (14) finally gives the value of the total atmospheric integral

$$\begin{aligned} \int_{r_1}^{r'} (n - 1)(r - r_1) dr &= \frac{R^2}{g^2} \\ &\cdot \left[\frac{(n_1 - 1)T_1^2 - (R\beta/g)(n^0 - 1)T^{0^2}}{1 - R\beta/g} \right] \end{aligned} \quad (15)$$

ATMOSPHERIC CORRECTION FOR RADIO RANGING

under normal conditions where the vertical distribution of temperature throughout the troposphere is substantially a linear function of height.

Integrals $\int_{r_1}^{r'} (e/T) dr$ and $\int_{r_1}^{r'} (e/T)^2 dr$

The amount and distribution of water vapor in the atmosphere varies greatly according to the prevailing conditions of evaporation and condensation. Usually, however, the vapor pressure decreases with height in much the same manner as the total pressure, though much more rapidly. For the average conditions in the middle latitudes, we can write, very approximately, but substantially in agreement with observed conditions during all seasons,

$$e = e_1(T/T_1)^{-4g/(R\beta)} \quad (16)$$

From (16),

$$\int_{r_1}^{r'} \left(\frac{e}{T} \right) dr = \frac{R}{4g} e_1 \quad (17)$$

$$\int_{r_1}^{r'} \left(\frac{e}{T^2} \right) dr = \left(\frac{1}{4g/R + \beta} \right) \left(\frac{e_1}{T_1} \right) \quad (18)$$

Equations 17 and 18 provide adequate estimates of the humidity integrals required for the determination of refractivity integral 7.

We can now combine the results from the preceding discussion and write, on the basis of equation 4, the following expression for the range correction:

$$\begin{aligned} \Delta s &= \frac{(n_0 - 1)RT_0}{p_0 g} p_1 \sec z_1 - \frac{(n_0 - 1)R^2 T_0}{r_1 p_0 g^2} \\ &\cdot \left[\frac{p_1 T_1 - (R\beta/g)p^0 T^0}{1 - R\beta/g} \right] \sec z_1 \tan^2 z_1 \\ &+ \left[\frac{(n_0 - 1)RT_0}{4p_0 g} \left(1 - \frac{R}{R_w} \right) - \frac{Rc_w}{4g} \right. \\ &\left. + \left(\frac{c_w'}{4g/R + \beta} \right) \frac{1}{T_1} \right] e_1 \sec z_1 \end{aligned} \quad (19)$$

Equation 19 is valid at radio microwave as well as laser frequencies; i.e., it gives the range correction for all the cases in which the refractivity is expressible by equation 6.

APPLICATION OF EQUATION 19 IN RADIO RANGING OF SATELLITES

Refractive Index of Air

The Essen and Froome formula adopted by the International Association of Geodesy [1963]

for the refractive index of air at radio microwave frequencies can be written, in metric units,

$$(n - 1)10^6 = 77.624(p/T) - 12.92(e/T) + 371900(e/T^2) \quad (20)$$

where p is the total pressure and e is the partial pressure of water vapor, both in millibars, and T is the absolute temperature in degrees Kelvin. We shall accordingly accept the numerical values

$$\begin{aligned} (n_0 - 1)T_0/p_0 &= 77.624 \times 10^{-6} \\ c_w &= 12.92 \times 10^{-6} \\ c_w' &= 371900 \times 10^{-6} \end{aligned}$$

for the constants in equation 19 pertinent to the refractivity of moist air.

Reduction of Local Gravity to the Centroid of the Atmospheric Column

The value of g as required in the first term of equation 19 can be derived from the approximate gravity formula

$$g = 98.07(1 - 0.0026 \cos 2\phi - 0.00031 \bar{H}) \times 10^1 \text{ cm sec}^{-2}$$

where ϕ is the latitude and \bar{H} is the height, in kilometers above sea level, of the center of gravity in a vertical column of the atmosphere. Since atmospheric density is nearly proportional to refractivity $(n - 1)$ of dry air, the height of the center of gravity above ground level can be expressed by the ratio

$$\bar{r} - r_1 = \int_{r_1}^{r'} (n - 1) \cdot (r - r_1) dr / \int_{r_1}^{r'} (n - 1) dr$$

and consequently, using (15) and (7a), we obtain

$$\begin{aligned} \bar{r} - r_1 &= \bar{H} - H = \left(\frac{R}{g - R\beta} \right) \\ &\cdot [T_1 - (R\beta/g)(p^0 T^0 / p_1)] \end{aligned} \quad (21)$$

Because of the poleward slope of the tropopause, and the seasonal variation of its height, there is a correlation between ground temperature T_1 and pressure p^0 at the tropopause, high

J. SAASTAMOINEN

temperatures being accompanied by low pressures, and vice versa. This tends to smooth out regional and seasonal variations in the height of the center of gravity, and equation 21, evaluated for the average conditions

$$\bar{H} = 7.3 + 0.9H$$

where H denotes the station height in kilometers above the sea level, appears to be accurate to within ± 0.4 km for all latitudes and all seasons. With this approximation, the expression for local gravity at the centroid of the atmospheric column becomes

$$g = 97.84(1 - 0.0026 \cos 2\phi - 0.00028H) \times 10^1 \text{ cm sec}^{-2} \quad (22)$$

Considering the present accuracy limitations of radio ranging, an average value

$$g = 97.84 \times 10^1 \text{ cm sec}^{-2}$$

can be accepted for all latitudes and all station heights.

Determination of Zenith Distance z_1

Since the effective ray path of radio waves is curved owing to the atmospheric refraction, the true zenith distance of a satellite computed from orbital elements is greater than the apparent zenith distance z_1 used in equation 19. Their approximate difference is given by the formula

$$\Delta z'' = \frac{16.0'' \tan z}{T} \left(p + \frac{4800e}{T} \right) \quad (23)$$

obtained by the methods developed for the determination of astronomical refraction [Saaastamoinen, 1970]. Pressures p and e are measured in millibars at the tracking station, and T is the absolute temperature in degrees Kelvin ($T = 273 + t$ °C).

Evaluation of the Second Term in Equation 19

The second term in equation 19 is a correction term that takes into account the effect of the spherical curvature of atmospheric layers. As in the previous case of equation 21, the numerical value of this term is largely independent of climatic conditions. An average value is therefore acceptable for all latitudes and all seasons.

TABLE 1. Coefficient $\frac{R}{r_1 g} \left[\frac{p_1 T_1 - (R\beta/g)p^0 T^0}{1 - R\beta/g} \right]$

Station Height, km above sea level	Coefficient of $\tan^2 z$
0	1.16
0.2	1.13
0.4	1.10
0.6	1.07
0.8	1.04
1	1.01
1.5	0.94
2	0.88
2.5	0.82
3	0.76
4	0.66
5	0.57
6	0.49

Range Correction Formula 19 in Numerical Form

For practical computation of the atmospheric correction for troposphere and stratosphere in radio ranging of satellites, we can now write equation 19 in the numerical form

$$\Delta s(\text{meters}) = 0.002277 \sec z \cdot [p + (1255/T + 0.05)e - 1.16 \tan^2 z] \quad (19a)$$

where z is the true zenith distance of the satellite corrected by subtracting refraction angle Δz , p is the total barometric pressure and e is the partial pressure of water vapor, both in millibars, and T is the absolute temperature in degrees Kelvin ($T = 273.2 + t$ °C). For other than sea-level stations, the numerical coefficient of the last term in (19a) should be replaced by the coefficient given in Table 1.

In the above derivation of the range correction formula, the omission of higher-order terms causes an error of the order of 0.1 meters in the range correction at a maximum zenith distance of 80°. Beyond this limit, formula 19a becomes grossly inaccurate and should not be applied.

REFERENCES

- International Association of Geodesy, Resolution 1 of the 13th General Assembly, *Bull. Geod.*, no. 70, 390, 1963.
 Saaastamoinen, J., The physical theory of astronomical refraction (abstract), *Eos Trans. AGU*, 51, 742, 1970.

Measured Physical and Optical Properties of the Passive Geodetic Satellite (Pageos) and Echo 1

DAVID S. McDUGAL AND ROBERT BENJAMIN LEE III

NASA Langley Research Center, Hampton, Virginia 23365

DARYL C. ROMICK

Goodyear Aerospace Corporation, Akron, Ohio 44306

Abstract. Two satellites used for geodesy, Pageos and Echo 1, have been observed in a continuing program since 1966 to determine the stability of their physical and optical properties. Measurements are made in the UBVRI spectral system. The amount of solar radiation reflected from a satellite's surface is measured photoelectrically and is calibrated against known stellar magnitudes by standard astronomical techniques. The calibrated satellite magnitudes are analyzed with respect to the sun-satellite-observer phase angle to infer the shape and size of the satellite and the reflective properties of the satellite's surface material. The physical and optical properties are used to determine proper position of the solar image on the satellite's surface, resulting in more precise geometric geodesy. Quantitative results from five observing periods indicate that, although local structural anomalies appear to exist, both satellites essentially maintained their nominal average 30.48-meter (50-foot) radius of curvature and specular reflecting characteristics.

The NASA Langley Research Center has been engaged in a program to define certain physical and optical properties of various inflatable satellites by using established ground-based photometric techniques. During the preliminary stages of the program, the Echo 1 was photometrically observed in the visual spectral band to demonstrate the feasibility of using the photometric techniques. Later (1964–1966), the NASA Satellite Photometric Observatory (SPO) was designed and constructed to extend the observations into four additional spectral bands (near-ultraviolet, blue, red, and near-infrared).

In 1966 the SPO was first used to photometrically observe the Pageos shortly after its launch to determine the following satellite properties:

1. Stellar magnitude.
2. Specular and diffuse surface reflectances, as well as total reflectance.
3. Mean radius of curvature and local variations in radius of curvature.

Since that time, the SPO has been used to observe the Pageos, Echo 1 and 2, and Explorers

19, 24, and 39 in order to determine the same satellite properties.

These observations of Pageos and Echo 1 have been used to define their suitability for geometric satellite triangulation as part of the requirement of the National Geodetic Satellites Program [Bowker, 1967] and to evaluate the optical stability of their vapor-deposited aluminum surfaces in space. In this paper, the photometric observations of the Pageos and Echo 1 are presented and are analyzed for six observation periods. The observations cover the years from 1966 to 1969 [Romick *et al.*, 1968; Romick *et al.*, 1969].

NOMENCLATURE

- A_{sp} weighting factor for the specular component of reflected light.
B blue spectral band, having an effective wavelength of $0.44 \mu\text{m}$.
 B_d weighting factor for the diffuse component of reflected light.
 D distance of the satellite from the observer, in kilometers.

PHOTOELECTRIC PHOTOMETRY OF PAGEOS AND ECHO 1

E_d	apparent diffuse illuminance of a satellite, in lumens/cm ² .
E_0	apparent illuminance of a zero-magnitude satellite, in lumens/cm ² .
E_{sat}	apparent total illuminance of a satellite, in lumens/cm ² .
E_{sp}	apparent specular illuminance of a satellite, in lumens/cm ² .
E_s	apparent illuminance of the sun, in lumens/cm ² .
$F(\Psi)$	Russell phase function.
I	near-infrared spectral band, having an effective wavelength of 0.90 μm .
m	apparent stellar magnitude.
m_d	diffuse stellar magnitude of a satellite.
m_{sat}	stellar magnitude of a satellite.
m_{sp}	specular stellar magnitude of a satellite.
m_s	stellar magnitude of the sun.
R	red spectral band, having an effective wavelength of 0.70 μm .
R_c	radius of curvature of a satellite, in meters.
S	specularity, equation 7.
U	near-ultraviolet spectral band, having an effective wavelength of 0.36 μm .
V	visual spectral band, having an effective wavelength of 0.55 μm .
γ	total reflectance of a satellite, in percent.
Ψ	phase angle, measured at the satellite between directions to the sun and observer, in degrees.

SATELLITES

The physical, optical, and orbital properties of Pageos and Echo 1, which are identical except for normalization height, are as follows [Teichman, 1965; Clemons, 1964]:

Inside material	Mylar 12.70 μm thick
Outside material	Evaporated aluminum 0.2 μm thick
Radius	15.24 meters
Normalization height	4248 km for Pageos, 1609 km for Echo 1
Reflectance (laboratory)	
U	0.88
B	0.90
V	0.90
R	0.88
I	0.88

THEORY

The illuminance or brightness of a satellite is dependent upon the satellite's surface re-

flectance, shape, and size. From careful measurements of the fluctuations in the illuminance of a satellite, various inferences can be drawn about these satellite properties. Before the properties can be deduced, the illuminance must be corrected for atmospheric extinction by using stellar calibration techniques [Hardie, 1962], earth albedo contributions, variations in the solar constant due to variations in the earth-sun distance, and variations in the distance from the satellite to the observer [Romick *et al.*, 1968]. Upon applying these corrections, the illuminance of a satellite is only dependent on the following factors:

1. Physical characteristics like shape and size.
2. Optical characteristics like the surface reflectance and specularity.
3. Normalized distance from the satellite to the observer.
4. Phase angle.
5. Intensity of the incident light.

Satellite photometry. For a specularly reflecting, spherical satellite, its apparent specular illuminance E_{sp} , previously given by Tousey [1956, 1957], is given below for either the U, B, V, R, or I spectral regimes:

$$E_{sp} = E_s \gamma (R_c)^2 / 4 D^2 \quad (1)$$

while its specular stellar magnitude m_{sp} in terms of its illuminance is

$$m_{sp} = -2.5 \log_{10} (E_{sp}/E_0) \quad (2)$$

Looking at equation 1, we can see that the illuminance of the satellite should be independent of phase angle Ψ , measured at the satellite between directions to the sun and observer, as shown in Figure 1.

For a perfectly diffusely reflecting, spherical satellite, its apparent diffuse illuminance E_d is

$$E_d = 2E_s \gamma R_c^2 F(\Psi) / 3D^2 \quad (3)$$

while its stellar magnitude m_d is

$$m_d = -2.5 \log_{10} (E_d/E_0) \quad (4)$$

where

$$F(\Psi) = [\sin \Psi + (\Pi - \Psi) \cos \Psi] / \Pi \quad (5)$$

$F(\Psi)$ is the Russell phase function [Russell, 1916], describing the dependence of the il-

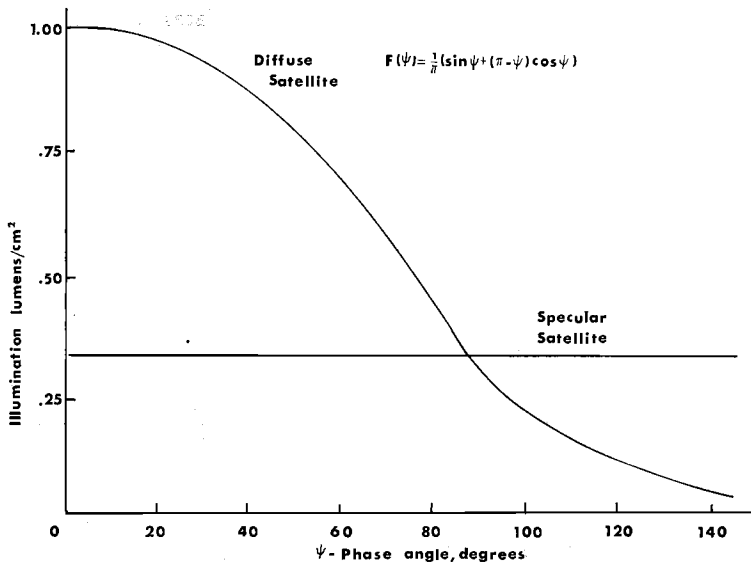


Fig. 1. Variation in illuminance for perfectly specular and diffusely reflecting satellite with phase angle.

luminance of a diffuse spherical satellite upon phase angle Ψ . The variation in its illuminance with phase angle is also shown in Figure 1. It should be noted that a diffuse satellite exhibits phases similar to those of the moon.

Equations 1 through 5 permit the photometric discrimination between the specular and diffuse reflecting surface properties of a spherical satellite. How closely a target satellite's illuminance conforms to that of a specular or diffuse satellite is determined by a linear regression technique. The regression equation used for this purpose is

$$10^{-0.4m_{sp}} = A_{sp}/4 + 2B_dF(\Psi)/3 \quad (6)$$

where A_{sp} and B_d are weighting factors for the specularly and diffusely reflected components of the illuminance. In the regression technique, a least-squares solution of equation 6 is fitted to the satellite data to obtain the best fit values for the intercept $A_{sp}/4$ and the slope $2B_d/3$ of equation 6. The values of A_{sp} and B_d are used to determine the specularity, which is the fraction of the sunlight reflected specularly. This is done by use of the equation

$$S = A_{sp}/(A_{sp} + B_d) \quad (7)$$

Next, the value of B_d is used to calculate the contribution due to diffuse reflection

$$m_d = -2.5 \log_{10} [2B_dF(\Psi)/3] \quad (8)$$

The diffuse contribution is then subtracted from the satellite's magnitude to yield its purely specular magnitude, m_{sp} described by the following equation:

$$m_{sp} = m_s - 2.5 \log_{10} (S\gamma R_c^2/4D^2) \quad (9)$$

The illuminance of a spherical satellite is dependent upon both the surface reflectance γ and the radius of curvature R_c , and it can be seen that either one can be obtained if the other is known or assumed.

If a reasonable value for R_c is assumed, the reflectance can be determined using equation 9, solved for γ :

$$\gamma = S^{-1} \text{ antilog } [(m_s - m_{sp})/2.5 - 2 \log_{10} R_c + 2 \log_{10} D + 0.60206] \quad (10)$$

Generally, the radius of curvature is assumed to be the design value for the satellite. Similarly, the radius of curvature can be calculated from a reasonable or laboratory-determined value for the reflectance γ by the following equation:

$$R_c (\text{ft}) = \text{antilog } [(m_s - m_{sp})/5 - 0.5 \log_{10} S\gamma + \log_{10} D + 0.30103] \quad (11)$$

With the aid of equation 11, the mean value of

PHOTOELECTRIC PHOTOMETRY OF PAGEOS AND ECHO 1

R_s can be obtained from a large number of satellite observations. The range and local variations in the radius of curvature R_s can be examined, in light of the satellite's original design, for implications of a possible new mean radius of curvature. In practice, iterative processes (utilizing knowledge of the satellite's physical and material properties) are used to converge on and arrive at the actual relationships of these two parameters. Reasonable physical limitations afford a set of boundary conditions that make this feasible and simplify the process.

MEASUREMENTS

The values of specularity, total reflectance, and radius of curvature are plotted as a function of time (years in orbit) in Figures 2, 3, and 4. The values of reflectance were determined by using equation 10 and assuming the radius of curvature to be 15.24 meters (50 feet), and the mean radius of curvature was calculated by using equation 11 and adopting the laboratory values of reflectance listed above.

Specularity. In Figure 2 the values of specularity are presented as a function of years in orbit for the visual band. The data represent a time history of vapor-deposited aluminum in space, since both the Pageos and Echo 1 were constructed with this aluminum surface. The fact that the specularity values are high and fairly constant with time indicates that the

aluminum surfaces of both satellites were optically stable in space. The specularity value for Echo 1 corresponding to 7.2 years in orbit was lower than the other values. This low value may be indicative of surface degradation caused by atmospheric effects, surface oxidation (since the satellite's mean orbital altitude fell below 1207 km), and by increased solar activity in 1967. Over-all, the specularity values for both satellites are found to be close to 96% of the laboratory-determined value of specularity for their aluminum surfaces.

Total reflectance. Figure 3 presents the values of total reflectance for the U, B, V, R, and I spectral bands. The Echo 1 reflectance data exhibit a decreasing trend after 6.5 years in orbit. This trend may be indicative of surface degradation related to the increased solar activity in 1967. The degradation is greatest for the shortest optical wavelengths, indicating the dulling and yellowing of the aluminum surface. The reflectance values for Pageos are essentially constant with time, indicating little if any surface degradation. The lower value of reflectance corresponding to 1.2 years in orbit may have been caused by poor atmospheric transparency during that time of observation. The reason for the I-band values being higher between 2 and 3 years in orbit than the previous values is unknown. Looking at the V-band data for both satellites, it can be said that vapor-deposited

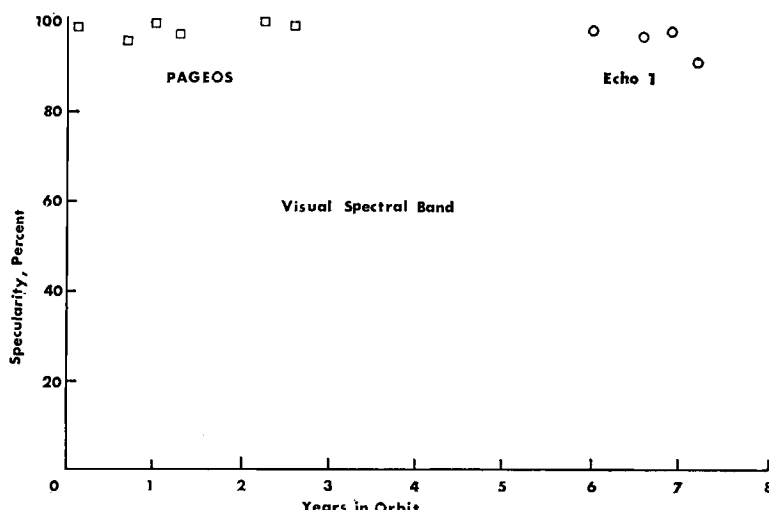
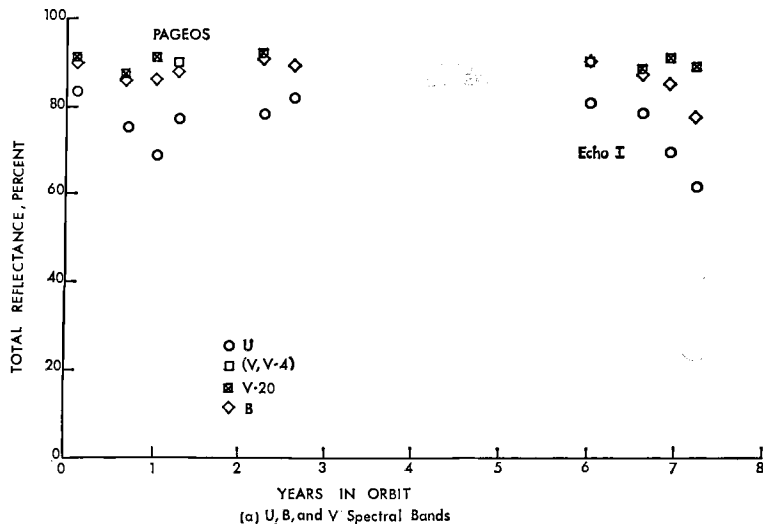


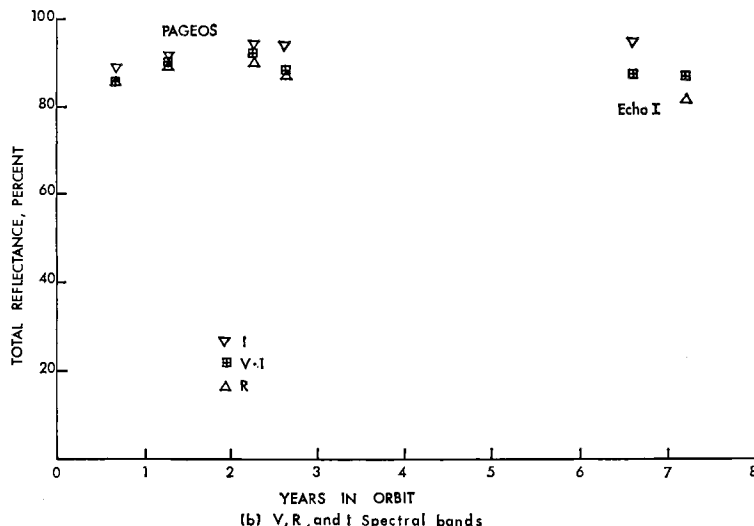
Fig. 2. Specularity values for Pageos and Echo 1 as a function of time in orbit.

McDOUGAL, LEE, AND ROMICK

257



(a) U, B, and V Spectral Bands



(b) V, R, and I Spectral Bands

aluminum was optically stable in space for wavelengths in the V band and that the V-band reflectances can be reliably and accurately used to define the mean radius of curvature for Echo 1 and Pageos.

Radius of curvature. In Figure 4, the mean radii of curvature are presented for both Pageos and Echo 1. Looking at the data, one can see that the satellites had mean radii close to their

design value of 15.24 meters. However, this does not necessarily mean that the satellites were spherical. There are obvious excursions, shown as circles in Figure 5, in the Pageos magnitude data taken after 2.7 years in orbit. These excursions are indicative of structural anomalies or distortions in the shape of Pageos. They were found to be as much as 3 magnitudes less than the average magnitude (represented by squares)

PHOTOELECTRIC PHOTOMETRY OF PAGEOS AND ECHO 1

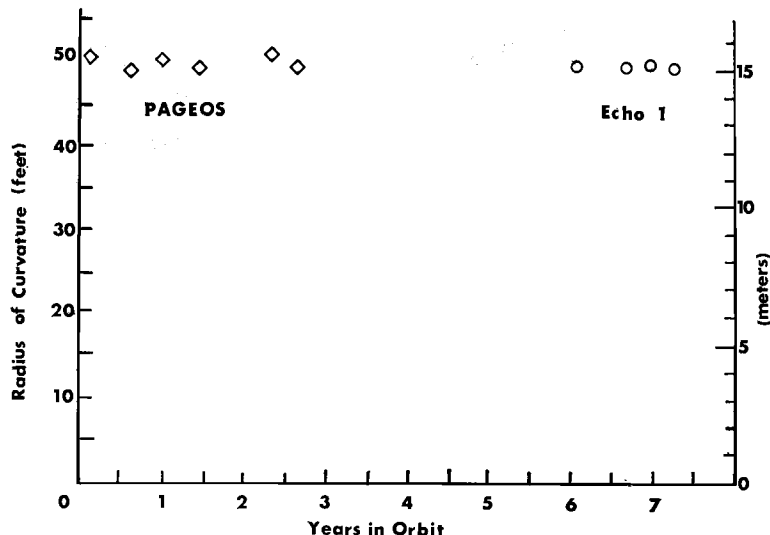


Fig. 4. Values of mean radius of curvature for Pageos and Echo 1 for the visual spectral band.

for Pageos and to occur infrequently (not every observation) for short durations. The excursions were not used in the satellite analyses. If they had been included, the corresponding mean radius of curvature and the deviation from this mean would have been 14.3 and ± 2.7 meters, respectively, compared to values of 14.9 and

± 1.8 meters for the average magnitude data for the Pageos.

The excursions may be indications that Pageos is no longer spherical and such a change in the satellite's shape may affect the accuracies of present or future geodetic measurements involving the Pageos. The excursions in the satellite

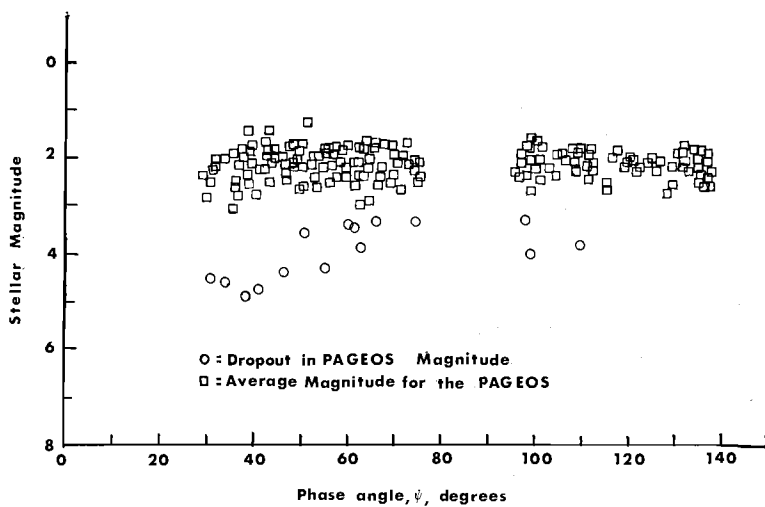


Fig. 5. Pageos time-shared V20-band photometric data, 1969.

McDOUGAL, LEE, AND ROMICK

259

illumination have also been noted by Kissell [1968].

Probable error. The probable errors for individual multicolor photometric observations of Pageos and Echo 1 were as follows:

1. Satellite magnitude, ± 0.02 .
2. Specularity, $\pm 2\%$.
3. Reflectance, $\pm 2\%$.
4. Satellite mean radius, ± 0.21 meter.

The values of the probable errors were determined in accordance with the theory discussed by Hostetler *et al.* [1967].

CONCLUSIONS

Multicolor photometric measurements of the sunlight reflected from the surfaces of the Pageos and Echo 1 were performed. In accordance with the results presented and discussed above, we conclude:

1. The vapor-deposited aluminum surfaces of Pageos and Echo 1 maintained their highly specular reflecting properties in space.
2. The surface reflectances for both satellites indicate little (if any) optical surface degradation occurred in the visual, red, and near-infrared spectral bands, whereas significant degradation did occur in the ultraviolet band and to a lesser degree in the blue.
3. The mean radii of curvature for Pageos and Echo 1 were found to be close to the design value of 15.24 meters. Structural anomalies have developed in the shape of Pageos, causing the

satellite to occasionally dim by several stellar magnitudes.

REFERENCES

- Bowker, D. E., Pageos project: Compilation of information for use of experimenter, *NASA Tech. Memo. X-1344*, 1967.
- Clemmons, D. L., The Echo 1 inflation system, *NASA Tech. Note D-2194*, 1964.
- Hardie, R. H., Photoelectric reductions, in *Astronomical Techniques*, edited by W. A. Hiltner, p. 178, University of Chicago Press, Chicago, Ill., 1962.
- Hostetler, R. L., R. H. Emmons, R. J. Preski, C. L. Rogers, and D. C. Romick, Ground-based photometric surveillance of the passive geodetic satellite, *NASA Contract. Rep. 791*, 1967.
- Johnson, H. L., Interstellar extinction in the galaxy, *Commun. Lunar Planet. Lab.*, 3(54), 79, 1965.
- Kissell, K. E., Diagnosis of spacecraft surface properties and dynamical motions by optical photometry, paper presented at the Cospar Symposium, Tokyo, Japan, May 1968.
- Romick, D. C., R. H. Emmons, R. J. Preski, and E. D. Kalasky, The modification and use of a ground-based photometer for evaluation of satellite materials, *NASA Contract. Rep. 66772*, 1968.
- Romick, D. C., R. H. Emmons, and R. J. Preski, Evaluation of satellite materials by use of ground-based photometric observatory, phase 2, *NASA Contract. Rep. 66899*, 1969.
- Russell, H. H., On the albedo of the planets and their satellites, *Astrophys. J.*, 43, 123, 1916.
- Teichman, L. A., The fabrication and testing of Pageos 1, *NASA Tech. Note D-4596*, 1968.
- Tousey, R., The visibility of an earth satellite, *Astronaut. Acta*, 2, 101, 1956.
- Tousey, R., Optical problems of satellites, *J. Opt. Soc. Amer.*, 47, 261, 1957.

6. Extraterrestrial Geodesy

Geodesy Results Obtainable with Lunar Retroreflectors

J. E. FALLER,¹ P. L. BENDER,² C. O. ALLEY,³ D. G. CURRIE,³ R. H. DICKE,⁴
W. M. KAULA,⁵ G. J. F. MACDONALD,⁶ J. D. MULHOLLAND,⁷
H. H. PLOTKIN,⁸ E. C. SILVERBERG,⁹ AND D. T. WILKINSON⁴

Abstract. Retroreflector packages have been carried to the moon by the Apollo 11, Apollo 14, and Apollo 15 missions, as well as by Luna 17. Laser ranging from the earth onto these packages should eventually yield information on polar motions and crustal movements accurate to a few centimeters, and on UT1 to 100 μ sec. Present (1971) error of the range measurements is 30 cm, but accuracy to 3 cm should be obtainable with improvements in methods and equipment.

In July 1969, the Apollo 11 astronauts placed an array of optical retroreflectors on the surface of the moon. In February of 1971, during the Apollo 14 mission, a second laser ranging retroreflector (LRRR) was placed on the lunar surface. During the Apollo 15 mission in July 1971, a third and larger laser ranging retroreflector

was placed in the area near Hadley Rille. The emplacement of these Apollo retroreflector packages on the lunar surface makes it possible, through laser ranging, to obtain very accurate measurements of the lunar distance [Alley *et al.*, 1965, 1970a, b; Faller *et al.*, 1969; Faller and Wampler, 1970]. These retroreflector arrays give rise to a returned laser signal with an intensity between 10 and 100 times greater than that reflected from the natural surface and eliminate the stretching out in time of the laser pulse that otherwise would result from the light being reflected back from different parts of the lunar surface. The fact that the three sites are well separated in longitude and latitude permits a completely geometrical separation of the lunar librations.

Each of the arrays is a wholly passive device containing small fused-silica corner cubes having a front face diameter of 3.8 cm. The Apollo 11 and 14 arrays are almost identical; each array contains 100 corner cubes. The Apollo 15 array contains 300 corner cubes. The larger signals obtainable with this array provide a greater frequency of returns and allow laser ranging with telescopes of smaller aperture.

¹ Department of Physics, 127 Science Center Tower, Wesleyan University, Middletown, Connecticut 06457.

² Joint Institute for Laboratory Astrophysics, National Bureau of Standards, University of Colorado, Boulder, Colorado 80302.

³ Department of Physics and Astronomy, University of Maryland, College Park, Maryland 20740.

⁴ Department of Physics, Princeton University, Princeton, New Jersey 08540.

⁵ Institute of Geophysics and Planetary Physics, University of California, Los Angeles, California 90024.

⁶ Council on Environmental Quality, Washington, D.C. 20506.

⁷ Astronomy Department, Physics Building 422, Austin, Texas 78712.

⁸ Optical Systems Branch, Goddard Space Flight Center, Greenbelt, Maryland 20770.

⁹ University of Texas, McDonald Observatory, Fort Davis, Texas 79734.

Full utilization of the Apollo arrays, as well as the French-Russian array carried on Luna 17, will entail an observing program that will last decades and will employ ground stations around the world. Lunar laser range measurements of 30-cm accuracy are being made to the Apollo 11, 14, and 15 retroreflector packages from the McDonald Observatory near Fort Davis, Texas. Retroreflected signals have also been obtained by the AFCRL Lunar Laser Observatory near Tucson, Arizona, the Pic du Midi Observatory in France, the Okayama Station of the Tokyo Astronomical Observatory in Japan, and the Crimean Astrophysical Observatory in the USSR. A new laser ranging station to begin operation sometime in 1973 is planned for Hawaii. This station will utilize separate transmitting and receiving optics (a small transmitting system and a large multilensed receiver telescope [Faller, 1971]) and will be capable of making range measurements to artificial satellites, as well as to the moon, to 3-cm accuracy.

An observing program resulting in an extended sequence of high-precision earth-moon distance measurements will over the years provide data from which a variety of information about the earth-moon system can be derived. The high-accuracy dynamical earth information from lunar range measurements, and probably also from laser range measurements to artificial satellites and from long baseline interferometry, will make possible major scientific progress in the following geophysical areas:

1. *The earth's core and inner mantle.* Turbulent eddies are believed to exist in the core. Mechanical or electromagnetic interaction of these eddies with the mantle may affect the axis of rotation and angular velocity of the mantle and crust. Observations of these changes provide clues to the nature of the core-mantle coupling, and hence to the properties of the core and lower mantle.

2. *Earthquake fault mechanisms.* Studies in the last few years have suggested that major earthquakes may be responsible for at least part of the excitation of the 14-month Chandler wobble of the earth. If so, much more accurate polar motion measurements may show features correlatable with earthquakes. This monitoring would at least give an integral constraint on the rock displacements associated with large

LUNAR RETROREFLECTORS

earthquakes. It may eventually give indication of asthenospheric flow before, or not associated with, an earthquake.

3. *Atmospheric circulation patterns.* Possible changes in the total angular momentum of the earth's atmosphere are believed to cause the annual and semiannual terms in the earth's rotation. Similar changes appear to be sufficient to cause observable changes in the earth's rotation even for periods as short as a few days.

4. *Large-scale crustal movements.* The remanent magnetic and seismological evidences for global plate tectonics are strong enough that simple confirmation of plate motions is not of great value. However, accurate measurements of motions may test whether the present rates of motion of major plates are the same as the average past rates deduced from displacements of geological features and remanent magnetism. More valuable would be measurements of differential motions within major plates, as are suggested, for example, by the recent geology and seismicity of the western United States.

To get the maximum information about crustal movements from the ranging program, at least six or eight stations on the major lithospheric plates are needed, as well as a number of additional stations to investigate the motions of the smaller plates and to look for distortion within the major plates. Some of these could be sites that are occupied only for a month or so every few years in order to observe the time-average motions. If one focuses instead on the questions of polar motion and fluctuations in the earth's rotation rate, the desirable number of regularly observing stations is roughly a dozen, since individual stations will frequently be shut down by weather for periods longer than those in which variations may be observable. However, the existence of two high-accuracy stations in Texas and Hawaii will make it possible to gain improved knowledge of both the polar motion and of fluctuations in the earth's rotation rate when the weather at the stations is good. As additional high-accuracy stations begin operating in other countries, observations of the crustal movements of the earth suggested by global plate tectonics will become possible.

The approximate formula for the topocentric distance ρ between an observing station on the

FALLER ET AL.

263

earth and the lunar retroreflector is

$$\rho = r - x_E - x_m \quad (1)$$

where r is the distance from the center of the earth to the center of the moon, and x_E and x_m are the projections of the observing station and retroreflector locations on the center-to-center line. This approximation is quite good, since other terms involving the observing station and retroreflector locations are only about 1% of $x_E + x_m$.

In the above approximation, the whole dependence of the range on the observing station coordinates or angular position of the earth is contained in x_E , where

$$x_E = \sigma \cos \delta \cos h + z \sin \delta \quad (2)$$

where σ is the distance from the axis of rotation, z is the height above the equatorial plane, and δ is the declination of the lunar center of mass. The local hour angle of the lunar center, $h \equiv z - \alpha$, is the local sidereal time minus the right ascension of the lunar center. It is zero when the moon crosses the meridian plane through the station, is -60° about four hours earlier, and is $+60^\circ$ about four hours later.

The uncertainties of the parameters in the lunar theory, in the retroreflector location, and in the librations all give mainly uncertainties in terms of period of 13.6 days or longer. Thus the 25-hour period $\cos h$ term in the range can be separated out. At the McDonald Observatory, the usual observing schedule is designed to do this. Measurements are made near meridian passage and roughly three hours earlier or later. From these observations, $\sigma \cos \delta$ and the time of meridian passage can be obtained.

When the range measurements near meridian passage have been fit by an improved lunar theory over a period of several years, the variations in $r - x_m$ and in α and δ will be known well enough so that the variations in σ and in t can be accurately calculated. This means that motion of the pole in the direction toward the station and the local time scale UTO can be determined, which will permit a check on the combined polar motion and earth rotation results compiled by the BIH and other organizations. The accuracies expected are within a fac-

tor of 2 or 3 of the basic range measurement accuracy.

With two or three regularly observing stations well separated geographically, both components of polar motion and universal time UT1 can be determined. Periods down to one day in the earth's rotation and polar motion can be found if the data are frequent enough, but a considerably larger number of stations is needed if short-period variations are to be monitored regularly. The effect of crustal movements on the locations of the stations would also be determined from the data. At the present time, with three U.S. arrays and one French-Russian array already on the moon, there is a very real scientific need for additional ground stations.

The major factor required in order to be able to start checking on present astronomical information about polar motion and earth rotation is the improvement of the basic lunar ephemeris. The initial range uncertainties for the Apollo retroreflectors were about 300 meters. So far, using data up through July 1970 for Apollo 11, it has been possible to improve the range prediction accuracy substantially. With the much higher frequency of data for Apollo 11 that has been obtained since October 1970 and data from Apollo 14 since February 1971, and most recently from Apollo 15 since August 1971, it should be possible to fit the lunar motion accurately as soon as the necessary analysis has been done.

The laser ranging method with its expected ± 3 cm or better range accuracy is capable of achieving an accuracy of a few centimeters for polar motion and crustal movements and of 100 μ sec for UT1. This compares with present accuracies of 1 or 2 meters for polar motion and about 5 msec for UT1 as determined by conventional astronomical observations. However, there is a strong need for continuation of present astronomical observations, at least through this decade, in order to permit an accurate comparison of the results.

The present (1971) accuracy of ± 30 cm for the lunar distance measurements at the McDonald Observatory [Silverberg and Currie, 1971] is determined mainly by problems in calibrating the electronic time delays in the system. A new calibration system to be installed later this year will in effect eliminate the time

delays by using the same photomultiplier and electronics for both the transmitted and the received pulse. This is expected to give ± 15 -cm accuracy by the beginning of 1972.

The ruby laser system being used in 1971 at McDonald gives 3-joule pulses with a repetition rate of 1 every 3 sec. The total pulse length between the 10% intensity points is 4 nsec. The rms variation in the observed transit time due to the laser pulse length and the jitter in the photomultiplier receiving the returned signal is 2 nsec, which results in the present ± 30 -cm statistical uncertainty for a single shot. Improvement to less than 1-nsec statistical uncertainty can be expected when the range residuals are averaged over a period of a few minutes.

The uncertainty in the range correction for the effect of the atmosphere was shown some time ago [Alley and Bender, 1968] to be less than 6 cm to zenith angles of 70° . This result was based on using the surface value of the atmospheric refractive index as a predictor for the correction, as is often done in radio work. Recently it has been pointed out [Hopfield, 1970, 1971; Saastamoinen, 1970] that very much better corrections for the optical case can be obtained by using the surface pressure as the predictor. It now seems likely that the total error in the range correction for zenith angles of up to 70° will be less than 1 cm for normal atmospheric conditions.

Present indications are that lasers having sufficient power to permit lunar ranging and having reduced beam divergence and pulse lengths of 0.2 nsec will be available shortly. With care, an accuracy of 0.1 nsec for the electronics seems achievable. The accuracy of range data that we can look forward to using subnanosecond laser pulses should thus be 3 cm or better.

LUNAR RETROREFLECTORS

REFERENCES

- Alley, C. O., and P. L. Bender, Information obtainable from laser range measurements to a lunar corner reflector, in *Continental Drift, Secular Motion of the Pole, and Rotation of the Earth*, Symp. 32 of the International Astronomical Union, pp. 86-90, edited by W. Markowitz and B. Guinot, Dordrecht, Netherlands, 1968.
- Alley, C. O., P. L. Bender, R. H. Dicke, J. E. Faller, P. A. Franken, H. H. Plotkin, and D. T. Wilkinson, Optical radar using a corner reflector on the moon, *J. Geophys. Res.*, **70**, 2267-2269, 1965.
- Alley, C. O., R. F. Chang, D. G. Currie, J. Mullendore, S. K. Poultney, J. D. Rayner, E. C. Silverberg, C. A. Steggerda, H. H. Plotkin, W. Williams, B. Warner, H. Richardson, and B. Bopp, Apollo 11 laser ranging retro-reflector: Initial measurements from the McDonald Observatory, *Science*, **167**, 368-370, 1970a.
- Alley, C. O., R. F. Chang, D. G. Currie, S. K. Poultney, P. L. Bender, R. H. Dicke, D. T. Wilkinson, J. E. Faller, W. M. Kaula, G. J. F. MacDonald, J. D. Mulholland, H. H. Plotkin, W. Carrion, and E. J. Wampler, Laser ranging retro-reflector: Continuing measurements and expected results, *Science*, **167**, 458-460, 1970b.
- Faller, J. E., and E. J. Wampler, The lunar laser reflector, *Sci. Amer.*, **222**(3), 38-49, March 1970.
- Faller, J. E., I. Winer, W. Carrion, T. S. Johnson, P. Spadin, L. Robinson, E. J. Wampler, and D. Wieber, Laser beam directed at the lunar retro-reflector array: Observations of the first returns, *Science*, **166**, 99-102, 1969.
- Faller, J. E., The Apollo retroreflector arrays and a new multilensed receiver telescope, *Space Res.*, **12**, in press, 1971.
- Hopfield, H. S., Tropospheric effect on electromagnetically measured range: Prediction from surface weather data (abstract), *Eos Trans. AGU*, **51**, 266, 1970.
- Hopfield, H. S., Tropospheric effect on electromagnetically measured range: Prediction from surface weather data, *Radio Sci.*, **6**, 357-367, 1971.
- Saastamoinen, J., The atmospheric correction for laser ranging of satellites (abstract), *Eos Trans. AGU*, **51**, 266, 1970.
- Silverberg, E. C., and D. G. Currie, A description of the lunar ranging station at McDonald Observatory, *Space Res.*, **12**, in press, 1971.

Lunar Gravity Model Obtained by Using Spherical Harmonics with Mascon Terms

MARSHALL H. KAPLAN AND BOHDAN G. KUNCIW

*Department of Aerospace Engineering
Pennsylvania State University, University Park, Pennsylvania 16802*

Abstract. The lunar gravitational potential must be accurately known in order to carry out near-surface orbital missions and perform precision landings automatically. Previous investigations by the Jet Propulsion Laboratory and Langley Research Center have concentrated on using a pure spherical harmonic expansion (Legendre polynomial series) to model this potential. This approach has not yielded entirely satisfactory results, because near-surface concentrations (mascons) do not permit rapid convergence of the series expansion. Mascons discovered through recent studies of gravimetry maps cause the moon to be gravitationally 'rough,' thus requiring use of high degree and order coefficients even to obtain a poor potential model. The work reported here is concerned with methods for obtaining models of lunar gravity by using a truncated spherical harmonic expansion with a finite number of mascon terms. To test this formulation, rates of change of the ascending node due to asphericity, mascons, sun and earth attraction, and solar pressure were used with measured data from the Lunar Orbiter series. Values of unknown coefficients in the potential model were calculated and were used to generate predictions of perturbation effects. Comparisons with Lunar Orbiter data indicate the validity of this approach. Determination of the lunar density distribution is also discussed.

The work reported here involves the investigation of a modified spherical harmonic expansion to describe the lunar gravity field. This technique may, however, be used to determine surface mass anomalies and gravity potential of any planetary body. The pure Legendre expansion does not require any knowledge of physical make-up of the central body, but only the time history of low-altitude satellite motion. This model has proved insufficient for the moon, thus indicating the need for other information about its physical structure. Our current knowledge of the moon indicates that mascons seem to occur only near the surface in correspondence to mare locations. Thus, major mascons are assumed to be located on the lunar nearside, since this is also the location of most mare regions. Gravimetry maps suggest mascon sites and give indications of their relative sizes.

Specifically, the gravity model used here is a truncated Legendre polynomial series with a finite number of mascon terms added. Although mascons have been considered as third-body perturbing sources [Wong *et al.*, 1969] in con-

nnection with the determination of Legendre coefficients of a pure spherical harmonic expansion, this particular formulation of gravity has not been used before. The mascons are treated as separate third-body, point-perturbing sources. Orbiter data is used to determine a small number of Legendre coefficients plus mascon magnitudes. Locations of mascon centers are predetermined from other information, such as gravimetry maps.

MODEL OF GRAVITATIONAL POTENTIAL

The general expression for the gravitational potential assumed here is

$$U = \frac{\mu}{r} \left[1 + \sum_{n=2}^{\infty} \sum_{m=0}^{n-1} \left(\frac{a}{r} \right)^n p_n m \cdot (\cos \phi) (C_{nm} \cos m\theta_U + S_{nm} \sin m\theta_U) \right] + \sum_{i=1}^q \frac{\mu_i}{|\mathbf{a}_i - \mathbf{r}|} \quad (1)$$

where each term in the mascon series represents a constrained third-body potential, a is the

mean lunar radius, and μ is the lunar gravity constant. Geometric relationships and nomenclature are illustrated in Figures 1 and 2. The x' , y' plane is the lunar equatorial. Of course, the Legendre series representing the moon without mascons is truncated at some low degree ($n = p$) in the practical case. Reduction of degree required for a satisfactory model is, in fact, one of the major objectives of this work. Values of the coefficients C_{nm} , S_{nm} , and μ_i are determined from artificial selenoid orbit data in conjunction with small perturbation analyses. The proper combination of values for the degree p and number of mascons q is, in principle, dependent on the desired accuracy of the potential U . However, the limited amount of data used and its associated accuracy put practical, low limits on p and q . Since only a few spherical harmonic terms and mascons can be included, accuracy of the model can be enhanced by proper selection. Validity of the available data is discussed in a later section.

DETERMINATION OF UNKNOWN COEFFICIENTS

In order to determine values of C_{nm} , S_{nm} , and μ_i , time histories of artificial selenoid orbits must be related to rates of change of orbital elements caused by perturbation forces. Because of limited time and funds, average rates of change over an orbital period were used instead of actual time variations of the elements. The use of such averaged rates reduces attainable resolution of mascon sizes and, in turn, limits the accuracy of the final model. In addition, a gravity model must be assumed in order to convert raw data into averaged rates over

an orbital cycle. The model used by JPL in reducing the raw radar tracking data [Lorell and Laing, 1970] to averages is a pure spherical harmonic expansion. Thus, an attempt is being made to determine mascon sizes and Legendre coefficient values in order to produce a more accurate model from somewhat contaminated raw data that has already been reduced by a poor model.

Assuming that average rates of change are given, expressions corresponding to each of the Kepler elements are needed. The instantaneous rates of change are obtained from Battin [1964]:

$$\begin{aligned} de/dt &= (r/h)[\sin \theta^*(1 + e \cos \theta^*)f_r \\ &\quad + (e + 2 \cos \theta^* + e \cos^2 \theta^*)f_\theta] \end{aligned} \quad (2a)$$

$$\begin{aligned} d\omega/dt &= (r/he)[- \cos \theta^*(1 + e \cos \theta^*)f_r \\ &\quad + \sin \theta^*(2 + e \cos \theta^*)f_\theta] \end{aligned} \quad (2b)$$

$$d\Omega/dt = [(\sin \theta)/(\sin i)]f_L/v_\theta \quad (2c)$$

$$di/dt = [(\cos \theta)/v_\theta]f_L \quad (2d)$$

where f_r , f_θ , f_L are the radial, transverse, and normal components of the perturbing force, respectively, and the ecliptic is taken as the reference plane. This force arises from lunar asphericity, mascons, attraction of sun and earth, and solar pressure. Other possible sources of perturbations, such as drag and attraction of other planets, have magnitudes below the noise level of actual tracking data and are therefore ignored. Since pure gravitational forces are conservative, the semi-major axis is unaffected by mascon attraction and is not in-

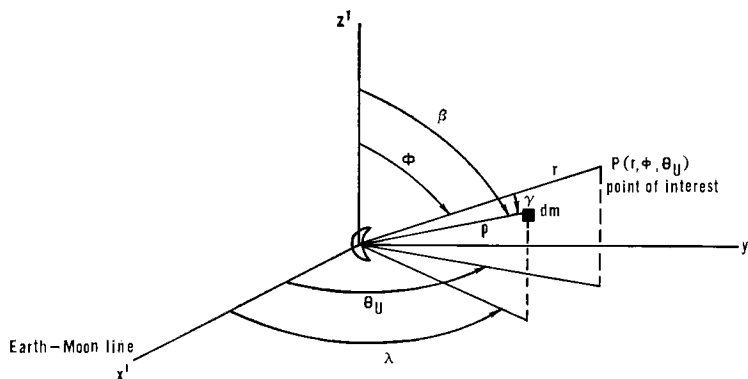


Fig. 1. Selenocentric coordinate system.

KAPLAN AND KUNCIW

267

cluded as a disturbed element. Perturbing forces are very small when compared to the lunar central attraction, μ/r^2 , and therefore effects on average rates of change of each perturbing source may be superimposed. Each of the above expressions is integrated over an orbital period for each source of perturbation. The effects are then added to give total average elemental rates. Actual values for these rates are obtained from reduced Lunar Orbiter data published by *Lorell and Laing* [1970]. Unknowns are obtained by selecting an equal number of sets of average rates and simultaneously solving the resulting linear equations in these unknowns. The sets of selected data should, if possible, reflect those elements that are most sensitive to third-body perturbations and less sensitive to solar pressure, which causes uncertainties in tracking data interpretation. Furthermore, selection of data from distinct orbital configurations and epochs will insure that the linear simultaneous equations in the unknowns will be independent, and a unique set of coefficient values will result.

Once each component of perturbation is expressed in terms of the argument of angular position θ and other orbital elements, the average rate of change of an element over one cycle is obtained from the general form:

$$\left\langle \frac{dE}{d\theta} \right\rangle = \frac{1}{2\pi} \int_0^{2\pi} \frac{dE}{d\theta} d\theta \quad (3)$$

where E is any of the elements e , ω , Ω , or i . During a single orbit, only first-order variations are considered. Thus, the orbital elements under the integral sign are kept constant, and integration involves only explicit functions of θ .

VALIDITY AND LIMITATIONS OF LUNAR ORBITER DATA

The actual data used for gravity analyses consist of Doppler and range tracking information. In raw form, these data are very precise, the noise level being orders of magnitude below information signal magnitudes [*Lorell*, 1969]. However, contamination and uncertainties have degraded the usefulness of the data in determining an accurate lunar gravity potential. Since the primary mission of Lunar Orbiter spacecraft was to photograph surface features, gravity measurements were secondary to operation and handling of the vehicles for camera-pointing

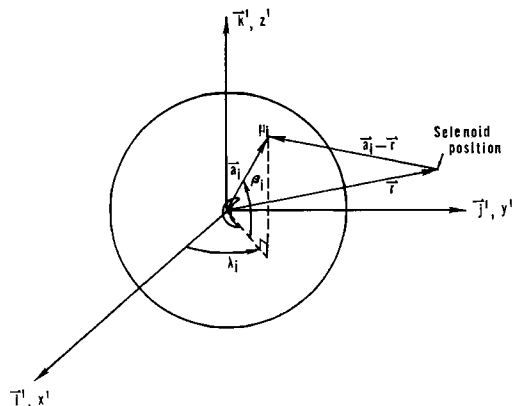


Fig. 2. Nomenclature for mascon locations.

requirements. Attitude control functions were performed by gas jets that did not apply pure couples about two of the three axes. Thus, most of the attitude maneuvers produced linear accelerations that have not been accounted for. Furthermore, only front-side data were obtainable because of occultation. This severely limits the quantity of desired information.

In order to reduce raw data into a useful form, a gravity model must be assumed a priori. The model used by JPL consists solely of spherical harmonics and thus results in considerable loss of resolution ability relative to mascon size determination.

Of course, to deduce lunar gravity from the raw tracking data, perturbations from other sources must be extracted. Solar and terrestrial attraction can be accurately modeled, whereas solar radiation pressure effects are somewhat uncertain. The complicated combination of vehicle attitude, configuration, reflectivity, and position relative to the lunar shadow allows only limited simulation of this effect. Such radiation pressure perturbations are estimated by the methods of *Bryant* [1961], which were also used by JPL.

In summary, the precision of raw tracking data has not been maintained through reduction to the determination of a gravity potential. Uncertainties in reduced data arise from inaccurate models of gravity and solar pressure, and from contamination due to uncoupled attitude control jets. These effects are equivalent to data uncertainties of the order of kilometers in position and meters per second in velocity.

Therefore, conclusions related to lunar gravity resulting from reduction of such data will be primarily of a qualitative nature.

AVERAGED RATES OF KEPLERIAN ELEMENTS

Orbital elements of lunar satellites are subject to perturbation from several sources. Disturbances with magnitudes above the data noise level are generated by asphericity, mascons, attraction of sun and earth, and solar pressure. In this analysis each source is considered separately, and effects of each are later superimposed.

Effects due to lunar asphericity (excluding mascons) are handled through the use of a spherical harmonic expansion, referred to as the 'asphericity disturbing potential,'

$$U'(r, \phi, \theta_U) = \frac{\mu}{r} \left[\sum_{n=2}^p \sum_{m=0}^n \left(\frac{a}{r} \right)^n p_n^m \cdot (\cos \phi) (C_{nm} \cos m\theta_U + S_{nm} \sin m\theta_U) \right]$$

which includes oblateness and triaxiality contributions. The associated perturbation force components are then obtained from

$$\begin{aligned} f_{U_r'} &= \partial U' / \partial r \\ f_{U_\theta'} &= (1/r) \partial U' / \partial \theta \\ f_{U_L'} &= [1/(r \sin \theta)] \partial U' / \partial i \end{aligned}$$

Of course, a transformation of coordinates from r, ϕ, θ_U to r, i, θ is required of U' before differentiation. The resulting force components are functions of r, i, θ, C_{nm} , and S_{nm} . Only terms up to third degree ($p = 3$) were considered, because higher-degree harmonics should contribute little to a moon without mascons. The elimination of higher harmonics is consistent with current theories on planetary structures. Asphericity effects are averaged through the use of equation 3, and resulting expressions are quite lengthy. Since only ascending node data were eventually used (see next section), averaged rates of change of e, ω , and i were not of concern. The expression for ascending node rate is constructed using

$$\left\langle \frac{d\Omega}{d\theta} \right\rangle_{U'} = \sum_{n=2}^3 \sum_{m=0}^n \left\langle \frac{d\Omega}{d\theta} \right\rangle_{U_{nm}},$$

where the seven terms have forms listed by Kunciw [1971].

LUNAR GRAVITY MODEL

Perturbations due to near-surface mascons are treated as third-body perturbing point sources with the constraint that they be located at the lunar surface. The attraction of the i th mascon on an orbiter is given as

$$\mathbf{f}_i = \frac{\mu_i(\mathbf{a}_i - \mathbf{r})}{|\mathbf{a}_i - \mathbf{r}|^3} \quad (4)$$

which is the gradient of the general mascon potential term in equation 1. For a given situation, components are taken and averaged rates of change due to mascons are obtained by equation 3. The most direct approach for handling this integration is by numerical methods via computer.

Perturbations due to the attraction of sun and earth may also be treated as third-body effects. However, simplifying approximations can be made, because $r_s \gg r$ and $r_E \gg r$. Expanding in powers of r/r_s , the force expression for solar attraction to first order is

$$\mathbf{f}_s = \frac{\mu_s}{r_s^2} \left[3 \left(\frac{\mathbf{r}_s \cdot \mathbf{r}}{r_s^2} \right) \frac{\mathbf{r}_s}{r_s} - \frac{\mathbf{r}}{r_s} \right]$$

Components of this are integrable in closed form. As with asphericity, the averaged rates for only ascending node are of interest. The expression is quite lengthy and is presented by Kunciw [1971] for both sun and earth attraction. Effects of solar radiation are handled as outlined by Bryant [1961]. The quality of simulation is limited by factors mentioned above.

Actual rates of change are obtained from reduced Lunar Orbiter data. The linear simultaneous equations in the unknowns are solved by computer, and resulting coefficients are then used to generate test rates of change. These are compared with corresponding orbiter data.

DISCUSSION OF RESULTS

Time histories of Kepler elements based on Lunar Orbiter data are plotted as normal points by Lorell and Laing [1970]. These points represent compressions of the raw data, each one corresponding to a short arc of observation, i.e., 4 to 12 hours of tracking. Data were reduced through the use of the JPL 2 spherical harmonic gravity model [Lorell, 1969].

Since the information is plotted as points and slopes and had to be measured from these plots,

KAPLAN AND KUNCIW

269

it was necessary to determine whether or not these points could be connected by smooth continuous curves that indicate secular rates of change. This was accomplished by regenerating time histories of elements with coefficients up to third degree (first twelve) from the JPL 2 model. A comparison between these and plots of normal points to indicate which slopes could be measured directly from normal point displays were used. On the basis of later results, this method of identifying measurable slopes appears to be valid. With the single exception of node position Ω , elemental slopes oscillate between normal points. Hence, rates of change could only be measured from normal point plots of Ω , and these were based on at least 6-day averages. Sixteen such slopes were measured, the selections being based on widely varying times and orbital situations to insure linear independence of the simultaneous equations to be solved for the unknown coefficients. Table 1 lists these reference rates of change, along with corresponding tracking arcs and values of epoch and time past epoch of the measurement.

Mascon positions were obtained from a lunar gravimetry map developed by *Muller and Sjogren* [1969] and are listed in descending order of acceleration magnitudes in Table 2. The 13 most significant acceleration anomalies from the region of complete gravimetry mapping are included. Smaller anomalies are known to exist over the entire surface and could not

be accounted for in this limited study. However, most of the major lunar mascons are thought to be located in the well-mapped region from which Table 2 is constructed. All mascons are represented as surface mass points with corresponding gravitational constants estimated from accelerations in Table 2 and also generated from the analysis to give magnitudes corresponding to rates of change of node position. Mascons are allowed to have positive or negative mass values in this analysis. There may, in fact, be significant low-density mass anomalies. Furthermore, since all mascons are not included, those that are considered tend to adjust in order to compensate.

Several combinations of C_{nm} , S_{nm} , and μ_i coefficients were tested and values were obtained in order to determine effects of adding mascon terms to a truncated spherical harmonic series. Table 3 lists the several test cases considered, and resulting coefficient values are included. Table 4 presents corresponding values of predicted rates of change of node position. Only those values that were generated after the unknowns were calculated are included. The remainder of the sixteen measured rates not appearing were used to generate the unknowns themselves.

Comparing independent slope predictions in Table 4 of PSU 1 and PSU 4 models with measured slopes in Table 1 indicates that the addition of one mascon to a simple oblate tri-

TABLE 1. Measured Element Rates of Change

Data Set	Lunar Orbiter Arc Ident.	Epoch		Time Past Epoch, days	Rate of Change of Node Position, deg/day
		Date	GMT		
1	1A	Aug. 14, 1966	1534	2	-0.460
2	1B	Aug. 25	1601	6	-0.500
3	2C	Dec. 8	2036	30	-0.500
4	3B	Feb. 12, 1967	1813	8	-0.500
5	3E	Aug. 30	1939	17	-0.875
6	4C	June 8	2239	8	-0.0333
7	4C	June 8	2239	3	-0.0500
8	5C	Aug. 9	0508	8	-0.0500
9	5D	Oct. 10	1937	40	-0.0400
10	1B	Aug. 25, 1966	1601	13	-0.444
11	1B	Aug. 25	1601	20	-0.444
12	2C	Dec. 8	2036	100	-0.500
13	2E	June 26, 1967	0701	80	-0.409
14	3B	Feb. 12	1813	24	-0.400
15	3E	Aug. 30	1939	12	-1.00
16	5D	Oct. 10	1937	70	-0.0375

TABLE 2. Mascon Locations and Sizes from Gravimetry

Mascon Ident.	Location		Accel., mgal	$\mu \times 10^{-8}$ (est.), km ³ /day ²
	Lat., deg	Long., deg		
μ_1	57	-14	-170	-6.2
μ_2	25	19	+165	+6.2
μ_3	33	-17	+155	+5.9
μ_4	44	21	-120	-4.4
μ_5	18	55	+100	+3.7
μ_6	50	-32	-90	-3.3
μ_7	-13	31	+90	+3.3
μ_8	60	62	-80	-2.9
μ_9	8	15	-70	-2.6
μ_{10}	-23	-37	+60	+2.2
μ_{11}	-33	-38	-50	-1.8
μ_{12}	8	-8	+50	+1.8
μ_{13}	-12	-13	-50	-1.8

axial model yields significant over-all improvement. Adding another mascon to PSU 4 gives the slightly improved PSU 5 model. However, as mascons are added, the limits of validity of the numerical quantities and gravimetry maps are quickly approached.

As a test of model validity, we compare predictions of PSU 2 and PSU 4 models, i.e., a second-degree spherical harmonic expansion

LUNAR GRAVITY MODEL

versus an oblate, triaxial body with one mascon. Over-all, predictions are about equivalent. However, the PSU 4 model contains only three terms, as compared with five for the PSU 2 version. This represents a qualitative demonstration of simplicity inherent in the hybrid model. Furthermore, a single mass anomaly can be modeled with one mascon term, while many spherical harmonics cannot do this as well. This is indicated by the PSU 3 model, in which Legendre terms through third degree are included. Predictions are degraded considerably from those of PSU 2, which contains only harmonics through second degree. The positive slope of the number 13 prediction is considered to be catastrophic. One explanation for this degradation might be that the seven added (third-degree) terms do not model mascons well enough to improve predictions and, in fact, degrade the simpler model. With this in mind, another interesting test of the hybrid method is represented by PSU 6, 7, and 8 models. Here Legendre terms through second degree are used with 5, 6, and 7 added mascons, respectively. In all three cases, predictions have the correct (negative) sign, and magnitudes are generally close to measured values. Thus, a simpler and more realistic gravity model appears to be

TABLE 3. Calculated Coefficients

Coefficients	Models							
	PSU 1	PSU 2	PSU 3	PSU 4	PSU 5	PSU 6	PSU 7	PSU 8
$C_{20} \times 10^4$	-2.8635	-2.3431	-2.3382	-2.5410	-2.4682	-2.2073	-2.2882	-2.2855
$C_{21} \times 10^4$		-0.0637	0.1113			-0.4209	0.0326	-0.0946
$S_{21} \times 10^4$		-0.0333	-0.0229			0.3538	0.3055	0.3180
$C_{22} \times 10^4$	0.3895	0.1492	0.0518	0.2152	0.1856	0.2852	0.2541	0.2464
$S_{22} \times 10^4$		-0.2216	-0.2264			-0.3790	-0.5122	-0.4820
$C_{30} \times 10^4$			-1.4117					
$C_{31} \times 10^4$			2.4634					
$S_{31} \times 10^4$			6.9560					
$C_{32} \times 10^4$			-39.1941					
$S_{32} \times 10^4$			13.0683					
$C_{33} \times 10^4$			1.7363					
$S_{33} \times 10^4$			0.2360					
$\mu_1 \times 10^{-8*}$				-0.0653	-0.0805	2.0499	-2.9693	-1.6733
$\mu_2 \times 10^{-8*}$					-0.0154	1.3408	-2.5309	-1.5045
$\mu_3 \times 10^{-8*}$						0.1066	1.2622	0.9535
$\mu_4 \times 10^{-8*}$						-3.3366	0.5592	-0.4076
$\mu_5 \times 10^{-8*}$							0.4944	1.5736
$\mu_6 \times 10^{-8*}$								1.2613
$\mu_7 \times 10^{-8*}$								2.5030
								1.8446
								0.0021

* km³/day²

TABLE 4. Predicted Node Position Rates (deg/day)

Data Set	PSU 1	PSU 2	PSU 3	PSU 4	PSU 5	PSU 6	PSU 7	PSU 8
3	-0.4899							
4	-0.6484			-0.5278				
5	-1.4198			-1.2417	-1.1958			
6	-0.0283	-0.0157		-0.0178	-0.0151			
7	-0.0354	-0.0250		-0.0294	-0.0273			
8	-0.0825	-0.0459		-0.0566	-0.0500			
9	-0.0595	-0.0547		-0.0591	-0.0597			
10	-0.7896	-0.6631		-0.6950	-0.6914			
11	-0.5179	-0.4206		-0.5193	-0.5126	-0.5798		
12	-0.5271	-0.4223		-0.5077	-0.5053	-0.6571	-0.4570	
13	-0.5782	-0.4844	0.2396	-0.4789	-0.4541	-0.4575	-0.4031	-0.4215
14	-0.4824	-0.5053	-0.4457	-0.4648	-0.4645	-0.4363	-0.8613	-0.7496
15	-1.0940	-1.1358	-1.2304	-1.0942	-1.0904	-1.0906	-0.8603	-0.9346
16	-0.0605	-0.0550	-0.0444	-0.0570	-0.0571	-0.1123	-0.0471	-0.0643

achievable by using a Legendre polynomial series of second degree with added mascon terms. It should also be noted that the PSU 4 model still gives better results than the 6, 7, and 8 models. This is explained by the fact that selection of mascon locations is critical. With the limited information available and data uncertainties, the selection process cannot yet be optimized.

Other indications of validity of the hybrid approach are the values calculated for Legendre and mascon coefficients. For example, in the PSU 4 model, the C_{20} and C_{22} values compare very well with those of JPL 2: -1.9189 and 0.1123, respectively. The gravity constant is 2

orders of magnitude lower than that given in Table 2. This is an indication that the single mascon had to absorb the effects of all mascons in predicting rates of change.

Predicted slopes from PSU 5 and normal point inputs of rates 15 and 16 in Table 1 are plotted in Figures 3 and 4, respectively, to give an indication of the form of data used and ability of a hybrid model to predict independent slopes. It should be noted that physical librations were not included, since their contributions to accuracy are negated by the uncertainty in slope measurement. These could be included when raw data are used directly. Furthermore, measurement and prediction accuracies are lim-

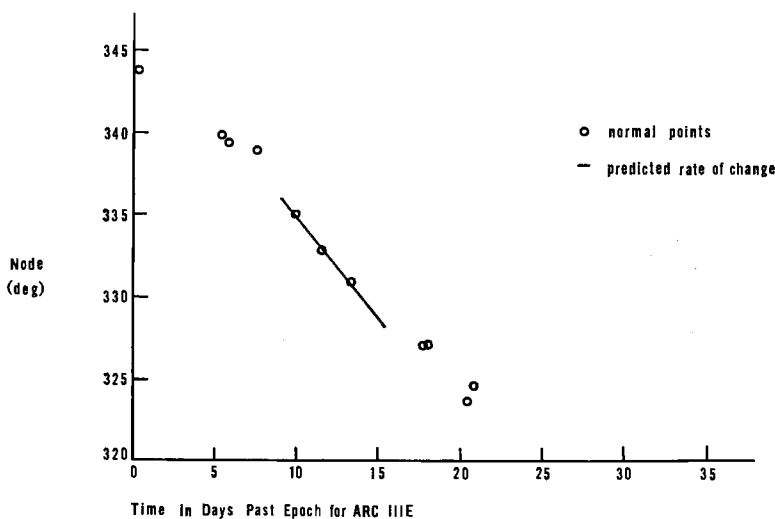


Fig. 3. Normal points and prediction for arc 3E.

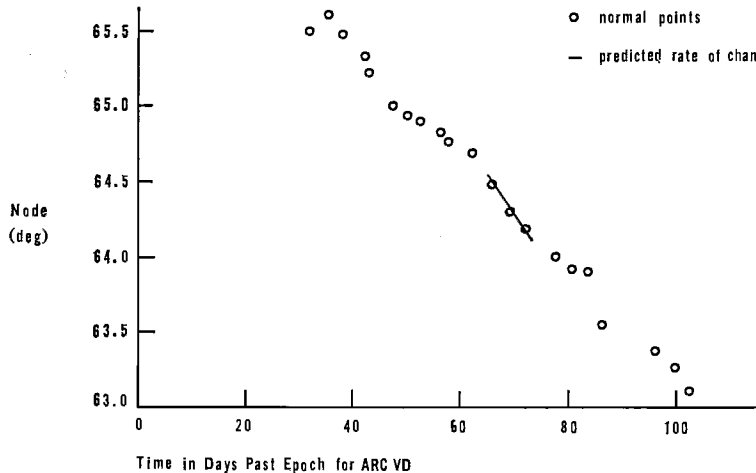


Fig. 4. Normal points and prediction for arc 5D.

ited to two significant figures. Substantial improvements in models would certainly be realized if complete and uncontaminated raw data were available and were reduced by hybrid models.

DETERMINATION OF LUNAR DENSITY DISTRIBUTION

The gravitational potential and density distribution of a planetary body are closely related. Given an accurate density model, gravity can be calculated immediately. However, the converse is not generally true, because a given gravity field can always arise from a surface mass distribution, implying that there is no unique density model corresponding to that potential. It would, nevertheless, be quite desirable to obtain this distribution for the moon. Such a knowledge would certainly aid in the lunar origin determination and might lead to a better understanding of its physical structure.

The density distribution can be approached through a gravity-density relationship [Battin, 1964], which assumes no mascons. Thus, a spherical harmonic gravity potential is obtainable from

$$U(r, \phi, \theta_U)$$

$$= G \iiint \frac{D(\rho, \beta, \lambda) \rho^2 \sin \beta d\rho d\beta d\lambda}{[r^2 + \rho^2 - 2r\rho \cos \gamma]^{1/2}} \quad (5)$$

where ρ is the radial distance to a point of interest below the lunar surface. Other variables

are defined in Figure 1. We can assume the density distribution function to have the form

$$D(\rho, \beta, \lambda) = \sum_{n=0}^{\infty} \sum_{m=0}^n M \left(\frac{\rho}{a} \right)^n P_n^m(\cos \beta) \cdot (B_{nm} \cos m\lambda + G_{nm} \sin m\lambda) \quad (6)$$

where M is the lunar mass. By noting that the denominator in the integrand of expression 5 is the generating function for a Legendre expansion, integration can be performed to give

$$U(r, \phi, \theta_U) = GM \sum_{n=0}^{\infty} \sum_{m=0}^n \left(\frac{1}{a} \right)^n \left(\frac{1}{r} \right)^{n+1} \left[\frac{a^{2n+3}}{2n+3} \right] \left[\frac{4\pi}{2n+1} P_n^m(\cos \phi) \cdot (B_{nm} \cos m\theta_U + G_{nm} \sin m\theta_U) \right]$$

Comparing this with the classical spherical harmonic expansion yields

$$\frac{a^3}{2n+3} \frac{4\pi}{2n+1} B_{nm} = C_{nm}$$

$$\frac{a^3}{2n+3} \frac{4\pi}{2n+1} G_{nm} = S_{nm}$$

Equation 6 can now be written as

$$D(\rho, \beta, \lambda) = \frac{M}{4\pi a^3/3} + \sum_{n=0}^{\infty} \sum_{m=0}^n M \left(\frac{\rho}{a} \right)^n P_n^m(\cos \beta) \cdot (B_{nm} \cos m\lambda + G_{nm} \sin m\lambda)$$

KAPLAN AND KUNCIW

273

This expression represents the lunar density distribution excluding mascons. These can be accounted for by noting their masses, locations, and sizes and by superimposing onto $D(\rho, \beta, \lambda)$. However, as was noted above, there is no unique solution for radial variations of density by gravity analysis from orbit. Although a radial variation $(\rho/a)^n$ is assumed here, a different one may be more suitable. Other sources of radial variation information are required to complete the density description.

CONCLUSIONS AND RECOMMENDATIONS

The primary purpose of this study was to develop a method for determining the lunar gravitational potential and to demonstrate its validity with existing data. Gravity is modeled with a truncated Legendre polynomial expansion plus a finite number of mascon terms. Several conclusions can be reached on the basis of the results.

It is logical to assume that the best lunar model lies between a pure spherical harmonic representation and an oblate, triaxial body with near-surface mascons. However, evidence indicates the latter extreme to be more representative of the moon. This is further supported by the work reported here. Furthermore, mascons have been modeled successfully as constrained third-body sources, and such a representation is compatible with spherical harmonics.

If a truly accurate gravity model of the moon is to be obtained, the hybrid model should be

used directly with raw tracking data. The model would be an oblate, triaxial body with many near-surface mascons.

Finally, the methods used here can be applied to other planetary bodies with near-surface mass anomalies. For the earth, crustal plates can be considered mass anomalies and can be treated as third bodies. Because of plate sizes, it would be necessary to subdivide them into several sections to achieve high resolution and accuracy.

Acknowledgment. One of us (Kunciw) was a National Science Foundation trainee during the performance of this work.

REFERENCES

- Battin, R. H., *Astronautical Guidance*, McGraw-Hill, New York, 1964.
- Bryant, R. W., The effect of solar radiation pressure on the motion of an artificial satellite, *NASA Tech. Note TN D-1063*, 1961.
- Kunciw, B. G., Accurate gravity and density models for the moon, M.S. thesis, Dept. of Aerospace Eng., Pa. State Univ., University Park, 1971.
- Lorell, J., Lunar orbiter gravity analysis, *Tech. Rep. 32-1387*, Jet Propul. Lab., Pasadena, Calif., 1969.
- Lorell, J., and P. A. Laing, Compilation of lunar orbiter tracking data used for long-term selenodesy, *Tech. Memo. 33-419*, Jet Propul. Lab., Pasadena, Calif., 1970.
- Muller, P. M., and W. L. Sjogren, Lunar gravimetry and mascons, *Appl. Mech. Rev.*, **22**, 955, 1969.
- Wong, L., G. Buechler, W. D. Downs, and R. H. Prislin, Dynamical determination of mascons on the moon (abstract), *Eos Trans. AGU*, **50**, 125, 1969.

Estimate of the Gravity Anomalies of Venus

P. BALDI, E. BOSCHI, AND M. CAPUTO

*Istituto di Fisica, and Istituto di Geodesia,
Università di Bologna, Bologna, Italy*

Abstract. We discuss the geodetic aspects and some physical features of the interior of Venus. The pressure, density, and temperature distributions are estimated. The gravity anomalies caused by convection currents, topography, and other effects are then estimated. We conclude that the tesseral harmonics of the field could be twice those found on the earth.

Among the terrestrial planets, Venus is the one for which it has been most difficult to infer physical features from geodetic characteristics. To begin with, the low rotation rate implies a very small flattening, and the absence of natural satellites does not allow the observation of any possible bulge. All this in turn negates speculation on physical properties of the planet such as strength, viscosity, and density distribution.

In this paper, we discuss some of the geodetic aspects of Venus using the mass, the radius, and the surface temperature of the planet. From these we shall attempt to deduce some of the physical properties of the planet and of its gravity anomalies, mainly those arising from convection currents and topography.

CONVECTION CURRENTS

To discuss some of the geodetic aspects of Venus, we first mention tentatively some physical aspects of the interior of the planet.

In some ways, the planet is similar to the earth, as can be seen from Table 1.

The pressure distribution can be estimated with some accuracy in the outer region of the planet by assuming a density distribution similar to that of the earth, starting from the surface, and by applying a factor ρ to match the total mass of the planet after subtracting from the earth the mass M_s of a small central core of radius equal to $R_E - R_v$ and properly reducing the remaining mass:

$$\rho_v = \rho^{-1} \rho_E$$

$$\rho_v = \frac{\text{reduced earth mass}}{\text{venus mass}} = 1.05$$

From this density distribution, we can compute the pressure distribution versus depth. We estimate that the error in the pressure for the outer part of the planet that is of interest to us, say the first 1000 km, is less than a few per cent or at most ten kbars. The pressure curve is shown in Figure 1.

The next parameter to consider for the discussion of the interior of the planet is temperature. Even for the earth, this parameter is poorly known; at 3000 km, an error of several hundred degrees is possible, but the estimates at lower depth have smaller uncertainties. The temperature at 700-km depth is about 3000°C according to different authors [Jeffreys, 1970; Kaula, 1968]. We know that the surface temperature of Venus is about 500°C more than the surface temperature of the earth [Marov, 1970]. We also assume the same radioactive content for Venus as for the Wasserburg model of the earth [Wasserburg *et al.*, 1964]. Since the upper limit of the temperature is important to our discussion, in the Venus 1 model we assume that the temperature gradient versus depth is that of the earth beginning at 20-km depth, where the earth is presumably at 500°C. The temperature curve is shown in Figure 2.

The gravity anomalies of the earth's gravity field, according to most authorities, are caused by density anomalies deeply seated in the mantle. Presumably these anomalies are associated with convection currents, and the low harmonic part of the gravity anomalies should be associated with large cells that probably extend to 700-km depth, where earthquakes

TABLE 1. Similarities of Earth and Venus

Planet	Mean Radius, km	Mass, grams	Density, g/cm ³	Temp. at 700 km, °C	Pressure at 700 km, kb
Earth	6370	$5.98 \cdot 10^{27}$	5.52	2950	256
Venus model 1	6056	$4.88 \cdot 10^{27}$	5.11	3000	210
Venus model 2	6056	$4.88 \cdot 10^{27}$	5.11	3450	210

cease to occur, indicating a more favorable condition for slow continuous motion. Tentatively, we can try to estimate the depth at which this region begins in Venus by comparing its pressure and temperature conditions with those of the earth and by taking into account that the melting point of most materials increases with pressure.

By considering Figures 1 and 2, we see that at 700-km depth in Venus the temperature and pressure are about $T = 3000^\circ\text{C}$ and $p = 210$ kbar; from this we can estimate that the physical conditions (near melting point) of basalt corresponding to 700-km depth in the earth are the same in Venus at 250-km depth, where $T = 2250^\circ\text{C}$, $p = 80$ kbar. This result is obtained by correcting the values obtained for the earth with the gradient of the pressure-temperature curves of basalt.

At this depth we can expect to have the same conditions as for the earth for convection currents to occur and therefore to cause gravity anomalies.

In a second model, we take temperature versus depth in Venus to be the same as that of the earth with an addition of 500°C at any point

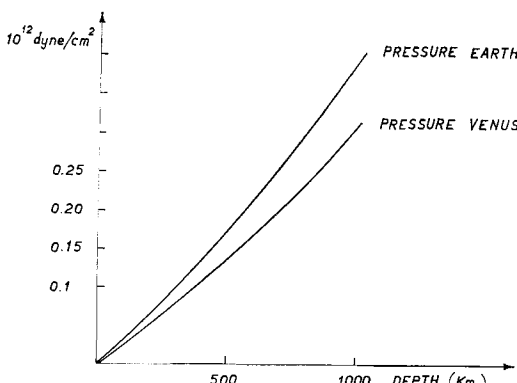


Fig. 1. Pressure versus depth in earth and Venus.

(Figure 3). This model should be considered as a limiting case because of the T^* dependence of conductivity that occurs above approximately 2000°C . We have a temperature of 3450°C at 700-km depth in Venus. From this we can estimate that the physical conditions (near the melting point) of basalt corresponding to 700-km depth in the earth are the same in Venus at 100-km depth, where $T = 2100^\circ\text{C}$, $p = 25$ kbar.

For the first model, dunite in the earth should be at a temperature below the melting point to a depth of 1000 km, whereas in Venus it should be at about the melting point from 500 km down.

For the second model, dunite in Venus should be at a temperature near the melting point from 200 km down.

We can repeat the considerations above assuming for Venus the temperature that results

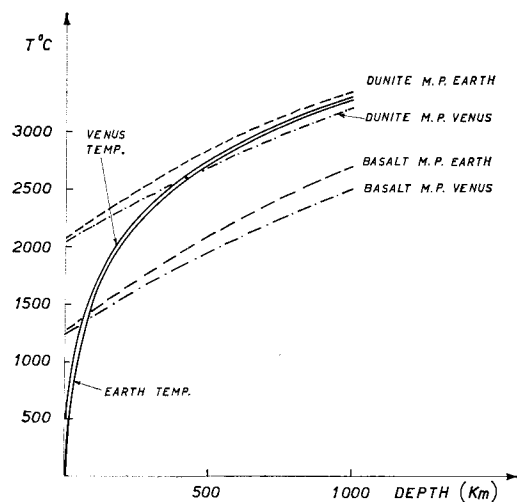


Fig. 2. Temperature versus depth from thermal history. The gradient for Venus is that of the earth beginning at 20 km.

BALDI, BOSCHI, AND CAPUTO

277

for the earth from electrical conductivity, with an addition of 500°C (Figure 4).

For the earth, dunite is at a temperature below the melting point to a depth of 1000 km, while basalt is at a temperature about the melting point from 600 km.

For Venus, instead, basalt and dunite are at a temperature near the melting point from 100 km and 700 km, respectively.

Because of the higher temperature, Venus should have faster convection currents and probably a greater density contrast at a depth lower than 700 km.

The existence of nonhydrostatic low-degree harmonic terms in the earth's gravitational field has been proved by satellite observations. The associated variations of the density in the mantle might have arisen during the earth's formation and been maintained since by the finite strength of the mantle, but we do not think this likely.

Alternatively, they may result from convection, in which case there should be a relation between the gravity anomalies and those surface features from which the existence of convection has been inferred, for example, the oceanic rises [Runcorn, 1964; Bott, 1967; Kaula, 1971]; because of the similarities between the two planets, we believe this to be the case for Venus.

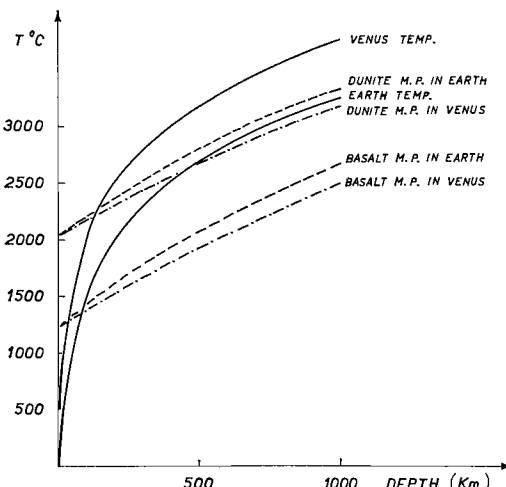


Fig. 3. Temperature versus depth from thermal history. In Venus the gradient is the same as that in the earth.

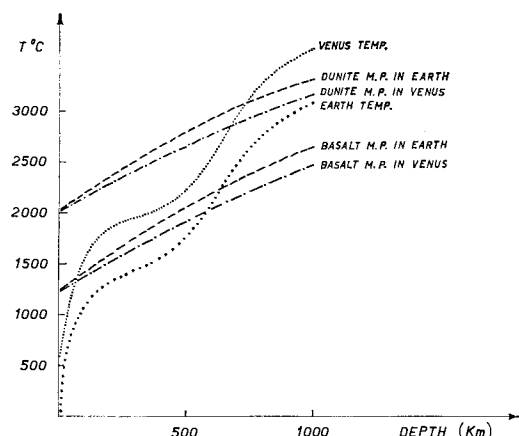


Fig. 4. Temperature versus depth estimated from conductivity.

The formula that gives the anomalies of the gravitational potential at the surface of the planet caused by density contrast d , described by the spherical harmonic coefficient H_{lm} at a depth H of a planet of radius a and mean density d_m is [Jeffreys, 1970]:

$$C_{lm} = \frac{3dH_{lm}}{(2l+1)ad_m} \left(1 - \frac{H}{a}\right)^{l+2}$$

A conservative guess is that the gravity anomalies in the model Venus 1, caused by the same kind of deep density anomalies as in the earth, could be at most twice that on the earth for a change of 450 km in H and the same density contrast.

In the second model, the gravity anomalies could be more than twice that on the earth for a change of 600 km in H .

Between the two models for temperature, the model in which we assume the superficial temperature gradient versus depth to be the same as in the earth will be considered a borderline model. Therefore we conclude that the gravity anomalies on Venus, caused by the same kind of deep density anomalies, could be larger than on the earth by a factor between 1.5 and 2.

A discovery of gravity anomalies of this magnitude could support a theory of convection currents in the interior of Venus. This could be detectable if we could obtain range rates to an accuracy 0.1 cm/sec with respect to a Venus orbiter.

TOPOGRAPHY

It has been observed by radar that on Venus there are elevations comparable to those found on the earth. The considerations that we have made above suggest that this topography is highly compensated isostatically. The physical conditions for isostatic compensation, which in the earth occurred in the past at about 30-km depth, on Venus should occur at much smaller depth, owing to the temperature condition, although the lower value of gravity would make the process slower. Isostasy might occur at, say, 10-km depth.

Even if we assume that the strength of the thin crust of Venus is the same as for the earth, which is hard to accept because of the higher temperature, then in spite of lower gravity (about 10% less) the gravity anomalies caused by topography would be much smaller than the corresponding anomalies in the earth and therefore would be difficult to detect with a satellite. This is of course true only for isostatically compensated topography.

GRAVITY ANOMALIES OF VENUS

If there is topography supported by dynamic forces, such as shallow convection currents, then there is the possibility of having correlated gravity anomalies. This of course could be detected by radar observations from satellites or from the earth.

REFERENCES

- Bott, M. H. P., Terrestrial heat flow and the mantle convection hypothesis, *Geophys. J. Roy. Astron. Soc.*, 14, 413, 1967.
Jeffreys, H., *The Earth*, 5th ed., p. 381, Cambridge University Press, London, 1970.
Kaula, W. M., *An Introduction to Planetary Physics*, John Wiley, New York, 1968.
Kaula, W. M., Prospects for planetary geodesy, *Eos Trans. AGU*, 52, 181, 1971.
Marov, M. Ya., The model of Venus atmosphere (tentative recommendation to Cospar Working Group 7), Cospar preprint, 1970.
Runcorn, S. K., Satellite gravity measurements and a laminar viscous flow model of the earth's mantle, *J. Geophys. Res.*, 69, 4389, 1964.
Wasserburg, G. J., G. J. F. McDonald, F. Hoyle, and W. A. Fowler, Relative contributions of uranium, thorium and potassium to heat production in the earth, *Science*, 143, 465, 1964.

Prospects for Planetary Geodesy¹

WILLIAM M. KAULA

*Department of Planetary and Space Science
Institute of Geophysics and Planetary Physics
University of California, Los Angeles 90024*

Abstract. Within the current decade, it can be anticipated that there will be significant improvement in knowledge of the physical librations and body tides of the moon, topographic variations of the inner planets, the low-degree harmonics of the gravity field of Mars, and the masses of Mercury and the outer planets. There will also be some improvement in knowledge of lunar topography, lunar gravitational variations, the oblatenesses of Venus and Mercury, and the oblateness of the outer planets. The principal need to attain further improvement for virtually all bodies is close-orbiting spacecraft. It is also desirable to improve radar capabilities.

This paper is essentially a supplement to Kaula [1971], which reviews progress in selenodesy and planetary geodesy over the past four years.

The objects of study in planetary geodesy can be divided into three classes on the basis of accessibility, which in turn is essentially a matter of distance. In Table 1, each of these classes is represented by a row. The columns in the table correspond to stages of technical implementation applicable to geodetic measurement of these bodies. 'Here' denotes work already accomplished, as reviewed by Kaula [1971]. 'Near' denotes work that is being carried out as part of an ongoing NASA project. 'Far' denotes work that is not yet incorporated in any flight project or instrumental development.

THE MOON

A resolution of about 40 km of features of the gravitational field of the moon has recently been obtained from Doppler tracking of Apollo 14 near pericenter, for which the altitude was only 16 km [Sjogren *et al.*, 1972]. However, for most of the front side of the moon, the resolu-

tion is probably no better than 200 km: i.e., about twice the altitude of the spacecraft used to infer the variations. This resolution implies tracking accuracy of about ± 1.0 mm/sec, using the procedure described by Kaula [1970] and assuming a power law $2 \times 10^{-4}/l^2$ for the rms magnitude $\delta_l(V^*)$ of the normalized dimensionless spherical harmonic coefficients of the moon's field:

$$l = 1738\pi/200 \approx 27 \quad (1)$$

$$\begin{aligned} \delta_l(v) &= (GM/a)^{1/2}(R/a)^{l+1} \delta_l(V^*) \\ &= (4.9 \times 10^{18}/1.84 \times 10^8)^{1/2} \\ &\quad \cdot (1.74/1.84)^{28} 2 \times 10^{-4}/27^2 \\ &= 0.009 \text{ cm/sec} \end{aligned} \quad (2)$$

We assume

$$\epsilon(v) \approx 10 \delta_l(v) = 0.09 \text{ cm/sec} \quad (3)$$

The main needs are now (1) near-side topographic elevations of comparable accuracy and resolution; and (2) far-side gravitational variations.

For topographic elevation needs, the spectrum of a surface coating equivalent to the potential is:

¹ Publication 961, Institute of Geophysics and Planetary Physics, University of California, Los Angeles 90024.

PROSPECTS FOR PLANETARY GEODESY

TABLE 1. Stages of Planetary Geodesy

Bodies	Distance, R_E	Here	Near	Far
Moon	$\sim 10^2$	Orbiters, ranging	Metric photography Laser altimetry Tidal gravimeter	Satellite-satellite tracking Gravity gradiometry
Inner Planets	$\sim 10^4$	Probes, ranging	Orbiters	Gravity gradiometry
Outer Planets	$\sim 10^5$	Passive techniques	Probes	Orbiters, ranging

$$\begin{aligned} \delta_i(\sigma) &= \frac{(2l+1)M}{4\pi R^2} \delta_i(V^*) \\ &= \frac{54 \times 7.35 \times 10^{25}}{4\pi(1.74 \times 10^8)^2} 2 \times 10^{-4}/27^2 \\ &= 2.87 \times 10^3 \text{ g/cm}^2 \end{aligned} \quad (4)$$

We assume

$$\epsilon(h) = 10 \delta_i(\sigma)/\rho = 86 \text{ meters} \quad (5)$$

An extraordinarily accurate system is thus not required to make isostatic corrections, etc., to an accuracy compatible with knowledge of the gravity field. The *J*-series Apollos, 15 through 17, carry 3-inch metric cameras and laser altimeters of ± 1 -meter accuracy with data points at 20 sec, or 32 km, intervals. The main limitation is the coverage afforded by these orbits: a total of only 6% of the moon's surface.

The *J*-series Apollos also carry out a satellite-to-satellite tracking experiment between the main spacecraft and a small subsatellite. The duration of the Apollo spacecraft in orbit around the moon, 120 hours, is not long enough, however, to get more than a small fraction of the farside gravity field in this manner [Esenwein *et al.*, 1971].

Other work in the 'here' and 'near' stages are ranging from the earth to the moon by laser, and gravimetry at the Apollo landing sites. Apollo 15 has landed a third retroreflector on the moon for laser ranging, thus enabling a strong determination of the physical librations about all three axes. Apollo 17 will land a precise tidal gravimeter, which should yield an estimate of the gross elastic properties of the moon, plus a mobile gravimeter to support geologic analyses of the region traversed by the astronauts in their mobile vehicle.

The completion of the Apollo flights will leave much feasible selenodesy undone. Measurements that could well be made from an unmanned

orbiter are laser altimetry and gravity gradiometry. To obtain 200-km resolution from a gradiometer orbiting at, say, 50-km altitude, the accuracy required under the same assumptions as in equations 2-5 would be:

$$\begin{aligned} \delta_i(\nabla \Delta g) &\approx [GM/a^3] \\ &\cdot [R/a]^{l+1} l(l+1) \delta_i(V^*) \\ &= [4.9 \times 10^{18}/(1.79 \times 10^8)^3] \\ &\cdot [1.74/1.79]^{28} 2 \times 10^{-4} \\ &= 1.6 \times 10^{-10} \text{ cm/sec}^2/\text{cm} \\ &= 0.16 \text{ EU} \end{aligned} \quad (6)$$

We assume

$$\epsilon(\nabla \Delta g) = 10 \delta_i(\nabla \Delta g) = 1.6 \text{ EU} \quad (7)$$

Such an accuracy is now believed to be quite feasible for an orbiting gradiometer [Bell *et al.*, 1971].

THE INNER PLANETS

The principal new data beyond that reviewed by Kaula [1971] are variations in the gravity field and topography of Mars obtained by the Mariner 9 orbiter. The orbit of Mariner 9 has an inclination to the equator of 64.4° , a semi-major axis of 3.72 Martian radii, and an eccentricity of 0.62. Despite the large semimajor axis, variations in the Martian gravity field equivalent to sixth-degree harmonics have been sensed. These variations are larger by a factor of 5 or 10 than what is predicted by equal stress scaling from the earth and moon [Lorell *et al.*, 1972]. Some more information about features near pericenter may be obtained from velocity residuals. Using the pericenter radius in place of semimajor axis in (2), putting 0.01 cm/sec for $\delta_i(v)$, and employing Martian parameters

WILLIAM M. KAULA

281

with $5 \times 10^{-5}/l^2$ for $\delta_i(V^*)$ (approximately the geometric mean of the moon and earth), we get:

$$\begin{aligned}\delta_i(v) &= [GM/a]^{1/2}(R/r_p)^{l+1} 5 \times 10^{-5}/l^2 \\ 0.01 &= 9.0 \times 0.736^{l+1}/l^2\end{aligned}\quad (8)$$

which yields $l = 8$, or features of about 1300-km extent. It is therefore to be hoped that future orbiting spacecraft will be placed in close circular orbits of fairly long duration.

Mariner 9 is also acquiring a lot more detail about topographic variations, through photography, occultations, and infrared measurements of atmospheric CO₂ content.

The 1973 Venus-Mercury flyby will yield a greatly improved determination of the mass of Mercury. Information will also be obtained on the radius of Mercury, to supplement the radar, and estimates of J_2 for both planets, but nothing more on variations in the two planets.

It can be anticipated that with improvements in the great radars and the occurrence of favorable oppositions, there will be a gradual improvement in knowledge of the rotation rates and topographic variations of the inner planets. The need is for more close-orbiting spacecraft, to obtain the variations in the gravitational fields. Improvements in the Deep Space Network tracking facility [*Jet Propulsion Laboratory, 1971*] being made primarily for missions to the outer planets would help obtain these details of inner planet structure.

THE OUTER PLANETS

Appreciable improvement in knowledge of outer planet masses is being made by the systematic analysis of the complete record of astronomic observations of their positions. Within the past year, there has been an appreciable downward revision of the upper limit on the mass of Pluto [*Seidelmann et al., 1971; Ash et al., 1971*]. An order-of-magnitude improvement in mass determination will occur when deep space probes pass close to these planets. So far, only the Pioneer F and G probes to Jupiter in 1973 are ongoing projects. More

ambitious 'grand tour' missions now appear to be postponed to the 1980's.

Because the major planets are so close to hydrostatic equilibrium, the prospect of obtaining significant information about their gravitational variations from probes is remote. What is needed, again, is orbiting satellites. A circum-Jupiter orbit is being considered as an optional use of instrumentation under development for possible grand tours. However, the major planets already have natural satellites, and probably the most economic means of obtaining improved knowledge of J_2 and J_4 , and hence of radial density variation in the planets, would be by enhancing the earth-based radar capability to the stage where it could track the natural satellites.

REFERENCES

- Ash, M. E., I. I. Shapiro, and W. B. Smith, The system of planetary masses, *Science*, **174**, 551-556, 1971.
- Bell, C. C., R. L. Forward, and H. P. Williams, Simulated terrain mapping with the rotating gravity gradiometer, in *Advances in Dynamic Gravimetry*, edited by W. T. Kattner, pp. 115-128, Instrum. Soc. Amer., Pittsburgh, Pa., 1971.
- Esenwein, G. F., F. I. Roberson, and D. L. Winterhalter, Apollo in lunar orbit, *Aeronaut. Astronaut.*, 52-63, April 1971.
- Jet Propulsion Laboratory, The Deep Space Network, *Tech. Rep. 32-1526*, Jet Propul. Lab., Pasadena, Calif., 252 pp., 1971.
- Kaula, W. M., Selenodesy and planetary geodesy, *Eos Trans. AGU*, **52**, IUGG 1-4, 1971.
- Kaula, W. M., The appropriate representation of the gravity field for satellite geodesy, in *Proceedings of the 4th Symposium on Mathematical Geodesy*, pp. 57-65, Com. Geod. Ital., Bologna, 1970.
- Lorell, J., G. H. Born, E. J. Christensen, J. F. Jordan, P. A. Laing, W. L. Martin, W. L. Sjogren, I. I. Shapiro, R. D. Reusenberg, and G. L. Slater, Mariner 9 celestial mechanical experiment: Gravity field and pole direction of Mars, *Science*, **175**, 317-320, 1972.
- Seidelmann, R. K., W. J. Klepczynski, R. L. Duncombe, and E. S. Jackson, Determination of the mass of Pluto, *Astron. J.*, **76**, 488-491, 1971.
- Sjogren, W. L., P. Gottlieb, P. M. Muller, and W. Wollenhaupt, Lunar gravity via Apollo 14 Doppler radio tracking, *Science*, **175**, 165-168, 1972.

7. Data Management

Considerations for an Earth Physics Information-Management Service

ROBERT W. MARTIN AND FREDERICK D. YOUNG

Smithsonian Astrophysical Observatory, Cambridge, Massachusetts 02138

Abstract. In a preliminary investigation into the feasibility of establishing a data center for earth physics, 12 disciplines were considered for inclusion. Estimation of the size of the data base for each indicated a need for storage of approximately 10^{10} characters. The computer-based system deemed most worthy of further investigation was the interactive concept with remote-terminal access. In an earlier study, we examined costs versus number of terminals, as well as much of the hardware and software requirements. Costs are not considered here, and only those aspects of the center's resources that a user would ordinarily encounter are considered. Users are divided into three classes according to how they would access information: with no terminal, with an interactive terminal, and with a multidevice terminal. All these users can be served by the same center without any particular difficulty, but the real benefactor is the user with an interactive terminal, because he can compile, debug, and run programs in one continuous session. Final points stressed are multiprogramming for dynamic resource sharing, hardware modularity for future expansion, and information protection for such a large community of users. We conclude that a survey should be conducted to gather more information from the potential users of such a system, and that a pilot project should be developed at some location where both earth-physics research and data-processing capabilities already exist.

Space techniques provide powerful methods for measuring physical quantities involved in the phenomena of the earth as a mechanical system. Results to date and the promise of future advances justify a vigorous earth-physics program within the national space effort.

Studies such as that at Williams College during the summer of 1969 have covered the instrumentation and procedures that will generate a broad spectrum of new information about the earth [Kaula, 1970]. Less attention has been directed to the problems associated with the organization, accessibility, and application of the information generated. This study addresses some aspects of information management for an earth-physics program.

The information-management concept envisioned here would usually not be concerned

with primary observational data. These data would presumably be handled by appropriate data banks, following current practice. The World Data Centers that have evolved from IGY and IQSY activities are examples of such existing capabilities. For the United States, the National Space Science Data Center (NSSDC) at Goddard Space Flight Center (GSFC) is another example.

Similarly, the many specialized scientific groups that use primary observations to derive fundamental earth physics results would be expected to continue their necessary roles. They would publish or otherwise make available the resultant information in their preferred media. The International Polar Motion Service (IPMS), the Bureau Internationale de l'Heure (BIH), and the United States Naval Observa-

tory (USNO) are examples of organizations of this type.

From such primary sources, the information-management activity considered here would assemble and transcribe in computer-accessible form an appropriate selection of information to support an earth physics applications program. For convenience in this report, the name earth physics information-management service (EPIMS) will denote this activity.

The available information about the earth, particularly that generated by space techniques, has by 1971 become very detailed. The involved formalism required to represent such detail dictates that many applications of this information must utilize a sizable computer. This is to be expected, because the fundamental information in almost all instances has been achieved by sophisticated computer operations. Thus, it is natural to inquire whether there is some efficient technique, still utilizing computer methods, that can be used to manage the accumulated information and make it conveniently available to all potential users. In this age, the printed page would not seem to be an efficient or optimum intermediary between computer-generated information about the earth and computer-formulated applications of this information.

Many computer-oriented information-management approaches can be envisioned. One intriguing possibility would offer interactive, remote-terminal access to a major computer in which the information would be retained in a convenient manner. If the peripheral equipment at the computer were sufficiently versatile, any organization with a terminal for computer access via telephone circuits could also call upon the earth physics information service. Many potential users already have such terminals.

The interactive feature of the system would allow an unfamiliar user to inquire as to what information is available and in what format, and how to reach it. He could use his remote terminal to write his own program, transforming the information into the form he requires and performing the desired calculations based on the data.

The main body of this study is divided into three parts: specifications for the data base, specifications for hardware and software for the computer center, and conclusions and recommendations.

The first part deals with the specifications that must be met by this information-management system. These specifications follow from the nature, format, and scope of available and anticipated information. These specifications must reflect an assessment as to which data will be in sufficient demand to justify treatment by the envisioned techniques.

DATA BASES AND PROCESSES FOR EARTH PHYSICS DISCIPLINES

Twelve general areas of investigation within the earth physics research field were considered for inclusion into EPIMS:

1. Time and frequency standards.
2. Earth's rotational motion.
3. Positional astronomy.
4. Geometrical geodesy.
5. Earth's gravitational potential.
6. Geology and global tectonics.
7. Atmosphere.
8. Ocean.
9. Ionosphere.
10. Earth's magnetic field.
11. Ground instruments.
12. Spacecraft.

The earth's gravitational potential provides a brief example of the detailed treatment of these topics.

The geopotential is most usefully represented by means of spherical-harmonic expansions. The definition of the expansion used should be clearly stated, and facilities should exist for converting the coefficients to one or another of the principal methods of normalization. Degrees of the harmonics up to about 25, or about 650 coefficients, can be expected in the near future. The geopotential or functions thereof can be requested for specific points, and programs should be made available to compute the following (see Table 1):

- A. Free-air gravity anomalies referenced to a specified surface, both at the earth's surface and in space.
- B. The height of the geoid above a specified reference surface.
- C. Deflections of the vertical at the earth's surface and in space.

In addition, requests for information on different types of gravity anomalies are anticipated: for example, isostatic anomalies. Thus,

TABLE 1. Information for the Earth's Gravitational Potential

Service	Description	Size (characters)	Classification
Spherical-harmonic coefficients	Provides several sets of currently used normalized coefficients of the spherical-harmonic expansion of the geopotential.	10^4	Base
Surface-gravity measurements	Provides one or more sets of surface-gravity data, probably as area means over $1^\circ \times 1^\circ$ or $5^\circ \times 5^\circ$ squares.	10^6	Base
Free-air gravity anomalies from the geopotential model	Computes gravity vector at specified coordinates, using standard representation.	10^6	Process
Geoid profile	Computes geoid height above a specified reference surface, using standard representation.	10^6	Process
Tidal geopotential variations	Represents tidal dependence of the geopotential.	10^6	Base
Annual geopotential variations	Represents annual, and eventually other, long-period variations of the geopotential.	10^6	Base

models for the elevation of the earth's topography and for the depth of compensation are required. Information on mean height above sea level is currently available for the entire surface of the earth, either as 5° by 5° area means or as a spherical-harmonic expansion up to degree 35.

Some collection of surface-gravity measurements should be tabulated, including the methods of reduction and averaging that have been used. The data will most likely be in the form of area means, possibly from 1° by 1° squares to 5° by 5° squares. Data programs should exist for converting the observations from one reference surface to another and for converting different types of gravity anomalies.

There are already some determinations of the time dependence of the spherical-harmonic coefficients in the geopotential. These should be included, when desired, in the potential representation.

As is indicated, twelve general areas of investigation were considered for EPIMS. The following tabulation gives initial estimates of the size of the data base (in number of characters of storage) for each:

Time and frequency standards	10^6
Earth's rotational motion	10^5
Positional astronomy	10^8
Geometrical geodesy	10^6
Earth's gravitational potential	10^6
Geology and global tectonics	10^8
Atmosphere	10^6

Ocean	10^7
Ionosphere	10^6
Earth's magnetic field	10^6
Ground instruments	10^6
Spacecraft	10^6

GENERAL PROBLEMS

We next consider the general problems involved in organizing a computer system for managing the data from an earth physics program. Areas treated include the concept of the center, access modes, availability and storage of information, features of the central computer, and protection of information.

To examine the concept of the center, let us consider the case of a scientist who wishes to work with a model of the atmosphere as part of his earth physics research. Depending on the size of his organization, he might have a good library or suitable computing facilities at his disposal. Or, through the efforts of a center such as NSSDC, he may know of results published by NASA. If he is successful in locating a suitable model, with additional time and effort he could perhaps obtain a computer-program version through yet another NASA facility such as the Computer Software and Management Information Center (Cosmic). With still a further expenditure of time, money, and effort, he could implement that program on the facilities at his own location or perhaps through a commercial service bureau. Hence, a typical scientist might, through considerable good fortune

EARTH PHYSICS INFORMATION-MANAGEMENT SERVICE

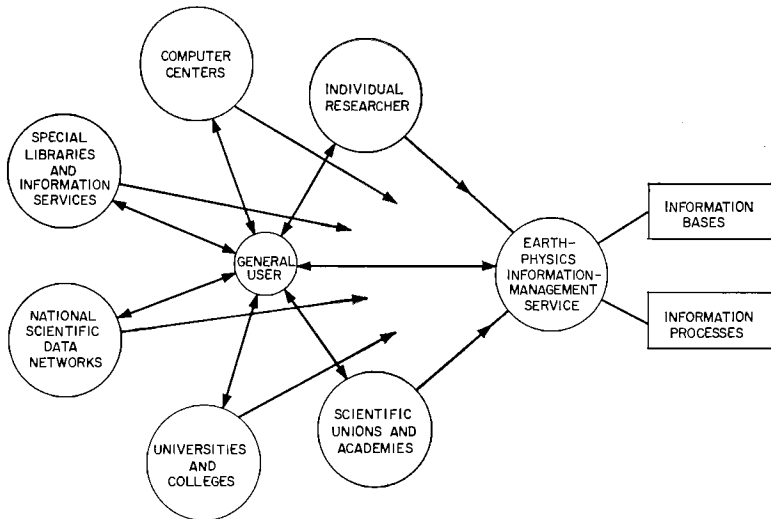


Fig. 1. Structure of EPIMS.

and with a minimum of three or four organizational contacts, achieve his original aims. The total inefficiency of this process is compounded by the number of researchers and organizations dealing in earth physics.

By combining the features of a computer service bureau and a special library through a centralized facility, EPIMS could achieve better results with considerably less effort and cost. Such a facility would provide a focus for both the active and the transient user in earth physics, as well as an interface service to the existing complex, heterogeneous, and sometimes confusing sources of information. Figure 1 shows a conceptual structure of the center and its interfaces.

We anticipate that EPIMS will become a general contact point for the scientific community for the coordination of earth physics information. As such, the center would interface with individuals and organizations having a wide range of capabilities and needs. In general, we could classify the access modes into three types: (1) no terminal, (2) interactive terminal, and (3) multidevice terminal.

The users who do not require or do not have a terminal to the center would largely be researchers who are not directly involved in earth physics or whose volume is so low as not to warrant a minimal terminal. In general, we expect that their requests would be received

by phone or mail, and the center must have adequate staffing and query terminals so that these requests can be processed in the same manner as would requests from a user who has his own console.

It will be necessary to publish a directory of services, data processes, and bases available, particularly to aid the nonterminal user. However, publication is not a goal of the center, except in this limited context.

Most users will employ EPIMS through one of a number of commercially available inquiry-response terminals, either teleprinter or cathode ray tube. We expect that a user would, in general, query the system through the console as to the availability of various information models, processes, and data bases. After this information search, he would find either a suitable model available to him with appropriate format options for his use or directive information on other possible sources to search. User-computer interactions would continue until this process had been exhausted.

In conversational computing, we can define an interaction cycle between the user and the computer system as composed of four basic elements: think, input, response, and output. We can define the action time as being the sum of the output, the think, and the input elements. When a user is interacting heavily with the system, it has been observed that the action

MARTIN AND YOUNG

287

time averages about 20 sec [*Hyman, 1967*] on a wide range of systems. It has further been observed that a response time exceeding 10 sec is unsatisfactory. A response time of up to 2 sec seems to provide the desired continuity for user-machine interaction.

Some users of EPIMS will have access either to a computer system or to a high-speed terminal that can act as a remote station. A group of users geographically close would warrant installation of terminal devices other than interactive consoles. In this context, a multi-device terminal would probably be made up of a line printer, a card punch, a card reader, and optional magnetic tape units. Data transmission would be carried on in the range of 2000 to 28,000 bits/sec. We expect there would be a limited number of such user facilities.

Considerations of information storage go beyond the physical volume required. It will be necessary to develop techniques, procedures, and guidelines to consider such matters as who should determine what is stored and available and why, how much information is required, and how long the information should be available.

Of necessity, the personnel and staff of an information center such as EPIMS will become technological and scientific gatekeepers. This extremely difficult role will require an awareness of the state of scientific development in many fields. The task will be laced with the subtleties required in dealing with a heterogeneous mix of national and international organizations and of individuals. If, for example, there are six currently accepted atmospheric models, but only two are considered necessary for such an information center, the care required to make such choices cannot be overstated.

From the nature of the computer-oriented information-management system being considered here, it is possible to specify in a general manner the major features of the desired computer system. It is evident that the hardware selected should permit the implementation of an interactive multiprogrammed system in a straightforward, optimum manner.

Multiprogramming is desirable from an economic point of view, since it allows dynamic sharing of the available resources among two or more programs. Specifically, it permits the overlap of computing and input-output opera-

tions, which should be a major asset for the type of system being considered. The reasons for specifying an interactive system are many. Interactive systems are usually associated with time-shared systems, mainly because time sharing has been emphasized by those seeking to provide interactive access to a computer. The concept of interactive computing and, consequently, time sharing derived its main impetus from the lack of satisfactory debugging capabilities in a batch-processing mode. Currently, the real benefit of interactive computing is the ability to compile, debug, and run programs in one continuous session at a console. This has had an unexpected impact on research. In fact, *Corbató and Vyssotsky [1965]* have stated, 'The availability of the MAC system has not only changed the way problems are attacked, but also important research has been done that would not have been undertaken otherwise.'

The hardware should be appropriately selected as an integral part of an interactive multiprogrammed system and should be modular as far as possible. Future expansion should include the possibility of multiple processors, as well as the upward expansion of the main memory. The desired modularity is indicated schematically in Figure 2.

Special problems with respect to protection of information arise when a computerized in-

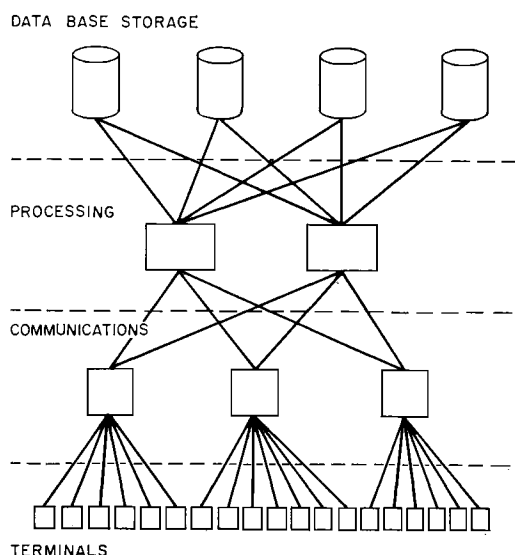


Fig. 2. Typical system configuration.

EARTH PHYSICS INFORMATION-MANAGEMENT SERVICE

formation system serves a large community of users, many of whom may be using the system simultaneously. There will be problems associated with the sharing of data and processes, as well as problems arising because groups of users may be working on cooperative efforts. Although 'privacy of information' may not be an issue here, since there should be no real conflict with respect to users' goals, protection is still highly desirable for several reasons:

1. Protection of processes limits the propagation of errors throughout the system while a user is debugging or utilizing what was thought to be a debugged process but is not.

2. Protection of information is necessary to prevent inadvertent (or malicious) changes or updating by improper authorities. This is quite necessary for reliable operation and reproducibility of results when identical tasks are being performed.

3. Protection is necessary for allocation of resources and usage records in order to ensure proper charging to users.

RECOMMENDATIONS AND CONCLUSIONS

After reviewing the information bases and processes available to the earth physics disciplines and the data-processing technology in existence today, we conclude that an earth physics information-management service is both desirable and feasible. Further, we feel that the potential benefits to both the general and the specialized user of earth physics information would be considerable. However, to ensure that the potential is there and can be met, we recommend the following:

1. A survey should be conducted of (a) data bases available, (b) data processes available, and (c) user interest and corresponding mode

of operation. The last part would be of a question-and-answer type designed to solicit both attitudes and information about current facilities that a given user might have for utilizing such a center. The surveyed users would represent the academic, government, and research communities.

2. A pilot operation of an earth physics information-management service should be developed at a location where a diversity of earth physics research talent and data-processing capabilities already exist. The initial data bases and processes provided would be those indicated in this study.

3. Both projects should be implemented in parallel, since the results of the survey could considerably augment the EPIMS data base but could still be inconclusive in terms of user attitude, which will develop with experience. Hence, operation of such a center will be the ultimate test of the concept.

Acknowledgment. This research was supported in part by grant NGR 09-015-107 from the National Aeronautics and Space Administration.

REFERENCES

- Corbato, F. J., and V. A. Vyssotsky, Introduction and overview of the Multics system, in *Conference Procedures, Fall Joint Computer Conference*, vol. 27, pp. 185-196, Spartan Books, Washington, D.C., 1965.
- Hyman, H., The time-sharing business, *Datamation*, 13, 49-57, 1967.
- Kaula, W. M. (Chairman), The terrestrial environment: Solid earth and ocean physics, Report of a study at Williamstown, Mass., *NASA Contract. Rep. CR-1579*, pp. 5-17, 6-10, 1970.
- Martin, R. W., and F. D. Young, Earth-physics data-management study, NASA final report, grant NGR 09-015-107, Cambridge, Mass., 69 pp., January 1971.

Summary

The papers in this monograph are extremely varied in subject, dealing not only with geodesy on the earth but also geodesy on the moon and on the other planets, and representing work done with either artificial or natural satellites. This summary is intended not only to give a glimpse at the key concepts of the individual papers, but to tie the papers more strongly together and to the art in general. The task is simpler if we keep to the same organization used in the main part of the volume, although ties between papers in different categories will be pointed out.

GEOMETRIC GEODESY: THEORY

Geodesy started as applied geometry, and throughout most of its history as the science of earth measurement has retained its geometric character. Until the latter part of the nineteenth century, the tools of the geodesist were scaled-up versions of the geometer's instruments: the tape, the transit, and the level. Even at the gateway to the era of artificial satellites and with worldwide gravity surveys going on around him, the geodesist still saw in these satellites primarily a new geometric tool—a new kind of beacon that was higher but still a beacon, to be used in exactly the same way that beacons have always been used.

With the accumulation of experience in satellite tracking and determination of satellite orbits has come a flexibility in the way artificial satellites are used. The first idea was that observations had to be made simultaneously from several stations to eliminate errors introduced by the satellite's motion. Although it is still believed that the highest accuracy is obtained by simultaneous observations, a considerable number of precise surveys are being made with satellite

positions calculated dynamically. The time interval and therefore the distance that the satellite can move between observations is selected on the basis of many factors besides orbital accuracy and may vary from a few milliseconds to several days. We will classify the survey methods, for convenience, into three modes:

- Simultaneous observation.
- Short arc.
- Long arc.

Obviously, there can be any combination of these modes also, but there is no need to complicate this summary by enumerating them. Nor is it necessary to make any fine distinction between short-arc and long-arc modes. We can classify a short-arc survey as that procedure in which all the observations necessary to fix a set of coordinates are made within a single revolution, and long-arc surveys as having the observations spread over more (usually considerably more) than one revolution.

The theory behind the simultaneous mode of survey is, in its major aspects, reasonably well fixed at present. Difficulties arise mostly in accounting for the very small but important error sources such as refraction, instrument time lag, and so on. These represent an irreducible residuum of errors that limit the attainable accuracy. But there is still considerable work going on in the theory of planning surveys. The problem of optimizing the distribution of observation stations is not as fully developed for satellite geodesy as for classical survey methods. It is therefore heartening that two papers on this subject are part of this volume. The one by Blaha is topological in nature and tries to find those surfaces that are the loci of observation stations and satellite

locations that produce poor geometry (for range measurement networks). He shows that surfaces to be avoided are generally of the second degree. This result is certainly of theoretical interest, although in practical work the occurrence of cases with avoidable bad geometry should not be frequent enough to warrant extensive application of Blaha's full analysis. Aardoom's paper attacks the same problem but on a more limited scale (for four distance-measuring equipment (DME) stations only) and with a more empirical approach; he solves the linearized equations for representative sets of station-satellite configurations. As one would expect, Blaha's and Aardoom's results agree where they can be compared. Aardoom, however, is more interested in finding good configurations than bad ones, so that the two papers taken together give a fair view of what the best and worst cases are like.

Perhaps a future paper will combine Blaha's and Aardoom's mathematics to provide a comprehensive survey. But an even more interesting extension would be one that optimizes the solution by finding configurations that produce the most accuracy for the least cost. Theories for surface surveys have been worked out by, among others, *Baarda* [1968]. A similar theory for satellite geodesy should be useful for planning. The situation selected by Aardoom and Blaha, a ranging network for simultaneous observations, is more restrictive than would be the case if short-arc methods were allowed also, and is considerably simpler than a network composed of both distance and direction measurements.

If the observations are not simultaneous, either the locations of the satellite at the time of observation must be known from independent sources, or the orbit must be determined along with the station locations. The latter case is usually equivalent to concurrent determinations of the observing station coordinates, the orbit, and the gravity field of the earth. The former is in principle the same as surveying by use of simultaneous observations. The paper by Baldini sets forth the theory for adjustment of quasi-simultaneous observations given the satellite directions, but does so from a viewpoint somewhat different from the usual one. Using satellite topocentric directions and a minimum of two astronomic station coordinates, he reduces

the satellite directions to an approximate earth-centered system, and subsequently adjusts the ground stations to the same system by minimizing deflections.

GEOMETRIC GEODESY: RESULTS

At the present time, there is only one global satellite geodesy project that is completely geometric in nature, i.e., makes use only of simultaneous observations and does not include orbital or gravity-field parameters as unknowns. This is the Worldwide Geometric Satellite Triangulation Program of the National Geodetic Survey. The current status of the project is given in the paper by Schmid in this volume. In order to fully appreciate the care and attention to detail that have gone into this project, a reading of earlier papers (e.g., the one referenced by Schmid) is essential. From Schmid's paper, we find that the project is concerned with determining the positions of 45 stations located so as to create an all-inclusive mesh with sides and angles as nearly uniform as sighting restrictions will allow. The rms error in the direction determined by a photograph is computed to be $\pm 0.24''$. Calculating the effects of all known or estimable errors on the accuracy of coordinates of a single station yields a position rms error of ± 4.2 meters. This is an excellent result, and is, we believe, considerably better than had been planned or expected at the start of the project when the shorter focal length BC-4 300-mm cameras were being used. The ± 4.2 meters probably reflects the ultimate accuracy achievable in this program.

Another project with almost, but not quite, the same independence of the orbit is the European Satellite Triangulation Program. A description of this program can be found in the proceedings of the 15th General Assembly of the IUGG, Moscow, 1971. The paper by Cazenave, Dargnies, et al. gives the results of a similar program carried out in 1968 by Centre National d'Etudes Spatiales and Smithsonian Astrophysical Observatory (SAO), using both laser DME and cameras. Thirteen stations were involved, but two were dropped because the number of simultaneous observations between them were small. Of the remaining 11 stations, two were equipped with laser DME.

HENRIKSEN, MANCINI, AND CHOVITZ

291

Where observations were not exactly simultaneous (by the lasers), interpolation was carried out. Standard deviations were ± 2 meters in each coordinate, or ± 3.5 meters over-all. This compares favorably with the value given by Schmid.

The next stage of progression from simultaneous observations toward totally independent observations is represented by the U.S. Corps of Engineers Secor program, its status being reported on by Rutscheidt and Dudley. Initially the Secor ranging equipment was intended to operate solely by simultaneous observations, four instruments at a time. It was found possible, however, to strengthen the solution by including short-arc observations, and the procedure at present mixes simultaneous and short-arc methods. Rutscheidt and Dudley's paper gives a few numerical results indicating that a ± 10 -meter accuracy can be achieved. The final results of the Secor equatorial belt will be obtained when orientation lines become available from the Pageos final adjustment.

Mueller et al. analyzed the Secor raw data thoroughly, solving many of the problems by dropping or modifying data as necessary to achieve internal consistency. Making an 'inner adjustment' and using other information on geoid heights, SAO coordinates for common stations, etc., they determined the rectangular coordinates of 10 Secor stations. Total (spherical) rms error varies apparently from about ± 12 meters to ± 16 meters based on limited amounts of data.

A particular mode of satellite surveying is more affected by placement of the observing stations than by the tracking instruments used. This principle is well illustrated by Baker's paper on 'mini-arc' determination. Baker's work was directed to problems anticipated in testing the satellite-borne altimeter tentatively to be launched by NASA in 1974 on the Geos C satellite. A precision of about ± 1 meter is expected from the altimeter. The orbit therefore ought to be known to better than ± 1 meter vertically in those orbital arc segments from which altimeter measurements will be made. This in turn effectively restricts segments to be used to the vicinity of high-precision tracking stations. The problem is then to find some way of computing the longest possible segments that have a vertical error much less than ± 1 meter, given the loca-

tions and equipment accuracy of the tracking stations. Baker's approach is to use a short arc (6 sec to 10 min, which he calls mini-arc) and to concentrate on minimizing the radial errors. A common procedure for computing short-arc orbits is to fit polynomials to the observed data. Experience shows that rms errors can be kept below ± 2 meters by this method over distances of up to 1000 km. To keep the rms error below 1 meter, and hopefully below 1 decimeter, Baker fits osculating orbits with first-order 'far-field' perturbations to very short segments, then combines the segments to produce the mini-arc. Actually, when we are concerned with eliminating errors of the order of a few centimeters, the rms error of the tracking instruments becomes a major factor, together with small local anomalies below the noise level of the tracking accuracy. The orbit-fitting approach of Baker can therefore be considered a forward step in the assault on a very difficult problem, but it probably is not the final solution.

A different approach is the long-arc mode employed by Marsh, Douglas, and Klosko. The method was dictated by the nature of the data available: observations of Geos 1 and Geos 2 flashes. The 25,000 observations were inserted into the equations of motion in sets covering 2-day long arcs, all parameters in the equations being fixed except the station coordinates and the orbital elements. The results, when compared to North American 1927 datum values for interstation distances, show differences of 5 to 10 meters. Comparison of coordinates of sites also occupied by the Jet Propulsion Laboratory showed similar agreement. What is significant about these results is the achievement of less than 10 meters error with the long-arc method. This compares very well with the simultaneous and short-arc results. Baker's values, in the centimeter region, are of course better, but these are at present completely theoretical and apply only to the orbit, not to the observing-station coordinates.

The paper by Bush is concerned with an analysis of expected survey and calibration results obtainable with Geos C. Using the existing range trackers, he found that the short-arc mode would suffice in tying the Atlantic and Pacific missile test ranges. His expected (spherical) standard deviations for station position are, over the arc from Cape Kennedy (Canaveral)

to Ascension, ± 15 meters, and over the Kwajalein to Cape Kennedy arc, ± 25 meters (referred to Vandenberg AF Base, California). These values are not really comparable to those in other papers. However, they are representative of results expected under difficult conditions of station and satellite availability and the use of only two or three successive passes in the short-arc solution.

PHYSICAL GEODESY: THEORY

The geoid can be found by the geometric method of astrogeodetic survey, but only in land areas and at considerable expense. (Astrogeodetic surveys at sea using instruments like the Geon of *von Arx* [1965] are still largely unproven, and the altimeter is yet in the future). A more indirect route, but one that can be used on land or sea and at less cost, is through the measurement of gravity. Before artificial satellites, derivation of the geoid from gravity data was almost solely by application of Stokes' formula, which gives the height of the geoid above a reference spheroid as a function of the gravity anomalies over the entire earth. In the early 1950's, deficiencies in Stokes' formula were being remarked, and modifications by *Molodensky* [1948], *Hirvonen* [1960], *Bjerhammar* [1960], and others were proposed and used.

With the advent of artificial satellites, a simpler approach to finding the grosser features of the geoid became available by applying the expression for the potential as a series of spherical harmonics. The reason this series is so useful for working with artificial satellite data is that it gives, when substituted into the equations of motion of a satellite, a set of differential equations that can be solved analytically (although not in closed form and not without considerable algebraic manipulation).

During the early years of satellite geodesy, the distinction between surface gravity and satellite gravity methods remained sharp, because surface data were too poorly distributed to yield good information about the gross features of the geoid, whereas satellite data were too coarse to offer any knowledge about the short-wavelength details. As data of both kinds grew better and more plentiful, it became obvious that the corresponding theories would have to be brought together so that the data could be combined. Various methods have been

presented for doing this, but only a few papers have been published comparing results of various methods. The most extensive computational comparison thus far is that by Hopkins in this volume. He numerically compares the methods of various authors using the same set of input data and examines the standard deviations of the results for the same spherical harmonic coefficients. However, since Hopkins' conclusions are entirely empirical, they give no indication as to the theoretical reasons behind the results. An analysis of the theoretical bases for the computational differences is obviously the next step. Analytic comparisons between a few of these and other methods have been made [e.g., *Pelinen*, 1969].

In studying the methods of combining satellite data with surface data, it should be remembered that the surface gravity data in their raw state are given for points at various distances above the reference ellipsoid. Before being compared with satellite data or introduced into the equations to be solved, these data are converted into gravity anomalies and averaged. This process can produce different levels of results depending on whether free-air, Bouguer, or isostatic anomalies are wanted. The geoid finally found by combining these data with satellite data will vary similarly. Khan, in his paper, evaluates the effects of these various kinds of gravity reductions on satellite-derived gravity values, up to coefficients of degree and order 16. He finds, as one might expect, that the lower-degree coefficients are not sensitive to the type of reduction employed, but that the effect increases as the wavelength decreases. This sort of analysis will become more important in the future as satellite data are more and more applied to problems in geology and tectonophysics.

While the Stokes' point-by-point integration and the spherical harmonic series are the most used and best known field representations, they are not the only ones possible and are certainly not the best for all purposes. The Stokes' formula requires knowledge of gravity all over the globe for the geoid at a given point to be found; the spherical harmonic method requires a knowledge of all the coefficients to get the total geoid height at a given point. The former is excellent for relative heights over short distances; the latter is best for relative average heights at large distances. *Koch* [1968] and

HENRIKSEN, MANCINI, AND CHOVITZ

293

Vinti [1971] have suggested using surface-layer mass distributions to generate short-wavelength gravity variations, and a number of papers have subsequently appeared exploring this approach. The paper by Koch in this volume describes the theoretical background. The difference between the models of Koch and Vinti is in the location of the surface layer. Vinti's placement on the surface of a sphere is simpler in concept, but, because the sphere is outside the earth at all points, causes difficulties in comparisons with surface gravity. Koch's method has been extensively covered by himself and by Morrison, who explores the way errors creep into satellite orbit computations when the anomalous gravity field is derived from surface layers. Obviously, no error would arise if the surface-layer representation were perfect. A well-known theorem guarantees that the surface layer will correctly generate the gravity field. But, as Morrison points out, in the actual computations the surface layer is approximated by a set of point masses, which generate errors. By using the point approximations, this method acquires characteristics of an approach described by Weightman [1967]. Weightman suggested that the gravity field might be more efficiently represented, over small parts of the earth's surface at least, by a suitable distribution of mass points than by Legendre functions. Weightman's point-mass distribution was, in its initial version, an entirely ad hoc affair, but further development has given his approach a more general aspect. Although the Koch-Morrison approach could be considered a special case of Weightman's, it should be remembered that the density layer method gives, theoretically, an exact representation of the field, but is computationally limited to point-mass approximation. Weightman's method tries to obtain the best field approximation with the fewest number of points, and in general uses a three-dimensional point distribution rather than a two-dimensional one. The paper in this volume by Balmino is an example of Weightman's method. Balmino finds that 126 points suffice to describe the same gravity field as the Smithsonian 1969 model, with an average error of 6 mgal. Since the Smithsonian field is defined by coefficients in a Legendre series, the approximation could in theory have been made exact by using more points. But the point-mass method is most efficient when describing very

local phenomena or very high-degree spherical harmonic functions. The application by Sjögren and Muller [1968] and by Wong *et al.* [1969] to lunar gravity are good examples.

In addition to the above approaches, there are beginning to appear theories derived from the communications sciences rather than the geophysical. The paper by Lundquist and Giacaglia describes one interesting approach to the problem of finding a more efficient mathematical description of the gravity field. Here, the sampling function is taken as the impulse response function of wave theory and is generalized to two dimensions on the sphere. Because it is similar to a unit response function, it can be used to define an arbitrary location of discrete data, and because it is a sampling function, it is efficient in presenting the information. Whether this particular sampling function is better than any other for the representation of the gravity field, it is too early to say, but there should be many promising avenues of exploration leading from Lundquist's and Giacaglia's work.

The papers by Schwarz and by Martin, Martin, and Smith attack the question of how finely the gravitational field can be resolved by satellite-to-satellite tracking.

Schwarz's approach is by numerical analysis of the distance between two satellites in close orbits, and of a geostationary satellite tracking a low-altitude one. His conclusion is that gravity variations between blocks 200 by 200 km can be distinguished from 200-km-high orbits. This would be equivalent to obtaining terms up to 90th degree and order.

The Martin, Martin, and Smith analysis considers only the case of a synchronous satellite tracking a lower one. Improved gravity field values result principally from the more continuous tracking possible and elimination of refraction effects. Their paper concentrates on the improvements expected in the lower-degree harmonics of the field.

PHYSICAL GEODESY: RESULTS

The initial geodetic objectives of the artificial satellites were modest, and in fact concentrated at first on the earth's flattening. As is well known, a value of 1/298.3 was found within a few months after the launching of the first satellite. Slight modifications to this value fol-

lowed, but values for higher-degree coefficients in the Legendre series expansion for the gravity potential came rapidly. Today, we have values up to degree and order 16, with a reasonable amount of confidence in those below degree 10. These values depend on the method of tracking used, the particular satellites tracked, on the locations of the observing stations, on the method of reduction, and on the theory employed, as well as on a number of minor factors such as the dates of the observations, and so on. For certain applications, differences in various sets of harmonic coefficients are not particularly important. For instance, some of the most consistent and best-analyzed gravity field values have for a long time been provided by the Naval Weapons Laboratory (NWL) as part of its support for the Transit navigation system. The NWL results differ somewhat from those of the others, but this is not as important as the fact that these NWL values provide a satisfactorily self-consistent navigation system. It will be found, on looking through the history of satellite geodesy, that self-consistency has been a major consideration in the use of satellite gravity data. The paper by Cazenave, Forestier, et al., for example, gives substantial improvements to Kozai's [1969] zonal harmonics up to 21st degree, the standard deviation being reduced by more than 70% in many cases. But the improvements are derived by observations on the particular satellites Dial, SAS, and People. Even if this new set was not an improvement physically, it would be just as useful for future tracking of these satellites, as long as it gave consistent results. The reason for emphasizing this point is that too much importance is sometimes placed on the differences in results, and insufficient attention is paid to the internal consistency of the data.

Of course this is not to say that such differences are immaterial. After we have filtered out the perturbations caused by factors that do not interest us, we can produce variance analyses that will disclose the factors that are important. The paper by Rapp on the accuracy of the spherical harmonic coefficients is an excellent example. Previously, Rapp [1968] gave some results that indicated low reliability of these coefficients for degree much higher than 12. His present paper goes further into the relation between the standard deviation of a co-

SUMMARY

efficient and the expected possible improvement in the coefficient. Depending on what criterion one uses for the ratio of the two, he finds a limiting value between 12 and 29 for the degree of a coefficient. He also uses correlation coefficients between the harmonic coefficients to estimate the latter's reliability.

An entirely different approach to the problem of how to assess errors in geodetic results is taken by Martin and Roy, who compare the timing and position errors and residuals of different models. They compare six different gravity fields, and select a field as best that is a compromise between the Smithsonian 1966 field and the 3.5 field of the Applied Physics Laboratory. Since their procedure is entirely computational and ad hoc, it does not have the generality of application of Rapp's. On the other hand, it is easy to use and, being simply a least-squares procedure, gives readily interpretable results.

Just as there are different means of evaluating the errors in gravity fields, so there are different methods of computing the gravity fields. These differences are well illustrated by comparing the reports by Strange et al., by Arnold, and by Cazenave, Forestier, et al. Strange and Arnold derive gravity-field values from both satellite and surface gravity data; Cazenave et al. uses only satellite data. The work of Strange et al. was concentrated on the United States; that of Arnold and Cazenave et al. was global. But Strange et al. used considerably more surface data than Arnold. As a consequence, the geoid for the United States is estimated by Strange et al. to have a precision of ± 2 meters, while the geoid of Arnold is estimated by the editors to have a precision of about $\pm 10\text{--}15$ meters. The methods used by the two are different also. Strange et al. used a combination of Stokes' method and a direct solution of the radial distance in the spherical harmonic. Arnold computed first the gravity anomalies and from these the geoid heights.

In refining determinations of the gravity field and the geoid, it is inevitable that some of the small variations of the earth from a rigid, uniformly rotating body will begin to have noticeable effects on the satellite orbits. At present, the changes in rate of rotation have not definitely been detected, but we can discern changes in the orientation of the rotational axis and in

HENRIKSEN, MANCINI, AND CHOVITZ

295

the shape of the earth as a function of time. The path of the earth's axis of rotation about a mean pole has a radius of about 10 meters. Since present satellite position errors can be kept within 1 to 2 meters (over short arcs), this Chandlerian motion should be detectable, and in fact it has been detected. The U.S. Naval Weapons Laboratory has monitored polar motion since 1969 through its influence on satellite orbit observations, and the paper by Beuglass and Anderle reports on the motion during 1970. Their technique is to evaluate polar motion by analyzing the combined tracking data from all Transit stations. D. Smith has proposed and is experimenting with measuring polar motion by tracking a satellite from two laser-ranging stations in the same meridian located on either side of the orbital plane. In this method, the high precision (better than ± 1 meter) of laser ranging is relied on rather than the averaging effect from a number of stations. The laser precision is in fact evaluated in the paper by Smith, Kolenkiewicz, and Dunn. It also explores the deformations of the earth caused by earth tides. These have an amplitude of about 10 to 20 cm, and their effects were previously detected by Kozai [1968] and Newton [1968], using satellite observations. Smith et al. have been able to verify these earlier results, deriving a value for the Love number of 0.35, compared to 0.29 by Kozai. This is well within the experimental error of the method.

Finally, we remark here on some small non-gravitational perturbations that affect balloon-type satellites. These, reported by Prior, are the effects of air drag and radiation pressure. A detailed analysis of these effects shows that the earth's albedo contributes an appreciable amount to the total radiation pressure. In order to account for air drag, Prior assumed an atmospheric (mostly hydrogen) pressure above 2300 km about 3 times that provided for by the 1966 U.S. standard atmosphere. Since the hydrogen density could conceivably be variable enough to account for the difference, the existence of this difference is not as important as the techniques used, which includes the effect of ion drag.

INSTRUMENTATION AND ENVIRONMENT

In geodesy, as in most other sciences, many major advances result from the introduction

of new instrumentation, and new epochs are marked off by progress in instrumentation rather than in theory. At the present time, we can see several new fields opening in satellite geodesy because new kinds of instruments are being introduced. Three of these are discussed in this volume: the satellite-borne altimeter, the satellite-borne gravity gradiometer, and satellite-to-satellite tracking.

The satellite-borne altimeter is the subject of three papers. The one by Stanley, Roy, and Martin is largely a description of what can be accomplished with an altimeter having an accuracy of better than 50 cm. In particular, they conclude that the geoid can be found to ± 1 meter worldwide. Although their analysis does not say so specifically, this value undoubtedly applies only to the geoid over the ocean. As they point out, one of the critical factors in attaining this high accuracy is the error in the orbit, and it is to reduce this error that Baker's paper, discussed before, addresses itself. An equally important factor, however, is the error in the altimeter's measurement of distance. This error, assumed to be a fixed value by Stanley, Roy, and Martin, is studied in detail in the papers by Pierson and Mehr and by Greene. Both consider correctly that the decisive factor affecting the error will be the shape of the radar pulse that returns to the altimeter after reflection from the ocean surface. The analysis by Pierson and Mehr is a continuation of their earlier studies. It uses an altimeter designed for NASA's Skylab as the archetype, and derives the effect of sea-surface topography on the emitted pulses. Their most important conclusion is that the waves may cause the return pulse to rise to a level of as much as 50 nsec before return energy from the nadir point reaches that level. At present, there are no experimental data that apply exactly to this situation. The closest available are experiments carried out by Yaplee and others at NRL, and by Genest and others at Raytheon (both cited in the Pierson and Mehr paper). As far as we can tell by extrapolation, the Pierson and Mehr predictions agree with these data. Much more experimental work is, however, necessary. Some of the problems introduced by 'early return' can be handled by putting proper judgment circuitry into the altimeter; Pierson and Mehr

believe that a split-gate detection method would be best.

Greene's paper deals with the same subject from a much broader viewpoint, considering not only pulse-shape induced errors but also errors caused by propagation and geometry. He considers an altimeter of the type to be carried in Geos C and a three-gate detector.

Such a variety of situations is covered by Greene that no short statement can summarize his results. An interesting one, however, is that the rms and bias errors for altimetry with pulse compression are a factor of 10 less than for altimetry without pulse compression.

Determining the geoid in ocean areas directly by altimetry has the advantage of supplying added information about sea state and other oceanographic data. The method is of little use over land, however, where other approaches must be tried. The ones most explored depend on a closer determination of the gravity field, and two recently developed possible procedures are considered in three papers. One is the satellite-borne gravity-gradient meter. Other designs have been proposed in the past, but none has shown much hope of getting to the 10^{-11} m/sec² per meter (10^{-2} Eotvos unit) required to be an improvement over other methods like more intensive and accurate tracking. The instrument described by Forward uses rotating, symmetrically placed masses, and is expected eventually to have the necessary accuracy, averaged over 30 sec. Forward's estimate is that this will extract gravity data out to (Legendre series terms of) degree 75. When one deals with gravity amplitudes as small as these, the use of Legendre series representation becomes unwieldy and without physical significance. This is particularly true in view of Rapp's results stated earlier. A better representation, perhaps like that described by Lundquist and Giacaglia, is then necessary.

The other new approach for finer determination of the gravity field is satellite-to-satellite tracking. The papers by Schwarz and by Martin, Martin, and Smith, being primarily concerned with the geodetic implications of the procedure rather than the instrumentation itself, have been discussed in the section on physical geodesy.

At present, timing is not a critical factor in geodetic satellite tracking. The use of good

quartz crystal clocks checked frequently against VLF time signals and periodically against portable cesium clocks brought to the stations should eliminate errors of more than 10 μ sec. This error is equivalent to a satellite motion of less than 0.1 meter, which is not significant compared to other errors. The situation is different, of course, when timing for very-long-baseline interferometry is considered. Markowitz, in his paper, gives a clear, concise account of timing service available and errors to be expected, and he confirms the above conclusions.

Satellite geodesy, like classical geodesy, is troubled by the effects of refraction on the measured angles and distances. These effects do not have the same critical role in satellite geodesy as they do in classical. First of all, most angle measurements in satellite geodesy are with respect to a coordinate system referred to the stars and are handled in such a way that only second-order effects need be accounted for. Second, distance measurements are almost always to points outside the atmosphere, so that only astronomical refraction need be considered; also, the effect of refraction on distance is less significant than that on angle. Third, lateral refraction is not a problem. Nevertheless, refraction is still an important error source, especially when radio waves longer than a decimeter are used, since at these wavelengths the ionosphere becomes influential. Hopfield [1969], Owens [1967], Bean [1959], Thayer [1967], and many others have studied the radio-refraction problem, and Saastamoinen's recent work is a notable addition to the literature. Saastamoinen deals with refraction at microwave (centimeter and shorter wavelength) frequencies, and ignores, therefore, the minute ionospheric contribution. It is worth considering, in this connection, the work done by Brettenbauer [1969] on astronomical refraction of light, which concludes that for tracking stations near sea level the atmospheric correction is independent of atmospheric conditions.

The paper by McDougal, Lee, and Romick ascertains the reflective properties of Pageos and Echo 1 and, from these, determines the optical centers of these satellites. The techniques used were refinements of those developed previously at the missile ranges, and are good enough to determine mean radii to about 0.2 meter.

EXTRATERRESTRIAL GEODESY

The term extraterrestrial covers geodesy-related activities that involve other planets than the earth, or other satellites than artificial ones. The connections among the papers presented are therefore tenuous. Each paper stands as an isolated example of current achievement in its own field.

The first one is on the tracking of retrodirective (corner-cube) reflectors on the moon. In the past, many scientists have suggested placing a radio beacon, optical beacon, or optical reflector on the moon to improve knowledge of the moon's librations, its orbit, and the shape of the earth. The only project of this kind to be put into effect thus far is that reported on by Faller et al. The principles of the technique are reviewed in their paper. The range-measurement errors given are on the order of 30 cm, but 3 cm is anticipated. These values are mostly based on theoretical considerations, that is, there are still no experimental data from the project to verify the estimates. Furthermore, until the error in the speed of light is reduced, the 3-cm estimate is out of the question.

The next two papers deal with the gravity fields of the moon and Venus, respectively. The first, by Kaplan and Kuncicw, is an independent continuation of work done by *Michael and Tolson* [1967] at NASA Langley Research Center, by *Sjögren and Muller* [1968] and others at Jet Propulsion Laboratory (JPL), and by *Wong* [1969] and others at Aerospace Corporation. The Langley group expressed the moon's gravity potential in spherical harmonics; the JPL and Aerospace groups used point masses or bodies of masses. Each method has its advantages, and the papers in the physical geodesy section of this volume discuss this question from the standpoint of earth geophysics. The moon's anomalous potential other than the flattening term appears now to be relatively much larger than that of the earth, and so the Legendre series representation loses some of its usefulness. Kaplan and Kuncicw meet the situation by selecting a judicious combination of both methods. Their results, judged by the rate of reduction of the Legendre series terms, seem to justify the approach.

In contrast, the paper by Baldi et al. on the

gravity anomalies of Venus is almost entirely theoretical in nature, deducing the gravity field of Venus from the mass, radius, and surface temperature of the planet. The viewpoint and conclusions are interesting, but, while the approach is valid for stellar structures in which there is considerable homogeneity and for which all applicable laws and boundary conditions can reasonably be assumed, this situation does not exist for any planet, except perhaps the earth itself. We cannot even at present depend on our knowledge of the moon to make reliable inferences of this nature, and much less is known about Venus than about the moon.

Kaula's paper is an estimate of future events in planetary geodesy based on presently planned NASA programs. He specifically points out what additional steps should be taken for increased knowledge: for example, close-orbiting artificial satellites for Mercury and Venus, capable of being accurately tracked.

A LOOK AT THE FUTURE

In sum, the papers in this volume indicate that satellite geodesy enjoys the prospects of a rich future. Probably the most important development in the next few years will be the emergence of a new variety of data gathering methods. The most significant of these is possibly satellite altimetry, which has the capability of supplying information on the geoid not attenuated by the satellite's altitude. The potential application of altimetry for oceanography as well will provide added impetus to the development and use of this source.

As geodetic knowledge of the earth is refined, the emphasis in theoretical research will turn to the application of geodetic information to geophysical models. It should be remembered that only a few years ago the subject of polar motion was not considered properly a part of geodesy, since it dealt with phenomena of magnitude less than could be measured by the geodetic techniques then current. Now, crustal motion, earth tides, and continental drift are all falling within the domain of geodetic analysis. It is anticipated and hoped that satellite geodesy will contribute to building up a comprehensive qualitative as well as quantitative model of the earth.

However, when attention is turned to the moon and planets, geodesy in a sense returns to

an earlier era. Here we will be concerned in the near future with determining gross shapes and rough gravitational distribution. Progress can be much more rapid than it was for the earth, the tools for data analysis having already been developed, provided only that the anticipated stream of data is not curtailed. But, even if it is, we feel that the future will not be bleak, since scientists will turn their attention to devising ingenious methods for extracting the maximum possible out of what is available.

REFERENCES

- Baarda, W., *A Testing Procedure for Use in Geodetic Networks*, Netherlands Geodetic Commission, Delft, Netherlands, 1968.
- Bean, B., and G. Thayer, Models of the atmospheric refractive index, *Proc. IRE*, 47(5), 740, 1959.
- Bjerhammar, A., *On the Determination of the Shape of the Earth*, Geodesy Division, Royal Institute of Technology, Stockholm, 1960.
- Brettenbauer, K., New results concerning the atmospheric effect on laser ranges to artificial satellites, paper presented at the International Symposium on Electromagnetic Distance Measurement and Atmospheric Refraction, Int. Ass. Geod. and Amer. Geophys. Union, Boulder, Colo., 1969.
- Hirvonen, R., New theory of the gravimetric geodesy, *Paper 56, Ser. A3*, Finnish Acad. of Sci., Helsinki, 1960.
- Hopfield, H., A two-quartic tropospheric refracting profile for correcting satellite data, paper presented at the International Symposium on Electromagnetic Distance Measurement and Atmospheric Refraction, Int. Ass. Geod. and Amer. Geophys. Union, Boulder, Colo., 1969.
- Koch, K. R., Alternate representation of the earth's gravitational field for satellite geodesy, *Boll. Geofis. Teor. Appl.*, 10, 318-325, 1968.
- Kozai, Y., Love's number of the earth derived from satellite observations, *Publ. Astron. Soc. Japan*, 20(1), 24-26, 1968.
- Kozai, Y., Revised zonal harmonics in the geopotential, *Smithson. Astrophys. Observ. Rep.* 295, 1969.
- Michael, W., and R. Tolson, The lunar orbiter project selenodesy experiment, in *The Use of Artificial Satellites for Geodesy*, vol. 2, edited by G. Veis, pp. 609-633, National Technical University, Athens, 1967.
- Molodensky, M., The external gravitational field of the figure of the earth (translated title), *Publ. 12(3)*, Akad. Nauk. SSSR, Moscow, 1948.
- Newton, R. R., A satellite determination of tidal parameters and earth deceleration, *Geophys. J. Roy. Astron. Soc.*, 14, 505-539, 1968.
- Owens, J. C., Optical refractive index of air: Dependence on pressure, temperature, and composition, *Appl. Optics*, 6(1), 51, 1967.
- Pellinen, L. P., Joint adjustment of gravimetric and satellite data in the determination of the earth's gravitational field, *Byull. Sta. Opt. Nablyudeniya Iskusstv. Sputnikov Zemli*, 55, 58-68, 1969.
- Rapp, R. H., A global $5^\circ \times 5^\circ$ anomaly field (abstract), *Eos Trans. AGU*, 49, 507, 1968.
- Sjögren, W., and P. Muller, Mascons: Lunar mass concentrations, *Science*, 161, 680-684, 1968.
- Thayer, G., Atmospheric effects on multiple-frequency range measurements, *ESSA Tech. Rep. IER 56-ITSA 53*, U.S. Government Printing Office, Washington, D.C., 1967.
- Vinti, J. P., Representation of the earth's gravitational potential, *Celestial Mechanics*, 4(3/4), 348-367, 1971.
- Von Arx, W. S., Practical astronomy from shipboard, *Sky and Telescope*, 29(6), 340-349, 1965.
- Weightman, J., Gravity, geodesy, and artificial satellites, in *The Use of Artificial Satellites for Geodesy*, vol. 2, edited by G. Veis, pp. 467-486, National Technical University, Athens, 1967.
- Wong, L., Dynamical determination of mascons on the moon (abstract), *EOS Trans. AGU*, 50(4), 125, 1969.